UNIVERSITY OF KWAZULU-NATAL

A NOVEL LIBRARY OF PYRIMIDINE BASED HYBRIDS AS POTENTIAL ANTIMALARIAL AGENTS: DESIGN, SYNTHESIS, CHARACTERIZATION AND *IN VITRO* BIOLOGICAL EVALUATION.

2021

BY: FRANCIS KAYAMBA

(STUDENT No: 216056692)

Submitted in fulfilment of the requirements for the degree of

Doctor of Philosophy in Pharmaceutical Chemistry

The discipline of Pharmaceutical Science, College of Health Science,

University of KwaZulu-Natal, Durban, South Africa

A NOVEL LIBRARY OF PYRIMIDINE BASED HYBRIDS AS POTENTIAL ANTIMALARIAL AGENTS: DESIGN, SYNTHESIS, CHARACTERIZATION AND *IN VITRO* BIOLOGICAL EVALUATION.

BY

FRANCIS KAYAMBA

216056692

2021

A thesis submitted to the School of Health Science, Discipline of Pharmaceutical science, Department of Pharmaceutical Chemistry, University of KwaZulu-Natal, Westville, for the degree of Doctor of Philosophy.

This thesis has been prepared according to **Format 4** (Thesis by publications) as outlined in the guidelines of the College of Health Sciences, University of KwaZulu-Natal. The chapters consist of a general introduction, chapters in discrete research papers and a final discussion. One chapters has been published, one chapter has been submitted in the peer-reviewed internationally accepted journal and remaining chapters have been written in manuscript format.

As the candidate's supervisor, I have approved this thesis for examination/submission:

Supervisor: Prof R. Karpoormath

Signed: [redacted] Date: 20/April/2021

Co-Supervisor: Prof V.O. Nyamori

Signed: [redacted] Date: 23/April/2021

Abstract

Malaria continues to be a fundamental health threat worldwide due to the rise of resistance in frontline medications, including artemisinin-based combination therapy (ACT). The condition requires new, innovative drug candidates to overcome existing challenges in the current treatment. The synthetic alteration involving existing pharmacophoric antimalarial drugs and natural products were utilized to construct an antimalarial candidate that could serve as a potent and effective lead compound for potential optimization. In continuing our ongoing research and the need to discover newer antimalarials, we endeavored to synthesize a novel library of antimalarial hybrids analogues comprising 4,6-diphenylpyrimidine core, a pharmacophoric moiety inspired by pyrimethamine and chalcone. Pyrimidine is a versatile heterocyclic building block of many drugs with vast medicinal properties such as antimicrobial, anti-inflammatory, analgesic, anticonvulsant, anticancer, and antioxidant. Fifty-three hybrids consisting of pyrimidine core fused with other significant antimalarial moieties, namely quinoline, cinnamoyl and 1,2,3-triazole through an alkane diamine linker, particularly piperazine, were synthesized. All the newly synthesised compounds were identified based on physicochemical and spectral data (IR, ^{1}H NMR, ^{13}C NMR and HRMS) per their predicted structures and preliminarily screened for antimalarial (*in vitro*) activities. Also, the binding affinities of two essential cytosolic *Plasmodium (P) falciparum* heat shock protein 70 homologues (*Pf*Hsp70-1 and *Pf*Hsp70-z) were examined.

Pyrimidine-quinoline hybrids (**Chapter 3**) demonstrated antimalarial ranging from 0.32 to 83 µM. Of this series, compounds **7a** and **7b** were the most potent with IC_{50} value of 0.32 ± 0.06 µM and IC_{50} 1.62 ± 1.14 µM, respectively with a safety profile of 9.79 to human kidney epithelial (HEK293) cells for **7a**. Equally, compounds **7a** and **7b** presented the highest binding affinity of two essential cytosolic *P. falciparum* heat shock protein 70 homologues; PfHsp70-1 and PfHsp70-z, with K_D in a lower nanomolar range (4.4-11.4 nM)

Pyrimidine-cinnamoyl hybrids (**Chapter 4**) exhibited antimalarial activity from 0.18 to 50 µM. Compounds **8a** and **8l** were the most active with IC_{50} value of 0.18 ± 0.02 µM and IC_{50} 0.21 ± 0.00 µM with the safety profile of 18.59 and 16.75 to human kidney epithelial (HEK293) cells, correspondingly. Compounds **8a** and **8l** showed the highest binding affinity of two essential cytosolic *P. falciparum* heat shock protein 70 homologues; PfHsp70-1 and PfHsp70-z, with K_D in a lower nanomolar range (9.69-10.8 nM).

Pyrimidine-1,2,3-triazole hybrids (**Chapter 5**) showed antimalarial activity from 0.04 to 2.41 µM. Compounds **8c**, **8e** and **8t** were the most promising with IC_{50} values ranging from 0.18 to

0.29 µM with a safety profile tenfold compared to human kidney epithelial (HEK293) cells. Similarly, compounds **8c**, **8e** and **8t** displayed the highest binding affinity of two essential cytosolic *P. falciparum* heat shock protein 70 homologues; PfHsp70-1 and PfHsp70-z, with K_D in a lower nanomolar range (11.3-90.0 nM).

The pyrimidine-1,2,3-triazole hybrid library demonstrated the most promising family as it had eight more potent compounds with IC_{50} values less than 0.50 µM, followed by the pyrimidine-cinnamoyl and lastly, pyrimidine-quinoline. All families exhibited PfHsp70-1 and PfHsp70-z enzyme activity in nanomolar concentration with a safety of 10-fold against human kidney epithelial (HEK293) mammalian cells.

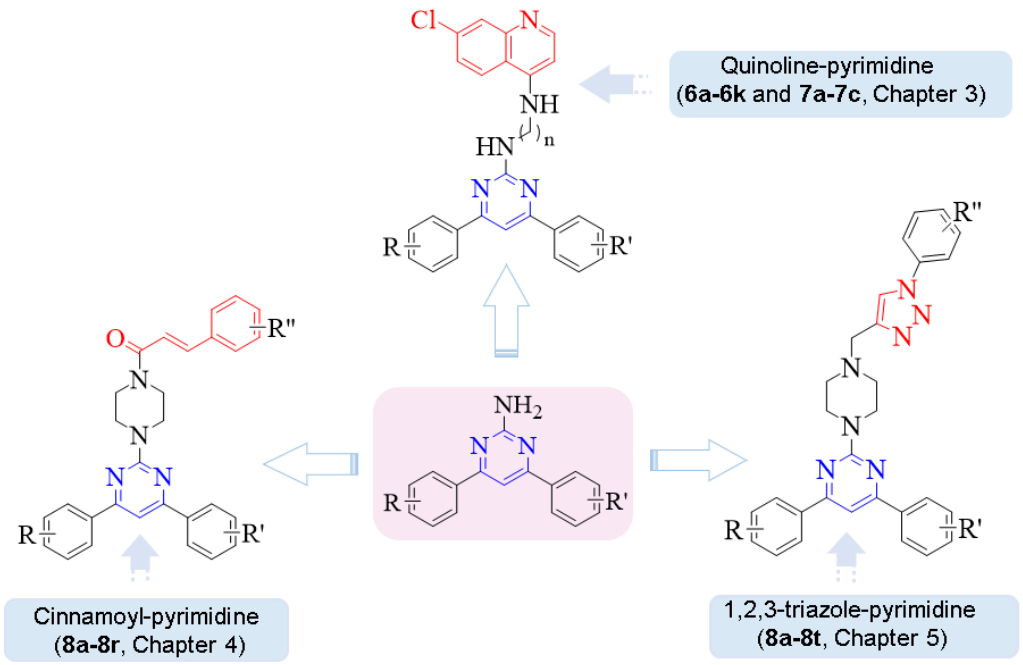

Keywords: cinnamoyl, 1,2,3-triazole, quinoline, pyrimidine, antimalarial, plasmodium, hybridization

DECLARATION 1 – PLAGIARISM

I, **Francis Kayamba,** declare that

i. The research reported in this thesis, except where otherwise indicated, is my original work.

ii. This thesis has not been submitted for any degree or examination at any other university.

iii. This thesis does not contain other person' data, pictures, graphs or other information, unless specifically acknowledged as being sourced from other persons.

iv. This thesis does not contain other persons' writing, unless specifically acknowledged as being sourced from other researchers. Where other written sources have been quoted, then:

   a. Their words have been re-written, but the general information attributed to them has been referenced.

   b. Where their exact words have been used, then their writing has been placed in italics and inside quotation marks and referenced.

v. Where I have reproduced a publication of which I am an author, co-author, or editor, I have indicated in detail which part of the publication was actually written by me.

vi. This thesis does not contain text, graphics or tables copied and pasted from the internet, unless specifically acknowledged, and the source being detailed in the thesis and in the reference's sections.

Signed: 

Date: 3rd April 2021

DECLARATION 2 – PUBLICATION

DETAILS OF CONTRIBUTION TO PUBLICATIONS that form part and/or include research presented in this thesis (include publications in preparation, submitted, in press and published and give details of the contributions of each author to the experimental work and writing of each publication).

Publications

1. **Francis Kayamba**, Srinivasulu Cherukupalli, Mbuso Faya, Ofentse Jacob Pooe, Vincent. O. Nyamori, Rajshekhar Karpoormath, "Lactate dehydrogenase and Malate dehydrogenase: potential antiparasitic targets for drug development studies". *Submitted to Bioorganic & Medicinal Chemistry Letters.*
   Contributions: I did the literature review and wrote the entire manuscript under the supervision of Dr Rajshekhar Karpoormath (Associate Professor) and Professor Vincent. O. Nyamori. The rest all the co-authors assisted with improvisation, writing up and summarizing the literature review (conclusion).

2. **Francis Kayamba**, T. Malimabe, I.K. Ademola, O.J. Pooe, N.D. Kushwaha, M. Mahlalela, R.L. van Zyl, M. Gordon, P.T. Mudau, T. Zininga, A. Shonhai, V.O. Nyamori, R. Karpoormath, "Design and synthesis of quinoline- pyrimidine inspired hybrids as potential plasmodial inhibitors," *European Journal of Medicinal Chemistry*, volume 217, page 113330 in 2021.
   Contributions: I devised the rationale and carried out all the experiments, characterization and manuscript writing under the supervision of Dr Rajshekhar Karpoormath (Associate professor) and Professor Vincent Nyamori. The antiplasmodial evaluation was conducted at Professor Robyn L van Zyl's laboratory, while the enzymes studies at Professor Tawanda Zininga's laboratory. The remaining co-authors assisted with designing the target molecules, as well as the results write-up and discussion.

3. **Francis Kayamba**, Teboho Malimabe, Ofentse Jacob Pooe, Robyn L van Zyl, Pertunia T Mudau, Tawanda Zininga, Addmore Shonhai, Vincent O. Nyamori, Karpoormath Rajshekhar "Promising class of Antiplasmodial agents; Design and synthesis of novel Pyrimidine–Cinnamoyl Hybrids". *Manuscript.*

Contributions: I devised the rationale and carried out all the experiments, characterization and manuscript writing under the supervision of Dr Rajshekhar Karpoormath (Associate professor) and Professor Vincent Nyamori. The antiplasmodial evaluation was conducted at Professor Robyn L van Zyl's laboratory, while the enzymes studies were conducted at Professor Tawanda Zininga's laboratory. The remaining co-authors assisted with designing the target molecules, as well as the results write-up and discussion.

4. **Francis Kayamba**, Teboho Malimabe, Ofentse Jacob Pooe, Robyn L van Zyl, Pertunia T Mudau, Tawanda Zininga, Addmore Shonhai, Vincent O. Nyamori, Karpoormath Rajshekhar "Synthesis and Antimalarial Activity of Novel 1,2,3-Triazole-Pyrimidine Hybrids". *Manuscript.*

   Contributions: I devised the rationale and carried out all the experiments, characterization and manuscript writing under the supervision of Dr Rajshekhar Karpoormath (Associate professor) and Professor Vincent Nyamori. The antiplasmodial evaluation was conducted at Professor Robyn L van Zyl's laboratory, while the enzymes studies were conducted at Professor Tawanda Zininga's laboratory. The remaining co-authors assisted with designing the target molecules, as well as the results write-up and discussion.

Conference contributions

1. **Oral presentation**: Synthesis of novel 4-nitropyrrole-based semicarbazide and thiosemicarbazide hybrids with antimicrobial and anti-tuberculosis activity. College of Health Sciences Annual Research Symposium, held at K-RITH, Nelson R Mandela School of Medicine Campus, Durban, South Africa, from 8th to 9th September **2017**.

2. **Poster presentation**: Design and synthesis of quinoline-pyrimidine inspired hybrids as potential plasmodial inhibitors. College of Health Sciences Annual Research Symposium, held at K-RITH, Nelson R Mandela School of Medicine Campus, Durban, South Africa, 1st November **2019**.

Other publications

1. N.D. Kushwaha, S.J. Zamisa, B. Kushwaha, A. Sharma, **Francis. Kayamba**, S.R. Merugu, A.M. Ganai, V.A. Obakachi, F. Albericio, R. Karpoormath, "Synthesis, crystal structure, spectroscopic and photophysical studies of novel fluorinated quinazoline derivatives", *Journal of Molecular Structure*; 1231 (**2021**) 129951.
2. Tirivashe Elton Chiwunze, Venkata Narayana Palakollu, Atal AS Gill, **Francis Kayamba**, Neeta Bachheti Thapliyal, Rajshekhar Karpoormath. "A highly dispersed multi-walled carbon nanotubes and poly (methyl orange) based electrochemical sensor for the determination of an antimalarial drug: Amodiaquine", *Materials Science and Engineering*: C 97 (**2019**), 285-292.
3. Srinivasulu Cherukupalli, Girish A Hampannavar, Sampath Chinnam, Balakumar Chandrasekaran, Nisar Sayyad, **Francis Kayamba**, Rajeshwar Reddy Aleti, Rajshekhar Karpoormath. "An appraisal on synthetic and pharmaceutical perspectives of pyrazolo [4, 3-d] pyrimidine scaffold", *Bioorganic & Medicinal Chemistry*: 26 (**2017**), 309-339.

Signed: 

Date: 3rd April, 2021

DEDICATION

Dedicated firstly, my beloved wife "Chipo" for her support, patience and endurance during my absence when undertaking my studies.

Also, to my two darling daughters, Mandy and Yandi, for your endurance and stamina when I was absent during the critical times in your life. I love you guys and owe this degree to you.

To my mother and father, in whom they tireless efforts have made me who I have become today.

My siblings, Ellie, Stephen, Mwewa, Vero, Paul and Joseph, for your love, support and encouragement.

And finally, my very good friends, Dr Chester Kalinda, Shem Sikombe and Nomfundo Ncobeni, for being there to support and encourage me during the course of the study. Your helping hand made this degree possible.

ACKNOWLEDGEMENT

I want to express my special thanks to my superiors, Professor Rajshekhar Karpoormath and Professor Vincent Nyamori, for their valued leadership, patience, and motivating suggestions which made this research and thesis a success. I was energized by your kindness and enthusiasm and faith in me all along. Thank you for your generosity and outstanding commitment.

Special thanks to the present and past group members of Synthetic and Medicinal Chemistry Research Group (SMCRG), in particular Dr Karunanidhi, Dr Hampannavar, Dr Sayyad and Dr Singh, for their valuable scientific contributions throughout the research, you're an inspiration, and I'm blessed to have you. In tough times, I was bounded by your constant encouragement and moral support. I'm short of words to say thank you.

My heartfelt thanks also go to Professor Robyn Van dan and her team from the Pharmacology Division, Department of Pharmacy and Pharmacology, Faculty of Health Sciences, University of Witwatersrand, Johannesburg 2193, South Africa, for performing the antiplasmodial screening.

Also, my heartfelt thanks to Dr Ofentse Jacob Pooe and his team For making the enzyme studies possible.

I would also like to take a moment to thank Dr Wesley Moran, my former supervisor, for laying the groundwork for this work.

I want to thank the technical staff, Mr Dilip Jagjivan and Dr Vuyisa Mzozoyana School of Physics and Chemistry and Ms Caryl Janse van Rensburg, Mass Spectrometry Laboratory, School of Chemistry, UKZN Pietermaritzburg, for their help in spectroscopic experiments.

My humble gratitude to the University of KwaZulu-Natal, South Africa, for approving of my Research proposal and providing all the necessary facilities for carrying my research work successfully.

My sincere Thanks and appreciation to all the supporting staff at Discipline of Pharmaceutical Sciences, College Of Health Sciences.

Additionally, I would like to thank my wife and friends for helping finalize this project within a limited time.

LIST OF ABBREVIATIONS AND ACROYNMS

^{13}C NMR	Carbon-13 nuclear magnetic resonance
^{1}H NMR	Proton nuclear magnetic resonance
3D-QSAR	Three-dimensional quantitative structure-activity relationship
A	Alanine
ACT	Artemisinin-based Combination Therapy
AIDS	Acquired Immune Deficiency Syndrome
AP	Atovaquone-proguanil
APAD	3-Acetylpyridine adenine dinucleotide
ARTS	Artemisinin combination therapy
ATP	Adenine triphosphates
BC	Before Christ
C	Cysteine
$CDCl_3$	Chloroform-d
$CHCl_3$	Chloroform
cm^{-1}	Wavenumber
COSY	Correlated nuclear magnetic resonance spectroscopy
CQ	Chloroquine
CRT	Chloroquine resistance transport
D	Aspartic acid
DCM	Dichloromethane
DHFR	*Dihydrofolate reductase*
DHODH	Plasmodial dihydroorotate dehydrogenase
DHPS	*Dihydropteroate synthase*
DMF	*N, N*-Dimethylformamide
DMSO	Dimethyl sulfoxide
DMSO-d_6	Dimethyl sulfoxide-d6
DNA	Deoxyribonucleic acid
DTT	Dichlorodiphenyltrichloroethane
DXP	1-Deoxy-D-xylulose-5-phosphate reductoisomerase
DZG	Dehydrozingerone
E	Glutamic acid
EIMS	Electron Ionization Mass Spectroscopy
ESI	Electrospray ionization
FPIX	Ferriprotoporphyrin IX
FTIR ATR	Fourier-transform infrared spectroscopy Attenuated total reflectance
G	Glycine (Gly)
GdnHCl	Guanidine Hydrochloride
H	Histidine(His)
HIV	Human immunodeficiency virus

hLDH	Human lactate dehydrogenase
HMBC	Heteronuclear multiple bond coherence
HRMS	High-resolution mass spectrometry
HSQC	Heteronuclear single quantum coherence
I	Isoleucine(lle)
IC_{50}	The drug concentration causing 50% inhibition
IC_{90}	The concentration of drug needed to inhibit 90% growth
IE	Electron Ionization
IPA	Isopropanol
K	Lysine
K_2CO_3	Potassium Carbonate
LDH	lactate dehydrogenase
M	Methionine(Met)
MDH	Malate Hydrogenase
MDR1	Multidrug Resistance Mutation
MeOH	Methanol
MHz	Megahertz
MTT	3-(4,5-Dimethylthiazol-2-yl)-2,5-Diphenyltetrazolium Bromide
MW	Microwave
N	Asparagine
NADH	Nicotinamide adenine dinucleotide
NADPH	Nicotinamide adenine dinucleotide phosphate
ND	Not determined
NOESY	Nuclear Overhauser Effect Spectroscopy
P	Proline(Pro)
p	*Falciparum*
PABA	Para-aminobenzoic acid
pfLDH	Plasmodium falciparum lactate dehydrogenase
PI4K	Phosphatidylinositol 4 kinase
$POCl_3$	Phosphoryl chloride
ppm	Parts per million
PRQ	Piperaquine
PS	Sulfadoxine-pyrimethamine
PZQ	Praziquantel
QSAR	Quantitative structure-activity relationship
R	Arginine (Arg)
RBC	Red blood cell
RNA	Ribonucleic acid
ROS	Reactive oxygen species
S	Serine
SA	South Africa
SAR	Structural activity relationship

SERCA	Sacro/endoplasmic reticulum Ca^{2+}-ATPase
SD	Standard Deviation
spp	Multiple species
T	Threonine
t-BuOH	*tert* Butyl alcohol
TCA	Tricarboxylic acid cycle
TgLDH	Toxoplasma gondii lactate dehydrogenase
THF	Tetrahydrofuran
TLC	Thin-layer chromatography
TMS	Tetramethylsilane
US	United States
V	Valine
v_{max}	Maximum frequency range
WHO	World Health organisation
Y	Tyrosine

TABLE OF CONTENTS

LIST OF FIGURES

Chapter 1

LIST OF TABLES

Chapter 1

CHAPTER 1

INTRODUCTION

1.1. Overview

Malaria ranks third among the major infectious diseases following pneumococcal acute respiratory and tuberculosis infections. It is mainly caused by a *single-cell eukaryotes* holoparasite of a *genus Plasmodium* of a phylum *Apicomplexa* member in the order *Haemosporida, which* transmits the disease in a person by a single bite of infected female anopheles *gambiae* mosquito injecting sporozoites into the bloodstream [1, 2]

The term malaria is an Italian word "*mala aria*" meaning "bad air" or "aria cattiva" coined after an atrocious fever that ravaged the Roman empire around five Before Christ (BC) [2]. A malaria mastery commenced in 1880 with Alphonse Lavern, a French military surgeon who discovered multiple phases of malaria in the peripheral human blood, such as pigmented spherical body, filiform components and exflagellation of a male gametocyte. These elements, which he recognized as protozoan parasites, namely Oscillaria malariae, were constant in patients with malaria and believed to cause disease [3]. He also noted that the drug quinine was effective to a certain extent against the parasites, mostly in the early stages. In 1885, Italian scientists Ettore Marchiafava and Angelo Celli proposed that the parasite described by Alphonse be called '*Plasmodium malariae'* due to its similarity with plasmodia. In 1889, Ronald Ross, a British doctor, discovered that malaria was transmitted by the mosquito, intermediate host, using an experimental model of bird malaria and female mosquito of Culex species. In 1898, Giovanni Battista Grassi, an Italian Zoologist, discovered that human malaria was caused only by Anopheles claviger and vectored by mosquitoes different from those of the birds. Ross and Grassi's findings revealed that malaria was transmitted by the bite of an infected mosquito. Grassi suggests malaria prevention by sensitizing people in prevailing regions to avoid outdoors at nightfall and avert mosquitoes from entering the houses [4, 5]. In subsequent years, dichlorodiphenyltrichloroethane (DTT) insecticide was introduced and used in more than ten nations to reduce and eliminate disease transmission. Unfortunately, the underdeveloped countries, such as Sub-Saharan nations, were not part of the elimination programme, which to date show the highest recorded malaria cases [6]. The progression, discoveries and mitigation of malaria is summarized in **Figure 1.1.**

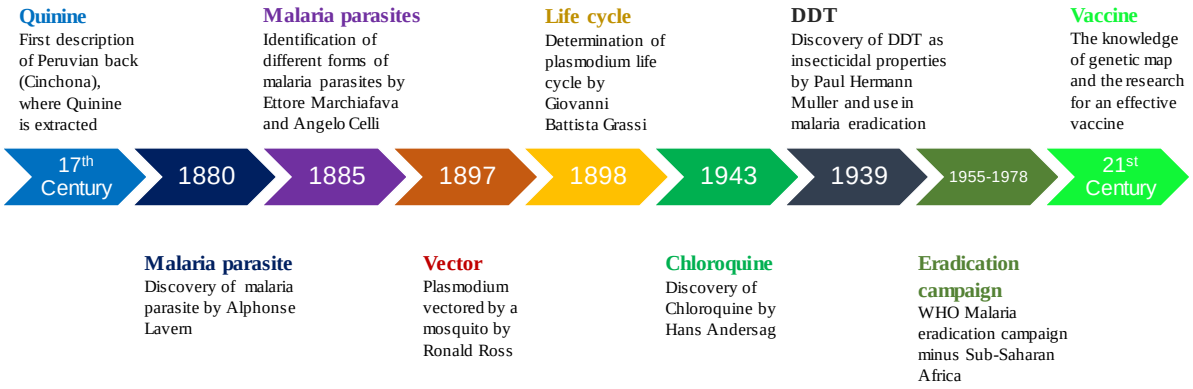

Figure 1.1. Main events on the revolution of malaria.

1.1.1 Malaria species

Five main *Plasmodium (p)* species are known to cause infection in humans viz *Plasmodium (P)*,

P. falciparum	Responsible for the majority of malaria cases with 99.7% in the African region, 62.8% in South-East Asia, 69% in the Eastern Mediterranean and 71.9% in the Western Pacific.
P. vivax	Predominant in the Americas, representing 74.1% of malaria cases.
P. ovale	Less common and found in tropical west Africa and rare frequency in Southeast Asia, Philippines and New Guinea.
P. malaria	low prevalence in the tropics.
P. knowles	It is rare, although most at risk are those living near macaques.

P. falciparum and P.vivax cause the majority of infections and deaths in humans [7, 8].

Malaria incidence in affected areas remains a health problem, an essential factor of morbidity and has economic implications costing endemic areas a huge amount of money for mitigation and treatment [9-11]. At the start, the clinical symptoms of malaria infection are mild, such as fever and headache, and they are difficult to diagnose [10, 11]. Malaria caused by *P. falciparum* can progress to severe illness if not handled within 24 hours, and it is often lethal.

1.1.2 Geographical synopsis of malaria infection

1.1.2.1 A global overview

Two hundred nineteen million people suffer from this disease every year, 90% in sub-Saharan Africa, two-thirds of the remaining cases occur in six countries – India, Brazil, Sri Lanka, Vietnam, Columbia and Solomon Islands. Four hundred and thirty-five thousand people died primarily in the World Health Organization (WHO) African region, accounting for 93% of the

deaths, mostly infants under five years and pregnant women. A decline in mortality rates in 2019 were as per the following; South East Asia WHO region (74%), Africa (67%) and Eastern Mediterranean regions (16%). About 3.1 billion people in Sub-Saharan African, in particular, remain at risk of malaria infection [12]. Malaria is more widespread in the poor tropical and subtropical regions of the world, as indicated in red in **Figure 1.2,** owing to the following reasons;

i. Favourable climate for the Anopheles mosquitoes to reproduce and continue throughout the year.
ii. These regions are infested with *P. falciparum* strain, contributing to severe malaria and death
iii. Lack of resources and socio-economic instability stall effective malaria control programs.

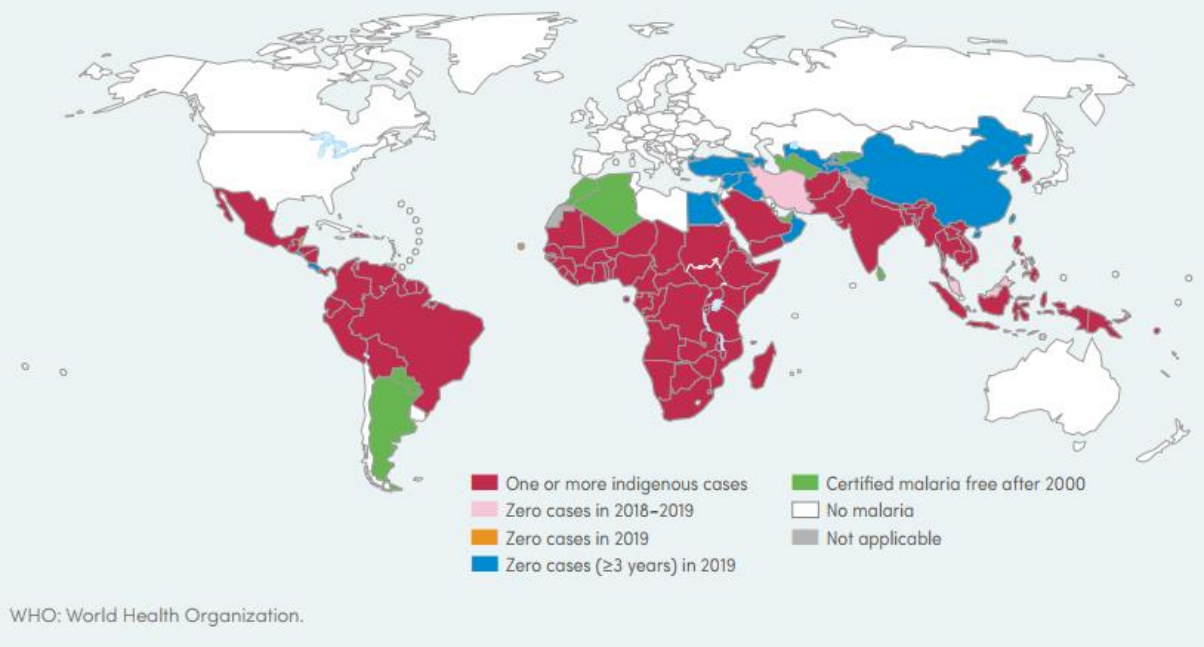

Figure 1.2. Global malaria geographical status of 2019 [12].

1.1.2.2 Malaria in South African

South Africa (SA) is still the only country in southern Africa to have successfully managed malaria-endemic, with only 10% of the population affected. It is common in three provinces, namely north-east Limpopo, along the border with Mozambique and Zimbabwe, Lowveld of Mpumalanga (including Kruger national park) and north of KwaZulu Natal [13, 14], as shown in red in Figure 1.3. Recently, the country recorded an upsurge in malaria cases with 9478 mortality cases and 76 fatalities in 2017/2018 as compared to 2015/2016 with 6 385 cases of malaria and 58 deaths, respectively [13]. The geographical spread of malaria in South Africa

is presented in **Figure 1.3**. Also, a non-endemic region such as Gauteng (green) has experienced an increase in malaria cases owing to travellers coming back from endemic malaria area such as Mozambique [15]. The incidence of malaria in SA is periodic and at its height during the rainy season from September to May, with the highest annual level of infections in January to April [13]. *P. falciparum* accounts for about 95% of malaria in SA [16].

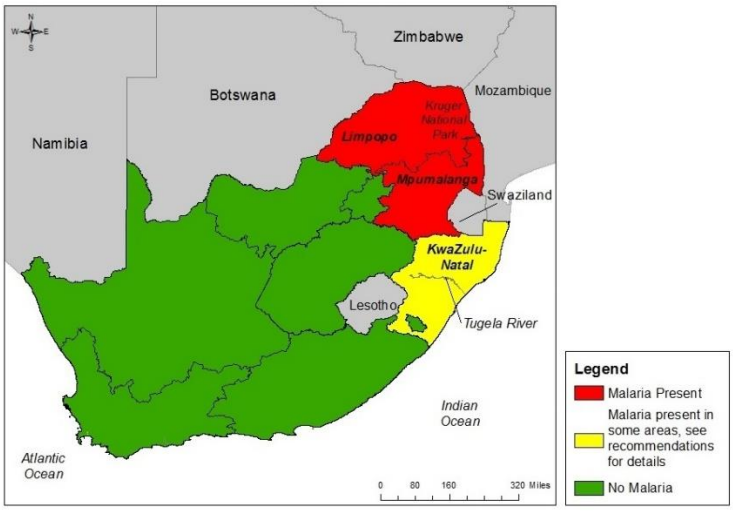

Figure 1.3. South African geographic distribution of malaria incidence.

The campaign to eradicate malaria in SA began around 1956 to reach a malaria-free nation, including endemic province, through the department of health. Measures such as residual spraying and disease modification of malaria helped to decrease malaria prevalence [16, 17]. Besides, the treatment and prevention measures enacted for malaria resulted in a reduction of cases and death by 85% and 81%, respectively, since the year 2000 [18].

1.2 Pathogenesis of malaria

Pathogenesis of malaria provides valuable insights into the relationship between the parasite, the host and the settings during infection.

1.2.1 The life cycle of the *Plasmodium* parasite

The *Plasmodium* life cycle begins when *Plasmodium* species (spp) parasites in the form of sporozoites are introduced into a human host through injecting saliva into the bloodstream during a blood feast of infected female anopheles ‘mosquito. The sporozoite then migrates to the liver, where they infect the hepatic cells (B), during which they propagate for nine to sixteen days by asexual fusion [19]. No symptoms are manifest at this time. The sporozoite matures into tissue schizonts containing thousands of merozoites, and while encapsulated in schizonts, they move to capillaries of the lungs through the heart. Some of the sporozoites in *P. vivax*

grow into hypnozoites that can be latent in the liver for up to 60 days. After five days, the schizonts then bursts into merozoites, releasing the merozoites into the bloodstream, thus entering the erythrocyte stage. Clinical symptoms such as fever begin to manifest when the cells raptures, releasing merozoites. Rapture of red blood cells (RBCs) enables invasion of other cells (intra-erythrocytic cycle) and release of erythrocyte and parasite debris, including malarial pigment (hemozoin) and glycophosphatidylinositol, the putative 'malaria toxin. In some infected blood cells, the merozoites replicate asexually and develop into gametocytes, which are circulated in the bloodstream and ingested during the next blood meal by the mosquito [20, 21]. The gametocytes ingested by the mosquito develop into gametes which progress into ookinetes that migrate to the mid-gut wall of the mosquito and form oocysts where they mature into thousands of sporozoites. The oocyst then bursts, releasing sporozoites that move to the mosquito salivary glands. The human cycle of infection prompts once the mosquito bites the next person [22, 23]. A schematic summary of the *P.falciparum* lifecycle is presented in **Figure 1.4.**

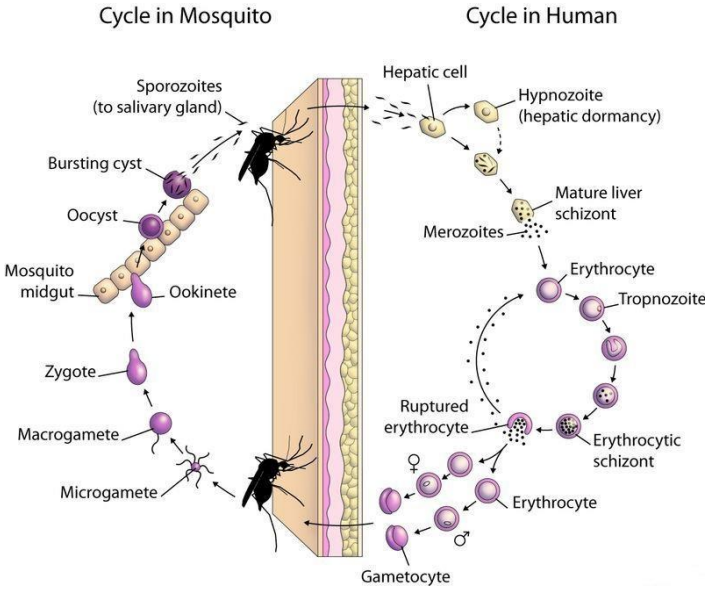

Figure 1.4. Schematic diagram of lifecycle of *P. falciparum.*

1.3 Malaria management

Although malaria is treatable and avertible, it is hard to control owing to the parasite adaptive nature and the disease-related vectors [24]. Malaria management involves three essential elements in the life cycle of *Plasmodium,* which are important for treatment and prevention. These elements include vector (mosquito), human (host) and agent (parasite) [25].

Vector (Mosquito)	Destroying the vector at the larval stage by eliminating breeding sites and also preventing mosquito bites in humans.
Human (host)	A malaria control chain where early diagnosis and timely therapy are important to reduce morbidity and mortality in incidence areas.
Agents	Control measures that deal with antimalarial agents are required to destroy the parasite at the asexual stage, stopping the progression of the infection and preventing blood meal transmission [24-26]. The various stages of management of malaria are illustrated in **Figure 1.5**.

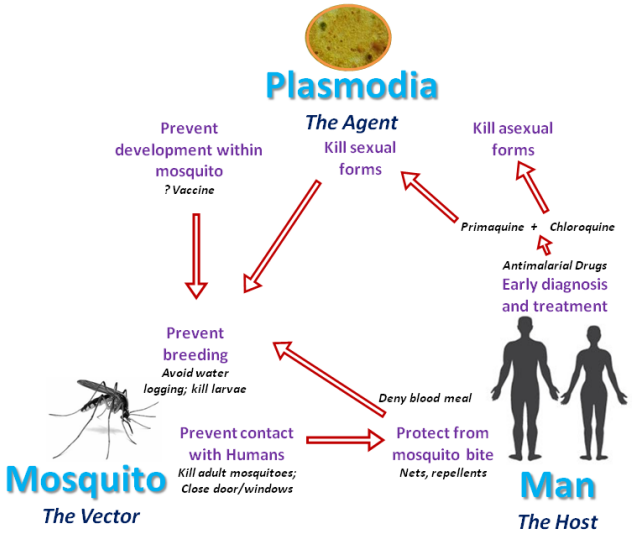

Figure 1.5. Management strategy of malaria [27].

In short, the management of malaria is reducing the infection to a point where it is no longer a threat and health concern. Treatment of malaria depends on the efficacy of the available drug therapies given at different essential stages to stop the *Plasmodium* life cycle [28].

1.3.1 Drug targets

Antimalarial drugs target different stages of the *Plasmodium* life cycle, most of which act on the intra-erythrocyte's stages of a parasite developmental stage associated with pathology that leads to clinical symptoms. In the intra-erythrocytes stage, the parasite assumes a mechanism essential to survive the host immune system while it steals its nutrients for survival. In discovering new drug entities, parasite-specific metabolites in biochemical pathways can be targeted without causing harm to the host, thereby reducing unwanted side effects [29-31]. The metabolic pathways that can be targeted for the development of new antimalarial agents

include, food vacuole, pyrimidine metabolism, apicoplast, folate metabolism, glycolysis and Heat shock protein 70 (Hsp70).

Food vacuole: Host haemoglobin is broken down by proteolytic enzymes such as aspartic and cysteine proteases in the food vacuole[28, 32]. Hampering the activity of these enzymes affect the parasites protein biosynthesis and the development of parasites in the erythrocyte stage. Besides, essential processes such as erythrocyte rapture and invasion are carried out by cysteine proteases; thus, inhibiting its activity would be detrimental to the parasite [33]. Antimalarial drugs based on quinoline acts on heme polymerase by preventing the polymerization of heme, a toxic pigment. When heme accumulates in the food vacuole, it is lethal to the parasite [34].

Pyrimidine metabolism: It is crucial in the production of purines and pyrimidine required for Ribonucleic acid (RNA) and Deoxyribonucleic acid (DNA) synthesis necessary for the growth and replication of parasites during the intraerythrocytic stage of the life cycle. It is an excellent target for the development of new antimalarial agents [35].

Apicoplast: Organelles are involved in a range of metabolic pathways, including fatty acid, isopentenyl diphosphate and heme synthesis required throughout the life cycle [36, 37]. These *Plasmodium*-specific anabolics and catabolic processes make them an ideal target for antimalarial drug discovery [38]. A parasite can survive without apicoplast; however, it cannot cause infection because apicoplast is necessary for synthesizing molecules needed for infection [35].

Folate metabolism: The pathway is essential because it involves two main enzymes, namely *dihydrofolate reductase* (DHFR) and *dihydropteroate synthase* (DHPS), which are crucial in DNA biosynthesis and metabolism of specific amino acids such as methionine and glycine [39]. The enzymes are highly *Plasmodium*-specific, making it possible to formulate particular inhibitors [40]. The target is essential for both chemotherapy and prophylaxes [41].

Plasmodium protein kinases: It enhances protein activity, stabilization and interaction with the ligand or localization of the phosphorylate substrate of the amino acids by adding phosphate groups from adenine triphosphates (ATP). Also, inhibiting the action of protein kinases is essential to prevent parasites invasion and intraerythrocytic development, making them good targets for antimalarial drug discovery [35].

Glycolysis: The anaerobic glycolytic biochemical pathway is crucial for the *Plasmodium* parasite as it serves as the only source of energy in the erythrocytes stage. Lack of a functional

tricarboxylic acid cycle (TCA) or Krebs cycle makes the parasites vulnerable because it relies on the fermentation pathway for energy for its metabolic processes. This process is facilitated by *p. Falciparum* lactate dehydrogenase (LDH), a key enzyme that converts pyruvate into L lactate, simultaneous oxidizing NADH cofactor to NAD+. *P. falciparum*-LDH differs considerably from its mammalian LDH isoform, suggesting that specific inhibitors for *P. falciparum*-LDH can be developed, thus making *P. falciparum*-LDH an idea antimalarial target [42-44].

Heat shock protein 70 (Hsp70): Plasmodial (Hsp70) chaperones, especially Hsp70-z (PfHsp70-z) and PfHsp70-1, which occur in the cytosol, are emerging as potential antimalarial targets. One of Hsps' most important functions is to aid the catalysis of protein folding. It is crucial for malaria parasites' survival, growth, and toxicity [45-47]. Hsps are thought to play an important role when malaria parasites infiltrate their host cells and develop in hepatocytes and red blood cells. Hsps are thought to preserve proteostasis in malaria parasites when exposed to unfavourable conditions in the host environment. Therefore, Inhibiting Hsp70 activity would be harmful to the parasite[48, 49].

Figure 1.6 illustrates various targets associated with antimalaria agents.

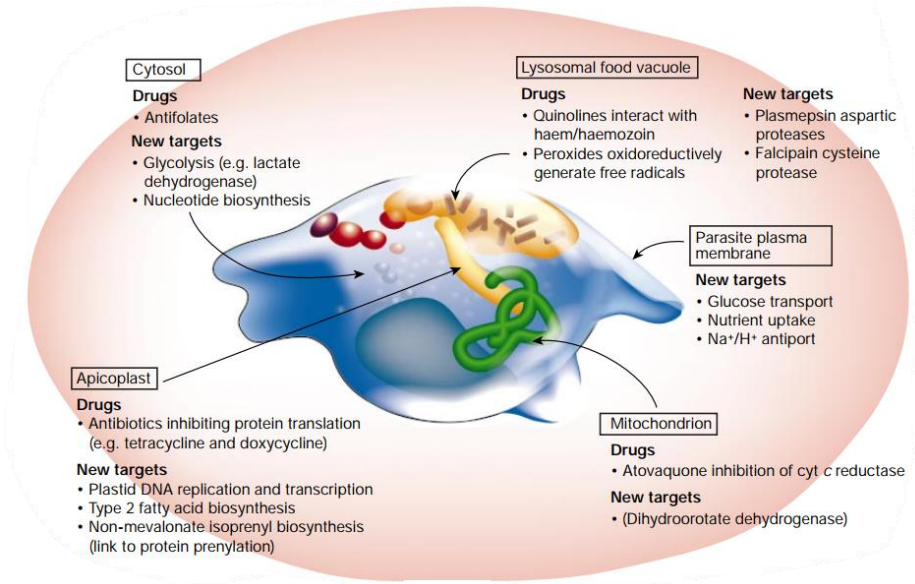

Figure 1.6. Malaria therapeutic targets with associated drugs [50].

1.3.2 Antimalarial drugs and their classification

Various antimalarial drugs act on different stages of the *Plasmodium* life cycle and are useful for chemotherapy and prophylaxis. The antimalarial drugs that have been used for treatment includes quinolines, artemisinin, antifolates and antibiotics [51].

1.3.2.1 Quinolines

Quinoline belongs to a class of heterocyclic aromatic compounds with benzene and pyridine fused at two abject carbons. Numerous variations on quinoline compounds have resulted in different class antimalarial compounds based on their structure, for example, 4-aminoquinolines, like chloroquine and amodiaquine, 8-aminoquinolines such as primaquine; 4-quinolinemethanols, e.g., mefloquine; quinoline-containing cinchona alkaloids, e.g., quinine and quinidine.

1.3.2.2 Mechanism of action for quinoline drugs

Quinoline based antimalarial prevent the detoxification process of the parasite during haemoglobin hydrolysis in the food vacuole during the intraerythrocytic stage. The breaking down of haemoglobin produces amino acids and a by-product called ferriprotoporphyrin IX (FPIX) heme. Accumulation of oxidised form of free FPIX heme is lethal to the parasite by causing lysis of the cell membrane and affect the function of lysosomal enzymes [52]. The parasite detoxifies it by polymerising at least 95% of FPIX into brown insoluble pigment known as hemozoin (non-toxic) using heme polymerase enzyme [53], as illustrated in **Figure 1.7**. Upon treatment with CQ, it forms FP-IX-CQ complex with free FP-IX, which then accumulates in the food vacuole, inducing oxidative stress, which may lead to peroxidation of the membrane lipids, oxidation of proteins and damage of DNA, thus causing demise to the parasite. CQ's basic side chain is critical for antimalarial activity because it promotes CQ accumulation in the food vacuole, inhibiting heme polymerization. [54, 55]. The SAR studies have shown that when an aryl group replaces the basic side chain of CQ, it improves *in vivo* antimalarial activity, which has given birth to other quinoline analogues [56].

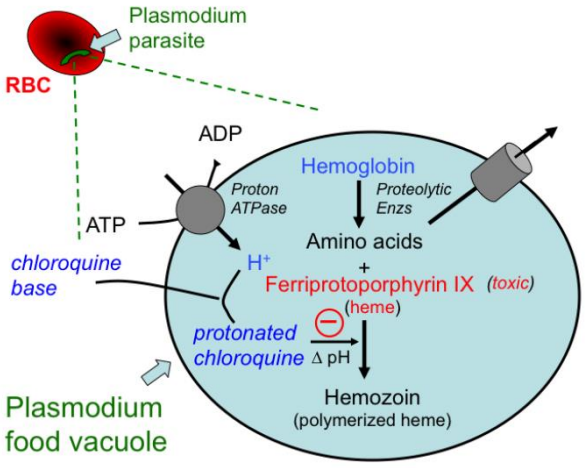

Figure 1.7. Proposed mechanism of CQ and other quinoline based antimalarial drugs.

Table 1. The structure of quinoline based antimalarial drugs and their associated side effects.

Classification	Drugs	Description	Side effects	References
Quinolines	Quinine 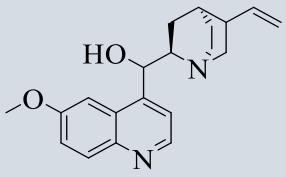	It was the first on antimalarial line-up drugs extracted from the cinchona tree by Pierre Joseph Pelletier and Joseph B. Caventou in 1850. It remained a frontline malaria drug until the 19th contrary.	Tinnitus, mild headache, muscle weakness, vomiting, hypoglycemia, cardiovascular effects, vertigo, visual disorders and hypotension	[57]
	Chloroquine 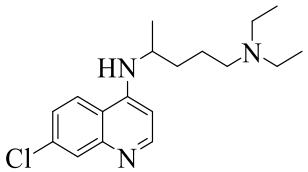	CQ was the first synthetic antimalarial drug discovered in 1934. It was an efficient and cheaper alternative to quinine.	Malaise, itching, headaches, visual impairment, gastrointestinal upset, cardiovascular effects and seizure	[58]
	Amodiaquine 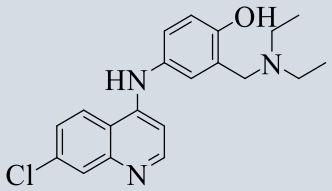	It was introduced in the 1970s as an alternative to CQ owing to it being active against CQ resistant strain for both *P. falciparum* and *P. vivax*. Used to treat uncomplicated malaria and less toxic to HIV patients with compromised immune systems	Abdominal cramps, nausea, vomiting and itchiness, headache, vertigo, insomnia, gastrointestinal upset, cardiovascular effects, depression, dreams and fatigue	[59]

	Mefloquine 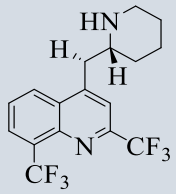	Introduced in the 1970s by the US army institute of research during Vietnam was another synthetic derivative of quinine with high hydrophobicity than CQ.	Abdominal pain, diarrhoea, vomiting, and nausea to neurological disorders such as hallucination, insomnia, convulsion and anxiety disorders	[60]
	Piperaquine 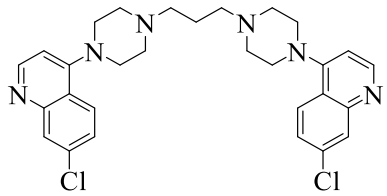	It was developed by the chinse in the 1960s and adopted as a frontline drug to address resistance in CQ. It was used for the prevention and treatment of malaria until the emergence of resistance in PRQ saw a decline in usage as monotherapy in 1990	nausea, headache, dizziness, and listlessness	[61]

1.3.2.3 Artemisinin

Artemisinin was discovered in 1972 by Tu Youyou, a Chinese scientist awarded a 2015 Nobel Prize in medicine. Artemisinin was from the herb Ding Hao, known as *Artemisia annua* in Latin. It was used for 200 years to treat intermittent fever by the ancient Chinese. The Chinese discovered that the extracts from Artemisia annua displayed good antimalarial activity in mice with lower toxicity than CQ and quinine, including being active against CQ resistant strain [62]. Structurally, artemisinin is a sesquiterpene lecton peroxide with poor solubility in water and oil and low oral bioavailability.

1.3.2.4 Mechanism

The endoperoxide bridge is crucial for antimalarial activity, demonstrated after artemisinin without endoperoxide was isolated from urine displayed reduced activity. According to studies, ART is permeable in the cell membrane, and because of its poor solubility, it can be transferred to all cell membranes. When art comes into contact with heme, it produces potentially hazardous oxidative oxygen species (ROS). ROS levels that are too high produce relatively non-specific damage. A portion of ART penetrates mitochondria in some species, where it may be potent and have specific damages, as illustrated in **Figure 1.8**. Mitochondria and ART interact in malaria parasites and Baker's yeast, causing mitochondrial dysfunction, but no mitochondrial activity was seen in mammalian cells. The process through which mitochondrial ART is activated is unknown [63-65]. Also, artemisinin and derivatives may inhibit Sacro/endoplasmic reticulum Ca^{2+}-ATPase (SERCA) owing to structural similarity with thapsigargin [66].

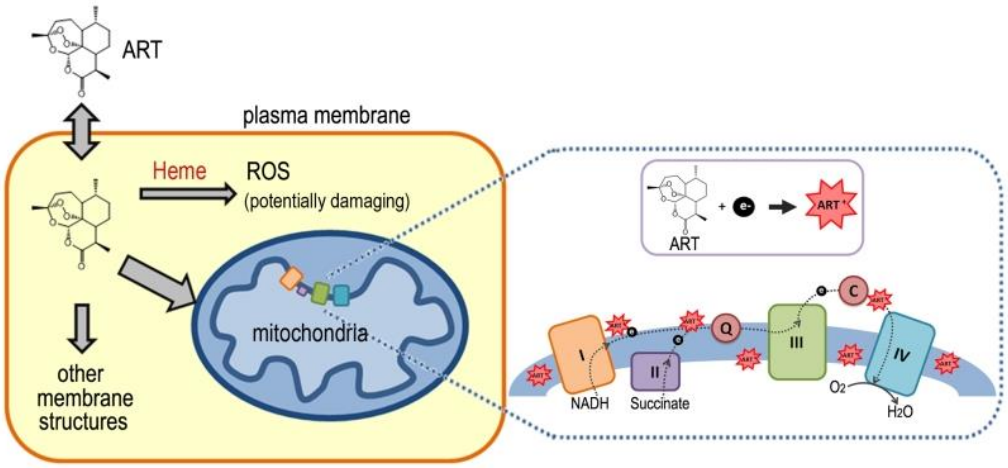

Figure 1.8. Proposed mechanism for artemisinin mediated through generation of ROS [65].

Table 2. The structure of artemisinin-based antimalarial drugs and their associated side effects.

Drug/ structure	Description	Side effects	Reference
Artemisinin 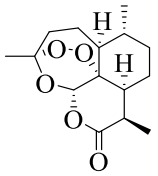 Dihydroartemisinin 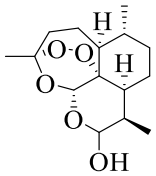 Artemether 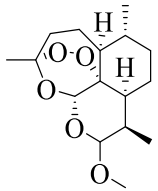 Artesunate 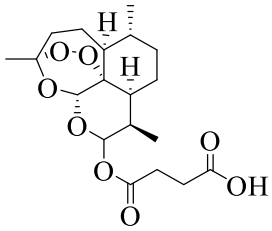 Artemiside 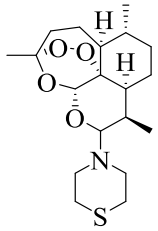 Artemisone 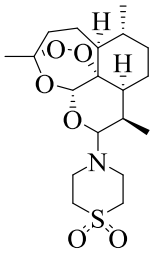	Antimalarial lactone derived from Qing Hao, a Chinese herb. Artemisinin was first isolated from a plant in 1971. Despite artemisinin displaying excellent antimalarial properties, it had poor solubility in water and oil and low oral bioavailability. Semi-synthetic analogues, namely artemether artesunate, artemisone and artemiside from dihydroartemisinin which showed improved solubility and antimalarial activity, were further developed.	Nausea, headaches, abnormal bleeding, itching and dark urine	[62, 64]

1.3.2.5 Antifolates

Antifolates are a class of drugs used against the synthesis of folic acid essential for parasite survival. Antifolates are used for both chemotherapy and prophylactic treatment. This antimetabolite inhibits the activity of dihydrofolate reductase (DHFR), preventing the formation of folic acid derivative tetrahydrofolate cofactors necessary for the synthesis of essential amino acids such as methionine and nucleic acid for cell development [67]. **Table 3** shows classes of antifolates antimalarial drugs: Type I and II

Table 3. Structure of antifolates antimalarial drugs; Type I and type II.

Type I antifolates	Type II antifolates
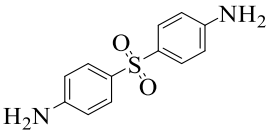 Dapsone 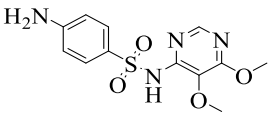 Sulfadoxine 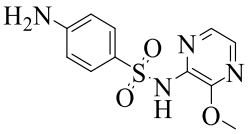 Sulfalene 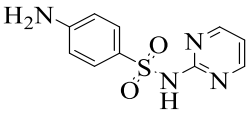 Sulfadiazine	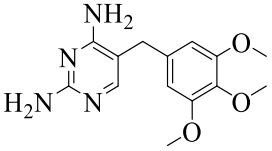 Trimethoprim 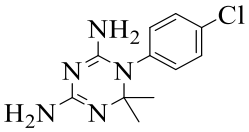 Cycloguanil 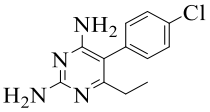 Pyrimethamine 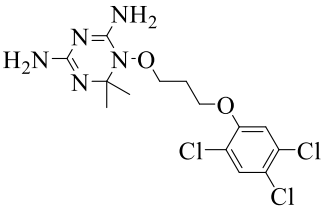 WR99210 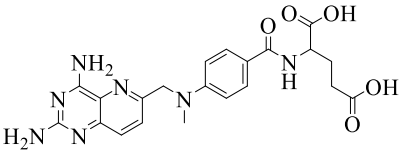 Methotrexate

Type 1 antifolates*:* Sulfonamides and sulfones are para-aminobenzoic acid (PABA) -like a structure that inhibits the synthesis of 7,8-dihydropteroate, a precursor of dihydrofolate, by competing with PABA for the active site of *dihydropteroate synthase* (DHPS).

Type 2 antifolates: These are antimetabolites with a pteridine ring-like structure that inhibits the parasite DHFR, catalysing the conversion of dihydrofolate to tetrahydrofolate using the nicotinamide adenine dinucleotide phosphate (NADPH).

1.3.2.6 Antibiotic drugs

Many antibiotics have shown good antiplasmodial efficacy, and those with moderate activity are used in conjunction with potent antimalarial medicines. Examples of these drugs with their associated side effects are displayed in (**Table 4**) [68]. Other antibiotics, such as azithromycin and clindamycin, have also demonstrated good antimalarial activity [69].

Since 1950, tetracycline has been used to treat malaria where its antiplasmodial activity targets the plasmodial mitochondrion and apicoplast, home to the genome, halting prokaryote-like RNA polymerases tRNAs and proteins, and preventing prokaryotic transcription of bacterial activity. It is recommended for the treatment of uncomplicated *P. falciparum* malaria in conjunction with other antimalarial agents, such as QN or ARTS. Doxycycline is effective for both the treatment and prevention of *P. falciparum* malaria in multidrug-resistant regions. Fosmidomycin is another antibiotic that displays antimalarial activity by inhibiting 1-deoxy-D-xylulose-5-phosphate reductoisomerase (DXP) essential for cellular function in the mammalian host by acting on apicoplast to prevent isoprenoid biosynthesis in the mevalonate pathway [70, 71].

Table 4. Malarial antibiotic drugs with associated side effects.

Classification	Drugs	Description	Side effects	References
Antibiotic	Tetracycline 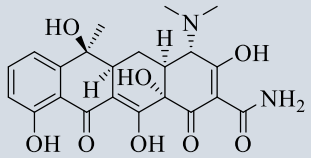 Doxycycline 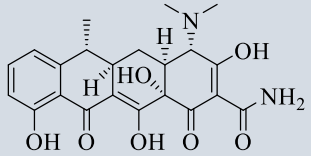	Tetracycline and its analogues such as, Doxycycline and minocycline, are antibiotics that displayed good antimalarial properties whose efficacy is achieved when combined with schizonticidal agents such as QN and ACTs. The targets include plasmodial mitochondrion and apicoplast, and bacterial activity targets prokaryotic translation.	photosensitivity, vaginitis, thin skin, nausea and vomiting Gastrointestinal effects, thrombophlebitis, hypoplasia, rash, dermatitis.	[68, 69]
	Atovaquone 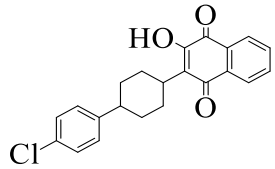	It is active against all species of *Plasmodium*. It is taken in synergy with proguanil, where they alter the electron transport and membrane potential necessary for proteins and small molecules transport in and out of the organelles. It also inhibits the cytochrome bc1 complex, which prevents the respiratory chain	Vomiting, diarrhoea, abdominal pain, headache, cough, rash, fever.	[72]

		required for the coenzyme Q regeneration, essential for pyrimidine biosynthesis.		

1.3.3 Drug toxicity

Drug toxicity is the harm posed by given therapy during the treatment, leading to different side effects. The toxicity of the drugs depends on the dosage, and its effects may cripple the entire system or vital organs like the liver. It happens when the side effect of the medicines supersedes the therapeutic effect of the dosage. Sometimes, the medicine may be both active and toxic at the same time [73]. Studies have shown that drug toxicity is among the leading cause of death in many countries [74-76]. Side effects of the antimalarial drug range from mild to severe. The diverse toxicity reaction of some antimalarial drugs has resulted in limitations in their usage. Sometimes toxicity occurs over a prolonged drug regimen or dosage. Studies have shown that side effects of antimalarial drugs would be severe in patients of specific groups such as small children, older adults, pregnant women, and those with compromised immune systems or who suffer from other diseases [77, 78]. Antimalaria drugs with their associated toxicity are mentioned in **tables 1- 4**.

1.3.4 Plasmodial drug resistance

Plasmodial resistance is a reduction in the efficacy of available antimalarial drugs enabling the parasite to persevere even after treatment. Efforts to mitigate and fight malaria have resulted in the parasitic mutation causing insensitivity to formally effective antimalarial drugs and severity of the sickness. Resistance is documented mainly in *P. falciparum* and *P. vivax* species, the strains responsible for human infection and fatality, in almost all available malarial drugs. Therefore, malaria remains a world health concern causing an increase in mortality and morbidity, which commands a height financial bill for replacement therapy. Resistance has often led to a compromise in using the current frontline antimalarial drugs for treatment [79]. Resistance is proliferated through the interactions of parasites with the human, carrier, drugs and the environment.

Drug properties: The drug pharmacokinetics and pharmacodynamics can lead to resistance by allowing the parasite to mutate for survival owing to the hydrophobicity of drugs with a long half-life that perpetuates in the system. This results in a change in the dose-response or concentration-effect relationship of the antimalarial drugs [80, 81].

Parasite properties: The parasites can evolve or mutate by adjusting the receptor of drugs, which has prompted an ascent in the incidence of resistance. The frequency of mutations corresponds directly to plasmodial resistance growth. The mutant can alter the permeability or transport of the membrane, consequently diminishing the drug absorption [82].

Drug interactions: Resistance which sprung from excessive use of antimalarial drugs, erroneous dosage, and deficient treatment [83].

Environment factors: The genetic expression of a parasite is influenced by the environment, such as host temperature and nutrients, which can bring about resistance, prompting a selective host response. The environmental factors, for example, physiological, biochemical, and behavioural processes, enhance growth and host exploitation of the parasite and thus virulence. The degree of transmission influences the proliferation of drug-resistant *Plasmodium*. The low-transmission region has an increased risk of developing drug resistance because infections usually manifest symptoms, and patients are treated promptly, thus increasing the exposure to antimalarial drugs. On the other hand, high transmission regions have a minimal risk of developing drug resistance owing to infections rarely showing symptoms, with patients barely exposed to antimalarial drugs [84]. Resistance has been reported in almost all antimalarial drugs, and the chronology of resistance against common antimalarial drugs is shown in **Table 5**

Table 5. Development of resistance against common antimalarial drugs in chronological order.

Antimalarial drug	Introduction year	First resistance case
Quinine	1820	1910
Chloroquine	1947	1957
Proguanil	1948	1949
Sulfadoxine/Pyrimethamine	1967	1967
Atovaquone	1977	1982
Mefloquine	1977	1985
Artemisinin	1972	2009

Chloroquine; *P. falciparum* CQ resistance first arose in Colombia and Thailand in the 1950s after World War II and quickly spread to other parts of the world such as South America, South-East Asia, and India in the 1960s and 70s. The case of chloroquine resistance was reported in Africa in the 1970s. At present, *P. falciparum* chloroquine-resistant strain has spread throughout malaria-endemic regions [85]. The tropical regions have shown chloroquine resistance,

but all ACT sensitive are highlighted in red in **Figure 1.9**. Furthermore, artemisinin resistance and ACT failure have been seen in Myanmar and Thailand, as represented by green and brown colours. Subtropical countries have no indigenous P. falciparum, while others are on the verge of eradicating malaria.

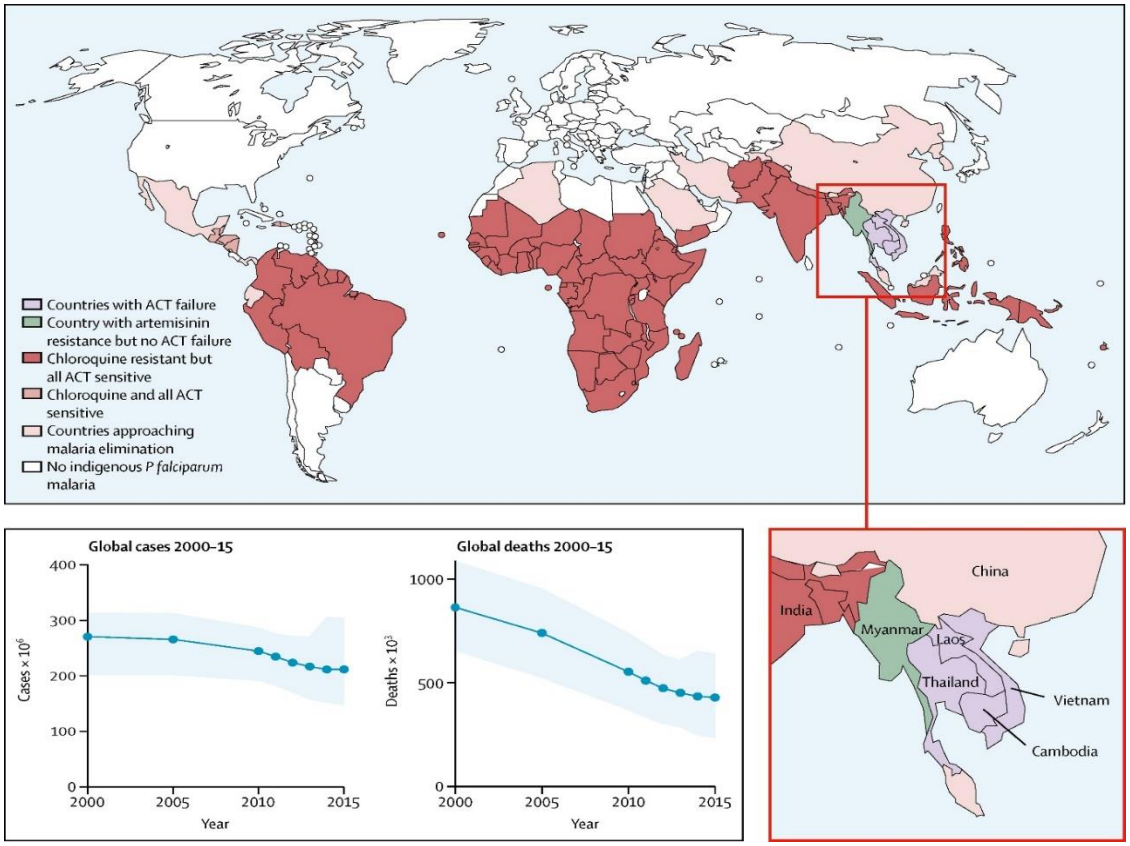

Figure 1.9. Global distribution in resistance of CQ.

Chloroquine resistance is aided by *P. falciparum*-CRT, an enzyme that impedes chloroquine efficacy by efflux it from the food vacuole, its site of function. *P. falciparum*-CRT prevents the transportation of CQ through the membrane, and its genetic mutation found at position 76, where Lysine is changed to Threonine (K76T), is a cornerstone for resistance [86]. Other resistance-related mutations occur at amino acid 72-75 that include C72S, M74I, N75E and N75K, which alters the membrane's pH gradient, making it unfavourable for CQ uptake in the food vacuole [87, 88].

Mefloquine; The overuse of quinine prompted mefloquine resistance before its development. Resistance in mefloquine is associated with the mutation of P. falciparum-MDR1 protein. Its ATP-binding domain faces the cytoplasm that promotes the uptake of drugs into the vacuole through the vacuole membrane [89, 90]. Furthermore, the mutation of ATP dependent-P-

glycoprotein pump homologue encoded by the MDT gene family aided mefloquine resistance. The *P. falciparum*-MDR1 gene is responsible for resistance to other mefloquine related drugs. Other resistance-related *P. falciparum*-mdr1 gene mutations include N86Y, Y184F, S1034C, N1042D and D1246Y [91].

Certain antimalarial drugs with comparable structure and biological action can show cross-resistance, such as mefloquine, quinine and halofantrine [92]. Also, CQ treatment has instigated cross-resistance in mefloquine in malaria-endemic regions. Although CQ and amodiaquine show cross-resistance, some CQ resistance parasites remain susceptible to amodiaquine [93]. The main mutation locations of the *P. falciparum*- CRT (A) are marked in a red point in **Figure 1.10**, whereas other mutants are indicated by yellow and black dots.

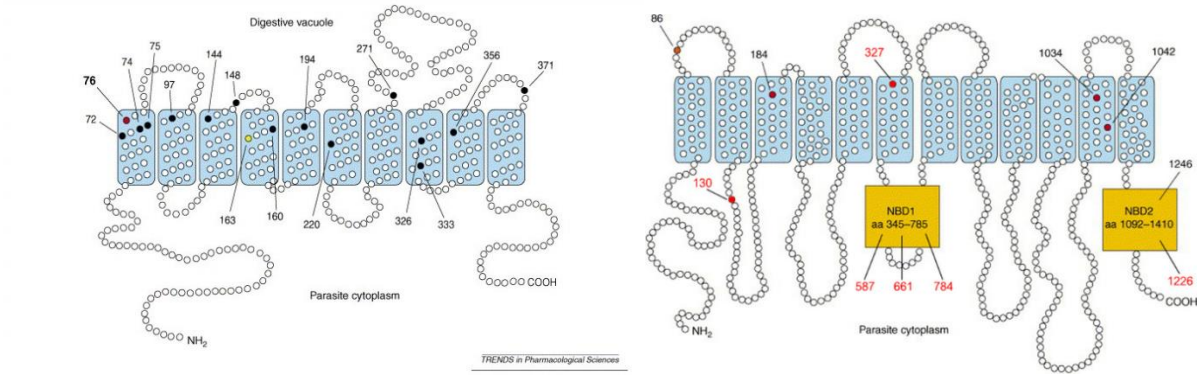

(A) (B)

Figure 1.10. *P. falciparum*- CRT (A) with the primary mutation at position 76 is shown by red spot and other mutants by yellow and black spots [94]. *P. falciparum*-MDR1(B) with the modification shown by red spots [95].

On the other hand, the first resistance occurrence of the antifolate viz pyrimethamine and proguanil combination therapy occurred in 1950. Resistance is associated with gene encoding mutation of the antifolates target enzymes *P. falciparum*-DHFR and *P. falciparum*-DHPS, which adversely affects the enzyme-binding affinity [96]. The resistance mutants of *P. falciparum*-DHFR began in Southeast Asia before spreading to Africa. The resistance of pyrimethamine in *P. falciparum* is caused by a four-point mutation of *P. falciparum*-DHFR, i.e. N51I, C59R, S108N and I164L [97]]. These mutations modify the binding pocket of the enzyme, thereby decreasing the binding potential of pyrimethamine. Resistance in cycloguanil is associated with double mutation, A16V / S108T in *P. falciparum*-DHFR; however, these mutants are prone to pyrimethamine [98].

The resistance of type I antifolate confers with a double mutation in *P. falciparum*-DHPS A437G / K540E amino acids [99]. Further, modifications at S436A/F, A581G and A613S/T improve the resistance of type I such as sulfone diapses, sulfadoxine, and sulphonamides as depicted in **Figure 1.11** [100].

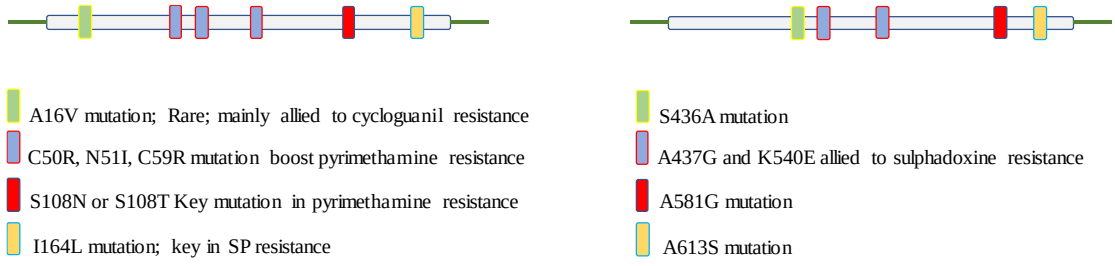

(A) (B)

Figure 1.11. Mutation in *P. falciparum*-DHFR (A) and *P. falciparum*-DHPS (B) associated with resistance in certain antifolates [101].

Resistance in artemisinin is conferred to mutation of the variant allele at L263E in the binding site of *P. falciparum*-ATP6 or of *P. falciparum*, thus impede its effective antimalarial action [102]. Also, resistance is brought about by triple point mutation at S1034C, N1042D and D1246Y in *P. falciparum*-MDR1 enzyme, a comparable mutation responsible for CQ resistance [103].

Atovaquone resistance arose from a mutation in the binding site of *P. falciparum* Cytochrome bc*1* (pfCYTbc1) at the Y268S position, thereby reducing the susceptibility of a drug to the parasite [104].

1.3.5 Combinational therapy

The prevalence of antimalarial drugs resistance has contributed to the limited use of mono-drug therapy to treat malaria. However, drug efficacy can be preserved by using combination therapy in which two or more drugs with different biochemical targets and modes of action are administered [105]. The benefit of combination therapy is that a pathogen can't resist two or more drugs; thus, decrease or delay resistance development. Drugs with no cross-resistance can be effective against the presence of a particular resistant mutant [106]. Artemisinin combination therapy (ACT) was first recommended as a first-line drug to treat uncomplicated malaria in Southeast Asia. WHO is increasingly recommending it as a frontline throughout the world. A quick-acting artemisinin-based compound with a short half-life is used in conjunction with a comparatively slower drug of a different class. This combination enables the artemisinin

derivative to continue at parasiticidal concentration until the parasite is wiped out, thereby ultimately protecting the artemisinin compound from resistance. The presence of a slower drug partner helps reduces the dosage scheme to three days; however, the short life of the artemisinin derivative only offers partial protection of the other drug counterpart. Examples of combination therapy are given in (**Table 6**).

Table 6. Examples of antimalarial ACT.

Sulfadoxine-pyrimethamine (SP)	It is branded as Fansidar, cheap, easy dosage and has fewer side effects. It was developed as an alternative to CQ resistance. Case of resistance in SP is reported. Fansidar efficacy can be retained when used in combination with CQ, mefloquine and amodiaquine [96, 107-109].
SP with CQ or amodiaquine	It was used to treat uncomplicated malaria. PS with CQ or amodiaquine is more efficient against all intraerythrocytic parasites. Fansidar/amodiaquine is more effective therapy than Fansidar-CQ, the only setback side effects such as agranulocytes and liver damage [110, 111].
SP/Quinine	Boosted drug efficacy, subsequently reducing dosage regimen quinine from seven to four days [112, 113].
SP/mefloquine	Branded as Fransimef and its use declined due to the emergence of resistance [114].
Quinine-antibiotics	Antibiotics used include tetracycline, doxycycline, clindamycin, and azithromycin show better efficacy against drug-resistant malaria. Quinine–clindamycin combination is safe for pregnant women and small children [115, 116].
Artemether-lumefantrine	Coartem Riamet and Lanart used to treat uncomplicated malaria. It was effective against *P. falciparum*-MDR.

Artesunate-amodiaquine	Coarsucam used in certain Africa nations as a frontline drug for uncomplicated malaria.
Artesunate-mefloquine	Artequin: used in Thailand for uncomplicated malaria as an alternative to mefloquine
Dihydroartemisinin-piperaquine	Artekin; used to address multi-drug malaria resistance in China, Vietnam, Thailand, and Cambodia.
Atovaquone-proguanil (AP)	Malarone; used for uncomplicated malaria therapy and prophylaxis, including treatment CQ resistant malaria. Three-day course drug regimen [117]. Safer for pregnant women and young children [118-120].

In addition to the combinational therapy strategy for delivering malaria medication as shown in **Table 6**, current drug development programmes focused on finding the novel mechanism of action acting on vast biological pathways such as haem detoxification, cyclic amine resistance locus, UDP-galactose and Acetyl CoA transporters, P-type sodium transporter ATPase 4, *P. falciparum* dihydrofolate reductase, phosphatidylinositol 4 kinase, and Plasmodial dihydroorotate dehydrogenase (DHODH). Potential antimalarial candidates under pre-clinical and clinical trials with their associated targets are presented in **Table 7**.

Table 7. Potent antimalarial candidate currently under clinical and pre-clinical trials

Antimalarial drug	Chemical class	Developmental stage	Mechanism of action/target
OZ439/ FQ	Trioxolane	Phase II b	Haem detoxification
GNF156	Imidazopiperazine	Phase IIb	Cyclic amine resistance locus, UDP-galactose and Acetyl CoA transporters
NITD609	Spiroindolone	Phase II study completion	P-type sodium transporter ATPase 4
P218	2,4-Diaminopyrimidine	VIS for prophylaxis	*P. falciparum* dihydrofolate reductase
MMV390048	2-Aminopyridine	Phase IIa	Phosphatidylinositol 4 kinase (PI4K)
UCT 943	2-Aminopyrazine	Pre-clinical trials	Phosphatidylinositol 4 kinase (PI4K)
DSM265	Triazolopyrimidine	Phase IIa	Plasmodial dihydroorotate dehydrogenase (DHODH)

1.4 Origin of my research

According to the available literature, malaria continues to be a health challenge in Asia, Americas and mainly in the Sub-Saharan region of Africa and accounting for 70% of the incidence. Also, countries such as SA that have low malaria incidence continues to face problems due to neighbouring malaria prevalence countries like Mozambique and Zimbabwe, as well as travellers' coming from endemic countries. Managing malaria in affected regions remain a challenge owing to lack of clinical experience, patients' adherence to treatment, inadequate availability of diagnostics or second-line drugs presents the risk of developing resistance to available drugs. This has significantly contributed to the growth of resistance to the current frontline drugs. This needs alternative therapy, which stimulates a rigorous and inclusive development strategy to offer lead optimized compounds to address the current malaria management challenge. A more comprehensive exploration of the pathogenesis of the parasite with related interactions with the host would also be crucial to identifying novel validated targets for antimalarial potential future lead optimization.

Pyrimidine is one of the well-known lead pharmacophores with a wide range of medicinal properties. The central nucleus in drugs, namely pyrimethamine, minoxide, thiamine, trimethoprim and sulfadiazine, possess antiparasitic, antihypertension, anti-inflammatory and antibacterial, respectively [121]. Furthermore, in P218, a possible antimalarial candidate under clinical trials, VIS for prophylaxis which began in December 2018, pyrimidine is an essential moiety. Antimalarial pyrimidine-based compounds target *P. falciparum*-DHFR, an enzyme that catalyses dihydrofolate reduction to tetrahydrofolate using NADPH as an electron donor. This reaction is essential for the *de novo* synthesis of purines and certain amino acids needed for DNA biosynthesis [122].

Natural products without adverse effects showing vast potential to modulate the immune response and inhibit the resistance mechanism were also exploited in a quest to develop lead candidates. Chalcones are natural products that, among other medicinal properties, have shown promising antimalarial properties. In addition to an enone (α, β-unsaturated carbonyl), the diphenyl groups on the chalcone were crucial for antimalarial activity. They were incorporated in the design linked to the fourth and sixth positions of the pyrimidine core, thus forming a modified pyrimidine pharmacophore as illustrated in **Figure 1.12**.

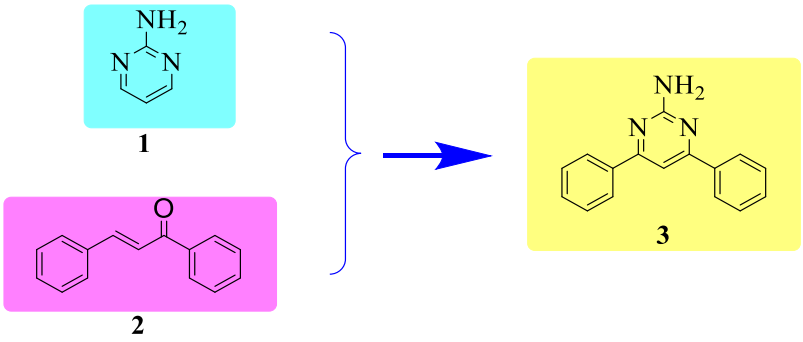

Figure 1.12. Rationally designed pyrimidine-based pharmacophore.

The modified pyrimidine pharmacophore (**3**) became the foundation we envisaged to synthesize the three series of hybrid molecules using the molecular hybridization approach as antimalarial agents, as shown and executed in chapters 3 - 5. This research work will be beneficial and enhances the importance of pyrimidine moiety incorporated with other pharmacophores, for example, cinnamoyl, triazole and quinolines for antimalarial activity.

Another pharmacological antimalarial scaffold, such as quinoline inspired from chloroquine, was used in the design and synthesis. Once known for antimalarial with a good toxicity index, CQ has been employed as a critical moiety in the search for reverse resistance by the hybridization approach. Structure-activity relationship (SAR) studies have shown that the basic tail of CQ and other related drugs such as amodiaquine and hydroxychloroquine is lipophilic, and it enhances the passage through the plasma membrane. Given this fact, diamine alkane linkers, including, piperazine will be incorporated in designing the molecule. Therefore, the design of hybrid analogues in chapter 3 contains a pyrimidine pharmacophore amalgamated to CQ linked through diamine alkane linkers.

Another new lead inspired by a natural source is the cinnamoyl derivative which resembles a Dehydrozingerone (DZG). Cinnamoyl derivative is a semi-structural analogue of curcumin. Cinnamoyl derivative, when merged to rifampicin framework through piperazinyl, increased its antibacterial activity by 10-fold. Cinnamoyl based compounds are known for their variety of pharmacological activities, namely antibacterial, anticancer, antifungal, antimalarial, anti-inflammatory, antidepressant, antioxidant etc. [123-126]. In chapter 5, the lead pyrimidine motif was hybridized to cinnamoyl derivative pharmacophore through a piperazine linker to afford potential antimalarial agents.

In the third series, the hybrid analogues were inspired by 1,2,3-triazole pharmacophore. The triazole scaffold, when merged to CQ derivative, enhanced the polymerization of heme. Triazoles also have displayed a spectrum of biological activity, including antimalarial properties. In chapter 4, we have foreseen the synthesis of the lead compound containing pyrimidine motif and 1,2,3-triazole scaffold linked by piperazine as potential antimalarial agents.

Therefore, in this research work, we anticipated the synthesis of quinoline, triazoles and cinnamoyl derivatives fused to a pyrimidine core using diamine alkane as a linker as potential antimalarial agents with anticipation to present inhibitors that would be active against the blood and liver stage of the parasite potential for both treatment and prophylaxis. Different substituents such as methoxy, fluoro, chloro, methyl and ethyl groups were used for bioisosteric replacements to afford a library of compounds in the hope to improve the antimalarial activity. Presented hereby is a library of hybrid molecules, all based on pyrimidine as a primary moiety. The pyrimidine motif was fused with quinoline for the first series, cinnamoyl core for the second core series and 1,2,3-triazole core for the third series, yielding three different families of compounds which are presented in three different chapters.

1.5 Research objectives

The emergence of resistance of the *Plasmodium* species on the frontline drugs has led to malaria emerge as a global health concern in modern-day drug therapy. Prioritisation of presenting new drugs that may address the shortcomings of current antimalarial chemotherapy deficiencies is required. The medicinal chemistry, central in drug discovery and development, seek to introduce new drug entities. It endeavours to synthesise novel chemical entities, modify existing scaffolds, amalgamate two or more bioactive molecules through hybridisation strategy, bioisosteric replacements, and optimisation of natural compounds in a quest to identify promising leads. Heterocyclic scaffolds with one or more heteroatoms have become essential in drug discovery, which is evident from the fact that more than 95% of the commercial drugs are based on heterocyclic scaffolds. The present study project was undertaken because of these facts. The aims and objectives of the current research work are;

1. To conduct a substantial literature survey to identify new chemical entities as promising antimalarial agents (Identification of a research gap and defining the scope of proposed work).

2. To synthesize a library of novel series of pyrimidine based molecular hybrids amalgamated with the following promising scaffolds:
   i. 1, 2, 3-triazole
   ii. Cinnamoyl and
   iii. Quinoline.
3. To purify the synthesized compounds through chromatographic methods viz. column (flash) chromatography.
4. To elucidate the structures of synthesized compounds using modern art instrumentation (^{1}H-NMR, ^{13}C-NMR, IR and High-resolution mass spectrometry).
5. To conduct the preliminary biological screening of the synthesized compounds for their antimalarial activity.
6. To investigate the binding affinities of two essential cytosolic *P. falciparum* heat shock protein 70 homologues; PfHsp70-1 and PfHsp70-z.

1.6 Layout/ structure of the thesis

The thesis entitled ‘‘**A novel library of pyrimidine-based hybrids as potential antimalarial agents; design, synthesis, characterization and *in vitro* biological evaluation**.” comprises the work done by the author in the Synthetic and Medicinal Chemistry Laboratory at the School of Pharmaceutical Sciences, University of KwaZulu Natal (Westville).

This thesis has been organized into **six chapters**. Out of six, three are presented as experimental manuscripts and one as a review manuscript.

Chapter I: Chapter one of this thesis deals with the introduction along with background and a brief overview of the literature of the proposed studies. This section gives an overview of the statement of the problem, research questions, the aim and objectives of the study. The brief methodology has been discussed to achieve specific aims and objectives.

Chapter II: Chapter two is a mini-review paper that has been communicated to “Bioorganic and Medicinal Chemistry Letters” Journal submission guidelines, entitled, “*Lactate dehydrogenase and Malate dehydrogenase: potential antiparasitic targets for drug development studies*”.

Chapter III: Chapter three looks at the design and synthesis of novel quinoline-pyrimidine using a molecular hybridisation approach. The synthesized compounds are characterized by NMR, FR

IR and FRMS and biologically evaluated for their antiprotozoal activity against a CQ-sensitive *P. falciparum*. The compounds were further investigated for *Pf*Hs70 activity.

Chapter IV: Chapter four looks at the design and synthesis of novel cinnamoyl-pyrimidine using a molecular hybridisation approach. The synthesised compounds are characterised by NMR, FR IR and FRMS and biologically evaluated for antiprotozoal activity against a CQ-sensitive *P. falciparum*. The compounds were further investigated for *Pf*Hs70 activity.

Chapter V: Chapter five looks at the design and synthesis of novel 1,2,3-triazole-pyrimidine using the molecular hybridisation approach. The synthesised compounds are characterised by NMR, FR IR and FRMS and biologically evaluated for antiprotozoal activity against a CQ-sensitive *P. falciparum.* The compounds were further investigated for *Pf*Hs70 activity

Chapter VI: Chapter six summarises the main conclusions and future recommendations of this work.

References

[1] E. A. Ashley, A. Pyae Phyo and C. J. Woodrow, "Malaria," *The Lancet,* vol. 391, no. 10130, pp. 1608-1621, 2018. https://doi.org/10.1016/S0140-6736(18)30324-6

[2] E. Hempelmann and K. Krafts, "Bad air, amulets and mosquitoes: 2,000 years of changing perspectives on malaria," *Malar J,* vol. 12, p. 232, Jul 9 2013. doi: 10.1186/1475-2875-12-232

[3] F. E. Cox, "History of the discovery of the malaria parasites and their vectors," *Parasit Vectors,* vol. 3, no. 1, p. 5, Feb 1 2010. doi: 10.1186/1756-3305-3-5

[4] E. Capanna, "Battista Grassi: a zoologist for malaria," *Focus,* vol. 3, no. 2, pp. 187-195, 2006. doi: DOI: 10.2436/20.7010.01.5.

[5] A. Neghme, "An appraisal of Giovan Battista Grassi: His work in biology and parasitology," *Exp Parasitol,* vol. 15, no. 3, pp. 260-278, 1964. doi: 10.1016/0014-4894(64)90022-0.

[6] S. Sadasivaiah, Y. Tozan and J. G. Breman, "Dichlorodiphenyltrichloroethane (DDT) for indoor residual spraying in Africa: how can it be used for malaria control?," (in eng), *Am J Trop Med Hyg,* vol. 77, no. 6 Suppl, pp. 249-263, Dec 2007.

[7] World Health Organisation, "Guidelines for the Treatment of Malaria-3rd edition," *World Health Organisation,* Geneva, Switzerland, 2015. https://www.ncbi.nlm.nih.gov/books/NBK294440/.

[8] K. C. K. Kathryn, N. Suh, S. Jay and Keystone, "Malaria," *Synthese,* vol. 170, no. 11, pp. 1693-1703, 2004. doi: 10.1053/cmaj.1030418

[9] Kathryn N. Suh, Kevin C. Kain and J. S. Keystone, "Malaria," *Canadian Medical Association Journal,* vol. 170, no. 11, pp. 1693-1702, 2004. doi: 10.1053/cmaj.1030418

[10] H. M. Keys, G. S. Noland, M. B. De Rochars, S. Blount and M. Gonzales, "Prevalence of malaria and lymphatic filariasis in bateyes of the Dominican Republic," *Infect Dis Poverty,* vol. 8, no. 1, p. 39, May 27 2019. doi: 10.1186/s40249-019-0547-3

[11] M. R. Galinski, E. V. Meyer and J. W. Barnwell, "Plasmodium vivax: modern strategies to study a persistent parasite's life cycle," *Adv Parasitol,* vol. 81, pp. 1-26, 2013. doi: 10.1016/B978-0-12-407826-0.00001-1

[12] World Health Organization, "World malaria report-2020," *World Health Organization,* Geneva, Switzerland, 2020. https://www.who.int/publications-detail-redirect/9789240015791.

[13] National Institute for communicable diseases. Service, "Malaria in South Africa 2017: An update," *National Institute for communicable diseases,* 2017. https://www.nicd.ac.za/malaria-in-south-africa-2017-an-update/

[14] L. Blumberg, J. Frean, D. Moonasar and C. South African Malaria Elimination, "Successfully controlling malaria in South Africa," *S Afr Med J,* vol. 104, no. 3 Suppl 1, pp. 224-227, Mar 2014. doi: 10.7196/samj.7600

[15] R. Maharaj, N. Morris, I. Seocharan, P. Kruger, D. Moonasar, A. Mabuza, E. Raswiswi and J. Raman, "The feasibility of malaria elimination in South Africa," *Malar J,* vol. 11, p. 423, Dec 19 2012. doi: 10.1186/1475-2875-11-423

[16] R. Maharaj, J. Raman, N. Morris, D. Moonasar, D. N. Durrheim, I. Seocharan, P. Kruger, B. Shandukani and I. Kleinschmidt, "Epidemiology of malaria in South Africa: from control to elimination," *S Afr Med J,* vol. 103, no. 10 Pt 2, pp. 779-783, Aug 29 2013. doi: 10.7196/samj.7441

[17] E. Khosa, L.R. Kuonza, P. Kruger and E. Maimela, "Towards the elimination of malaria in South Africa: a review of surveillance data in Mutale Municipality, Limpopo Province, 2005 to 2010," *Malar J,* vol. 12, p. 7, Jan 8 2013. doi: 10.1186/1475-2875-12-7

[18] D. Moonasar, T. Nuthulaganti, P. S. Kruger, A. Mabuza, E. S. Rasiswi, F. G. Benson and R. Maharaj, "Malaria control in South Africa 2000-2010: beyond MDG6," *Malar J,* vol. 11, p. 294, Aug 22 2012. doi: 10.1186/1475-2875-11-294

[19] T. R. Schleicher, J. Yang, M. Freudzon, A. Rembisz, S. Craft, M. Hamilton, M. Graham, G. Mlambo, A. K. Tripathi, Y. Li, P. Cresswell, P. Sinnis, G. Dimopoulos and E. Fikrig, "A mosquito salivary gland protein partially inhibits Plasmodium sporozoite cell traversal and transmission," *Nat Commun,* vol. 9, no. 1, p. 2908, Jul 25 2018. doi: 10.1038/s41467-018-05374-3

[20] J. Akter, D. S. Khoury, R. Aogo, L. I. M. Lansink, A. Sheelanair, B.S. Thomas, P. Laohamonthonkul, C. P. S. Pernold, M. W. A. Dixon, M.S.F. Soon, L. G. Fogg, J. A. Engel, T. Elliott, I. Sebina, K. R. James, D. Cromer, M. P. Davenport and A. Haque, "Plasmodium-specific antibodies block in vivo parasite growth without clearing infected

red blood cells," *PLoS Pathog,* vol. 15, no. 2, p. e1007599, Feb 2019. doi: 10.1371/journal.ppat.1007599.

[21] M. Olivier, K. Van Den Ham, M. T. Shio, F. A. Kassa, and S. Fougeray, "Malarial pigment hemozoin and the innate inflammatory response," *Front Immunol,* vol. 5, p. 25, 2014. doi: 10.3389/fimmu.2014.00025.

[22] M. B. Wells and D. J. Andrew, "Anopheles Salivary Gland Architecture Shapes Plasmodium Sporozoite Availability for Transmission," *mBio,* vol. 10, no. 4, Aug 6 2019. doi: 10.1128/mBio.01238-19.

[23] B. B. Kojin and Z. N. Adelman, "The Sporozoite's Journey Through the Mosquito: A Critical Examination of Host and Parasite Factors Required for Salivary Gland Invasion," *Front Ecol Evol,* vol. 7, 2019. doi: 10.3389/fevo.2019.00284.

[24] R. W. Steketee, "Good news in malaria control… now what?," *Am J Trop Med Hyg,* vol. 80, no. 6, pp. 879-880, 2009. https://pubmed.ncbi.nlm.nih.gov/19478241/.

[25] Nature, "Control of Malaria," *Nature,* pp. 419-417, 2002. https://www.malariasite.com/control-of-malaria/.

[26] A. Ramsay, P. Olliaro and J. C. Reeder, "The need for operational research and capacity-building in support of the Global Technical Strategy for Malaria 2016-2030," *Malar J,* vol. 15, p. 235, Apr 25 2016. doi: 10.1186/s12936-016-1302-x.

[27] S. Kar and S. J. Kar, "Control of malaria," vol. 9, no. 7, pp. 511-512, 2010. https://www.nature.com/articles/nrd3207?platform=hootsuite.

[28] P. Winstanley and S. Ward, "Malaria Chemotherapy," *Adv in Parasitol,* pp. 47-76. 2006. doi: :10.1016/S0065-308X(05)61002-0.

[29] Z. Zhang and W. Tang, "Drug metabolism in drug discovery and development," *Acta Pharm Sin B,* vol. 8, no. 5, pp. 721-732, Sep 2018. doi: 10.1016/j.apsb.2018.04.003

[30] A. H. Fairlamb, R. G. Ridley, and H. J. Vial, "Drugs against parasitic diseases: R&D methodologies and issues. Discoveries and drug development," *World Health Organization,* 2003.

[31] A. Guidi, G. Petrella, V. Fustaino, F. Saccoccia, S. Lentini, R. Gimmelli, G. Di Pietro, A. Bresciani, D. O. Cicero, and G. Ruberti, "Drug effects on metabolic profiles of Schistosoma mansoni adult male parasites detected by 1H-NMR spectroscopy," *PLoS Negl Trop Dis,* vol. 14, no. 10, p. e0008767, Oct 2020. doi: 10.1371/journal.pntd.0008767

[32] V. L. Lew, T. Tiffert and H. Ginsburg, "Excess haemoglobin digestion and the osmotic stability of Plasmodium falciparum-infected red blood cells," *Blood,* vol. 101, no. 10, pp. 4189-4194, May 15 2003. doi: 10.1182/blood-2002-08-2654

[33] P. J. Rosenthal, "Cysteine proteases of malaria parasites," *Int J Parasitol,* vol. 34, no. 13-14, pp. 1489-1499, Dec 2004. doi: 10.1016/j.ijpara.2004.10.003

[34] D. J. Sullivan, Jr., "Quinolines block every step of malaria heme crystal growth," *Proc Natl Acad Sci U S A,* vol. 114, no. 29, pp. 7483-7485, Jul 18 2017. doi: 10.1073/pnas.1708153114

[35] A. Mukherjee and G. C. Sadhukhan, "Anti-malarial drug design by targeting apicoplasts: new perspectives," *Pharmacopuncture,* vol. 19, no. 1, p. 7, 2016. doi: 10.3831/KPI.2016.19.001.

[36] M. J. Boucher and E. Yeh, "Disruption of Apicoplast Biogenesis by Chemical Stabilization of an Imported Protein Evades the Delayed-Death Phenotype in Malaria Parasites," *mSphere,* vol. 4, no. 1, Jan 23 2019. doi: 10.1128/mSphere.00710-18.

[37] D. E. Goldberg and P. A. Sigala, "Plasmodium heme biosynthesis: To be or not to be essential?," *PLoS Pathog,* vol. 13, no. 9, p. e1006511, 2017. doi: 10.1371/journal.ppat.1006511.

[38] T. Uddin, G. I. Mcfadden, and C. D. Goodman, "Validation of putative apicoplast-targeting drugs using a chemical supplementation assay in cultured human malaria parasites," *Antimicrob Agents Chemother,* vol. 62, no. 1, 2018. doi 10.1128/AAC.01161-17.

[39] J. E. Hyde, "Exploring the folate pathway in Plasmodium falciparum," *Acta Trop,* vol. 94, no. 3, pp. 191-206, 2005. doi: 0.1016/j.actatropica.2005.04.002

[40] A. Nzila, S. A. Ward, K. Marsh, P. F. Sims, and J. E. Hyde, "Comparative folate metabolism in humans and malaria parasites (part I): pointers for malaria treatment from cancer chemotherapy," *Trends Parasitol,* vol. 21, no. 6, pp. 292-298, 2005. doi: 10.1016/j.pt.2005.04.002

[41] J. E. Hyde and I. B. Muller, "Targeting folate metabolism in the human malaria parasite Plasmodium falciparum," *Curr Enzyme Inhib,* vol. 8, no. 2, pp. 150-169, 2012. doi: 10.2174/157340812800793255.

[42] H. Ginsburg, "Malaria parasite stands out," *Nature,* vol. 466, no. 7307, pp. 702-703, 2010. https://www.nature.com/articles/466702a.

[43] K. Muraleedharan and M. Avery, "Advances in the discovery of new antimalarials," *Curr Protein Pept Sci*, no. 3, vol. 17, pp. 275-279, 2007. doi: 10.2174/138920371799160226180543.

[44] S. A. Cobbold and M. J. Mcconville, "The Plasmodium Tricarboxylic Acid Cycle and Mitochondrial Metabolism," in *Encyclopedia of Malaria*, 2014, pp. 1-18. https://doi.org/10.1007/978-1-4614-8757-9_13-1.

[45] T. Zininga, I. Achilonu, H. Hoppe, E. Prinsloo, H. W. Dirr and A. Shonhai, "Plasmodium falciparum Hsp70-z, an Hsp110 homologue, exhibits independent chaperone activity and interacts with Hsp70-1 in a nucleotide-dependent fashion," *Cell Stress Chaperones*, vol. 21, no. 3, pp. 499-513, May 2016. doi: 10.1007/s12192-016-0678-4

[46] T. Zininga, I. Achilonu, H. Hoppe, E. Prinsloo, H. W. Dirr, and A. J. P. O. Shonhai, "Overexpression, purification and characterisation of the Plasmodium falciparum Hsp70-z (PfHsp70-z) protein," *PLoS One*, vol. 10, no. 6, p. e0129445, 2015. doi: 10.1371/journal.pone.0129445.

[47] T. Zininga, C. P. Anokwuru, M. T. Sigidi, M. P. Tshisikhawe, I. I. D. Ramaite, A. N. Traore, H. Hoppe, A. Shonhai, and N. Potgieter, "Extracts Obtained from Pterocarpus angolensis DC and Ziziphus mucronata Exhibit Antiplasmodial Activity and Inhibit Heat Shock Protein 70 (Hsp70) Function," *Molecules*, vol. 22, no. 8, Jul 28 2017. doi: 10.3390/molecules22081224

[48] I. L. Cockburn, A. Boshoff, E. R. Pesce and G. L. Blatch, "Selective modulation of plasmodial Hsp70s by small molecules with antimalarial activity," *Biol Chem*, vol. 395, no. 11, pp. 1353-1362, Nov 1 2014. doi: 10.1515/hsz-2014-0138

[49] T. Zininga, S. Makumire, G. W. Gitau, J. M. Njunge, O. J. Pooe, H. Klimek, R. Scheurr, H. Raifer, E. Prinsloo, J. M. Przyborski, H. Hoppe, and A. Shonhai, "Plasmodium falciparum Hop (PfHop) Interacts with the Hsp70 Chaperone in a Nucleotide-Dependent Fashion and Exhibits Ligand Selectivity," *PLoS One*, vol. 10, no. 8, p. e0135326, 2015. doi: 10.1371/journal.pone.0135326

[50] R. G. Ridley, "Medical need, scientific opportunity and the drive for antimalarial drugs," *Nature*, vol. 415, no. 6872, pp. 686-693, 2002. https://doi.org/10.1038/415686a.

[51] H. Gelband, C. B. Panosian and K. J. Arrow, "Saving lives, buying time: economics of malaria drugs in an age of resistance," vol. 412, pp. 686-693, 2004. doi: 10.17226/11017.

[52] X. Nqoro, N. Tobeka and B. A. Aderibigbe, "Quinoline-based hybrid compounds with antimalarial activity," *Molecules,* vol. 22, no. 12, p. 2268, 2017. doi: 10.3390/molecules22122268.

[53] N. J. White, "Antimalarial drug resistance," *J Clin Invest,* vol. 113, no. 8, pp. 1084-1092, 2004. doi: 10.1172/JCI21682.

[54] A. R. Parhizgar and A. Tahghighi, "Introducing new antimalarial analogues of chloroquine and amodiaquine: a narrative review," *Iran J Med Sci,* vol. 42, no. 2, p. 115, 2017. https://www.ncbi.nlm.nih.gov/pmc/articles/PMC5366359/

[55] S. Kondaparla, U. Debnath, A. Soni, V. R. Dola, M. Sinha, K. Srivastava, S. K. Puri and S.B. Katti, "Synthesis, biological evaluation, and molecular modelling studies of chiral chloroquine analogues as antimalarial agents," *Antimicrob Agents Chemother,* vol. 62, no. 12, 2018. doi: 10.1128/AAC.02347-17

[56] V. R. Dola, A. Soni, P. Agarwal, H. Ahmad, K. S. R. Raju, M. Rashid, M. Wahajuddin, K. Srivastava, W. Haq and A. Dwivedi, "Synthesis and evaluation of chirally defined side-chain variants of 7-chloro-4-aminoquinoline to overcome drug resistance in malaria chemotherapy," *Antimicrob Agents Chemother*, vol. 61, no. 3, 2017. doi: https://doi.org/10.1128/AAC.01152-16.

[57] G. Gachelin, P. Garner, E. Ferroni, U. Tröhler, and I. Chalmers, "Evaluating Cinchona bark and quinine for treating and preventing malaria," *J R Soc Med,* vol. 110, no. 1, pp. 31-40, 2017. doi: 10.1177/0141076816681421

[58] G. T. Edwin, M. Korsik and M. H. Todd, "The past, present and future of anti-malarial medicines," *Malar J,* vol. 18, no. 1, pp. 1-21, 2019. doi.org/10.1186/s12936-019-2724-z

[59] M. Cairns, B. Cisse, C. Sokhna, C. Cames, K. Simondon, E. Ba, J.-F. Trape, O. Gaye, B. Greenwood and P. Milligan, "Amodiaquine dosage and tolerability for intermittent preventive treatment to prevent malaria in children," *Antimicrob Agents Chemother,* vol. 54, no. 3, pp. 1265-1274, 2010. doi: 10.1128/AAC.01161-09.

[60] S. J. Lee, F. O. Ter Kuile, R. N. Price, C. Luxemburger and F. Nosten, "Adverse effects of mefloquine for the treatment of uncomplicated malaria in Thailand: A pooled analysis of 19, 850 individual patients," *PloS one,* vol. 12, no. 2, p. e0168780, 2017.

[61] T. M. Davis, T. Y. Hung, K. Sim, H. A. Karunajeewa and K. F. Ilett, "Piperaquine: a resurgent antimalarial drug," *Drugs,* vol. 65, no. 1, pp. 75-87, 2005. doi: 10.2165/00003495-200565010-00004.

[62] X. Z. Su and L. H. Miller, "The discovery of artemisinin and the Nobel Prize in Physiology or Medicine," *Sci China Life Sci,* no. 11, vol 58 pp. 11752-1179, 2015. doi: 10.1007/s11427-015-4948-7.

[63] J. L. Bridgford, S. C. Xie, S. A. Cobbold, C. F. A. Pasaje, S. Herrmann, T. Yang, D. L. Gillett, L. R. Dick, S. A. Ralph and C. Dogovski, "Artemisinin kills malaria parasites by damaging proteins and inhibiting the proteasome," *Nat Commun,* vol. 9, no. 1, pp. 1-9, 2018. doi.org/10.1038/s41467-018-06221-1

[64] C. X. Liu, "Discovery and development of artemisinin and related compounds," *Chin Herb Med,* vol. 9, no. 2, pp. 101-114, 2017. doi.org/10.1016/S1674-6384(17)60084-4

[65] C. Sun and B. Zhou, "The molecular and cellular action properties of artemisinins: what has yeast told us?," *Microbial Cell,* vol. 3, no. 5, p. 196, 2016. doi: 10.15698/mic2016.05.498

[66] U. Eckstein-Ludwig, R. Webb, I. Van Goethem, J. East, A. Lee, M. Kimura, P. O'neill, P. Bray, S. Ward, and S. Krishna, "Artemisinins target the SERCA of Plasmodium falciparum," *Nature,* vol. 424, no. 6951, pp. 957-961, 2003. doi: 10.1038/nature01813.

[67] Y. Yuthavong, "Basis for antifolate action and resistance in malaria," *Microbes Infect,* vol. 4, no. 2, pp. 175-182, 2002. doi: 10.1016/s1286-4579(01)01525-8

[68] M. P. Draper, B. Bhatia, H. Assefa, L. Honeyman, L. K. Garrity-Ryan, A. K. Verma, J. Gut, K. Larson, J. Donatelli, and A. Macone, "In vitro and in vivo antimalarial efficacies of optimized tetracyclines," *Antimicrob Agents Chemother,* vol. 57, no. 7, pp. 3131-3136, 2013. doi: 10.1128/AAC.00451-13.

[69] T. Gaillard, J. Dormoi, M. Madamet and B. Pradines, "Macrolides and associated antibiotics based on similar mechanism of action like lincosamides in malaria,"*Malar J,* vol. 15, no. 1, pp. 1-11, 2016. doi: 10.1186/s12936-016-1114-z.

[70] J. Wiesner and H. Jomaa, "1-Deoxy-d-Xylulose 5-Phosphate Pathway," in *Encyclopedia of Malaria,* 2013, pp. 1-12. https://link.springer.com/content/pdf/10.1007%2F978-1-4614-8757-9_10-1.pdf.

[71] R. K. Dhiman, M. L. Schaeffer, A. M. Bailey, C. A. Testa, H. Scherman and D. C. Crick, "1-Deoxy-D-xylulose-5-phosphate reductoisomerase (IspC) from Mycobacterium tuberculosis: towards understanding mycobacterial resistance to fosmidomycin," *J bacteriol*, vol. 187, no. 24, pp. 8395-8402, 2005. doi: 10.1128/JB.187.24.8395-8402.2005.

[72] T. S. Skinner-Adams, G. M. Fisher, A. G. Riches, O. E. Hutt, K. E. Jarvis, T. Wilson, M. Von Itzstein, P. Chopra, Y. Antonova-Koch and S. Meister, "Cyclization-blocked proguanil as a strategy to improve the antimalarial activity of atovaquone," *Commun Bio,* vol. 2, no. 1, pp. 1-14, 2019. https://doi.org/10.1038/s42003-019-0397-3

[73] I. P. Stolerman, Drug Toxicity. *Encyclopedia of Psychopharmacology*, 2010. https://www.springer.com/gp/book/9783540687061

[74] M. S. Shiels, A. B. De González, A. F. Best, Y. Chen, P. Chernyavskiy, P. Hartge, S. Q. Khan, E. J. Pérez-Stable, E. J. Rodriquez, and S. Spillane, "Premature mortality from all causes and drug poisonings in the USA according to socioeconomic status and rurality: an analysis of death certificate data by County from 2000–15," *The Lancet Public Health,* vol. 4, no. 2, pp. e97-e106, 2019. doi: 10.1016/S2468-2667(18)30208-1.

[75] H. Hedegaard, A. M. Miniño, and M. Warner, "Drug overdose deaths in the United States, 1999-2018," *NCHS Data Brief*, no 356 pp.1-8.2020. https://pubmed.ncbi.nlm.nih.gov/32487285/

[76] H. Hedegaard, A. M. Miniño and M. Warner, "Urban-rural differences in drug overdose death rates, by sex, age, and type of drugs involved, 2017," *NCHS Data Brief*, 2019. no 345. https://pubmed.ncbi.nlm.nih.gov/31442197/

[77] K. A. J. Al Khaja and R. P. Sequeira, "Drug treatment and prevention of malaria in pregnancy: a critical review of the guidelines," *Malar J,* vol. 20, no. 1, p. 62, Jan 23 2021. doi: 10.1186/s12936-020-03565-2

[78] World Health Organization, "Guideline for the treatment of malaria-3rd edtion " *World Health Organization,* 2015. https://www.afro.who.int/publications/guidelines-treatment-malaria-third-edition

[79] A. N. Cowell and E. A. Winzeler, "The genomic architecture of antimalarial drug resistance," *Briefings in functional genomics,* vol. 18, no. 5, pp. 314-328, 2019.

[80] Q. Li and M. Hickman, "The Impact of Pharmacokinetic Mismatched Antimalarial Drug Combinations on the Emergence and Spread of Drug-Resistant Parasites," *Basic*

Pharmacokinetic Concepts and Some Clinical Applications, vol. 1, pp. 1-32, 2015. doi: 10.5772/59506

[81] E. Klein, "Antimalarial drug resistance: a review of the biology and strategies to delay emergence and spread," *Int J Antimicrob Agents,* vol. 41, no. 4, pp. 311-317, 2013. doi: 10.1016/j.ijantimicag.2012.12.007

[82] B. A. Wilson, N. R. Garud, A. F. Feder, Z.J. Assaf and P. S. Pennings, "The population genetics of drug resistance evolution in natural populations of viral, bacterial and eukaryotic pathogens," *Mol Ecol,* vol. 25, no. 1, pp. 42-66, 2016. doi: 10.1111/mec.13474.

[83] A. Corsonello, A. M. Abbatecola, S. Fusco, F. Luciani, A. Marino, S. Catalano, M.G. Maggio and F. Lattanzio, "The impact of drug interactions and polypharmacy on antimicrobial therapy in the elderly," *Clin Microbiol Infect,* vol. 21, no. 1, pp. 20-26, 2015. doi: 10.1016/j.cmi.2014.09.011.

[84] J. Bengtsson-Palme, E. Kristiansson and D. J. Larsson, "Environmental factors influencing the development and spread of antibiotic resistance," *FEMS Microbiol Rev,* vol. 42, no. 1, p. fux053, 2018. doi: 10.1093/femsre/fux053.

[85] D. Ménard and D. A. Fidock, "Accelerated evolution and spread of multidrug-resistant Plasmodium falciparum takes down the latest first-line antimalarial drug in Southeast Asia," *Lancet Infect Dis,* vol. 19, no. 9, pp. 916-917, 2019. doi: 10.1016/S1473-3099(19)30394-9.

[86] R. Afoakwah, J. N. Boampong, A. Egyir-Yawson, E. K. Nwaefuna, O. N. Verner, and K. K. Asare, "High prevalence of PfCRT K76T mutation in Plasmodium falciparum isolates in Ghana," *Acta Tropica,* vol. 136, pp. 32-36, 2014.

[87] S. Griffing, L. Syphard, S. Sridaran, A. M. Mccollum, T. Mixson-Hayden, S. Vinayak, L. Villegas, J. W. Barnwell, A. A. Escalante, and V. Udhayakumar, "pfmdr1 amplification and fixation of pfcrt chloroquine resistance alleles in Plasmodium falciparum in Venezuela," *Antimicrob Agents Chemother,* vol. 54, no. 4, pp. 1572-1579, 2010. doi: 10.1128/AAC.01243-09.

[88] M. Bushman, L. Morton, N. Duah, N. Quashie, B. Abuaku, K. A. Koram, P. R. Dimbu, M. Plucinski, J. Gutman, and P. Lyaruu, "Within-host competition and drug resistance in the human malaria parasite Plasmodium falciparum," *Proc Biol Sci* , vol. 283, no. 1826, p. 20153038, 2016. doi: 10.1098/rspb.2015.3038

[89] T. M. Dokunmu, C. U. Adjekukor, O. F. Yakubu, A. O. Bello, J. O. Adekoya, O. Akinola, E. O. Amooand A. H. Adebayo, "Asymptomatic malaria infections and Pfmdr1 mutations in an endemic area of Nigeria," *Malar J,* vol. 18, no. 1, pp. 1-7, 2019. doi.org/10.1186/s12936-019-2833-8.

[90] C. Wongsrichanalai, A. L. Pickard, W. H. Wernsdorfer and S. R. Meshnick, "Epidemiology of drug-resistant malaria," *Lancet Infect Dis* , vol. 2, no. 4, pp. 209-218, 2002. doi: 10.1016/s1473-3099(02)00239-6.

[91] M. I. Veiga, S. K. Dhingra, P. P. Henrich, J. Straimer, N. Gnädig, A.-C. Uhlemann, R. E. Martin, A. M. Lehane, and D. A. Fidock, "Globally prevalent PfMDR1 mutations modulate Plasmodium falciparum susceptibility to artemisinin-based combination therapies," *Nat Commun,* vol. 7, no. 1, pp. 1-12, 2016. doi: 10.1038/ncomms11553.

[92] X. C. Ding, D. Ubben, and T. N. Wells, "A framework for assessing the risk of resistance for antimalarials in development," *Malar J,* vol. 11, no. 1, pp. 1-11, 2012.

[93] V. C. Corey, A. K. Lukens, E. S. Istvan, M. C. Lee, V. Franco, P. Magistrado, O. Coburn-Flynn, T. Sakata-Kato, O. Fuchs, and N.F. Gnädig, "A broad analysis of resistance development in the malaria parasite," *Nat Commun,* vol. 7, no. 1, pp. 1-9, 2016. doi: 10.1038/ncomms11901

[94] S. Pulcini, H. M. Staines, A. H. Lee, S. H. Shafik, G. Bouyer, C. M. Moore, D. A. Daley, M.J. Hoke, L. M. Altenhofen, and H. J. Painter, "Mutations in the Plasmodium falciparum chloroquine resistance transporter, PfCRT, enlarge the parasite's food vacuole and alter drug sensitivities," *Sci Rep,* vol. 5, no. 1, pp. 1-16, 2015. doi: 10.1038/srep14552

[95] M. Imwong, A. M. Dondorp, F. Nosten, P. Yi, M. Mungthin, S. Hanchana, D. Das, A.P. Phyo, K.M. Lwin, and S. Pukrittayakamee, "Exploring the contribution of candidate genes to artemisinin resistance in Plasmodium falciparum," *Antimicrob Agents Chemother,* vol. 54, no. 7, pp. 2886-2892, 2010. doi: 10.1128/AAC.00032-10

[96] D. W. Juma, P. Muiruri, K. Yuhas, G. John-Stewart, R. Ottichilo, J. Waitumbi, B. Singa, C. Polyak, and E. Kamau, "The prevalence and antifolate drug resistance profiles of Plasmodium falciparum in study participants randomized to discontinue or continue cotrimoxazole prophylaxis," *PLoS Negl Trop Dis,* vol. 13, no. 3, p. e0007223, 2019. doi: 10.1371/journal.pntd.0007223

[97] N. C. Iriemenam, M. Shah, W. Gatei, A. M. Van Eijk, J. Ayisi, S. Kariuki, J. V. Eng, S. O. Owino, A. A. Lal, and Y. O. Omosun, "Temporal trends of sulphadoxine-pyrimethamine (SP) drug-resistance molecular markers in Plasmodium falciparum parasites from pregnant women in western Kenya," *Malar J,* vol. 11, no. 1, pp. 1-15, 2012. doi: 10.1186/1475-2875-11-134

[98] S. Gesase, R. D. Gosling, R. Hashim, R. Ord, I. Naidoo, R. Madebe, J. F. Mosha, A. Joho, V. Mandia, and H. Mrema, "High resistance of Plasmodium falciparum to sulphadoxine/pyrimethamine in northern Tanzania and the emergence of dhps resistance mutation at Codon 581," *PLoS One,* vol. 4, no. 2, p. e4569, 2009. doi: 10.1371/journal.pone.0004569

[99] A. Nzila, "The past, present and future of antifolates in the treatment of Plasmodium falciparum infection," *J Antimicrob Chemother,* vol. 57, no. 6, pp. 1043-1054, 2006. doi: 10.1093/jac/dkl104

[100] C. H. Sibley, J. E. Hyde, P. F. Sims, C.V. Plowe, J. G. Kublin, E. K. Mberu, A. F. Cowman, P. A. Winstanley, W. M. Watkins and A. M. Nzila, "Pyrimethamine–sulfadoxine resistance in Plasmodium falciparum: what next?," *Trends Parasitol,* vol. 17, no. 12, pp. 570-571, 2001. doi: 10.1016/s1471-4922(01)02085-2.

[101] R. Abdul-Ghani, H. F. Farag, and A. F. Allam, "Sulfadoxine-pyrimethamine resistance in Plasmodium falciparum: a zoomed image at the molecular level within a geographic context," *Acta Tropica,* vol. 125, no. 2, pp. 163-190, 2013. doi: 10.1016/j.actatropica.2012.10.013

[102] S. G. Valderramos, D. Scanfeld, A. C. Uhlemann, D. A. Fidock, and S. Krishna, "Investigations into the role of the Plasmodium falciparum SERCA (PfATP6) L263E mutation in artemisinin action and resistance," *Antimicrob Agents Chemother,* vol. 54, no. 9, pp. 3842-3852, 2010. doi: 10.1128/AAC.00121-10

[103] A. B. S. Sidhu, S. G. Valderramos, and D. A. Fidock, "pfmdr1 mutations contribute to quinine resistance and enhance mefloquine and artemisinin sensitivity in Plasmodium falciparum," *Mol Microbiol,* vol. 57, no. 4, pp. 913-926, 2005. doi: 10.1111/j.1365-2958.2005.04729.x

[104] C. N. Nguetse, A. A. Adegnika, T. Agbenyega, B. R. Ogutu, S. Krishna, P. G. Kremsner, and T. P. Velavan, "Molecular markers of anti-malarial drug resistance in Central, West

and East African children with severe malaria," *Malar J*, vol. 16, no. 1, pp. 1-9, 2017. doi: 10.1186/s12936-017-1868-y

[105] I. Adam, Y. Ibrahim, and G. I. Gasim, "Efficacy and safety of artemisinin-based combination therapy for uncomplicated Plasmodium falciparum malaria in Sudan: a systematic review and meta-analysis," *Malar J*, vol. 17, no. 1, pp. 1-8, 2018. doi: 10.1186/s12936-018-2265-x

[106] L. E. Heller and P. D. Roepe, "Artemisinin-based antimalarial drug therapy: molecular pharmacology and evolving resistance," *Trop Med Infect Dis*, vol. 4, no. 2, p. 89, 2019. doi: 10.3390/tropicalmed4020089

[107] W. Zheng, H. Jiang, Z. Xiong, Z. Jiang, and H. Chen, "Efficacy of Pyrimethamine/Sulfadoxine versus Chloroquine for the Treatment of Uncomplicated Falciparum Malaria in Children Aged Under 5 Years," *Iran J Parasitol*, vol. 8, no. 1, p. 1, 2013. https://pubmed.ncbi.nlm.nih.gov/23682255/

[108] L. C. Okell, J. T. Griffin, and C. Roper, "Mapping sulphadoxine-pyrimethamine-resistant Plasmodium falciparum malaria in infected humans and in parasite populations in Africa," *Sci Rep*, vol. 7, no. 1, pp. 1-15, 2017. doi: 10.1038/s41598-017-06708-9

[109] M. T. Alam, S. Vinayak, K. Congpuong, C. Wongsrichanalai, W. Satimai, L. Slutsker, A. A. Escalante, J. W. Barnwell, and V. Udhayakumar, "Tracking origins and spread of sulfadoxine-resistant Plasmodium falciparum dhps alleles in Thailand," *Antimicrob Agents Chemother* , vol. 55, no. 1, pp. 155-164, 2011. doi: 10.1128/AAC.00691-10

[110] H. Mcintosh, "Chloroquine or amodiaquine combined with sulfadoxine-pyrimethamine for treating uncomplicated malaria," *Cochrane Database Syst Rev*, no. 4, 2001. doi: /10.1002/14651858.CD000386.pub2

[111] A. Hasugian, E. Tjitra, A. Ratcliff, H. Siswantoro, E. Kenangalem, R. Wuwung, H. Purba, K. Piera, F. Chalfien, and J. Marfurt, "In vivo and in vitro efficacy of amodiaquine monotherapy for chloroquine-resistant P. vivax," *Antimicrob Agents Chemother* , vol. 53, no. 3, pp. 1094–1099, 2008. doi: 10.1128/AAC.01511-08

[112] P. B. Matsiegui, M. A. Missinou, M. Necek, S. Issifou, and P. G. Kremsner, "Short course of quinine plus a single dose of sulfadoxine/pyrimethamine for Plasmodium falciparum malaria," *Wien Klin Wochenschr*, vol. 118, no. 19, pp. 610-614, 2006. doi: 10.1007/s00508-006-0657-3

[113] A. Hall, E. Doberstyn, V. Mettaprakong, and P. Sonkom, "Falciparum malaria cured by quinine followed by sulfadoxine-pyrimethamine," *Br Med J,* vol. 2, no. 5961, pp. 15-17, 1975. doi: 10.1136/bmj.2.5961.15

[114] A. J. Magill, J. Zegarra, C. Garcia, W. Marquiño, and T. K. Ruebush Ii, "Efficacy of sulfadoxine-pyrimethamine and mefloquine for the treatment of uncomplicated Plasmodium falciparum malaria in the Amazon basin of Peru," *Rev Soc Bras Med Trop,* vol. 37, no. 3, pp. 273-278, 2004. doi: 10.1590/s0037-86822004000300015

[115] W. Metzger, B. Mordmüller, W. Graninger, U. Bienzle, and P. G. Kremsner, "High efficacy of short-term quinine-antibiotic combinations for treating adult malaria patients in an area in which malaria is hyperendemic," *Antimicrob Agents Chemother,* vol. 39, no. 1, pp. 245-246, 1995. doi: 10.1128/aac.39.1.245

[116] C. O. Obonyo and E. A. Juma, "Clindamycin plus quinine for treating uncomplicated falciparum malaria: a systematic review and meta-analysis," *Malar J,* vol. 11, no. 1, pp. 1-11, 2012. doi: 10.1186/1475-2875-11-2.

[117] E. Meltzer and E. Schwartz, "Atovaquone-proguanil chemoprophylaxis in the era of Tafenoquine," *J Travel Med,* vol. 26, no. 4, p. tay133, 2019. doi: 10.1093/jtm/tay133

[118] Center for Disease Control and Prevention "Malaria; How to choose a Drug to Prevent Malaria," *Center for Disease Control and Prevention,* 2018. https://www.cdc.gov/malaria/travelers/drugs.html

[119] World Health Organization, "Chapter 7. Malaria," *World Health Organization,* 2009. https://www.who.int/ith/2017-ith-chapter7.pdf

[120] K. R. Tan, J. K. Fairley, M. Wang, and J. R. Gutman, "A survey on outcomes of accidental atovaquone-proguanil exposure in pregnancy," *Malar J,* vol. 17, no. 1, p. 198, May 15 2018. doi: 10.1186/s12936-018-2352-z

[121] T. P. Selvam, C. R. James, P. V. Dniandev and S. K. Valzita, "A mini-review of pyrimidine and fused pyrimidine marketed drugs," *Pharm,* vol. 2, no. 4, 2012. https://updatepublishing.com/journal/index.php/rip/article/view/271.

[122] E. Bilsland, L. Van Vliet, K. Williams, J. Feltham, M. P. Carrasco, W. L. Fotoran, E. F. G. Cubillos, G. Wunderlich, M. Grøtli, F. Hollfelder, V. Jackson, R. D. King, and S. G. Oliver, "Plasmodium dihydrofolate reductase is a second enzyme target for the antimalarial action

of triclosan," *Sci Rep,* vol. 8, no. 1, pp. 1038-1038, 2018. doi: 10.1038/s41598-018-19549-x

[123] N. Rastogi, K. S. Goh, L. Horgen, W. W. J. F. I. Barrow, and M. Microbiology, "Synergistic activities of antituberculous drugs with cerulenin and trans-cinnamic acid against Mycobacterium tuberculosis," *FEMS Immunol Med Microbiol,* vol. 21, no. 2, pp. 149-157, 1998. doi: 10.1111/j.1574-695X.1998.tb01161.x.

[124] R. Pasupureddy, S. Verma, A. Pant, R. Sharma, S. Seshadri, V. Pande, A. K. Saxena, R. Dixit, and K. C. J. E. P. Pandey, "Crucial residues in falcipains that mediate haemoglobin hydrolysis," *Exp Parasitol,* vol. 197, pp. 43-50, 2019. doi: 10.1016/j.exppara.2019.01.005.

[125] K. V. Sashidhara, M. Kumar, R. K. Modukuri, R. K. Srivastava, A. Soni, K. Srivastava, S. V. Singh, J. Saxena, H. M. Gauniyal, S. K. J. B. Puri, and M. Chemistry, "Antiplasmodial activity of novel keto-enamine chalcone-chloroquine based hybrid pharmacophores," *Bioorg Med Chem,* vol. 20, no. 9, pp. 2971-2981, 2012. doi: 10.1016/j.bmc.2012.03.011

[126] H. B. Rasmussen, S. B. Christensen, L. P. Kvist, and A. J .P. M. Karazmi, "A simple and efficient separation of the curcumins, the antiprotozoal constituents of Curcuma longa," *Planta Med,* vol. 66, no. 04, pp. 396-398, 2000. doi: 10.1055/s-2000-8533.

CHAPTER 2

Lactate dehydrogenase and Malate dehydrogenase: Potential antiparasitic targets for drug development studies

Graphical Abstract

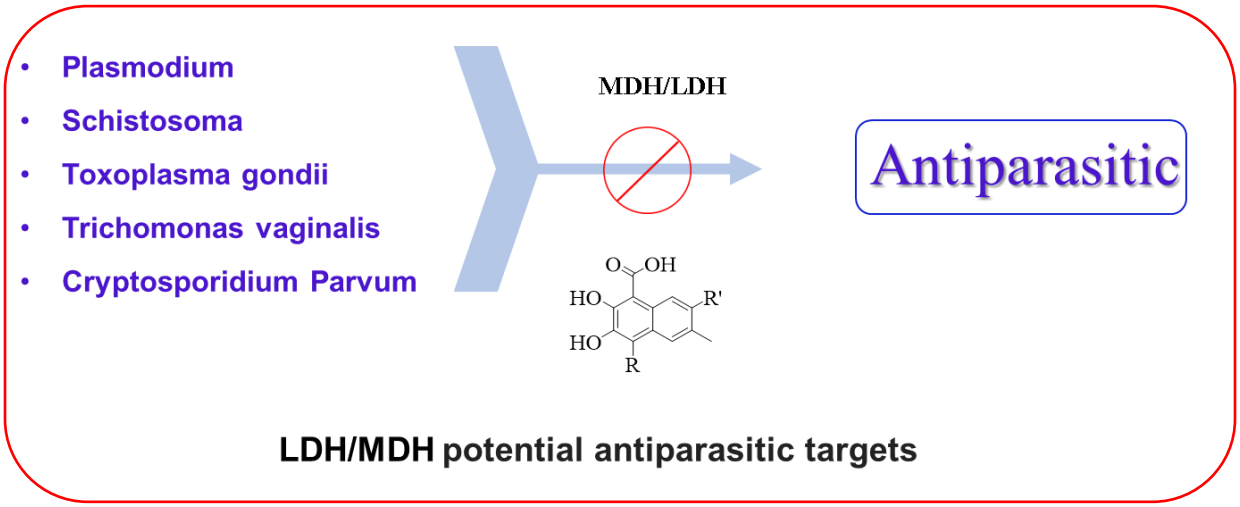

Abstract

Parasitic diseases remain a major public health concern for humans, claiming millions of lives annually. Although different treatments are required for these diseases, drug usage is limited due to the development of resistance and toxicity. The victory over these impediments necessitates alternate therapy. As per our literature review, parasitic Lactate dehydrogenases (LDH) and Malate dehydrogenases (MDH) have shown unique pharmacological selective and specificity compared to other isoforms, thus highlighting them as viable therapeutic targets involved in aerobic and anaerobic glycolytic pathways. LDH and MDH are important therapeutic targets for invasive parasites because they play a critical role in the progression and development of parasitic diseases. Any strategy to impede these enzymes would be fatal to the parasites, paving the way for developing and discovering novel antiparasitic agents. This review aims to highlight the importance of parasitic LDH and MDH as therapeutic drug targets in selected obligate apicoplast parasites. To the best of our knowledge, this review presents the first comprehensive review of LDH and MDH as potential antiparasitic targets for drug development studies.

Keywords: lactate dehydrogenase, malate dehydrogenase, *Plasmodium falciparum*, *Schistosoma haematobium, cryptosporidium parvum.*

2.1 Introduction

Parasites are causative agents of many diseases that infect many living organisms. Despite various control strategies, parasitic diseases such as malaria, leishmaniasis, cryptosporidiosis, trypanosomiasis, schistosomiasis are still prevalent in tropical regions, with annual mortality rates of at least 500 000 [1]. Their continued ability to develop resistance towards first-line drugs necessitates the need for new drug treatment regimens [2]. The glycolytic pathway plays a central role in the generation of ATP in the life cycles of most protozoan parasites; thus, the disruption of the glycolytic pathway is regarded as a promising target, especially for novel drugs [3-7]. Specifically, Lactate dehydrogenase (LDH) and Malate dehydrogenase (MDH) have been identified as key and potential enzymatic targets in the parasite's glycolytic pathway. LDH facilitates the interconversion of pyruvate and lactate while oxidizing nicotinamide adenine dinucleotide (NADH) to NAD+. The regeneration of NAD+ enables the reproduction of ATP, which is vital for cell survival and development [8-10]. MDH is a homologue of LDH, and together with LDH, it contributes to the energy generation in some parasites [11, 12]. The primary function of MDH is the interconversion between malate and oxaloacetate by hydride transfer of NAD+ or NADP+ as cofactors (**Figure 2.1**) [3]. As described above, lactate and oxaloacetate can serve as substrates in the generation of ATP for energy production. MDH also plays a significant role in other metabolic pathways, including aspartate biosynthesis, malate-aspartate shuttle, gluconeogenesis, and lipogenesis. Phylogenetic studies show that MDH and LDH emerged from early gene duplication preceding in all three domains of life in a eukaryotic cell [14]. As such, LDH is contained only in the cytosol, while MDHs are present in the cytosol, mitochondria, chloroplasts, and peroxisomes.

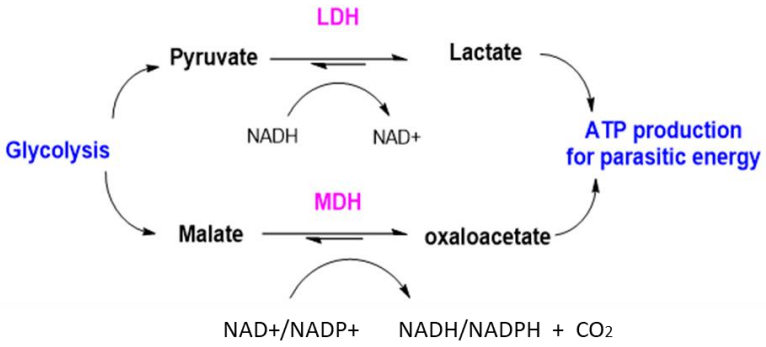

Figure 2.1. The catalytic reactions of parasite LDH and MDH for energy generation.

These two enzymes have a highly preserved tertiary structure representing a dynamic, active site important for mediating the ligand-binding specificity. Furthermore, the site-directed mutagenesis studies indicated an easy conversion between LDH and MDH specificity by mutation of certain amino acids at specific sites [15, 16]. As a result, they have distinct characteristics differentiating them from Human LDH (hLDH) and Human MDH (hMDH), making them suitable therapeutic targets. As such, LDH and MDH have many roles in parasitic diseases caused by Plasmodium [11], Trichomonas [7], Toxoplasma Gondii [6], Schistosoma [5] as well as Cryptosporidium parvum [3], which are described further in detail in this review.

Most importantly, all the parasites mentioned above lack functional mitochondrion to generate ATP through aerobic respiration [17]. The production of energy depends entirely on the catalytic routes of LDH and MDH. Thus this heavy reliance makes the glycolytic pathway of these parasites an ideal target. As a result, any attempt to stop or downregulate the activities of LDH and MDH would have cidal implications for the parasites. Developing compounds with both LDH and MDH inhibitory action would be a promising strategy in the fight against these maladies. A class of compounds such as oxamate and gossypol have exhibited dual inhibition of LDH and MDH (**Table 1**). Given that LDH is a vital target in certain parasites, it can be deduced that MDH would be essential. The parasites with their known inhibitors are highlighted in **Table 1**. The inhibition of LDH and MDH in certain parasites may be a promising strategy for developing new antiparasitic agents.

Table 1. Parasites with their potential inhibitors.

Parasites	**Potential Compounds**	**Target enzyme**	**Activity IC_{50} (µM)**	**Reference**
Plasmodium	Azole, Gossypol	LDH	0.14	[18-20]
	Oxamate	LDH/MDH	1.75/2.66	
Trichomonas vaginalis	Quinolines-1,2,3-triazolylcarboxamides	LDH	100.00	[21]
Toxoplasma Gondii	Gossypol	LDH1/LDH2	0.70/0.10	[22]
Schistosoma	Benziimidazole	LDH	nd	[23]
	Praziquantel			

Cryptosporidium parvum	Gosspol, FX11, NSC10447, NSC158011	LDH	11.80 - 79.60	[3, 24]

nt =not determined

The dual functionality of LDH and MDH as relevant targets in discovery drugs is one feature of certain parasites that have been neglected. They have been shown to be complementary, and when viewed together rather than separately, they can yield positive results. Formulating compounds that target both enzymes in the parasite glycosidic pathway would thus be more valuable. Therefore, this review endeavours to address the gaps identified in the literature on LDH and MDH as therapeutic targets.

2.2 An appraisal of the inhibitory action of parasite-LDH and MDH by top inhibitors

In the treatment of parasitic disease, the emergence of drug resistance continues to be a challenge. Malaria, for example, have already demonstrated resistance to first-line drugs like artemisinin and artemisinin-based combination therapy (ACT) [25]. In schistosomiasis, PZQ resistance has been reported, though the evidence is still inconclusive [26]. Toxoplasmosis has also been shown to be resistant to mainstay drugs pyrimethamine and sulfadiazine [27]. One of the intriguing and promising novel targets are LDH and MDH, with compounds such as gossypol, oxamate, azole and quinoline already shown to be essential and active against them. Thus, this section delves into the structure of the LDH and MDH enzymes and their top inhibitors.

2.2.1 *Plasmodium*

Malaria still claims about 409,000 lives, with an estimated 229 million cases every year, chiefly in sub-Saharan Africa [28]. *Plasmodium* has shown resistance on nearly all mainstay antimalarial drugs, and comprehension of the resistance mechanism is still challenging. More regrettable still, no effective commercial vaccine has been developed [29].

Insights into the *Plasmodium sp.* glycolytic pathway may provide the basis to create a new antimalarial candidate and sidestep resistance. The absence of a practical TCA cycle in *Plasmodium* mitochondrion makes the parasite heavily rely on the fermentation of glucose and minimal oxidation for energy [30]. This process is facilitated by *Pf*LDH, which has been validated as a novel and potential antimalarial target [31]. *Pf*LDH utilizes a rotenone-insensitive single-subunit NADH cofactor (NDH-II) different from its mammalian counterpart, which uses NADH cofactor NDH-I suggesting an antimalarial that can selectively be targeted [16]. This process is

key as the parasite enters the agamic stage of the *Plasmodium* life cycle in the erythrocytic stage [30]. Bozdech and colleagues previously demonstrated that all glycolytic enzymes are upregulated at the early trophozoite stage during the asexual cycle, coinciding with the time of maximal metabolic activity by the parasite [32]. RNA transcriptional data demonstrated that *Pf*LDH expression is highest during the intracellular lifecycle stage and lowest at the schizont stage. Thus, LDH is vital in the development of trophozoite, the success of the asexual metabolic process and infection [33]. An infected cell consumes about 20-fold more energy, and thus hampering *PfDLH* activity would be lethal to the parasite [30].

*Pf*LDH shares ~90-92% phylogenetic similarities in catalytic residues and cofactor binding sites with *P. vivax, P. malariae* and *P. ovale*. The crystal structure of *Pf*LDH revealed a unique five amino acids insertion loop next to its binding site indicated in blue (**Figure 2.2**). It modifies the dislodgment of the nicotinamide ring and increases the volume of the active site. The loop enhances the selective inhibitory activity, thus presenting a unique kinetic behaviour making PfLDH an ideal antimalarial target [34, 35].

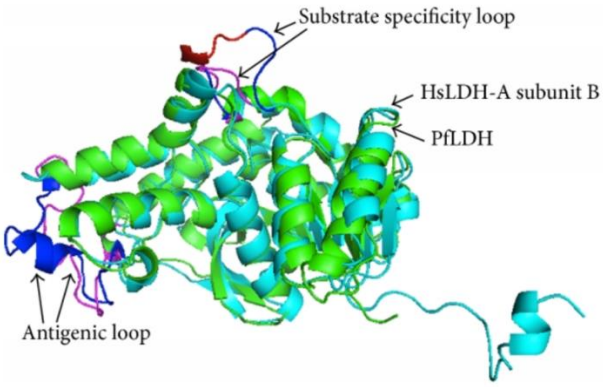

Figure 2.2. A comparative alignment of structural Human (H)LDH (cyan) versus *Pf*LDH (green) [36].

The binding of NADH in the PfLDH pocket is obstructed by steric hindrance of the nicotinamide group resulting from weaker Hydrogen (H) bond formed between the carbonyl oxygen of the amide and PfLDH. Thus, 3-acetylpyridine adenine dinucleotide (APAD), a synthetic analogue of NADH, is preferred, about 200 to 300-fold more affinity than NADH derivative towards *Pf*LDH [37]. Also, PfMDH has been demonstrated to be a crucial plasmodium enzyme that complements *Pf*LDH activity in the fermentation process. *Pf*MDH catalyzes the interconversion of malate to oxaloacetate using APAD [11]. A stall of the production of ATP in *P. falciparum* may require

inhibition of both *Pf*LDH and *Pf*MDH. Although *Pf*MDH and *Pf*LDH are similar in structure, they differ in substrate-binding [34]. **Figure 2.3** highlights a class of compounds that were shown to be potent against *Pf*LDH. Interestingly, oxamic derivatives are the only class of compounds known to display dual inhibitory against *Pf*LDH (IC_{50}=1.75 ± 0.26 µM) and *Pf*MDH (IC_{50}=2.66 ± 0,26 µM) [11].

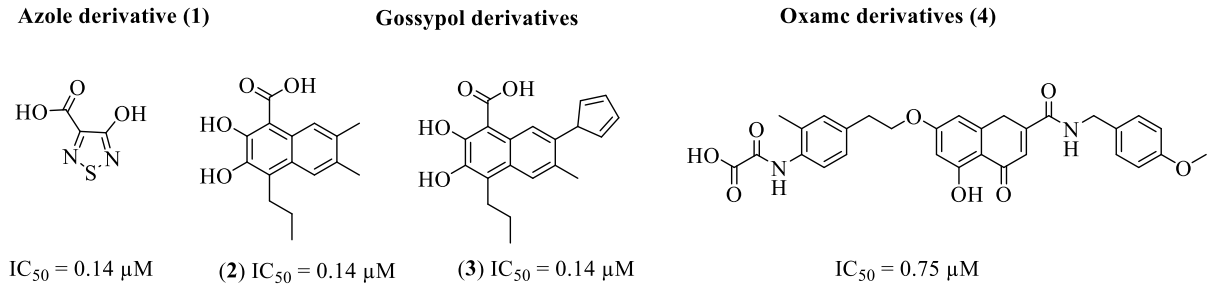

Figure 2.3. Chemical structures of some known potent *Pf*LDH inhibitors.

Azole derivatives displayed remarkable selective activity against the *Pf*LDH with IC_{50} of 0.14 µM, as shown by compound **1**. However, these compounds are discredited by their smaller size because they get completely immersed in the active site pocket. Gossypol derivatives are another class of compounds that showed good activity against *Pf*LDH with an IC_{50} value of 0.1 µM, as revealed by compounds **2** and **3**, respectively. They are highly cytotoxic, and further derivatization neither improved selectivity nor activity. Lastly, oxamate derivatives are the only group of compounds that showed good activity against *Pf*LDH and *Pf*MDH with IC_{50} values of 1.75 and 2.66 µM, respectively, corresponding to compound **4** [18]. In view of facts, the azole, gossypol and oxamate would be vital moieties in formulating new anti-malarial candidates focusing on *Pf*LDH as a target.

Krettli *et al*. (2011) [35] conducted an *in-silico, and in vitro* screening of 50 commercially available drugs against *Pf*LDH, which revealed atorvastatin, itraconazole and parconazole possessed antimalarial activity, as depicted in **Table 2**. This entails that the drugs can alongside potentially inhibit *Pf*LDH in antimalarial activity and may be promising candidates when used in synergy with other antimalarial drugs. For instance, atorvastatin showed an excellent synergistic effect with quinine [35].

Table 2. Potent commercially available drugs against PfLDH [35].

Drug	**IC_{50} (µM)**

Atorvastatin	13.1 ± 4.5
Itraconazole	9.3 ± 0.8
Posaconazole	2.6 ± 0.3

Similarly, chloroquine (CQ) and other quinoline antimalarial drugs demonstrated mild anti-*PfLDH* activity by selectively forming Hydrogen bonds with Met30, Ile31 Thr101, Ala244, Ser245 and Pro246 amino acids exclusive to *Pf*LDH. Although CQ and other quinoline antimalarial drugs were not direct inhibitors of *Pf*LDH, their anti-*Pf*LDH activity added to the overall efficacy. Also, studies have indicated that CQ lodges in the NADH cofactor binding pocket of *Pf*LDH like the adenyl group of NADH, making it a potential competitor of NADH [38]. Despite resistance in most quinoline based antimalarial drugs, quinoline can still be considered a key moiety as a starting point in the formulation of new antimalarial with complementary inhibition of *Pf*LDH.

2.2.2 *Schistosoma*

Schistosomiasis is a waterborne disease caused by the blood flukes of the genus *Schistosoma*, which infects 250 million people and an annual mortality of about 11,750 occurring Middle East, Asia, South America and chiefly in the poor tropical region of Saharan Africa. Praziquantel (PZQ) drug has been used as a first-line treatment choice for both treatment and prevention of schistosomiasis, with efficacy across all parasite life-stages. However, the mass administration of PZQ has enabled an environment ideal for the emergence of drug-resistant parasites, thus, highlighting the need to seek alternative chemotherapy [39, 40].

Similarly, *Schistosomiasis* LDH (SLDH) is a crucial enzyme in the glycolytic biochemical pathway, and it has been recognized as a potential target for both chemotherapy and prevention. Although studies are still underway, SLDH has shown similar biological functions as the other LDH isoforms. Its role is characterized by the production of lactate and NAD+ from pyruvate and NADH cofactor. The lactate generated perpetuates the anaerobic respiration of the parasite, which is the sole source of energy the parasites highly rely on [41]. As the *schistosomula* worm matures into an adult in the host bloodstream, it triggers more production of lactate to meet the energy demand [42]. Impeding the activity of SLDH will starve the parasite to death, and this serves as a promising strategy for the development of schistosomiasis therapeutic drugs.

Further probing on the mode of action of these molecules will be cardinal for mechanistic elucidation and the development of new therapeutic anti-schistosomiasis candidates. A s*chistosome* species, *Schistosoma mansoni* (Sm) LDH, has been revealed to have significant amino acid preservation responsible for substrate, coenzyme binding and catalysts with similarities ranging from 25% -58% with other LDH isoforms [43]. In addition, studies have indicated that antiserum antibody inhibited all LDH of *Schistosoma* species; *Japoanicium* (j), *mansoni* (m) and *haematobium* (h) did not show any effect against the LDH from the rabbit muscles signifying a selective inhibition [44]. Because of the facts mentioned, SLDH possesses disparities with other LDH isoforms both in amino acid residue and inhibitory activity, a promising trait suggesting that potential anti-schistosomiasis candidate is highly specific and selective to be developed.

An *in vitro* screening revealed that PZQ and levamisole inhibited both the reduction and oxidation reaction of *Cotylophoron cotylophorum* (Cc) LDH activity. Furthermore, activity against CcLDH increased following treatment with derivatives of benzimidazole, mebendazole, fenbendazole and albendazole [23]. Therefore, because PZQ has been shown to be a strong inhibitor of SjLDH, it can be extrapolated that benzimidazole and levamisole may be promising potent SLDH scaffolds. **Figure 2.4** shows compounds that are active against SLDH.

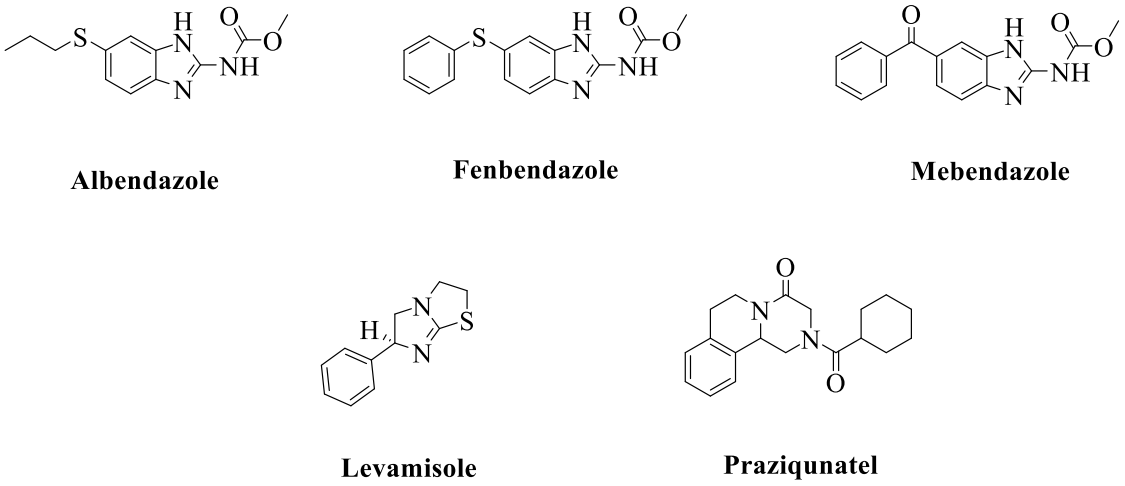

Figure 2.4. Drugs that are potent inhibitors of SLDH.

2.2.3 *Toxoplasma gondii*

Toxoplasma gondii (*T. gondii*) is a single-cellular parasite known to cause Toxoplasmosis, that the parasite infects a diversity of warm-blooded animals, including humans and domestic cats [27]. Toxoplasmosis has formally been reported to infect over one million people contracted mainly

through ingesting food, water, vegetables and fruits infected with sporulated oocyst or tissue cysts from raw meat [45]. In humans, it is considered as an opportunistic disease that mostly affects and shows severe symptoms in individuals with weakened immune systems and pregnant women [46]. Toxoplasmosis infections are distributed statistically as follows; Brazil, 77.5%; Sao Tome and Principe, 75.2%; Iran, 63.9%; Colombia, 63.5%; and Cuba, 61.8% [42, 47].

It is noted that *T. gondii* has two distinguishable LDHs; TgLDH1 and TgLDH2 expressed at different stages in its life cycle [121]. These isoforms carry an amino acid sequence of 71% similarity. TgLDH efficiently uses APAD (an NADH analogue) as a cofactor for the fermentation process to generate energy that is crucial for the growth and survival of the parasite [22]. Halting this process would serve as a way of formulating and developing new anti-toxoplasmosis drugs [49].

Like *Pf*LDH, the structure of TgLDH1 and TgLDH2 have five amino acid specificity loop adjacent to an active site which enables it to be the rate step determinant in the catalytic action [50]. TvLDH2 insertion is similar to that of *Pf*LDH, vaguely different from TgLDH1. These unique, distinguishable feature of TgLDHs makes cofactor binding site of substrate different [50, 51]. The activity of the two TgLDHs are crucial in the two central asexual stages of the parasite called tachyzoite and bradyzoite [52]. The first stage is characterized by the rapid growth of the tachyzoites. In the second stage, the residual tachyzoites instigate the development of tissue cysts, which slowly matures into bradyzoite [53]. This transformation is significant in the transition and pathogenesis of the parasite. Tachyzoites and bradyzoites have different energy requirements and use different LDH in their biochemical metabolism [6]. Bradyzoites are not susceptible to drugs because their stage lacks a functional TCA cycle and respiratory chain. They have demonstrated resistance to both the immune system and chemotherapy and are responsible for recurring infections. The pair LDHs expressed at different life stages give the parasite an adaptive trait for diverse metabolic requirements necessary for a rapid replication of the tachyzoite stage or a quiescent lifestyle typical of the bradyzoites [49 54].

The Tachyzoite stage has been attributed to acute infection liable for distributing the parasites to the brains and other tissue. The Tachyzoite stages use LDH1 for the generation of its energy, in the bradyzoites, a differentiation stage, LDH1 is transcripted into LDH2. LDH2 uses three-fold more energy than LDH1 [6, 54]. The bradyzoite stages are responsible for making the infection

chronic. The growth of bradyzoites gradually forms latent tissue cysts, enabling perseverance for longevity in the host and cause the transmission to another host without recycling through its sexual stage [6, 54]. An immune deficiency of the host may cause the bradyzoites to revert to tachyzoites and resuscitated infection. Both enzymes show almost identical catalytic activities without any significant differences in enzyme kinetics. To probe the role of TgLDH during the tachyzoite and the bradyzoite stages, Avery *et al*. (2017), engineered a knockdown strain which was used to express LDH1 or LDH2 of which it slowed the growth rates *in vitro,* reduced virulence, and decreased the development of cyst burdens *in vivo* [6]. The erasure of both LDH1 and LDH2 brought a more severe defect in chronic stage cyst burdens. Lactate dehydrogenases in *T. gondii* are key to virulence, bradyzoite differentiation, and chronic disease and showed the potential of LDH mutants as vaccine strains. No known drugs have yet been tested against LDH1 [6].

These differences will allow the development of specific and selective inhibitors of LDH1and LDH2 [51]. Below is a list of compounds that show activity against both TgLDH1 and TgLDH2 (**Figure 2.5**).

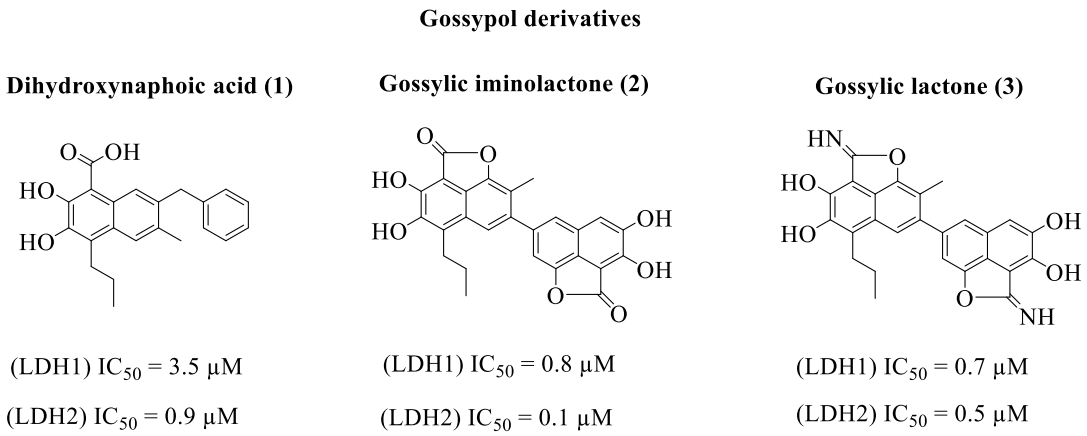

Figure 2.5. Some potent compounds for TgLDH: LDH1 and LHD2.

As highlighted in the figure above, gossypol derivatives were active against both TgLDHs, LDH1 and LDH2. Despite showing good activity of as low as 0.5 µM and 0.7 µM against LDH2 and LDH2, respectively, their toxicity profile disadvantaged them [22]. Gossypol derivatives displayed activity against LDH1 and LDH2, indicating a good starting point for the development of potent anti-TgLDH for both LDH1 and LDH2 as well as PfLDH. Thus, gossypol will be an essential scaffold in search of new anti-TgLDH drugs.

2.2.4 *Trichomonas vaginalis*

Trichomonas vaginalis (*T. vaginalis*) is a motile protozoan that resides in the urogenital tract responsible for the transmission of a common sexually transmitted infection (STI) called trichomoniasis [55]. It affects both men and women, and World Health Organization (WHO) reports annual newly recorded cases of about 270 million worldwide and around 3.7 million in the United States alone [56]. Trichomoniasis is not life-threatening and curable, but it can be devastating and raises the risk of adverse pregnancy outcomes such as premature labour and low birth-weight of infants, prostate and cervix neoplasia, pelvic inflammation and vaginitis. It is also known to increase the HIV viral load, thus increase the chance of spreading the disease during unprotected sex [55, 57].

Likewise, understanding the *T. vaginalis* glycolytic pathway is crucial for the development of anti-*T. vaginalis* agents. *T. vaginalis* only contains a motile and symptom-causing trophozoite stage undergoing cell division. The trophozoites differ in magnitude and form, with a typical length and width of 10 m and 7 µm, respectively. It has been shown that chemical and temperature agitation in trophozoites assist the conversion to pseudocysts, though it is poorly studied [58]. The energy for the amitochondriate is produced by substrate-level glycolytic phosphorylation and metabolic fermentation [54]. The hydrogenosomes, the energy powerhouse, are responsible for the anaerobic generation of lactate and hydrogen (H_2) using TvLDH gas via the oxidation of pyruvate (**Figure 2.6**). Pyruvate, together with CO_2, is proceeded from malate, a primary hydrogenosomes substrate by oxidative decarboxylated using a NAD-dependent malic enzyme TvMDH. The process is a complementary action facilitated by TvMDH and TvLDH, respectively, in the cytosol**.** As illustrated in **Figure 2.6**, NAD+ produced from the conversion of pyruvate to lactate aided by TvLDH and NADH cofactor becomes essential in oxidative recycling of malate in the hydrogenosomes [59].

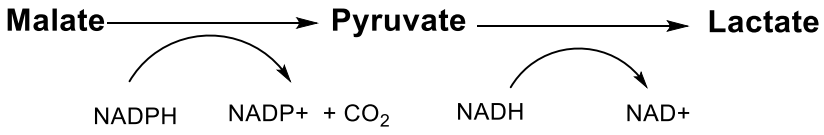

Figure 2.6. The biochemical pathway used to produce Lactate in Tv.

Trichomonas has two LDHs designed as TvLDH1 and TvLDH2, although the distinctive features between the two are not well known. TvLDH is present in all trichomonas species, and their

Hydrogenosomes possess unique reducing properties that would be a basis for chemotherapeutic development. Traditional drugs such as metronidazole are useful for antitrichomonal action where its nitro group is reduced in the hydrogenosomes metabolism [21].

The crystal structures of TvLDH and TvMDH that it possesses Arg91 crucial for coordinating the C-4 carboxyl of oxaloacetate malate, which is replaced by Leu91 in TvLDH. TvLDH1 and TvLDH2 revealed about 49.2 and 49.5% similarity in amino acid sequence, respectively and shared ~323 amino acid positions to the TvMDH. TvLDH has about 33.5-44.5% similarity in amino acid sequence with its counterparts. The similarities between TvLDH and TvMDH suggest that agents that would inhibit the activity of TvLDH are more likely to be potent against TvMDH. Another vital interchange observed is that Trp230 in TvMDH occupies Gly230 in TvLDH.

Furthermore, TvMDH and TvLDH are distinguished by two amino acids residues at deposits Gly229 and Ser239. These residues enhance hydrophobic interaction with lactate-pyruvate substrates. It is noteworthy to mention that TvLDH1 also display high activity on oxaloacetate, which is a rare property for LDH [21]. The disparities in the amino acid sequence of the TvLDH and TvMDH with other LDHs isoform allows the development of ligands that are highly specific and selective towards Tv LDH and MDH [21].

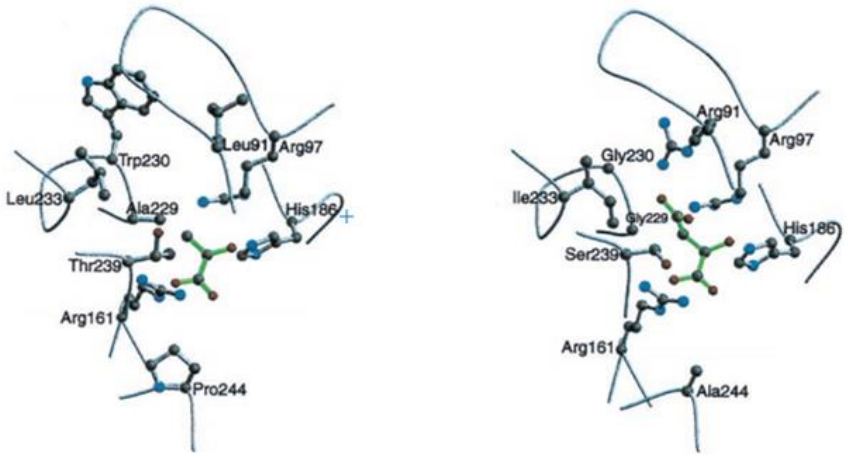

TvLDH TvMDH

Figure 2.7. Crystal structure of TvLDH1 and TvMDH.

No known drugs or molecules have been identified that inhibit TvLDH and TvMDH. Since 1960, only metronidazole and other 5-nitroimidazoles, such as tinidazole have been used to treat Tv [60].

However, like other drugs, these also suffer a fate of resistance. An imperative need to trade on new roads and develop novel anti-Tv agents is necessary. The glycolytic pathway crucial to the parasites has been informative and lay a foundation to create new drugs and evade resistance [27].

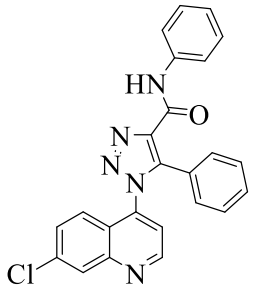

IC_{90} = 100 μM

Figure 2.8. Quinolines-1,2,3-triazolylcarboxamides (QTCA-2), a potential inhibitor of TvLDH.

Compound QTCA-2 showed promising activity against TvLDH with an IC_{90} value of 100 μM prompting an *in-silico* screening that gave the binding free energy of -3.9 $Kcalmol^{-1}$ through H-bonds with Arg48 and Thr239 and hydrophobic interaction through Ile16 and ile128. Other key amino acids involved in the ligand target interaction included Gly11, Gly14, Gln15, Asp41, Val86, Ala87, Ser88, Gly129, Asn130 and Phe238 [41]. Like in *Pf*LDH, 7-chloroquinoline would be a crucial moiety in the formulation of TvLDH agents.

2.2.5 *Cryptosporidium Parvum*

Cryptosporidium parvum (*C. parvum*) is a gastrointestinal parasite mainly responsible for a waterborne diarrheal called cryptosporidiosis worldwide, especially in the USA [61]. Effective treatment and vaccination of the parasite have not been approved yet, in any case, at present, only nitazoxanide is endorsed for treatment [24].

Like in other parasites, *C. parvum* depends on anaerobic respiration for the survival of parasites. It equally utilizes the enzyme, CpLDH to facilitate and attain its energy requirement [3]. The structure of CpLDH possesses a conserved Met163 residue that allows a better packing environment for the acetyl group of APAD+. Lastly, there is a minute rotation of the pyridine ring around the glycoside bond connecting N1 and C1, which moves the methyl group away from the carbonyl oxygen atom of Ile138 and Met163. For the LDH/APAD+/pyruvate structure, this torsion

angle is 132.2°, smaller than the one required for the three complexes that bind NAD+/NAD, which needs a 144.8° to 146.0° angle. Although all these changes are relatively small, together, there are enough to explain the higher activity that CpLDH shows towards APAD+ [61].

The structural elucidation of CpLDH revealed that it holds an antigenic loop at residue amino 210-225 like *Pf*LDH and TgLDH. Three amino acid deposits Il100, Pro101 and Gly102 of CpLDH bulge out, forming the surface of the binding site cavity. CpLDH is not susceptible to inhibition by excess pyruvates up to 20 µM as in its human counterpart because of the smaller conformation loop in the active site [122]. CpLDH has been revealed to be closely related to CpMDH in structure and enzymatic properties. Arginine occupies the residue at 102 of the CpMDH active site, and this single mutation is sufficient to alter and increase the substrate specificity by 3-fold [62]. Thus, any strategy to inhibit the activity of CpLDH may inhibit CpMDH as well due to the overall similarity in the architecture of CpLDH and CpMDH [61].

Ligands such as pyruvate, oxamate and lactate would occupy a similar position in the binding site of CpLDH like PfLDH. The residues crucial for the interaction are Arg171 and His195, and for selectivity is Tsp107 [61, 63]. Selectivity for ligands are more profound despite amino acids sequential similarities in the active site, subtle structural or conformation differences of CpLDH and CpMDH [122]. **Figure 2.9** highlights potent CpLDH compounds.

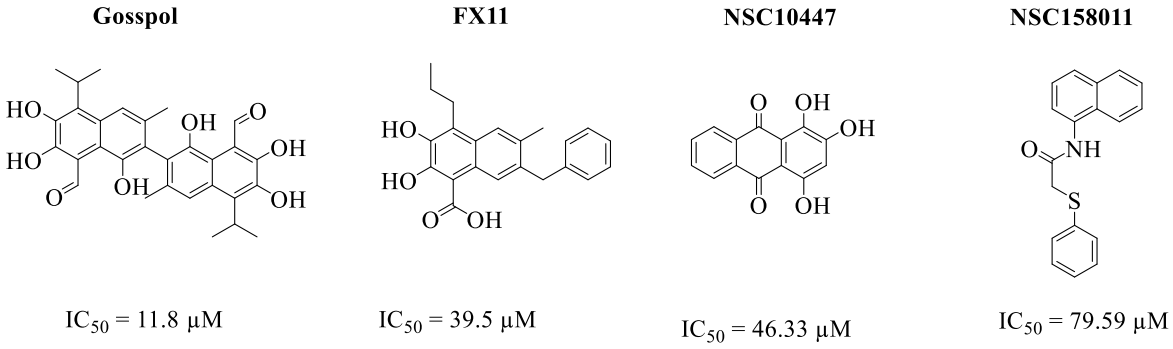

Figure 2.9. Compounds that were potent against CpLDH [113,134].

2.3 Conclusion and future perspectives

In conclusion, glycosidic enzymes, especially LDH and MDH, have proven to be crucial in the energy metabolic pathways of parasites mentioned above and are attractive as potential novel targets. We discovered that most studies have only considered the activity of LDH, however, some

have found that compounds that were active against the LDH would also be active against MDH due to the close resemblance between the two. Moreover, LDH and MDH are examples of recently evolved convergent enzymes that are complementary. Literature audit revealed that moieties like gossypol, oxamate, azole, and quinoline have already been active against the parasites mentioned above, especially plasmodium. In addition, this compiles a thorough understanding of LDH and MDH structures of the parasite is needed to yield hit compounds that would have dual inhibition in search of new drugs. With the current emergence of resistance on the mainstay drugs, these targets would be an excellent starting point for developing LDH and MDH-focused antiparasitic candidates to tackle certain parasitic diseases in future.

Reference

[1] K. E. Galbreath, E. P. Hoberg, J. A. Cook, B. Armién, K. C. Bell, M. L. Campbell, J. L. Dunnum, A. T. Dursahinhan, R. P. Eckerlin, S. L. Gardner, S. E. Greiman, H. Henttonen, F.A. Jiménez, A.V.A. Koehler,B. Nyamsuren, V. V. Tkach, F. Torres-Pérez, A. Tsvetkova, and A. G. Hope "Building an integrated infrastructure for exploring biodiversity: field collections and archives of mammals and parasites," *J Mammal,* vol. 100, no. 2, pp. 382-393, 2019, doi: 10.1093/jmammal/gyz048.

[2] K. Pisarski, "The Global Burden of Disease of Zoonotic Parasitic Diseases: Top 5 Contenders for Priority Consideration," *Trop Med Infect Dis,* vol. 4, no. 1, p. 44, 2019, doi: 10.3390/tropicalmed4010044.

[3] K. Li, S. M. Nader, X. Zhang, B. C Ray, C. Y. Kim, A. Das and W. H Witola "Novel lactate dehydrogenase inhibitors with in vivo efficacy against Cryptosporidium parvum," *PLoS Pathog,* vol. 15, no. 7, pp. e1007953-e1007953, 2019, doi: 10.1371/journal.ppat.1007953.

[4] L. Liu, C. Fei, H. Dong, K. Zhangl. J. Fu, T. Li and F. Xue, "Lactate dehydrogenase: An important molecule involved in acetamizuril action against Eimeria tenella," *J Integ Agric,* vol. 19, no. 5, pp. 1332-1339, 2020, doi: 10.1016/s2095-3119(19)62845-5.

[5] Y. Li, W. Gan, W. Zhan, P. Feng, H. Chen, Y, Zheng and X. Hu "Antibodies against Schistosoma japonicum lactate dehydrogenase B enhance enzyme active," *Mol Biochem Parasitol,* vol. 226, pp. 1-8, Dec 2018, doi: 10.1016/j.molbiopara.2018.08.005.

[6] A. E. Abdelbaset, B. A. Fox, M. H. Karram, M. R. Abd Ellah, D. J. Bzik, and M. Igarashi, "Lactate dehydrogenase in Toxoplasma gondii controls virulence, bradyzoite differentiation, and chronic infection," *PloS one,* vol. 12, no. 3, pp. e0173745-e0173745, 2017, doi: 10.1371/journal.pone.0173745.

[7] M. S. Setzer, K. G. Byler, I. V. Ogungbe, and W. N. Setzer, "Natural Products as New Treatment Options for Trichomoniasis: A Molecular Docking Investigation," *Sci Pharm,* vol. 85, no. 1, p. 5, 2017, doi: 10.3390/scipharm85010005.

[8] F. Jafary, M. R. Ganjalikhany, A. Moradi, M. Hemati, and S. Jafari, "Novel Peptide Inhibitors for Lactate Dehydrogenase A (LDHA): A Survey to Inhibit LDHA Activity via Disruption of Protein-Protein Interaction," *Sci Rep,* vol. 9, no. 1, p. 4686, Mar 18 2019, doi: 10.1038/s41598-019-38854-7.

[9] J. E. Masterson and S. D. Schwartz, "The enzymatic reaction catalyzed by lactate dehydrogenase exhibits one dominant reaction path," *Chem Phys*, vol. 442, no. 17, pp. 132-136, 2014, doi: 10.1016/j.chemphys.2014.02.018.

[10] Y. Feng, Y. Xiong, T. Qiao, X. Li, L. Jia, and Y. Han, "Lactate dehydrogenase A: A key player in carcinogenesis and potential target in cancer therapy," *Cancer Med*, vol. 7, no. 12, pp. 6124-6136, 2018, doi: 10.1002/cam4.1820.

[11] A. Pradhan, A. K. Tripathi, P. V. Desai, P. K. Mukherjee, M. A. Avery, L. A. Walker and B. L. Tekwani, "Structure and function of Plasmodium falciparum malate dehydrogenase: role of critical amino acids in the co-substrate binding pocket," *Biochimie*, vol. 91, no. 11-12, pp. 1509-17, Nov-Dec 2009, doi: 10.1016/j.biochi.2009.09.005.

[12] A. K. Tripathi, P. V. Desai, A. Pradhan, S. I. Khan, M. A. Avery, L. A. Walker and B. L. Tekwani, "An alpha-proteobacterial type malate dehydrogenase may complement LDH function in Plasmodium falciparum. Cloning and biochemical characterization of the enzyme," *Eur J Biochem*, vol. 271, no. 17, pp. 3488-502, Sep 2004, doi: 10.1111/j.1432-1033.2004.04281.x.

[13] B. Zhang, J. Tornmalm, J. Widengren, H. Vakifahmetoglu-Norberg, and E. Norberg, "Characterization of the Role of the Malate Dehydrogenases to Lung Tumor Cell Survival," *J Cancer*, vol. 8, no. 11, pp. 2088-2096, 2017, doi: 10.7150/jca.19373.

[14] M. E. Glasner, D. P. Truong, and B. C. Morse, "How enzyme promiscuity and horizontal gene transfer contribute to metabolic innovation," *FEBS J*, vol. 287, no. 7, pp. 1323-1342, Apr 2020, doi: 10.1111/febs.15185.

[15] G. Wu, A. Fiser, B. ter Kuile, A. Sali and M. Müller, "Convergent evolution of Trichomonas vaginalis lactate dehydrogenase from malate dehydrogenase," *Proc Nat Acad Sci USA*, vol. 96, no. 11, pp. 6285-6290, 1999, doi: 10.1073/pnas.96.11.6285.

[16] T. Takahashi-Íñiguez, N. Aburto-Rodríguez, A. L. Vilchis-González, and M. E. Flores, "Function, kinetic properties, crystallization, and regulation of microbial malate dehydrogenase," *J Zhejiang Uni Sci B*, vol. 17, no. 4, pp. 247-261, 2016, doi: 10.1631/jzus.B1500219.

[17] T. O. Alabduladhem and B. Bordoni, "Physiology, Krebs Cycle," StatPearls Publishing LLC, 2021.

https://pubmed.ncbi.nlm.nih.gov/32310492/#:~:text=The%20cycle%20serves%20as%20a,%2C%20and%20alpha%2Dketoglutarate%20dehydrogenase.

[18] A. Kohlmann, S. G. Zech, F. Li, T. Zhou, R. M. Squillace, L. Commodore, M. T. Greenfield, X. Lu, D. P. Miller, W. Huang, J. Qi, R. M. Thomas, Y. Wang, S. Zhang, R. Dodd, S. Liu, R. Xu, Y. Xu, J. J. Miret, V. Rivera, T. Clackson, W. C. Shakespeare, X. Zhu, and D. C. Dalgarno, "Fragment growing and linking lead to novel nanomolar lactate dehydrogenase inhibitors," *J Med Chem*, vol. 56, no. 3, pp. 1023-40, Feb 14 2013, doi: 10.1021/jm3014844.

[19] R. Conners, F. Schambach, J. Read, A. Cameron, R. B. Sessions, L. Vivas, A. Easton, S. L Croft and R. L. Brady, "Mapping the binding site for gossypol-like inhibitors of Plasmodium falciparum lactate dehydrogenase," *Mol Biochem Parasitol*, vol. 142, no. 2, pp. 137-48, Aug 2005, doi: 10.1016/j.molbiopara.2005.03.015.

[20] S. R. Choi, A. Pradhan, N. L. Hammond, A. G. Chittiboyina, B. L. Tekwani, and M. A. Avery, "Design, Synthesis, and Biological Evaluation of Plasmodium falciparum Lactate Dehydrogenase Inhibitors," *J Med Chem*, vol. 50, no. 16, pp. 3841-3850, 2007, doi: 10.1021/jm070336k.

[21] P. A. Steindel, E. H. Chen, J. D. Wirth, and D. L. Theobald, "Gradual neofunctionalization in the convergent evolution of trichomonad lactate and malate dehydrogenases," *Protein Sci*, vol. 25, no. 7, pp. 1319-1331, 2016, doi: 10.1002/pro.2904.

[22] C. Dando, E. R. Schroeder, L. A. Hunsaker, L. M. Deck, R. E. Royer, X. Zhou, S. F. Parmley and D. L. Vander Jagt, "The kinetic properties and sensitivities to inhibitors of lactate dehydrogenases (LDH1 and LDH2) from Toxoplasma gondii: comparisons with pLDH from Plasmodium falciparum," *Mol Biochem Parasitol*, vol. 118, no. 1, pp. 23-32, 2001, doi: 10.1016/s0166-6851(01)00360-7

[23] G. A. Picanço, N. F. Lima, T. C. Gomes, C. M. Fraga, D. S. M. M. Alves, R. Castillo, T. L. Costa, R. S. Lino-Junior, J. Ambrosio and M. C. Vinaud, "Partial inhibition of the main energetic pathways and its metabolic consequences after in vivo treatment with benzimidazole derivatives in experimental neurocysticercosis," *J Parasitol*, vol. 146, no. 12, pp. 1578-1582, Oct 2019, doi: 10.1017/S0031182019000933.

[24] H. Zhang, F. Guo, and G. Zhu, "Cryptosporidium Lactate Dehydrogenase Is Associated with the Parasitophorous Vacuole Membrane and Is a Potential Target for Developing

Therapeutics," *PLoS Pathog,* vol. 11, no. 11, pp. e1005250-e1005250, 2015, doi: 10.1371/journal.ppat.1005250.

[25] World Health Organization, "Artemisinin resistance and artemisinin-based combination therapy efficacy: status report," *World Health Organization,* 2018. https://www.who.int/docs/default-source/documents/publications/gmp/who-cds-gmp-2019-17-eng.pdf

[26] N. Vale, M. J. Gouveia, G. Rinaldi, P. J. Brindley, F. Gärtner, and J. M. Correia da Costa, "Praziquantel for Schistosomiasis: Single-Drug Metabolism Revisited, Mode of Action, and Resistance," *Antimicrob Agents Chemother,* vol. 61, no. 5, pp. e02582-16, 2017, doi: 10.1128/AAC.02582-16.

[27] M. Montazeri, S. Mehrzadi, M. Sharif, S. Sarvi, A. Tanzifi, S. A. Aghayan and A. Daryani, "Drug Resistance in Toxoplasma gondii," *Front Microbiol,* vol. 9, p. 2587, 2018, doi: 10.3389/fmicb.2018.02587.

[28] World Health Organization, "World malaria report 2020: 20 years of global progress and challenges," ed. Geneva, Switzerland: World Health Organization, 2020. https://apps.who.int/iris/handle/10665/337660.

[29] E. Ashley, A. Pyae Phyo, and C. Woodrow, "Malaria," *Lancet,* vol. 391, pp. 1608-1621, 2018, doi: 10.1016/S0140-6736(18)30324-6.

[30] R. Shivapurkar, T. Hingamire, A. S. Kulkarni, P. R. Rajamohanan, D. S. Reddy, and D. Shanmugam, "Evaluating antimalarial efficacy by tracking glycolysis in Plasmodium falciparum using NMR spectroscopy," *Sci Rep,* vol. 8, no. 1, pp. 18076-18076, 2018, doi: 10.1038/s41598-018-36197-3.

[31] S. Saxena, L. Durgam, and L. Guruprasad, "Multiple e-pharmacophore modelling pooled with high-throughput virtual screening, docking and molecular dynamics simulations to discover potential inhibitors of Plasmodium falciparum lactate dehydrogenase (PfLDH)," *J Biomol Struct Dyn,* vol. 37, no. 7, pp. 1783-1799, Apr 2019, doi: 10.1080/07391102.2018.1471417.

[32] Z. Bozdech, M. Llinas, B. L. Pulliam, E. D. Wong, J. Zhu, and J. L. DeRisi, "The transcriptome of the intraerythrocytic developmental cycle of Plasmodium falciparum," *PLoS Biol,* vol. 1, no. 1, p. E5, Oct 2003, doi: 10.1371/journal.pbio.0000005.

[33] P. Ngotho, A. B. Soares, F. Hentzschel, F. Achcar, L. Bertuccini, and M. Marti, "Revisiting gametocyte biology in malaria parasites," *FEMS Microbiol Rev*, vol. 43, no. 4, pp. 401-414, 2019, doi: 10.1093/femsre/fuz010.

[34] J. D. Wirth, J. I. Boucher, J. R. Jacobowitz, S. Classen, and D. L. Theobald, "Functional and Structural Resilience of the Active Site Loop in the Evolution of Plasmodium Lactate Dehydrogenase," *Biochemistry*, vol. 57, no. 45, pp. 6434-6442, 2018, doi: 10.1021/acs.biochem.8b00913.

[35] J. Penna-Coutinho, W. A. Cortopassi, A. A. Oliveira, T. C. C. França, and A. U. Krettli, "Antimalarial activity of potential inhibitors of Plasmodium falciparum lactate dehydrogenase enzyme selected by docking studies," *PloS One*, vol. 6, no. 7, pp. e21237-e21237, 2011, doi: 10.1371/journal.pone.0021237.

[36] A. Alam, M. K. Neyaz, and S. I. Hasan, "Exploiting unique structural and functional properties of malarial glycolytic enzymes for antimalarial drug development," *Malar Res Treat*, vol. 2014, pp. 451065-451065, 2014, doi: 10.1155/2014/451065.

[37] C. F. Markwalter, K. M. Davis, and D. W. Wright, "Immunomagnetic capture and colourimetric detection of malarial biomarker Plasmodium falciparum lactate dehydrogenase," *Anal Biochem*, vol. 493, pp. 30-34, 2016, doi: 10.1016/j.ab.2015.10.003.

[38] W. A. Cortopassi, A. A. Oliveira, A. P. Guimarães, M. N. Rennó, A. U. Krettli, and T. C. França, "Docking studies on the binding of quinoline derivatives and hematin to Plasmodium falciparum lactate dehydrogenase," *J Biomol Struct Dyn*, vol. 29, no. 1, pp. 207-218, 2011, doi: 10.1080/07391102.2011.10507383.

[39] C. H. King, E. M. Muchiri, and J. H. Ouma, "Evidence against rapid emergence of praziquantel resistance in Schistosoma haematobium, Kenya," *Emerg Infect Dis*, vol. 6, no. 6, p. 585, 2000, doi: 10.3201/eid0606.000606.

[40] H. You, R. J. Stephenson, G. N. Gobert, and D. P. McManus, "Revisiting glucose uptake and metabolism in schistosomes: new molecular insights for improved schistosomiasis therapies," *Front Genet*, vol. 5, pp. 176-176, 2014, doi: 10.3389/fgene.2014.00176.

[41] Â. S. Lopesa, R. N. Nevesa, M. Samara. D. A. Gelson, P. D. Alvesb, A. Maria, C. Lucielli, S. Karine, R. B. Fabiana, K. S. Tiaga and C. S. Borsuka "Quinolines-1, 2, 3-triazolylcarboxamides exhibit antiparasitic activity in Trichomonas vaginalis," *Biotechnol Res Innov*, vol. 3, no. 2, pp. 265-274, 2019, doi: 10.1016/j.biori.2019.06.003.

[42] X. Du, M. K. Jones, S. S. K. Nawaratna, S. Ranasinghe, C. Xiong, P. Cai, D. P. McManus and H. You, "Gene Expression in Developmental Stages of Schistosoma japonicum Provide Further Insight into the Importance of the Schistosome Insulin-Like Peptide," *Int J Mol Sci,* vol. 20, no. 7, p. 1565, 2019, doi: 10.3390/ijms20071565.

[43] R. Guerra-Sa, G. R. Franco, S. D. Pena, and V. Rodrigues, "Lactate dehydrogenase: sequence and analysis of its expression during the life cycle of Schistosoma mansoni," *Mem Inst Oswaldo Cruz,* vol. 93, pp. 205-206, 1998, doi: 10.1590/S0074-02761998000700035.

[44] W. F. Henion, T. E. Mansour, and E. Bueding, "The immunological specificity of lactic dehydrogenase of Schistosoma mansoni," *Exp Parasitol,* vol. 4, no. 1, pp. 40-44, 1955, doi: 10.1016/0014-4894(55)90021-7.

[45] A. M. Alizadeh, S. Jazaeri, B.Shemshadi, F. Hashempour-Baltork, Z. Sarlak, Z. Pilevar and H. Hosseini, "A review on inactivation methods of Toxoplasma gondii in foods," *Pathog Glob Health,* vol. 112, no. 6, pp. 306-319, 2018, doi: 10.1080/20477724.2018.1514137.

[46] A. H. Al-Adhroey, A. A. K. O. Mehrass, A. A. Al-Shammakh, A. D. Ali, M. Y. M. Akabat, and H. M. Al-Mekhlafi, "Prevalence and predictors of Toxoplasma gondii infection in pregnant women from Dhamar, Yemen," *BMC Infect Dis,* vol. 19, no. 1, pp. 1089-1089, 2019, doi: 10.1186/s12879-019-4718-4.

[47] A. M. Alizadeh, S. Jazaeri, B. Shemshadi, F. Hashempour-Baltork, Z. Sarlak, Z. Pilevar and H. Hosseini, "The global serological prevalence of Toxoplasma gondii in felids during the last five decades (1967-2017): a systematic review and meta-analysis," *Parasit Vector,* vol. 13, no. 1, pp. 82-82, 2020, doi: 10.1186/s13071-020-3954-1.

[48] N. Xia, T. Zhou, X. Liang, S. Ye, P. Zhao, J. Yang, Y. Zhou, J. Zhao and B Shen, "A Lactate Fermentation Mutant of Toxoplasma Stimulates Protective Immunity Against Acute and Chronic Toxoplasmosis," *Front Immunol* vol. 9, pp. 1814-1814, 2018, doi: 10.3389/fimmu.2018.01814.

[49] M. Lunghi, R. Galizi, A. Magini, V. B. Carruthers, and M. Di Cristina, "Expression of the glycolytic enzymes enolase and lactate dehydrogenase during the early phase of Toxoplasma differentiation is regulated by an intron retention mechanism," *Mol Microbiol,* vol. 96, no. 6, pp. 1159-1175, 2015, doi: 10.1111/mmi.12999.

[50] I. Coppens, T. Asai, and S. Tomavo, "Biochemistry and metabolism of Toxoplasma gondii: Carbohydrates, lipids and nucleotides," *Elsevier*, 2014, pp. 257-295. doi: 10.1016/B978-0-12-396481-6.00008-8.

[51] K. L. Kavanagh, R. A. Elling, and D. K. Wilson, "Structure of Toxoplasma gondii LDH1: active-site differences from human lactate dehydrogenases and the structural basis for efficient APAD+ use," *Biochemistry*, vol. 43, no. 4, pp. 879-889, 2004, doi: 10.1021/bi035108g.

[52] M. Attias, D. E. Teixeira, M. Benchimol, R. C. Vommaro, P. H. Crepaldi, and W. De Souza, "The life-cycle of Toxoplasma gondii reviewed using animations," *Parasit Vector*, vol. 13, no. 1, pp. 588-588, 2020, doi: 10.1186/s13071-020-04445-z.

[53] F. Al-Anouti, S. Tomavo, S. Parmley, and S. Ananvoranich, "The expression of lactate dehydrogenase is important for the cell cycle of Toxoplasma gondii," *J Biol Chem*, vol. 279, no. 50, pp. 52300-52311, 2004, doi: 10.1074/jbc.M409175200.

[54] V. Jeffers, Z. Tampaki, K. Kim, and W. J. Sullivan, Jr., "A latent ability to persist: differentiation in Toxoplasma gondii," *Cell Mol Life Sci*, vol. 75, no. 13, pp. 2355-2373, 2018, doi: 10.1007/s00018-018-2808-x.

[55] Center of Disease Prevention and Control, "Trichomoniasis - CDC Fact Sheet," ed: Center of Disease Prevention and Control, 2020. https://www.cdc.gov/std/trichomonas/stdfact-trichomoniasis.htm

[56] H. Lin, K. Huang, C. Chung, H. Lin, R. Chen, C. Tsao, W. Chien and T. Chiueh, "Infection with Trichomonas vaginalis increases the risk of psychiatric disorders in women: a nationwide population-based cohort study," *Parasit Vector*, vol. 12, no. 1, pp. 88-88, 2019, doi: 10.1186/s13071-019-3350-x.

[57] M. Bradic and J. M. Carlton, "Does the common sexually transmitted parasite Trichomonas vaginalis have sex?," *PLoS Pathog*, vol. 14, no. 3, pp. e1006831-e1006831, 2018, doi: 10.1371/journal.ppat.1006831.

[58] D. Beri, P. Yadav, H. R. N. Devi, C. Narayana, D. Gadara, and U. Tatu, "Demonstration and Characterization of Cyst-Like Structures in the Life Cycle of Trichomonas vaginalis," *Front Cell Infect Microbiol*, vol. 9, pp. 430-430, 2020, doi: 10.3389/fcimb.2019.00430.

[59] I. Hrdý, R. Cammack, P. Stopka, J. Kulda, and J. Tachezy, "Alternative pathway of metronidazole activation in Trichomonas vaginalis hydrogenosomes," *Antimicrob Agents Chemother*, vol. 49, no. 12, pp. 5033-5036, 2005, doi: 10.1128/AAC.49.12.5033.

[60] D. Leitsch, "Recent Advances in the Trichomonas vaginalis Field," *F1000Res*, vol. 5, pp. F1000 Faculty Rev-162, 2016, doi: 10.12688/f1000research.7594.1.

[61] W. J. Cook, O. Senkovich, A. Hernandez, H. Speed, and D. Chattopadhyay, "Biochemical and structural characterization of Cryptosporidium parvum Lactate dehydrogenase," *Int J Biol Macromol*, vol. 74, pp. 608-619, 2015, doi: 10.1016/j.ijbiomac.2014.12.019.

[62] D. Madern, X. Cai, M. S. Abrahamsen, and G. Zhu, "Evolution of Cryptosporidium parvum lactate dehydrogenase from malate dehydrogenase by a very recent event of gene duplication," *Mol Biol Evol*, vol. 21, no. 3, pp. 489-497, 2004, doi: 10.1093/molbev/msh042.

[63] M. J. Varga, M. W. Dzierlenga, and S. D. Schwartz, "Structurally linked dynamics in lactate dehydrogenases of evolutionarily distinct species," *Biochemistry*, vol. 56, no. 19, pp. 2488-2496, 2017, doi: 10.1021/acs.biochem.7b00245.

CHAPTER 3

Design and synthesis of quinoline-pyrimidine inspired hybrids as potential plasmodial inhibitors

Graphical Abstract

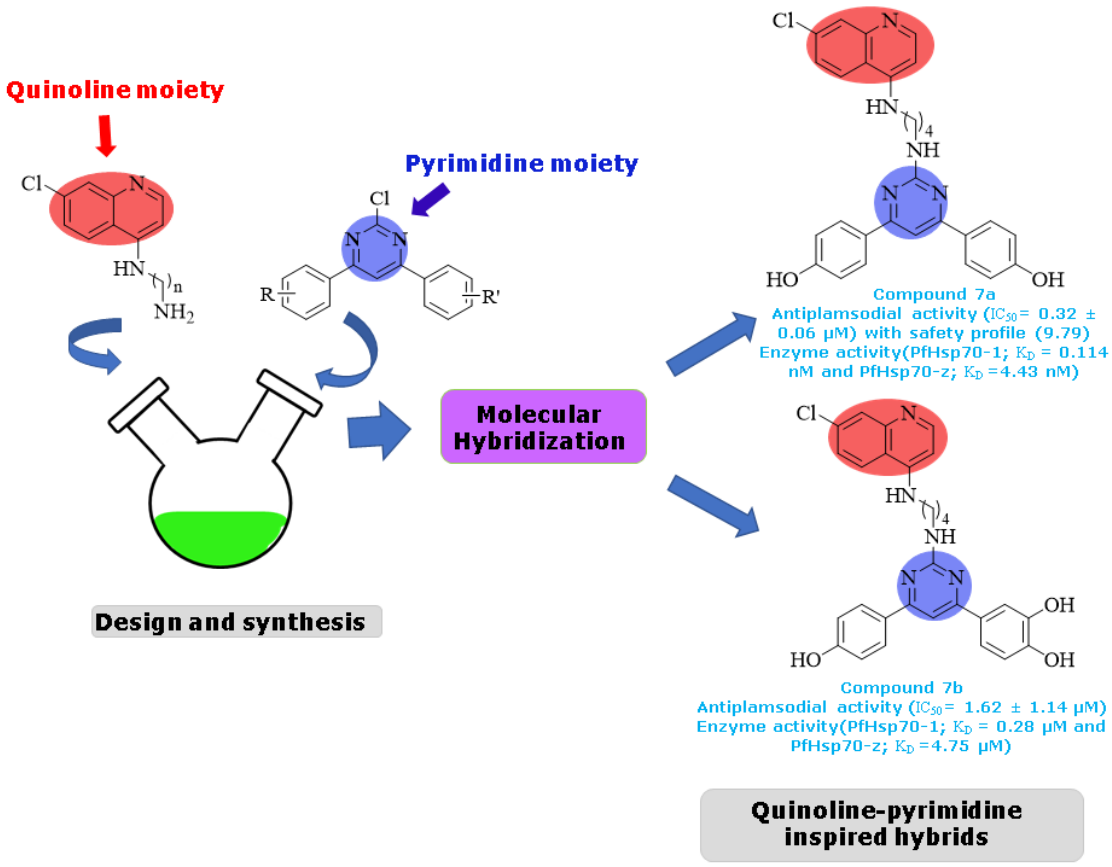

European Journal of Medicinal Chemistry 217 (2021) 113330

Contents lists available at ScienceDirect

European Journal of Medicinal Chemistry

journal homepage: http://www.elsevier.com/locate/ejmech

Design and synthesis of quinoline-pyrimidine inspired hybrids as potential plasmodial inhibitors

Francis Kayamba [a], Teboho Malimabe [b, c], Idowu Kehinde Ademola [d], Ofentse Jacob Pooe [e], Narva Deshwar Kushwaha [a], Mavela Mahlalela [a], Robyn L. van Zyl [b, c], Michelle Gordon [d], Pertunia T. Mudau [f], Tawanda Zininga [f, g], Addmore Shonhai [g], Vincent O. Nyamori [h], Rajshekhar Karpoormath [a, *]

[a] Department of Pharmaceutical Chemistry, College of Health Sciences, University of KwaZulu-Natal, Durban, 4000, South Africa
[b] Pharmacology Division, Department of Pharmacy and Pharmacology, Faculty of Health Sciences, University of Witwatersrand, Johannesburg, 2193, South Africa
[c] WITS Research Institute for Malaria (WRIM), Faculty of Health Sciences, University of Witwatersrand, Johannesburg, 2193, South Africa
[d] School of Laboratory Medicine and Medical Sciences, College of Health Science, University of KwaZulu-Natal, Durban, 4000, South Africa
[e] Discipline of Biochemistry, School of Life Sciences, University of KwaZulu-Natal, Durban, 4000, South Africa
[f] Department of Biochemistry University of Venda, School of Mathematical and Natural Sciences, Thohoyandou, 0950, South Africa
[g] Department of Biochemistry, Stellenbosch University, Stellenbosch, 7600, South Africa
[h] School of Chemistry and Physics, University of KwaZulu-Natal, Westville Campus, Durban, 4000, South Africa

ARTICLE INFO

Article history:
Received 29 October 2020
Received in revised form
18 February 2021
Accepted 24 February 2021
Available online 3 March 2021

Keywords:
Molecular hybrids
Quinoline
Pyrimidine
Antimalarial agents
Malaria
Antiprotozoal
Piperazine
PfHsp70

ABSTRACT

Presently, artemisinin-based combination therapy (ACT) is the first-line therapy of *Plasmodium falciparum* malaria. With the emergence of malaria parasites that are resistant to ACT, alternative antimalarial therapies are urgently needed. In line with this, we designed and synthesised a series of novel *N*-(7-chloroquinolin-4-yl)-*N'*-(4,6-diphenylpyrimidin-2-yl)alkanediamine hybrids (**6a-7c**) and evaluated their inhibitory activity against the NF54 chloroquine-susceptible strain as a promising class of antimalarial compounds. The antiplasmodial screening revealed that seven analogues showed promising to good activity with half-maximal inhibitory concentration (IC_{50}) = 0.32 μM–4.30 μM. Compound **7a** with 1,4-diamine butyl linker and 4-hydroxyl phenyl on fourth and sixth position of pyrimidine core showed the most prominent activity with an IC_{50} value of 0.32 ± 0.06 μM, with a favourable safety profile of 9.79 to human kidney epithelial (HEK293) cells. The remaining six analogues showed moderate activity with IC_{50} values ranging from 7.50 μM to 83.01 μM. We further investigated the binding affinities of the molecules to two essential cytosolic *P. falciparum* heat shock protein 70 homologues; PfHsp70-1 and PfHsp70-z. Compound **7a** exhibited the highest binding affinity for both PfHsp70s with K_D in a lower nanomolar range (4.4–11.4 nM). Furthermore, molecular docking revealed that compounds **6**, **6k**, **7b** and **7a** exhibited better fitness in PfHsp70-1 with compound **7a** showing the highest and lowest binding scores of −9.8 kcal/mol. Therefore, we speculate that PfHsp70-1 is one of the targets of these inhibitors. The bioisoteric replacement of the groups at phenyl ring at the fourth and sixth position of the pyrimidine core had a constructive association with antiplasmodial activity. The promising antiplasmodial activity of the synthesised analogues illustrates how crucial molecular hybridisation is as a strategy in the development of quinoline-pyrimidine hybrids as prospective antiprotozoal agents.

1. Introduction

The evolution of *Plasmodium* strains has caused uncertainty in the treatment of malaria, and thousands of people are still dying as a result of the advent of resistance on current treatment such as artemisinin combination therapies (ACTs) and chloroquine (CQ) [1]. Malaria is predominately spread by *P. falciparum* which is more prevalent in Africa. An estimate of 228 million people were infected with malaria in 2018, killing approximately 405 000 people, of which over 90% were in Sub-Saharan Africa. Children under the age

* Corresponding author.
E-mail address: karpoormath@ukzn.ac.za (R. Karpoormath).

https://doi.org/10.1016/j.ejmech.2021.113330
0223-5234/

Abstract

Presently, artemisinin-based combination therapy (ACT) is the first-line therapy of *Plasmodium falciparum* malaria. With the emergence of malaria parasites that are resistant to ACT, alternative antimalarial therapies are urgently needed. In line with this, we designed and synthesised a series of novel *N*-(7-chloroquinolin-4-yl)-*N*'-(4,6-diphenylpyrimidin-2-yl)alkanediamine hybrids (**6a-k and 7a-c**) and evaluated their inhibitory activity against the NF54 chloroquine-susceptible strain as a promising class of antimalarial compounds. The antiplasmodial screening revealed that seven analogues showed promising good activity with half-maximal inhibitory concentration (IC_{50}) = 0.32 to 4.30 µM. Compound **7a** with 1,4-diamine butyl linker and 4-hydroxyl phenyl on fourth and sixth position of pyrimidine core showed the most prominent activity with an IC_{50} value of 0.32 ± 0.06 µM, with a favourable safety profile of 9.79 to human kidney epithelial (HEK293) cells. The remaining six analogues showed moderate activity with IC_{50} values ranging from 7.50 to 83.01 µM. We further investigated the binding affinities of the molecules to two essential cytosolic *P. falciparum* heat shock protein 70 homologues; PfHsp70-1 and PfHsp70-z. Compound **7a** exhibited the highest binding affinity for both PfHsp70s with K_D in a lower nanomolar range (4.4-11.4 nM). Furthermore, molecular docking revealed that compounds **6**, **6k**, **7b** and **7a** exhibited better fitness in PfHsp70-1, with compound **7a** showing the highest and lowest binding scores of -9.8 kcal/mol. Therefore, we speculate that PfHsp70-1 is one of the targets of these inhibitors. The bioisosteric replacement of the groups at phenyl ring at the fourth and sixth position of the pyrimidine core had a constructive association with antiplasmodial activity. The promising antiplasmodial activity of the synthesised analogues illustrates how crucial molecular hybridisation is as a strategy in the development of quinoline-pyrimidine hybrids as prospective antiprotozoal agents.

Keywords: molecular hybrids, quinoline, pyrimidine, antimalarial agents, malaria, antiprotozoal, piperazine, PfHsp70

3.1 Introduction

The evolution of *Plasmodium* strains has caused uncertainty in the treatment of malaria, and thousands of people are still dying as a result of the advent of resistance on current treatment such as artemisinin combination therapies (ACTs) and chloroquine (CQ) [1]. Malaria is predominately spread by *P. falciparum* which is more prevalent in Africa. An estimate of 228 million people were infected with malaria in 2018, killing approximately 405 000 people, of which over 90% were in Sub-Saharan Africa. Children under the age of five and pregnant women are the major victims of the scourge, especially those in poor tropical regions. About 3.2 billion people remain at risk of the epidemic [2, 3]. Thus, necessitating the need for alternative therapy in the absence of an efficient antimalarial vaccine [4].

An audit of antimalarial pharmacophores revealed that, in addition to other vast medicinal properties, the pyrimidine moiety displayed admirable antimalarial properties. It has proven to be key in some drugs and lead antimalarial candidates at an advanced stage of clinical trials. Amongst the leading antimalarial pharmacophores are proguanil, pyrimethamine, P218 and WR9920. Most antimalarial pyrimidine-based drugs hold prospects as prophylactic agents. These compounds target *P. falciparum* dihydrofolate reductase, which is implicated in the folic acid pathway that is essential for DNA biosynthesis [5]. Chalcones are another class of analogues well-known for excellent antimalarial therapy; where for example, licochalcone, a natural flavonoid product was active against CQ-susceptible (3D7) and CQ-resistance (Dd2) strains [6, 7]. The phenyl groups of chalcone were important for antiplasmodial activity as indicated by SAR studies, and as such, we tried to integrate these pharmacophores into the modified potent molecule [8]. Given this context, we expected that a promising antiplasmodial agent would be the combination of active pharmacophores inspired by pyrimethamine and chalcone to produce a 4,6-diphenylpyrimidine. **Figure 3.1** shows CQ and other potential antimalarial compounds that were crucial in designing this novel series.

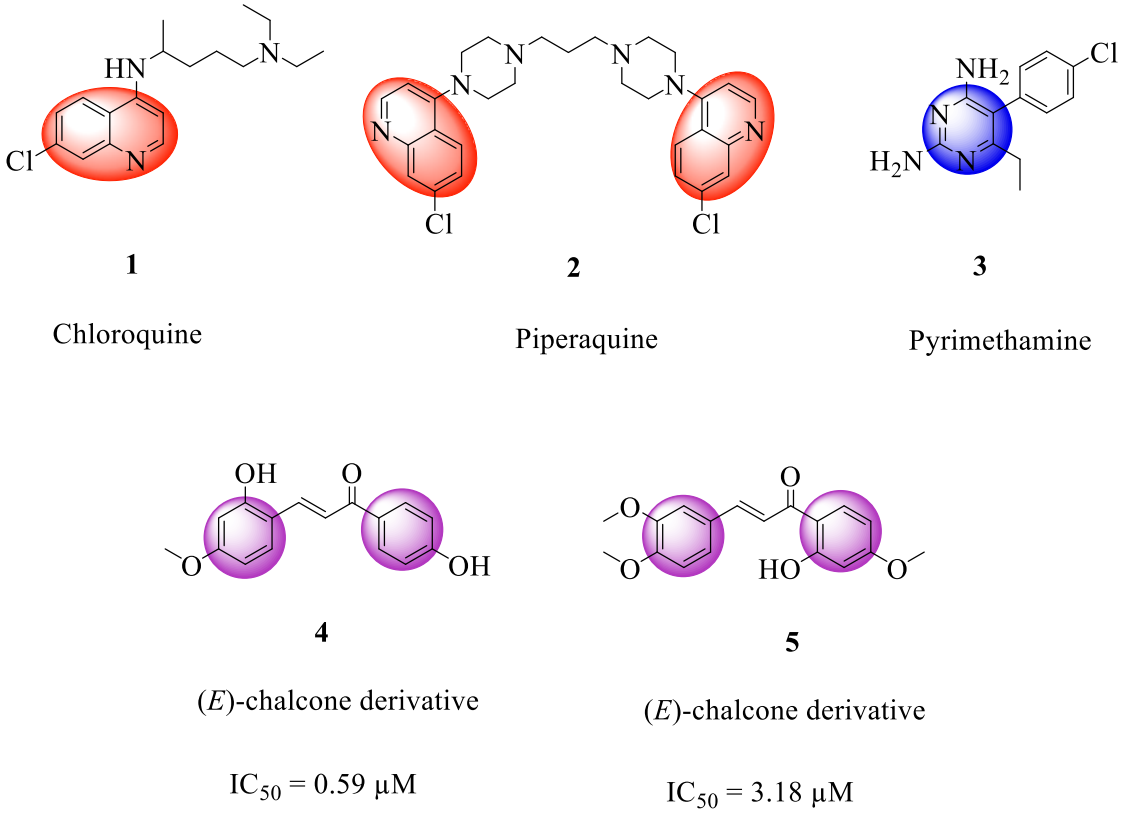

Figure 3.1. Marketed drugs and chalcone based potential antimalarial compounds.

While antimalarial drugs, such as piperaquine and CQ, based on a quinoline backbone, are inexpensive with a robust therapeutic index, they have lost efficacy as stand-alone drugs due to the emergence of resistance [9, 10] mediated by a mutated form of the *Plasmodium falciparum* chloroquine resistance "transporter" [11, 12]. Although prospects for CQ reapplication as an antimalarial remain [13], its role as an agent against avian influenza H5N1 and ZIKV viral infections is gaining more attention [14-16]. SAR studies of CQ revealed that the basic chain is crucial for antimalarial activity by improving the drug's lipophilic, allowing easy passage through the malarial plasma membrane [17]. In light of this, incorporating various linkers such as piperazine and different alkyl diamine holds promise towards making effective antimalarial agents. In view of the aforementioned, we synthesised a hybrid molecule, as illustrated in **Figure 3.2**, by a molecular hybridisation approach using two robust moieties, viz pyrimidine and quinoline, to present a safer and alternative therapy for malaria. We anticipated presenting an antimalarial candidate effective against both the liver and blood-stages of *Plasmodium*; for potential use for both treatment and prophylaxis.

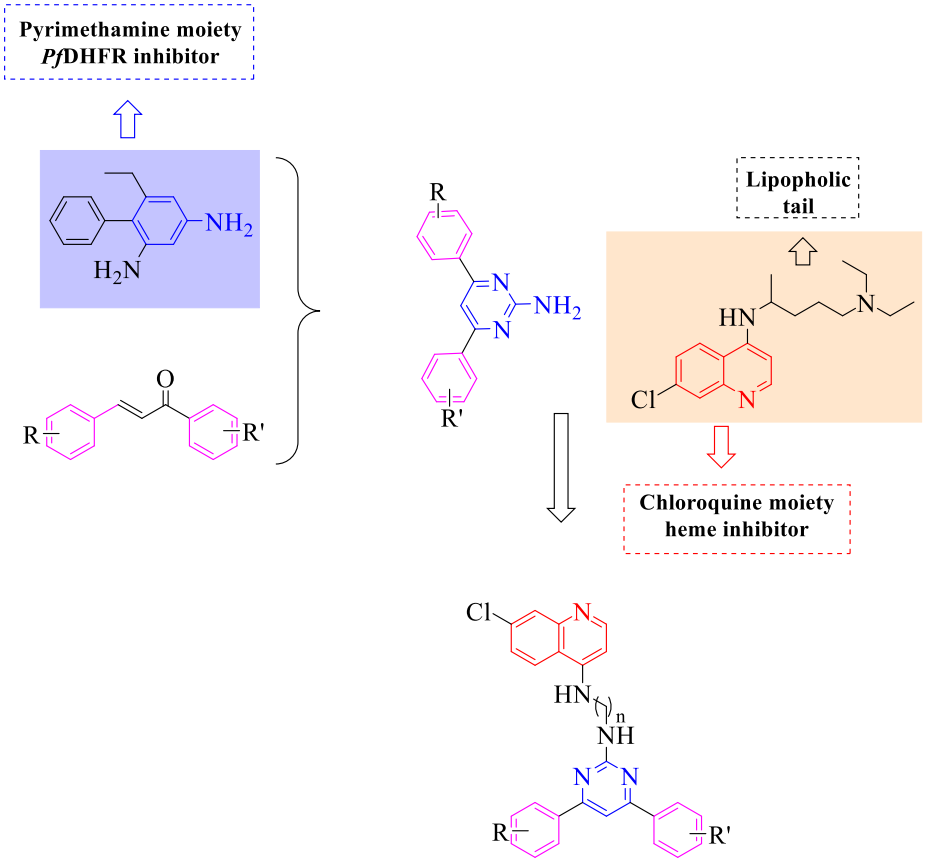

Figure 3.2. Rational design of pyrimidine-quinoline hybrid molecules.

3.2 Chemistry

The novel library of quinoline-pyrimidine hybrids **6(a-k**) was synthesised using a versatile synthetic pathway. The intermediate *(E)*-chalcones **1(a-f)** were prepared by aldol condensation reaction as previously reported, using assorted commercially available benzaldehydes and acetophenones using sodium hydroxide basic condition in a good yield of 95% [18]. The cyclisation of chalcone using guanidine hydrochloride and sodium hydroxide base afforded numerous 4,6-diphenylpyrimidin-2-amine **2(a-e)** analogues according to scheme 1. The known **Sandmeyer reaction** applies to substituting an aromatic amine of compound **2** to hydroxyl (4,6-diphenylpyrimidin-2-ol **3(a-e)** via diazonium salt intermediate formation. Sodium nitrate in acetic acid initiates the diazonium salt formation and then substitution of diazo salt with water. 2-Chloro-4,6-diphenylpyrimidine analogues **4(a-f)** were synthesised from assorted **3** analogues using $POCl_3$ with catalytic DMF as illustrated in **Scheme 1**.

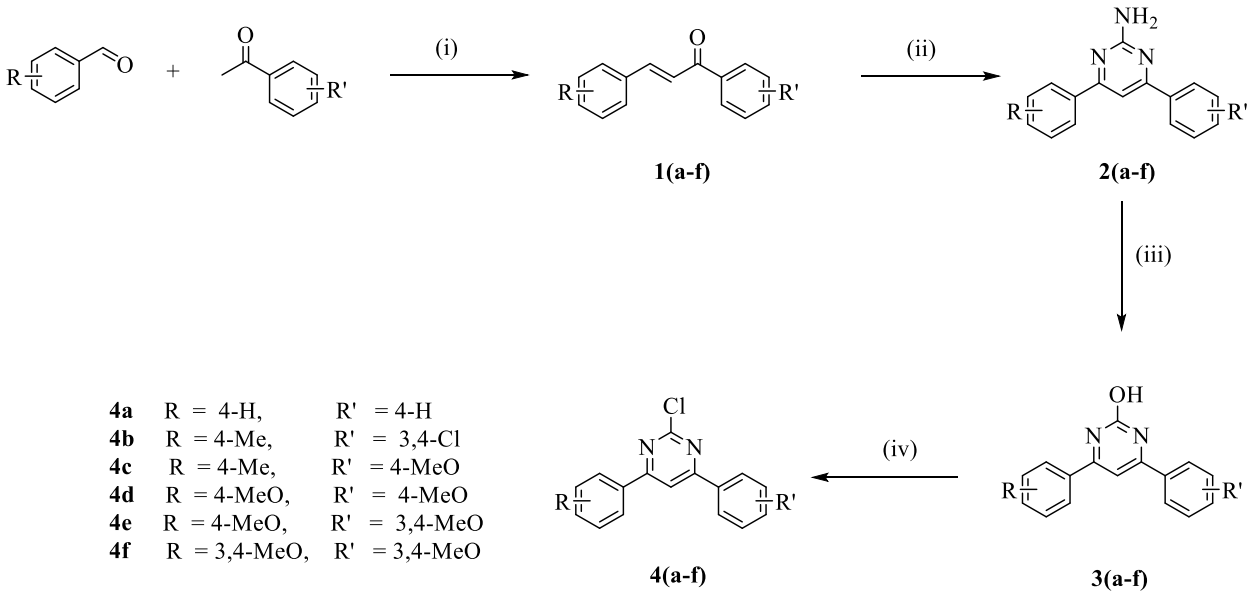

Scheme 1. Reaction conditions: (i) EtOH, NaOH, sonicate, 35°C, 1 hour; (ii) Guanidine hydrochloride, NaOH, EtOH, reflux, 24 hours; (iii) Acetic acid, $NaNO_2$, H_2O, rt, 3 hours; (iv) $POCl_3$, DMF, 100°C, reflux, 6 hours.

The synthesis and characterisation of a series of quinoline-diamine compounds **5(a-e)** were as per reported methods [8]. Various **5(a-e)** compounds were further coupled with various **4(a-e)** compounds using K_2CO_3 to afford a library of the targeted pyrimidine-quinoline hybrids analogues (**6a-7c)**. The methoxy substituents on the phenyl group of final compounds **6g**, **6i** and **6j** were further demethylated using HBr acid in a microwave to afford compounds **7a, 7b and 7c,** respectively, in good yield as depicted in **Scheme 2**.

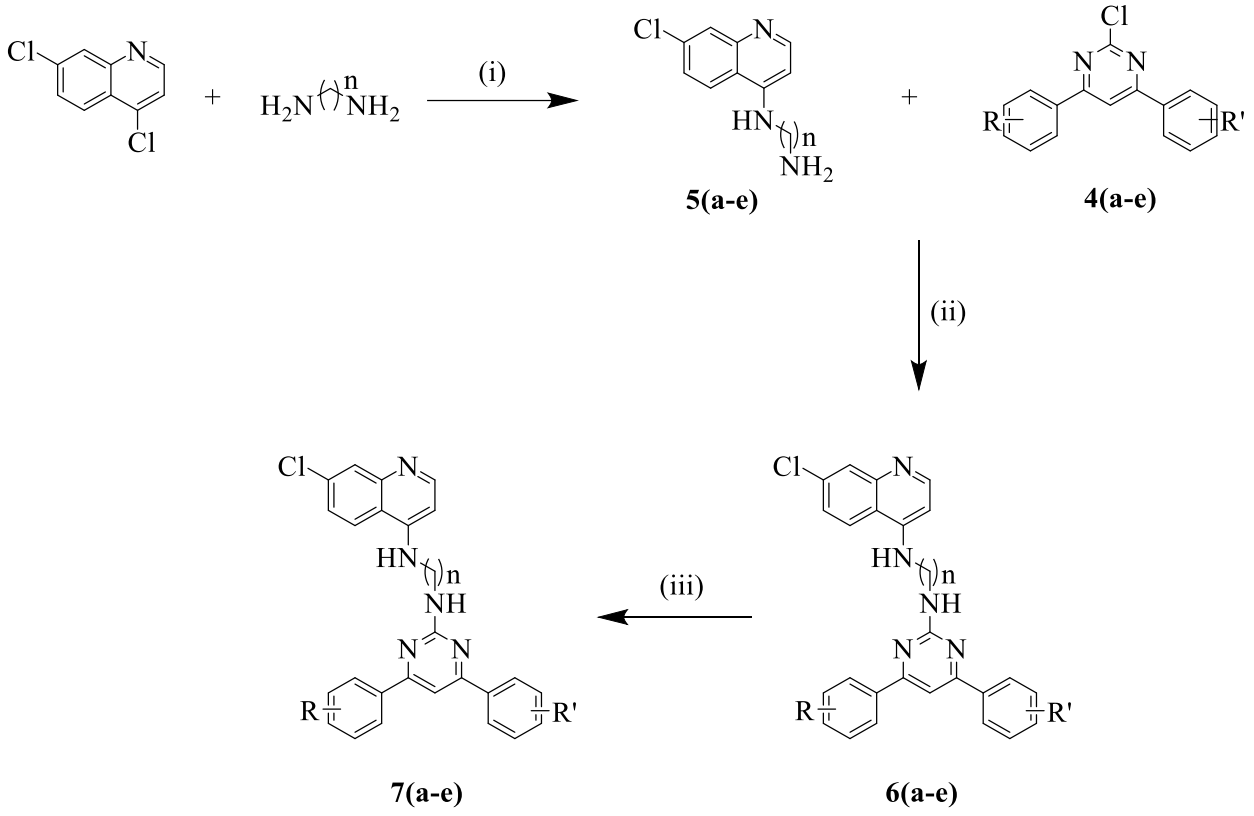

Scheme 2; Reaction conditions: (i) Isopropanol (IPA), reflux, 100°C, 16 hours; (ii) K_2CO_3, Dimethylformamide (DMF), Microwave (MW), 120°C, 40 mins; (iii) HBr, MW, 100°C, 20 mins.

3.3 Results and discussion

3.3.1 Synthesis and spectral studies

Structural analysis based on proton nuclear magnetic resource (^{1}H NMR) spectrum of compound **1b** revealed two characteristic doublets resonating at chemical shifts (δ) 7.80-7.77 ppm (Ph-CH=CH) and 7.52-7.49 ppm (Ph-CH=CH) with J = 15.62 Hz and 15.61 Hz, respectively, signifying the formation of a *trans*-olefinic conformation. Other resonating signals were observed on the spectrum at δ 3.89 and 2.39 ppm representing methoxy and methyl substituents on the phenyl groups of the (*E*)-chalcone. The two doublet signals of the olefin disappear on the ^{1}H NMR spectrum of compound **2b**, and two distinctive singlets at signal δ 7.35 ppm (pyr-H) in the aromatic region and the amino signal at δ 5.22 ppm (pyr-NH_2) appeared indicating the formation of a pyrimidine core. The structure of the 2-hydroxyl pyrimidine analogue is signified by the vanishing of the amino signal and presence of hydroxyl (OH) signal downfield at δ 11.89 ppm on the H^1 NMR spectrum of compound **3**. The spectrum of the chlorinated compound **4** is characterised by the disappearance of OH signal and minor shifts on pyr-H from δ 7.35 ppm to 7.60 ppm. The ^{1}H

NMR spectrum (400 and 600 MHz, DMSO-d_6) of the targeted compound(s), as presented by compound **7d,** is characterised by the presence of two individual peaks; broad singlet resonating at δ 5.04 ppm (-NH) and triplet at 5.55 ppm (-NH) of an aliphatic alkane diamine linker signified coupling of quinoline and pyrimidine motifs. Other distinctive peaks, as aforementioned, included δ 2.46 ppm, 3.52 ppm, 4.06 ppm and 4.07 ppm representing methyl, methylene, methoxy and methylene, respectively. The outstanding signals from 6.47-8.44 ppm represent the aromatic protons for phenyl and piperazine moieties. The spectral properties of the final compound **7g** were confirmed by 2D NMR and further supported by their respective ^{13}C NMR. The most prominent peak for ^{13}C NMR of the final compound for pyr-H (C9) and methylene for diamine butane line resonate at signal δ ranging from 100.53-99.89 pm and 27.42-42.99 ppm, respectively. The methoxy (MeO) peak signal resonates at 55.40 ppm, and the remaining carbon signals correspond to the aromatic carbons. **Figure 3.3** represents the structures of the final compounds annotated as compounds **6 (a-k)** and **7 (a-c**).

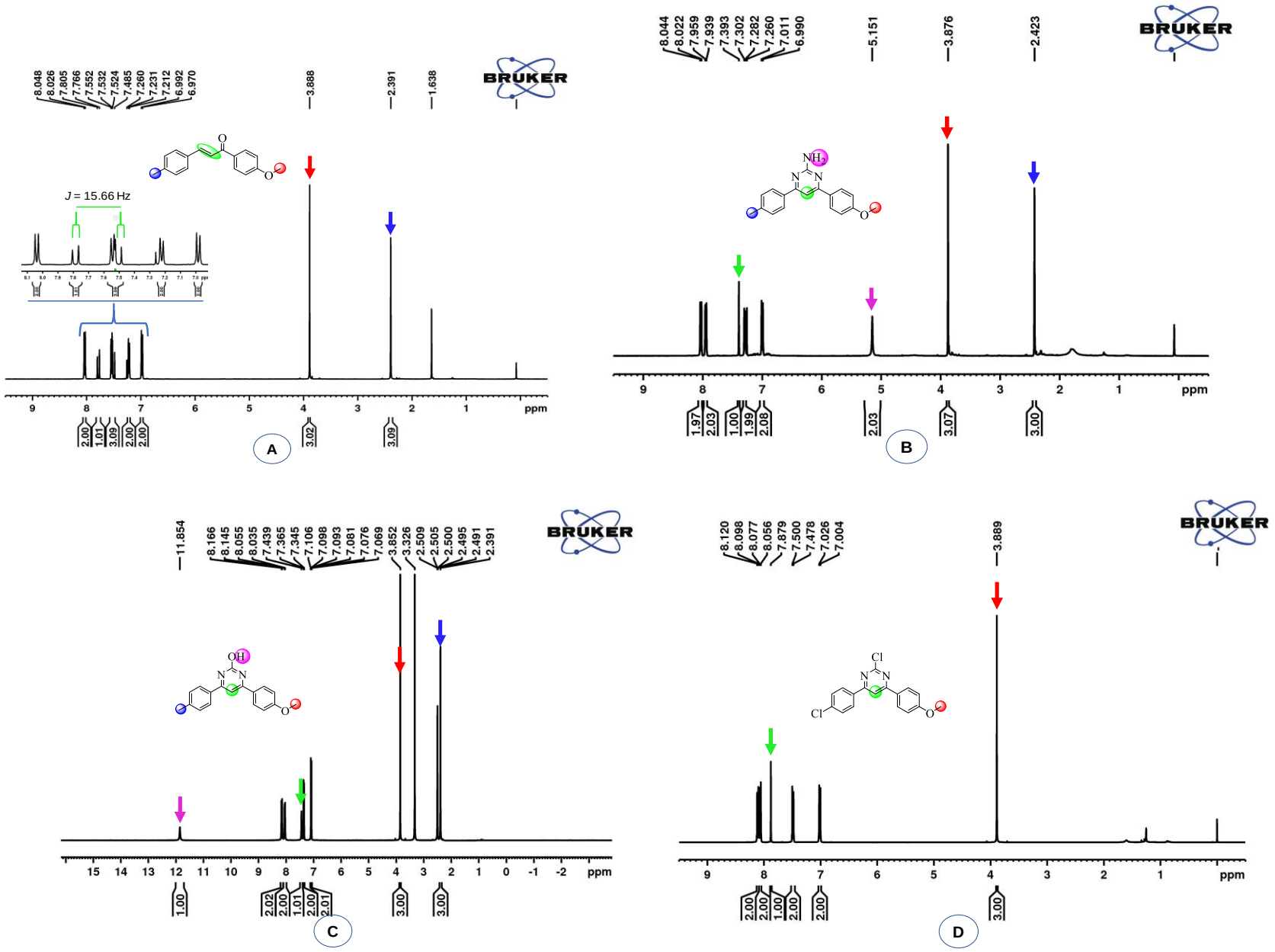
BRUKER
8.048
8.026
7.805
7.766
7.552
7.532
7.524
7.485
7.260
7.231
7.212
6.992
6.970
3.888
2.391
1.638
J = 15.66 Hz
ppm
2.00
1.01
3.09
2.00
2.00
3.02
3.09
A
8.044
8.022
7.959
7.939
7.393
7.302
7.282
7.260
7.011
6.990
5.151
3.876
2.423
NH2
ppm
1.97
2.03
1.00
1.99
2.08
2.03
3.07
3.00
B
11.854
8.166
8.145
8.055
8.035
7.439
7.365
7.345
7.106
7.098
7.093
7.081
7.076
7.069
3.852
3.326
2.509
2.505
2.500
2.495
2.491
2.391
OH
ppm
1.00
2.02
2.00
1.01
2.00
2.01
3.00
3.00
C
8.120
8.098
8.077
8.056
7.879
7.500
7.478
7.026
7.004
3.889
Cl
Cl
ppm
2.00
2.00
1.00
2.00
2.00
3.00
D

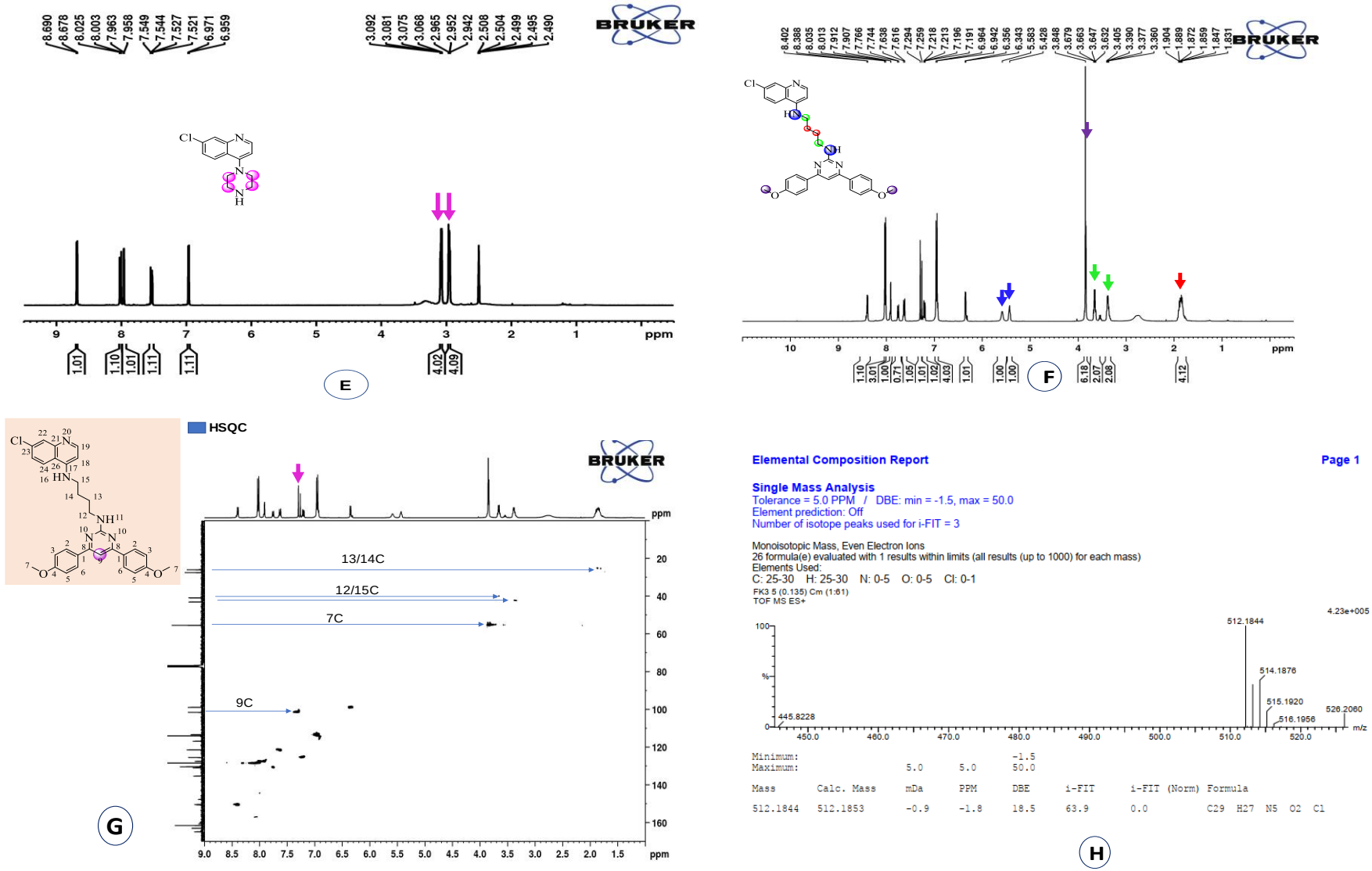

Figure 3.3. ^{1}H-NMR for intermediates derivative: chalcone (A), 4,6-diphenylpyriidin-2-amine (B), 4,6-diphenylpyrimidin-2-ol (C), 2-chloro-4,6-diphenylpyrimidine (D), 4,6-diphenyl-2-(piperazin-1-yl)pyrimidine (E). The ^{1}H NMR and HSQC of the final compounds; N^{1}-(4,6-bis(4-methoxyphenyl)pyrimidin-2-yl)-N^{4}-(7-chloroquinolin-4-yl)butane-1,4-diamine (**7g**) (F and G). HRMS of compound **8b**.

3.3.2 Antiplasmodial activity

The synthesised novel analogues of (**6a-k and 7a-c**) were assessed for potency against the NF54 CQ-susceptible strain of *P. falciparum* maintained *in vitro* at the blood stage. Table 1 presents the antiplasmodial activity of the hybrid analogues (**6a-k and 7a-c**) and standard reference drugs (CQ and quinine). Compound **7a** showed promising activity with IC_{50} values less than 0.5 µM, while the remaining analogues displayed moderate activity in micromolar levels against the CQ-susceptible strain (NF54). The IC_{50} values of the compounds were determined from log sigmoid dose-response curves using GraphPad Prism® 5.0.0 (GraphPad Software, Inc San Diego, CA). Given the antiplasmodial activity, we assessed a reasonable number of analogues to establish a brief structure-activity relationship (SAR) towards identifying the groups accounting for the activity. The bioisosteric replacement on the phenyl rings on the fourth and sixth position of pyrimidine core, and linker coupling the pyrimidine and quinoline positively correlated with the antiprotozoal activity, as shown in **Table 1**.

Table 1. *In vitro* antiplasmodial activity of compounds (**6a-6k**) and (**7a-7c**).

Compound No	n	R	R'	Antimalarial		Cytotoxicity		Selective Index
				IC_{50} (µM)	SD	IC_{50} (µM)	SD	
6a	p	4-H	4-H	7.50	1.49	nd	nd	nd
6b	4	4-Me	4-Cl	9.49	1.12	nd	nd	nd
6c	p	4-Me	4-Cl	13.12	1.28	nd	nd	nd
6d	2	4-Me	4-MeO	4.30	1.01	nd	nd	nd
6e	3	4-Me	4-MeO	2.71	1.22	nd	nd	nd
6f	p	4-Me	4-MeO	2.63	1.28	nd	nd	nd
6g	4	4-MeO	4-MeO	83.01	1.46	nd	nd	nd
6h	p	4-MeO	4-MeO	7.69	1.42	nd	nd	nd
6i	4	3,4-MeO	4-MeO	2.61	1.00	nd	nd	nd
6j	p	3,4-MeO	4-MeO	17.81	1.18	nd	nd	nd
6k	p	3,4-MeO	3,4-MeO	6.17	1.22	nd	nd	nd
7a	4	4-OH	4-OH	0.32	0.06	3.16	0.75	9.79
7b	4	3,4-OH	4-OH	1.62	1.14	nd	nd	nd
7c	p	3,4-OH	4-OH	2.66	1.04	nd	nd	nd

Quinine	0.108	0.003	134.35	1.45	1243.98
Chloroquine	0.012	0.002	101.19	25.72	8432.50
Camptothecin	nd	nd	nd	0.20	0.01

IC_{50}: Concentration at 50% inhibition of the parasite's growth
Selective Index: IC_{50} values of cytotoxic activity/IC_{50} values of antimalarial activity
nd: not determined
p: Piperazine
SD: Standard Derivative

From the screened compounds, only compounds **7a** showed substantial plasmodial inhibitory activity with IC_{50} = 0.32 ± 0.06 µM, while the other six promising hybrids, namely compounds **6d**, **6e**, **6f**, **6i**, **7b** and **7c** portrayed moderate activity with IC_{50} ranging from 0.50 to 4.30 µM (**Table 1**). The remaining compounds (**6a**, **6b**, **6c**, **6g**, **6h**, **6j** and **6k)** displaying IC_{50} values > 5 µM were considered inactive. Compound **6i** had a moderate activity with an IC_{50} value of 2.61 ± 1.00 µM, and compounds **6g** and **6j** appraised inactive with IC_{50} values of 83.01 ± 1.46 µM and 17.81 ± 1.18 µM, respectively. However, demethylation of the methoxy groups from these compounds resulted in improved aqua solubility that consequently increased the antiplasmodial activity of **7a**, **7b** and **7c** with IC_{50} values of 0.32 ± 0.06 µM, 1.62 ± 1.14 µM and 2.66 ± 1.04 µM, respectively of which compound **7a** had the most prominent activity.

Diamino alkane linker based derivatives

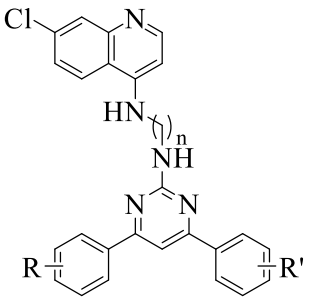

6b n = 4, R = 4-Me, R' = 4-Cl
6d n = 2, R = 4-Me, R' = 4-MeO
6e n = 3, R = 4-Me, R' = 4-MeO
6g n = 4, R = 4-MeO, R' = 4-MeO
6i n = 4, R = 4-MeO, R' = 3,4-MeO
7a n = 4, R = 4-OH, R' = 4-OH
7b n = 4, R = 4-OH, R' = 3,4-OH

Piperazine linker based derivatives

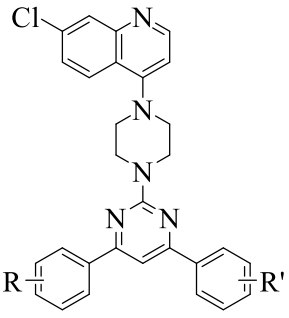

6a R = 4-H, R' = 4-H
6c R = 4-Me, R' = 4-Cl
6f R = 4-Me, R' = 4-MeO
6h R = 4-MeO, R' = 4-MeO
6j R = 4-MeO, R' = 3,4-MeO
6k R = 3,4-MeO, R' = 3,4-MeO
7c R = 4-OH, R' = 3,4-OH

Figure 3.4. Structures of the final compounds **6 (a-k)** and **7 (a-c).**

As observed, compounds **6a, 6c**, **6h** and **6k** owning a piperazine linker were considered inactive with IC_{50} values > 5 µM. However, compounds **6g** and **7c** with piperazine linker revealed moderate activity with IC_{50} values of 2.63 ± 1.28 µM and 2.66 ± 1.04 µM, respectively. It can be suggested that the piperazine linker could have been significant, and the difference in activity could allude to bioisosteric replacements at phenyl groups of the 4,6-diphenylpyrimidine core. Of the piperazine linker-based compounds, **6j** had the least activity with an IC_{50} value of 17.81 ± 1.18 µM, but its demethylation boosted the activity by almost seven-fold as illustrated by compound **7c** with IC_{50} of 2.66 ± 1.04 µM. In addition, substituting chloro with a methoxy group of the 4-(4-chlorophenyl)-6-(p-tolyl)pyrimidine core of compound **6c** yielded improved activity four-fold as illustrated by compound **6f**. Insignificant variation in activity is observed as more methoxy groups are added as shown by compound **6h** and **6k** with IC_{50} values of 7.69 ± 1.42 µM and 6.17 ± 1.22 µM individually. Compounds **6d** and **6e** respectively bearing 1,3-diamino propane and 1,2-diamino ethane, and both containing a 4-(4-methoxyphenyl)-6-(p-tolyl)pyrimidine motif only displayed moderate activity with IC_{50} values of 4.30 ± 1.01 µM and 2.71± 1.22 µM. Compounds **6b**, **6g**, **6i**, **7a** and **7b** having a 1,4-diamino butane linker presented a broader variation in the activity. Note that compound **6g** bearing two methoxy substituents on fourth positions of the phenyl groups of the 4,6-diphenylpyrimidine core had the least activity (Table 1). Adding an extra methoxy group to the third position increased the activity by nine-fold as defined by compound **6i** (IC_{50} = 2.61 ± 1.00 µM). Compound **6b** housing methyl and chloro substituents on 4-(4-chlorophenyl)-6-(p-tolyl)pyrimidine core was nine times more active than compound **6g**, though four times less active than **6i** despite both having methoxy substituents on the 4,6-diphenypyrimindine nucleus. The demethylation of methoxy groups of 4,6-bis(4-methoxyphenyl)pyrimidine of compound **6g** core heightened the activity by over two hundred-fold as demonstrated by **7a,** the most active compound**.** Although compound **6i** showed moderate activity, demethylation of the methoxy groups of the 4-(3,4-dimethoxyphenyl)-6-(4-methoxyphenyl)pyrimidine core compounds only mildly improved the activity of compound **7b** (2.61 vs 1.62 µM).

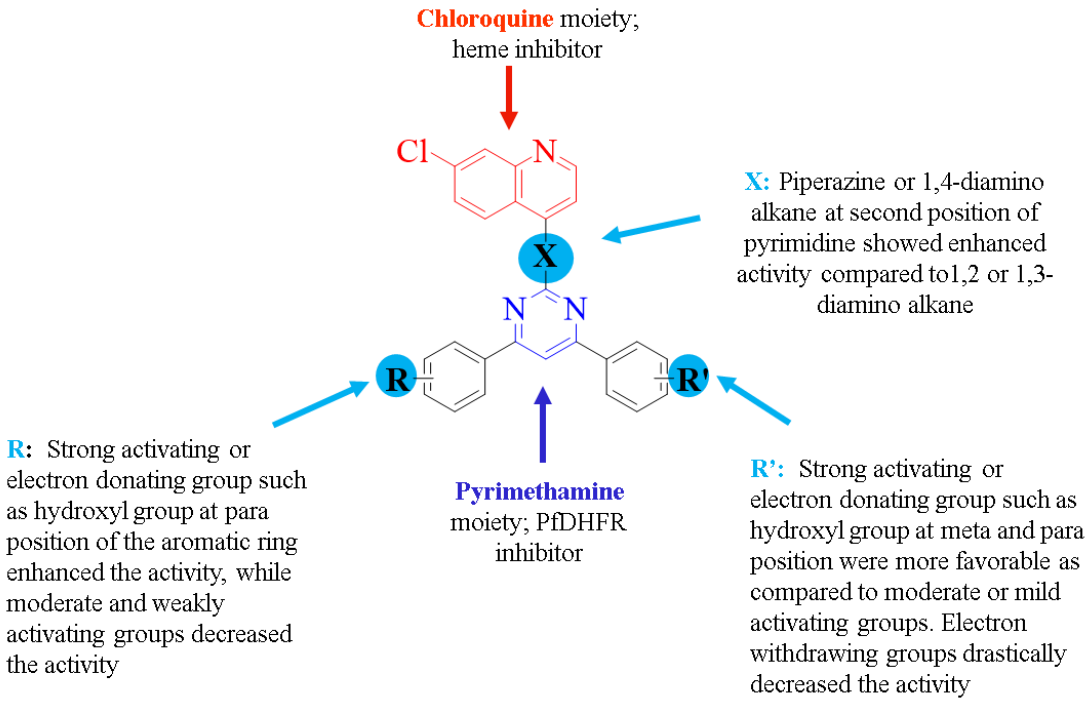

Figure 3.5. Structure Activity Relationship (SAR) for quinoline-pyrimidine derivatives.

It should be noted that, in contrast to other substituents such as methyl, chlorine and methoxy, the hydroxyl significantly influenced the antiplasmodial activity as defined in the activity of compounds **6b**, **6g**, **6i**, **7a** and **7b** analogues with the same 1,4-diamino butane linker (**Figure 3.5**). Given the above, it can be concluded that diamino alkane linkers, particularly 1,4-diamino butane and piperazine were crucial for the activity. Also, substituting phenyl groups of 4, 6-diphenylprimidine core with electron-donating groups, particularly hydroxyl groups, positively correlated with antiplasmodial activity.

Pyrimidinones have previously been shown to possess the antiplasmodial activity and target the essential parasite protein folding pathway of *P. falciparum* Hsp70 [19]. As such, we investigated the binding affinities of these compounds against the recombinant forms of two essential cytosolic *P. falciparum* Hsp70s; PfHsp70-1 and PfHsp70-z [18]. To determine binding kinetics, we employed surface plasmon resonance (SPR) analysis, as previously conducted [20, 21]. The SPR sensorgrams generated (**Figure 3.6**) were fitted to a simple 1:1 Langmuir kinetic binding model (**Table 2**). Generally, both parasite Hsp70s interacted with the four molecules in a concentration-dependent manner (**Figure 3.6**). The rates of dissociation were comparable for all the molecules. Estimated K_D values were within the lower micromolar to the upper nanomolar range, suggesting

a fairly high affinity of the compounds for the two essential cytosol localized *P. falciparum* Hsp70s (Table 2). Interestingly, PfHsp70-1 exhibited higher binding affinity (K_D values within lower nanomolar range) for compounds **6h** and **6k** compared to PfHsp70-z, which exhibited a four and two orders of magnitude reduction in affinity for the same compounds**,** respectively (Table 2). Compound **7a** exhibited a higher binding affinity for PfHsp70-z with one order of magnitude difference in comparison to its affinity for PfHsp70-1 (**Table 2**). On the other hand, compound **7b** had a lower affinity (K_D= 0.281 µM) for PfHsp70-1; and higher affinity (K_D=4.75 µM) for PfHsp70-z, respectively. Altogether, this suggests that compound **7a** showed the highest propensity to recognize both proteins. Notably, the observed varied preference of some of the compounds for the two PfHsp70 proteins highlights that despite their apparent sequence conservation, PfHsp70s possess unique motifs for selective targeting.

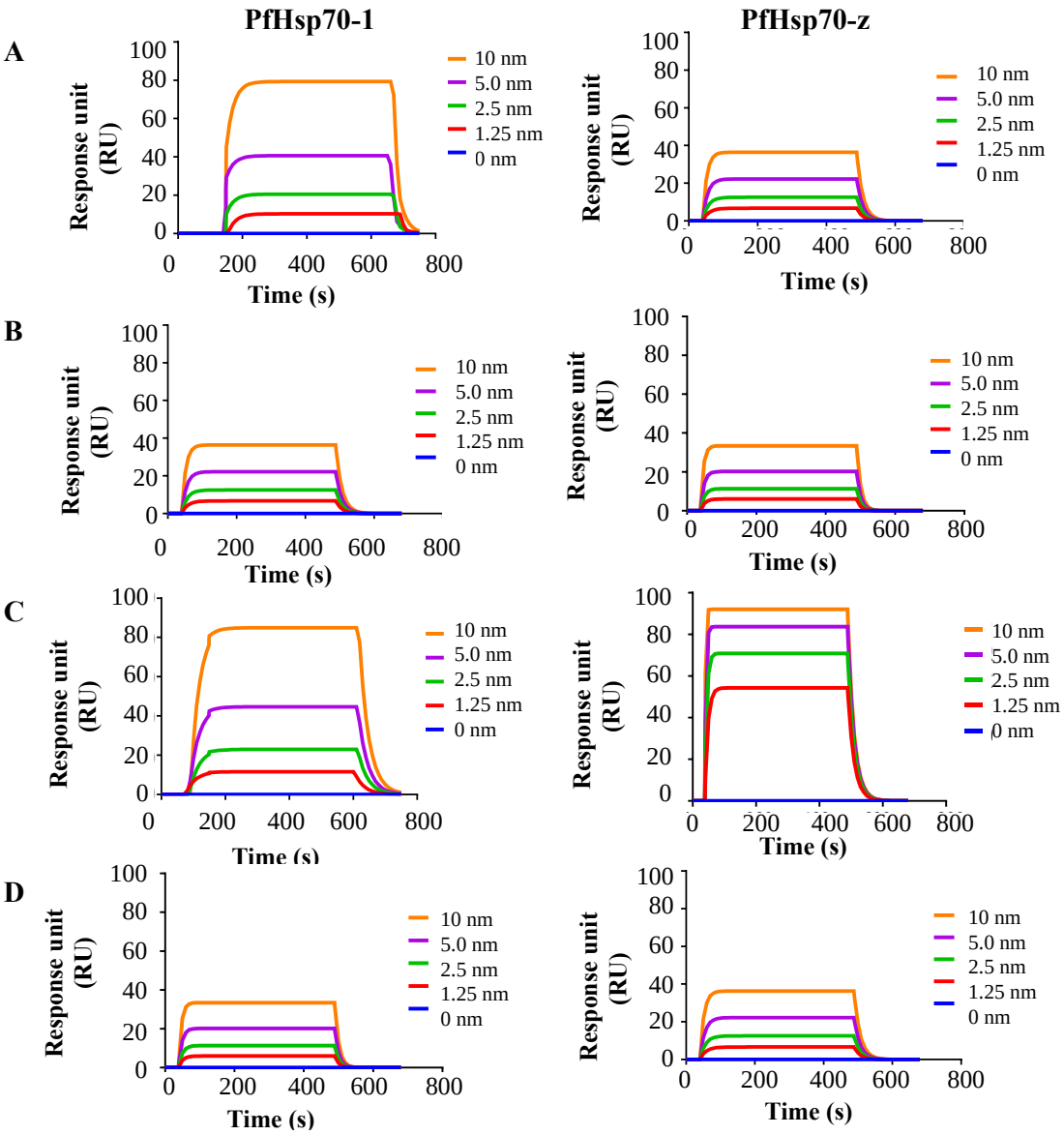

Figure 3.6. Selected synthetic compounds bind *P. falciparum* Hsp70s directly. Plots represent interaction of PfHsp70-1 or PfHsp70-z) as investigated against varying levels of the selected compounds (**6h, 6k, 7a or 7b**).

Shown in **Figure 3.6** are the representative SPR sensorgrams representing direct protein-compound interaction. The sensorgrams were analysed to generate the kinetics in Table 2. Binding affinity was evaluated as follows: (A) PfHsp70-1-**6h** (K_D= 2.19 nM) and PfHsp70-z-**6h** (K_D= 0.137 µM); (B) PfHsp70-1-**6k** (K_D= 0.261 nM) and PfHsp70-z-**6k** (K_D=2.05 µM); (C) PfHsp70-1-**7a** (K_D= 0.114 nM) and PfHsp70-z-**7a** (K_D=4.43 nM); (D) PfHsp70-1-**7b** (K_D= 0.281 µM) and PfHsp70-z-**7b** (K_D=4.75 µM), respectively.

Table 8. Kinetics data for the interaction of molecules with *P. falciparum* recombinant Hsp70 proteins.

Analyte	**Ligand**	K_a **(1/(M*s))** ± est. error	K_d **(1/s)** ± est. error	K_D **(M)** ± est. error	X^2
6h	PfHsp70-1	3.30 (±0.67) e^{+06}	1.32 (±0.12) e^{-02}	2.19 (±0.70) e^{-09}	1.1
	PfHsp70-z	5.99 (±0.90) e^{+03}	8.24 (±0.76) e^{-02}	1.37 (±0.89) e^{-05}	7.1
6k	PfHsp70-1	2.68 (±0.68) e^{+06}	7.00 (±0.11) e^{-02}	2.61 (±0.57) e^{-08}	2.4
	PfHsp70-z	1.34 (±0.99) e^{+04}	7.48 (±0.60) e^{-02}	2.05 (±0.59) e^{-06}	6.9
7a	PfHsp70-1	7.73 (±0.54) e^{+06}	8.81 (±0.24) e^{-02}	1.14 (±0.44) e^{-08}	4.7
	PfHsp70-z	2.70 (±0.53) e^{+07}	1.20 (±0.44) e^{-01}	4.43 (±0.92) e^{-09}	3.2
7b	PfHsp70-1	2.79 (±0.67) e^{+05}	7.84 (±0.92)e^{-02}	2.81 (±0.35) e^{-07}	8.8
	PfHsp70-z	1.91 (±0.77) e^{+04}	9.06 (±0.83)e^{-02}	4.75 (±0.55) e^{-06}	7.9

SPR based kinetics for the direct interaction of PfHsp70-1 and Hsp70-z with the various compounds are represented by the rate of association (*Ka*), rate of dissociation (Kd) and the steady-state affinity (K_D), respectively. The ligand represents the respective immobilised protein on the CMD 3D 500L chip surface to which the analyte was injected at a flow rate of 50 µl/min in triplicate. Data was analysed after double referencing (refractive index changes on-chip surface without protein immobilised and for buffer injected without analyte) as a baseline. Data are represented as mean ± standard error of measurement. Chi-square (χ^2) values show the 1:1 Langmuir curve fitting residuals.

Furthermore, the cytotoxicity screening of the most potent molecule, **7a**, against human embryonic kidney epithelial (HEK-293) cells was studied (**Table 1**). The selective index (SI) of 9.79 was calculated for the most potent compound by dividing the IC_{50} value of the cytotoxic activity divided by the IC_{50} value of the antimalarial activity. The observed activity suggests that while selectively killing the parasite, compound **7a** has a limited cytotoxic effect against mammalian cells at therapeutic dosages, where a safety index of 10 is regarded as safe.

3.3.3 Molecular docking scores

To measure the compounds' fitness at the active catalytic sites of the two enzymes, a molecular docking analysis was performed. The four compounds were docked into the ATPase active sites of the enzymes (PfHsp70-1 and PfHsp70-z) to calculate and examine the fitness/affinity of the compounds. Based on the computational data, it is likely that the compounds bind to the ATPase domain for both proteins in a similar fashion to ATP binding. Suggesting that they could be competitive inhibitors to ATP binding for PfHsp70-1 and PfHsp70-z. **Table 2.** represents the binding modes and docking results of the compounds for each enzyme. Notably, the four compounds showed relatively good binding scores for PfHsp70-1. Compounds **7a** and **6k** showed the highest and lowest binding scores of -9.8 kcal/mol and -8.7 kcal/mol, respectively. The docking result for PfHsp70-z revealed that compound **7b** exhibited the highest docking score of -8.9 kcal/mol; while, compounds **7a** and **6k** showed the lowest values of -8.1 kcal/mol. The results suggest that the four compounds exhibited better fitness in PfHsp70-1 than PfHsp70-z. To better understand the binding affinity and structural mechanisms of inhibition of the four compounds against the two enzymes, molecular dynamics study on the compounds' best binding modes to the enzymes were investigated since molecular docking scores might give false-positive results.

3.3.3.1 Binding energies/affinities of the molecules to PfHsp70-1 and PfHsp70-z

To calculate the binding free energies of all the finals compounds to the enzymes, the Molecular Mechanics/Generalized Born Surface Area (MMGBSA) computational technique was employed. Table 3 shows the results of the thermodynamic binding free energy profiles for the compounds to the two enzymes. All the compounds showed high binding energies/affinity for PfHsp70-1, ranging from -46.752 to -56.270 kcal/mol, with compounds **7a** and **7b** having the highest free energies of -56.270 kcal/mol and -53.968 kcal/mol, respectively. Compound **6k** exhibited higher binding energy (-49.182 kcal/mol) than **6h** (-46.752 kcal/mol). This result is in consistent with the docking results indicating that compounds **7a** and **7b** had the highest docking score for PfHsp70-1. In the PfHsp70-z systems, compounds **7b** and **6k** showed the highest binding affinities of -52.097 kcal/mol and -49.122 kcal/mol. This is also in consistent with the docking result that showed compound **7b** to have the highest docking score.

Molecules	PfHsp70-1	PfHsp70-z
7a	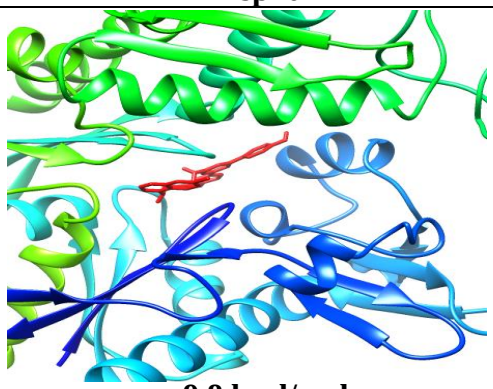 -9.8 kcal/mol	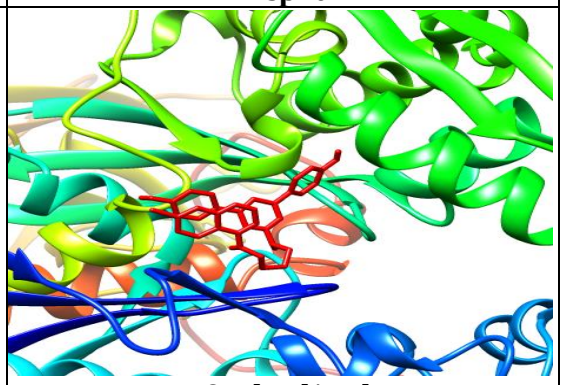 -8.1 kcal/mol
7b	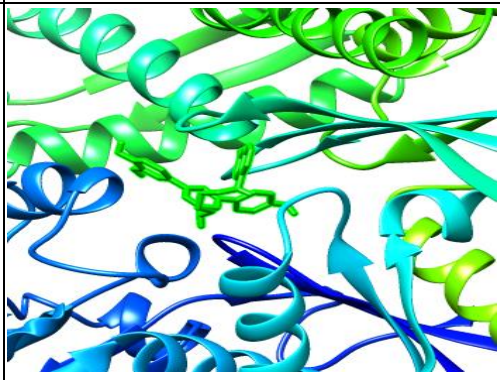 -9.1 kcal/mol	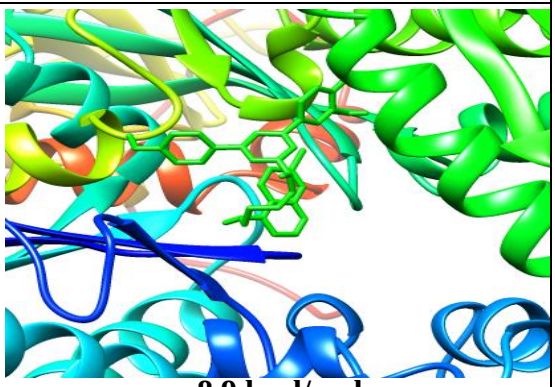 -8.9 kcal/mol
6h	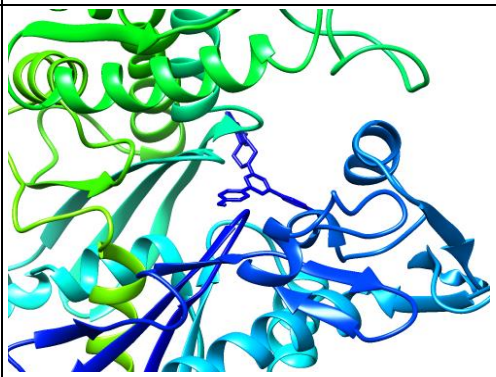 -9.0 kcal/mol	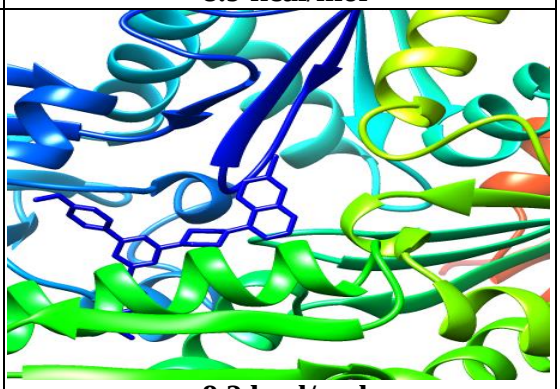 -8.2 kcal/mol
6k	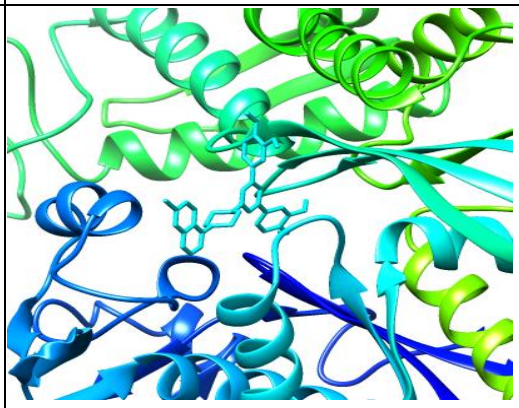 -8.7 kcal/mol	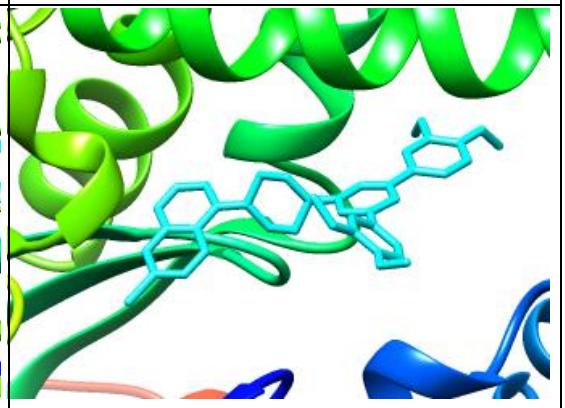 -8.1 kcal/mol

Figure 3.7. Binding modes and docking scores of the molecules to PfHsp70-1 and PfHsp70-z.

Furthermore, as shown in Table 3, compounds **6k** and **7b** showed no difference in their binding affinities for the two enzymes. Generally, PfHsp70-1 showed strong binding energies for compounds, **6h**, **6k**, **7a** and **7b**, than PfHsp70-z. The high binding affinities recorded suggest possible inhibitory activities of compounds (**6h**, **6k**, **7a** and **7b**) against the protein folding role of PfHsp70-1.

Table 3. Thermodynamic binding free energy profiles for the compounds.

Energy Components (kcal/mol)					
Complex	**Δ E_{vdW}**	**ΔE_{elec}**	**ΔG_{gas}**	**ΔG_{solv}**	**ΔG_{bind}**
PfHsp70-1					
6a	-48.805±4.167	-10.005±3.324	-46.179±8.117	20.574±1.104	-41.485±7.544
6b	-33.255±4.705	-8.775±2.751	-39.685±2.216	15.111±2.212	-37.323±4.245
6c	-37.742±4.235	-9.155±1.545	-41.331±4.114	17.008±2.101	-40.137±3.038
6d	-38.188±7.884	-9.288±6.002	-42.078±4.555	21.000±2.414	-36.685±5.422
6e	-42.131±7.134	-38.322±10.231	64.111±9.313	40.120±4.223	-47.363±4.205
6f	-35.777±6.155	-19.578±3.688	-58.124±4.574	25.435±2.585	-34.898±5.985
6g	-37.903±3.241	-21.588±2.411	-60.004±2.660	27.747±2.575	-35.999±4.257
6h	-58.681±4.387	-8.298±6.244	-66.978±7.441	20.226±4.431	-46.752±5.806
6i	-35.113±4.585	-22.200±3.471	-51.745±3.747	24.155±3.886	-33.219±3.888
6j	-35.989±5.100	-24.681±3.812	-57.818±5.558	24.988±4.515	-34.910±4.378
6k	-59.352±5.864	-21.389±6.159	-80.741±7.015	31.559±5.613	-49.182±6.582
7a	-65.317±4.753	-36.744±10.146	-102.061±12.488	45.791±5.010	-56.270±9.413
7b	-58.507±4.406	-42.327±13.445	100.834±12.429	46.867±6.614	-53.968±7.005
7c	-60.688±3.181	-31.581±8.435	-87.481±7.700	39.928±6.781	-42.823±7.880
PfHsp70-z					
6a	-40.243±2.723	-23.212±3.104	-72.126±4.332	31.432±3.424	-32.073±3.023
6b	-34.123±4.111	-14.423±3.933	-44.133±2.811	21.331±5.121	-30.332±1.932
6c	-41.272±3.928	-23.092±7.834	-73.023±4.933	34.422±5.474	-41.324±3.339
6d	-37.223±3.983	-21.223±7.215	-51.443±4.113	30.551±5.441	-37.525±5.251

6e	-35.245±4.145	-23.254±5.444	-47.982±2.254	32.268±4.141	-33.125±3.331
6f	-21.113±3.112	-17.723±2.863	-32.141±4.223	19.321±2.113	-29.222±3.432
6g	-22.343±4.422	-19.424±2.128	-28.321±3.252	20.441±3.938	-26.234±2.224
6h	-47.397±3.501	-16.487±5.949	-63.884±7.430	28.353±5.285	-35.531±4.910
6i	-23.111±2.165	-22.214±3.819	-19.231±4.122	17.654±4.525	-24.212±2.333
6j	-42.785±3.423	-18.447±4.551	-55.957±5.541	25.415±5.998	-31.258±4.233
6k	-61.985±4.948	-23.126±9.433	-85.111±11.737	35.990±8.178	-49.122±6.131
7a	-48.129±4.947	-28.574±12.986	-76.703±14.429	41.877±7.891	-34.826±9.645
7b	-60.543±3.675	-33.094±9.310	-93.636±8.713	41.539±5.474	-52.097±5.016
7c	-29.105±5.500	-20.117±2.234	-45.777±424	23.425±4.646	-30.411±4.008

ΔEele electrostatic energy, ΔEvdW van der Waals energy, ΔGbind total binding free energy, ΔGsol solvation free energy, ΔEgas gas-phase free energy

3.3.3.2 Ligand-receptor interaction profiles of the molecules

The receptor-ligand interaction plots examined the molecular interactions between the bound compounds and the amino acid residues at the active sites of an enzyme [1]. To examine the mechanistic inhibitory characteristics of the four compounds, the interaction between the compounds and the active site amino residues of the enzymes were assessed. **Figure 3.8** and **Figure 3.9** shows the 2D representation of the interactions plots between the compounds and the different amino acid residues of PfHsp70-1 and PfHsp70-z, respectively. Van der Waals, H-bond, pi-anion and pi-alkyl are the interactions observed in the PfHsp70-1 complexes. Structurally related compounds **6k** and **6h** showed pi-anion interactions with cysteine residues, Cys206 and Cys77, respectively (**Figure 3.8**).

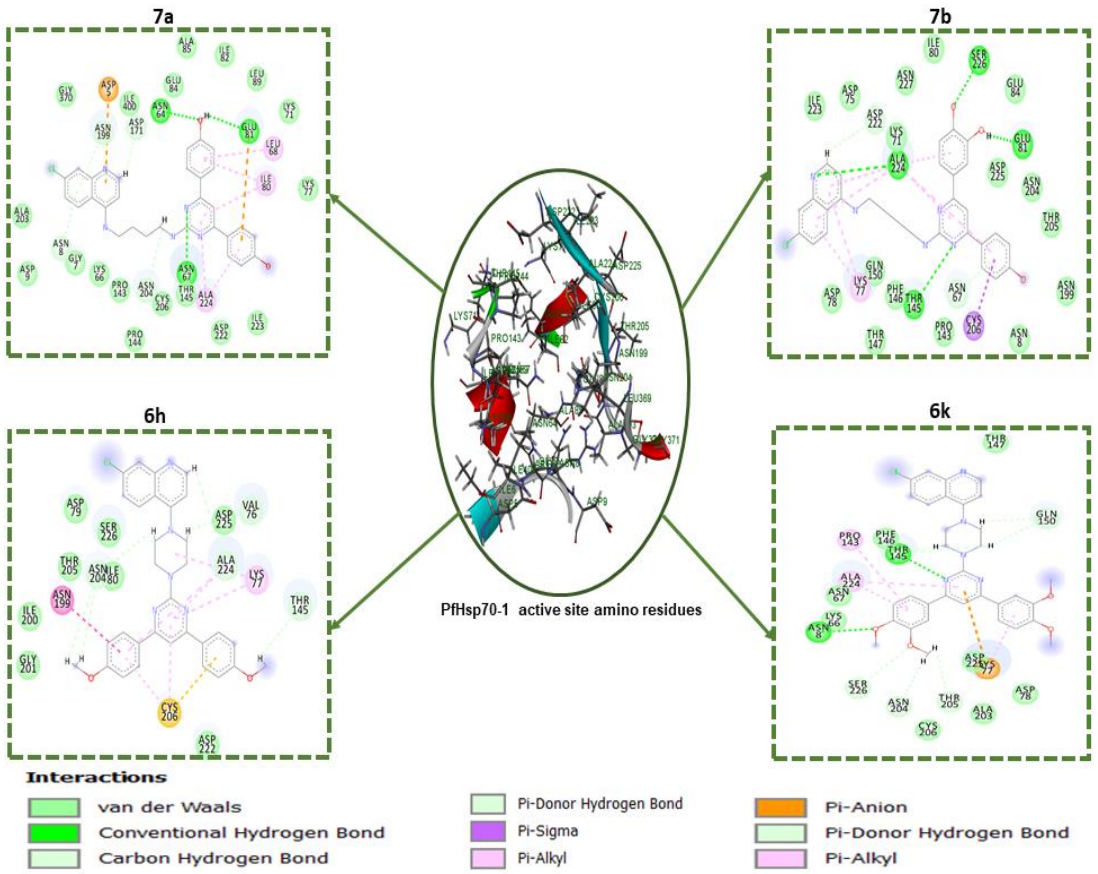

Figure 3.8. A depiction of protein-ligand interactions plots with different amino acid residues.

While compound **7a** had pi-anion interaction with Asp5, however, compound **6h** showed no pi-anion interaction but had a pi-sigma interaction with Cys206. These data revealed that binding energies are proportional to the number of H-bond and the total number of interactions observed in the four compounds, where compounds **7a**, **7b**, **6k** and **6h** have total interaction numbers of 29, 23, 17 and 15, respectively. A slightly different interaction was observed in PfHsp70-z complexes. Unlike the pi-anion interaction observed in PfHsp70-1, a pi-cation interaction was observed in PfHsp70-z. Furthermore, pi-pi stacked and donor-donor interactions were also observed. All the compounds showed a significant number of H-bond interactions required for stability. A donor-donor interaction was only observed in compound **7b**. The difference in the number and type of interactions observed for the two proteins (PfHsp70-1 and PfHsp70-z) could explain the higher binding energies observed in the PfHsp70-1 complexes.

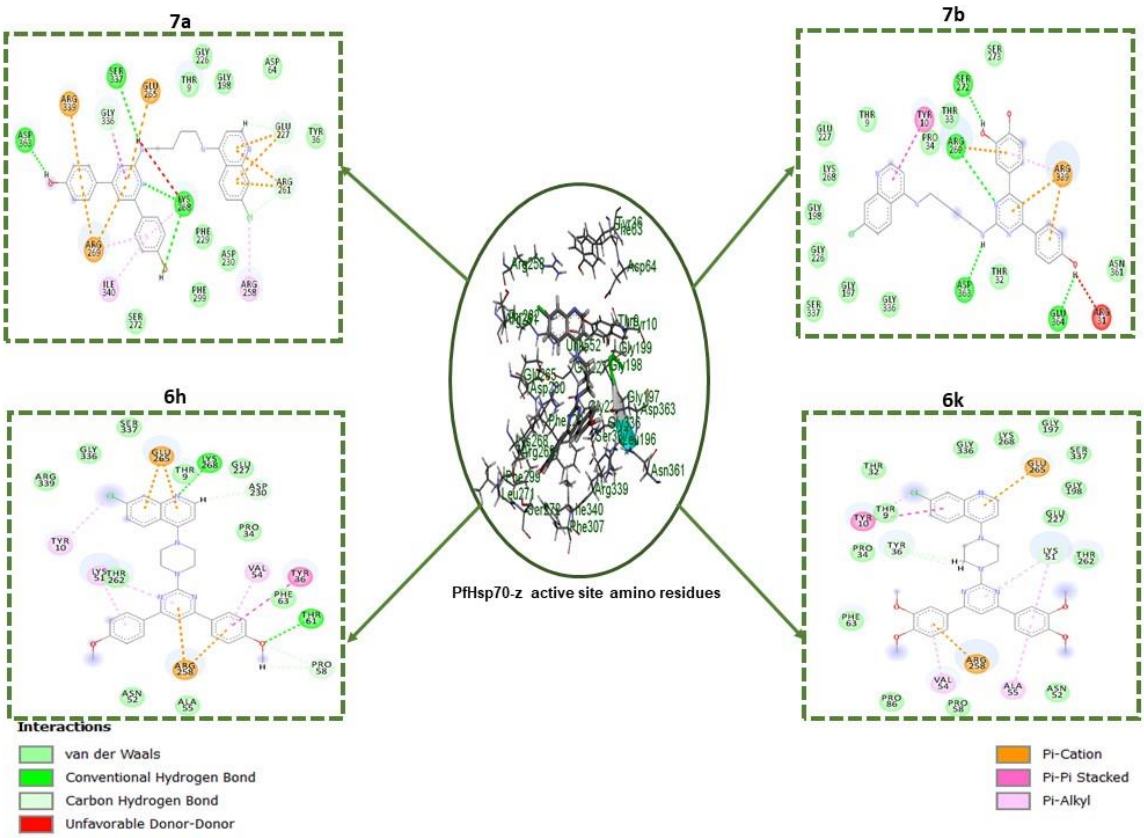

Figure 3.9. A depiction of protein-ligand interactions plots with different amino acid residues.

3.3.3.3 Stability and Flexibility of the Enzymes bound Complexes

To examine the stability and dynamics of enzyme-ligand complexes, 100 ns molecular dynamic (MD) simulations were performed. Root means square deviation (RMSD), a radius of gyration (RoG), root means square fluctuation (RMSF) and solvent accessible surface area (SASA) of alpha carbon (Cα) atoms were monitored and analyzed along with the entire duration of 100 ns of the MD simulation for the unbound and bound enzyme systems. For PfHsp70-1, the RoG plots revealed the binding of the four compounds lowers the mean RoG values of the four compounds (**7a**; 35.243 Å, **7b**; 34.553 Å, **6h**; 34.183 Å, **6k**; 31.432 Å) when compared to the unbound PfHsp70-1 systems; 35.973 Å (**Figure 3.10-1a**). A similar reduction in average RoG values after the binding of the Brath goo compounds (**7a**; 28.272 Å, **7b**; 28.231 Å, **6h**; 28.354 Å, **6k**; 27.642 Å) was also observed in PfHsp70-z complexes when compared with the average value of the unbound PfHsp70-z system, 28.321 Å (**Figure 3.10-1**). This finding suggests the binding of the compounds stabilizes the enzymes.

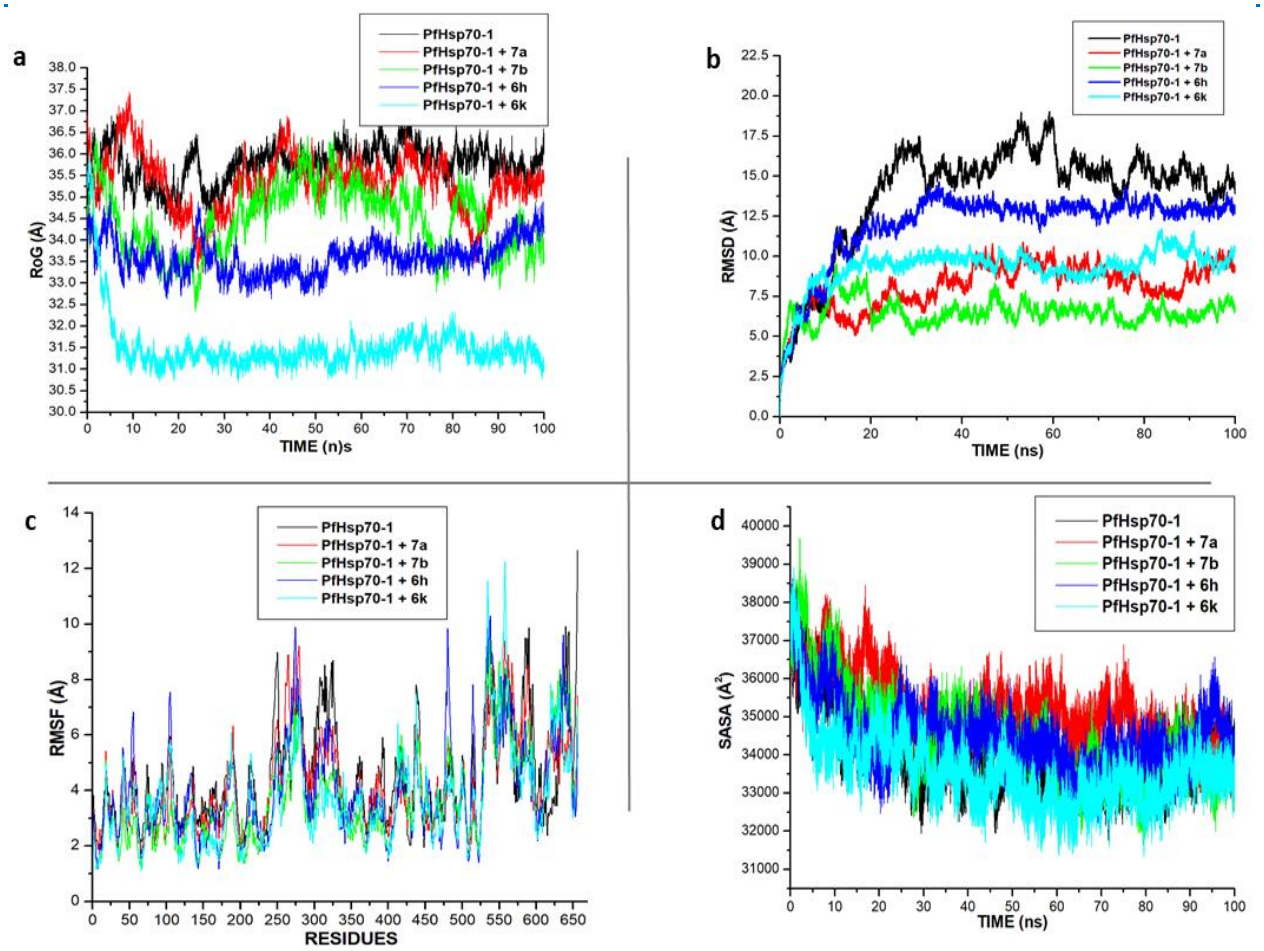

Figure 3.10-1. Plots of alpha C atoms of the PfHsp70-1, **7a**, **7b**, **6h** and **6k**, a) RoG plots b) RMSD, c) RMSF and d) SASA plots systems calculated throughout 100 ns MD simulations.

Figure 3.10-2 shows the plot of the RMSD values, which is a measurement of the enzyme complexes' convergence and stability [23]. The plot shows that all the four compounds and the unbound systems reach convergence after about 8 ns. The RMSD plots for the complexes revealed that the four complexes are more stable (lower RMSD values) than the unbound systems of PfHsp70-1 and PfHsp70-z. This also suggests that the alpha carbon fluctuation of the compounds converged well during MD simulation. Likewise, the RMSF of the complexes were studied to examine the flexibility and stability of individual amino residues of the proteins. RMSF monitors the behaviour of the active residues of a protein. Higher and lower fluctuation values indicated more and less flexible movements, respectively. As shown in **Figure 3.10-2**, c, residues 200 - 300, 305 - 345 and 5525 - 600 fluctuate more in all the four compounds and the unbound PfHsp70-1 systems. While most of the residues (150 - 250) involved in ligand binding fluctuate less. The plot further revealed that the average RMSF values of the compounds (**7b** (3.743 Å), **7a** (3.771 Å), **6h**

(3.989 Å) and **6k** (4.023 Å)) were lower (less fluctuation) than the unbound system with average RMSF value of 4.212 Å. For the PfHsp70-z systems, more flexibility was observed at residues 230 – 260, 375 – 400 and 450 – 475. Unlike the PfHsp70-1 system, compounds **7a** and **7b** exhibited higher average RMSF values (2.942 Å and 2.729 Å, respectively) than registered by unbound PfHsp70-1 (2.547 Å). Compounds **6h** and **6k** exhibited less fluctuation than the unbound enzyme, with average values of 2.4675 Å and 2.501 Å, respectively.

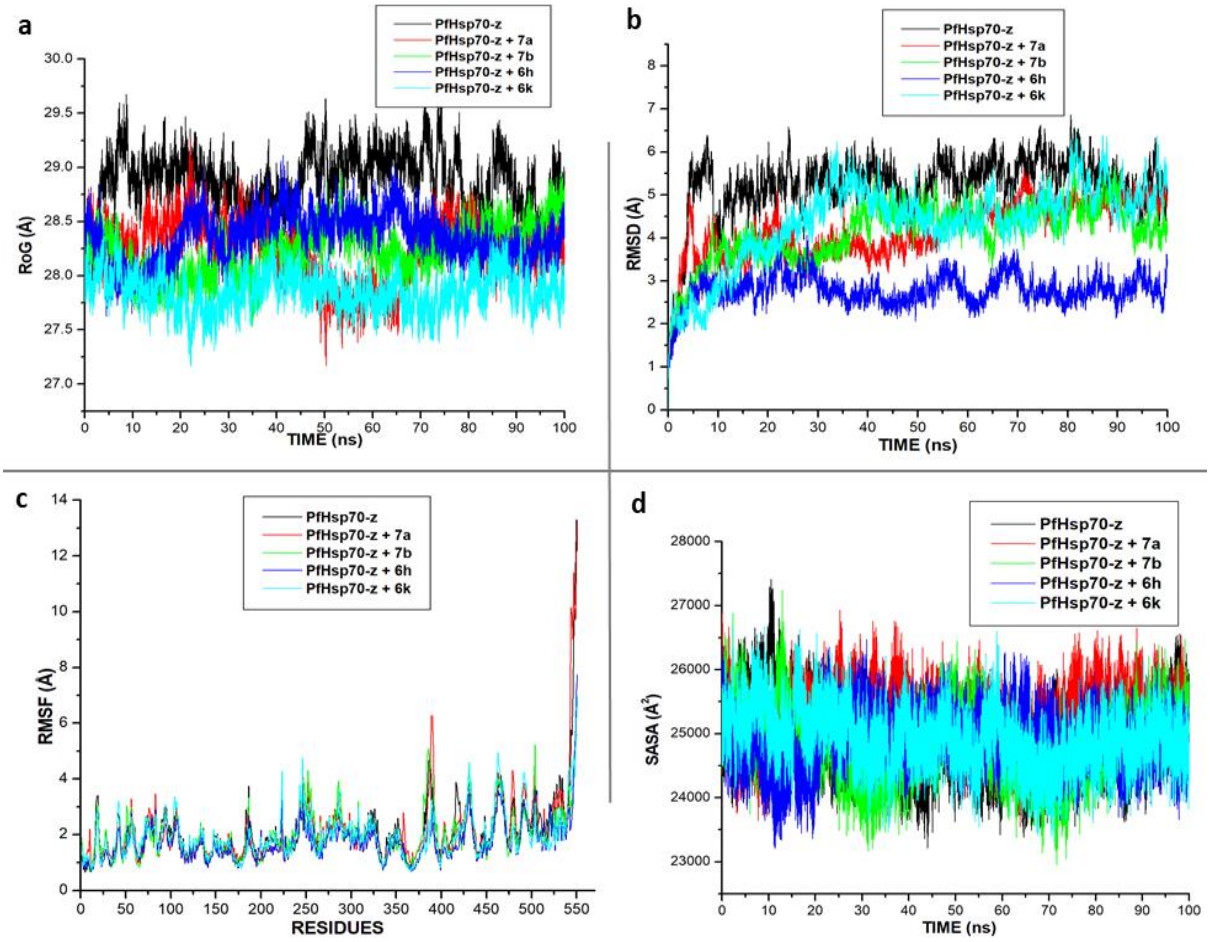

Figure 3.10-2. Plots of alpha C atoms of the PfHsp70-z, **7a**, **7b**, **6h** and **6k,** a) RoG plots b) RMSD, c) RMSF and d) SASA plots systems calculated throughout 100 ns MD simulations.

SASA is another parameter to quantify the enzymes' exposure to the solvent environment [24]. The four compounds exhibited an increase in the exposure of the enzyme to solvent molecules, as their respective bindings raised the average SASA values compared to the unbound PfHsp70-1 (**Figure 3.10-2, d**). SASA mean values of 35100 Å^2, 34200 Å^2, 34550 Å^2, 33800 Å^2 and 33700 Å^2 were recorded for compounds **7a**, **7b**, **6h**, **6k,** and unbound PfHsp70-1. The average SASA

values for compounds **7a**, **7b**, **6h**, **6k** and the unbound PfHsp70-z systems are 25900 $Å^2$, 25100 $Å^2$, 25600 $Å^2$, 24700 $Å^2$ and 24800 $Å^2$ (**Figure 3.10-2. d**). The increased SASA values reported for the compounds showed the binding of the compounds further exposed the enzyme to a solvent molecule. This suggests that the structural integrity of the enzyme was not distorted after 100 ns.

3.3.3.4 Assessing the drug-likeness of the compounds

Pharmacokinetic properties of the compounds were predicted using the SwissADME serve [25]. Lipinski's rule of five is a set of rules that assess both the physical and chemical properties of potential drugs to ascertain their safety as an orally active drug [26]. As shown in Table 5, the four compounds (**6h**, **6k**, **7a** and **7b**) had no more than 5 hydrogen bond donors, no more than 10 hydrogen bond acceptors, thus passed the drug-likeness test and are poorly soluble in water. The result showed that the four compounds' partition coefficients (log P) are around 5. Greater logP usually indicates the probability of a drug to permeate the lipid membrane is low [27]. Compounds **7a** and **7b** were predicted to be poorly absorbed in the gastrointestinal tract (GIT), while compounds **6h** and **6k** were predicted to be highly absorbed. This suggests that the highly absorbed compounds would attain optimal concentrations in the systemic circulation than the lowly absorbed compounds. The blood-brain barrier (BBB) is a protective gate that prevents the passage of toxic compounds into the brain or the central nervous system [25]. For the four test compounds (**6h**, **6j**, **7a** and **7b**), the number of hydrogen donors ranged between 0 to 5 while hydrogen acceptors 5 to 7. Thus, indicating that all the test compounds could be considered orally active. None of the four compounds were predicted to permeate the BBB. Bioavailability score is a measurement of the rate of absorption and quantity of a given amount of unchanged drug that goes to the systemic circulation [28]. The four compounds showed a relatively high score of 0.55, which suggests they all might reach their sites of activity with higher concentrations required for therapeutic effect.

Table 4. Pharmacokinetic and physicochemical properties of the molecules**.**

Comp	***M. Formula***	***M. Weight (g/mol)***	***H-bond donor***	***H-bond acceptor***	***Lipophilicity (iLOGP)***	***Water Solubility***	***GIT Absorption***	***BBB Permeability***	***Bioavailability Score***	***Drug likeness (Lipinski)***
7a	$C_{29}H_{26}ClN_5O_2$	512.00	4	5	5.03	Poor	Low	No	0.55	Yes

7b	$C_{29}H_{26}ClN_5O_3$	528.00	5	6	4.69	Poor	Low	No	0.55	Yes
6h	$C_{31}H_{28}ClN_5O_2$	538.04	0	5	5.20	Poor	High	No	0.55	Yes
6k	$C_{33}H_{32}ClN_5O_4$	598.09	0	7	5.16	Poor	High	No	0.55	Yes

3.4 Conclusion

In summary, pyrimidine-quinoline analogy inspired chloroquine and pyrimethamine antimalarial drugs were designed, synthesised by molecular hybridisation approach and screened for their antiplasmodial activity. The facile preparation with excellent yields of these compounds makes the synthetic pathway attractive and versatile. Among the tested compounds, only compound **7a** displayed the best antiplasmodial activity (IC_{50} =0.32 ± 0.06 μM), with a selectivity index of 9.79, which is considered safe. Interestingly, compound **7a** bound to both parasite Hsp70 chaperones with significant affinity, suggesting that one possible mechanism of action of this compound could be to abrogate the protein folding pathway of the parasite. This hypothesis was further supported by the observed molecular docking scores. Brief SAR studies revealed that strong activating or electron-donating groups on the meta and para position of the aromatic group enhanced the activity. Similarly, piperazine or 1,4-diamino butane linkers were essential for the activity. The authors believe that the outcome or observation of this research work would assist the researchers in designing potent antimalarial agents.

Declaration of Competing Interest

The authors declare no known conflicting financial or personal interests that could have appeared to influence the work reported in this paper.

Acknowledgement

The authors would like to express their heartfelt gratitude to the Discipline of Pharmaceutical Sciences, College of Health Sciences, University of KwaZulu-Natal (UKZN), Durban, South Africa, for providing all the necessary facilities. R.K. gratefully acknowledges National Research Foundation-South Africa (NRF-SA) for funding this project (grant nos. 103728, 112079 and 129247). The authors would also like to acknowledge Dr Vuyisa Mzozoyana (UKZN) for NMR spectroscopic experimental data.

3.5 Experimental

3.5.1 Chemistry protocol

All the chemicals used in this research work were purchased from Sigma-Aldrich and Merck Millipore, South Africa. The commercially available chemicals benzaldehyde and acetophenone were purchased from Sigma-Aldrich (South Africa). All the solvents, except those of laboratory-reagent grade, were dried and purified when necessary according to previously published methods. The progress of the reactions and the purity of the compounds were monitored by thin-layer chromatography (TLC) on pre-coated silica gel plates procured from E. Merck and Co. (Darmstadt, Germany) using 36% ethyl acetate in n-hexane as the mobile phase and iodine vapour as the visualising agent.

The melting points of the synthesised compounds were determined using a Thermo Fisher Scientific (IA9000, UK) digital melting point apparatus and are uncorrected. The IR spectra were recorded on a Bruker Alpha FT-IR spectrometer (Billerica, MA, USA) using the ATR technique. The ^{1}H NMR and ^{13}C NMR spectra were recorded on a Bruker AVANCE 400 and 600 MHz (Bruker, Rheinstetten/Karlsruhe, Germany) spectrometers using $CDCl_3$ and DMSO-*d6*. The chemical shifts are reported in units with respect to TMS as an internal standard. HRMS spectra were recorded on an Autospec mass spectrometer with electron impact at 70 eV.

3.5.1.1 A typical procedure for the synthesis of (*E*) chalcone (1b-1f)

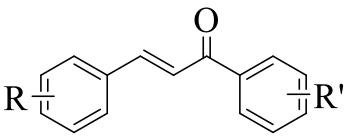

1b R = 4-Me, R' = 4-Cl

1c R = 4- Me, R' = 4-MeO

1d R = 4-MeO, R' = 4-MeO

1e R = 3,4-MeO, R' = 4-MeO

1f R = 3,4-MeO, R' =3,4-MeO,

To a stirring solution of acetophenone (5 g, 32.34 mmol) in EtOH (30 ml), a 60% NaOH solution (12 g NaOH/ H_2O (20 mL)) was added. The reaction was stirred at room temperature for 30 minutes. Benzaldehyde (4.7 g, 38.81 mmol) was then added, and the reaction was sonicated for 1 hour at 35^{o}C. The progression of the reaction was monitored by TLC. Excess ethanol was removed under vacuum, and the reaction mixture was added into 100 g of ice and stirred. The precipitates formed were filtered, washed with excess water and dried under vacuum. The crude product was purified by recrystallisation in EtOH to obtain the following pure compounds in good yield.

(E)-1-(4-chlorophenyl)-3-(p-tolyl)prop-2-en-1-one **(1b)**: Yellow solid, yield: 90 %, mp = 162-164 °C; ^{1}H NMR (400 MHz, $CDCl_3$, *δ*, ppm): 7.96 (d, *J* = 8.57 Hz, 2H, ArH), 7.78 (d, *J* = 15.65 Hz, 1H, ph,-CH=C**H**), 7.54 (d, *J* = 8.08 Hz, 2H, ArH), 7.47 (d, *J* = 8.36 Hz, 2H, ArH), 7.46-7.42 (d, *J* = 15.65 Hz, 1H, ph,-C**H**=CH), 7.23 (d, *J* = 7.96 Hz, 2H ArH), 2.40 (s, 3H, CH_3); ^{13}C NMR (400 MHz, $CDCl_3$, *δ*, ppm): 189.28, 145.48, 141.38, 139.09, 136.09, 136.65, 131.96, 129.90, 129.77, 128.92, 128.58, 120.46, 21.59 (CH_3).

(E)-1-(4-methoxyphenyl)-3-(p-tolyl)prop-2-en-1-one (**1c**): Yellow solid, yield: 96.3%, mp = 125-128 °C; ^{1}H NMR (400 MHz, $CDCl_3$, *δ*, ppm): 8.04 (d, *J* = 8.76 Hz, 2H, ArH), 7.89 (d, *J* =15.60 Hz, 1H, ph-C**H**=CH), 7.54 (d, *J* = 7.95 Hz, 2H, ArH), 7.51 (d, *J* = 15.63 Hz, 1H, ph-CH=C**H**), 7.22 (d, *J* = 7.97, Hz,, 2H ArH), 6.98 (d, *J* = 8.77 Hz, 2H, ArH), 3.88 (s,3H, CH_3), 2.39 (s, 3H,CH_3); ^{13}C NMR (400 MHz, $CDCl_3$, *δ*, ppm): 189.43, 163.92, 144.64, 141.40, 132.92, 131.81, 131.34, 130.24, 128.96, 121.46, 114.39, 56.06(OCH_3), 22.09 (CH_3).

(E)-1,3-bis(4-methoxyphenyl)prop-2-en-1-one (**1d**): Yellow solid, yield: 85.7%, mp = 102-104 °C; ^{1}H NMR (400 MHz, $CDCl_3$, *δ*, ppm): 8.03 (d, *J* = 8.75 Hz, 2H, ArH), 7.78 (d, *J* = 15.58 Hz, 1H, ph-C**H**=CH), 7.60 (d, *J* = 8.66 Hz, 2H, ArH), 7.43 (d, *J* = 15.58 Hz, 1H, ph-CH=C**H**), 6.96 (dd, *J* = 17.58, 8.72 Hz, 4H, ArH), 3.89 (s,3H, OCH_3), 3.85 (s, 3H, OCH_3); ^{13}C NMR (400 MHz, $CDCl_3$, *δ*, ppm): 189.39, 163.84, 162.09, 162.09, 144.39, 131.95, 131.28, 130.67, 128.40, 120.15, 114.96, 114.36, 56.05 (OCH_3), 55.98 (OCH_3).

(E)-3-(3,4-dimethoxyphenyl)-1-(4-methoxyphenyl)prop-2-en-1-one (**1e**): Yellow solid, yield: 80.6%, mp = 92-94 °C; ^{1}H NMR (400 MHz, $CDCl_3$, *δ*, ppm): 8.03 (d, *J* = 8.81 Hz, 2H, ArH), 7.75 (d, *J* = 15.56 Hz, 1H, ph-CH=C**H**), 7.40 (d, *J* = 15.56 Hz, 1H, ph-C**H**=CH), 7.23 (dd, *J* = 8.31, 1.64 Hz, 1H, ArH), 7.16 (s, 1H, ArH), 6.98 (d, *J* =8.81 Hz, 1H, ArH), 6.89 (d, *J* = 8.27 Hz, 1H, ArH), 3.94 (s, 3H, OCH_3), 3.92 (s, 3H, OCH_3), 3.88 (s, 3H, OCH_3); ^{13}C NMR (400 MHz, $CDCl_3$, *δ*, ppm): 189.37, 163.86, 151.83, 149.80, 144.71, 131.89, 131.29, 128.65, 123.53, 120.42, 114.36, 111.70, 110.68, 56.56 (OCH_3), 56.54 (OCH_3), 56.05 (OCH_3).

(E)-1,3-bis(3,4-dimethoxyphenyl)prop-2-en-1-one (**1f**): Yellow solid, yield: 99%, mp = 109-111°C; ^{1}H NMR (400 MHz, $CDCl_3$, *δ*, ppm): 7.76 (d, *J* = 15.54 Hz, 1H, ph-CH=C**H**), 7.69 (d, *J* = 8.36 Hz, 1H, ArH), 7.62 (s, 1H, ArH) 7.41 (d, *J* = 15.54 Hz, 1H, ph-C**H**=CH), 7.24 (d, *J* = 8.44 Hz, 1H, ArH), 7.16 (s, 1H, ArH), 6.92 (dd, *J* = 11.73, 8.31 Hz, 2H, ArH), 3.89-3.95 (m, 9H, CH_3),

3.92 (s, 3H, CH_3); ^{13}C NMR (400 MHz, $CDCl_3$, δ, ppm): 189.26, 153.70, 151.86, 149.81, 144.73, 132.13, 128.64, 123.46, 123.43, 120.25, 111.72, 111.43, 110.81, 110.50, 56.65 ($2OCH_3$), 56.57 ($2OCH_3$).

3.5.1.2 A typical procedure for the synthesis of 4,6-diphenylpyrimidin-2-amine(2a-2f)

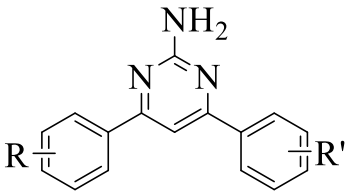

2a	R = 4-H,	R' = 4-H
2b	R = 4-Me,	R' = 4-Cl
2c	R = 4- Me,	R' = 4-MeO
2d	R = 4-MeO,	R' = 4-MeO
2e	R = 3,4-MeO,	R' = 4-MeO
2f	R = 3,4-MeO,	R' =3,4-MeO,

The reaction mixture of (*E*)-chalcone (**1**) (8 g, 31.16 mmol), guanidine hydrochloride (4.8 g, 49. 86 mmol) and 60% NaOH (12 g NaOH/H_2O (20 mL)) in EtOH (30 mL) was refluxed for 24 hours. The progression of the reaction was monitored using TLC. Excess ethanol was removed under vacuum using rotavapor, and the reaction mixture was then added in 100 g ice water. The precipitate formed was filtered, washed with excess water and dried. The crude compound was purified by column chromatography using EtOAc/hexane (1:4) eluent to obtain the following pure compounds.

4,6-diphenylpyrimidin-2-amine **(2a)**: Yellow solid, yield: 65 %, mp = 136-138℃; ^1H NMR (400 MHz, $CDCl_3$, δ, ppm): 8.07-8.05 (m, 4H, ArH), 7.51-7.49 (m, 6H, ArH), 7.46 (s, 1H, ArH), 5.35 (s, 2H, NH_2).

4-(4-chlorophenyl)-6-(p-tolyl)pyrimidin-2-amine (**2b**): Yellow solid, yield: 62%, mp = 162-165℃; ^1H NMR (400 MHz, $CDCl_3$, δ, ppm): 8.00 (d, *J* = 8.36 Hz, 2H, ArH), 7.95 (d, *J* = 7.96 Hz, 2H, ArH), 7.46 (d, *J* = 8.36 Hz, 2H, ArH), 7.37 (s, 1H, ArH), 7.30 (d, *J* = 7.38 Hz, 2H, ArH), 5.31 (s, 2H , NH_2), 2.43 (s, 3H, CH_3) ; ^{13}C NMR (400 MHz, $CDCl_3$, δ, ppm): 166.40, 164.76, 163.63, 140.93, 136.52, 136.25, 134.74, 129.53, 128.95, 128.42, 127.04, 103.64, 21.44 (CH_3).

4-(4-methoxyphenyl)-6-(p-tolyl)pyrimidin-2-amine (**2c**): Yellow solid, yield: 58%, mp = 127-129℃; 8.03 (d, *J* = 8.64 Hz, 2H, ArH), 8.00 (d, *J* = 8.36 Hz, 2H, ArH), 7.46 (d, *J* =8.36 Hz, 2H, ArH), 7.37 (s, 1H, Pyr-H), 7.00 (d, *J* = 8.56 Hz, 2H, ArH) 5.20 (s, 2H, NH_2), 3.88 (s, 3H, CH_3);

^{13}C NMR (400 MHz, $CDCl_3$, δ, ppm): 165.88, 164.64, 163.55, 161.76, 136.47, 136.47, 129.91, 128.96, 128.64, 128.40, 114.14, 103.18, 55.43 (OCH_3).

4,6-bis(4-methoxyphenyl) pyrimidin-2-amine (**2d**); Yellow solid, yield: 65 %, mp = 171-173 ℃; ^{1}H NMR (400 MHz, $CDCl_3$, δ, ppm): 8.04 (d, *J* = 8.66 Hz, 4H, ArH), 7.36 (s, 1H, Pyr-H) 7.00 (d, *J* = 8.69 Hz,4H, ArH), 5.36 (s, 2H, NH_2), 3.87 (s, 6H, $2CH_3$); ^{13}C NMR (400 MHz, $CDCl_3$, δ, ppm): 165.19, 162.97, 161.77, 129.78, 128.69, 114.15, 102.64, 55.43 (OCH_3).

4-(3,4-dimethoxyphenyl)-6-(4-methoxyphenyl) pyrimidin-2-amine (**2e**) : Yellow solid, yield: 61 %, mp = 157-159 ℃; ^{1}H NMR (400 MHz, $CDCl_3$, δ, ppm): 8.04 (d, *J* = 8.86 Hz, 2H, ArH), 7.71 (d, *J* = 1.92 Hz, 1H, ArH), 7.63 (dd, *J* = 8.55, 2.0 Hz,1H, ArH), 7.36 (s, 1H, Pyr-H), 7.00 (d, *J* = 8.84 Hz, 1H, ArH), 6.96 (d, *J* = 8.45 Hz, 1H, ArH), 5.35 (s, 2H, NH_2), 4.00 (s, 3H, CH_3), 3.95 (s, 3H, CH_3), 3.87 (s, 3H, CH_3).

4,6-bis(3,4-dimethoxyphenyl)pyrimidin-2-amine (**2f**): Yellow solid, yield: 67 %, ^{1}H NMR (400 MHz, $CDCl_3$, δ, ppm): 7.71 (s, 2H, ArH), 7.62 (dd, *J* = 8.45, 1.69 Hz, 2H, ArH), 7.37 (s, 1H, Pyr-H), 6.96 (d, *J* = 8.40 Hz, 1H, ArH), 5.25 (s, 2H, NH_2), 4.00 (s, 6H, $2CH_3$), 3.95 (s, 6H, $2CH_3$).

3.5.1.3 A typical procedure for the synthesis of 4,6-diphenylpyrimidin-2-ol (3a-3f)

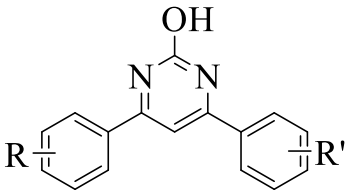

3a	R = 4-H,	R' = 4-H
3b	R = 4-Me,	R' = 4-Cl
3c	R = 4- Me,	R' = 4-MeO
3d	R = 4-MeO,	R' = 4-MeO
3e	R = 3,4-MeO,	R' = 4-MeO
3f	R = 3,4-MeO,	R' =3,4-MeO,

4,6-Diphenylpyrimidin-2-amine (**2**) (4 g, 12.76 mmol) was dissolved in acetic acid (100 mL), and whilst stirring a solution of 10 eq $NaNO_2$ dissolved in H_2O (50 ml) was slowly added at room temperature. The reaction mixture was further stirred for 3 hours. The progression of the reaction was monitored using TLC. The precipitate formed was filtered and washed with excess water and dried under a vacuum. The crude product was recrystallized in EtOH to obtain the following pure compounds in good yield.

4,6-diphenylpyrimidin-2-ol (**3a**): Yellow solid, yield: 85 %, mp = 231-234 ℃; ^{1}H NMR (400 MHz, DMSO-d$_6$, *δ*, ppm): 11.96 (s, 1H, Pyr-O**H**), 8.17(d, *J* = 6.56 Hz, 4H, ArH), 7.57-7.55 (m, 7H, ArH); ^{13}C NMR (400 MHz, DMSO-d$_6$, *δ*, ppm): 134.78, 131.42, 128.79, 127.54, 100.40.

4-(4-chlorophenyl)-6-(p-tolyl)pyrimidin-2-ol (**3b**): Yellow solid, yield: 89 %, mp = <300 ℃; ^{1}H NMR (400 MHz, DMSO-d$_6$, *δ*, ppm): 11.83 (s, 1H, Pyr-O**H**), 8.14 (d, *J* = 8.56 Hz, 1H, ArH), 8.13 (d, *J* = 8.76 Hz, 2H, ArH), 7.79-7.77 (m, 1H, ArH), 7.69 (d, *J* = 1.56 Hz, 2H, ArH), 7.08 (d, *J* = 8.84 Hz, 2H, ArH), 3.88 (s, 3H, OCH$_3$), 3.85 (s, 6H, 2OCH$_3$).

4-(4-methoxyphenyl)-6-(p-tolyl)pyrimidin-2-ol (**3d**): Yellow solid, yield: 91 %, mp = 235-237 ℃;, ^{1}H NMR (400 MHz, DMSO-d$_6$, *δ*, ppm): 11.85 (s, 1H, Pyr-O**H**), 8.16 (d, *J* = 8.74 Hz, 2H, ArH), 8.04 (d, *J* = 7.97 Hz, 2H, ArH), 7.44 (s, 1H, pyr-H), 7.35 (d, *J* = 7.98 Hz, 2H, ArH), 7.09 (d, *J* = 8.97 Hz, 2H, ArH), 3.85 (s, 3H, OCH$_3$), 2.39(s, 3H, CH$_3$); ^{13}C NMR (400 MHz, DMSO-d$_6$, *δ*, ppm): 162.05, 141.51, 129.39, 129.35, 127.46, 114.18, 55.46 (OCH$_3$), 55.99 (CH$_3$).

4,6-bis(4-methoxyphenyl)pyrimidin-2-ol (**3d**): Yellow solid, yield: 90 %, mp = <300 ℃; ^{1}H NMR (400 MHz, DMSO-d$_6$, *δ*, ppm): 11.82 (s, 1H, Pyr-O**H**), 8.14 (d, *J* = 8.53 Hz, 2H, ArH), 7.41 (s, 1H, pyr-H), 7.09 (d, *J* = 8.91 Hz, 2H, ArH), 3.85 (s, 6H, 2OCH$_3$), ^{13}C NMR (400 MHz, DMSO-d$_6$, *δ*, ppm): 162.00, 129.32, 114.18, 55.46 (2OCH$_3$).

4-(3,4-dimethoxyphenyl)-6-(4-methoxyphenyl)pyrimidin-2-ol **(3e)**: Yellow solid, yield: 89 %, mp = 235-237 ℃; ^{1}H NMR (400 MHz, DMSO-d$_6$, *δ*, ppm): 11.83 (s, 1H, Pyr-O**H**), 7.79 (d, *J* = 7.29 Hz, 2H, ArH), 7.70 (d, *J* = 7.71 Hz, 2H, ArH), 7.41 (s, 1H, ArH), 7.10 (d, *J* = 8.2 Hz, 2H, ArH), 3.88 (s, 3H, OCH$_3$), 3.85(s, 3H, OCH$_3$); ^{13}C NMR (400 MHz, DMSO-d$_6$, *δ*, ppm): 162.00, 151.74, 148.77, 129.37, 129.31, 121.10, 114.7, 111.47, 110.43, 97.91, 55.71 (OCH$_3$), 55.45 (2OCH$_3$).

4,6-bis(3,4-dimethoxyphenyl)pyrimidin-2-ol **(3f)**: Yellow solid, yield: 93 %, mp = <300℃; ^{1}H NMR (400 MHz, DMSO-d$_6$, *δ*, ppm): 11.83 (s, 1H, Pyr-O**H**), 7.79 (d, *J* = 7.29 Hz, 2H, ArH), 7.70 (d, *J* = 7.71 Hz, 2H, ArH), 7.41 (s, 1H, ArH), 7.10 (d, *J* = 8.2 Hz, 2H, ArH), 3.88 (s, 6H, 2OCH$_3$), 3.85(s, 6H, 2OCH$_3$); ^{13}C NMR (400 MHz, DMSO-d$_6$, *δ*, ppm): 151.73, 148.72, 121.18, 111.42, 110.43, 55.66 (4OCH$_3$); HRMS (ESI, *m/z*) [M+Na] calculated for $C_{20}H_{20}N_2O_5$, 391.1270; found 391.1279.

3.5.1.4 A typical procedure for the synthesis of 2-chloro-4,6-diphenylpyrimidine

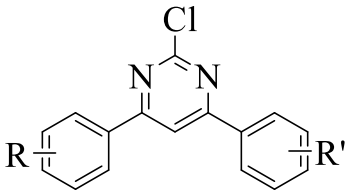

4a	R = 4-H,	R' = 4-H
4b	R = 4-Me,	R' = 4-Cl
4c	R = 4- Me,	R' = 4-MeO
4d	R = 4-MeO,	R' = 4-MeO
4e	R = 3,4-MeO,	R' = 4-MeO
4f	R = 3,4-MeO,	R' =3,4-MeO

A solution of 4,6-diphenylpyrimidin-2-ol (4g, 16.11 mmol) and 0.4 mL DMF in $POCl_3$ (20 mL) was refluxed for 6 hours. The reaction completion was monitored by TLC. The reaction was added into ice water, and the precipitate formed was filtered, washed with water and dried under vacuum. The crude compound was purified by column chromatography using EtOAc/hexane (1:9) eluent to obtain pure compounds.

2-chloro-4,6-diphenylpyrimidine **(4a)**: Yellow solid, yield: 93 %, mp = 115-116 °C; ^{1}H NMR (400 MHz, $CDCl_3$, δ, ppm): 8.07-8.05 (m, 4H, ArH), 7.51-7.49 (m, 6H, ArH), 7.46 (s, 1H, ArH), 5.35 (s, 2H, NH_2).

2-chloro-4-(4-chlorophenyl)-6-(p-tolyl)pyrimidine (**4b**): Yellow solid, yield: 89%, ^{1}H NMR (400 MHz, $CDCl_3$, δ, ppm): 8.09 (d, *J* = 8.52 Hz, 2H, ArH), 8.04 (d, *J* = 8.16 Hz, 2H, ArH), 7.94 (s, 1H, Pyr-H), 7.50 (d, *J* = 8.52 Hz, 2H, ArH), 7.33 (d, *J* = 8.00 Hz, 2H, ArH), 2.44 (s, 3H, CH_3); ^{13}C NMR (400 MHz, $CDCl_3$, δ, ppm): 166.77, 165.13, 161.05, 141.46, 136.88, 133.16, 131.65, 128.83, 128.30, 127.68, 126.37, 109.20, 20.51(CH_3).

2-chloro-4-(4-chlorophenyl)-6-(4-methoxyphenyl)pyrimidine (**4c**): Yellow solid, yield: 95%, ^{1}H NMR (400 MHz, $CDCl_3$, δ, ppm): 8.11 (d, *J* = 8.84 Hz, 2H, ArH), 8.07 (d, *J* = 8.56 Hz, 2H, ArH), 7.88 (s, 1H, Pyr-H), 7.49 (d, *J* = 8.68 Hz, 2H, ArH), 7.02 (d, *J* = 8.92 Hz, 2H, ArH), 3.89 (s, 3H, OCH_3); ^{13}C NMR (400 MHz, $CDCl_3$, δ, ppm): 167.27, 165.95, 162.75, 162.02, 137.82, 134.25, 129.30, 129.16, 128.67, 127.81, 114.46, 109.62, 55.50 (OCH_3).

2-chloro-4,6-bis(4-methoxyphenyl)pyrimidine (**4d**): Yellow solid, yield: 93%, mp = 187-190°C; ^{1}H NMR (400 MHz, $CDCl_3$, δ, ppm): 8.10 (d, *J* = 8.48 Hz, 3H, ArH), 7.87 (d, *J* = 8.84 Hz, 1H, ArH), 7.85 (s, 1H, Pyr-H), 7.01 (dd, *J* = 8.50 Hz, 1.74 Hz, 4H, ArH), 3.88 (s, 6H, 2OCH_3); ^{13}C

NMR (400 MHz, $CDCl_3$, δ, ppm): 166.74, 166.52, 162.51, 161.84, 161.58, 131.61, 129.10, 128.19, 127.90, 114.39,113.67, 109.01, 55.49(OCH_3), 55.44 (OCH_3).

2-chloro-4,6-bis(4-methoxyphenyl)pyrimidine (**4e**): Yellow solid, yield: 93 %, mp = 187-190℃; ^{1}H NMR (400 MHz, $CDCl_3$, δ, ppm): 8.10 (d, *J* = 8.48 Hz, 3H, ArH), 7.87 (d, *J* = 8.84 Hz, 1H, ArH), 7.85 (s, 1H, Pyr-H), 7.01 (dd, *J* = 8.50 Hz, 1.74 Hz, 4H, ArH), 3.88 (s, 6H, 2OCH_3); ^{13}C NMR (400 MHz, $CDCl_3$, δ, ppm): 166.74, 166.52, 162.51, 161.84, 161.58, 131.61, 129.10, 128.19, 127.90, 114.39, 113.67, 109.01, 55.49(OCH_3), 55.44 (OCH_3).

2-chloro-4-(3,4-dimethoxyphenyl)-6-(4-methoxyphenyl)pyrimidine (**4f**): Yellow solid, yield: 89 %, mp = 138-141℃; ^{1}H NMR (400 MHz, $CDCl_3$, δ, ppm): 8.12 (d, *J* = 8.88 Hz, 2H, ArH), 7.87 (d, *J* = 8.84 Hz, 1H, ArH), 7.85 (s, 1H, Pyr-H), 7.01 (d, *J* = 8.88, 2H, ArH), 6.96 (d, *J* = 8.36, 1H, ArH), 4.00 (s, 3H, OCH_3), 3.95 (s, 3H, OCH_3), 3.88 (s, 3H, OCH_3); ^{13}C NMR (400 MHz, $CDCl_3$, δ, ppm): 164.28, 164.24, 162.78, 161.40, 150.90, 149.06, 131.44, 131.04, 120.01, 113.92, 110.87, 110.05, 99.65, 56.00 (OCH_3), 55.95 (OCH_3), 55.39 (OCH_3).

2-chloro-4,6-bis(3,4-dimethoxyphenyl)pyrimidine (**4g**): Yellow solid, yield: 78 %, mp = 180-183℃; ^{1}H NMR (400 MHz, $CDCl_3$, δ, ppm): 7.86 (s, 1H, ArH), 7.74 (s, 2H, ArH), 7.69 (d, *J* = 7.12 Hz, 2H, ArH), 6.97 (d, *J* = 7.76 Hz, 2H, ArH), 4.00 (s, 6H, 2OCH_3), 3.96 (s, 6H, 2OCH_3).

3.5.1.5 A typical procedure for the synthesis of 4,6-diphenyl-2-(piperazin-1-yl)pyrimidine

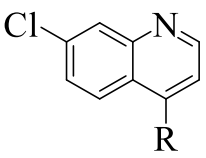

5a R = ethane-1,2-diamine

5d R = propane-1,3-diamine

5c R = butane-1,4-diamine

5d R = piperazin-1-yl

A reaction mixture of 2-chloro-4,6-diphenylpyrimidine (4.0 g, 15 mmol) and piperazine (13.92 g, 150 mmol) in isopropanol (20 mL) was refluxed for 20 hours. The progression of the reaction was monitored by TLC. The reaction mixture was added to 2 M NaOH (100 mL) solution, and the precipitate formed was filtered, washed with water and diethyl ether, and dried under vacuum. The crude product was purified by recrystallised in EtOAc to obtain the following pure compounds.

N^1-(7-chloroquinolin-4-yl)ethane-1,2-diamine (**5a**): Yellow solid, yield: 97 %, mp = 137-139 ℃; ^{1}H NMR (400 MHz, DMSO-d_6, δ, ppm): 8.33 (d, J = 5.48 Hz, 1H, ArH), 8.20 (d, J = 9.01 Hz, 1H, ArH), 7.76 (d, J = 1.84 Hz, 1H, ArH), 7.40 (dd, J = 9.00 Hz, 1.85 Hz, 1H, ArH), 7.26 (s, 1H, -NH), 6.50 (d, J = 5.56 Hz, 1H, ArH), 3.27 (br.s, 2H, CH_2), 2.79 (t, J = 6.38 Hz, 2H, CH_2); ^{13}C NMR (400 MHz, DMSO-d_6, δ, ppm): 152.35, 152.27, 150.06, 149.02, 134.24, 127.41, 124.78, 117.80, 99.25, 45.58.

N^1-(7-chloroquinolin-4-yl)propane-1,3-diamine (**5b**): Yellow solid, yield: 98 %, mp = 88-90℃; ^{1}H NMR (400 MHz, DMSO-d_6, δ, ppm): 8.32 (d, J = 5.06 Hz, 1H, ArH), 8.17 (d, J = 8.92 Hz, 1H, ArH), 7.75 (d, J = 4.92Hz, 1H, ArH), 7.68 (br.s, 1H, -NH), 7.40 (d, J = 7.20 Hz, 1H, ArH), 6.48 (d, J = 5.54 Hz, 1H, ArH), 3.30 (t, J = 6.90Hz, 2H, ArH), 2.66 (t, J = 6.60 Hz, 2H, CH_2), 1.74 (q, J = 6.75 Hz, 2H, CH_2), ^{13}C NMR (400 MHz, DMSO-d_6, δ, ppm): 151.83, 151.70, 150.36,148.45, 133.64, 126.84, 126.84, 124.22, 123.89, 122.04, 98.61, 40.20.

N^1-(7-chloroquinolin-4-yl)butane-1,4-diamine (**5c**): White solid, yield: 99 %, mp = 121-124 ℃; ^{1}H NMR (400 MHz, DMSO-d_6, δ, ppm): 8.32 (d, J = 5.48 Hz, 1H, ArH), 8.19 (d, J = 9.01 Hz, 1H, ArH), 7.76 (d, J = 1.64 Hz, 1H, ArH), 7.39 (dd, J = 8.94, 1.64, Hz, 1H, ArH), 7.36 (br.s, 1H, -NH), 6.44 (d, J = 5.56 Hz, 1H, ArH), 3.23 (t, J = 6.90 Hz, 2H, CH_2), 2.54 (t, J = 6.98 Hz, 2H, CH_2), 1.62 (q, J = 6.98 Hz, 2H, CH_2), 1.44 (p, J = 7.35 Hz, 2H, CH_2); ^{13}C NMR (400 MHz, DMSO-d_6, δ, ppm): 151.25, 149.91, 148.02, 133.19, 126.38, 123.72, 123.43, 116.77, 98.13, 41.79(CH_2), 40.88 (CH_2), 29.49 (CH_2), 24.67 (CH_2).

7-chloro-4-(piperazin-1-yl)quinoline (**5d**): Yellow solid, yield: 100 %, mp = 113-115 ℃;^{1}H NMR (400 MHz, DMSO-d_6, δ, ppm): 8.68 (d, J = 5.00 Hz, 1H, ArH), 8.01 (d, J = 9.00 Hz, 1H, ArH), 7.96 (d, J = 2.16 Hz, 1H, ArH), 7.53 (dd. J = 8.98 Hz, 2.26 Hz, 1H, ArH), 3.09-3.07 (m, 4H, 2CH_2), 2.97-2.94 (m, 4H, 2CH_2); ^{13}C NMR (400 MHz, DMSO-d_6, δ, ppm): 156.42, 151.17, 151.88, 149.61, 148.78, 141.29, 135.36, 133.53, 128.69, 128.11, 128.02, 126.04, 125.80, 125.69, 124.25, 122.03, 121.31, 109.37, 109.37, 51.86, 44.69.

3.5.1.6 A typical procedure for the synthesis of N^1-(7-chloroquinolin-4-yl)-N2-(4,6-diphenylpyrimidin-2-yl) ethane-1,2-diamine

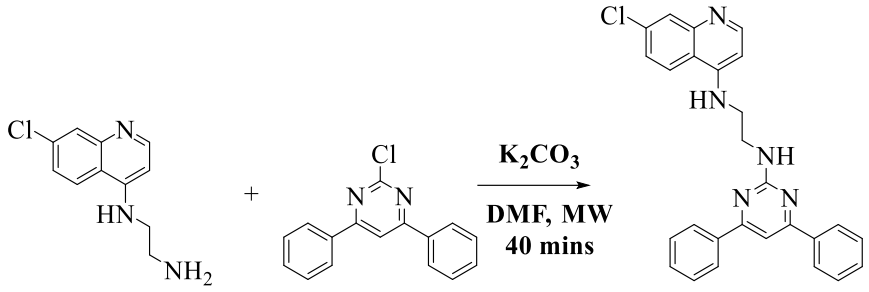

A solution of 2-chloro-4,6-diphenylpyrimidine **(6)** (120.65 mg, 0.45 mmol)**,** *N*^{1}-(7-chloroquinolin-4-yl) ethane-1,2-diamine **(5)** (100 mg, 0.45 mmol) and K_2CO_3 (125.03 mg, 0.91 mmol) in DMF (2 mL) was discharged to a microwave at temperature 120 ºC, pressure 150 Psi and power 150 Watts for 40 minutes. The progression of the reaction was monitored using TLC. The reaction mixture was added to ice water. The precipitate formed was filtered, washed with water and dried under vacuum. The compound was purified using silica gel in a chromatographic column with eluent 1% MeOH in DCM to afford the following pure compounds.

7-chloro-4-(4-(4,6-diphenylpyrimidin-2-yl)piperazin-1-yl)quinoline (**6a**): Yellow solid, yield: 65 % , mp = 169-172 ℃; ^{1}H NMR (400 MHz, $CDCl_3$, *δ*, ppm): 8.76 (d, *J* = 4.35 Hz, 1H, ArH), 8.14 (d, *J* = 3.63 Hz, 3H, ArH), 8.08-8.07 (m, 2H, ArH), 7.82 (d, *J* = 3.44 Hz, 1H, ArH), 7.51-7.48 (m, 8H, ArH), 6.89 (d, *J* = 8.45 Hz, 1H, ArH), 4.33-4.19 (m, 4H, $2CH_2$), 3.36-3.29 (m, 4H, $2CH_2$); ^{13}C NMR (400 MHz, $CDCl_3$, *δ*, ppm): 163.76, 157.09, 151.13, 150.64, 141.49, 134.83, 129.77, 129.11, 127.48, 127.28, 126.89, 124.60, 123.09, 122.09, 111.96, 103.09, 98.16, 56.37, 40.20, 21.47.

N^1*-(4-(4-chlorophenyl)-6-(p-tolyl)pyrimidin-2-yl)-N*^{4}*-(7-chloroquinolin-4-yl)butane-1,4-diamine* (**6b**): Yellow solid, yield: 84 %, mp = 192-194 ℃; ^{1}H NMR (400 MHz, $CDCl_3$, *δ*, ppm): 8.50 (d, *J* = 5.32 Hz, 1H, ArH), 7.94 (d, *J* = 1.99 Hz, 1H, ArH), 7.70 (d, *J* =8.43 Hz, 2H, ArH), 7.65 (d, *J* = 7.97 Hz, 2H, ArH), 7.54 (d, *J* = 8.96 Hz, 1H, ArH), 7.41 (d, *J* = 8.44 Hz, 2H, ArH), 7.29 (dd, *J* = 8.92, 2.07 Hz, 1H, ArH), 7.24 (d, *J* = 8.24 Hz, 3H, ArH), 6.36 (d, *J* = 5.34 Hz, 1H, ArH), 5.36 (t, *J* = 5.95 Hz, 1H, NH), 5.03 (br.s, 1H, NH), 3.55 (q, *J* = 3.55 Hz, 2H, CH_2), 3.55 (q, *J* = 5.55 Hz, 2H, CH_2), 2.40 (s, 3H, CH_3), 1.85-1.79 (m, 4H, $2CH_2$); ^{13}C NMR (400 MHz, $CDCl_3$, *δ,* ppm): 160.03, 151.87, 149.66, 148.95, 139.99, 135.92, 135.76, 134.91, 134.46, 130.69, 129.15, 128.76,

128.29, 125.81, 117.08, 114.71, 99.03, 42.98(CH_2), 41.16(CH_2), 27.45(CH_2), 25.93 (CH_2), 21.44 (CH_3).

7-chloro-4-(4-(4-(4-chlorophenyl)-6-(p-tolyl)pyrimidin-2-yl)piperazin-1-yl)quinoline (**6c**)*:* Yellow solid, yield: 82%, mp = 215-217 °C; ^{1}H NMR (400 MHz, $CDCl_3$, *δ*, ppm): 8.74 (d, *J* = 4.90 Hz, 1H, ArH), 8.07 (m, 4H, ArH), 8.01 -8.06 (d, *J* = 8.16 Hz, 2H, ArH), 7.47 (d, *J* = 8.49 Hz, 3H, ArH), 7.40 (s, 1H, ArH), 7.31 (d, *J* = 8.04 Hz, 2H, ArH), 6.88 (d, *J* = 5.00 Hz, 1H, ArH), 4.31 (t, *J* = 4.58 Hz, 4H, 2CH_2), 3.35(t, *J* = 4.86 Hz, 4H, 2CH_2), 2.44 (s, 3H, CH_3); ^{13}C NMR (400 MHz, $CDCl_3$, *δ,* ppm): 163.96, 162.21, 157.09, 151.99, 150.21, 140.96, 136.56, 136.49, 135.05, 129.47, 128.98, 128.39, 127.03, 126.35, 125.15, 122.02, 1032.16, 101.90, 52.33, 44.00, 21.46.

N^1-(7-chloroquinolin-4-yl)-N^2-(4-(4-methoxyphenyl)-6-(p-tolyl)pyrimidin-2-yl)ethane-1,2-diamine **(6d)**: Yellow solid, yield: 88%, mp = 154-157 °C; ^{1}H NMR (400 MHz, $CDCl_3$, *δ*, ppm): 8.43 (d, *J* = 3.67 Hz, 1H, ArH), 8.15 (s, 1H, ArH), 8.01 (br s, 4H, ArH), 7.81 (s, 1H, ArH), 7.40 (s, 1H, ArH), 7.34 (d, *J* = 7.09 Hz, 3H, ArH), 7.11-7.02 (m, 3H, ArH), 6.46 (br, s, 1H, NH), 6.30 (d. *J* = 5.28 Hz, 1H, ArH), 5.90 (br s, 1H, NH), 4.05-4.04 (m, 2H, CH_2), 3.97 (s, 3H, CH_3), 3.51-3.50 (m, 2H, CH_2), 2.46 (s, 3H, CH_3); ^{13}C NMR (400 MHz, $CDCl_3$, *δ,* ppm): 163.89, 157.23, 151.26, 150.77, 134.97, 129.90, 129.24, 127.62, 127.42, 127.02, 124.74, 112.10, 103.23, 98.29, 56.50, 40.33, 21.60, 14.25.

N^1-(7-chloroquinolin-4-yl)-N^3-(4-(4-methoxyphenyl)-6-(p-tolyl)pyrimidin-2-yl)propane-1,3-diamine (**6e**): Yellow solid, yield: 76%, mp = 97-99 °C; ^{1}H NMR (400 MHz, $CDCl_3$, *δ*, ppm): 8.42 (s, 1H, ArH), 8.09 (d, *J* = 1.99 Hz, 1H, ArH), 7.91 (t, *J* = 16.44 Hz, 5H, ArH), 7.42 (d, *J* = 8.73 Hz, 1H, ArH), 7.28 (s, 2H, ArH), 7.00-6.94 (m, 2H, ArH), 6.37 (d, *J* = 4.89 Hz, 1H, ArH), 5.69 (br.s, 1H, -NH), 5.48 (t, *J* = 4.89 Hz, 1H, -NH), 3.96 (s, 3H, OCH_3), 3.81 (q, *J* = 6.16 Hz, 2H, CH_2), 3.52-3.48 (m, 2H, ArH), 2.44 (s, 3H, CH_3), 2.10 (q, *J* = 6.09 Hz, 2H, CH_2); ^{13}C NMR (400 MHz, $CDCl_3$, *δ*, ppm): 166.06, 164.01, 163.17, 156.82, 140.94, 135.07, 129.58, 128.99, 127.06, 126.68, 125.26, 122.97, 121.37, 111.83, 102.59, 56.32 (OCH_3), 40.59 (C-NH_2) , 38.75(C-NH_2) , 28.89(CH_2), 21.44 (CH_3).

7-chloro-4-(4-(4-(4-methoxyphenyl)-6-(p-tolyl)pyrimidin-2-yl)piperazin-1-yl)quinoline **(6f)**: Yellow solid, yield: 83 %, mp = 191-193 °C; FTIR (ATR, *Vmax*, cm-1): 3038 (C-H), 2998 (C-H of CH_3), 2956 (C-H of CH_3), 1438-1565 (C=C of Ar), 1237 (C-O), 773 (C-Cl), ^{1}H NMR (400 MHz, $CDCl_3$, *δ*, ppm): 8.74 (d, *J* = 4.96 Hz, 1H, ArH), 8.12 (d, *J* = 8.80 Hz, 2H, ArH), 8.08 (s,

1H, ArH), 8.06 (d, *J* = 5.69 Hz, 1H, ArH), 8.04 (d, *J* = 8.09 Hz, 3H, ArH) 7.47 (dd, *J* = 8.99, 1.99 Hz, 1H, ArH), 7.40 (s, 2H, CH_2), 7.30 (d, *J* = 8.04 Hz, 2H, ArH), 7.01 (d, *J* = 8.79 Hz, 2H, ArH), 6.88 (d, *J* = 5.02 Hz, 1H, ArH), 4.31-4.29 (m, 4H, $2CH_2$), 3.89 (s, 3H, OCH_3), 3.35 (t, q =4.83 Hz,4H, $2CH_2$) 2.43 (s, 3H, CH_3); ^{13}C NMR (400 MHz, $CDCl_3$, *δ,* ppm): 164.71, 162.12, 157.13, 151.96, 151.25, 150.17, 149.17, 135.06, 130.93, 128.94, 126.35, 125.19, 122.00, 120.24, 110.96, 110.13, 109.14, 101.48, 56.11(2OMe), 56.04 (2OMe), 52.38 ($2CH_2$), 44.03 ($2CH_2$), 21.44 (CH_3).

N^1-(4,6-bis(4-methoxyphenyl)pyrimidin-2-yl)-N^4-(7-chloroquinolin-4-yl)butane-1,4-diamine (**6g**): Yellow solid, yield: 83 %, mp = 144-145 ℃; FTIR (ATR, *Vmax*, cm-1): 3256 (N-H), 3069, 2932 (C-H, CH_3), 1573-1450 (C=C, Ar) 1239 (C-O), 763 (C-Cl); ^{1}H NMR (400 MHz, $CDCl_3$, *δ*, ppm): 8.38 (d, *J* = 5.57 Hz, 1H, ArH),), 8.03 (d, *J* = 8.81 Hz, 3H, ArH), 7.91 (d, *J* = 2.10 Hz, 1H, ArH), 7.76 (d, *J* = 8.69 Hz, 1H, ArH), 7.62 (d, *J* = 8.97 Hz, 1H, ArH), 7.30 (s, 1H, ArH), 7.21 (dd, *J* = 7.20, 2.04 Hz, 1H, ArH) 6.96 (d, *J* = 8.72 Hz, 5H, ArH), 6.35 (d, *J* = 5.61 Hz, 1H, ArH), 5.55 (br.s, 1H, NH), 5.40 (t, *J* = 6.01Hz, 1H, NH), 3.85 (s, 6H, $2OCH_2$), 3.66 (m, 1H, NH),), 5.56- 5.48 (m, 1H, NH), 3.19 (s, 6H, $2CH_3$), 3.81-3.60 (m, 2H, CH_2), 3.51 (q, *J* = 6.27 Hz, 2H, CH_2), 3.51 (q, *J* = 6.10 Hz, 2H, CH_2), 1.91-1.82 (m, 4H, $2CH_2$); ^{13}C NMR (400 MHz, $CDCl_3$, *δ,* ppm): 164.91, 162.99, 161.58, 150.40, 135.35, 130.97, 130.41, 128.45, 127.51, 125.47, 121.41, 116.86, 114.03, 113.37, 101.53, 99.89, 55.40 2(OCH_3), 42.99 (C-NH), 40.84 (C-NH), 27.42 (CH_2), 25.96 (CH_2); HRMS (ESI, *m/z*) $[M+Na]^+$; calculated for $C_{31}H_{30}ClN_5O_2$, 562.1972, found 562.1986.

4-(4-(4,6-bis(4-methoxyphenyl)pyrimidin-2-yl)piperazin-1-yl)-7-chloroquinoline (**6h**): Yellow solid, yield: 87 %, mp = 191-195 ℃; FTIR (ATR, *Vmax*, cm-1): 3037, 2996 (C-H, CH_3), 1604-1419 (C=C, Ar) 1242 (C-O), 812 (C-Cl); ^{1}H NMR (400 MHz, $CDCl_3$, *δ*, ppm): 8.74 (d, *J* = 4.98 Hz, 1H, ArH), 8.11 (d, *J* = 8.85 Hz, 3H, ArH), 8.13-8.01 (m, 2H, ArH), 7.86 (d, *J* = 8.84 Hz, 1H, ArH), 7.47 (dd, *J* = 9.05, 2.01 Hz, 1H, ArH), 7.37 (s, 1H, ArH), 7.01 (d, *J* = 8.81 Hz, 4H, ArH), 6.88 (d, *J* = 5.03 Hz, 1H, ArH), 4.31-4.29 (m, 4H, $2CH_2$), 3.88 (s, 6H, $2CH_3$), 3.35 (t, *J* = 4.88 Hz, 4H, $2CH_3$), 1.29 (s, 3H, CH_3); ^{13}C NMR (400 MHz, $CDCl_3$, *δ,* ppm): 164.71, 162.12, 157.13, 151.96, 151.25, 150.17, 149.17, 135.06, 130.93, 128.94, 126.35, 125.19, 122.00, 120.24, 110.96, 110.13, 109.14, 101.48, 56.11(2OMe), 56.04 (2OMe), 52.38 ($2CH_2$), 44.03 ($2CH_2$); HRMS (ESI, *m/z*) $[M+H]^+$; calculated for $C_{31}H_{28}ClN_5O_2$, 538.2010, found 538.2030.

N1-(7-chloroquinolin-4-yl)-N4-(4-(3,4-dimethoxyphenyl)-6-(4-methoxyphenyl)pyrimidin-2-yl)butane-1,4-diamine (**6i**)*;* Yellow solid, yield: 93% mp = 130-132 ℃; FTIR (ATR, *Vmax*, cm-

[1]): 3080 (C-H), 2935 (C-H of CH_3), 2956 (C-H of CH_3), 1438-1601 (C=C of Ar), 1179, 1260 (C-O), 773 (C-Cl), ^{1}H NMR (400 MHz, $CDCl_3$, *δ*, ppm): 8.39 (d, *J* = 5.52 Hz, 1H, ArH), 7.99 (d, *J* = 8.77 Hz, 3H, ArH), 7.89 (brs.1H, ArH), 7.73 (d, *J* = 8.72 Hz, 1H, ArH), 7.46-7.42 (m, 1H, ArH), 7.28 (s, 1H, ArH), 6.96 (d, *J* = 8.80 Hz, 1H, ArH), 6.35 (t, *J* = 4.47 Hz, 1H, ARH), 5.83-5.76 (m, 1H, NH), 5.56-5.49 (m, 1H, NH), 3.87 (s, 6H, $2OCH_3$), 3.85 (s, 3H, OCH_3), 3.78 (t, *J* = 5.76 Hz, 2H, $2CH_2$), 3.48 (t, *J* = 5.81 Hz, 2H, CH_2), 2.07 (q, *J* = 5.81 Hz, 2H, CH_2); ^{13}C NMR (400 MHz, $CDCl_3$, *δ,* ppm): 164.71, 162.13, 157.13, 151.96, 151.25, 150.17, 149.17, 135.06, 130.93, 128.94, 126.35, 125.19, 122.00, 120.24, 110.96, 110.13, 109.14, 101.48, 56.11 (2OMe), 56.04 (OMe), 52.38 ($2CH_2$), 44.03 ($2CH_2$).

7-chloro-4-(4-(4-(3,4-dimethoxyphenyl)-6-(4-methoxyphenyl)pyrimidin-2-yl)piperazin-1-yl)quinoline (**6j**): Yellow solid, yield: 79 % mp = 201-204 ℃; FTIR (ATR, *Vmax*, cm-1): 3276 (C-N), 3073, 2839 (C-H of CH_3), 1572-1430 (C=C Ar) 1298 (C-O), 763 (C-Cl), ^{1}H NMR (400 MHz, $CDCl_3$, *δ*, ppm): 8.74 (d, *J* = 4.97 Hz, 1H, ArH), 8.12 (d, *J* = 8.81 Hz, 2H, ArH), 8.02-8.10 (m, 2H, ArH), 7.74-7.70 (m, 2H, ArH), 7.47 (dd, *J* = 9.01, 1.99 Hz, 1H, ArH), 7.36 (s, 1H, ArH), 7.02 (d, *J* = 8.77 Hz, 2H, ArH), 6.98 (d, *J* = 8.27 Hz, 1H, ArH), 6.89 (d, *J* = 5.02 Hz, 1H, ArH), 4.31 (t, *J* = 4.40 Hz, 4H, $2CH_2$), 4.01 (s, 3H, CH_3), 3.96 (s, 3H, CH_3), 3.89 (s, 3H, CH_3), 3.36 (t, *J* = 4.40 Hz, 4H, $2CH_2$); ^{13}C NMR (400 MHz, $CDCl_3$, *δ,* ppm): 161.64, 157.15, 151.98, 151.19, 150.20, 149.15, 135.04, 130.99, 130.56, 128.95, 128.58, 126.33, 125.20, 122.03, 120.22, 114.04, 110.96, 110.07, 109.15, 101.25, 56.08, 56.04, 52.38, 44.03.

4-(4-(4,6-bis(3,4-dimethoxyphenyl)pyrimidin-2-yl)piperazin-1-yl)-7-chloroquinoline (**6k**): Yellow solid, yield: 88 %, mp = 249-251 ℃; FTIR (ATR, *Vmax*, cm-1): 3080 (C-H), 2935 (C-H of CH_3), 2956 (C-H of CH_3), 1438-1601 (C=C of Ar), 1179, 1260 (C-O), 773 (C-Cl), ^{1}H NMR (400 MHz, $CDCl_3$, *δ*, ppm): 8.74 (d, *J* = 4.96 Hz, 1H, ArH), 8.08 (m, 2H, ArH), 7.75-7.70 (m, 4H, ArH) 7.47 (dd, *J* = 9.01, 1.99 Hz, 1H, ArH), 7.36 (s, 1H, ArH), 6.98 (d, *J* = 8.40 Hz, 2H, ArH), 6.89 (d, *J* = 5.01 Hz, 1H, ArH), 4.30 (t, *J* = 4.10Hz, 4H, $2CH_2$), 4.01 (s, 6H, $2OCH_3$), 3.96 (s, 6H, $2OCH_3$), 3.36 (t, *J* = 4.73 Hz, 4H, $2CH_2$); ^{13}C NMR (400 MHz, $CDCl_3$, *δ,* ppm): 164.71, 162.13, 157.13, 151.96, 151.25, 150.17, 149.17, 135.06, 130.93, 128.94, 126.35, 125.19, 122.00, 120.24, 110.96, 110.13, 109.14, 101.48, 56.11(2OMe), 56.04 (2OMe), 52.38 ($2CH_2$), 44.03 ($2CH_2$).

3.5.1.7 A typical procedure for the synthesis of 4-(2-(4-(7-chloroquinolin-4-yl)piperazin-1-yl)-6-(4-hydroxyphenyl)pyrimidin-4-yl)benzene-1,2-diol

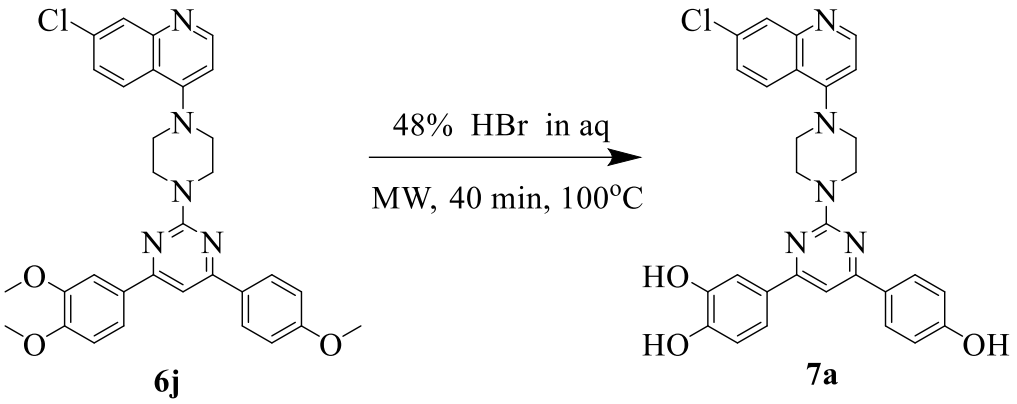

7a (50 mg, 0.10 mmol) in 48% aqueous HBr (2 mL) was discharged into a microwave and radiated at temperature 100 ºC, pressure 300 PSI and power 300 watts for 40 minutes. Using TLC, the development of the product was monitored. The precipitate formed was filtered and washed with water and diethyl ether. The crude product was recrystallized in ethanol to afford the following pure compounds in good yield.

4,4'-(2-((4-((7-chloroquinolin-4-yl)amino)butyl)amino)pyrimidine-4,6-diyl)diphenol (**7a**); Yellow solid, yield: 93 %, mp = 214-216 ℃; FTIR (ATR, V_{max}, cm^{-1}): 3351 (O-H), 3256 (N-H), 3061, 2944 (C-H, CH_3), 1443-1576 (C=C, Ar), 1281 (C-O), 791 (C-Cl);^{1}H NMR (400 MHz, $CDCl_3$, δ, ppm): 13.06 (s, 1H, ph-OH), 10.37 (br, s, 1H, ph-OH), 9.39-9.37 (m, 1H, NH), 8.55 (d, J = 9.21 Hz, ArH), 8.52 (br, s, 1H, NH), 8.24-8.05 (m, 4H, ArH), 7.90 (d, J = 2.05 Hz, 1H, ArH), 7.71 (dd, J = 9.08, 2.07 Hz, 1H, ArH), 7.66 (s, 1H, ArH), 7.30-7.23 (m, 4H, ArH), 6.36 (d, J = 5.32 Hz, 1H, ArH), 5.36 (t, J = 5.94 Hz, 1H, ArH), 6.93 (d, J = 7.16Hz, 5H, ArH), 5.62-2.61(m, 4H, $2CH_2$), 1.83 -1.80 (m, 4H, $2CH_2$); ^{13}C NMR (400 MHz, $CDCl_3$, δ, ppm): 160.68, 158.96, 155.90, 143.31, 138.84, 138.55, 134.17, 131.27, 129.70, 127.36, 127.33, 126.01, 119.51, 116.74, 115.83, 115.03, 114.89, 102.66, 100.54, 99.19, 99.13, 43.45, 40.95, 26.55, 25.43; HRMS (ESI, *m/z*) $[M+H]^+$; calculated for $C_{29}H_{26}ClN_5O_2$, 512.1853; found 512.1844.

4-(2-((4-((7-chloroquinolin-4-yl)amino)butyl)amino)-6-(4-hydroxyphenyl)pyrimidin-4-yl)benzene-1,2-diol (**7b**): Yellow solid, yield: 89 %, mp = 221 -223 ℃;FTIR (ATR, *Vmax*, cm^{-1}): 3418 (O-H), 3228 (N-H), 2927 (C-H of CH_3), 1439-1568 (C=C of Ar), 1273 (C-O), 759 (C-Cl); ^{1}H NMR (400 MHz, $CDCl_3$, δ, ppm): 9.90 (br.s, 2H, 2ph-OH), 8.80 (br, s, 1H, ph-OH), 8.50 (d, J

= 9.13 Hz, 1H, ArH), 8.41 (d, *J* = 6.64 Hz, 1H, ArH), 8.03 (d, *J* = 8.66 Hz, 4H, ArH), 8.24-8.05 (m, 4H, ArH), 7.87 (d, *J* = 1.96 Hz, 1H, ArH), 7.64 (dd, *J* = 9.12, 2.12 Hz, 1H, ArH), 7.44 (s, 1H, ArH), 7.09 (t, *J* = 5.87 Hz, 1H, NH), 6.82 (br s, 4H, (1NH, 3ArH), 6.76 (d, *J* = 6.66 Hz, 1H, ArH), 3.59-3.194 (m, 6H, $2CH_2$), 2.06 (t, *J* = 6.60 Hz, 2H, ArH); ^{13}C NMR (400 MHz, $CDCl_3$, *δ*, ppm): 163.08, 160.17, 154.32, 145.95, 137.11, 128.97, 128.78, 126.47, 125.67, 122.67, 116.60, 115.78, 114.92, 99.91, 99.15, 41.49, 40.61, 38.98, 28.23.

4-(2-(4-(7-chloroquinolin-4-yl)piperazin-1-yl)-6-(4-hydroxyphenyl)pyrimidin-4-yl)benzene-1,2-diol (**7c**): Yellow solid, yield: 94 %, mp = < 300 °C; FTIR (ATR, *Vmax*, cm^{-1}): 3418 (O-H), 3228 (N-H), 2927 (C-H of CH_3), 1439-1568 (C=C of Ar), 1273 (C-O), 759 (C-Cl); ^{1}H NMR (400 MHz, $CDCl_3$, *δ*, ppm): 9.93 (s, H, ph-O<u>H</u>), 9.43 (br s, 1H, ph-O<u>H</u>), 9.08 (s, H, 2ph-O<u>H</u>), 8.73 (d, *J* = 4.96 Hz, 1H, ArH), 8.20 (d, *J* = 9.00 Hz, 1H, ArH), 8.13 (d, *J* = 8.55 Hz, 2H, ArH), 8.01(d, *J* = 1.97 Hz, 1H, ArH), 7.73 (d, *J* = 2.04 Hz, 1H, ArH), 7.62-7.56 (m, 2H, ArH), 7.53 (s, 1H, ArH), 7.10 (d, *J* = 5.12 Hz, 1H, ArH), 6.90 (d, *J* = 8.56 Hz, 2H, ArH), 6.87 (d, *J* = 8.28 Hz, 1H, ArH), 4.19 (br.s, 4H, $2CH_2$); ^{13}C NMR (400 MHz, $CDCl_3$, *δ*, ppm): 164.63, 164.30, 162.03, 160.36, 157.13, 148.64, 145.95, 134.42, 129.81, 129.30, 129.13, 128.01, 126.86, 128.01, 126.86, 126.37, 121.73, 119.50, 116.06, 116.00, 115.89, 115.24, 114.85, 109.92, 100.28, 52.22, 43.99, 40.53.

3.6 Pharmacological evaluation

3.6.1 Antiplasmodial activity

The chloroquine-sensitive strain of *P. falciparum* (NF54) was maintained continuously *in vitro* in supplemented RPMI-1640 culture media at 37 °C and gassed with a mixture of 5% CO_2, 3% O_2 and 92% N_2 [29]. 5% D-sorbitol was used to synchronise the culture in the ring stage [30]. To determine the antimalarial activity of the compounds, the synchronised ring-stage parasites were adjusted to a final parasitaemia of 2% and 2% haematocrit, to which serial dilutions of the compounds and positive control, quinine were added after a 24 hours incubation. Negative controls included uninfected erythrocytes and drug-free parasitised erythrocytes. Following a further 48 h incubation period, the plates were frozen at -70 °C for 1 hour and thawed for 1 hour. Lysate (25 µl) were transferred to a second plate, to which 100 µL Malstat™ and 20 µL nitroblue tetrazolium-phenazine ethosulphate (1:1) mixture was added to each well and incubated for 40 min at 37 °C to quantify the parasite lactate dehydrogenase (pLDH) activity [31]. Thereafter, 5% acetic acid was added to each well, and the absorbance of the formazan products read at 620 nm as an indicator of

parasite viability. The percentage parasite growth, taking the appropriate controls into account, were calculated and used to determine the concentration required to inhibit parasite growth by 50% (IC_{50} value) from log sigmoid dose-response curves using the GraphPad Prism® 5.0.0 software. Each experiment was repeated in triplicate [32, 33].

3.6.2 Toxicity assays

3.6.2.1 Cell viability assay

Human embryonic kidney epithelial (HEK-293) cells were maintained at 37 °C in a humidified environment with a 5% CO_2 as a monolayer in Dulbecco's modified Eagle's medium (DMEM) supplemented with 10% fetal bovine serum, 100 IU/ml penicillin and 100 µg/ml streptomycin. A cell suspension (10 000 cells/well) was incubated at 37 °C for 48 hours with serial dilutions of compounds/positive control. A final concentration of less than 1% DMSO had no effect on the viability of the cells. Thereafter, 40 µL of (3-(4, 5-dimethylthiazolyl-2)-2, 5-diphenyltetrazolium bromide (MTT; 5mg/ml in phosphate buffer saline (pH 7.3)) was added to each well and incubated for a further 2 hours. DMSO was used to dissolve the formazan crystals and then quantified spectrophotometrically at an absorbance of 540 nm with a reference wavelength of 690 nm (Labsystems Multiskan RC) [34]. Percent cellular viability was determined using the appropriate controls and used to calculate the IC_{50} values which were compared to the positive control, camptothecin. The experiment was repeated in triplicate [35, 36].

3.6.2.2 Determination of binding affinity of select synthetic compounds to *P. falciparum* Hsp70

Recombinant forms of two essential cytosol localized *P. falciparum* Hsp70s; PfHsp70-1 and PfHsp70-z were expressed in *E. coli* and purified using nickel affinity chromatography following a previously described approach [21]. The binding affinities of the proteins for four selected compounds were determined by SPR analysis using the BioNavis™ 420A ILVES MP-SPR (BioNavis, Tampere, Finland) at 25 ºC as previously described [21]. A running buffer, degassed PBS Tween 20 (4.3 mM Na_2HPO_4, 1.4 mM KH_2PO_4, 137 mM NaCl, 3 mM KCl, 0.005 % (v/v) Tween 20, and 20 mM EDTA; pH 7.4) was used. The recombinant proteins were immobilised as ligands at 0.5 µg/ml onto functionalized 3D carboxymethyl dextran sensors (CMD 3D 500L; BioNavis, Tampere, Finland). Immobilization of ligands was achieved through amine coupling after 1-ethyl-3-(3-dimethylaminopropyl) carbodiimide (EDC) [Sigma Aldrich, Germany] and N-

hydroxy-succinimide (NHS) [Sigma Aldrich, Germany] activation following a protocol provided by the manufacturer (BioNavis, Tampere, Finland) to achieve <200 RUs. A reference channel without immobilized protein served as a control for non-specific binding and changes in refractive index. As analyte, compounds (**6h**, **6k**, **7a**, and **7b**) were prepared into aliquots of 0, 1.25, 2.5, 5 and 10 nM injected three times at a flow rate of 50 µL/min into each flow cell. Injections with buffer only were used as controls. Association between ligand and analyte was allowed for 3 min, and dissociation was monitored for a total of 10 min. Kinetics steady-state equilibrium constant data was processed after double referencing of the sensorgrams and concatenating the responses of all five analyte concentrations by global fitting using TraceDrawer software version 1.8 (Ridgeview Instruments, Sweden).

3.7 Molecular docking

The molecular docking software utilized in this study was the Autodock Vina Plugin available on Chimera [37], with default docking parameters. Homology model of PfHsp70-1 (PlasmoDB accession number: PF3D7_0818900) and PfHsp70-z (PlasmoDB accession number: PF3D7_0708800.1) were also built using chimera software [38]. Gasteiger charges were added to the compounds, and the non-polar hydrogen atoms were merged to carbon atoms. The PCs were then docked into the active site pocket of PfHsp70-1 and PfHsp70-z (by defining the grid box with a spacing of 1 Å and size of 35 × 43 × 45 and 43 x 40 x 32 pointing in x, y and z directions, respectively). The four compounds' systems were then subjected to molecular dynamics simulations.

3.7.1.1 Molecular Dynamic (MD) Simulations

The MD simulation was performed as described by Idowu *et al.* (2019) with little modification. The simulations were performed using the GPU version provided with the AMBER package (AMBER 18), in which the FF18SB variant of the AMBER force field [39] was used to describe the systems.

ANTECHAMBER was used to generate atomic partial charges for the compounds by utilizing the Restrained Electrostatic Potential (RESP) and the General Amber Force Field (GAFF) procedures. The Leap module of AMBER 18 allowed for the addition of hydrogen atoms, as well as Na^+ counter ions for neutralization of all (both PfHsp70-1 and PfHsp70-z) systems. The amino acids were numbered, numbering residues 1-658 for PfHsp70-1 and 1-567 for PfHsp70-z. The systems

were then suspended implicitly within an orthorhombic box of TIP3P water molecules such that all atoms were within 8Å of any box edge [40].

An initial minimization of 2000 steps were carried out with an applied restraint potential of 500 kcal/mol for both solutes, were performed for 1000 steps using the steepest descent method followed by 1000 steps of conjugate gradients. An additional full minimization of 1000 steps were further carried out using the conjugate gradient algorithm without restraint. A gradual heating MD simulation from 0 K to 300 K was executed for 50 ps, such that the systems maintained a fixed number of atoms and fixed volume. The solutes within the systems were imposed with a potential harmonic restraint of 10 kcal/mol and collision frequency of 1.0 ps. Following heating, an equilibration estimating 500 ps of each system was conducted; the operating temperature was kept constant at 300 K. Additional features such as several atoms and pressure were also kept constant, mimicking an isobaric-isothermal ensemble. The system's pressure was maintained at 1 bar using the Berendsen barostat [41, 42].

The total time for the MD simulations conducted were 100 ns. In each simulation, the SHAKE algorithm was employed to constrict the bonds of hydrogen atoms [43]. The step size of each simulation was 2 fs, and an SPFP precision model was used. The simulations coincided with the isobaric-isothermal ensemble (NPT), with randomized seeding, the constant pressure of 1 bar maintained by the Berendsen barostat [42], a pressure-coupling constant of 2 ps, a temperature of 300 K and Langevin thermostat 44] with a collision frequency of 1.0 ps.

3.7.1.2 Post-Dynamic Analysis

Analysis of Root Mean Square Deviation (RMSD), Root Means Square Fluctuation (RMSF), Solvent accessible surface area (SASA) and Radius of Gyration (RoG) was done using the CPPTRAJ module employed in the AMBER 18 suit. All raw data plots were generated using the Origin data analysis software [45].

3.7.1.3 Binding Free Energy Calculations

To estimate and compare the binding affinity of the systems, the free binding energy was calculated using the Molecular Mechanics/GB Surface Area method (MM/GBSA) (Ylilauri, M., Pentikäinen, 2013). Binding free energy was averaged over 100000 snapshots extracted from the 100 ns

trajectory. The free binding energy (ΔG) computed by this method for each molecular species (complex, ligand, and receptor) can be represented as:

$$\Delta G_{bind} = G_{complex} - G_{receptor} - G_{ligand} (1)$$

$$\Delta G_{bind} = E_{gas} + G_{sol} - TS\ (2)$$

$$E_{gas} = E_{int} + E_{vdw} + E_{ele}\ (3)$$

$$G_{sol} = G_{GB} + G_{SA}\ (4)$$

$$G_{SA} = \gamma SASA\ (5)$$

The term E_{gas} denotes the gas-phase energy, which consists of the internal energy E_{int}; Coulomb energy E_{ele} and the van der Waals energies E_{vdw}. The E_{gas} was directly estimated from the FF14SB force field terms. Solvation free energy, G_{sol}, was estimated from the energy contribution from the polar states, GGB, and non-polar states, G. The non-polar solvation energy, SA. GSA, was determined from the solvent-accessible surface area (SASA), using a water probe radius of 1.4 Å. In contrast, the polar solvation, GGB, the contribution was estimated by solving the GB equation. S and T denote the total entropy of the solute and temperature, respectively.

References

[1] D. Ménard and D. A. Fidock, "Accelerated evolution and spread of multidrug-resistant Plasmodium falciparum takes down the latest first-line antimalarial drug in Southeast Asia," *Lancet Infect Dis*, vol. 19, no. 9, pp. 916-917, 2019. doi: 10.1016/S1473-3099(19)30394-9.

[2] A. Oxner, M. Vellanki, A. Myers, F. Bangura, S. Bangura, A. M. Koroma, R. Massaquoi, F. Gbao, D. Kamanda, J. Gassimu and R. Kahn., "Reducing mortality from severe malaria in Sierra Leonean children by applying the World Health Organization's standard malarial protocol with additional sublingual glucose: A continuous quality improvement report," *Int J Infect Dis*, vol. 96, pp. 61-67, Jul 2020, doi: 10.1016/j.ijid.2020.04.046.

[3] World Health Organization, "World malaria report,". Geneva, Switzerland: World Health Organization, 2020, https://www.who.int/publications-detail-redirect/9789240015791.

[4] L. Schuerman, "RTS, S malaria vaccine could provide major public health benefits," *The Lancet*, vol. 394, no. 10200, pp. 735-736, 2019, doi: 10.1016/S0140-6736(19)31567-3.

[5] M. V. Raimondi, O. Randazzo, M. L. Franca, G. Barone, E. Vignoni, D. Rossi and S. Collina, "DHFR Inhibitors: Reading the Past for Discovering Novel Anticancer Agents," *Molecules*, vol. 24, no. 6, Mar 22 2019, doi: 10.3390/molecules24061140.

[6] L. C. Mishra, A. Bhattacharya, and V. K. Bhasin, "Phytochemical licochalcone A enhances the antimalarial activity of artemisinin in vitro," *Acta Trop*, vol. 109, no. 3, pp. 194-8, Mar 2009, doi: 10.1016/j.actatropica.2008.11.006.

[7] M. Chen, T. G. Theander, S. B. Christensen, L. Hviid, L. Zhai, and A. Kharazmi, "Licochalcone A, a new antimalarial agent, inhibits in vitro growth of the human malaria parasite Plasmodium falciparum and protects mice from P. yoelii infection," *Antimicrob Agents Chemother*, vol. 38, no. 7, pp. 1470-5, Jul 1994, doi: 10.1128/aac.38.7.1470.

[8] K. Devi, V. Rajendran, T. M. Rangarajan, R. P. Singh, P. C. Ghosh, and M. Singh, "Synthesis and Evaluation of Antiplasmodial Activity of 2,2,2-Trifluoroethoxychalcones and 2-Fluoroethoxy Chalcones against Plasmodium falciparum in Culture," *Molecules*, vol. 23, no. 5, May 14 2018, doi: 10.3390/molecules23051174.

[9] N. C. Phong, M. Chavchich, H. H. Quang, N. N. San, G. W. Birrell, I. Chuang, N. J. Martin, N. D. Manh and M. D. Edstein, "Susceptibility of Plasmodium falciparum to artemisinins and Plasmodium vivax to chloroquine in Phuoc Chien Commune, Ninh Thuan

Province, south-central Vietnam," *Malar J,* vol. 18, no. 1, p. 10, Jan 17 2019, doi: 10.1186/s12936-019-2640-2.

[10] L. Sitali, M. C. Mwenda, J. M. Miller, D. J. Bridges, M. B. Hawela, E. Chizema-Kawesha, J. Chipeta, and B. Lindtjørn, "En-route to the 'elimination' of genotypic chloroquine resistance in Western and Southern Zambia, 14 years after chloroquine withdrawal," *Malar J,* vol. 18, no. 1, p. 391, Dec 3 2019, doi: 10.1186/s12936-019-3031-4.

[11] S. Pulcini, H. M. Staines, A. H. Lee, S. H. Shafik, G. Bouyer, C. M. Moore, D. A. Daley, M. J. Hoke, L. M. Altenhofen, H. J. Painter, J. Mu, D. J. P. Ferguson, M. Llinás, R. E. Martin, D. A. Fidock, R. A. Cooper and S. Krishna, "Mutations in the Plasmodium falciparum chloroquine resistance transporter, PfCRT, enlarge the parasite's food vacuole and alter drug sensitivities," *Sci Rep,* vol. 5, p. 14552, Sep 30 2015, doi: 10.1038/srep14552.

[12] M. Mishra, V. Singh, and S. Singh, "Structural Insights Into Key Plasmodium Proteases as Therapeutic Drug Targets," *Front Microbiol,* vol. 10, p. 394, 2019, doi: 10.3389/fmicb.2019.00394.

[13] Z. O. Ibraheem, R. A. Majid, H. M. Sidek, S. M. Noor, M. F. Yam, M. F. Abd Rachman Isnadi and R. Basir, "In Vitro Antiplasmodium and Chloroquine Resistance Reversal Effects of Andrographolide," *Evid Based Complement Alternat Med,* vol. 2019, p. 7967980, 2019, doi: 10.1155/2019/7967980.

[14] P. E. Bunney, A. N. Zink, A. A. Holm, C. J. Billington, and C. M. Kotz, "Orexin activation counteracts decreases in nonexercise activity thermogenesis (NEAT) caused by high-fat diet," *Physiol Behav,* vol. 176, pp. 139-148, Jul 1 2017, doi: 10.1016/j.physbeh.2017.03.040.

[15] R. Delvecchio, L. M. Higa, P. Pezzuto, A. L. Valadão, P. P. Garcez, F. L. Monteiro, E. C. Loiola, A. A. Dias, F. J. M. Silva, M. T. Aliota, E. A. Caine, J. E. Osorio, M. Bellio, D. H . O'Connor, S. Rehen, R. Santana de Aguiar, A. Savarino, L. Campanati and A. Tanuri, "Chloroquine, an Endocytosis Blocking Agent, Inhibits Zika Virus Infection in Different Cell Models," *Viruses,* vol. 8, no. 12, Nov 29 2016, doi: 10.3390/v8120322.

[16] S. Zhang, C. Yi, C. Li, F. Zhang, J. Peng, Q. Wang, X. Liu, X. Ye, P. Li, M. Wu, Q. Yan, W. Guo, X. Niu, L. Feng, W. Pan, L. Chen and L. Qu, "Chloroquine inhibits endosomal viral RNA release and autophagy-dependent viral replication and effectively prevents

maternal to fetal transmission of Zika virus," *Antiviral Res*, vol. 169, p. 104547, Sep 2019, doi: 10.1016/j.antiviral.2019.104547.

[17] G. T. Edwin, M. Korsik, and M. H. Todd, "The past, present and future of anti-malarial medicines," *Malar J*, vol. 18, no. 1, pp. 1-21, 2019. doi: 10.1186/s12936-019-2724-z.

[18] C. L. Perrin and K. L. Chang, "The Complete Mechanism of an Aldol Condensation," *J Org Chem*, vol. 81, no. 13, pp. 5631-5, Jul 1 2016, doi: 10.1021/acs.joc.6b00959.

[19] A. N. Chiang, J. C. Valderramos, R. Balachandran, R. J. Chovatiya, B. P. Mead, C. Schneider, S. L. Bell, M. G. Klein, D. M. Huryn, X. S. Chen, and B. W. Day, "Select pyrimidinones to inhibit the propagation of the malarial parasite, Plasmodium falciparum," *Bioorg Med Chem*, vol. 17, no. 4, pp. 1527-33, Feb 15 2009, doi: 10.1016/j.bmc.2009.01.024.

[20] T. Zininga, L. Ramatsui, P. B. Makhado, S. Makumire, I. Achilinou, H. Hoppe, H. Dirr and A. Shonhai, "(-)-Epigallocatechin-3-Gallate Inhibits the Chaperone Activity of Plasmodium falciparum Hsp70 Chaperones and Abrogates Their Association with Functional Partners," *Molecules*, vol. 22, no. 12, Dec 5 2017, doi: 10.3390/molecules22122139.

[21] T. Zininga, O. J. Pooe, P. B. Makhado, L. Ramatsui, E. Prinsloo, I. Achilonu, H. Dirr and A. Shonhai, "Polymyxin B inhibits the chaperone activity of Plasmodium falciparum Hsp70," *Cell Stress Chaperones*, vol. 22, no. 5, pp. 707-715, Sep 2017, doi: 10.1007/s12192-017-0797-6.

[22] I. Kehinde, P. Ramharack, M. Nlooto, and M. Gordon, "Molecular dynamic mechanism(s) of inhibition of bioactive antiviral phytochemical compounds targeting cytochrome P450 3A4 and P-glycoprotein," *J Biomol Struct Dyn*, pp. 1-11, Oct 16 2020, doi: 10.1080/07391102.2020.1821780.

[23] B. Hess, "Convergence of sampling in protein simulations," *Phys Rev E Stat Nonlin Soft Matter Phys*, vol. 65, no. 3 Pt 1, p. 031910, Mar 2002, doi: 10.1103/PhysRevE.65.031910.

[24] S. E. Boyce, N. Tirunagari, A. Niedziela-Majka, J. Perry, M. Wong, E. Kan, L. Lagpacan, O.Barauskas, M. Hung, M. Fenaux, T. Appleby, W. J. Watkins, U. Schmitz and R. Sakowicz, "Structural and regulatory elements of HCV NS5B polymerase--β-loop and C-terminal tail--are required for activity of allosteric thumb site II inhibitors," (in eng), *PLoS One*, vol. 9, no. 1, p. e84808, 2014, doi: 10.1371/journal.pone.0084808.

[25] D. J. Begley and M. W. Brightman, "Structural and functional aspects of the blood-brain barrier," *Prog Drug Res*, vol. 61, no. 61, pp. 39-78, 2003. doi:10.1007/978-3-0348-8049-7_2

[26] C. Lipinski, F. Lombardo, B. W. Dominy and P. J. Feeney, "Experimental and computational approaches to estimate solubility and permeability in drug discovery and development settings," *Adv. Drug Deliv. Rev*, vol. 46, no. 1-3, p. 3, 2001, doi: 10.1016/j.addr.2012.09.019.

[27] M. Remko, A. Boháč, and L. Kováčiková, "Molecular structure, pK a, lipophilicity, solubility, absorption, polar surface area, and blood-brain barrier penetration of some antiangiogenic agents," *J Struct Chem,* vol. 22, no. 3, pp. 635-648, 2011, doi: 10.1007/s11224-011-9741-z.

[28] R. P. Heaney, "Factors Influencing the Measurement of Bioavailability, Taking Calcium as a Model," *J Nutr,* vol. 131, no. 4, pp. 1344S-1348S, 2001, doi: 10.1093/jn/131.4.1344S.

[29] W. Trager and J. B. Jensen, "Human malaria parasites in continuous culture," *Science,* vol. 193, no. 4254, pp. 673-5, Aug 20 1976, doi: 10.1126/science.781840.

[30] C. Lambros and J. P. Vanderberg, "Synchronization of Plasmodium falciparum Erythrocytic Stages in Culture," *J Parasitol,* vol. 65, no. 3, pp. 418-420, 1979, doi: 10.2307/3280287.

[31] M. T. Makler, J. M. Ries, J. A. Williams, J. E. Bancroft, R. C. Piper, B. L. Gibbins and D. J. Hinrichs, "Parasite lactate dehydrogenase as an assay for Plasmodium falciparum drug sensitivity," *Am J Trop Med Hyg,* vol. 48, no. 6, pp. 739-41, Jun 1993, doi: 10.4269/ajtmh.1993.48.739.

[32] J. Reader, M. Botha, A. Theron, S. B. Lauterbach, C. Rossouw, D. Engelbrecht, M. Wepener, A. Smit, D. Leroy, D. Mancama, T. L. Coetzer and L. Birkholtz, "Nowhere to hide: interrogating different metabolic parameters of Plasmodium falciparum gametocytes in a transmission blocking drug discovery pipeline towards malaria elimination," *Malar J,* vol. 14, p. 213, May 22 2015, doi: 10.1186/s12936-015-0718-z.

[33] A. D. Forkuo, C. Ansah, K. B. Mensah, K. Annan, B. Gyan, A. Theron, D. Mancama and C. W. Wright, "*In vitro* anti-malarial interaction and gametocytocidal activity of cryptolepine," *Malar J,* vol. 16, no. 1, p. 496, Dec 28 2017, doi: 10.1186/s12936-017-2142-z.

[34] T. Mosdam, "Rapid colourimetric assay for cellular growth and survival: Application to proliferation and cytotoxic assay," *J. Immunol. Methods,* vol. 65, pp. 55-63, 1983, doi: 10.1016/0022-1759(83)90303-4.

[35] K. M. Krawczyk, D. Matak, L. Szymanski, C. Szczylik, C. Porta, and A. M. Czarnecka, "Culture in embryonic kidney serum and xeno-free media as renal cell carcinoma and renal cell carcinoma cancer stem cells research model," *Cytotechnology,* vol. 70, no. 2, pp. 761-782, Apr 2018, doi: 10.1007/s10616-017-0181-5.

[36] J. C. Domingue, M. Ao, J. Sarathy, A. George, W. A. Alrefai, D. J. Nelson and M. C. Rao, "HEK-293 cells expressing the cystic fibrosis transmembrane conductance regulator (CFTR): a model for studying the regulation of Cl- transport," (in eng), *Physiol Rep,* vol. 2, no. 9, Sep 1 2014, doi: 10.14814/phy2.12158.

[37] Z. Yang, K. Lasker, D. Schneidman-Duhovny, B. Webb, C. C. Huang, E. F. Pettersen, T. D. Goddard, E. C. Meng, A. Sali and T. E. Ferrin, "UCSF Chimera, MODELLER, and IMP: an integrated modelling system," *J Struct Biol,* vol. 179, no. 3, pp. 269-78, Sep 2012, doi: 10.1016/j.jsb.2011.09.006.

[38] A. Sali and T. L. Blundell, "Comparative protein modelling by satisfaction of spatial restraints," *J Mol Biol,* vol. 234, no. 3, pp. 779-815, Dec 5 1993, doi: 10.1006/jmbi.1993.1626.

[39] P. C. Nair and J. O. Miners, "Molecular dynamics simulations: from structure-function relationships to drug discovery," *In Silico Pharmacol,* vol. 2, p. 4, 2014, doi: 10.1186/s40203-014-0004-8.

[40] W. L. Jorgensen, J. Chandrasekhar, J. D. Madura, R. W. Impey, and M. L. Klein, "Comparison of simple potential functions for simulating liquid water," *J Chem Phys,* vol. 79, no. 2, pp. 926-935, 1983, doi: 10.1063/1.445869.

[41] P. Gonnet, "P-SHAKE: a quadratically convergent SHAKE in O (n2)," *J Comput Phys,* vol. 220, no. 2, pp. 740-750, 2007, doi: 10.1016/j.jcp.2006.05.032.

[42] J. E. Basconi and M. R. Shirts, "Effects of Temperature Control Algorithms on Transport Properties and Kinetics in Molecular Dynamics Simulations," *J Chem Theory Comput,* vol. 9, no. 7, pp. 2887-99, Jul 9 2013, doi: 10.1021/ct400109a.

[43] J. P. Ryckaert and A. Bellemans, "Molecular dynamics of liquid alkanes," *Far Dis Chem Soci,* vol. 66, pp. 95-106, 1978, doi: 10.1016/0021-9991(77)90098-5.

[44] J. Izaguirre, D. Catarello, J. Wozniak, and R. Skeel, "Langevin stabilization of molecular dynamics," *J Chem. Phys*, vol. 114, pp. 2090–2098, 2001, doi: 10.1063/1.1332996.

[45] E. Seifert, "OriginPro 9.1: scientific data analysis and graphing software-software review," *J Chem Inf Model*, vol. 54, no. 5, p. 1552, May 27 2014, doi: 10.1021/ci500161d.

CHAPTER 4

Promising class of antiplasmodial agents: Design and synthesis of novel Pyrimidine–Cinnamoyl hybrids

Graphical Abstract

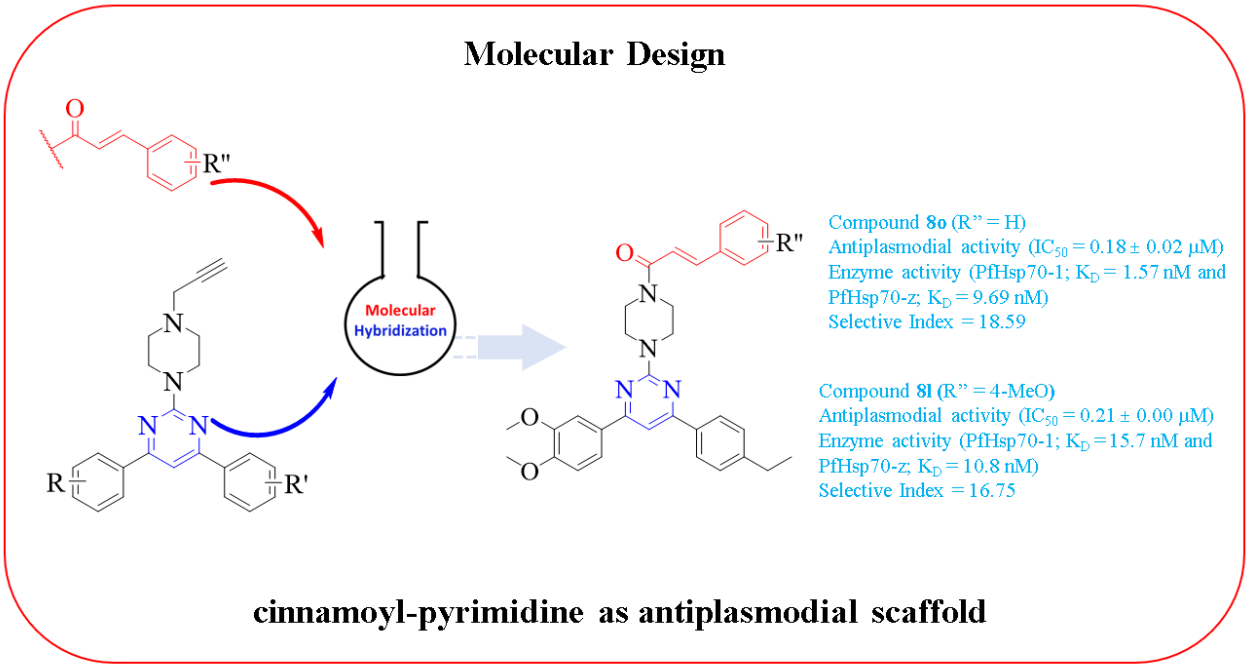

Abstract

Malaria remains a challenge in epidemic areas owing to the emergence of resistance against artemisinin-based combination therapy (ACT), presently the first-line drugs. This necessitates the urgent need for an alternative and new affordable antimalarial drug for treatment. In line with our ongoing research, we present an efficacious novel class of antiplasmodial molecular hybrids; (*E*)-1-(4-(4,6-diphenylpyrimidin-2-yl)piperazin-1-yl)-3-phenyl prop-2-en-1-one derivatives (**8a-n**). *In vitro* antimalarial inhibitory activity of the synthesized compounds was evaluated against the NF54 chloroquine-sensitive strain. From the antiprotozoal screening, thirteen compounds presented active to promising activity with half-maximal inhibitory concentration (IC_{50}) values ranging from 0.18 to 4.09 µM, using quinine and chloroquine as standard drugs. Compound **8o** and **8l** emerged as the most active compounds with IC_{50} values of 0.18 ± 0.02 µM and 0.21 ± 0.001 µM with an associated good safety index of 18.59 and 16.75 to human kidney epithelial (HEK293) cells, respectively. We further evaluated the binding affinities of the molecules to two essential cytosolic *P. falciparum* heat shock protein 70 homologues; PfHsp70-1 and PfHsp70-z. Compounds **8o** and **8l** exhibited an excellent binding affinity for both PfHsp70s with K_D in a lower nanomolar range (1.57 -15.7 nM and 9.69-10.8 nM). Therefore, we envisioned that PfHsp 70-1 is one of the targets of these inhibitors. The synthesized analogues present a new chemical architecture which is structurally unrelated to the current regime of antimalarial drugs representing a valid strategy to combat resistance in *P. falciparum* species to currently available drugs. The presence of activating or electron-donating groups at a para position on the phenyl ring of 4,6-diphenylpyrimidine moiety and cinnamoyl group had a positive correlation for biological activity, suggesting the importance of molecular hybridisation approach for the development of newer cinnamoyl clubbed with 4,6-diphenyl pyrimidine hybrids as potential antiprotozoal agents.

Keywords: PfHsp-70, Antiplasmodial activity, Malaria, Pyrimidine, Cinnamoyl, resistance

4.1 Introduction

The emergence of plasmodial resistance on the mainstay drugs, for example, artemisinin-based combination therapy (ACT) and chloroquine (CQ), remains a challenge for the global health unit [1, 2]. A WHO 2019 report on malaria indicated that malaria infected about 228 million people by 2018. About 405 000 people died, 94% of whom were from Sub Saharan Africa, and about [3, 4] 3.2 billion people continue to be at risk of contracting the disease. Likewise, in Saharan Africa, about 11 million pregnant women were affected by malaria, at least causing about 900 000 low birthweights. Children under 5 were the most prone, with deaths of 272 000 accounting for 67% globally [4]. Acute malaria is deadly, continuing to claim millions of lives unless it is diagnosed and treated in good time [1, 5]. The absence of an antimalarial vaccine leaves drug treatment as the only option for therapy [6-8]. Malaria continues to exacerbate in pestilence areas with the emergence of resistance and lack of vaccines, thus necessitates an urgent need for an alternative and efficient drug.

A medicinal chemistry pharmacophore [9] audit reviewed that curcumin (**1**), a natural product obtained from *Curcuma longa* roots, has huge promising pharmacological properties such as antimicrobial [10, 11], anti-inflammatory, antioxidant [12], antiproliferative and antiangiogenic activities. [13-15]. Structurally, it possesses a cinnamoyl moiety with enone conjugate, which has been identified to be crucial for bioactivity [16]. Additionally, curcumin has exhibited antimalarial activity against the blood form CQ-resistance plasmodial strain with IC_{50} of 5 µM [11]. Additionally, a series of curcumin analogues earned patents for anti-plasmodium properties [17, 18]. Licochalcone A (**2**), another natural compound with cinnamoyl moiety, likewise displayed good antiplasmodial activity [17]. Chemosensitizer containing cinnamoyl moiety have been used with CQ to evade resistance by enabling CQ by-pass *P. falciparum-chloroquine resistance transporter*, a key efflux enzyme responsible for resistance [18]. The enone conjugate in chalcone (cinnamoyl moiety) was crucial in inhibiting cysteine protease, [19] an enzyme required for haemoglobin degradation as a source of amino acids needed for parasite biochemical pathways [20, 21].

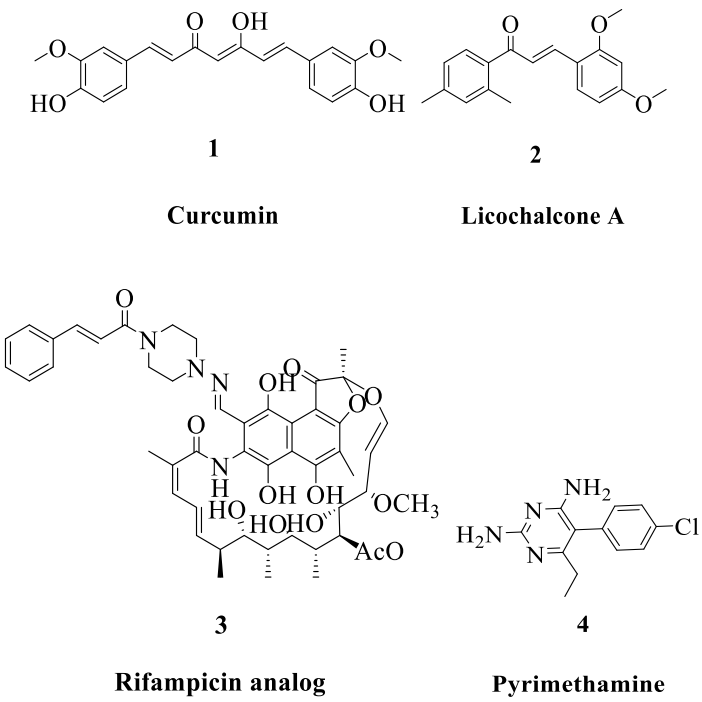

Figure 4.1. Commercial drugs and natural products that have antimalarial properties.

A commercial drug such as rifampin (**3**), an antibiotic drug, has displayed significant antimalarial activity against the CQ resistance and sensitive strains with IC_{50} of 3.2 µM and 1.3 µM, respectively [22]. Rifampin house a cinnamoyl motif which essentially improved its antibiotic activity by 10-fold [23]. Also, when administered in combination with amodiaquine and artemisinin, for antimalarial, the activity of rifampicin against CQ-resistance strain of *P. falciparum* improved tremendously and, in another instance, it enhanced the sensitivity of CQ for antimalarial activity due to its high tolerance level [24, 25].

Pyrimidine is an important biologically active nucleus with a significant range of activities, including antimalarial [22, 24-27]. For instance, pyrimethamine (**4**), a malaria drug, house a pyrimidine core that inhibits *dihydrofolate reductase* (DHFR), preventing deoxyribonucleic acid (DNA) biosynthesis and thereby killing the *Plasmodium* parasite [27]. Several compounds with pyrimidine and cinnamoyl nuclei that shown significant antimalarial compounds are listed in **Figure 4.2**.

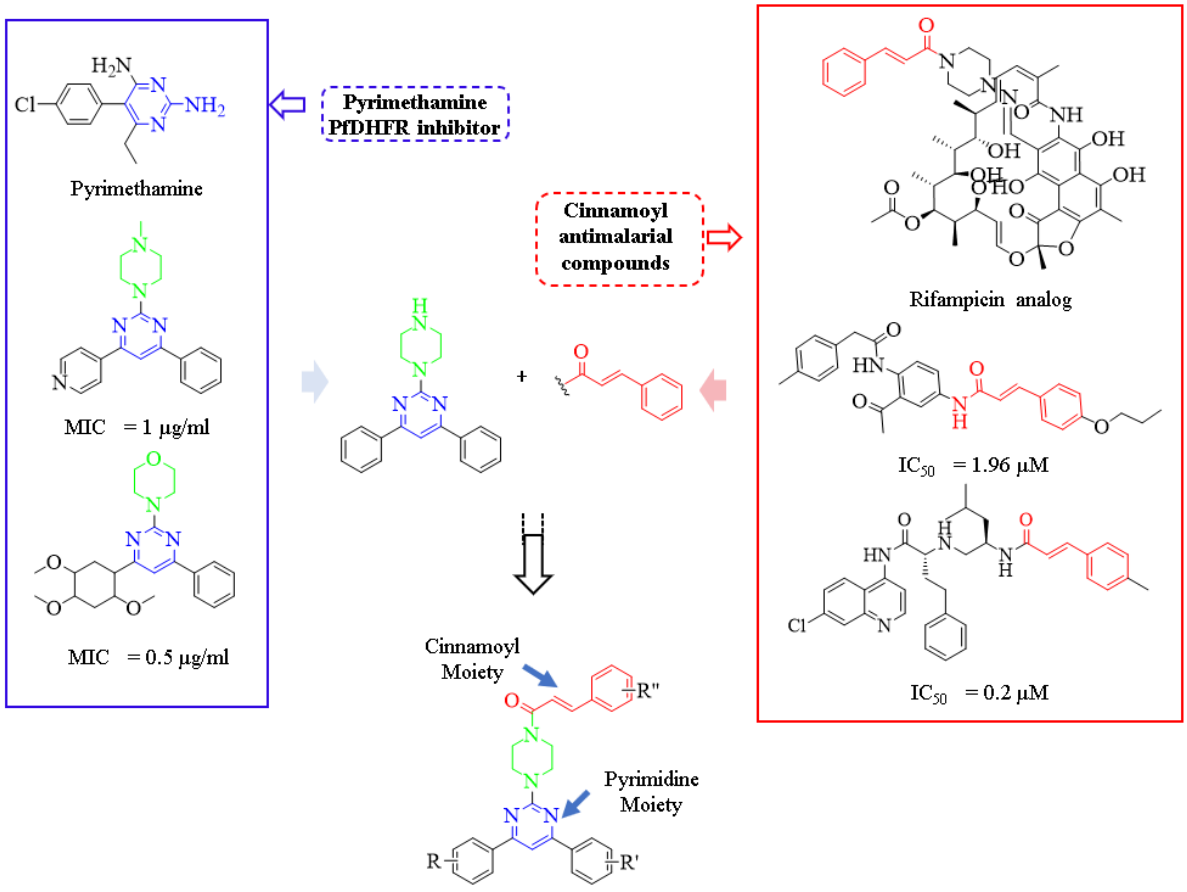

Figure 4.2. Rational design of the molecular hybrid based on pyrimidine and cinnamoyl motif linked by piperazine.

In addition, other pyrimidine antimalarial derivatives revealed that a cyclohexyl (piperazine) at the second position of the pyrimidine nucleus was crucial for antimalarial activity [26-29]. Also, piperazine primarily enhanced the antimalarial activity by 3-fold of 7 quinoline-pyrimidine hybrids compared to CQ than an alkylene diamine aliphatic as a linker against CQ-resistant Dd2 strain, signifying it as a significant antimalarial pharmacophore [30]. This is in line with our recently published manuscript, Karpoormath *et al*. (2021), a pyrimidine-based moiety (4,6-diphenylpyrimidine) proved to be key in the antimalarial activity [31].

Given the facts and as per our ongoing research, we employed the molecular hybridization strategy to present compounds speculated to have DHFR and protease cysteine inhibitory properties. We perceived that the hybrid molecule of cinnamoyl and pyrimidine motifs linked by piperazine could lead to evasion of plasmodial resistance and give a feasible approach for discovering new

antimalarial therapies. Therefore, our quest anticipates delivering a single molecule with dual therapeutic action with enhanced efficacy and bioavailability [29].

4.2 Chemistry

The multi-step synthetic route and structural elucidation of 2-chloro-4,6-diphenylpyrimidine derivatives were accomplished as reported in our previous work in the chapter 3 section. Synthesis of a library of intermediates and novel cinnamoyl-pyrimidine hybrids **8 (a-r**) was performed using expedient multi-step organic synthetic routes described in **Schemes 1** and **2**. The *(E)* chalcones (**1)** were synthesized using assorted commercially available benzaldehyde and acetophenone by a simple Aldol condensation reaction in NaOH ethanolic basic conditions as per reported protocol [2]. The cyclisation of assorted *(E)* chalcones using guanidine. HCl, via NaOH basic catalyzed reaction, afforded a series of 4,6-diphenylpyrimidin-2-amines derivatives (**2**). 2-Aminepyrimidine derivatives (**2**) were then oxidized to 4,6-diphenylpyrimidin-2-ol (**3)** by diazonium salt intermediate formation using sodium nitrate in acetic acid. Chlorination of **3** to obtain 2-chloro-4,6-diphenylpyrimidines (**4)** was completed using $POCl_3$ with catalytic DMF. Refluxing of **4** with excess piperazine in IPA yielded a series of 4,6-diphenyl-2-(piperazine-1-yl) pyrimidine (**5),** as shown in scheme 1.

Scheme 3

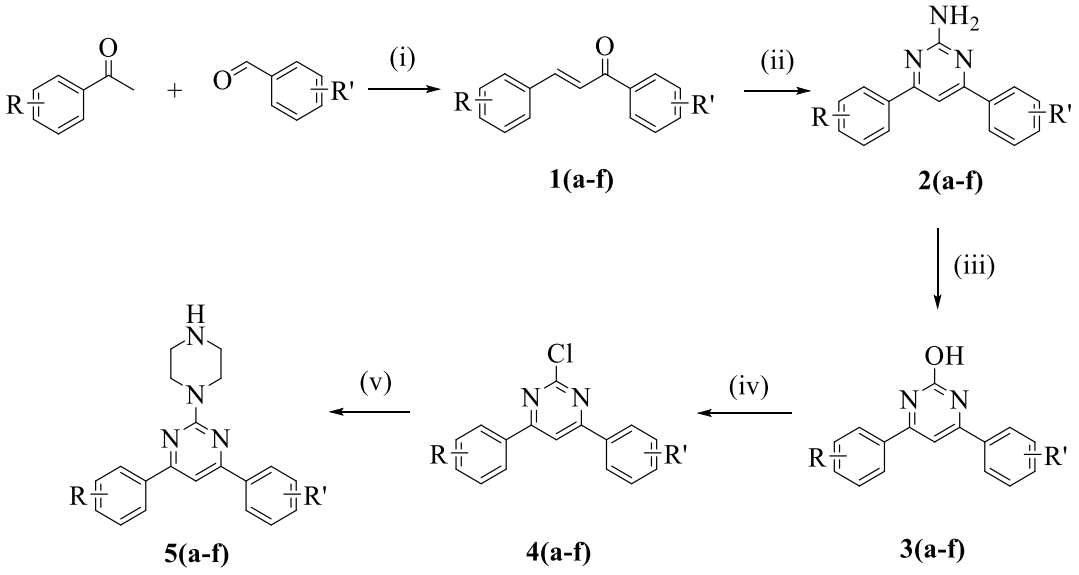

Reaction conditions: (i) NaOH, EtOH, rt, 2 hours (ii) GdnHCl, NaOH, reflux, 16 hours (iii) $NaNO_2$, Acetic acid, rt, 3 hours (iv) $POCl_3$, DMF, reflux, 6 hours. (v) Piperazine, isopropyl alcohol (IPA), reflux, 16 hours.

The cinnamoyl chloride (**7**) analogues were synthesised by chlorination using versatile reagents such as oxalyl dichloride with catalytic DMF in DCM as previously reported procedure [3]. A library of the final compounds **8(a-r)** in good yield (73- 93%) was afforded by amidification coupling of assorted cinnamoyl chlorides derivatives (**7**) and 4,6-diphenyl-2-(piperazin-1-yl)pyrimidine (**5)** using triethylamine catalyst in DCM as illustrated in **Scheme 2**.

Scheme 4

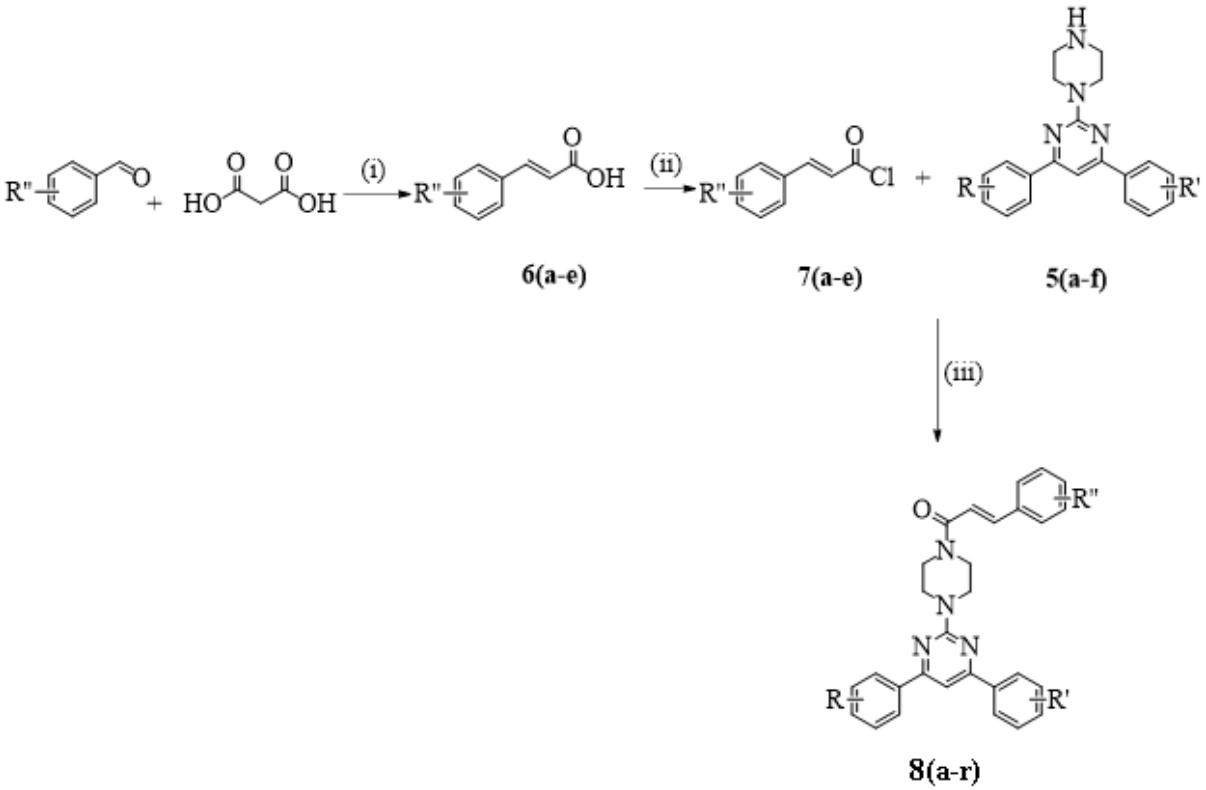

Reaction conditions: (i) Pyridine, piperidine, reflux, 16 hours (ii) DMF, DCM, 0ºC- rt, 1hour (iii) Et_3N, DCM, 0ºC – rt, 3 hours.

4.3 Results and discussion

4.3.1 Synthesis and spectral studies

The designed molecular structures of the final compounds coincided with the IR, ^{1}H-NMR and ^{13}C- NMR spectral data obtained and HRMS for verification. The ^{1}H NMR of compound **1b** presented two discrete doublets (d) signals at δ 7.78 ppm (Ph-C<u>H</u>=CH) and 7.50 ppm (Ph-CH=C<u>H</u>) with J = 15.62 Hz and 15.61 Hz respectively, signifying the formation of an olefin with a trans conformation. The spectrum also exhibited two singlets at about δ 3.89 and 2.39 ppm, indicating methoxy and methyl substituents on the diphenyl group of the (*E*)-Chalcone. ^{1}H NMR spectrum of compound **2** presents the appearance of two typical signals at δ 7.34 ppm and 5.22 ppm signifying a pyrimidine aromatic proton (Pyr-H) and 2-amino group (Pyr-NH_2) of pyrimidine core and the disappearance of the olefin signals. The formation of a 2-hydroxyl pyrimidine derivative (**3**) is indicated by the disappearance of the amino signal at δ 5.22 ppm and the presence of a broad singlet (br.s) signal at 11.85 ppm. The proton spectrum of 2-chloropyrimidine is characterized by the disappearance of hydroxyl (OH) signal, and minor shifts were noted of Pyr-H at δ 7.35 ppm to 7.60 ppm. 4,6-Diphenyl-2-(piperazin-1-yl) pyrimidine (**5**) ^{1}H NMR spectrum had two distinctive peaks; a broad singlet (s) at 3.93 ppm and quartet (q) at 2.57ppm (J = 4.42 Hz), accounting for all the four methylene protons of piperazinyl group. Cinnamic acid (**6**) ^{1}H NMR was defined by three distinctive signals; two doublets (d) at resonating δ 7.58 ppm (d, J = 16.05 Hz) and δ 6.55 ppm (d, J = 16.04 Hz) signifying an (*E*) olefinic conformation and, broad singlet(s) at δ 12.46 ppm for carboxylic hydroxyl (OH). The ^{1}H NMR (400 and 600 MHz, DMSO-d_6) of the final compound **8c** is defined by two definite doublets (d) peaks at δ 7.74 ppm (J = 15.45) and 6.96 ppm (J = 15.41 Hz), indicating the formation of (*E*) olefinic cinnamoyl group. The presence of two broad singlets (br.s) signals at δ 3.98 ppm and 3.85/3.74 ppm account for the four methylene' of piperazinyl linker, and likewise, a sharp singlet (s) signal at δ 3.85 ppm and 2.34 ppm accounting for a methoxy and methyl groups on fourth positions of diphenyl group on the pyrimidine. The outstanding protons of the aromatic group appear as diverse signals as singlets, doublets or multiple in the aromatic region (8.27 ppm -7.08 ppm). The ^{1}H NMR data of the respective compounds concurred with their corresponding ^{13}C NMR data. The most noteworthy signals resonated at δ 43.80-53.13, 55.39 and 21.44 ppm accounting for the four methylene of piperazinyl, methoxy and methyl carbons, respectively. A distinctive signal is also observed resonating at 100 ppm, indicating a (Pyr-H) carbon. Further, the characteristic signals resonated at δ 140.46 ppm and 120.76 ppm

accounted for olefinic carbons, while signals at δ 164.92- 164.55 ppm and 162.12-161.54 ppm accounted for aromatic carbon attached methoxy and (C-N). Signal resonating at 123.49-137.44 ppm accounted for the remaining aromatic carbon.

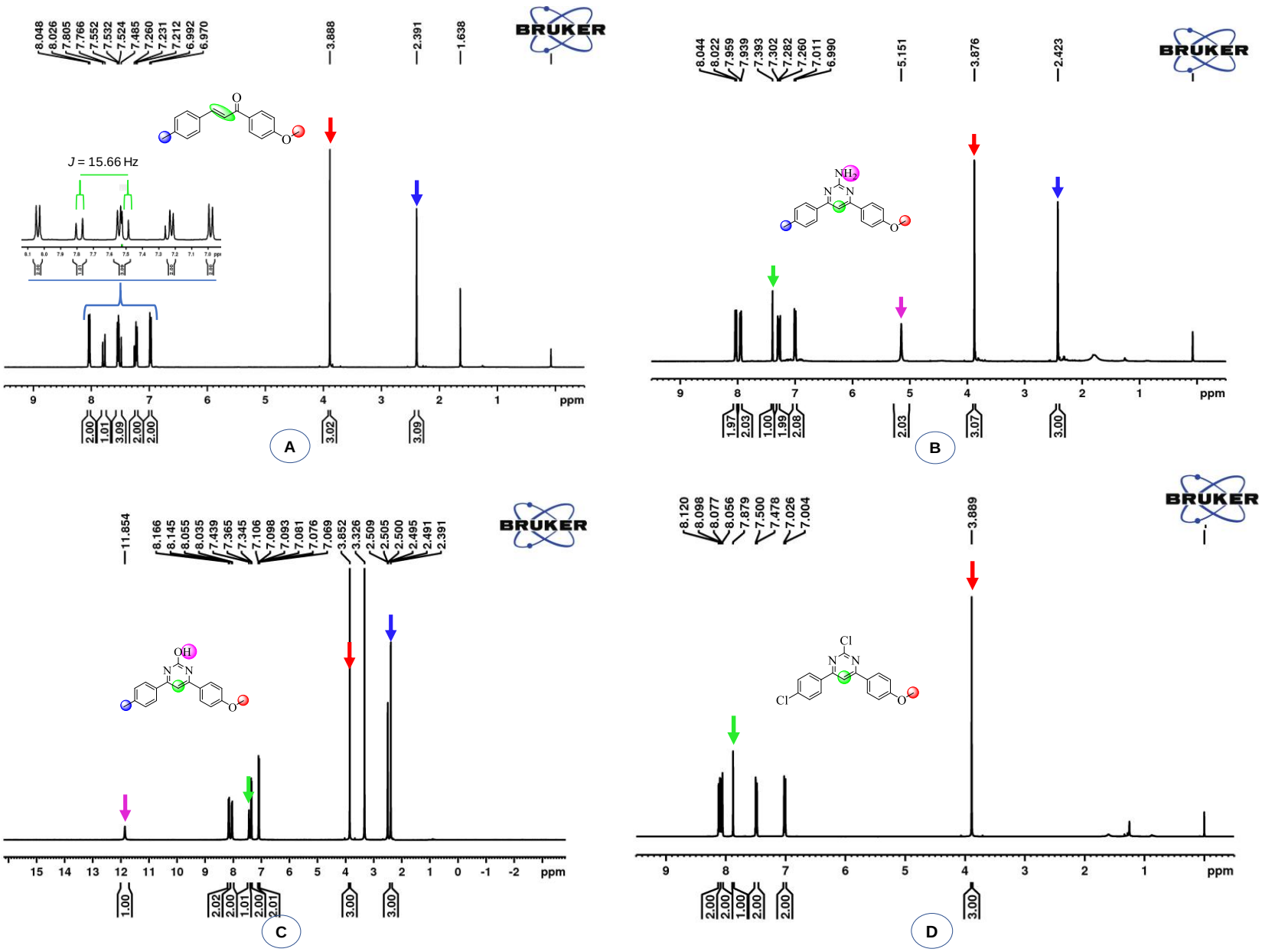
8.048
8.026
7.805
7.766
7.552
7.532
7.524
7.485
7.260
7.231
7.212
6.992
6.970
3.888
2.391
1.638
J = 15.66 Hz
ppm
2.00
1.01
3.09
2.00
2.00
3.02
3.09
A
8.044
8.022
7.959
7.939
7.393
7.302
7.282
7.260
7.011
6.990
5.151
3.876
2.423
ppm
1.97
2.03
1.00
1.99
2.08
2.03
3.07
3.00
B
11.854
8.166
8.145
8.055
8.035
7.439
7.365
7.345
7.106
7.098
7.093
7.081
7.076
7.069
3.852
3.326
2.509
2.505
2.500
2.495
2.491
2.391
ppm
1.00
2.02
2.00
1.01
2.00
2.01
3.00
3.00
C
8.120
8.098
8.077
8.056
7.879
7.500
7.478
7.026
7.004
3.889
ppm
2.00
2.00
1.00
2.00
2.00
3.00
D

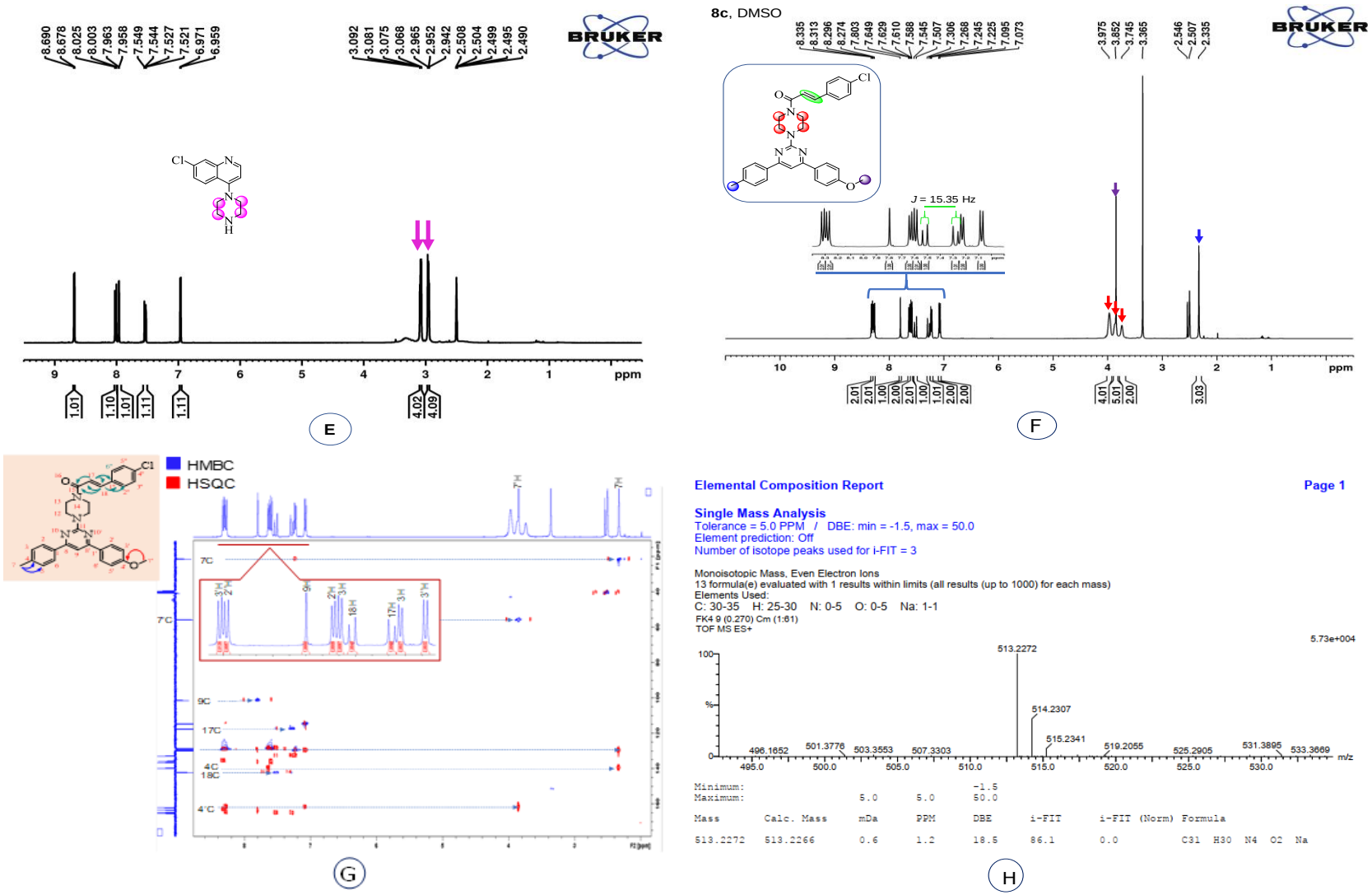

Figure 4.3. [1]H-NMR for intermediates derivative: chalcone (A), 4,6-diphenylpyriidin-2-amine (B), 4,6-diphenylpyrimidin-2-ol (C), 2-chloro-4,6-diphenylpyrimidine (D), 4,6-diphenyl-2-(piperazin-1-yl)pyrimidine (*E*), [I]H NMR, HMBC and HSQC (**8d**); (*E*)-3-(4-chlorophenyl)-1-(4-(4-(4-methoxyphenyl)-6-(p-tolyl)pyrimidin-2-yl)piperazin-1-yl)prop-2-en-1-one (**8d**) (F and G). HRMS of final product compound **8c** (H).

4.3.2 Antimalarial activity

The synthesized analogues (**8a-8r**) were evaluated for potent activity against NF54 CQ-sensitive strain of *Plasmodium falciparum* (*P. falciparum*) as per the earlier reported method, and the conditions of the assay are cited in the supporting information. All the hybrid analogues inhibited the plasmodial species, and the data obtained for **5b** and **8**(**a-r**) and CQ and quinine (standard reference drugs) is depicted in **Table 1**. Thirteen analogues displayed good to promising activity in micromolar level against the NF54 CQ-sensitive strain assay. The IC_{50} of these compounds were calculated from concentration-response plots using GraphPad Prism 5.0.0 software.

Table 1. *In vitro* antimalarial activity of compounds

Compound ID	Antimalarial		Cytotoxicity		Selective Index
	IC_{50} (µM)	SD	IC_{50} (µM)	SD	
5b	5-50	nd	nd	nd	nd
8a	6.02	1.72	nd	nd	nd
8b	2.72	1.10	nd	nd	nd
8c	1.72	1.15	nd	nd	nd
8d	2.33	1.12	nd	nd	nd
8e	0.60	0.19	0.93	0.36	1.54
8f	4.09	1.39	nd	nd	nd
8g	2.71	1.12	nd	nd	nd
8h	3.58	1.32	nd	nd	nd
8i	5-50	nd	nd	nd	nd
8j	5-50	nd	nd	nd	nd
8k	7.43	0.23	3.69	0.45	0.50
8l	0.21	0.00	3.55	0.16	16.75
8m	0.20	0.04	0.87	0.11	4.34
8n	1.56	1.08	nd	nd	nd
8o	0.18	0.02	3.36	0.31	18.59
8p	0.72	1.01	nd	nd	nd
8q	3.67	1.35	nd	nd	nd
8r	5-50	nd	nd	nd	nd
Quinine	0.11	0.003	134.35	1.45	1243.98
Chloroquine	0.01	0.002	101.19	25.72	8432.50
Camptothecin	nd	nd	0.2	0.01	nd

IC_{50}: Concentration at 50% inhibition of the parasite's growth

Selective Index: IC_{50} values of cytotoxic activity/IC_{50} values of antimalarial activity

nd: not done.

SD: Standard Deviation

Out of all the evaluated compounds, **8l**, **8m** and **8o** showed the most significant antiprotozoal inhibition, with IC_{50} values below 0.5 µM corresponding to 0.21 ± 0.00 µM, 0.20 ± 0.04 µM and 0.18 ± 0.02 µM respectively, with **8o** being the most prominent. Nine compounds (**8b**, **8c**, **8d**, **8e**, **8f**, **8g**, **8h, 8p** and **8q**) displayed moderate activity with IC_{50} (0.50 to 5.0 µM) while the activity of the remaining five compounds (**8a**, **8i**, **8j**, **8k** and **8r**) were considered inactive with IC_{50} greater than 5 µM. Quinine and chloroquine, respectively, were two and eighteen times more active than the most potent compounds (**8o**). This highlights the potential of these hybrids as antimalarials. Three pyrimidine-cinnamoyl of the compound class were considered potent, with the most active IC_{50} values as low as 0.18 µM, two-fold more active than our last reported compounds [31]. This indicates that a cinnamoyl amalgamated pyrimidine demonstrated to be more promising and shows how versatile a pyrimidine is as an antimalarial pharmacophore as it can be observed by other reported activity. Also, as noted by the improved activity of these hybrids, it shows how a cinnamoyl core is significant to the antimalarial activity in line with Bianca *et al*. report [31, 39].

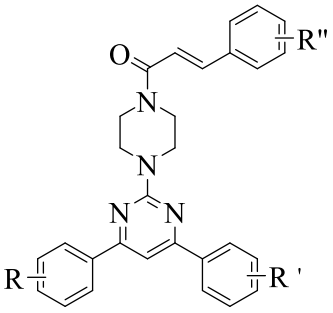

8a R = 4-Cl, R' = 4-MeO, R" = H
8b R = 4-Me R' = 4-MeO, R" = H
8c R = 4-Me, R' = 4-MeO, R" = 4-Cl
8d R = 4-Me, R' = 4-MeO, R" = 4-Me
8e R = 4-Me, R' = 4-MeO, R" = 3,4-diMeO
8f R = 4-MeO, R' = 4-MeO, R" = H
8g R = 4-MeO, R' = 4-MeO, R" = 4-Cl
8h R = 4-MeO, R' = 4-MeO, R" = 4-Me
8i R = 4-MeO, R' = 4-MeO, R" = 4-MeO
8j R = 4-MeO, R' = 4-MeO, R" = 3,4-diMeO
8l R = 3,4-diMeO, R' = 4-Et, R" = H
8m R = 3,4-diMeO, R' = 4-Et R" = 4-Cl
8n R = 3,4-diMeO, R' = 4-Et, R" = 4-Me
8o R = 3,4-diMeO, R' = 4-Et R" = 4-MeO

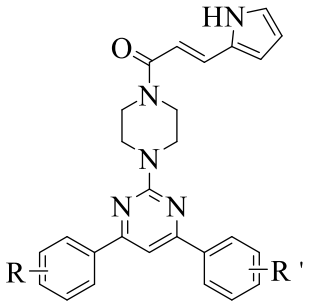

8k R = 4-MeO, R' = 4-MeO
8p R = 3,4-diMeO, R = 4-Et

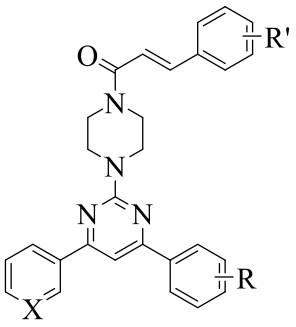

8q R = 4-Cl, R =Me

Figure 4.4. The structures of the pyrimidine-cinnamoyl derivatives **8(a-q)**.

Since a substantial number of hybrid analogues were evaluated for activity, a purposeful SAR to determine the members that significantly impact the activity of the synthesized series was established. The bioisosteric substitution on the phenyl groups on the 4,6-diphenylprimidine and cinnamoyl motifs positively correlated with the antiprotozoal activity. The compounds housing a 4-(3,4-dimethoxyphenyl)-6-(4-ethylphenyl)pyrimidine motif showed promising results ranging from 0.18 to 1.56 µM. Compounds **8o**, **8i** and **8m** were the most active with IC_{50} less than 0.5 µM (**Table 1**), while compounds **8n** and **8p** showed moderate activity with IC_{50} values of 0.72 and 1.56 µM, respectively. Bioisosteric replacement on the cinnamoyl motif afforded a variation in the activity. An activating and a mild withdrawing group such as methoxy and chloro respectively at position four of the phenyl group showed the most activity illustrated by compounds **8m** and **8o**.

Similarly, there was no observed significant difference for unsubstituted phenyl on the cinnamoyl group of compound **8l** compared to **8m** and **8o**. However, replacing the phenyl with a heteroaromatic group such as pyrrole reduced the activity three-fold, as demonstrated by **8h** and

8p. For compounds with 4,6-bis(4-methoxyphenyl) pyrimidine core, they displayed moderate to inactive with IC_{50} ranging 2.71 to 7.43 µM. Here also, the bioisosteric replacements on the cinnamoyl motif presented a difference in the activity. Compounds **8f**, **8g** and **8h** displayed moderate activity with IC_{50} 2.71 to 4.09 µM. Mild activating and withdrawal groups such as methyl and chloro induced moderate activity. Unsubstituted phenyl on the cinnamoyl also showed moderate activity with IC_{50} 4.09 µM, however, substituting the phenyl group with the pyrrole group reduced the activity by about two-fold depicted by compound **8f** and **8k**. The antimalarial action was centred on the cinnamoyl and pyrimidine cores joined by a piperazine linker. The antimalarial activity was further increased by bioisosteric substitution on the phenyl group of cinnamoyl and the 4,6-diphenylpyrimidine motif, which was crucial in identifying the potent candidate linked with activity.

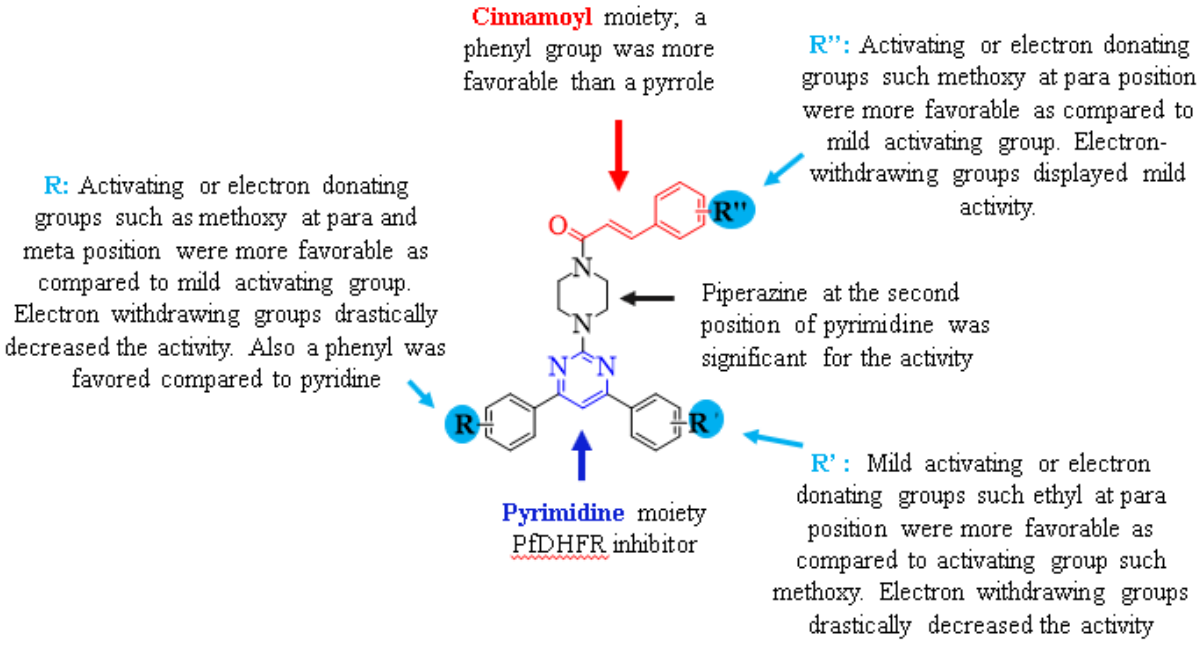

Figure 4.5. Structure Activity Relationship of Cinnamoyl -pyrimidine compounds.

Compounds bearing a 4-(4-methoxyphenyl)-6-(p-tolyl)pyrimidine nucleus had IC_{50} values ranging from 0.60 to 9.02 µM. Activating and mild electron-withdrawing groups on the phenyl group of cinnamoyl core portrayed moderate activity with IC_{50} values ranging from 0.6 to 2.33 as illustrated by compounds **8c**, **8d** and **8e**. A non-substituted phenyl of the cinnamoyl group (**8b**) showed moderate activity (2.72 µM), still, the substitution of a methyl group at the fourth position reduced

activity by about two-fold while dimethoxy substitution at the third and fourth position enhanced the activity about five-times. Substitution of a mild activating group such as methyl at the fourth position was inactive. Replacing the phenyl with heteroaromatic compounds such as pyridine on the fourth position of diphenylpyrimidine core did not affect the activity as demonstrated by compounds (**8a** and **8q**). It can be deduced that substitution on the phenyl of the diphenyl pyrimidine and cinnamoyl were crucial to the antiprotozoal activity.

Additionally, the cytotoxicity screening of the most potent molecules **8k, 8l, 8m, 8o** against mammalian cells has been studied, and the results are shown in **Table 1**. The selective index (SI) of the most potent compound was determined using the IC_{50} value of the cytotoxic activity divided by IC_{50} values of antimalarial activity formulae, was obtained to be 0.50, 16.75, 4.34 and 18.59 corresponding to **8k, 8l, 8m** and **8o**. Quinine and Chloroquine had a safe index of approximately seventy and 400-times, respectively, compared to the most active compound **8o**. Compound **8o** and compound 8l have a good safety index that can selectively kill the parasite tenfold with limited cytotoxic effect against mammalian cells at therapeutic dosages.

4.4 *In-vitro* binding affinity studies

The direct protein-small molecule binding affinities to determine the direct binding of the compounds **8o** and **8l** to the *P. falciparum* Hsp70s (PfHsp70-1 and PfHsp70-z) were determined using SPR. Based on the sensorgrams generated it was observed that the compounds **8o** and **8l** bound to both proteins in a concentration dependent manner (Table 2). The steady-state binding affinities in the lower nanomolar ranger to PfHsp70-1 and higher to PfHsp70-z (Table 2). The compounds **8o** and **8l** are both bound to PfHsp70-1 with high affinity in the lower nanomolar range compared to one order of magnitude difference in their binding affinities to the PfHsp70-z counterpart. This suggests that these compounds prefer *Pf*Hsp70-1 binding.

Table 29. Relative affinities for association of *Pf*Hsp70-1/*Pf*Hsp70-z with compounds **8o** and **8l**.

Ligand	**Analyte**	***Ka* (1/M*s)**	***Kd* (1/s)**	**K_D (M)**	**X^2**
PfHsp70-1	**8o**	5.92 (±0.02) e^{6}	9.29 (±0.21) e^{-2}	1.57 (±0.7) e^{-9}	1.2
	8l	7.97 (±0.1) e^{6}	7.72 (±0.7) e^{-2}	9.69 (±0.5) e^{-9}	2.0
PfHsp70-z	**8o**	6.24 (±0.4) e6	9.79 (±0.8) e-2	1.57 (±0.8) e-8	1.0

	8l	8.28 (±0.2) e6	8.97(±0.07) e-2	1.08 (±0.2) e-8	2.1

Standard errors of measurement are shown in parenthesis.

4.5 Conclusion

In summary, we here present a library of novel pyrimidine-cinnamoyl hybrids merged by piperazine and their associated antiplasmodial activity. The readily available chemical reagents and reactants, and excellent yields (80-90%) make this synthetic strategy attractive and methodical. Compounds **8l** and **8o,** in particular, showed the most prominent antimalarial activity, with IC_{50} values 0.18 ± 0.02 µM and 0.21 ± 0.00 µM, respectively, and a favourable selective index of 16.75 and 18.59. Furthermore, compounds **8o** and **8l** had a high affinity for both parasites Hsp70-1 and Hsp70-z, signifying that one of the compounds' potential modes of action is to disrupt the parasite's protein folding pathway. The findings of this study propose how beneficial it is to incorporate a piperazine linker to amalgamate the fragments of pyrimidine and cinnamoyl moiety and of the designed compounds, thus laying a good foundation for further lead optimization. The antimalarial activity can be improved by the variation of the phenyl substituents and or comprehensive supplemental functionalism, which promise an investigation.

Declaration of Competing Interest

The authors declare no known conflicting financial or personal interests that could have influenced the work reported in this paper.

Acknowledgement

The authors would like to express their heartfelt gratitude to the Discipline of Pharmaceutical Sciences, College of Health Sciences, University of KwaZulu-Natal (UKZN), Durban, South Africa, for providing all the necessary facilities. R.K. gratefully acknowledges National Research Foundation-South Africa (NRF-SA) for funding this project (grant nos. 103728, 112079 and 129247). The authors would also like to acknowledge Dr Vuyisa Mzozoyana (UKZN) for NMR spectroscopic experimental data.

4.6 Chemistry section

4.6.1 Chemical protocols

All the chemicals reagents utilized in this research work were acquired from Sigma-Aldrich and Merck Millipore, South Africa. The commercially accessible chemicals benzaldehyde and

acetophenone were obtained from Sigma- Aldrich (South Africa). All and sundry of the solvents, except those of laboratory-reagent grade, were dried and purified when required following previously published procedures. The chemical reactions' progression and the compounds' purity were monitored by thin-layer chromatography (TLC) on pre-coated silica gel plates secured from E. Merck and Co. (Darmstadt, Germany) using 36% ethyl acetate in n-hexane as the mobile phase and iodine vapour as the visualizing agent.

The melting points of the synthesized compounds were measured by a Thermo Fisher Scientific (IA9000, UK) digital melting point apparatus and are uncorrected. The IR spectra were recorded on a Bruker Alpha FT-IR spectrometer (Billerica, MA, USA) using the ATR technique. The ^{1}H NMR and ^{13}C NMR spectra were recorded on a Bruker AVANCE 400 and 600 MHz (Bruker, Rheinstetten/Karlsruhe, Germany) spectrometers using $CDCl_3$ and DMSO-*d6*. The chemical shifts are reported in δ ppm units using TMS, an internal standard. HRMS spectra were recorded on an Autospec mass spectrometer with electron impact at 70 eV.

4.6.1.1 A typical procedure for the synthesis of *(E)* chalcones.

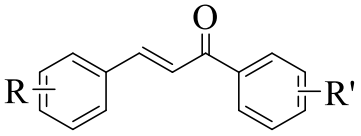

1a R = 4-Cl, R' = 4-MeO
1b R = 4-Me, R' = 4-MeO
1c R = 4-MeO, R' = 4-MeO
1d R = 3,4-diMeO, R' = 4-Et

To a stirring solution of acetophenone (5 gm, 32.34 mmol) in EtOH (30 ml) was added 60% NaOH solution (12 g NaOH/ H_2O (20 mL). The reaction was stirred at room temperature for 30 minutes, after which benzaldehyde (4.7 g, 38.81 mmol) was added, and the reaction mixture sonicated for 1 hour at 35°C. The development of the product was monitored by TLC. Excess ethanol was removed under vacuum, and the reaction mixture was added into 100 g of ice and stirred. The precipitates formed were filtered, washed with excess cold water and dried. The crude product was purified by recrystallisation in EtOH to obtain the pure following compounds.

(E)-3-(4-chlorophenyl)-1-(4-methoxyphenyl) prop-2-en-1-one (**1a**): Yellow solid, yield: 96%, mp = 130-133 °C; ^{1}H NMR (400 MHz, $CDCl_3$, *δ*, ppm): 8.03 (d, *J* = 8.85 Hz, 2H, ArH), 7.74 (d, *J* = 15.65 Hz, 1H, Ph-C**H**=CH), 7.57 (d, *J* = 8.49 Hz, 2H, ArH), 7.51 (d, *J* = 15.63 Hz, 1H, Ph-CH=C**H**), 7.38 (d, *J* = 8.49, Hz, 2H ArH), 6.98 (d, *J* = 8.84, Hz, 2H ArH), 3.89 (s, 3H, OCH_3); ^{13}C

NMR (100 MHz, $CDCl_3$, δ ppm): 188.40, 163.55, 142.47, 136.18, 133.58, 130.91, 122.27, 113.91, 55.53 (OCH_3).

(E)-1-(4-methoxyphenyl)-3-(p-tolyl)prop-2-en-1-one (**1b**): Yellow solid. yield: 98%, mp = 125-128 °C; ^{1}H NMR (400 MHz, $CDCl_3$, δ, ppm): 8.04 (d, J = 8.76 Hz, 2H, ArH), 7.89 (d, J =15.60 Hz, 1H, Ph-C**H**=CH), 7.54 (d, J = 7.95 Hz, 2H, ArH), 7.51 (d, J = 15.63 Hz, 1H, Ph-CH=C**H**), 7.22 (d, J = 7.97, Hz, 2H ArH), 6.98 (d, J = 8.77 Hz, 2H, ArH), 3.88 (s, 3H, CH_3), 2.39 (s, 3H,CH_3); ^{13}C NMR (100 MHz, $CDCl_3$, δ ppm): 189.43 (C=O), 163.92, 144.64, 141..40, 132.92, 131.81, 131.34, 130.24, 128.96, 121.46, 114.39, 56.06(OCH_3), 22.09 (CH_3).

(E)-1,3-bis(4-methoxyphenyl)prop-2-en-1-one (**1c**): Yellow solid, yield: 86%, mp = 102-104 °C; ^{1}H NMR (400 MHz, $CDCl_3$, δ, ppm): 8.03 (d, J = 8.75 Hz, 2H, ArH), 7.78 (d, J = 15.58 Hz, 1H, Ph-C**H**=CH), 7.60 (d, J = 8.66 Hz, 2H, ArH), 7.43 (d, J = 15.58 Hz, 1H, Ph-CH=C**H**), 6.96 (dd, J = 17.58, 8.72 Hz, 4H, ArH), 3.89 (s,3H, OCH_3), 3.85 (s, 3H, OCH_3); ^{13}C NMR (100 MHz, $CDCl_3$, δ ppm): 189.39 (C=O), 163.84, 162.09, 144.39, 131.95, 131.28, 130.67, 128.40, 120.15, 114.96, 114.36, 56.05 (OCH_3), 55.98 (OCH_3).

(E)-3-(3,4-dimethoxyphenyl)-1-(4-methoxyphenyl)prop-2-en-1-one (**1f**): Yellow solid, yield: 81%, mp = 80-83 °C; ^{1}H NMR (400 MHz, $CDCl_3$, δ, ppm): 8.03 (d, J = 8.81 Hz, 2H, ArH), 7.75 (d, J = 15.56 Hz, 1H, Ph-C**H**=CH), 7.40 (d, J = 15.56 Hz, 1H, Ph-CH=C**H**), 7.23 (dd, J = 8.31, 1.64 Hz, 1H, ArH), 7.16 (s, 1H, ArH), 6.98 (d, J =8.81 Hz, 1H, ArH), 6.89 (d, J = 8.27 Hz, 1H, ArH), 3.94 (s, 3H, OCH_3), 3.92 (s, 3H, OCH_3), 3.88 (s, 3H, OCH_3); ^{13}C NMR (100 MHz, $CDCl_3$, δ ppm): 189.37 (C=O), 163.86, 151.83, 149.80, 144.71, 131.89, 131.29, 128.65, 123.53, 120.42, 114.36, 111.70, 110.68, 56.56 (OCH_3), 56.54 (OCH_3), 56.05 (OCH_3).

4.6.1.2 A typical procedure for the synthesis of 4,6-diphenylpyrimidin-2-amine.

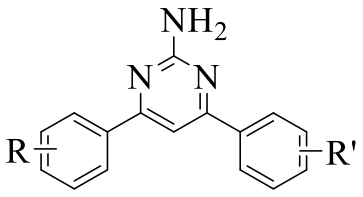

2a R = 4-Cl, R' = 4-MeO
2b R = 4-Me, R' = 4-MeO
2c R = 4-MeO, R' = 4-MeO
2d R = 3,4-diMeO, R' = 4-Et

The reaction mixture of (*E*) chalcone (8 g, 31.16 mmol), Guanidine.HCl (4.8 g, 49. 86 mmol) and 60% NaOH (12 g NaOH/H_2O (20 mL)) in EtOH (30 mL) was refluxed for 24 hours. The

development of the product was monitored using TLC. Excess ethanol was removed under vacuum using rotavapor. The reaction mixture was then added in 100 g ice water, and the precipitate formed was filtered, washed with excess cold water and dried. The crude compound was purified by column chromatography using EtOAc/Hexane (1:4) eluent to obtain the following pure compounds.

4-(4-chlorophenyl)-6-(4-methoxyphenyl)pyrimidin-2-amine (**2a**): Yellow solid, yield: 58%, mp = 127-129°C; ^{1}H NMR (400 MHz, $CDCl_3$, δ, ppm): 8.03 (d, J = 8.78 Hz, 2H, ArH), 7.95 (d, J = 8.06 Hz, 2H, ArH), 7.39 (s, 1H, Pyr-H), 7.29 (d, J = 7.98 Hz, 2H, ArH), 7.00 (d, J = 8.76 Hz, 2H, ArH), 5.15 (s, 2H, NH_2), 3.88 (s, 3H, CH_3), 2.42 (s, 3H, CH_3); ^{13}C NMR (100 MHz, $CDCl_3$, δ ppm): 189.43, 163.92, 144.64, 141.40, 132.92, 131.34, 130.24, 128.96, 121.46, 114.39, 56.06 (OCH_3), 22.89 (CH_3).

4-(4-methoxyphenyl)-6-(p-tolyl)pyrimidin-2-amine (**2b**): Yellow solid, yield: 64%, mp = 127-129°C; ^{1}H NMR (400 MHz, $CDCl_3$, δ, ppm): 8.03 (d, J = 8.64 Hz, 2H, ArH), 8.00 (d, J = 8.36 Hz, 2h, ArH), 7.46 (d, J =8.36 Hz, 2H, ArH), 7.37 (s, 1H, Pyr-H), 7.00 (d, J = 8.56 Hz, 2H, ArH) 5.20 (s, 2H, NH_2), 3.88 (s, 3H, CH_3); ^{13}C NMR (100 MHz, $CDCl_3$, δ ppm): 165.88, 164.64, 163.55, 161.76, 136.47, 136.47, 129.91, 128.96, 128.64, 128.40, 114.14, 103.18, 55.43 (OCH_3).

4,6-bis(4-methoxyphenyl) pyrimidin-2-amine (**2c**): Yellow solid, yield: 65%, mp = 171-173 °C; ^{1}H NMR (400 MHz, $CDCl_3$, δ, ppm): 8.04 (d, J = 8.66 Hz, 4H, ArH), 7.36 (s, 1H, Pyr-H), 7.00 (d, J = 8.69 Hz,4H, ArH), 5.36 (s, 2H, NH_2), 3.87 (s, 6H, $2CH_3$); ^{13}C NMR (100 MHz, $CDCl_3$, δ ppm): 165.19, 162.97, 161.77, 129.78, 128.69, 114.15, 102.64, 55.43 (OCH_3).

4-(3,4-dimethoxyphenyl)-6-(4-ethylphenyl)pyrimidin-2-amine (**2d**): Yellow solid, yield: 61%; ^{1}H NMR (400 MHz, $CDCl_3$, δ, ppm): 8.26 (d, J = 8.23 Hz, 2H, ArH), 7.97 (dd, J = 7.98 Hz,1.94 Hz, 1H, ArH), 7.89 (s, 1H, Pyr-H), 7.88 (d, J = 8.20 Hz, 1H, ArH), 7.38 (d, J = 8.26 Hz, 2H, ArH), 7.10 (d, J = 8.59 Hz, 1H, ArH), 3.92 (s, 3H, OCH_3), 3.86 (s, 3H, OCH_3), 2.70 (q, J = 5.68 Hz, 2H, $2CH_2$), 1.23 (t, J = 7.58 Hz, 3H CH_3); ^{13}C NMR (100 MHz, $CDCl_3$, δ ppm): 165.07, 164.63, 162.12, 151.08, 149.11, 146.83, 135.80, 131.15, 128.18, 127.11, 120.94, 110.10, 101.30, 56.04(OCH_3), 56.02 (OCH_3), 28.81 (CH_2), 15.52 (CH_3).

4-(furan-2-yl)-6-(pyridin-3-yl)pyrimidin-2-amine (**2f**): Yellow solid, yield: 65%; ^{1}H NMR (400 MHz, DMSO-d_6, δ, ppm): 8.36 (s, 1H, ArH) 8.75 (d, J = 3.92 Hz, 1H, ArH), 8.52 (d, J = 8.00 Hz,

1H, ArH), 8.24 (d, *J* = 8.52 Hz, 2H, ArH), 7.82 (s, 1H, Pyr-H), 7.63 (d, *J* = 8.60 Hz, 2H, ArH), 7.59 (dd, *J* = 7.96 Hz, 4.80 Hz, 1H, ArH); ^{13}C NMR (100 MHz, DMSO-d_6, δ ppm): 151.93, 148.61, 136.43, 135.02, 129.41, 128.91, 123.78.

4.6.1.3 A typical procedure for the synthesis of 4,6-diphenylpyrimidin-2-ol

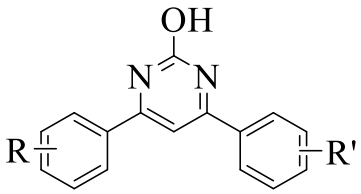

3a R = 4-Cl, R' = 4-MeO
3b R = 4-Me, R' = 4-MeO
3c R = 4-MeO, R' = 4-MeO
3d R = 3,4-diMeO, R' = 4-Et

4-(4-chlorophenyl)-6-(4-methoxyphenyl)pyrimidin-2-ol (**3a**): Yellow solid, yield: 83%, mp = 235-237 °C; ^{1}H NMR (400 MHz, DMSO-d_6, δ, ppm): 11.94 (s, 1H, Pyr-O**H**), 8.18 (dd, *J* = 18.36 Hz, 8.53Hz, 4H, ArH), 7.62 (d, *J* = 8.60 Hz, 2H, ArH), 7.56 (s, 1H, Pyr-H), 7.10 (d, *J* = 8.89 Hz, 2H, ArH), 3.85 (s, 3H, OCH_3); ^{13}C NMR (100 MHz, DMSO-d_6, δ ppm): 162.11, 136.20, 129.37, 128.81, 127.49, 114.23, 55.48 (OCH_3).

4-(4-methoxyphenyl)-6-(p-tolyl)pyrimidin-2-ol (**3b**): Yellow solid, yield: 88%, mp = 235-237 °C; ^{1}H NMR (400 MHz, DMSO-d_6, δ, ppm): 11.85 (s, 1H, Pyr-O**H**), 8.16 (d, *J* = 8.74 Hz, 2H, ArH), 8.04 (d, *J* = 7.97 Hz, 2H, ArH), 7.44 (s, 1H, Pyr-H), 7.35 (d, *J* = 7.98 Hz, 2H, ArH), 7.09 (d, *J* = 8.97 Hz, 2H, ArH), 3.85 (s, 3H, OCH_3), 2.39 (s, 3H, CH_3); ^{13}C NMR (100 MHz, DMSO-d_6, δ ppm): 162.05, 141.51, 129.39, 129.35, 127.46, 114.18, 55.46 (OCH_3), 55.99 (CH_3).

4,6-bis(4-methoxyphenyl)pyrimidin-2-ol (**3c**): Yellow solid, yield: 79%; ^{1}H NMR (400 MHz, DMSO-d_6, δ, ppm): 11.82 (s, 1H, Pyr-O**H**), 8.14 (d, *J* = 8.53 Hz, 2H, ArH), 7.41 (s, 1H, Pyr-H), 7.09 (d, *J* = 8.91 Hz, 2H, ArH), 3.85 (s, 6H, $2OCH_3$); ^{13}C NMR (100 MHz, DMSO-d_6, δ ppm): 162.00, 129.32, 114.18, 55.46 ($2OCH_3$).

4-(3,4-dimethoxyphenyl)-6-(4-ethylphenyl)pyrimidin-2-ol (**3d**): Yellow solid, yield: 93%; ^{1}H NMR (400 MHz, DMSO-d_6, δ, ppm): 12.02 (s, 1H, Pyr-O**H**), 8.26 (d, *J* = 8.23 Hz, 2H, ArH), 7.97 (dd, *J* = 7.98 Hz,1.94 Hz, 1H, ArH), 7.89 (s, 1H, Pyr-H), 7.88 (d, *J* = 8.20 Hz, 1H, ArH), 7.38 (d, *J* = 8.26 Hz, 2H, ArH), 7.10 (d, *J* = 8.59 Hz, 1H, ArH), 3.92 (s, 3H, OCH_3), 3.86 (s, 3H, OCH_3), 2.70 (q, *J* = 5.68 Hz, 2H, $2CH_2$), 1.23 (t, *J* = 7.58 Hz, 3H CH_3); ^{13}C NMR (100 MHz, DMSO-d_6, δ ppm): 165.07, 164.63, 162.12, 151.08, 149.11, 146.83, 135.80, 131.15, 128.18, 127.11, 120.94, 110.10, 101.30, 56.04(OCH_3), 56.02 (OCH_3), 28.81 (CH_2), 15.52 (CH_3).

4-(furan-2-yl)-6-(pyridin-3-yl)pyrimidin-2-ol (**3f**): Yellow solid, yield: 90%; ^{1}H NMR (400 MHz, DMSO-d$_6$, δ, ppm), 12.21 (s, 1H, Pyr-O**H**), 9.36 (s, 1H, ArH) 8.75 (d, *J* = 3.92 Hz, 1H, ArH), 8.52 (d, *J* = 8.00 Hz, 1H, ArH), 8.24 (d, *J* = 8.52 Hz, 2H, ArH), 7.82 (s, 1H, Pyr-H), 7.63 (d, *J* = 8.60 Hz, 2H, ArH), 7.59 (dd, *J* = 7.96 Hz, 4.80 Hz, 1H, ArH); ^{13}C NMR (100 MHz, DMSO-d$_6$, δ ppm): 151.93, 148.61, 136.43, 135.02, 129.41, 128.91, 123.78.

A solution of 10 eq $NaNO_2$ in H_2O (50 mL) was slowly added to a stirring solution of 4,6-diphenylpyrimidin-2-amine (4 g, 12.76 mmol) in acetic acid (50 mL)) at room temperature. The reaction mixture was further stirred for 3 hours. The formation of the product was monitored using TLC. The precipitate formed was filtered, washed with excess cold water and dried. The crude product was recrystallised in EtOH to obtain the following pure compounds.

4.6.1.4 A typical procedure for the synthesis of 2-chloro-4,6-diphenylpyrimidine

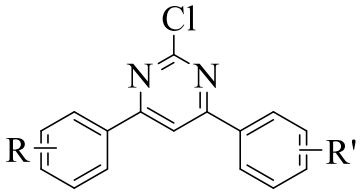

4a R = 4-Cl, R' = 4-MeO
4b R = 4-Me, R' = 4-MeO
4c R = 4-MeO, R' = 4-MeO
4d R = 3,4-diMeO, R' = 4-Et

A reaction mixture of 4,6-diphenylpyrimidin-2-ol (4gm, 16.11 mmol) and 0.4 mL DMF in $POCl_3$ (20 mL) was refluxed for 6 hours. The development of the product was monitored using TLC. The reaction mixture was added into 100 gm ice, and the precipitate formed was filtered, washed with water and dried. The crude compound was purified by column chromatography using EtOAc/Hexane (1:9) eluent to obtain the following pure compounds.

2-chloro-4-(4-chlorophenyl)-6-(p-tolyl)pyrimidine (**4b**): Yellow solid, yield: 88% ; ^{1}H NMR (400 MHz, $CDCl_3$, δ, ppm): 8.09 (d, *J* = 8.52 Hz, 2H, ArH), 8.04 (d, *J* = 8.16 Hz, 2H, ArH), 7.94 (s, 1H, Pyr-H), 7.50 (d, *J* = 8.52 Hz,2H, ArH), 7.33 (d, *J* = 8.00 Hz, 2H, ArH), 2.44 (s, 3H, CH_3); ^{13}C NMR (100 MHz, $CDCl_3$, δ ppm): 166.77, 165.13, 161.05, 141.46, 136.88, 133.16, 131.65, 128.83, 128.30, 127.68, 126.37, 109.20, 20.51(CH_3).

2-chloro-4-(4-chlorophenyl)-6-(4-methoxyphenyl)pyrimidine (**4c**): Yellow solid, yield: 95%; ^{1}H NMR (400 MHz, $CDCl_3$, δ, ppm): 8.11 (d, *J* = 8.84 Hz, 2H, ArH), 8.07 (d, *J* = 8.56 Hz, 2H, ArH), 7.88 (s, 1H, Pyr-H), 7.49 (d, *J* = 8.68 Hz, 2H, ArH), 7.02 (d, *J* = 8.92 Hz, 2H, ArH), 3.89 (s, 3H,

OCH_3); ^{13}C NMR (100 MHz, $CDCl_3$, δ ppm): 167.27, 165.95, 162.75, 162.02, 137.82, 134.25, 129.30, 129.16, 128.67, 127.81, 114.46, 109.62, 55.50 (OCH_3).

2-chloro-4,6-bis(4-methoxyphenyl)pyrimidine (**4e**): Yellow solid, yield: 93%, mp = 187-190°C; ^1H NMR (400 MHz, $CDCl_3$, δ, ppm): 8.10 (d, J = 8.48 Hz, 3H, ArH), 7.87 (d, J = 8.84 Hz, 1H, ArH), 7.85 (s, 1H, Pyr-H), 7.01 (dd, J = 8.50 Hz, 1.74 Hz, 4H, ArH), 3.88 (s, 6H, $2OCH_3$); ^{13}C NMR (100 MHz, $CDCl_3$, δ ppm): 166.74, 166.52, 162.51, 161.84, 161.58, 131.61, 129.10, 128.19, 127.90, 114.39, 113.67, 109.01, 55.49 (OCH_3), 55.44 (OCH_3).

2-chloro-4-(3,4-dimethoxyphenyl)-6-(4-methoxyphenyl)pyrimidine (**4f**): Yellow solid, yield: 89%, mp = 138-141°C; ^1H NMR (400 MHz, $CDCl_3$, δ, ppm): 8.12 (d, J = 8.88 Hz, 2H, ArH), 7.87 (d, J = 8.84 Hz, 1H, ArH), 7.85 (s, 1H, Pyr-H), 7.01 (d, J = 8.88 Hz, 2H, ArH), 6.96 (d, J = 8.36 Hz, 1H, ArH), 4.00 (s, 3H, OCH_3), 3.95 (s, 3H, OCH_3), 3.88 (s, 3H, OCH_3); ^{13}C NMR (100 MHz, $CDCl_3$, δ ppm): 164.28, 164.24, 162.78, 161.40, 150.90, 149.06, 131.44, 131.04, 120.01, 113.92, 110.87, 110.05, 99.65, 56.00 (OCH_3), 55.95(OCH_3), 55.39(OCH_3).

2-chloro-4,6-bis(3,4-dimethoxyphenyl)pyrimidine (**4g**): Yellow solid, yield: 78%, mp = 180-183°C; ^1H NMR (400 MHz, $CDCl_3$, δ, ppm): 7.86 (s, 1H, ArH), 7.74 (s, 2H, ArH), 7.69 (d, J = 7.12 Hz, 2H, ArH), 6.97 (d, J = 7.76 Hz, 2H, ArH), 4.00 (s, 6H, $2OCH_3$), 3.96 (s, 6H, $2OCH_3$).

4.6.1.5 A typical procedure for the synthesis of 4,6-diphenyl-2-(piperazin-1-yl)pyrimidine

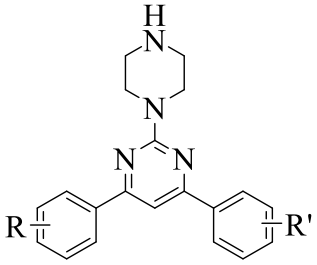

5a	R = 4-Cl,	R' = 4-MeO
5b	R = 4-Me,	R' = 4-MeO
5c	R = 4-MeO,	R' = 4-MeO
5d	R = 3,4-MeO,	R' = 4-Et

A reaction mixture of 2-chloro-4,6-diphenylpyrimidine (4.0 g, 15 mmol) and piperazine (13.92 g, 150 mmol) in isopropanol (20 mL) was refluxed for 20 hours. Using TLC, the progression of the reaction was monitored. The reaction mixture was added to 2 M NaOH (100 mL), the precipitate formed was filtered, washed with water/diethyl ether and dried under vacuum. The product was purified by recrystallisation in EtOAc to afford the following pure compound(s).

4-(4-chlorophenyl)-6-(4-methoxyphenyl)-2-(piperazin-1-yl)pyrimidine (**5a**): Yellow solid, yield: 98%; ^{1}H NMR (400 MHz, $CDCl_3$, δ, ppm): 8.25 (d, J = 8.76 Hz, 2H, ArH), 8.17 (d, J = 8.08 Hz, 1H, ArH), 7.70 (s, 1H, Pyr-H), 7.33 (d, J = 8.04 Hz, 2H, ArH), 3.93 (br s, 4H, $2CH_2$), 3.84 (s, 3H, OCH_3), 2.57 (q, J = 4.42 Hz, 4H, $2CH_2$).

4-(4-methoxyphenyl)-2-(piperazin-1-yl)-6-(p-tolyl)pyrimidine (**5b**): Yellow solid, yield: 98%; ^{1}H NMR (400 MHz, $CDCl_3$, δ, ppm): 8.26 (d, J = 8.79 Hz, 2H, ArH), 8.18 (d, J = 8.09 Hz, 2H, ArH), 7.70 (s, 2H, Pyr-H), 7.33 (d, J = 8.04 Hz, 2H, ArH), 7.07 (d, J = 8.79 Hz, 2H, ArH), 3.94 (br s, 4H, $2CH_2$), 3.85 (s, 3H, OCH_3), 2.58 (br s, 4H, $2CH_2$), 2.38 (s, 3H, CH_3); ^{13}C NMR (100 MHz, DSMO-d_6, δ ppm): 164.90, 164.23, 164.09, 161.57, 161.50, 141.76, 140.55, 139.46, 134.58, 132.46, 129.60, 129.47, 128.77, 128.29, 128.09, 127.05, 117.15, 114.11, 113.48, 100.68, 55.42 (OCH_3), 21.05, 21.03 (CH_3); HRMS (ESI, *m/z*) $[M+H]^+$; calculated for $C_{22}H_{24}N_4O$, 361.2028; Found 361.2067.

4,6-bis(4-methoxyphenyl)-2-(piperazin-1-yl)pyrimidine (**5c**): Brown solid, yield: 86%, mp =151-153 °C; FTIR (ATR, ν_{max}, cm^{-1}): 3277 (N-H of NH), 2926-2845 (C-H of CH_3), 1172-1094 (C-N of pyr), 1256 (C-O of OCH_3),1563 (C=N of pyr), 1605(C=C of Ar); ^{1}H NMR (400 MHz, DSMO-d_6, δ, ppm): 8.25 (d, J = 8.37 Hz, 4H, ArH), 7.67 (s, 1H, Pyr-H), 7.06 (d, J = 8.38 Hz, 4H ArH), 3.93 (br s, 4H, $2CH_2$), 3.84(s, 6H, $2OCH_3$), 3.37 (s, 2H, CH_2), 2.18 (s, 1H, CH), 2.60 (br s, 4H, $2CH_2$); ^{13}C NMR (100 MHz, $CDCl_3$, δ ppm): 163.70, 161.48, 161.28, 129.65, 128.58, 122.28, 113.92, 99.88, 55.28 ($2OCH_3$), 51.03 (CH_2), 46.11($2CH_2$), 43.26 ($2CH_2$).

4-(3,4-dimethoxyphenyl)-6-(4-ethylphenyl)-2-(piperazin-1-yl)pyrimidine (**5d**): Yellow solid, yield: 95%, mp = 130-133°C; ^{1}H NMR (400 MHz, $CDCl_3$, δ, ppm): 8.25 (d, J = 8.23 Hz, 2H, ArH), 7.96 (d, J = 7.98, 1.94 Hz, 1H, ArH), 7.88 (s, 1H, Pyr-H), 7.86 (d, J = 8.20 Hz, 2H, ArH), 7.28 (d, J = 8.26 Hz, 2H, ArH), 7.09 (d, J = 8.59 Hz, 1H, ArH), 4.33 (br s, 4H, $2CH_2$), 3.91 (s, 3H, OCH_3), 3.85 (s, 3H, OCH_3), 3.76 (br s, 4H, $2CH_2$), 2.70 (q, J = 7.57, 2H, CH_2), 1.23 (q, J = 7.58Hz, 3H, CH_3); ^{13}C NMR (100 MHz, DMSO-d_6, δ ppm): 164.38, 164.28,160.92, 151.37, 148.83, 146.95, 134.44, 129.28, 128.08, 127.42, 127.28, 120.58, 111.48, 110.39, 101.95, 56.79, 55.79(OCH_3), 55.65 (OCH_3), 49.38 ($2CH_2$), 37.29 ($2CH_2$), 28.06 (CH_2), 15.46 (CH_3).

4-(furan-2-yl)-2-(piperazin-1-yl)-6-(pyridin-3-yl)pyrimidine (**5e**): Yellow solid, yield: 93 %; ^{1}H NMR (400 MHz, $CDCl_3$, δ, ppm): 8.75 (d, J = 3.94 Hz, 2H, ArH), 8.52 (d, J = 8.06 Hz, 1H, ArH),

8.24 (d, *J* = 8.55 Hz, 2H, ArH), 7.82 (s, 1H, Pyr-H), 7.63 (d, *J* = 8.61 Hz, 2H, ArH), 7.68 (d, *J* = 7.98 Hz, 1H, ArH), 3.93 (br s, 4H, $2CH_2$), 2.56 (br s, 4H, $2CH_2$).

4.6.1.6 A typical procedure for the synthesis of cinnamic acid

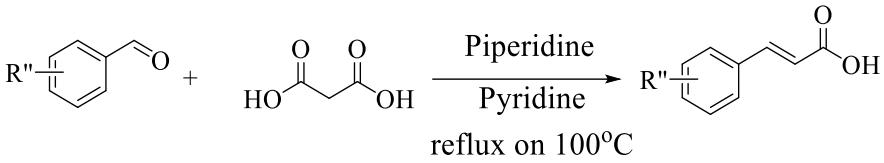

Benzaldehyde (2.0 g, 14.22 mmol), malonic acid (3.3g, 31.30 mmol) and piperidine (1.5 g, 17.07 mmol) in pyridine (30 mL) was reflux for 24 hours. The progression of the reaction was tracked by TLC. The crude was then added to a 2 M HCl solution. The precipitate formed was filtered, washed with water and dried to obtain the following pure compounds. No purification was needed.

(E)-3-(p-tolyl)acrylic acid (**6a**): yield: 98%, Creamy white fluffy solid, mp = 195-198 °C; ^{1}H NMR (400 MHz, DMSO-*d*6, *δ*, ppm): 12.31 (s, 1H, OH), 7.58-7.54 (m, 3H, ArH), 7.23 (d, *J* = 7.67 Hz, 2H, ArH), 6.46 (d, *J* = 16.01 Hz, 1H, Ph-CH=C**H**), 2.33 (s, 3H, CH_3); ^{13}C NMR (100 MHz, DMSO-*d*6, *δ* ppm):144.38, 140.59, 140.43, 131.98, 129.97, 128.65, 118.57, 21.46.

(E)-3-(4-chlorophenyl)acrylic acid (**6b**): Creamy white fluffy solid, yield: 97%, mp = 140-143 °C ; ^{1}H NMR (400 MHz, DMSO-*d*6, *δ*, ppm): 12.46 (s, 1H, OH), 7.72 (d, *J* = 8.51 Hz, 2H, ArH), 7.58 (d, *J* = 16.05 Hz, 1H, Ph-C**H**=CH), 7.46 (d, *J* = 8.48 Hz, 2H, ArH), 6.55 (d, *J* = 16.04 Hz, 1H, Ph-CH=C**H**); ^{13}C NMR (100 MHz, DMSO-*d*6, *δ* ppm): 167.88, 142.97, 135.17, 133.74, 130.40, 129.39, 120.56.

(E)-3-(furan-2-yl)acrylic acid (**6c**):Yellow solid, yield: 89%, mp =142-144 °C; ^{1}H NMR (400 MHz, DMSO-*d*6, δ, ppm): 12.40 (s, 1H), 7.83 (s, 1H), 7.38 (d, *J* =16 Hz, 1H), 6.93 (d, *J* = 3.5 Hz, 1H), 6.62 ppm (t, *J* = 3.5 Hz, 1H), 6.15 (d, *J* = 16 Hz, 1H); ^{13}C NMR (100 MHz, DMSO-*d*6, δ, ppm): 167.7, 150.7, 146.1, 131.2, 116.3, 115.9, 113.1.

4.6.1.7 A typical procedure for the synthesis of cinnamoyl chloride

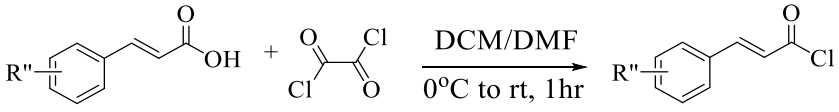

To a stirring solution of cinnamic acid (0.2 g, 1.10 mmol) and 2 drops DMF in anhydrous dichloromethane (DCM, 5 mL), oxalyl chloride (0.21g, 1.6 mmol) was added at 0°C in an ice bath under N_2. After 10 mins, the reaction was stirred at room temperature for 50 mins. The progression of the reaction was tracked by TLC. The crude product was dried under vacuum on rotavapor under N_2. The crude product was used for the next step without further purification.

4.6.1.8 A typical procedure for the synthesis of (*E*)-1-(4-(4-(4-methoxyphenyl)-6-(p-tolyl) pyrimidine-2-yl)piperazin-1-yl)-3-phenylprop-2-en-1-one

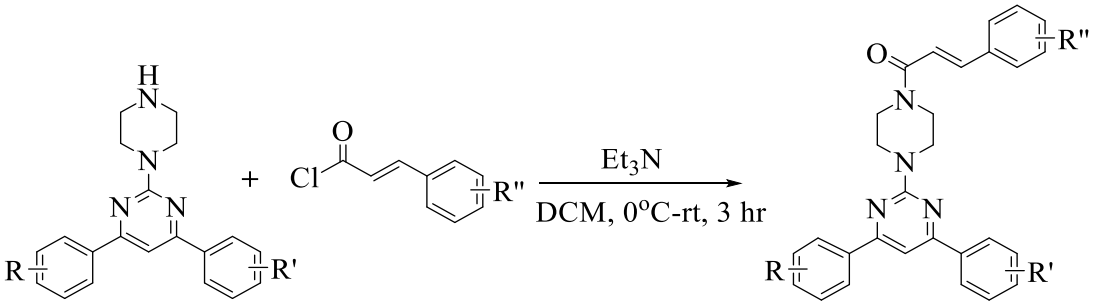

4,6-Diphenyl-2-(piperazin-1-yl) pyrimidine (0.2 g, 0.63 mmol) dissolved in DCM (3 mL) was added to a stirring solution of cinnamoyl chloride (0.16 g, 0.95 mmol) and Et_3N (0.25 mL) in DCM (5 mL) at 0°C under N_2. After 10 mins, the reaction mixture was allowed to stir for 3 hours at room temperature under N_2. The progression of the reaction was tracked using TLC. DCM and Et_3N were removed under rotavapor. The crude compound was purified by column chromatography using DCM (100%) as an eluent to obtain the following pure compounds.

Spectra Data for compound 8 (a-r)

(E)-1-(4-(4-(4-chlorophenyl)-6-(4-methoxyphenyl)pyrimidin-2-yl)piperazin-1-yl)-3-phenylprop-2-en-1-one (**8a**): Yellow solid, yield: 86%, mp = 216-219 °C; IR (ATR-FTIR, ν_{max}, cm^{-1}): ν = 2950-2840 (C-H, CH_3), 1676-1624 (C=C, olefin), 1282 (C-O, OCH_3), 983 (C=C, alkene), ^{1}H NMR (400 MHz, $CDCl_3$, δ, ppm): 8.32 (d, J =8.58 Hz, 2H, ArH), 8.28 (d, J = 8.81 Hz, 2H, ArH), 7.80 (s, 1H, ArH), 7.69 (d, J =8.57 Hz, 2H, ArH), 7.56 (d, J =15.44 Hz, 1H, Ph-C**H**=CH), 7.44-7.40 (m, 3H, ArH), 7.34 (d, J = 15.40 Hz, 1H, Ph-CH=C**H**), 7.08 (d, J =8.84 Hz, 2H, ArH), 3.98 (br s, 4H, $2CH_2$), 3.85 (s, 3H, OCH_3), 3.85-3.74 (m. 3H, $2CH_2$); ^{13}C NMR (100 MHz, DSMO-d_6, δ ppm): 164.63, 164.35, 162.91, 161.54, 161.43, 141.61, 136.12, 135.37, 135.14, 129.54, 129.34, 128.82, 128.75, 128.67, 128.01, 118.26, 114.02, 100.90, 55.35 (OCH_3).

(E)-1-(4-(4-(4-methoxyphenyl)-6-(p-tolyl)pyrimidin-2-yl)piperazin-1-yl)-3-phenylprop-2-en-1-one (**8b**): Creamy white solid, yield: 90%, mp = 185-187 ℃; IR (ATR-FTIR, ν_{max}, cm^{-1}): *v* = 3010 (C-H of Olefin), 2997-2840 (C-H of CH_3), 1643-1605 (C=C OF Ar), 1251 (C-O, OCH_3), 980 (C-H of Olefin); ^1H NMR (400 MHz, $CDCl_3$, *δ*, ppm): 8.10 (d, *J* = 8.90 Hz, 2H, ArH), 8.02 (d, *J* = 8.19 Hz, 2H, ArH), 7.73 (d, *J* = 15.43 Hz, 1H, Ph-C**H**=CH), 7.57-7.55 (m, 1H, ArH), 7.40-7.38 (m, 4H, ArH), 7.30 (d, *J* = 7.99 Hz, 2H, ArH), 7.01 (d, *J* = 8.89 Hz, 2H, ArH), 6.96 (d, *J* = 15.43 Hz, 1H, Ph-CH=C**H**), 4.10 (br s, 4H, $2CH_2$), 3.89 (s, 3H, OCH_3), 2.43 (s, 3H, CH_3); ^{13}C NMR (100 MHz, DSMO-d_6, *δ* ppm): 164.61, 164.11, 163.98, 161.47, 161.41, 141.60, 140.44, 135.14, 134.50, 129.55, 129.51, 129.03, 128.76, 128.76, 128.68, 128.53, 128.02, 126.97, 118.26, 114.00, 100.61, 55.34(OCH_3), 20.98 (CH_3); HRMS (ESI, *m/z*) $[M+H]^+$; calculated for $C_{31}H_{30}N_4O_2$, 513.2267; Found 513.2272.

(E)-3-(4-chlorophenyl)-1-(4-(4-(4-methoxyphenyl)-6-(p-tolyl)pyrimidin-2-yl)piperazin-1-yl)prop-2-en-1-one (**8c**): Brown solid, yield: 71%, mp = 169-172 ℃; IR (ATR-FTIR, ν_{max}, cm^{-1}): *v* =3128 (C-C, Olefin), 2938-2840 (C-H, CH_3), 1607 (C=C, olefin), 1212.33-1236.35 (C-O, OCH_3), 980 (C-C, Olefin); ^1H NMR (400 MHz, $CDCl_3$, *δ*, ppm): 8.10 (d, *J* = 8.90 Hz, 2H, ArH), 8.01 (d, *J* = 8.18 Hz, 2H, ArH), 7.67 (d, *J* = 15.43 Hz, 1H, Ph-C**H**=CH), 7.48 (d, *J* = 8.46 Hz, 2H, ArH), 7.38-7.35 (m, 3H, ArH), 7.30 (d, *J* =7.96 Hz, 2H, ArH), 7.01 (d, *J* = 8.89 Hz, 2H, ArH), 6.92 (d, *J* = 15.43 Hz, 1H, Ph-CH=C**H**), 4.10 (br s, 4H, $2CH_2$), 3.88 (s, 3H, CH_3), 3.80 (br s, 4H, $2CH_2$), 2.43 (s, 3H, CH_3); ^{13}C NMR (100 MHz, $CDCl_3$, *δ* ppm): 165.06, 164.43, 164.70, 161.99, 161.65, 141.61, 140.69, 135.50, 135.29, 133.21, 131.48, 129.42, 129.10, 128.99, 128.88, 128.68, 128.58, 126.58, 117.69, 114.04, 113.35, 101.54, 55.43(OCH_3), 21.45 (CH_3).

(E)-1-(4-(4-(4-chlorophenyl)-6-(4-methoxyphenyl)pyrimidin-2-yl)piperazin-1-yl)-3-(p-tolyl)prop-2-en-1-one (**8d**): Yellow solid, yield: 88%, mp = 207-209 ℃; IR (ATR-FTIR, ν_{max}, cm^{-1}): *v* =2994.33 (C-H, olefin), 2916.03, 2834.98 (C-H, CH_3), 1649.56 (C=C, olefin), 783.05 (C-Cl). ^1H NMR (400 MHz, $CDCl_3$, *δ*, ppm): 8.07 (dd, *J* = 15.64 Hz, 8.77 Hz, 4H, ArH), 7.71 (d, *J* =15.91 Hz, 1H, Ph-C**H**=CH), 7.47-7.44 (m, 4H, ArH), 7.35 (s, 1H, ArH), 7.20 (d, *J* = 7.94 Hz, 2H, ArH), 7.01 (d, *J* = 8.89 Hz, 2H, ArH), 6.90 (d, *J* = 15.40 Hz, 1H, Ph-C**H**=CH), 4.09 (br s, 4H, $2CH_2$), 3.88 (s, 3H, OCH_3), 3.80 (br s, 4H, $2CH_2$), 2.38 (s, 3H, CH_3); ^{13}C NMR (100 MHz, $CDCl_3$, *δ* ppm): 164.96, 164.73, 164.59, 161.95, 151.70, 149.32, 147.13, 140.66, 135.37, 134.06, 134.05,

130.27, 130.22, 129.25, 128.52, 127.63, 120.85, 119.69, 112.04, 110.89, 101.45, 56.20 (OCH_3), 28.55 (CH_3).

(E)-3-(3,4-dimethoxyphenyl)-1-(4-(4-(4-methoxyphenyl)-6-(p-tolyl)pyrimidin-2-yl)piperazin-1-yl)prop-2-en-1-one (**8e**): Creamy white solid, yield: 93%, mp = 124-128 ℃; IR (ATR-FTIR, ν_{max}, cm^{-1}): *v* = 2996.75 (C-H, olefin), 2911.69-2836.59 (C-H, CH_3), 1723.52, 1643.39 (C=C, olefin), 1237.32 (C-O, OCH_3); ^{1}H NMR (400 MHz, $CDCl_3$, *δ*, ppm): 8.10 (d, *J* = 8.90 Hz, 2H, ArH), 8.01 (d, *J* = 8.19 Hz, 2H, ArH), 7.68 (d, *J* = 15.32 Hz, 1H, Ph-C**H**=CH), 7.38 (s, 1H, ArH), 7.30 (d, *J* = 7.99 Hz, 2H, ArH), 7.15-7.13 (m, 2H, ArH), 7.06 (d, *J* = 1.89 Hz, 1H, ArH), 7.00 (d, *J* = 8.87 Hz, 2H, ArH), 6.88 (d, *J* = 8.33 Hz, 1H, ArH), 6.81 (d, *J* = 15.32 Hz, 1H, Ph-CH=C**H**), 4.10 (br s, 4H, $2CH_2$), 3.94 (s, 3H, OCH_3), 3.92 (s, 3H, OCH_3), 3.88 (s, 3H, OCH_3), 3.83 (br s, 4H, $2CH_2$), 2.43(s, 3H, CH_3).

(E)-1-(4-(4,6-bis(4-methoxyphenyl)pyrimidin-2-yl)piperazin-1-yl)-3-phenylprop-2-en-1-one (**8f**): Creamy white solid, yield: 86%, mp = 170-172 ℃; IR (ATR-FTIR, ν_{max}, cm^{-1}): 3005 (C-H, olefin), 2929-2940 (C-H, CH_3), 1646-1606 (C=C, olefin), 1265 (C-O, OCH_3), 983 (C-C, Olefin); ^{1}H NMR (400 MHz, $CDCl_3$, *δ*, ppm): 8.10 (d, *J* = 8.88 Hz, 4H, ArH), 7.74 (d, *J* = 15.45 Hz, 1H, Ph-C**H**=CH), 7.56-7.55 (m, 1H, ArH), 7.40-7.35 (m, 3H, ArH), 7.01 (d, *J* = 8.92 Hz, 4H, ArH), 6.96 (d, *J* = 15.41 Hz, 1H, Ph-CH=C**H**), 4.10 (br s, 4H, $2CH_2$), 3.88 (s, 6H, OCH_3), 3.80 (br s, 4H, $2CH_2$); ^{13}C NMR (100 MHz, $CDCl_3$, *δ* ppm): 165.77, 164.58, 161.97, 161.61, 143.03, 135.29, 130.55, 129.70, 128.85, 128.56, 127.82, 117.12, 114.03, 101.04, 55.43 ($2OCH_3$).

(E)-1-(4-(4,6-bis(4-methoxyphenyl)pyrimidin-2-yl)piperazin-1-yl)-3-(4-chlorophenyl)prop-2-en-1-one (**8g**): Yellow solid, yield: 89%, mp = 169-172 ℃; IR (ATR-FTIR, ν_{max}, cm^{-1}): *v* = 3003.37 (C-H, Olefin), 2931- 2840 (C-H, CH_3), 1714 (C=O), 1650 (C=C, Ar), 1254, 1236 (C-O, OCH_3), 784 (C-Cl).^{1}H NMR (400 MHz, $CDCl_3$, *δ*, ppm): 8.27 (d, *J* = 8.36 Hz, 4H, ArH), 7.81-7.78 (m, 2H, ArH), 7.72 (s, 1H, ArH), 7.56-7.48 (m, 3H, ArH), 7.38 (d, *J* = 15.42 Hz, 1H, Ph-CH=C**H**), 7.08 (d, *J* = 8.36 Hz, 4H, ArH), 3.98 (br s, 4H, $2CH_2$), 3.85 (s, 6H, $2CH_3$), 3.75 (br s, 4H, $2CH_2$); ^{13}C NMR (100 MHz, $CDCl_3$, *δ* ppm): 164.46, 163.83, 161.47, 161.40, 140.22, 134.16, 134.01, 130.07, 129.78, 128.80, 128.68, 119.19, 114.02, 100.23, 55.36 (OCH_3).

(E)-1-(4-(4,6-bis(4-methoxyphenyl)pyrimidin-2-yl)piperazin-1-yl)-3-(p-tolyl)prop-2-en-1-one (**8h**): Creamy white solid, yield: 74%, mp = 172-174 ℃; IR (ATR-FTIR, ν_{max}, cm^{-1}): *v* = 2995-

2840 (C-H, CH_3), 1643-1606 (C=C, olefin), 1234 (C-O, OCH_3), 980 (C-C, Olefin); ^{1}H NMR (400 MHz, $CDCl_3$, δ, ppm): 8.27 (d, J = 8.66 Hz, 4H, ArH), 7.72 (s, 1H, ArH), 7.64 (d, J = 7.85 Hz, 2H, Ar), 7.52 (d, J = 15.34 Hz, 1H, Ph-C**H**=CH), 7.30 (s, 1H, ArH), 7.26-7.22 (m, 2H, ArH), 7.08 (d, J = 8.74 Hz, 4H, ArH), 3.97 (br s, 4H, $2CH_2$), 3.85 (s, 6H, $2OCH_3$), 3.74-3.64 (m, 4H, $2CH_2$); ^{13}C NMR (100 MHz, $CDCl_3$, δ ppm): 164.74, 163.80, 161.44, 161.38, 141.64, 139.33, 132.42, 129.37, 129.12, 128.66, 128.23, 128.03, 117.11, 114.00, 100.19, 55.35 (OCH_3), 20.97 (CH_3).

(E)-1-(4-(4,6-bis(4-methoxyphenyl)pyrimidin-2-yl)piperazin-1-yl)-3-(4-methoxyphenyl)prop-2-en-1-one (**8i**): Brown solid, yield: 71%, IR (ATR-FTIR, ν_{max}, cm^{-1}): v = 3127 (C-C, olefin), 2930-2848 (C-H, CH_3), 1653 (C=C, olefin), 1258 (C-O, OCH_3), 986(C-C, olefin); ^{1}H NMR (400 MHz, $CDCl_3$, δ, ppm): 8.09 (d, J = 8.87 Hz, 4H, ArH), 7.72-7.68 (d, J = 15.35 Hz, 1H, Ph-C**H**=CH), 7.52-7.49 (d, J = 8.70 Hz, 2H, ArH), 7.34 (s, 1H, ArH), 7.02-6.70 (d, J =8.87 Hz, 4H, ArH), 6.92-6.90 (d, J = 8.73 Hz, 2H, ArH), 6.84-6.80 (d, J = 15.35 Hz, 1H, Ph-CH=C**H**), 4.09 (br s, 4H, $2CH_2$), 3.88 (s, 6H, $2OCH_3$), 3.84 (s, 3H, OCH_3), 3.81 (br s, 4H, $2CH_2$); ^{13}C NMR (100 MHz, $CDCl_3$, δ ppm): 166.03, 164.57, 161.60, 142.72, 130.58, 129.39, 128.88, 128.03, 114.59, 114.27, 114.02, 101.00, 55.43 ($2OCH_3$), 55.38 (OCH_3).

(E)-1-(4-(4,6-bis(4-methoxyphenyl)pyrimidin-2-yl)piperazin-1-yl)-3-(3,4-dimethoxyphenyl)prop-2-en-1-one (**8j**): Yellow solid, yield: 81%, mp = 116-118 ℃; IR (ATR-FTIR, ν_{max}, cm^{-1}): v =2998 (C-H, Olefin), 2929-2836 (C-H, CH_3), 1643 (C=C, of Ar), 1234 (C-O, OCH_3); ^{1}H NMR (400 MHz, $CDCl_3$, δ, ppm): 8.27 (d, J = 8.38 Hz, 4H, ArH), 7.73 (s, 1H, ArH), 7.50 (d, J = 15.22 Hz, 1H, Ph-C**H**=CH), 7.40 (s, 1H, ArH), 7.24-7.19 (m, 2H, ArH), 7.08 (d, J = 8.80 Hz, 4H, ArH), 6.98 (d, J = 8.28 Hz, 1H, ArH), 3.98 (br s, 4H, $2CH_2$), 3.85-3.72 (m, 16H, $2CH_3$, $4CH_3$); ^{13}C NMR (100 MHz, $CDCl_3$, δ ppm): 167.11, 164.91, 163.81, 161.40, 150.32, 142.01, 129.61, 129.54, 128.68, 127.98, 122.47, 121.51, 115.55, 114.01, 111.61, 110.24, 100.17, 55.69 (OCH_3), 55.55(OCH_3), 55.44 (OCH_3), 55.36(OCH_3).

(E)-1-(4-(4,6-bis(4-methoxyphenyl)pyrimidin-2-yl)piperazin-1-yl)-3-(furan-2-yl)prop-2-en-1-one (**8k**): Yellow solid, yield: 91%, mp = 176-178 ℃; IR (ATR-FTIR, ν_{max}, cm^{-1}): v = 3060 (C-H, olefin), 2935-2842(C-H, CH_3), 1658 (C=C, olefin), 1260 (C-O, OCH_3), 988 (C-C, Olefin); ^{1}H NMR (400 MHz, $CDCl_3$, δ, ppm): 8.09 (d, J =8.85 Hz, 4H, ArH), 7.52 (d, J =15.08 Hz, 1H, Ph-C**H**=CH), 7.47 (s, 1H, ArH), 7.34 (s, 1H, ArH), 7.01 (d, J = 8.86 Hz, 4H, ArH), 7.94 (d, J =15.91

Hz, 1H, Ph-C**H**=CH), 7.81(d, *J* =8.48Hz, 2H, ArH), 6.88 (d, *J* = 15.08 Hz, 1H, Ph-CH=C**H**), 6.57 (d, *J* = 3.32 Hz, 1H, ArH), 6.47 (dd, *J* = 1.72 Hz, 1H, ArH), 4.08 (s, 4H, $2CH_2$), 3.88 (s, 6H, OCH_3), 3.79 (br s, 4H, $2CH_2$); ^{13}C NMR (100 MHz, $CDCl_3$, δ ppm):165.47, 164.57, 161.97, 161.60, 151.71, 143.95, 130.56, 129.82, 128.55, 114.53, 114.02, 113.92, 112.23, 101.00, 55.42 ($2OCH_3$); HRMS (ESI, *m/z*) $[M+Na]^+$; calculated for $C_{31}H_{29}ClN_4O_3$, 519.009; Found 519.2008.

(E)-1-(4-(4-(3,4-dimethoxyphenyl)-6-(4-ethylphenyl)pyrimidin-2-yl)piperazin-1-yl)-3-phenylprop-2-en-1-one (**8l**): Creamy white solid, yield: 92%, mp =174-176 °C; ^1H FTIR (ATR, ν_{max}, cm^{-1}): 2997-2856 (C-H, CH_3), 1646 (C=C, olefin), 1264 (C-O, OCH_3), 982 (C-C, Olefin), NMR (400 MHz, $CDCl_3$, δ, ppm): 8.20 (d, *J* = 7.91 Hz, 2H, ArH), 7.90 (d, *J* = 8.49 Hz, 1H, ArH), 7.84 (s, 1H, ArH), 7.75-7.74 (m, 3H, ArH), 7.55 (d, *J* = 15.34 Hz, 1H, Ph-C**H**=CH), 7.43-7.33 (m, 6H, ArH), 7.08 (d, *J* = 8.44 Hz, 1H, ArH), 3.99 (br s, 4H, $2CH_2$), 3.90 (s, 3H, CH_3), 3.85 (s, 3H, CH_3), 3.85-3.76 (m, 4H, $2CH_2$), 2.68 (qt, *J* = 7.58 Hz, 2H, CH_2), 1.23(t, *J* = 7.59 Hz, 3H, CH_3); ^{13}C NMR (100 MHz, $CDCl_3$, δ ppm): 165.17, 164.74, 164.60(C=O), 151.71, 149.32, 147.13, 142.09, 135.67, 135.38, 130.28, 130.02, 129.24, 128.52, 128.50, 127.63, 120.86, 118.81, 112.05, 110.91, 101.44, 56.26($2CH_2$), 28.56(CH_2), 15.91(CH_2), 2(OCH_3).

(E)-3-(4-chlorophenyl)-1-(4-(4-(3,4-dimethoxyphenyl)-6-(4-ethylphenyl)pyrimidin-2-yl)piperazin-1-yl)prop-2-en-1-one (**8m**): Creamy white fluffy solid, yield: 79%, mp = 109- 110 °C; IR (ATR-FTIR, ν_{max}, cm^{-1}): *v* =2965-2836 (C-H, CH_3), 1649-1613 (C=C, olefin), 1260 (C-O, OCH_3), 982 (C=C, alkene); ^1H NMR (400 MHz, $CDCl_3$, δ, ppm): 8.21 (d, *J* =8.25 Hz, 2H, ArH), 7.93-7.90 (dd, *J* =8.47Hz, 1.97 Hz, 1H, ArH), 7.79 (d, *J* =8.54 Hz, 2H, ArH), 7.75 (s, 1H, ArH), 7.54 (d, *J* = 15.39 Hz, 1H, Ph-CH=C**H**), 7.48 (d, *J* =8.51 Hz, 2H, ArH), 7.40 (s, 1H, ArH), 7.37 (d, *J* =8.00 Hz, 2H, ArH), 7.09 (d, *J* =8.54 Hz, 1H, ArH), 3.98 (br s, 4H, $2CH_2$), 3.90 (s, 3H, CH_3), 3.85 (s, 3H, CH_3), 3.75 (br s, 4H, $2CH_2$), 2.69 (q, *J* = 7.56 Hz, 2H, CH_2), 1.22 (t, *J* = 7.61 Hz, 3H, CH_3); ^{13}C NMR (100 MHz, DMSO-d_6, δ ppm):164.44, 164.21, 164.08, 161.44, 151.17, 148.79, 146.66, 140.21, 134.84, 134.15, 133.99, 129.77, 129.71, 128.77, 128.06, 127.15, 120.35, 119.17, 111.49, 110.29, 100.94, 55.68 (OCH_3), 55.62(OCH_3), 28.07 (CH_2), 15.47 (CH_3).

(E)-1-(4-(4-(3,4-dimethoxyphenyl)-6-(4-ethylphenyl)pyrimidin-2-yl)piperazin-1-yl)-3-(p-tolyl)prop-2-en-1-one (**8n**): Creamy white solid, yield: 87%, mp = 159-161°C; IR (ATR-FTIR, ν_{max}, cm^{-1}): 3080 (C-H, olefin), 3003-2835 (C-H, CH_3), 1771-1712 (C=O), 1652 1606 (C=C,

olefin), 1257 (C-O, OCH_3), 981 (C-C, Olefin); ^{1}H NMR (400 MHz, $CDCl_3$, δ, ppm): 8.04 (d, *J* = 8.16 Hz, 2H, ArH), 7.73-7.69 (m, 3H, ArH), 7.45 (d, *J* = 8.05 Hz, 1H, ArH), 7.33 (d, *J* = 8.12 Hz, 2H, ArH), 7.20 (d, *J* = 7.95 Hz, 2H, ArH), 6.98 (d, *J* = 8.35 Hz, 1H, ArH), 6.91 (d, *J* = 15.36 Hz, 1H, Ph-C**H**=CH), 4.10 (br s, 4H, $2CH_2$), 4.01 (s, 3H, OCH_3), 3.96 (s, 3H, OCH_3), 3.80 (br s, 4H, $2CH_2$), 2.68(qt, *J* = 7.59 Hz, 2H, CH_2), 1.22(t, *J* = 7.58 Hz, 3H, CH_3); ^{13}C NMR (100 MHz, DMSO-d_6, δ ppm):164.75, 164.21, 164.08, 161.44, 151.17, 148.79, 146.65, 141.66, 139.32, 134.86, 132.42, 129.73, 129.36, 128.03, 127.15, 120.35, 117.10, 111.49, 110.30, 100.92, 55.68 (OCH_3), 55.61 (OCH_3), 28.89 (CH_2), 20.96 (CH_2), 15.47 (CH_3).

(E)-1-(4-(4-(3,4-dimethoxyphenyl)-6-(4-ethylphenyl)pyrimidin-2-yl)piperazin-1-yl)-3-(4-methoxyphenyl)prop-2-en-1-one (**8o)**: Creamy white fluffy solid, yield: 89%, mp = 114-116 ℃; IR (ATR-FTIR, ν_{max}, cm^{-1}): *v*= 3080 (C-C, Olefin), 2934-3840 (C-H, CH_3), 1603 (C=C, of Ar), 1259 (C-O, OCH3), 980 (C-C, Olefin); ^{1}H NMR (400 MHz, $CDCl_3$, δ, ppm): 8.20 (d, *J* = 7.57 Hz, 2H, ArH), 7.90 (d, *J* = 8.37 Hz, 1H, ArH), 7.86 (s, 1H, ArH), 7.74 (s, 1H, ArH), 7.69 (d, *J* = 8.02 Hz, 2H, ArH), 7.51 (d, *J* = 15.25 Hz, 1H, Ph-C**H**=CH), 7.36 (d, *J* = 7.59 Hz, 2H, ArH), 7.18 (d, *J* = 15.32 Hz, 1H, Ph-CH=C**H**), 7.09 (d, *J* = 8.69Hz, 1H, ArH), 6.97 (d, *J* = 7.69 Hz, 2H, ArH), 3.98 (s,br, 4H, $2CH_2$), 3.90 (s, 3H, OCH_3), 3.85(s, 3H, OCH_3), 3.80 (s, 3H, OCH_3), 3.75-3.71(m, 4H, $2CH_2$), 2.69 (q, *J* = 7.47 Hz, 2H, CH_2), 1.23(*t*, *J* = 7.53 Hz, 3H, CH_3); ^{13}C NMR (100 MHz, $CDCl_3$, δ ppm): 164.89, 164.20, 164.07, 161.44,160.42, 151.17, 148.79, 146.61, 141.43, 134.85, 129.75, 129.63, 129.19, 128.00, 127.77, 127.32, 127.10, 120.33, 115.58, 114.17, 111.52, 110.37, 100.90, 55.69 (OCH_3), 55.60 (OCH_3), 55.23 (OCH_3), 15.39 (CH_2), 15.36 (CH_3).

(E)-1-(4-(4-(3,4-dimethoxyphenyl)-6-(4-ethylphenyl)pyrimidin-2-yl)piperazin-1-yl)-3-(furan-2-yl)prop-2-en-1-one (**8p**): Creamy white fluffy solid, yield: 86%, mp = 179-182 ℃; IR (ATR-FTIR, ν_{max}, cm^{-1}): *v* = 2938-2840 (C-H, CH_3), 1256 (C-O), 984 (C-C, Olefin); ^{1}H NMR (400 MHz, $CDCl_3$, δ, ppm): 8.20 (d, *J* =8.24 Hz, 2H, ArH), 7.91 (dd, *J* =8.49 Hz, 1.91 Hz, 1H, ArH), 7.82 (dd, *J* = 10.40 Hz, 1.93 Hz, 1H, ArH), 7.75 (s, 2H, ArH), 7.41 -7.36 (m, 3H, ArH), 7.09 (d, *J* =8.54 Hz, 1H, ArH), 7.00 (d, *J* =15.24 Hz, 1H, Ph-CH=C**H**), 6.88 (d, *J* = 3.32 Hz, 1H, ArH), 6.62 (dd, *J* = 1.71 Hz, 1H, ArH), 3.97(br s, 4H, $2CH_2$), 3.90 (s. 3H, OCH_3), 3.84 (s. 3H, OCH_3), 3.84 (br s, 4H, $2CH_2$), 2.69 (q, *J* = 7.54 Hz, 2H, CH_2), 1.23 (t, *J* = 7.57 Hz, 3H, CH_3); ^{13}C NMR (100 MHz, $CDCl_3$, δ ppm):165.75,, 165.49, 165.18, 164.74, 162.01, 151.69, 151.22, 149.16, 147.04, 143.95,

143.03, 135.56, 130.88, 129.85, 128.84, 128.25, 127.81, 127.123, 120.22, 114.49, 113.96, 112.24, 110.97, 110.04, 101.77, 55.04, 25.82, 15.51.

(E)-1-(4-(4-(4-chlorophenyl)-6-(pyridin-3-yl)pyrimidin-2-yl)piperazin-1-yl)-3-(p-tolyl)prop-2-en-1-one (**8q**): Yellow solid, yield: 84%, mp = 172-174 ℃; IR (ATR-FTIR, ν_{max}, cm^{-1}): *v* =3080.95 (C-H, olefin), 2997-2859(C-H, CH_3), 1640 (C=O), 1242 (C-O), 982 (C-C, Olefin), 783(C-Cl, ArCl); ^{1}H NMR (400 MHz, $CDCl_3$, *δ*, ppm): 9.46 (s, 1H, ArH), 8.72 (d, *J* = 4.08 Hz, 1H, ArH), 8.62 (d, *J* =7.89 Hz, 1H, ArH), 8.33 (d, *J* =8.37 Hz, 2H, ArH), 7.94 (s, 1H, ArH), 7.63-7.55 (m, 5H, ArH), 7.51 (d, *J* = 15.34 Hz, 1H, Ph-C**H**=CH), 7.27 (d, *J* = 15.68 Hz, 1H, Ph-CH=C**H**), 7.22 (d, *J* = 7.69 Hz, 2H, ArH), 3.98 (br s, 4H, $2CH_2$), 3.87-3.74 (m, 4H, $2CH_2$), 2.33 (s, 3H, CH_3); ^{13}C NMR (100 MHz, DSMO-d_6, *δ* ppm): 164.79, 163.59, 162.79, 161.45, 151.44, 148.44, 141.69, 139.36, 135.75, 135.73, 134.57, 132.55, 132.40, 129.49, 129.38, 129.12, 128.17, 128.02, 123.75, 118.07, 117.07, 101.89, 20.96 (CH_3); HRMS (ESI, *m/z*) $[M+H]^+$; calculated for $C_{29}H_{26}ClN_5O$, 496.1904; Found 496.2116.

(E)-1-(4-(4-(furan-3-yl)-6-(pyridin-3-yl)pyrimidin-2-yl)piperazin-1-yl)-3-phenylprop-2-en-1-one (**8r**): Yellow solid, yield: 89%, mp = 163-165 ℃; IR (ATR-FTIR, ν_{max}, cm^{-1}): *v* = 3077 (C-C, Olefin), 2932.13-2840 (C-H, CH_3), 1660 (C=C, olefin), 1259 (C-O, OCH_3); ^{1}H NMR (400 MHz, $CDCl_3$, *δ*, ppm): 9.30 (s, 1H, ArH), 8.73 (s, 1H, ArH), 8.39 (d, *J* = 7.97Hz, 2H, ArH), 8.06 (d, *J* =8.57 Hz, 2H, ArH), 7.74 (d, *J* = 15.41 Hz, 1H, Ph-C**H**=CH), 7.56-7.54 (m, 2H, ArH), 7.48 (d, *J* = 8.57 Hz, 2H, ArH), 7.39 (d, *J* = 8.73 Hz, 4H, ArH), 6.95 (d, *J* = 15.42 Hz, 1H, Ph-CH=C**H**), 4.10 (s,br, 4H, $2CH_2$), 3.90-3.83 (m, 4H, $2CH_2$); ^{13}C NMR (100 MHz, $CDCl_3$, *δ* ppm): 165.76, 164.58, 163.22, 161.98, 151.33, 148.37, 143.24, 136.92, 136.01, 135.20, 134.51, 129.78, 129.03, 128.87, 128.43, 127.83, 123.59, 116.91, 102.02.

4.7 Pharmacological Evaluation

4.7.1 Antimalarial activity

The chloroquine-sensitive strain of *P. falciparum* (NF54) was maintained continuously *in vitro* in supplemented RPMI-1640 culture media at 37 ˚C and gassed with a mixture of 5% CO_2, 3% O_2 and 92% N_2 [36]. 5% D-sorbitol was used to synchronise the culture in the ring stage [37]. Determination of the antimalarial activity of different compounds, the synchronised ring-stage parasites were adjusted to a final parasitaemia of 2% and 2% haematocrit, to which serial dilutions

of the derivatives and positive control, quinine were added after 24-hour incubation. Negative controls included uninfected erythrocytes and drug-free parasitised erythrocytes. Following a further 48 h incubation period, the plates were frozen at -70˚C for 1 hour and thawed for 2 hours. Twenty-five microliters of lysate was transferred to a non-sterile plate, to which 100 µL Malstat™ and 20 µL nitroblue tetrazolium and phenazine ethosulphate (1:1) mixture was added to each well and incubated for 40 min at 37 ˚C to quantify the parasite lactate dehydrogenase (pLDH) activity [38]. Thereafter, 5% acetic acid was added to each well, and the absorbance of the formazan products read at 620 nm, as an indicator of parasite viability. The percentage parasite growth, taking the appropriate controls into account were calculated and used to determine the concentration required to inhibit parasite growth by 50% (IC_{50} value) from log sigmoid dose-response curves using the GraphPad Prism® 5.0.0 software. Each experiment was repeated in triplicate [39, 40].

4.7.2 Toxicity assays

4.7.2.1 Cell viability assay

Human embryonic kidney epithelial (HEK-293) cells were maintained at 37 ˚C in a humidified chamber with a 5% CO_2 as a monolayer in Dulbecco's modified Eagle's medium (DMEM) supplemented with 10% of fetal bovine serum, 100 IU mL^{-1} penicillin and 100 µg mL^{-1} streptomycin. A cell suspension (10 000 cells per well) was incubated at 37 ˚C for 48 h with serial dilutions of compounds/positive control. A final concentration of less than 1% DMSO had no effect on the viability of the cells. Thereafter, 40 µL of (3-(4, 5-dimethylthiazolyl-2)-2, 5-diphenyltetrazolium bromide (MTT; 5mg mL^{-1} in phosphate buffer saline (pH 7.3)) was added to each well and incubated for a further 2 hours. DMSO was used to dissolve the formazan crystals and then quantified by reading the absorbance at 540 nm with a reference wavelength of 690 nm (Labsystems Multiskan RC) [41]. Percent cellular viability was determined using the appropriate controls and used to calculate the IC_{50} values which were compared to the positive control, camptothecin. The experiment was repeated in triplicate [42, 43].

4.7.2.2 Binding affinity assays using select synthetic compounds to *P. falciparum* Hsp70

Ligand-compound interaction studies were undertaken to define a possible antiplasmodial mechanism of action. Heat shock proteins are essential to parasite survival, in this study, we

investigated the *P. falciparum* heat shock protein 70's; PfHsp70-1 and PfHsp70-z, as possible antiplasmodial "protein-compound" interactive partners. Recombinant PfHsp70-1 and PfHsp70-z were produced in *E. coli* with a 6x Histidine tag and purified using a nickel affinity protein purification using a previously described method [44]. Binding affinities between the ligand and selected compound were investigated by SPR analysis using the BioNavis™ 420A ILVES MP-SPR (BioNavis, Tampere, Finland) [45]. Degassed PBS Tween 20 (4.3 mM Na_2HPO_4, 1.4 mM KH_2PO_4, 137 mM NaCl, 3 mM KCl, 0.005 % (v/v) Tween 20, and 20 mM EDTA; pH 7.4) was used as a system running buffer. PfHsp70-1 and PfHsp70-z were immobilized as ligands at 0.5 μg/mL onto functionalized 3D carboxymethyl dextran sensors chips (CMD 3D 500L; BioNavis, Tampere, Finland). Immobilization of ligands was achieved through amine coupling after 1-ethyl-3-(3-dimethylaminopropyl) carbodiimide (EDC) [Sigma Aldrich, Germany] and N-hydroxy-succinimide (NHS) [Sigma Aldrich, Germany] activation following a protocol provided by the manufacturer (BioNavis, Tampere, Finland) to achieve < 200 RUs. A reference channel without immobilized protein served as a control for non-specific binding and changes in refractive index. As analytes, compounds (Compound **8o** and **8l**) were prepared into aliquots of 0, 1.25, 2.5, 5 and 10 nM injected three times at a flow rate of 50 μL/min into each flow cell. Injections with buffer only were used as controls. Association between ligand and compounds was allowed for 3 min, and dissociation was monitored for a total of 10 min. Kinetics steady-state equilibrium constant data was processed after double referencing of the sensorgrams and concatenating the responses of all five analyte concentrations by global fitting using TraceDrawer software version 1.8 (Ridgeview Instruments, Sweden).

References

[1] World Health Organization, "High burden to high impact: a targeted malaria response," World Health Organization, 2018. https://www.who.int/publications-detail-redirect/WHO-CDS-GMP-2018.25.

[2] M. Legros and S. Bonhoeffer, "Evolution of drug resistance in malaria parasites," *Malar J*, vol. 11, no. 1, p. P63, 2012/10/15 2012, doi: 10.1186/1475-2875-11-S1-P63.

[3] World Health Organization, "World malaria report 2020: 20 years of global progress and challenges," Geneva, Switzerland: World Health Organization, 2020. https://apps.who.int/iris/handle/10665/337660.

[4] World Health Organization, "World malaria report," Geneva, Switzerland: World Health Organization, 2020, https://apps.who.int/iris/handle/10665/337660.

[5] J. L. Espinoza, "Malaria resurgence in the Americas: An underestimated threat," *Pathog*, vol. 8, no. 1, p. 11, 2019, doi: 10.3390/pathogens8010011.

[6] S. J. Draper, B. K. Sack, C. R. King, C. M. Nielsen, J. C. Rayner, M. K. Higgins, C. A. Long, R. A. Seder and S. J. Draper, "Malaria vaccines: Recent advances and new horizons," *Cell Host Microbe*, vol. 24, no. 1, pp. 43-56, Jul 11 2018, doi: 10.1016/j.chom.2018.06.008.

[7] M. N. Wykes, "Why haven't we made an efficacious vaccine for malaria?", *EMBO Rep*, vol. 14, no. 8, p. 661, Aug 2013, doi: 10.1038/embor.2013.103.

[8] Centre for Disease Control and Presentations. *Global Health, Vaccines*. Centre for Disease Control and Presentations, 2019. https://www.cdc.gov/globalhealth/immunization/default.htm.

[9] S. C. Parija, "Drug resistance in malaria: A predicament," *Trop Parasitol*, vol. 6, no. 1, p. 1, Jan-Jun 2016, doi: 10.4103/2229-5070.175022.

[10] D. C. Sharma, "Turmeric (Curcuma Longa) Wsr to Curcumin," *World J Pharm Res*, pp. 740-753, 2017, doi: 10.20959/wjpr20177-8826.

[11] R. C. Reddy, P. G. Vatsala, V. G. Keshamouni, G. Padmanaban, and P. N. Rangarajan, "Curcumin for malaria therapy," *Biochem Biophys Res Commun*, vol. 326, no. 2, pp. 472-4, Jan 14 2005, doi: 10.1016/j.bbrc.2004.11.051.

[12] Q. Elliott, Z. Wang, R. A. Setien, J. Puttkammer, A. Ugrinov, J. Lee, D. C. Webster, and Q. R. Chu, "Furfural-derived diacid prepared by photoreaction for sustainable materials synthesis," *ACS Sustainable Chem Eng,* vol. 6, no. 7, pp. 81368141, 2018, doi: 10.1021/acssuschemeng.8b02415.

[13] H. Hatcher, R. Planalp, J. Cho, F. M. Torti, and S. V. Torti, "Curcumin: from ancient medicine to current clinical trials," *Cell Mol Life Sci,* vol. 65, no. 11, pp. 163152, Jun 2008, doi: 10.1007/s00018-008-7452-4.

[14] L. Vera-Ramirez, P. Pérez-Lopez, A. Varela-Lopez, M. Ramirez-Tortosa, M. Battino, and J. L. Quiles, "Curcumin and liver disease," *Biofactors,* vol. 39, no. 1, pp. 88-100, Jan-Feb 2013, doi: 10.1002/biof.1057.

[15] L. E. Wright, J. B. Frye, B. Gorti, B. N. Timmermann, and J. L. Funk, "Bioactivity of turmeric-derived curcuminoids and related metabolites in breast cancer," *Curr Pharm Des,* vol. 19, no. 34, pp. 6218-25, 2013, doi: 10.2174/1381612811319340013.

[16] B. Pérez, C. Teixeira, J. Gut, P. J. Rosenthal, J. R. Gomes, and P. Gomes, "Corrigendum: Cinnamic acid/chloroquinoline conjugates as potent agents against chloroquine-resistant Plasmodium falciparum," *Chem Med Chem,* vol. 8, no. 8, pp. 1238-1238, 2013, doi: 10.1002/cmdc.201300258.

[17] M. Larsen, H. Kromann, A. Kharazmi, and S. F. Nielsen, "Conformationally restricted antiplasmodial chalcones," *Bioorg Med Chem Lett,* vol. 15, no. 21, pp. 4858-61, Nov 1 2005, doi: 10.1016/j.bmcl.2005.07.012.

[18] L. L. Franco, M. V. de Almeida, L. F. R. E. S. Vieira, A. M. Pohlit, and M. S. Valle, "Synthesis and antimalarial activity of dihydroperoxides and tetraoxanes conjugated with bis(benzyl)acetone derivatives," *Chem Biol Drug Des,* vol. 79, no. 5, pp. 790-7, 2012, doi: 10.1111/j.1747-0285.2012.01345.x.

[19] H. B. Rasmussen, S. B. Christensen, L. P. Kvist, and A. Karazmi, "A simple and efficient separation of the curcumins, the antiprotozoal constituents of Curcuma longa," *Planta medica,* vol. 66, no. 04, pp. 396-398, 2000, doi: 10.1055/s-2000-8533.

[20] R. Pasupureddy, S. Verma, A. Pant, R. Sharma, S. Seshadri, V. Pande, A. K. Saxena, R. Dixit and K. C. Pandey, "Crucial residues in falcipains that mediate haemoglobin hydrolysis," *Expl Parasitol,* vol. 197, pp. 43-50, 2019/02/01/ 2019, doi: 10.1016/j.exppara.2019.01.005.

[21] K. V. Sashidhara, M. Kumar, R. K. Modukuri, R. K. Srivastava, A. Soni, K. Srivastava, S. V. Singh, J K Saxena, H. M. Gauniyal and S. K. Puri, "Antiplasmodial activity of novel keto-enamine chalcone chloroquine based hybrid pharmacophores," *Bioorg Med Chem*, vol. 20, no. 9, pp. 2971-81, May 1 2012, doi: 10.1016/j.bmc.2012.03.011.

[22] B. Pradines, C. Rogier, T. Fusai, J. Mosnier, W. Daries, E Barret and D Parzy, "In vitro activities of antibiotics against Plasmodium falciparum are inhibited by iron," *Antimicrob Agents Chemother*, vol. 45, no. 6, p. 1746, 2001, doi: 10.1128/AAC.45.6.1746-1750.2001.

[23] N. Rastogi, K. S. Goh, L. Horgen, and W. W. Barrow, "Synergistic activities of antituberculous drugs with cerulenin and trans-cinnamic acid against Mycobacterium tuberculosis," *FEMS Immunol Med Microbiol*, vol. 21, no. 2, pp. 149-157, 1998, doi: 10.1111/j.1574-695X.1998.tb01161.x.

[24] J. A. Badejo, O. O. Abiodun, O. Akinola, C. T. Happi, A. Sowunmi, and G. O. Gbotosho, "Interaction between rifampicin, amodiaquine and artemether in mice infected with chloroquine-resistant Plasmodium berghei," *Malar J*, vol. 13, no. 1, p. 299, 2014, doi: 10.1186/1475-2875-13-299.

[25] M. Strath, T. Scott-Finnigan, M. Gardner, D. Williamson, and I. Wilson, "Antimalarial activity of rifampicin in vitro and in rodent models," *Trans R Soc Trop Med Hyg*, vol. 87, no. 2, pp. 211-216, 1993/03/01/ 1993, https://doi.org/10.1016/0035-9203(93)90497-E.

[26] A. Agarwal, K. Srivastava, S. K. Puri, and P. M. Chauhan, "Syntheses of 2,4,6trisubstituted triazines as antimalarial agents," (in eng), *Bioorg Med Chem Lett*, vol. 15, no. 3, pp. 531-3, Feb 1 2005, doi: 10.1016/j.bmcl.2004.11.052.

[27] J. Morgan, R. Haritakul, and P. Keller, "Antimalarial activity of 2,4-diaminopyrimidines," *Let Drug Des Discov*, vol. 5, no. 4, pp. 277-280, 2008, doi: 10.2174/157018008784619843.

[28] V. R. Dola, A. Soni, P. Agarwal, H. Ahmad, K. S. R. Raju, M. Rashid, M. Wahajuddin, K. Srivastava, W. Haq, A. K. Dwivedi, S. K. Puri, and S. B. Katti, "Synthesis and evaluation of chirally defined side-chain variants of 7chloro-4-aminoquinoline to overcome drug resistance in malaria chemotherapy," *Antimicrob Agents Chemother*, vol. 61, no. 3, 2017. https://doi.org/10.1128/AAC.01152-16

[29] S. Manohar, U. C. Rajesh, S. I. Khan, B. L. Tekwani, and D. S. Rawat, "Novel 4aminoquinoline-pyrimidine based hybrids with improved in vitro and in vivo antimalarial

activity," *ACS Med Chem Lett,* vol. 3, no. 7, pp. 555-559, 2012/07/12 2012, doi: 10.1021/ml3000808.

[30] S. Manohar, M. Tripathi, and D. S. Rawat, "4-aminoquinoline based molecular hybrids as antimalarials: an overview," *Curr Top Med Chem,* vol. 14, no. 14, pp. 1706-33, 2014, doi: 10.2174/1568026614666140808125728.

[31] F. Kayamba, T. Malimabe, I. K. Ademola, N. D. Kushwaha, M. Mahlalela, R. L. van Zyl, M. Gordon, P. T. Mudau, T. Zininga, A. Shonhai, V. O. Nyamori and R. Karpoormath, "Design and synthesis of quinoline-pyrimidine inspired hybrids as potential plasmodial inhibitors,", *Eur J Med Chem,* vol. 217, p. 113330, Mar 3 2021, doi: 10.1016/j.ejmech.2021.113330.

[32] F. Toda, K. Tanaka, and K. Hamai, "Aldol condensations in the absence of solvent: acceleration of the reaction and enhancement of the stereoselectivity," *J Chem Soc Perkin Trans. I,* no. 11, pp. 3207-3209, 1990, doi: 10.1039/P19900003207.

[33] D. Giles, K. Roopa, F. R. Sheeba, P. M. Gurubasavarajaswamy, G. Divakar, and T. Vidhya, "Synthesis pharmacological evaluation and docking studies of pyrimidine derivatives," *Eur J Med Chem,* vol. 58, pp. 478-84, Dec 2012, doi: 10.1016/j.ejmech.2012.09.050.

[34] J. Dickson, L. Flores, M. Stewart, R. LeBlanc, H. N. Pati, M. Lee, and H. Holt, "Synthesis and cytotoxic properties of chalcones: an interactive and investigative undergraduate laboratory project at the interface of chemistry and biology," ASC *J Chem Edu,* vol. 83, no. 6, p. 934, 2006, doi: 10.1021/ed083p934.

[35] L. Mohammadkhani and M. M. Heravi, "Oxalyl chloride: A versatile reagent in organic transformations," *Chem Select,* vol. 4, no. 20, pp. 6309-6337, 2019, doi: 10.1002/slct.201900120.

[36] W. Trager and J. B. Jensen, "Human malaria parasites in continuous culture," *Science,* vol. 193, no. 4254, pp. 673-5, Aug 20 1976, doi: 10.1126/science.781840.

[37] C. Lambros and J. P. Vanderberg, "Synchronization of plasmodium falciparum erythrocytic stages in culture," *J Parasitol,* vol. 65, no. 3, pp. 418-420, 1979, doi: 10.2307/3280287.

[38] M. T. Makler, J. M. Ries, J. A. Williams, J. E. Bancroft, R. C. Piper, B. L. Gibbins and D. J. Hinrichs, "Parasite lactate dehydrogenase as an assay for Plasmodium falciparum drug

sensitivity," *Am J Trop Med Hyg*, vol. 48, no. 6, pp. 739-41, Jun 1993, doi: 10.4269/ajtmh.1993.48.739.

[39] A. D. Forkuo, C. Ansah, K. B. Mensah, K. Annan, B. Gyan, A. Theron, D. Mancama and C. W. Wright, "*In vitro* anti-malarial interaction and gametocytocidal activity of cryptolepine," *Malar J*, vol. 16, no. 1, p. 496, 2017, doi: 10.1186/s12936017-2142-z.

[40] J. Reader, M. Botha, A. Theron, S. B. Lauterbach, C. Rossouw, D. Engelbrecht, M. Wepener, A. Smit, D. Leroy, D. Mancama, T. L. Coetzer and L. Birkholtz, "Nowhere to hide: interrogating different metabolic parameters of Plasmodium falciparum gametocytes in a transmission blocking drug discovery pipeline towards malaria elimination," *Malar J*, vol. 14, p. 213, May 22 2015, doi: 10.1186/s12936-015-0718-z.

[41] T. Mosdam, "Rapid colourimetric assay for cellular growth and survival: Application to proliferation and cytotoxic assay," *J. Immunol. Methods*, vol. 65, pp. 55-63, 1983, doi: 10.1016/0022-1759(83)90303-4.

[42] J. C. Domingue, M. Ao, J. Sarathy, A. George, W. A. Alrefai, D. J. Nelson and M. C. Rao, "HEK-293 cells expressing the cystic fibrosis transmembrane conductance regulator (CFTR): a model for studying the regulation of Cl- transport," *Physiol Rep*, vol. 2, no. 9, Sep 1 2014, doi: 10.14814/phy2.12158.

[43] K. M. Krawczyk, D. Matak, L. Szymanski, C. Szczylik, C. Porta, and A. M. Czarnecka, "Culture in embryonic kidney serum and xeno-free media as renal cell carcinoma and renal cell carcinoma cancer stem cells research model," *Cytotechnology*, vol. 70, no. 2, pp. 761-782, Apr 2018, doi: 10.1007/s10616-017-0181-5.

[44] T. Zininga, S. Makumire, G. W. Gitau, J. M. Njunge, O. J. Pooe, H. Klimek, R. Scheurr, H. Raifer, E. Prinsloo, J. M. Przyborski, H. Hoppe and A. Shonhai, "Plasmodium falciparum Hop (PfHop) interacts with the hsp70 chaperone in a nucleotide-dependent fashion and exhibits ligand selectivity," *PLoS One*, vol. 10, no. 8, p. e0135326, 2015, doi: 10.1371/journal.pone.0135326.

[45] T. Zininga, O. J. Pooe, P. B. Makhado, L. Ramatsui, E. Prinsloo, I. Achilonu, H. Dirr and A. Shonhai, "Polymyxin B inhibits the chaperone activity of Plasmodium falciparum Hsp70," *Cell Stress Chaperones*, vol. 22, no. 5, pp. 707-715, Sep 2017, doi: 10.1007/s12192-017-0797-6.

CHAPTER 5

Synthesis and antimalarial activity of novel 1,2,3-triazole-pyrimidine hybrids

Graphical Abstract

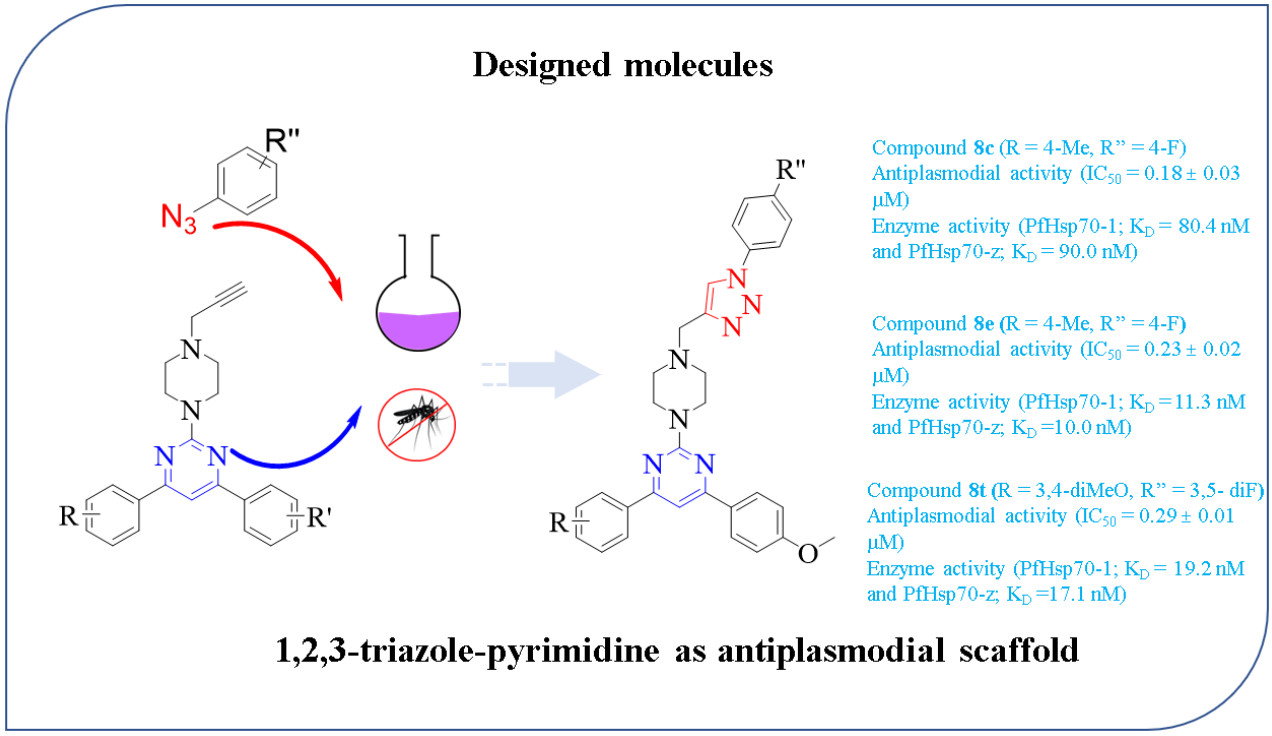

Abstract

To provide an optimized lead antimalarial candidate to address the emergence of resistance in the mainstay drugs, including the Artemisinin combination therapy (ACT), this studies endeavoured to develop and synthesize a novel class of 2-(4-((3H-pyrazol-5-yl)methyl)piperazin-1-yl)-4,6-diphenylpyrimidine hybrids (**8a-t**). *In vitro*, antimalarial evaluation of the synthesized compounds yielded a half-maximal inhibitory concentration (IC_{50}) range from 0.18 to 2.41 µM. Seven compounds were active (IC_{50} value < 0.5 µM) with compound **8p** having IC_{50} values as low as 0.04 ± 2.23 µM. In particular, three compounds **8c, 8e** and **8t** equally displaying prominent activity with IC_{50} of 0.18 ± 0.03 µM, 0.22 ± 0.02 µM and 0.29 ± 0.01 µM had safety profile of 13.40, 9.11 and 61.15 respectively to human kidney epithelial (HEK293) cells. The remaining compounds showed promising activity with IC_{50} values ranging from 0.59 to 2.41 µM. The molecules' binding affinities to two vital cytosolic *P. falciparum* heat shock protein 70 homologues, PfHsp70-1 and PfHsp70-z, were also studied. Compound **8e** displayed the highest binding affinity for both PfHsp70s with K_D in a lower nanomolar range (10-11.3 nM). A constructive link between the antimalarial activity and variation on the phenyl group with activating groups on 4,6-diphenypyrimidine and deactivating groups on 1,2,3-triazole of the hybrid analogues was suggested through structure-activity relationship (SAR) studies. These 1,2,3-triazole-pyrimidine derivatives have the potential to be considered for further evaluation as the starting point for the development of new antimalarial candidates.

Keywords: Malaria, pyrimidine, 1,2,3-triazoles, molecular hybridization, PfHsp70, antiplasmodial, hybrids

5.1 Introduction

Almost all antimalarial frontline drugs developed resistance against *P. falciparum*[1,2], hence, resulting in malaria being a global health threat costing millions of United States dollars in management and treatment [3–6]. As per the WHO recent report in 2019, approximately 229 million people were infected with malaria, with more than 409 000 deaths, 93% of which were from sub-Sahara Africa. Malaria consequences mostly impact pregnant women and children less than five years in endemic areas. About 200 million people still live in abject fear of the malady [7–9]. Since no effective vaccine has yet been developed, therefore the management of malaria exclusively relies on drug therapy [7,10–12].

1,2,3-Triazole scaffold has received considerable attention in drug design, such as antimicrobial [13,14], anticancer [15] and antitubercular agent [16,17]. It also played a crucial role as a recognition cap group in inhibiting histone deacetylase (HDAC), a promising anticancer target [18]. 1,2,3-Triazole was an essential motif of β-lactam-triazole derivatives (**4**) and compound (**1**) that was active against the CQ resistance and sensitive strains with a good toxicity profile (**Figure 5. 1**) [1,19]. Other triazole derivatives displayed promising antimalarial activity and toxicity profile against HepG2 cells [20]. Furthermore, studies by Walter et al. indicated that 1,2,3-triazole is a potential heme inhibitor that allegedly enhances antimalarial activity [21,22].

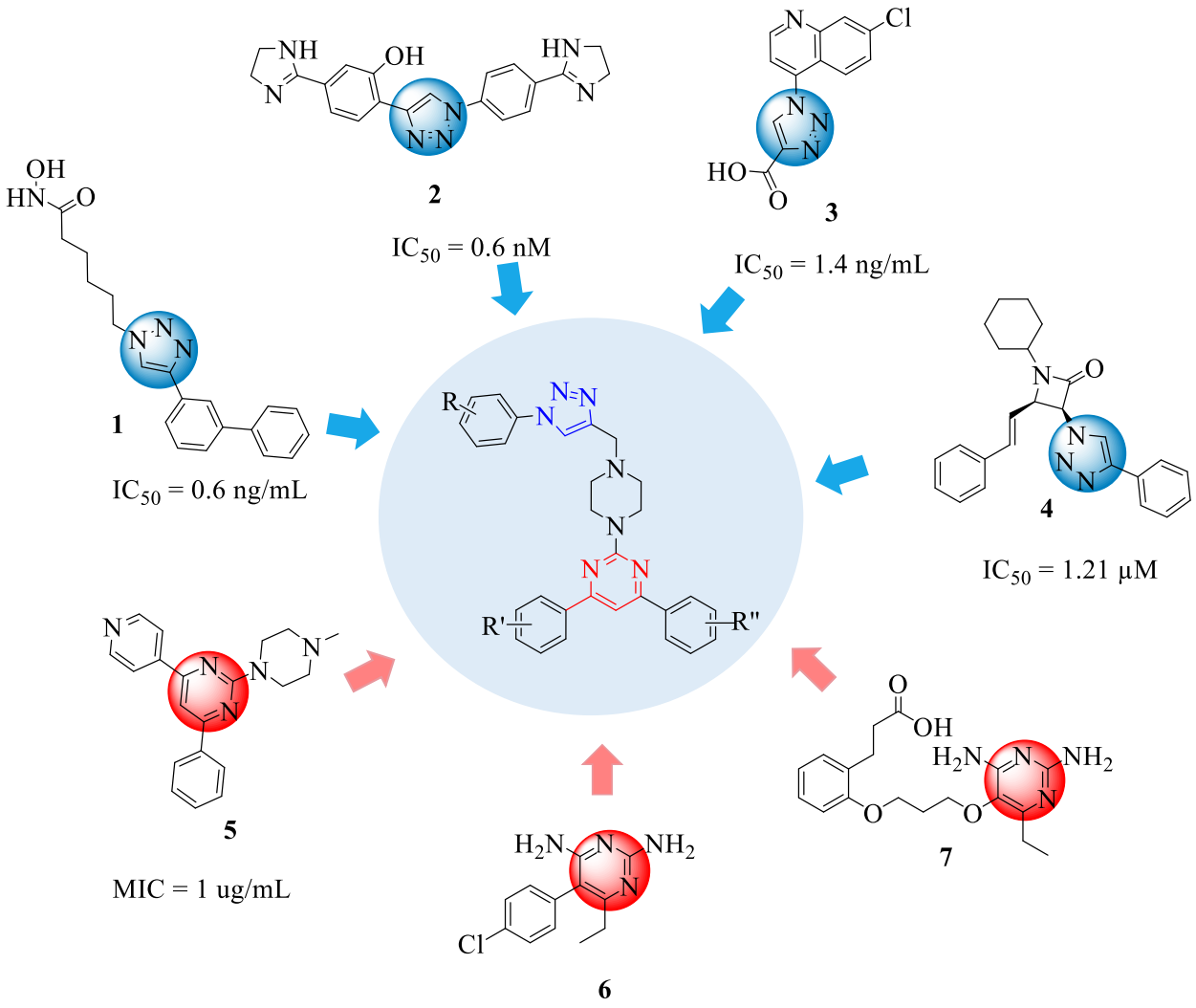

Figure 5.1. Rational design of novel 1,2,3-triazole–pyrimidine hybrids.

Antimalarials with good antimalarial activity, such as pyrimethamine (**6**) and P218 (**7**), have pyrimidine as a key scaffold [23–27]. Such antimalarials are noted for inhibiting the enzyme *Plasmodium falciparum* dihydrofolate reductase (*P. falciparum*-DHFR), impeding the plasmodial folic acid process crucial to the de novo synthesis of purines and pyrimidine needed for the deoxyribonucleic acid (DNA) biosynthesis. This process is important for the survival and growth of the malaria parasite; otherwise, halting it would be lethal to the parasite [23,28,29]. In other pyrimidine-based antimalarial compounds such as 5, substituting a cyclohexyl(piperazine) at position two on the pyrimidine nucleus was crucial for the activity [23,24,30]. Also, we recently demonstrated that a 4,6-diphenylpyrimidine nucleus was essential for antimalarial activity, which we endeavoured to incorporate as part of our ongoing research to develop a library of antimalarial

compounds [31]. In addition, a piperazine linker enhanced the antimalarial activity of 7-quinoline-pyrimidine hybrids by 3-fold against CQ-resistant Dd2 strain compared to the hybrids that had the alkane diamine aliphatic linker indicating how crucial it is as antimalarial pharmacophore [32].

Given the facts and as per our ongoing research, we aimed to apply modern concepts of molecular hybridization to design a library of novel hybrids bearing 1,2,3-triazole and 4,6-diphenylpyrimidine as modified motif using piperazine as a linker. In line with this, we anticipated to provide a single molecule with dual therapeutic action with improved antimalarial efficacy and bioavailability against both liver and blood stages [30].

5.2 Chemistry

The preparation of a library of novel 2-(4-((3H-pyrazol-5-yl)methyl)piperazin-1-yl)-4,6-diphenylpyrimidine hybrids **8(a-t**) was executed using the efficient and versatile synthetic route as described in **Scheme 1** and **2**. The synthesis of the starting material, *(E)* chalcones (**1)** was achieved utilizing different commercially accessible benzaldehyde and acetophenone by an easy aldol condensation reaction in sodium hydroxide ethanolic basic conditions as per stated methods [33–35]. Different (*E*) chalcones were cyclized to produce 4,6-diphenylpyrimidin-2-amines derivatives (**2**) through NaOH basic catalyzed using guanidine hydrochloride reaction. Sandmeyer reaction was applied to oxidize the amino pyrimidine (compound **2**) to hydroxyl (4,6-diphenylpyrimidin-2-ol **3(a-e)** which was initiated through the formation of diazonium salt intermediate using sodium nitrate in acetic acid and then substitution of diazo salt with water. Assorted compounds (**3**) were utilized to afford analogues of 2-chloro-4,6-diphenylpyrimidines **4(a-e)** using $POCl_3$ with catalytic DMF in a 90% yield. 4,6-diphenyl-2-(piperazine-1-yl) pyrimidines **5(a-e)** were obtained by refluxing various **4** with excess piperazine in IPA. Analogues of 4,6-diphenyl-2-(4-(prop-2-yn-1-yl) piperazin-1-yl) pyrimidine (**6**) derivatives were synthesized using propargyl bromide and Et_3N catalyst in DMF from compound (**5**) derivatives showed in **Scheme 1**.

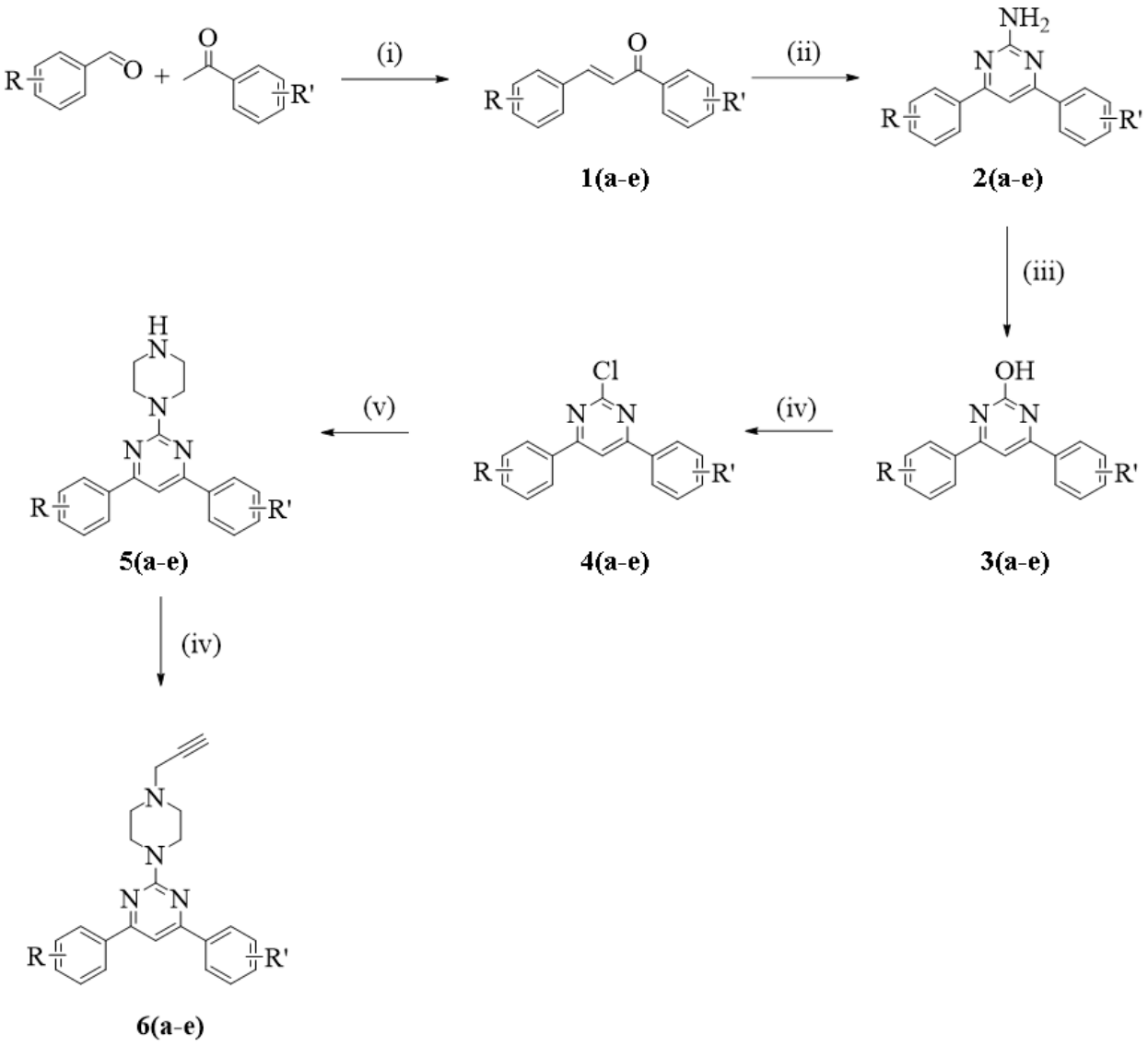

Reaction Conditions: (i) NaOH, EtOH, rt, 2 hours; (ii) Guanidine hydrochloride, NaOH, reflux, 16 hours; (iii) $NaNO_2$, AcOH, rt, 3 hours; (iv) $POCl_3$, DMF, reflux, 6 hours; (v) Piperazine, IPA, reflux, 16 hours; (vi) Propargyl bromide, Et_3N, DMF, 0°C- rt, 3 hours.

Different acyl azides were prepared from various commercially available aniline via diazonium salt formation using sodium nitrite and sodium azide in HCl/H_2O. These were immediately used in the second step. Finally, through copper-catalyzed azide-alkyne cycloaddition of variety acyl azides and compound **6** derivatives using click reaction were the final compounds:4,6-diphenyl-2-(4-((1-phenyl-1H-1,2,3-triazol-4-yl)methyl)piperazin-1-yl)pyrimidine derivatives (**8**) prepared as illustrated in **Scheme 2** [36].

Scheme 5

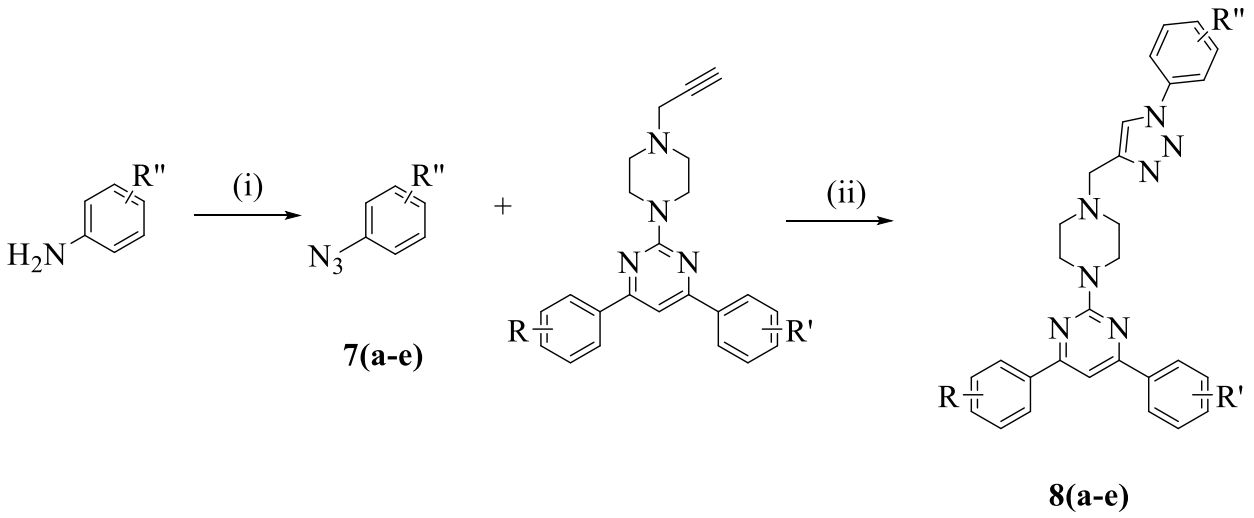

Reaction Conditions: (i) $NaNO_2$, HCl: H_2O, NaN_3, O°C, 1 hour; (ii) $CuSO_4.5H_2O$, sodium ascorbate, H_2O:*t*-BuOH, K_2CO_3, rt, 4 hours.

5.3 Results and discussion

5.3.1 Synthesis and Spectral studies

Structural elucidation of the final compounds was accomplished using spectral data IR, ^{1}H NMR and ^{13}C NMR and further ascertain using HRMS. The ^{1}H NMR spectrum of starting material **1c** had two distinct doublets (d) peaks at δ7.74 ppm (Ph-CH=CH) and 7.51 ppm (Ph-CH=CH) with *J* = 15.65 Hz and 15.63 Hz, respectively indicating the formation of the *trans* olefin. Also present were a definite singlet(s) signal at 3.89 ppm for methoxy protons, and various residual peaks viz; singlets(s) and doublets (d) lay in the aromatic region 8.04 ppm - 6.97 ppm accounting for phenyl protons. In the ^{1}H NMR spectrum of compound **2d,** the olefinic peak vanishes, and two characteristic singlets appeared at δ 7.39 ppm and 5.15 ppm signifying a pyrimidine aromatic proton (pyr-H) and 2-amino group (pyr-NH_2) of pyrimidine core. The disappearance of amino peak at 5.15 ppm and the appearance of singlet(s) signal at 11.85 ppm ascertain the formation of a hydroxyl group (OH) of 4,6-diphenylpyrimidin-2-ol derivative (**3**). The formation of 2-chloro-4,6-diphenylpyrimidine derivative (**4**) was characterized by the vanishing of OH peak and a small shift of (pyr-H) from δ 7.39 ppm to 7.62 ppm. 4,6-Diphenyl-2-(piperazin-1-yl) pyrimidine (**5**) ^{1}H NMR spectrum was presented by two new distinctive peaks; a broad singlet (br s) at 3.93 ppm and quartet (q) at 2.57ppm (*J* = 4.42 Hz) corresponding to the four methylene protons of piperazinyl group.4,6-

diphenyl-2-(4-(prop-2-yn-1-yl) piperazin-1-yl) pyrimidine ^{1}H NMR spectrum was characterized by the appearance of two new discrete peaks at δ 3.36 ppm and 3.17 ppm signifying for two methylene (-CH_2-) and alkyne (-C≡C<u>H</u>) protons respectively. The ^{1}H NMR (400 and 600 MHz, DMSO-d_6) of the final compound **8m** is distinguished by disappearance alkyne (-C≡C<u>H</u>) proton and appearance of a new prominent triazole peak at δ 8.76 ppm signifying the formation of 1,2,3-triazole. Other notable peaks as aforementioned are presented by two broad singlets(br s) signals resonating at δ 4.10 ppm and 3.80 ppm affirming the presence of four methylene protons of piperazinyl linker. Also, a sharp singlet(s) signal at δ 3.88 ppm accounting for 4-methoxy substituted phenyl on 4-phenylpyrimidine was observed. The outstanding protons of the aromatic group appear as mixed signals as singlets, doublets or multiplets in the aromatic region (8.27 ppm -7.08 ppm). The ^{1}H NMR data of the individual compounds agreed with their matching ^{13}C NMR data. The most notable signals resonated at δ 43.79-53.09 ppm, 53.46 ppm and 55.41 ppm conforming to the four piperazinyl methylene, methylene(-CH_2-) and 4-methoxy of a substituted phenyl, respectively. Furthermore, the remaining signal resonating at 100.92-164.92 ppm accounted for the aromatic carbons.

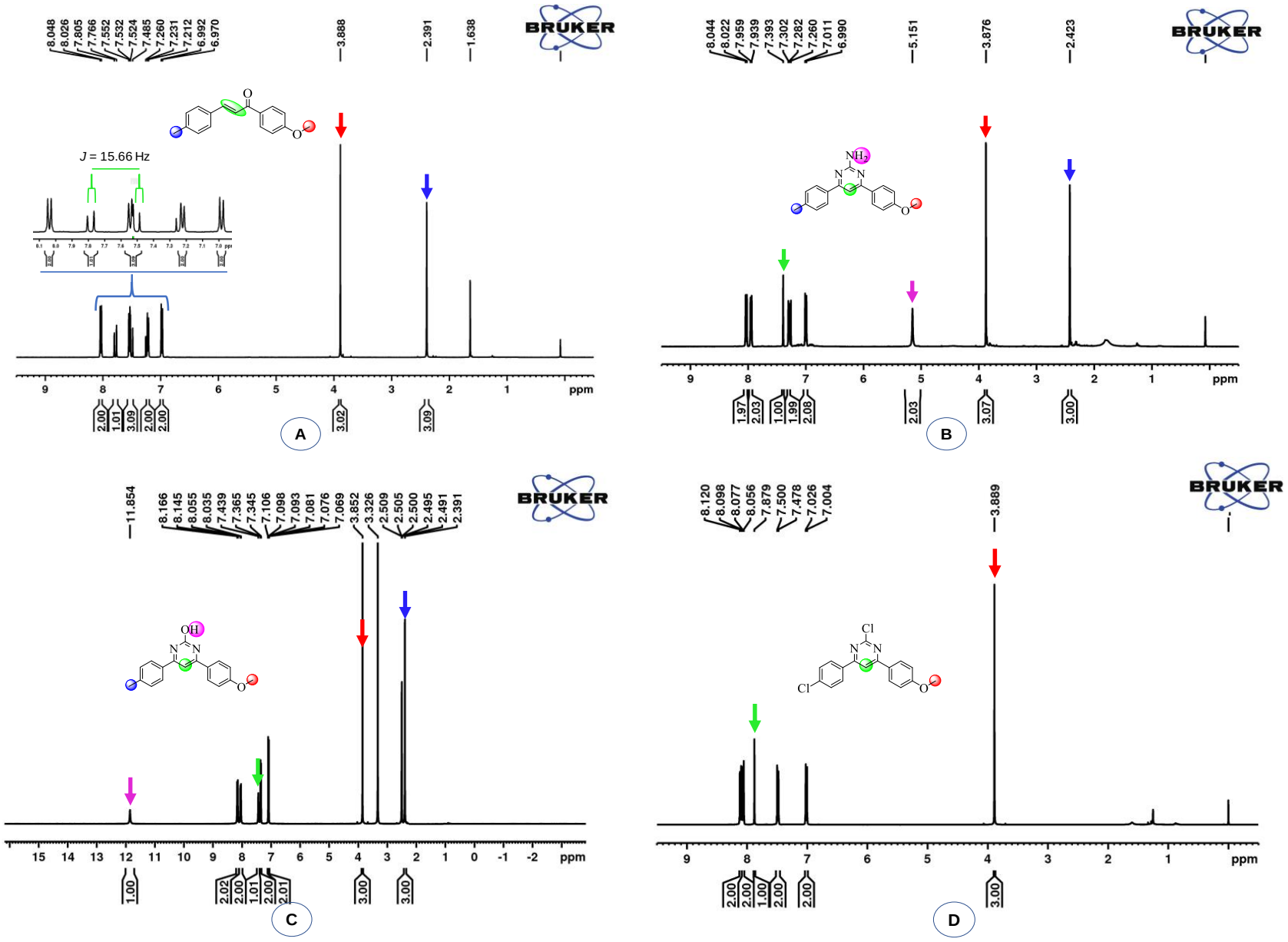
8.048
8.026
7.805
7.766
7.552
7.532
7.524
7.485
7.260
7.231
7.212
6.992
6.970
3.888
2.391
1.638
BRUKER
J = 15.66 Hz
ppm
2.00
1.01
3.09
2.00
2.00
3.02
3.09
A
8.044
8.022
7.959
7.939
7.393
7.302
7.282
7.260
7.011
6.990
5.151
3.876
2.423
BRUKER
NH2
ppm
1.97
2.03
1.00
1.99
2.08
2.03
3.07
3.00
B
11.854
8.166
8.145
8.055
8.035
7.439
7.365
7.345
7.106
7.098
7.093
7.081
7.076
7.069
3.852
3.326
2.509
2.505
2.500
2.495
2.491
2.391
BRUKER
OH
ppm
1.00
2.02
2.00
1.01
2.00
2.01
3.00
3.00
C
8.120
8.098
8.077
8.056
7.879
7.500
7.478
7.026
7.004
3.889
BRUKER
Cl
Cl
ppm
2.00
2.00
1.00
2.00
2.00
3.00
D

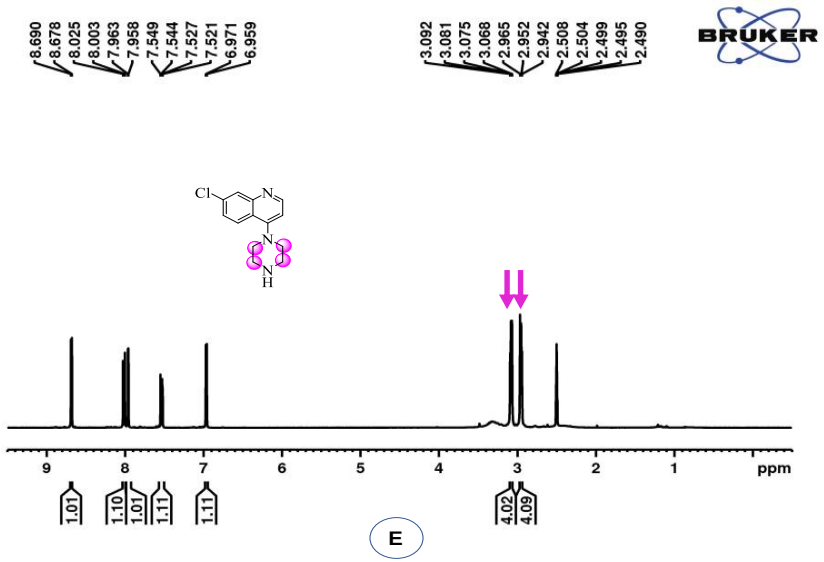
8.690
8.678
8.025
8.003
7.963
7.958
7.549
7.544
7.527
7.521
6.971
6.959
3.092
3.081
3.075
3.068
2.965
2.952
2.942
2.508
2.504
2.499
2.495
2.490
BRUKER
Cl
N
N
H
9
8
7
6
5
4
3
2
1
ppm
1.01
1.10
1.01
1.11
1.11
4.02
4.09
E

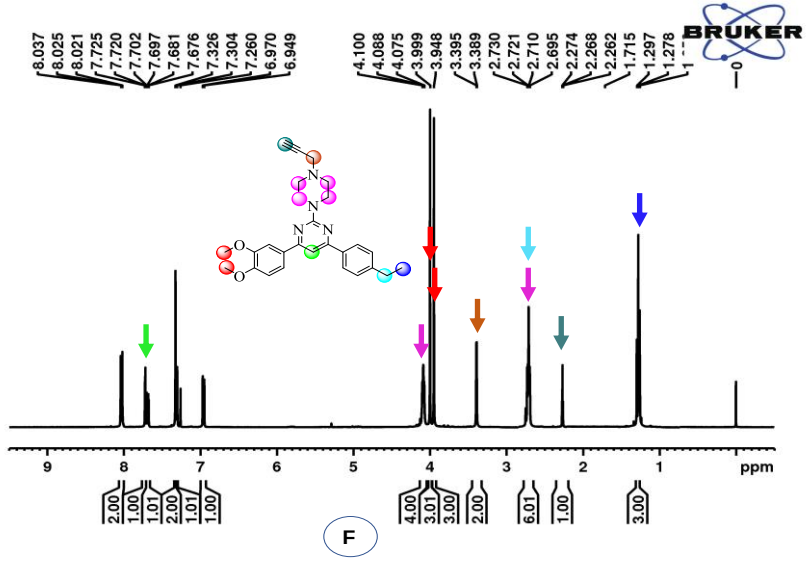
8.037
8.025
8.021
7.725
7.720
7.702
7.697
7.681
7.676
7.326
7.304
7.260
6.970
6.949
4.100
4.088
4.075
4.075
3.999
3.948
3.395
3.389
2.730
2.721
2.710
2.695
2.274
2.268
2.262
1.715
1.297
1.278
BRUKER
O
O
O
N
N
N
N
9
8
7
6
5
4
3
2
1
ppm
2.00
1.00
1.01
2.00
1.01
1.00
4.00
3.01
3.00
2.00
6.01
1.00
3.00
F

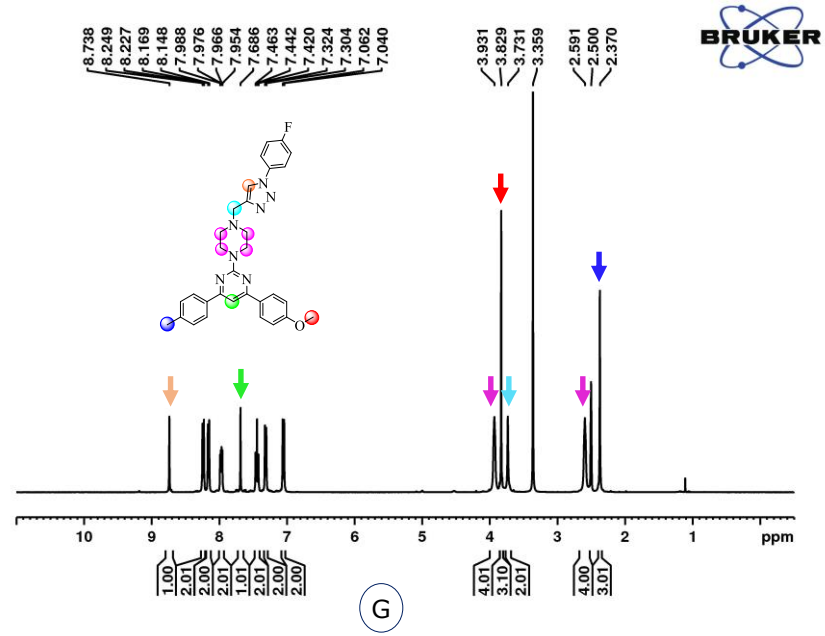
8.738
8.249
8.227
8.169
8.148
7.988
7.976
7.966
7.954
7.686
7.463
7.442
7.420
7.324
7.304
7.062
7.040
3.931
3.829
3.731
3.359
2.591
2.500
2.370
BRUKER
F
O
N
N
N
N
N
N
10
9
8
7
6
5
4
3
2
1
ppm
1.00
2.01
2.00
2.01
1.01
2.01
2.00
2.00
4.01
3.10
2.01
4.00
3.01
G

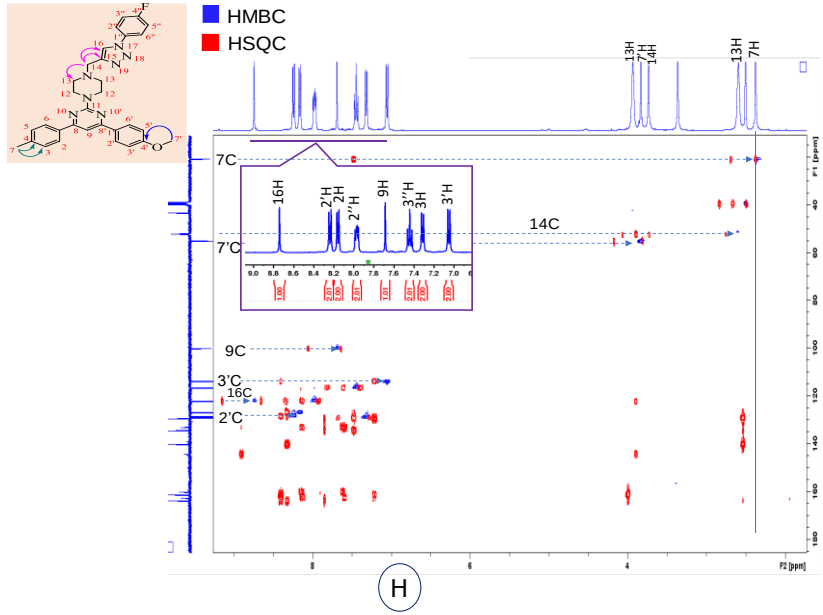
HMBC
HSQC
13H
7H
14H
13H
7H
7C
7'C
16H
2'H
2H
2''H
9H
3''H
3H
3'H
14C
9C
3'C
16C
2'C
H

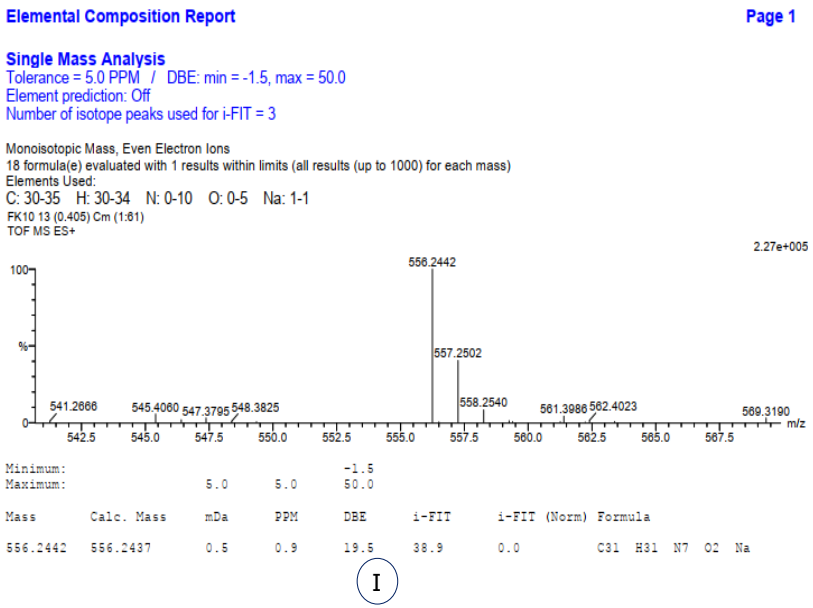

Figure 5.2. ^{1}H-NMR for intermediates derivative: chalcone (A), 4,6-diphenylpyriidin-2-amine (B), 4,6-diphenylpyrimidin-2-ol (C), 2-chloro-4,6-diphenylpyrimidine (D), 4,6-diphenyl-2-(piperazin-1-yl)pyrimidine (E) and 4,6-diphenyl-2-(4-prop-2-yn-1-yl)piperazin-1-yl)pyrimidine(F). 1 HMNR , HMBE and HSQC for final compound ; 2-(4-((1-(4-fluorophenyl)-1H-1,2,3-triazol-4-yl)methyl)piperazin-1-yl)-4-(4-methoxyphenyl)-6-(p-tolyl)pyrimidine (**8h**) (G and H). HRMS for compound **8m** (I).

A new library of the synthesized compounds (**8a-8t**) were screened *in vitro* for potential antimalarial activity against NF54 CQ-sensitive strain of *P. falciparum* according to a formerly reported procedure, and the method and conditions of the biological assay are described in the supporting information. All the hybrid molecules displayed significant antimalarial activity, and the vital data of the individual molecule (**8a-8t**) with corresponding activity plus standard reference drugs (CQ and Quinine) are presented in Table 1. All the hybrid molecules showed promising to moderate action in micromolar against NF54 CQ-sensitive strain assay. The IC_{50} values of these hybrid molecules were determined using a dose response-inhibition plot on a GraphPad Prism 5.0.0 software (Table 1). A brief SAR was conducted to establish group(s) that were significant to the antimalarial activity from the hybrid analogues that were evaluated. Notably, the variation in substituents on the phenyl aromatic rings of the final compounds had a positive connection with the inhibition action against the antiplasmodial activity.

Table 1. Antimalarial and cytotoxicity screening of the synthesized compounds.

Compound ID	Antimalarial		Cytotoxicity		Selective Index
	(IC_{50} µM)	SD	(IC_{50} µM)	SD	
8a	1.58	1.15	nd	nd	nd
8b	0.32	1.13	nd	nd	nd
8c	0.18	0.03	2.43	0.75	13.40
8d	0.59	1.03	nd	nd	nd
8e	0.23	0.02	2.05	1.11	9.11
8f	1.14	1.03	nd	nd	nd
8g	2.41	1.26	nd	nd	nd
8h	0.64	1.05	nd	nd	nd
8i	0.60	1.05	nd	nd	nd
8j	0.65	1.06	nd	nd	nd
8k	0.70	1.09	nd	nd	nd
8l	0.75	1.02	nd	nd	nd
8m	0.93	1.08	nd	nd	nd
8n	0.09	1.96	nd	nd	nd
8o	0.07	1.52	nd	nd	nd
8p	0.04	2.23	nd	nd	nd
8q	0.91	1.17	nd	nd	nd
8r	2.06	0.10	5.19	0.91	2.51
8s	0.72	1.23	nd	nd	nd
8t	0.29	0.01	17.00	4.50	61.15

Quinine	0.11	0.003	134.35	1.45	1243.98
Chloroquine	0.01	0.002	101.19	25.72	8432.50
Camptothecin	nd	nd	0.02	0.01	nd

IC_{50}: Concentration at 50% inhibition of the parasite's growth

Selective Index: IC_{50} values of cytotoxic activity/IC_{50} values of antimalarial activity

nd: not done

SD: Standard Deviation

From the antimalarial evaluation, seven compounds (**8b**, **8c**, **8e**, **8n**, **8o**, **8p** and **8t**) displayed good activity with IC_{50} values low than 0.5 µM, ranging from 0.04 µM to 0.32 µM (Table 1). Compound **8o**, **8p** and **8n** emerged as the more prominent with IC_{50} values corresponding to 0.07 ± 1.52 µM, 0.04 ± 2.23 µM and 0.09 ± 1.96 µM. The rest of the hybrids equally displayed promising activity with IC_{50} between 0.59 to 2.41 µM. The activity of most active compounds (**8o)** was two-fold and eighteen-fold less active than that of reference drugs: Quinine and Chloroquine, respectively. This demonstrates how promising these candidates are as antimalarial compounds. Five pyrimidine-1,2,3-triazole compound class were considered potent, with the most active IC_{50} values as low as 0.18 uM, two-fold more active than our last reported compounds [31]. This indicates that a 1,3,-triazole fused with pyrimidine demonstrated to be more auspicious and shows how versatile a pyrimidine is as an antimalarial pharmacophore as it can be observed by other reported activity [31, 34]. Also, as noted by the improved activity of these hybrids, it shows how a 1,2,3-triazole core is significant to the antimalarial activity in line with Royo *et al.* report [17].

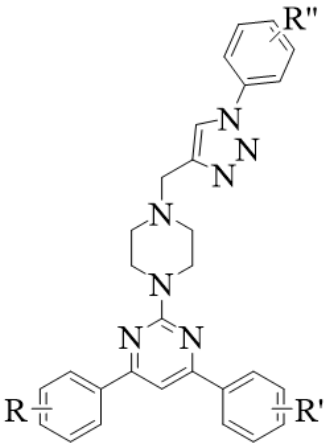

8(**a**-**t**)

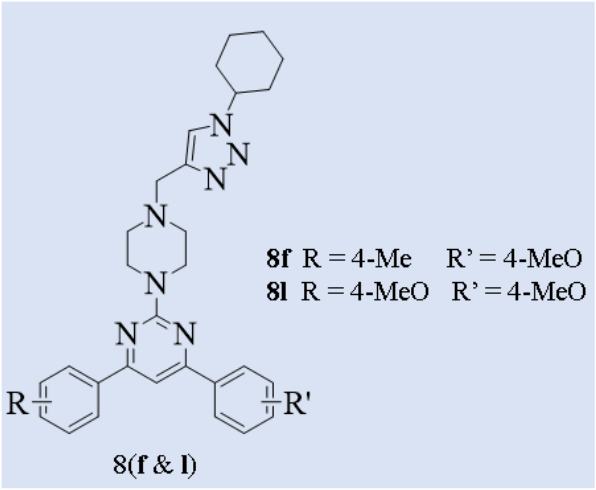

8(**f** & **l**)

8a	R = 4-Me	R' = 4-MeO	R" = H
8b	R = 4-Me	R' = 4-MeO	R" = 4-Cl
8c	R = 4-Me	R' = 4-MeO	R" = 4-F
8d	R = 4-Me	R' = 4-MeO	R" = 4-NO_2
8e	R = 4-Me	R' = 4-MeO	R" = 3-CF_3
8g	R = 4-Cl	R' = 4-MeO	R" = H
8b	R = 4-Cl	R' = 4-MeO	R" = 4-Cl
8i	R = 4-Cl	R' = 4-MeO	R" = 4-F
8j	R = 4-Cl	R' = 4-MeO	R" = 4-NO_2
8k	R = 4-Cl	R' = 4-MeO	R" = 4-CF_3
8m	R = 4-MeO	R' = 4-MeO	R" = H
8n	R = 4-MeO	R' = 4-MeO	R" = 4-Cl
8o	R = 4-MeO	R' = 4-MeO	R" = 4-F
8p	R = 4-MeO	R' = 4-MeO	R" = 4-NO_2
8q	R = 4-MeO	R' = 4-MeO	R" = 3-CF_3
8r	R =3, 4-MeO	R' = 4-MeO	R" = H
8s	R = 3, 4-MeO	R' = 4-MeO	R" = 4-Cl
8t	R = 3, 4-MeO	R' = 4-MeO	R" = 3,5-diF

Figure 5.3. Structure of the pyrimidine-1,2,3-triazole compound **8(a-t)**.

The most active hybrids constituting the 4,6-bis(4-methoxyphenyl)pyrimidine motif showed minor variation with the bioisosteric replacement on the phenyl group of the 1-phenyl-1H-1,2,3-triazole core. Substitution with a strong deactivating group, for instance, a nitro (NO_2) at the para position, emerged as the most prominently active compound with IC_{50} = 0.04 ± 2.24 µM as presented by **8p**. Similarly, a strong and mild deactivating such as fluoro (F) and chloro (Cl) displayed good activity with IC_{50} 0.07 ± 1.96 µM and 0.09 ± 1.52 µM corresponding to **8o** and **8n** respectively (Figure 3). The non-substituted phenyl of 1-phenyl-1H-1,2,3-triazole (**8m**) nucleus is about twenty-three-fold less active than the most active compounds (**8p**), signifying how essential the substitutions on this motif are to the activity. Hybrids possessing the 4-(p-tolyl)-6-(4-methoxyphenyl)pyrimidine equally displayed the array of activity with different substitutions on the 1-phenyl-1H-1,2,3-triazole core. In this group of compounds, **8b**, **8c** and **8e** had activity below 0.5 µM with **8c** with a strong deactivating group (F) exhibited the promising antimalarial activity

with IC_{50} = 0.18 ± 0.03 µM. Other important groups on the 1-phenyl-1H-1,2,3-triazole core were Cl and trifluoromethane (CF_3), which equally had activity less than 0.5 µM. Minor difference in the activity is noted with either phenyl (**8a**) or cyclohexyl (**8f**) on the triazole core. However, substitution on the phenyl of the 1-phenyl-1H-1,2,3-triazole core with F increased the activity nine times compared to a non-substituted phenyl. A strong deactivating group such as NO_2 only showed moderate activity, as illustrated by **8d**. In addition, **8c** displayed a good safety profile of 13.40, where it is 10-fold more active as an antimalarial agent against human cell line. The rest of the compounds displayed activity ranging from IC_{50} values 0.59 to 2.41µM.

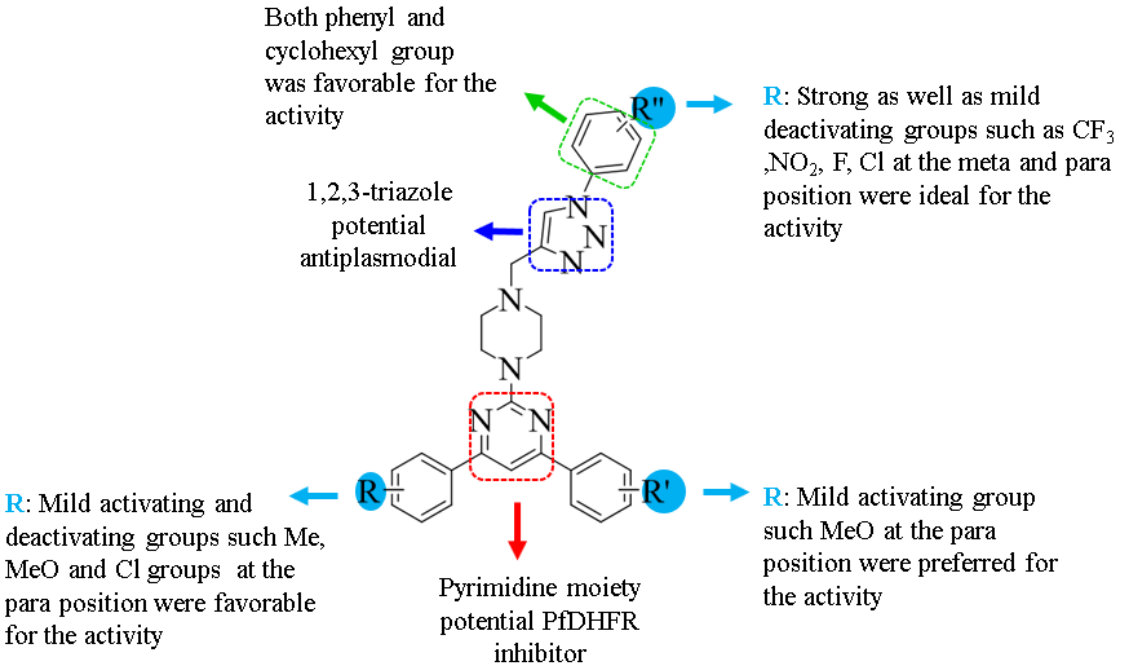

Figure 5.4. Structure-Activity Relationship (SAR) of 1,2,3-triazole-pyrimidine hybrids.

All compounds housing a 4-(4-methoxyphenyl)-6-(p-tolyl)pyrimidine core and 1-phenyl-1H-1,2,3-triazole only showed promising activity with IC_{50} ranging from 0.60 to 2.41 µM. A cyclohexyl on the first position of triazole (**8l**) was three-fold more active than the phenyl group (**8g**), however strong deactivating (F) substituents on the phenyl group (**8i**) enhanced the activity four- times. The analogues with the 4-(3,4-dimethoxyphenyl)-6-(4-ethylphenyl)pyrimidine core displayed varied activity for phenyl substituents on the 1,2,3-triazole nucleus. Notably, a compound possessing 3,5-difluoro (diF) on the phenyl group of 1,2,3-triazole core displayed promising activity with 0.29 ± 0.01 µM corresponding to compound **8t**. While a non-substituted benzyl group and *p*-chloro substituent equally showed moderate activity with IC_{50} 2.06 ± 0.10 µM

and 0.72 ± 1.23 µM agreeing with **8r** and **8s** respectively. In view of the presented results, it can be deduced that both a phenyl group and its substitutions and aliphatic cycloalkyl group on 1,2,3-triazole moiety were essential for the antiplasmodial activity. Strong deactivating groups such as F, NO_2, CF_3, and mild activating like Cl were significant for the activity on the phenyl group of the 1-phenyl-1H-1,2,3-triazole moiety. An activating group such a methoxy, particularly on the para position, was suitable for the activity. Although other substitutions on the phenyl(s) of the 4,6-diphenylpyrimidine core were vital, *p*-methyl/ *p*-methoxy and *p*-methoxy were the most significant and displayed the most activity.

Furthermore, some active compounds were evaluated against human embryonic kidney epithelial (HEK-293) cells (Table 1). The selective index (SI) of compounds **8c**, **8e** and **8t** were calculated to be 13.40, 9.11 and 61.15 by dividing the IC_{50} value of the cytotoxic activity by the IC_{50} value of the antimalarial activity. The safe index of Quinine and Chloroquine was about ninety-fold and six hundred-fold than that of the most potent compound. **8c**, respectively. The observed activity suggests that while selectively killing the parasite, compound **8c**, **8e** and **8t** has a limited cytotoxic effect against mammalian cells at therapeutic dosages; where a safety index of 10 is regarded as safe. It can be deduced that the 1,2,3-triazole and pyrimidine core linked through a piperazine linker are central to the antimalarial activity. Bioisoteric replacement on the phenyl group of 1,2,3-triazole and 4,6-diphenylpyrimidine motif further enhanced the antimalarial activity which important in identify the potent candidate associated with activity.

5.4 *In-vitro* binding affinity studies

The analysis of the direct protein-compound binding affinities was conducted using SPR. The steady-state affinity of the compounds **8c**, **8e** and **8t** on the recombinant *P. falciparum* Hsp70-1 and Hsp70-z were in the lower nanomolar range (Table 2). Both compounds **8e** and **8t** had marginally higher binding affinities to both PfHsp70-1 and PfHsp70-z. However, compound **8c** had lower binding affinities to both recombinant proteins. This suggests that compound **8c** had the least specificity among these compounds.

Table 2. Steady-state binding affinities for the association of PfHsp70-1/PfHsp70-z with compounds.

Ligand	Analyte	*Ka* (1/M*s)	*Kd* (1/s)	K_D (M)	X^2

PfHsp70-1	**8c**	7.84 (±0.04) e^{6}	6.31 (±0.20) e^{-2}	8.04 (±0.9) e^{-8}	8.9
	8e	6.36 (±0.30) e^{6}	7.17 (± 0.1) e^{-2}	1.13 (±0.5) e^{-8}	4.5
	8t	2.22 (±0.05) e^{6}	4.26 (±0.30) e^{-2}	1.92 (±0.30) e^{-8}	4.2
PfHsp70-z	**8c**	8.2 (±0.40) e^{5}	7.38 (±0.80) e^{-2}	9.0 (±0.80) e^{-8}	1.0
	8e	9.52 (±0.20) e^{6}	9.54 (±0.70) e^{-2}	1.00 (±0.2) e^{-8}	4.3
	8t	3.30 (±0.30) e^{6}	5.64 (±0.04) e^{-2}	1.71 (±0.30) e^{-8}	5.9

The standard error of measurement is shown in parenthesis.

5.5 Conclusion

1,2,3-triazole-pyrimidine hybrids through a piperazine linker present a novel series of promising antimalarial candidates. The hybrids were synthesized in high yields (70-100%) using a simple and striking approach involving easily available chemical reagents and reactants. Particularly, compound **8p** emerged as the most promising hit exhibiting good antimalarial activity against IC_{50} 0.04 ± 2.24 µM. Selected cytotoxicity screening of other active compounds performed revealed that compounds **8c**, **8e** and **8t** with IC_{50} values with IC_{50}= 0.18 ± 0.03 µM, 0.23 ± 0.02 µM and IC_{50} 0.29 ± 0.01 µM had a safety profile of 13.40, 9.11 and 61.151. The findings of this study propose the benefits of how a piperazine linker was essential in the amalgamation of 1,2,3-triazole and pyrimidine fragments sprung as novel antiplasmodial molecular hybrids. As evidenced by the study, a further variation of the phenyl substituents with other activating or deactivating groups on both 1-phenyl-1H-1,2,3-triazole and 4,6-diphenypyrimidine core could guarantee improved antimalarial activity.

Declaration of Competing Interest

The authors declare no known conflicting financial or personal interests that could have appeared to influence the work reported in this paper.

Acknowledgement

The authors would like to express their heartfelt gratitude to the Discipline of Pharmaceutical Sciences, College of Health Sciences, University of KwaZulu-Natal (UKZN), Durban, South Africa, for providing all the necessary facilities. R.K. gratefully acknowledges National Research Foundation-South Africa (NRF-SA) for funding this project (grant nos. 103728, 112079 and

129247). The authors would also like to acknowledge Dr Vuyisa Mzozoyana (UKZN) for NMR spectroscopic experimental data.

5.6 Experimental section

5.6.1 Chemical protocols

All the chemicals' reagents utilized in this research work were acquired from Sigma-Aldrich and Merck Millipore, South Africa. The commercially accessible chemicals Benzaldehyde and acetophenone were obtained from Sigma- Aldrich (South Africa). All and sundry of the solvents, except laboratory-reagent grade, were dried and purified when required as per formerly published procedures. The progression of the chemical reactions and the compounds' purity were monitored by thin-layer chromatography (TLC) on pre-coated silica gel plates secured from E. Merck and Co. (Darmstadt, Germany) using 36% ethyl acetate in n-hexane as the mobile phase and iodine vapour as the visualizing agent.

The synthesised compounds' melting points were resolved by a Thermo Fisher Scientific (IA9000, UK) digital melting point apparatus. The IR spectra were recorded on a Bruker Alpha FT-IR spectrometer (Billerica, MA, USA) using the ATR technique. The ^{1}H NMR and ^{13}C NMR spectra were recorded on a Bruker AVANCE 400 and 600 MHz (Bruker, Rheinstetten/Karlsruhe, Germany) spectrometers using $CDCl_3$ and DMSO-*d6*. The chemical shifts were reported in δ ppm units using TMS, an internal standard. HRMS spectra were recorded on an Autospec mass spectrometer with electron impact at 70 eV.

5.6.1.1 A typical procedure for the synthesis of (*E*) chalcones 1(a-d)

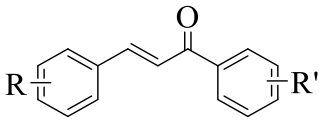

1a R = 4-Cl, R' = 4-MeO
1b R = 4-Me, R' = 4-MeO
1c R = 4-MeO, R' = 4-MeO
1d R = 3,4-MeO, R' = 4-Et

To a stirring solution of acetophenone (5 g, 32.34 mmol) in EtOH (30 ml) was added 60% NaOH solution (12 g NaOH/ H_2O (20 mL)). The reaction was stirred at room temperature for 30 minutes, after which benzaldehyde (4.7 g, 38.81 mmol) was added, and the reaction mixture sonicated for 1 hour at 35^{o}C. The development of the product was monitored by TLC. Excess ethanol was removed under vacuum, and the reaction mixture was added into 100 gm of ice and stirred. The

precipitates formed were filtered, washed with excess water and dried. The crude product was purified by recrystallisation in EtOH to obtain the pure following compounds.

(E)-3-(4-chlorophenyl)-1-(4-methoxyphenyl) prop-2-en-1-one (**1a**): Yellow solid, yield: 96%, mp = 130-133 °C; ^{1}H NMR (400 MHz, $CDCl_3$, δ, ppm): 8.03 (d, J = 8.85 Hz, 2H, ArH), 7.74 (d, J = 15.65 Hz, 1H, Ph-C**H**=CH), 7.57 (d, J = 8.49 Hz, 2H, ArH), 7.51 (d, J = 15.63 Hz, 1H, Ph-CH=C**H**), 7.38 (d, J = 8.49, Hz, 2H ArH), 6.98 (d, J = 8.84, Hz, 2H ArH), 3.89 (s, 3H, OCH_3); ^{13}C NMR (400 MHz, $CDCl_3$, δ, ppm): 188.40, 163.55, 142.47, 136.18, 136.18, 133.58, 130.91, 122.27, 113.91, 55.53 (OCH_3).

(E)-1-(4-methoxyphenyl)-3-(p-tolyl)prop-2-en-1-one (**1b**): Yellow solid. yield: 98%. mp = 125-128 °C; ^{1}H NMR (400 MHz, $CDCl_3$, δ, ppm): 8.04 (d, J = 8.76 Hz, 2H, ArH), 7.89 (d, J=15.60 Hz, 1H, Ph-C**H**=CH), 7.54 (d, J= 7.95 Hz, 2H, ArH), 7.51 (d, J= 15.63 Hz, 1H, Ph-CH=C**H**), 7.22 (d, J = 7.97, Hz, 2H ArH), 6.98 (d, J=8.77 Hz, 2H, ArH), 3.88 (s,3H, CH_3), 2.39 (s, 3H,CH_3); ^{13}C NMR (400 MHz, $CDCl_3$, δ, ppm): 189.43 (C=O), 163.92, 144.64, 141.40, 132.92, 131.81, 131.34, 130.24, 128.96, 121.46, 114.39, 56.06 (OCH_3), 22.09 (CH_3).

(E)-1,3-bis(4-methoxyphenyl)prop-2-en-1-one (**1c**): Yellow solid, yield: 100 %. mp = 102-104 °C; ^{1}H NMR (400 MHz, $CDCl_3$, δ, ppm): 8.03 (d, J = 8.75 Hz, 2H, ArH), 7.78 (d, J=15.58 Hz, 1H, Ph-C**H**=CH), 7.60 (d, J = 8.66 Hz, 2H, ArH) 7.43 (d, J=15.58 Hz, 1H, Ph-CH=C**H**), 6.96 (dd, J= 17.58, 8.72 Hz, 4H, ArH), 3.89 (s,3H, OCH_3), 3.85 (s, 3H, OCH_3); ^{13}C NMR (400 MHz, $CDCl_3$, δ, ppm): 189.39 (C=O), 163.84, 162.09, 162.09, 144.39,131.95,131.28, 130.67, 128.40, 120.15, 114.96, 114.36, 56.05 (OCH_3), 55.98 (OCH_3).

5.6.1.2 A typical procedure for the synthesis of 4,6-diphenylprimidin-2-amine.

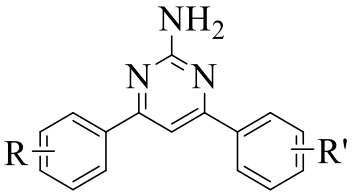

2a	R = 4-Cl,	R' = 4-MeO
2b	R = 4-Me,	R' = 4-MeO
2c	R = 4-MeO,	R' = 4-MeO
2d	R = 3,4-MeO,	R' = 4-Et

The reaction mixture of (*E*) chalcone (8 gm, 31.16 mmol), Guanidine.HCl (4.8 g, 49. 86 mmol) and 60% NaOH (12 g NaOH/H_2O (20 mL) in EtOH (30 mL) was refluxed for 24 hours. The development of the product was monitored using TLC. Excess ethanol was removed under vacuum

using rotavapor. The reaction mixture was then added in 100 g ice water, and the precipitate formed was filtered, washed with excess cold water and dried. The crude compound was purified by column chromatography using EtOAc/Hexane (1:4) eluent to obtain the following pure compounds.

4-(4-chlorophenyl)-6-(4-methoxyphenyl)pyrimidin-2-amine (**2a**): Yellow solid, yield: 56 %, mp = 127-129 °C; ^{1}H NMR (400 MHz, $CDCl_3$, *δ*, ppm): 8.03 (d, *J* = 8.78 Hz, 2H, ArH), 7.95 (d, *J* = 8.06 Hz, 2H, ArH), 7.39 (s, 1H, Pyr-H), 7.29 (d, *J* = 7.98 Hz, 2H, ArH), 7.00 (d, *J* = 8.76 Hz, 2H, ArH), 5.15 (s, 2H, NH_2), 3.88 (s, 3H, CH_3), 2.42 (s, 3H, CH_3). ^{13}C NMR (100 MHz, $CDCl_3$, *δ*, ppm): 189.43, 163.92, 144.64, 141.40, 132.92, 131.34, 130.24, 128.96, 121.46, 114.39, 56.06 (OCH_3), 22.89 (CH_3).

4-(4-methoxyphenyl)-6-(p-tolyl)pyrimidin-2-amine (**2b**): Yellow solid, yield 63% mp = 127-129 °C; ^{1}H NMR (400 MHz, $CDCl_3$, *δ*, ppm): 8.03 (d, *J* = 8.64Hz, 2H, ArH), 8.00 (d, *J* = 8.36 Hz, 2H, ArH), 7.46 (d, *J* =8.36 Hz, 2H, ArH), 7.37 (s, 1H, Pyr-H), 7.00 (d, *J* = 8.56 Hz, 2H, ArH) 5.20 (s, 2H, NH_2), 3.88 (s, 3H, CH_3). ^{13}C NMR (100 MHz, $CDCl_3$, *δ*, ppm): 165.88, 164.64, 163.55, 161.76, 136.47, 129.91, 128.96, 128.64, 128.40, 114.14, 103.18, 55.43 (OCH_3).

4,6-bis(4-methoxyphenyl) pyrimidin-2-amine (**2c**); Yellow solid, yield: 61 % mp = 171-173 °C; ^{1} H NMR (400 MHz, $CDCl_3$, *δ*, ppm): 8.04 (d, *J* = 8.66 Hz, 4H, ArH), 7.36 (s, 1H, Pyr-H), 7.00 (d, *J* = 8.69 Hz, 4H, ArH), 5.36 (s, 2H, NH_2), 3.87 (s, 6H, $2CH_3$); ^{13}C NMR (100 MHz, $CDCl_3$, *δ*, ppm): 165.19, 162.97, 161.77, 129.78, 128.69, 114.15, 102.64, 55.43 (OCH_3).

4-(3,4-dimethoxyphenyl)-6-(4-ethylphenyl)pyrimidin-2-amine (**2d**): Yellow solid, yield: 59 % , ^{1}H NMR (400 MHz, $CDCl_3$, *δ*, ppm): 8.26 (d, *J* = 8.23 Hz, 2H, ArH), 7.97 (dd, *J* = 7.98 Hz,1.94 Hz, 1H, ArH), 7.89 (s, 1H, pyr-H), 7.88 (d, *J* = 8.20 Hz, 1H, ArH), 7.38 (d, *J* = 8.26 Hz, 2H, ArH), 7.10 (d, *J* = 8.59 Hz, 1H, ArH), 3.92 (s, 3H, OCH_3), 3.86 (s, 3H, OCH_3), 2.70 (q, *J* = 5.68 Hz, 2H, $2CH_2$), 1.23 (t, *J* = 7.58 Hz, 3H CH_3); ^{13}C NMR (100 MHz, $CDCl_3$, *δ*, ppm): 165.07, 164.63, 162.12, 151.08, 149.11, 146.83, 135.80, 131.15, 128.18, 127.11, 120.94, 110.10, 101.30, 56.04 (OCH_3), 56.02 (OCH_3), 28.81 (CH_2), 15.52 (CH_3).

5.6.1.3 A typical procedure for the synthesis of 4,6-diphenylpyrimidin-2-ols.

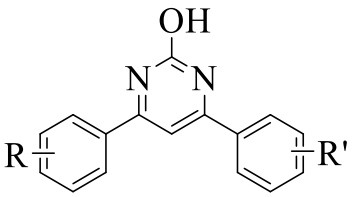

3a R = 4-Cl, R' = 4-MeO
3b R = 4-Me, R' = 4-MeO
3c R = 4-MeO, R' = 4-MeO
3d R = 3,4-MeO, R' = 4-Et

To the stirring solution of 4,6-diphenylpyrimidin-2-amine (4 g, 12.76 mmol) in acetic acid (50 mL) was slowly added a solution of 10 eq $NaNO_2$ in H_2O (50 mL) at room temperature. The reaction mixture was further stirred for 3 hours. The development of the product was monitored using TLC. The precipitate formed was filtered, washed with excess water and dried. The crude product was recrystallized in EtOH to obtain the following pure compounds.

4-(4-chlorophenyl)-6-(4-methoxyphenyl)pyrimidin-2-ol (**3a**): Yellow solid, yield: 97%, mp = 235-237 °C; ^{1}H NMR (400 MHz, DMSO-d_6, δ, ppm): 11.94 (s, 1H, Pyr-O**H**), 8.18 (dd, *J* = 18.36 Hz, 8.53Hz, 4H, ArH), 7.62 (d, *J* = 8.60 Hz, 2H, ArH), 7.56 (s, 1H, pyr-H), 7.10 (d, *J* = 8.89 Hz, 2H, ArH), 3.85 (s, 3H, OCH_3); ^{13}C NMR (100 MHz, DMSO-d_6, δ, ppm): 162.11, 136.20, 129.37, 128.81, 127.49, 114.23, 55.48 (OCH_3).

4-(4-methoxyphenyl)-6-(p-tolyl)pyrimidin-2-ol (**3b**): Yellow solid, yield: 95%, mp = 235-237 °C; ^{1}H NMR (400 MHz, DMSO-d_6, δ, ppm): 11.85 (s, 1H, Pyr-O**H**), 8.16 (d, *J* = 8.74 Hz, 2H, ArH), 8.04 (d, *J* = 7.97 Hz, 2H, ArH), 7.44 (s, 1H, pyr-H), 7.35 (d, *J* = 7.98 Hz, 2H, ArH), 7.09 (d, *J* = 8.97 Hz, 2H, ArH), 3.85 (s, 3H, OCH_3), 2.39 (s, 3H, CH_3); ^{13}C NMR (100 MHz, DMSO-d_6, δ, ppm): 162.05, 141.51, 129.39, 129.35, 127.46, 114.18, 55.46 (OCH_3), 55.99 (CH_3).

4,6-bis(4-methoxyphenyl)pyrimidin-2-ol (**3c**): Yellow solid, yield: 100%, mp = °C; ^{1}H NMR (400 MHz, DMSO-d_6, δ, ppm): 11.82 (s, 1H, Pyr-O**H**), 8.14 (d, *J* = 8.53 Hz, 2H, ArH), 7.41 (s, 1H, pyr-H), 7.09 (d, *J* = 8.91 Hz, 2H, ArH), 3.85 (s, 6H, $2OCH_3$); ^{13}C NMR (100 MHz, DMSO-d_6, δ, ppm): 165.19, 162.00, 161.77, 129.32, 128.69, 114.18, 102.64, 55.46 ($2OCH_3$).

4-(3,4-dimethoxyphenyl)-6-(4-ethylphenyl)pyrimidin-2-ol (**3d**): Yellow solid, yield: 100% , ^{1} HNMR (400 MHz, DMSO-d_6, δ, ppm): 12.02 (s, 1H, Pyr-O**H**), 8.26 (d, *J* = 8.23 Hz, 2H, ArH), 7.97 (dd, *J* = 7.98 Hz, 1.94 Hz, 1H, ArH), 7.89 (s, 1H, pyr-H), 7.88 (d, *J* = 8.20 Hz, 1H, ArH), 7.38 (d, *J* = 8.26 Hz, 2H, ArH), 7.10 (d, *J* = 8.59 Hz, 1H, ArH), 3.92 (s, 3H, OCH_3), 3.86 (s, 3H,

OCH_3), 2.70 (q, *J* = 5.68 Hz, 2H, $2CH_2$), 1.23 (t, *J* = 7.58 Hz, 3H CH_3); ^{13}C NMR (100 MHz, DMSO-d_6, *δ*, ppm): 165.07, 164.63, 162.12, 151.08, 149.11, 146.83, 135.80, 131.15, 128.18, 127.11, 120.94, 110.10, 101.30, 56.04 (OCH_3), 56.02 (OCH_3), 28.81 (CH_2), 15.52 (CH_3).

5.6.1.4 A typical procedure for the synthesis of 2-chloro-4,6-diphenylpyrimidines.

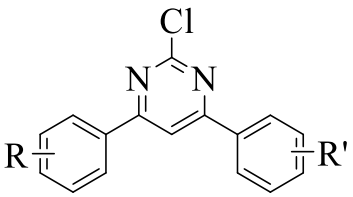

4a	R = 4-Cl,	R' = 4-MeO
4b	R = 4-Me,	R' = 4-MeO
4c	R = 4-MeO,	R' = 4-MeO
4d	R = 3,4-MeO,	R' = 4-Et

A solution of 4,6-diphenylpyrimidin-2-ol (4 g, 16.11 mmol) and 0.4 mL DMF in $POCl_3$ (20 mL) was refluxed for 6 hours. The development of the product was monitored using TLC. The reaction mixture was added into 100 g ice, and the precipitate formed was filtered, washed with water and dried. The crude compound was purified by column chromatography using EtOAc/Hexane (1:9) eluent to obtain the following pure compounds.

2-chloro-4-(4-chlorophenyl)-6-(4-methoxyphenyl)pyrimidine (**4a**): Yellow solid, yield: 98 %, ; ^1H NMR (400 MHz, $CDCl_3$, *δ*, ppm): 8.11 (d, *J* = 8.84 Hz, 2H, ArH), 8.07 (d, *J* = 8.56 Hz, 2H, ArH), 7.88 (s, 1H, Pyr-H), 7.49 (d, *J* = 8.68 Hz, 2H, ArH), 7.02 (d, *J* = 8.92 Hz, 2H, ArH), 3.89 (s, 3H, OCH_3); ^{13}C NMR (400 MHz, $CDCl_3$, *δ*, ppm): 167.27, 165.95, 162.75, 162.02, 137.82, 134.25, 129.30, 129.16, 128.67, 127.81, 114.46, 109.62, 55.50 (OCH_3); HRMS (ESI, *m/z*).

2-chloro-4-(4-chlorophenyl)-6-(p-tolyl)pyrimidine (**4b**): Yellow solid, yield: 97 %; ^1H NMR (400 MHz, $CDCl_3$, *δ*, ppm): 8.09 (d, *J* = 8.52 Hz, 2H, ArH), 8.04 (d, *J* = 8.16 Hz, 2H, ArH), 7.94 (s, 1H, Pyr-H), 7.50 (d, *J* = 8.52 Hz, 2H, ArH), 7.33 (d, *J* = 8.00 Hz, 2H, ArH), 2.44 (s, 3H, CH_3); ^{13}C NMR (100 MHz, $CDCl_3$, *δ*, ppm): 166.77, 165.13, 161.05, 141.46, 136.88, 133.16, 131.65, 128.83, 128.30, 127.68, 126.37, 109.20, 20.51 (CH_3).

2-chloro-4,6-bis(4-methoxyphenyl)pyrimidine (**4c**): Yellow solid, yield: 100 % mp = 187-190 ℃; ^1H NMR (400 MHz, $CDCl_3$, *δ*, ppm): 8.10 (d, *J* = 8.48 Hz, 3H, ArH), 7.87 (d, *J* = 8.84 Hz, 1H, ArH), 7.85 (s, 1H, Pyr-H), 7.01 (dd, *J* = 8.50 Hz, 1.74 Hz, 4H, ArH), 3.88 (s, 6H, $2OCH_3$); ^{13}C

NMR (400 MHz, $CDCl_3$, δ, ppm): 166.74, 166.52, 162.51, 161.84, 161.58, 131.61, 129.10, 128.19, 127.90, 114.39, 113.67, 109.01, 55.49 (OCH_3), 55.44 (OCH_3).

2-chloro-4-(3,4-dimethoxyphenyl)-6-(4-ethylphenyl)pyrimidine (**4d**): Yellow solid, yield: 98%, mp = 138-141 °C; ^{1}H NMR (400 MHz, $CDCl_3$, δ, ppm): 8.12 (d, J = 8.88 Hz, 2H, ArH), 7.87 (d, J = 8.84 Hz, 1H, ArH), 7.85 (s, 1H, Pyr-H), 7.01 (d, J = 8.88, 2H, ArH), 6.96 (d, J = 8.36, 1H, ArH), 3.95 (s, 3H, OCH_3), 3.88 (s, 3H, OCH_3), 2.70 (q, J = 5.68 Hz, 2H, $2CH_2$), 1.23 (t, J = 7.58 Hz, 3H CH_3); ^{13}C NMR (100 MHz, $CDCl_3$, δ, ppm): 164.28, 164.24, 162.78, 161.40, 150.90, 149.06, 131.44, 131.04, 120.01, 113.92, 110.87, 110.05, 99.65, 56.04 (OCH_3), 56.02 (OCH_3), 28.81 (CH_2), 15.52 (CH_3).

5.6.1.5 A typical procedure for the synthesis of 4,6-diphenyl-2-(piperazin-1-yl)pyrimidines.

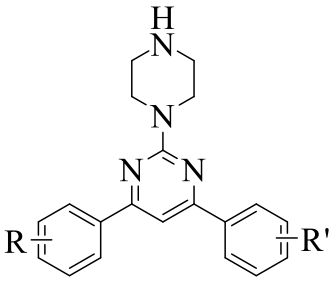

5a	R = 4-Cl,	R' = 4-MeO
5b	R = 4-Me,	R' = 4-MeO
5c	R = 4-MeO,	R' = 4-MeO
5d	R = 3,4-MeO,	R' = 4-Et

A reaction mixture of 2-chloro-4,6-diphenylpyrimidine (4.0 g, 15 mmol) and piperazine (13.92 g, 150 mmol) in isopropanol (20 mL) was refluxed for 20 hours. Using TLC, the progression of the reaction was monitored. The reaction mixture was added to 2 M NaOH (100 mL), the precipitate formed filtered, washed with water/diethyl ether and dried under vacuum. The product was purified by recrystallisation in EtOAc to afford the following pure compound(s).

4-(4-chlorophenyl)-6-(4-methoxyphenyl)-2-(piperazin-1-yl)pyrimidine (**5a**): Yellow solid, yield: 100 %, ^{1} H NMR (400 MHz, $CDCl_3$, δ, ppm): 8.25 (d, J = 8.76 Hz, 2H, ArH), 8.17 (d, J = 8.08 Hz, 1H, ArH), 7.70 (s, 1H, pyr-H), 7.33 (d, J = 8.04 Hz, 2H, ArH), 3.93 (br s, 4H, $2CH_2$), 3.84 (s, 3H, OCH_3), 2.57 (q, J = 4.42 Hz, 4H, $2CH_2$).

4-(4-methoxyphenyl)-2-(piperazin-1-yl)-6-(p-tolyl)pyrimidine (**5b**): Yellow solid, yield: 100%; ^{1}H NMR (400 MHz, $CDCl_3$, δ, ppm): 8.26 (d, J = 8.79 Hz, 2H, ArH), 8.18 (d, J = 8.09 Hz, 2H, ArH),

7.70 (s, 2H, pyr-H), 7.33 (d, *J* = 8.04 Hz, 2H, ArH), 7.07 (d, *J* = 8.79 Hz, 2H, ArH), 3.94 (br s, 4H, $2CH_2$), 3.85 (s, 3H, OCH_3), 2.58 (br s, 4H, $2CH_2$), 2.38 (s, 3H, CH_3).

4,6-bis(4-methoxyphenyl)-2-(piperazin-1-yl)pyrimidine (**5c**): Brown solid, yield: 100%, mp = 151-153 °C; FTIR (ATR, ν_{max}, cm^{-1}): 3277 (N-H of NH), 2926-2845 (C-H of CH_3), 1172-1094 (C-N of pyr), 1256 (C-O of OCH_3), 1563 (C=N of pyr), 1605 (C=C of Ar), ^{1}H NMR (400 MHz, DSMO-d_6, δ, ppm): 8.25 (d, *J* = 8.37 Hz, 4H, ArH), 7.67 (s, 1H, Pyr-H), 7.06 (d, *J* = 8.38 Hz, 4H ArH), 3.93 (br s, 4H, $2CH_2$), 3.84 (s, 6H, $2OCH_3$), 3.37 (s, 2H, CH_2), 2.18 (s, 1H, CH), 2.60 (br s, 4H, $2CH_2$); ^{13}C NMR (100 MHz, $CDCl_3$, δ, ppm): 163.70, 161.48, 161.28, 129.65, 128.58, 122.28, 113.92, 99.88, 55.28 ($2OCH_3$), 51.03 (CH_2), 46.11($2CH_2$), 43.26 ($2CH_2$).

4-(3,4-dimethoxyphenyl)-6-(4-ethylphenyl)-2-(piperazin-1-yl)pyrimidine (**5d**): Yellow solid, yield: 100%, mp = 130-133 °C; ^{1}H NMR (400 MHz, $CDCl_3$, δ, ppm): 8.25 (d, *J* = 8.23 Hz, 2H, ArH), 7.96 (d, *J* = 7.98, 1.94 Hz, 1H, ArH), 7.88 (s, 1H, pyr-H), 7.86 (d, *J* = 8.20 Hz, 2H, ArH), 7.28 (d, *J* = 8.26 Hz, 2H, ArH), 7.09 (d, *J* = 8.59 Hz, 1H, ArH), 4.33 (br s, 4H, $2CH_2$), 3.91 (s, 3H, OCH_3), 3.85 (s, 3H, OCH_3), 3.76 (br s, 4H, $2CH_2$), 2.70 (q, *J* = 7.57, 2H, CH_2), 1.23 (q, *J* = 7.58Hz, 3H, CH_3); ^{13}C NMR (100 MHz, DMSO-d_6, δ, ppm): 164.38, 164.28,160.92, 151.37, 148.83, 146.95, 134.44, 129.28, 128.08, 127.42, 127.28, 120.58, 111.48, 110.39, 101.95, 56.79, 55.79 (OCH_3), 55.65 (OCH_3), 49.38 ($2CH_2$), 37.29 ($2CH_2$), 28.06 (CH_2), 15.46 (CH_3).

5.6.1.6 Typical procedure for synthesis of 4,6-diphenyl-2-(4-(prop-2-yn-1-yl)piperazin-1-yl)pyrimidines.

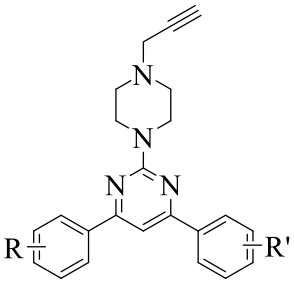

6a	R = 4-Cl,	R' = 4-MeO
6b	R = 4-Me,	R' = 4-MeO
6c	R = 4-MeO,	R' = 4-MeO
6d	R = 3,4-MeO,	R' = 4-Et

To a stirring solution of 4,6-bis(4-methoxyphenyl)-2-(piperazin-1-yl)pyrimidine (2 g, 5.32 mmol) in DMF (20 mL) was added propargyl bromide (0.69 g, 5.85 mmol) and Et_3N (1.1 g , 10.63 mmol) at 0^{o}C. The reaction was further stirred at room temperature for 3 hours, and, using the TLC, the progression of the reaction was monitored. The reaction mixture was then added to 100 g ice,

stirred, and the precipitate formed was filtered under vacuum, washed with water and dried. The compound was purified by recrystallization using EtOH to obtain the following compound(s).

4-(4-chlorophenyl)-6-(4-methoxyphenyl)-2-(4-(prop-2-yn-1-yl)piperazin-1-yl)pyrimidine (**6a**). Yellow solid, yield: 100%, mp = 148-151°C; ^{1}H NMR (400 MHz, $CDCl_3$, δ, ppm): 8.26 (d, J = 8.79 Hz, 2H, ArH), 8.18 (d, J = 8.09 Hz, 2H, ArH), 7.70 (s, 1H, pyr-H), 7.33 (d, J = 8.04 Hz, 2H, ArH), 7.07 (d, J = 8.79 Hz, 2H, ArH), 3.94 (br s, 4H, $2CH_2$), 3.85 (s, 3H, OCH_3), 3.36 (s, 2H, CH_2), 3.17 (s, 1H, CH), 2.58 (br s, 2H, $2CH_2$).

4-(4-methoxyphenyl)-2-(4-(prop-2-yn-1-yl)piperazin-1-yl)-6-(p-tolyl)pyrimidine (**6b**)*:* Yellow solid, Yield: 98 %; ^{1}H NMR (400 MHz, DMSO-d_6, δ, ppm): 8.25 (d, J = 8.76 Hz, 2H, ArH), 8.17 (d, J = 8.08 Hz, 2H, ArH), 7.70 (s, 1H, pyr-H), 7.33 (d, J = 8.04 Hz, 2H, ArH), 7.07 (d, J = 8.80 Hz, 2H, ArH), 3.94 (br s, 4H, $2CH_2$), 3.85 (s, 3H, OCH_3), , 3.86 (s, 3H, OCH_3), 3.36 (d, J = 1.76 Hz, 2H, CH_2),3.17 (s, 1H, CH), 2.58 (t, J = 4.42 Hz, 4H, $2CH_2$), 2.39 (s, 3H, CH_3); ^{13}C NMR (100 MHz, DMSO-d_6, δ, ppm): 164.88, 164.78, 161.41, 151.86, 149.33, 147.45, 134.93, 128.57, 127.77, 121.07, 111.97, 110.89, 102.44, 56.28 ($2OCH_3$), 56.14 (OCH_3).

4,6-bis(4-methoxyphenyl)-2-(4-(prop-2-yn-1-yl)piperazin-1-yl)pyrimidine (**6c**): Yellow solid, yield: 100%; ^{1}H NMR (400 MHz, $CDCl_3$, δ, ppm): 8.14 (d, J = 8.52 Hz, 4H, ArH), 7.40 (s, 1H, pyr-H), 7.97 (dd, J = 7.98,1.94 Hz, 1H, ArH), 7.89 (s, 1H, pyr-H), 7.88 (d, J = 8.20 Hz, 1H, ArH), 7.39 (d, J = 8.26 Hz, 2H, ArH), 7.10 (d, J = 8.59 Hz, 1H, ArH), 3.94 (br s, 4H, $2CH_2$), 3.92 (s, 3H, OCH_3), 3.86 (s, 3H, OCH_3), 3.80 (br s, 4H, $2CH_2$), 3.36 (s, 2H, CH_2), 3.17 (s, 1H, CH), 2.70 (q, J = 5.68 Hz, 2H, $2CH_2$), 1.23 (t, J = 7.58 Hz, 3H CH_3).

4-(3,4-dimethoxyphenyl)-6-(4-ethylphenyl)-2-(4-(prop-2-yn-1-yl)piperazin-1-yl)pyrimidine (**6d**): Yellow solid, yield: 96%, mp = 133-136 °C; ^{1}H NMR (400 MHz, $CDCl_3$, δ, ppm): 8.26 (d, J = 8.23 Hz, 2H, ArH), 7.97 (dd, J = 7.98 Hz, 1.94 Hz, 1H, ArH), 7.89 (s, 1H, pyr-H), 7.88 (d, J = 8.20 Hz, 1H, ArH), 7.38 (d, J = 8.26 Hz, 2H, ArH), 7.10 (d, J = 8.59 Hz, 1H, ArH), 3.94 (br s, 4H, $2CH_2$), 3.92 (s, 3H, OCH_3), 3.86 (s, 3H, OCH_3), 3.83 (br s, 4H, $2CH_2$), 3.36 (s, 2H, CH_2), 3.17 (s, 1H, CH), 2.70 (q, J = 5.68 Hz, 2H, $2CH_2$), 1.23 (t, J = 7.58 Hz, 3H CH_3); ^{13}C NMR (100 MHz, $CDCl_3$, δ, ppm): 165.07, 164.63, 162.12, 151.08, 149.11, 146.83, 135.80, 131.15, 128.18, 127.11, 120.94, 110.10, 101.30, 56.04, 56.02, 51.99, 47.14, 43.75, 29.70, 28.81, 15.52.

5.6.1.7 A typical procedure for the synthesis of azidobenzenes.

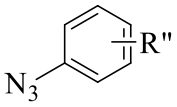

R" = 3 - NO_2
= 4 - F
= 4 - Cl
= 3, 5- difluoro
= 4 - CF_3

A solution of $NaNO_2$ (1.84 g, 26.65 mmol) in H_2O (5.5 mL) was slowly added to a stirring solution of aniline (2.0 g, 15.68 mmol) in 4 HCl (30 mL) at 0^oC. The reaction mixture was further stirred for 30 mins at 0^oC, after which an aqueous solution of NaN_3 (1.73 g, 26.65 mmol) in H_2O (5 mL) was added over 5 mins. The reaction mixture was stirred at room temperature for 30 mins. The reaction completion was monitored by TLC. The crude compound was extracted in Et_2O (2 x20 mL), and the collected organic layer was dried using Na_2SO_4. Et_2O was removed under rotavapor to obtain the azidobenzenes compounds.

5.6.1.8 Typical procedure for synthesis of 4,6-diphenyl-2-(4-((1-phenyl-1H-1,2,3-triazol-4-yl)methyl)piperazin-1-yl)pyrimidine derivatives

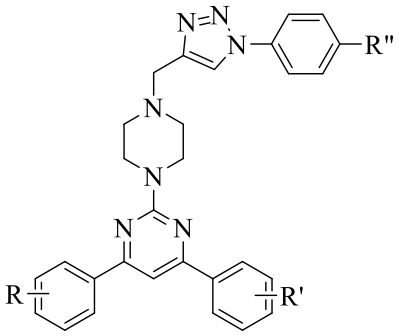

A reaction mixture of 4,6-diphenyl-2-(4-(prop-2-yn-1-yl) piperazin-1-yl)pyrimidine (0.25 g, 0.60 mmol), excess sodium azide, $CuSO_4.5H_2O$(24 mg, 0.15 mmol) and sodium ascorbate (29 mg, 0.15 mmol) in (H_2O/*t*-BuOH; =>1:2) (4mL) is stirred at room temperature for 6 hours. Reaction progression monitored by TLC. The reaction mixture is added into 100 g of ice water, stirred, and the precipitate formed is filtered, washed with water and diethyl ether. The compound is purified using column chromatography .1:9.9 => MeOH and DCM.

4-(4-chlorophenyl)-6-(4-methoxyphenyl)-2-(4-((1-phenyl-1H-1,2,3-triazol-4-yl)methyl)piperazin-1-yl)pyrimidine (**8a**): Yellow solid, yield: 83%, mp = 187-189 °C; FTIR (ATR, ν_{max}, cm^{-1}): 2997-2836 (C-H of CH_3), 1123-1141 (C-N of pyr), 1252-1235 (C-O of OCH_3), 1564 (C=N of pyr),

1695-1602 (C=C of Ar), 811 (C-Cl); ^{1}H NMR (400 MHz, DMSO, *δ*, ppm): 8.76 (s, 1H, ArH), 8.27 (dd, *J* =17.44 Hz, 8.51 Hz, 4H, ArH),7.93 (d, *J* =7.95 Hz, 2H, ArH), 7.75 (s, 1H, ArH), 7.61-7.56 (m, 4H, ArH), 7.48 (t, *J* = 7.34 Hz, 1H, ArH), 7.06 (d, *J* = 8.59 Hz, 2H ArH), 3.94 (br s, 4H, $2CH_2$), 3.84 (s, 3H, OCH_3), 3.74(s, 2H, CH_2), 2.60 (br s, 4H, $2CH_2$); ^{13}C NMR (400 MHz, DMSO, *δ*, ppm): 164.24, 162.80, 161.46, 161.44, 144.39, 136.70, 136.17, 135.25, 129.79, 129.39, 128.76, 128.69, 128.62, 128.43, 122.02, 119.90, 113.96, 100.50, 55.31 (OCH_3), 52.56 (CH_2), 52.20.

4-(4-chlorophenyl)-2-(4-((1-(4-fluorophenyl)-1H-1,2,3-triazol-4-yl)methyl)piperazin-1-yl)-6-(4-methoxyphenyl)pyrimidine (**8b**): Yellow solid, yield: 86%, mp = 164-167 ℃; FTIR (ATR, ν_{max}, cm^{-1}): 2997-2856 (C-H of CH_3), 1264 (C-O of OCH_3), 1576 (C=N of pyr), 1645 (C=C of Ar), 1028, (C-F), 804 (C-Cl); ^{1}H NMR (400 MHz, $CDCl_3$, *δ*, ppm): 8.73 (s, 1H, ArH), 8.29 (d, *J* =7.58 Hz, 2H, ArH), 8.25 (d, *J* =7.75 Hz, 2H, ArH), 7.97 (br s, 2H, ArH), 7.74 (s, 1H, ArH), 7.57 (d, *J* =7.24 Hz, 2H, ArH), 7.44 (br s, 1H, ArH), 7.07 (d, *J* = 7.54 Hz, 2H ArH), 3.93 (br s, 4H, $2CH_2$), 3.84 (s, 3H, OCH_3), 3.74 (s, 2H, CH_2), 2.60 (br s, 4H, $2CH_2$); ^{13}C NMR (100 MHz, DMSO, *δ*, ppm): 164.23, 162.79, 161.44, 160.26, 144.42, 136.16, 135.25, 133.26, 129.39, 128.75, 128.61, 122.26, 122.17, 116.72, 116.49, 113.95, 100.49, 55.30 (OCH_3), 52.53 (CH_2), 52.18 ($2CH_2$), 43.41 ($2CH_3$).

4-(4-chlorophenyl)-2-(4-((1-(4-chlorophenyl)-1H-1,2,3-triazol-4-yl)methyl)piperazin-1-yl)-6-(4-methoxyphenyl)pyrimidine (**8c**): Creamy white solid, yield: 96%, mp = 211-213 ℃; 3386 (N-H of N_2), 2937-2841 (C-H of CH_3), 1604 (C=C of Ar), 1254 (C-O of OCH_3), 803.4 (C-Cl); ^{1}H NMR (400 MHz, $CDCl_3$, *δ*, ppm): 8.05 (d, *J* = 8.52 Hz, 2H, ArH), 8.01 (d, *J* = 8.28 Hz, 2H, ArH), 7.72 (d, *J* = 7.80 Hz, 2H, ArH), 7.48 (d, *J* = 7.87 Hz, 2H, ArH), 7.42 (d, *J* = 8.10 Hz, 2H, ArH), 7.28 (s, 1H, ArH), 6.98 (d, *J* = 8.32 Hz, 2H, ArH), 4.11 (br s, 4H, ArH), 3.95 (s, 3H, OCH_3), 3.87 (s, CH_2, CH_2), 2.80 (br s, 4H, $2CH_2$); ^{13}C NMR (100 MHz, $CDCl_3$, *δ*, ppm): 165.05, 163.82, 162.05, 161.80, 136.76, 136.42, 134.63, 130.42, 130.06, 128.93, 128.68, 128.45, 121.76, 114.13, 101.20, 55.53 (OCH_3), 53.00 ($2CH_2$), 43.37 ($2CH_2$).

4-(4-((4-(4-(4-chlorophenyl)-6-(4-methoxyphenyl)pyrimidin-2-yl)piperazin-1-yl)methyl)-1H-1,2,3-triazol-1-yl)phenyl nitrate (**8d**): Brick red solid, yield: 97%, mp = 146-149 ℃; FTIR (ATR, ν_{max}, cm^{-1}): 3373 (N-H of NH_2), 2932-2843 (C-H of CH_3), 1656 (C=C of Ar), 1505-1536 (N-O of NO_3), 1258 (C-O of OCH_3), 803 (C-Cl); ^{1}H NMR (400 MHz, DMSO, *δ*, ppm): 8.96 (s, 1H, ArH), 8.43 (d, *J* = 7.92 Hz, 2H, ArH), 8.29-8.23 (m, 6H ArH), 7.73 (s, 1H, ArH), 7.56 (d, *J* = 7.52 Hz,

2H, ArH), 7.05 (d, *J*= 7.71 Hz, 2H ArH), 3.93 (br s, 4H, $2CH_2$), 3.83 (s, 6H, $2CH_3$), 3.77 (s, 2H, CH_2), 2.61 (br s, 4H, $2CH_2$); ^{13}C NMR (100 MHz, $CDCl_3$, *δ*, ppm): 164.23, 162.79, 161.45, 146.51, 140.94, 136.14, 135.27, 129.38, 128.76, 128.69, 128.67, 128.62, 125.48, 120.40, 120.05, 113.96, 100.50, 55.31 (OCH_3), 52.24 ($2CH_2$), 52.13 ($2CH_2$), 43.44 ($2CH_3$).

4-(4-chlorophenyl)-6-(4-methoxyphenyl)-2-(4-((1-(3-(trifluoromethyl)phenyl)-1H-1,2,3-triazol-4-yl)methyl)piperazin-1-yl)pyrimidine (**8e**): Yellow solid, yield: 89%, mp = 155-157 ℃; FTIR (ATR, ν_{max}, cm^{-1}): 3370 (N-H of NH_2), 2965-2843 (C-H of CH_3), 1508-1538 (N-O of NO_3), 1234 (C-O of OCH_3), 1032 (C-F), 817 (C-Cl); ^{1}H NMR (400 MHz, $CDCl_3$, *δ*, ppm): 8.08-7.98 (m, 7H, ArH), 7.72-7.66 (m, 2H, ArH), 7.44 (d, *J* = 8.51 Hz, 2H, ArH), 7.29 (s. 1H, ArH), 6.99 (d, *J* = 8.75 Hz, 2H, ArH), 4.06 (br s, 4H, $2CH_2$), 3.87 (s, 3H, OCH_3), 3.86 (s, 2H, CH_2), 2.70 (br s, 4H, $2CH_2$); ^{13}C NMR (100 MHz, $CDCl_3$, *δ*, ppm): 165.09, 163.89, 162.24, 161.83, 146.01, 137.61, 136.96, 136.43, 132.80, 130.75, 130.63, 128.99, 128.74, 128.53, 125.49, 125.45, 123.69, 120.90, 117.54, 117.50, 114.18, 101.20, 55.59 (OCH_3), 53.63 (CH_2), 53.26 ($2CH_2$), 43.97 ($2CH_2$) (CH_3).

4-(4-chlorophenyl)-2-(4-((1-cyclohexyl-1H-1,2,3-triazol-4-yl)methyl)piperazin-1-yl)-6-(4-methoxyphenyl)pyrimidine (**8f**): Creamy white solid, yield: 70%, mp = 207-209 ℃; FTIR (ATR, ν_{max}, cm^{-1}): 3391 (N-H of NH_2), 2931-2842 (C-H of CH_3), 1651 (C=C of Ar), 1259 (C-O of OCH_3), 805 (C-Cl); ^{1}H NMR (400 MHz, $CDCl_3$, *δ*, ppm): 8.07 (d, *J* = 8.12Hz, 2H, ArH), 8.03 (d, *J* = 8.12 Hz, 2H, ArH), 7.52 (s, 1H, ArH), 7.43 (d, *J* = 8.15 Hz, 2H, ArH), 7.28 (s, 1H, ArH), 6.99 (d, *J* = 8.41Hz, 2H, ArH), 4.45 (t, *J* = 11.6 Hz, 1H, CH), 4.03 (br s, 4H, $2CH_2$), 3.86 (s, 3H, OCH_3), 3.75 (s, 2H, CH_2), 2.64 (br s, 4H, $2CH_2$), 2.22 (d, *J* = 8.15 Hz, 2H, CH_2), 1.92 (d, *J* = 8.15 Hz, 2H, CH_2), 1.76 (qt, *J* = 12.57 Hz, 3H, CH, CH_2), 1.46 (q, *J* = 12.83 Hz, 2H, CH_2), 1.27 (q, *J* = 12.83 Hz, 2H, CH_2); ^{13}C NMR (100 MHz, $CDCl_3$, *δ*, ppm): 164.98, 163.77, 162.19, 161.73, 136.91, 136.31, 130.57, 128.88, 128.66, 126.45, 114.09, 100.92, 60.17 (CH), 55.50 (OCH_3), 53.77 (CH_2), 53.11 (CH_2), 43.87 (CH_2), 33.70 (CH_2), 25.29 (CH_2).

4-(4-methoxyphenyl)-2-(4-((1-phenyl-1H-1,2,3-triazol-4-yl)methyl)piperazin-1-yl)-6-(p-tolyl)pyrimidine (**8g**): Yellow solid, yield: 83%, mp = 185-187 ℃; FTIR (ATR, ν_{max}, cm^{-1}): 3465(C-N), 2963-2836 (C-H of CH_3), 1127-1171 (C-N of pyr), 1260 (C-O of OCH_3), 1562 (C=N of pyr), 1601 (C=C of Ar); ^{1}H NMR (400 MHz, DMSO, *δ*, ppm): 8.76 (s, 1H, ArH), 8.25 (d, *J* =8.27 Hz, 2H, ArH), 8.16 (d, *J* =7.71 Hz, 2H, ArH), 7.93 (d, *J* =7.72 Hz, 2H, ArH), 7.69 (s, 1H,

ArH), 7.59 (t, *J* = 7.56Hz, 2H, ArH), 7.48 (t, *J* = 7.14 Hz, 1H, ArH),7.31 (d, *J* = 7.67 Hz, 2H ArH),7.05 (d, *J* = 8.35 Hz, 2H ArH), 3.94 (br s, 4H, $2CH_2$), 3.83 (s, 3H, OCH_3), 3.74 (s, 2H, CH_2), 2.60 (br s, 4H, $2CH_2$), 2.33 (s, 3H, CH_3); ^{13}C NMR (100 MHz, DMSO, *δ*, ppm): 164.00, 163.38, 161.52, 161.32, 144.42, 136.71, 134.57, 129.79, 129.59, 129.18, 128.60, 128.43, 126.70, 122.02, 119.91, 113.94, 100.22, 55.28 (OCH_3), 52.58 (CH_2), 52.24 ($2CH_2$), 43.42 ($2CH_3$), 20.93 (CH_3).

2-(4-((1-(4-fluorophenyl)-1H-1,2,3-triazol-4-yl)methyl)piperazin-1-yl)-4-(4-methoxyphenyl)-6-(p-tolyl)pyrimidine (**8h**): Brown yellow solid, yield: 98%, mp = 186-188 ℃; FTIR (ATR, ν_{max}, cm^{-1}): 3382 (N-H of N_2), 2930-2846 (C-H of CH_3), 1656 (C=C of Ar), 1257 (C-O of OCH_3), 803.85 (C-Cl); ^{1}H NMR (400 MHz, $CDCl_3$, *δ*, ppm): 8.07 (d, *J* = 8.73 Hz, 2H, ArH), 7.99 (d, *J* = 8.07 Hz, 2H, ArH), 7.93 (s, 1H, ArH), 7.72 (dd, *J* = 4.31 Hz, 13.47 Hz, 2H, ArH), 7.32 (s, 1H, ArH) 7.27 (d, *J*= 8.18 Hz, 2H, ArH), 7.21 (t, *J* = 8.48Hz, 2H, ArH), 6.98 (d, *J* = 8.78 Hz, 2H, ArH), 4.06 (br s, 4H, ArH), 3.86 (s, 3H, OCH_3), 3.84 (s, CH_2, CH_2), 2.69 (br s, 4H, $2CH_2$), 2.41 (s, 3H, CH_3); ^{13}C NMR (100 MHz, $CDCl_3$, *δ*, ppm): 165.02, 164.65, 163.72, 162.22, 161.60, 161.24, 145.48, 140.55, 135.63, 133.52, 130.84, 129.44, 128.64, 127.07, 122.60, 122.51, 121.14, 116.93, 116.70, 114.06, 101.08, 55.50 (OCH_3), 53.61, 53.21, 43.90, 21.52 (CH_3).

2-(4-((1-(4-chlorophenyl)-1H-1,2,3-triazol-4-yl)methyl)piperazin-1-yl)-4-(4-methoxyphenyl)-6-(p-tolyl)pyrimidine (**8i**): Yellow solid, yield: 95%, mp = 153-155 ℃; FTIR (ATR, ν_{max}, cm^{-1}): 2997-2835 (C-H of CH_3), 1723-1603 (C=C of Ar), 1234 (C-O of OCH_3), 814 (C-Cl); ^{1}H NMR (400 MHz, DMSO, *δ*, ppm): 8.08 (d, *J*= 8.68 Hz, 2H, ArH), 8.00 (d, *J*= 8.03Hz, 2H, ArH), 7.95 (s, 1H, ArH), 7.70 (d, *J* = 8.73Hz, 2H, ArH), 7.50 (d, *J* = 8.70Hz, 2H, ArH), 7.32 (s, 1H, ArH), 7.28 (d, *J* = 8.12 Hz, 2H, ArH), 6.99 (d, *J* = 8.72 Hz, 2H, ArH), 4.06 (br s, 4H, ArH), 3.87 (s, 3H, OCH_3), 3.84 (s, CH_2, CH_2), 2.69 (br s, 4H, $2CH_2$), 2.41 (s, 3H, CH_3); ^{13}C NMR (400 MHz, DMSO, *δ*, ppm): 165.02, 164.65, 162.22, 161.61, 145.65, 140.56, 135.71, 135.63, 134.53, 130.84, 130.03, 129.44, 128.64, 127.08, 121.71, 120.84, 114.06, 101.08, 55.50 (OCH_3), 53.60 (CH_2), 53.21 ($2CH_2$), 43.91 ($2CH_2$), 21.53 (CH_3).

4-(4-methoxyphenyl)-2-(4-((1-(4-nitrophenyl)-1H-1,2,3-triazol-4-yl)methyl)piperazin-1-yl)-6-(p-tolyl)pyrimidine (**8j**): Brick red solid, yield: 100%, mp = 203-205 ℃; FTIR (ATR, ν_{max}, cm^{-1}): 2929-2836 (C-H of CH_3), 1644 (C=C of Ar), 1535-1505 (N-O of NO_2), 1254 (C-O of OCH_3); ^{1}H NMR (400 MHz, DMSO, *δ*, ppm): 8.97 (s, 1H, ArH), 8.43(d, *J* = 6.91 Hz, 2H, ArH), 8.24 (br s,

4H, ArH), 8.15 (d, *J* = 6.15 Hz, 2H, ArH), 7.67 (s, 1H, ArH), 7.67 (s, 2H, ArH), 7.05 (d, *J* = 6.79 Hz, 2H, ArH), 3.94 (br s, 4H, ArH), 3.83 (br s, 5H, CH_2, OCH_3), 2.62 (br s, 4H, $2CH_2$), 2.37 (s, 3H, CH_3); ^{13}C NMR (100 MHz, DMSO, *δ*, ppm): 165.05, 164.68, 162.22, 161.65, 147.28, 146.49, 141.35, 140.62, 135.61, 130.82, 129.47, 128.65, 127.08, 125.74, 125.67, 120.77, 120.50, 119.52, 114.09, 101.14, 55.53 (OCH_3), 53.53, 53.26, 43.9221.54, (CH_3).

4-(4-methoxyphenyl)-6-(p-tolyl)-2-(4-((1-(3-(trifluoromethyl)phenyl)-1H-1,2,3-triazol-4-yl)methyl)piperazin-1-yl)pyrimidine (**8k**): Yellow solid, yield: 88%, mp = 169-171 ℃; FTIR (ATR, ν_{max}, cm^{-1}): 3347 (N-H of NH_2), 2937-2812 (C-H of CH_3), 1607 (C=C of Ar) 1253 (C-O of OCH_3), 1032 (C-F); ^{1}H NMR (400 MHz, $CDCl_3$, *δ*, ppm): 8.07 (d, *J* = 8.04Hz, 2H, ArH), 8.04 (s, 2H, ArH), 7.99 (d, *J* = 7.89 Hz, 2H, ArH), 7.71-7.64 (m. 1H, ArH), 7.32 (s, 1H, ArH), 7.27 (d, *J* = 8.64 Hz, 2H, ArH), 4.07 (br s, 4H, ArH), 3.86 (s, 3H, OCH_3), 3.85 (s, CH_2, CH_2), 2.70 (br s, 4H, $2CH_2$), 2.41 (s, 3H, CH_3); ^{13}C NMR (100 MHz, $CDCl_3$, *δ*, ppm): 165.03, 164.66, 162.23, 161.61, 145.97, 140.56, 137.55, 135.63, 132.37, 130.84, 130.68, 129.45, 128.64, 127.08, 125.40, 125.36, 123.60, 120.86, 117.48, 114.07, 100.10, 55.50 (OCH_3), 53.59, 53.24, 43.81, 21.42 (CH_3).

2-(4-((1-cyclohexyl-1H-1,2,3-triazol-4-yl)methyl)piperazin-1-yl)-4-(4-methoxyphenyl)-6-(p-tolyl)pyrimidine (**8l**): Cream white solid, yield: 90%, mp = 205-207 ℃; FTIR (ATR, ν_{max}, cm^{-1}): 2960-2850 (C-H of CH_3), 1653 (C=C of Ar), 1510-1546 (N-O of NO_3), 1453 (C-H of CH_3), 1216-1259 (C-O of OCH_3); ^{1}H NMR (400 MHz, $CDCl_3$, *δ*, ppm): 8.07 (d, *J* = 8.76 Hz, 2H ArH), 7.99 (d, *J* = 8.08 Hz, 2H, ArH), 7.52 (s, 1H, ArH), 7.31 (s, 1H, ArH), 7.27 (d, *J* = 8.45 Hz, 2H, ArH), 6.98 (d, *J* = 8.76 Hz, 2H, ArH), 4.44 (t, *J* = 11.75 Hz, 1H, CH), 4.04 (br s, 4H, $2CH_2$), 3.86(s, 3H, OCH_3), 3.75 (s, 2H, CH_2), 2.64 (br s, 4H, $2CH_2$), 2.41 (s, 3H, CH_3), 2.22 (d, *J* = 11.05 Hz, 2H, CH_2), 1.92 (d, *J* = 13.53 Hz, 2H, CH_2), 1.83-1.69 (m, 3H, CH, CH_2), 1.46 (q, *J* =12.95 Hz, 2H, CH_2), 1.30-0.25 (m, 1H, CH); ^{13}C NMR (100 MHz, $CDCl_3$, *δ*, ppm): 164.89, 164.52, 162.15, 161.47, 140.40, 135.56, 130.79, 129.32, 128.53, 126.97, 120.20, 113.94, 100.91, 60.05, 55.39, 53.71, 53.07, 43.79, 33.61, 25.20, 25.17, 21.42 (CH_3); HRMS (ESI, *m/z*) $[M+Na]^+$; calculated for $C_{31}H_{37}N_7O$, 546.2957; found 546.2963.

4,6-bis(4-methoxyphenyl)-2-(4-((1-phenyl-1H-1,2,3-triazol-4-yl)methyl)piperazin-1-yl)pyrimidine (**8m**); Creamy white solid, yield: 100% , mp = 176-179 ℃; FTIR (ATR, ν_{max}, cm^{-1}): 3418(N-H of NH_2), 2924-2772 (C-H of CH_3), 11723-1141 (C-N of pyr), 1255-1234 (C-O of

OCH_3), 1564 (C=N of pyr), 1605 (C=C of Ar); ^{1}H NMR (400 MHz, DMSO, *δ*, ppm): 8.66 (s, 1H, ArH), 8.14 (d, *J* =8.73 Hz, 4H, ArH),7.83 (d, *J* =7.83 Hz, 2H, ArH), 7.56 (s, 1H, ArH), 7.49 (t, *J* = 7.78Hz, 2H, ArH), 7.38 (t, *J* =7.38 Hz, 1ArH), 6.96 (d, *J* = 8.76 Hz, 4H ArH), 3.83 (br s, 4H, $2CH_2$), 3.73 (s, 6H, $2OCH_3$), 3.64 (s, 2H, CH_2), 2.40 (br s, 4H, $2CH_2$); ^{13}C NMR (400 MHz, DMSO, *δ*, ppm): 163.69, 161.49, 161.28, 144.46, 136.72, 129.81, 129.67, 128.58, 128.45, 122.06, 119.91, 113.93, 99.81, 55.29 (OCH_3), 52.61 (CH_2), 52.27 ($2CH_2$), 43.43.($2CH_3$); HRMS (ESI, *m/z*) $[M+Na]^+$; calculated for $C_{31}H_{31}N_7O_2Na^+$, 556.2431*;* found 556.2442.

4-(4-((1-(4-fluorophenyl)-1H-1,2,3-triazol-4-yl)methyl)piperazin-1-yl)-4,6-bis(4-methoxyphenyl)pyrimidine (**8n**):Brown solid, yield: 89%, mp = 173-176 ℃; FTIR (ATR, ν_{max}, cm^{-1}): 3421 (N-H of NH_2), 2963-2836 (C-H of CH_3), 1170-1070 (C-N of pyr), 1258 (C-O of OCH_3), 1562 (C=N of pyr), 1603 (C=C of Ar); ^{1}H NMR (400 MHz, DMSO, *δ*, ppm): 8.74 (s, 1H, ArH), 8.23 (d, *J* = 8.78 Hz, 4H, ArH), 7.99-7.96 (m, 2H ArH), 7.66 (s, 1H, ArH), 7.44(*t*, *J* = 8.77 Hz, 4H, ArH), 7.05 (d, *J* = 8.78 Hz, 4H ArH), 3.93 (br s, 4H, $2CH_2$), 3.83 (s, 6H, $2OCH_3$), 3.74 (s, 2H, CH_2), 2.60 (br s, 4H, $2CH_2$); ^{13}C NMR (100 MHz, $CDCl_3$, *δ*, ppm): ^{13}C NMR (400 MHz, DMSO, *δ*, ppm): 163.68, 162.71, 161.47, 161.27, 160.27, 133.29, 129.66, 128.57, 122.28, 122.19, 116.74, 116.51, 113.92, 99.81, 55.28 ($2OCH_3$), 52.24 (CH_2), 52.22($2CH_2$), 43.41 ($2CH_2$).

4,6-bis(4-methoxyphenyl)-2-(4-((1-(4-nitrophenyl)-1H-1,2,3-triazol-4-yl)methyl)piperazin-1-yl)pyrimidine (**8o**): Brown solid, yield: 91%, mp = 162-165 ℃; FTIR (ATR, ν_{max}, cm^{-1}): 3376 (N-H of NH_2), 2930-2845 (C-H of CH_3), 1508-1534 (N-O of NO_3), 1257(C-O of OCH_3); ^{1}H NMR (400 MHz, $CDCl_3$, *δ*, ppm): 8.07 (d, *J* = 8.84Hz, 4H, ArH), 8.05 (s, 2H, ArH), 7.99 (d, *J* = 7.38 Hz, 1H, ArH), 7.71-7.65 (m, 2H, ArH), 7.29 (s, 1H, ArH), 6.99 (d, *J* = 8.83 Hz, 4H, ArH), 4.07 (br s, 4H, $2CH_2$), 3.87 (s, 8H, CH_2, $2CH_3$), 2.70 (br s, 4H, $2CH_2$); ^{13}C NMR (100 MHz, $CDCl_3$, *δ*, ppm): 164.59, 162.23, 161.63, 137.59, 132.42, 131.35, 130.93, 130.73, 128.66, 125.45, 125.41, 123.65, 117.53, 117.49, 114.09, 113.42, 100.69, 55.54 ($2OCH_3$), 53.61 (CH_2), 53.27($2CH_2$), 43.94 ($2CH_2$).

4,6-bis(4-methoxyphenyl)-2-(4-((1-(3-(trifluoromethyl)phenyl)-1H-1,2,3-triazol-4-yl)methyl)piperazin-1-yl)pyrimidine (**8p**): Yellow solid, yield: 89%, mp = 140-143 ℃; FTIR (ATR, ν_{max}, cm^{-1}): 3399 (N-H of NH_2), 2934-2843 (C-H of CH_3), 1172-1140 (C-N of pyr), 1255-1233 (C-O of OCH_3),1563 (C=N of pyr), 1653(C=C of Ar); ^{1}H NMR (400 MHz, DSMO-d_6, *δ*,

ppm): 8.96 (s, 1H, ArH), 8.43 (d, *J* = 9.04 Hz, 2H, ArH), 8.25-8.21 (m, 6H ArH), 7.65 (s, 1H, ArH), 7.05 (d, *J* = 8.79 Hz, 4H ArH), 3.93 (br s, 4H, $2CH_2$), 3.83 (s, 6H, $2OCH_3$), 3.77(s, 2H, CH_2), 2.60 (br s, 4H, $2CH_2$); ^{13}C NMR (100 MHz, DSMO-d_6, *δ*, ppm): 163.69, 161.48, 161.29, 146.53, 145.13, 140.94, 130.90, 129.67, 128.58, 125.50, 122.55, 120.42, 113.93, 99.82, 55.30 (OCH_3), 52.48 (CH_2), 52.22 ($2CH_2$), 43.42 ($2CH_2$).

4-(3,4-dimethoxyphenyl)-6-(4-ethylphenyl)-2-(4-((1-phenyl-1H-1,2,3-triazol-4-yl)methyl)piperazin-1-yl)pyrimidin (**8q**): Brown solid, yield: 98%, FTIR (ATR, ν_{max}, cm^{-1}): 3376 (N-H, for NH_3), 2930-2845 (C-H of CH_3), 1505-1534 (N-O of NO_3), 1257(C-O of OCH_3); ^{1}H NMR (400 MHz, DSMO-d_6, *δ*, ppm): 8.82 (s, 2H, ArH), 7.95 (d, *J* = 7.92 Hz, 2H, ArH), 7.62 (s, 2H, ArH), 7.38 (s, 1H, ArH), 7.28 (d, *J* = 7.92 Hz, 2H, ArH), 6.91 (d, *J* = 8.90 Hz, 2H, ArH), 6.85-6.76 (m, 3H ArH), 4.42 (br s, 4H, $2CH_2$), 3.97 (s, 3H, OCH_3), 3.91 (s, 3H, OCH_3), 3.82 (s, 2H, CH_2), 2.68 (q, *J* = 7.55 Hz, 2H, CH_2), 2.31 (br s, 4H, $2CH_2$), 2.16 (s, 3H, CH_3), 1.25 (t, *J* = 7.61 Hz, CH_3); ^{13}C NMR (100 MHz, DSMO-d_6, *δ*, ppm): 165.27, 164.40, 162.37, 162.25, 161.10, 151.63, 149.35, 147.61, 135.37, 134.89, 132.20, 132.15, 130.17, 129.67, 128.46, 127.66, 127.324, 120.46, 117.70, 112.46, 112.24, 111.08, 109.98, 104.80, 104.65, 104.39, 109.39, 109.93, 56.37, 56.27, 56.520, 53.27, 14.73, 37.87, 28.92, 15.56.

2-(4-((1-(4-chlorophenyl)-1H-1,2,3-triazol-4-yl)methyl)piperazin-1-yl)-4-(3,4-dimethoxyphenyl)-6-(4-ethylphenyl)pyrimidine (**8r**): Brown solid, yield: 99%, mp = 167 -170 ℃; FTIR (ATR, ν_{max}, cm^{-1}): 3377 (N-H of NH_2), 2935-2842 (C-H of CH_3), 1658 (C=C of Ar), 1505-1536 (N-O of NO_3), 1230 (C-O of OCH_3), 817 (C-Cl); ^{1}H NMR (400 MHz, DSMO-d_6, *δ*, ppm): 8.79 (s, 1H, ArH), 8.18 (d, *J* = 8.02 Hz, 2H, ArH), 7.97 (d, *J* = 8.64 Hz, 2H ArH), 7.88 (d, *J* =8.46 Hz, 2H, ArH), 7.81 (s, 1H, ArH), 7.69 (s, 1H, ArH), 7.66 (d, *J* =8.64 Hz, 2H, ArH), 7.35(d, *J*= 7.98 Hz, 2H ArH), 7.07 (d, *J* =8.50 Hz, 1H, ArH), 3.94 (br s, 4H, $2CH_2$), 3.88 (s, 3H, OCH_3), 3.83 (s, 3H, OCH_3), 3.75 (s, 2H, CH_2), 2.70-2.62 (m, 6H, $3CH_2$), 1.21 (t, *J* = 7.56 Hz, 3H, CH_3); ^{13}C NMR (100 MHz, DSMO-d_6, *δ*, ppm): 164.09, 163.97, 161.48, 151.06, 148.72, 146.52, 135.54, 134.90, 132.69, 129.77, 127.98, 127.07, 121.58, 120.90, 120.25, 111.43, 110.24, 100.56, 55.64 (OCH_3), 55.57 (OCH_3), 28.02 (CH_2), 15.43 (CH_3).

4-(3,4-dimethoxyphenyl)-6-(4-ethylphenyl)-2-(4-((1-(4-(trifluoromethyl)phenyl)-1H-1,2,3-triazol-4-yl)methyl)piperazin-1-yl)pyrimidine (**8s**): Brown solid, yield: 100%, mp = FTIR (ATR, ν_{max}, cm^{-1}): 2958-2836 (C-H of CH_3), 1644-1603 (C=C of Ar), 1506-1536 (N-O of NO_3), 1253 (C-

O of OCH_3), 1027 (C-F); ^{1}H NMR (400 MHz, $CDCl_3$, δ, ppm): 8.95 (s, 1H, ArH), 8.31 (s, 1H, ArH), 8.30-8.28 (m, 1H ArH), 8.18 (d, *J* = 8.17 Hz, 2H, ArH), 7.89-7.80 (m, 4H, ArH), 7.70 (s, 1H, ArH), 7.35 (d, *J* = 8.14 Hz, 2H, ArH), 7.07 (d, *J* = 8.57 Hz, 2H, ArH), 3.95 (br s, 4H, $2CH_2$), 3.88 (s, 3H, OCH_3), 3.83 (s, 3H, OCH_3), 3.77 (s, 2H, CH_2),2.67 (q, *J* = 7.62 Hz, 2H, CH_2), 2.62(br s, 4H, $2CH_2$), 1.21 (t, *J* = 7.61 Hz, CH_3); ^{13}C NMR (100 MHz, DSMO-d_6, δ, ppm): 164.10, 163.99, 161.49, 151.08, 148.73, 146.54, 137.19, 134.90, 131.24, 130.68, 130.35, 129.79, 127.99, 127.08, 124.98, 123.70, 120.26, 116.58, 116.54, 111.44, 110.25, 100.57, 55.65(OCH_3), 55.57(OCH_3), 52.27 (CH_2), 43.45 (CH_2), 28.04 (CH_2), 15.44 (CH_3).

2-(4-((1-(3,5-difluorophenyl)-1H-1,2,3-triazol-4-yl)methyl)piperazin-1-yl)-4-(3,4-dimethoxyphenyl)-6-(4-ethylphenyl)pyrimidine (**8t**): Creamy white solid, yield: 100 %, mp = 176-179 °C; FTIR (ATR, ν_{max}, cm^{-1}): 3422 (N-H of NH_3), 2933-2856 (C-H of CH_3), 1603 (C=C of Ar), 1506-1536 (N-O of NO_3), 1453 (C-H of CH_3), 1258 (C-O of OCH_3), 1024 (C-F). 806 (C-Cl); ^{1}H NMR (400 MHz, $CDCl_3$, δ, ppm): 8.18 (d, *J* = 6.84 Hz, 2H ArH), 7.88 (d, *J* = 7.32 Hz, 2H ArH), 7.81 (s, 1H, ArH), 7.69 (s, 1H, ArH), 7.36-7.31 (m, 6H, ArH), 7.07 (d, *J* = 7.88 Hz, 2H ArH), 3.88 (br s, 7H, $2CH_2$, OCH_3), 3.83 (br s, 5H, CH_2, OCH_3), 2.67 (d, *J* = 6.76 Hz, 6H, $3CH_2$),1.21 (s, 3H, CH_3); ^{13}C NMR (100 MHz, $CDCl_3$, δ, ppm): 164.09, 163.98, 161.50, 151.07, 148.74, 146.53, 136.12, 134.91, 129.81, 128.71,128.03, 127.99, 127.83, 127.09, 120.27, 111.44, 110.27, 100.57, 55.67 (OCH_3), 55.57 (CH_2), 52.83 (OCH_3), 28.04(CH_2), 15.46 (OCH_3).

5.7 Pharmacological Evaluation

5.7.1 Antimalarial activity

The chloroquine-sensitive strain of *P. falciparum* (NF54) was maintained continuously *in vitro* in supplemented RPMI-1640 culture media at 37 ˚C and gassed with a mixture of 5% CO_2, 3% O_2 and 92% N_2 [37]. D-sorbitol was used to synchronize the culture in the ring stage [38]. Determination of the antimalarial activity of different compounds, the synchronized ring-stage parasites were adjusted to a final parasitaemia of 2% and 2% haematocrit, to which serial dilutions of the derivatives and positive control, quinine were added after a 24 hours incubation. Negative controls included uninfected erythrocytes and drug-free parasitized erythrocytes. Following a further 48 hours incubation period, the plates were frozen at -70˚C for 1 hour and thawed for 2 hours. Twenty-five microlitres of lysate was transferred to a non-sterile plate, to which 100 µL Malstat™ and 20 µL nitroblue tetrazolium and phenazine ethosulphate (1:1) mixture was added to

each well and incubated for 40 min at 37 ˚C to quantify the parasite lactate dehydrogenase (pLDH) activity [39]. Thereafter, 5% acetic acid was added to each well and the absorbance of the formazan products read at 620 nm as an indicator of parasite viability. The percentage parasite growth, taking the appropriate controls into account, were calculated and used to determine the concentration required to inhibit parasite growth by 50% (IC_{50} value) from log sigmoid dose-response curves using the GraphPad Prism® 5.0 software. Each experiment was repeated in triplicate [40,41].

5.7.2 Toxicity assays

5.7.2.1 Cell viability assay

Human embryonic kidney epithelial (HEK-293) cells were maintained at 37 ˚C in a humidified environment with a 5% CO_2 as a monolayer in Dulbecco's modified Eagle's medium (DMEM) supplemented with 10% of fetal bovine serum, 100 IU mL^{-1} penicillin and 100 µg mL^{-1} streptomycin. A cell suspension (10 000 cells per well) was incubated at 37 ˚C for 48 h with serial dilutions of compounds/positive control. A final concentration of less than 1% DMSO had no effect on the viability of the cells. Thereafter, 40 µL of (3-(4, 5-dimethylthiazolyl-2)-2, 5-diphenyltetrazolium bromide (MTT; 5 mg mL^{-1} in phosphate buffer saline (pH 7.3) was added to each well and incubated for a further 2 hours. DMSO was used to dissolve the formazan crystals and then quantified by reading the absorbance at 540 nm with a reference wavelength of 690 nm (Labsystems Multiskan RC) [42]. Percent cellular viability was determined using the appropriate controls and used to calculate the IC_{50} values compared to the positive control, camptothecin. The experiment was repeated in triplicate [43,44].

5.7.2.2 Binding affinity assays using select synthetic compounds to *P. falciparum* Hsp70

The direct protein compound binding studies were conducted using SPR. The recombinantly produced PfHsp70-1 and PfHsp70-z [45–47] were immobilized on as ligands on CMD 3D 500L; (BioNavis, Tampere, Finland) [48]. As controls, a channel without immobilized protein was used to monitor nonspecific changes in refractive index. As analytes, compounds (Compound **8c, 8e** and **8t**) were prepared into aliquots of 0, 1.25, 2.5, 5 and 10 nM that were injected at a flow rate of 50 µL/min onto the immobilized protein in each flow cell. For double referencing, injections with buffer only were also used as controls. The interaction was allowed for a total of 13 minutes for association and dissociation events. The steady-state equilibrium constant data were processed

from the generated sensorgrams using TraceDrawer software version 1.8 (Ridgeview Instruments, Sweden).

References

[1] P. Singh, S. Sachdeva, R. Raj, V. Kumar, M. P. Mahajan, S. Nasser, L. Vivas, J. Gut, P.J. Rosenthal, T. Feng, K. Chibale, Antiplasmodial and cytotoxicity evaluation of 3-functionalized 2-azetidinone derivatives, *Bioorg. Med. Chem. Lett*. 21 (2011) 4561–4563. https://doi.org/10.1016/j.bmcl.2011.05.119.

[2] N. J. White, Review series Antimalarial drug resistance, *J. Clin. Invest*. 113 (2004). https://doi.org/10.1172/JCI200421682.1084.

[3] Q. Anne-Maryse, Pierre-Louis Jumana, E. Isabel, S. Challa, The Malaria Control Success Story Anne-Maryse, (2008).

[4] T. Okorosobo, G.M. Mwabu, J.N. Orem, Economic burden of malaria in six countries of Africa, J. Bus. Mark. Manag. (2011).

[5] D. Menard, A. Dondorp, Antimalarial Drug Resistance : A threat to malaria elimination, cold spring harb. Perspect. Med. 2009 (2017). http://perspectivesinmedicine.cshlp.org/.

[6] R. B. Y. The, A. General, Malaria, Comptrol. Audit. Gen. Ordered. (2013).

[7] World Health Organisation, World malaria report 2020- WHO: 20 years of global progress and challenges, Geneva, Switzerland, 2020. https://www.mmv.org/newsroom/publications/world-malaria-report-2020?gclid=Cj0KCQiAv6yCBhCLARIsABqJTjYQ5UgQmOuMIr3YNko1HARzcENfzQ8RTa2YLaZ9RvrRwQHX0l75s2kaAsksEALw_wcB.

[8] K. A. J. Al Khaja, R. P. Sequeira, Drug treatment and prevention of malaria in pregnancy: a critical review of the guidelines, *Malar J*, 20 (2021) 1–13. https://doi.org/10.1186/s12936-020-03565-2.

[9] E. B. Chaponda, D. Chandramohan, C. Michelo, S. Mharakurwa, J. Chipeta, R.M. Chico, High burden of malaria infection in pregnant women in a rural district of Zambia : a cross-sectional study, *Malar. J*. 14 (2015) 1–12. https://doi.org/10.1186/s12936-015-0866-1.

[10] A. Bartoloni, L. Zammarchi, Clinical aspects of uncomplicated and severe malaria, *Mediterr J Hematol Infect Dis*. (2012). https://doi.org/10.4084/MJHID.2012.026.

[11] U. M. Chukwuocha, P. C. Okorie, G. N. Iwuoha, S. N. Ibe, I. N. Dozie, B. E. Nwoke, Awareness, perceptions and intent to comply with the prospective malaria vaccine in parts of South Eastern Nigeria, *Malar J*, vol. 17, pp. 1–7, 2018. https://doi.org/10.1186/s12936-018-2335-0.

[12] S. Mahmoudi, H. Keshavarz, "Malaria vaccine development: the need for novel approaches: A Review Article," *Iran J Parasitol*, no. 1, vol. 13, pp. 1–10, 2018. https://www.ncbi.nlm.nih.gov/pmc/articles/PMC6019592/.

[13] V. Sumangala, B. Poojary, N. Chidananda, J. Fernandes, N.S. Kumari, Synthesis and antimicrobial activity of 1,2,3-triazoles containing quinoline moiety, *Arch Pharm Res*, vol. 33, pp. 1911–1918, 2010. https://doi.org/10.1007/s12272-010-1204-3.

[14] P. López-Rojas, M. Janeczko, K. Kubinski, Á. Amesty, M. Masłyk, A. Estévez-Braun, "Synthesis and antimicrobial activity of 4-substituted 1,2,3-triazole-coumarin derivatives," *Molecules*. vol. 23. pp 1–18, 2018. https://doi.org/10.3390/molecules23010199.

[15] B. Ewa, K. E. Chrobak, "Chemistry Novel triazoles of 3-acetylbetulin and betulone as anticancer agents," vol. 60 pp. 2051–2061, 2018. https://doi.org/10.1007/s00044-018-2213-x.

[16] R. S. Keri, S. A. Patil, Triazole : "A promising antitubercular agent," no. 4, vol 86, pp. 410–423, 2015. https://doi.org/10.1111/cbdd.12527.

[17] S. Zhang, Z. Xu, C. Gao, Q. Ren, L. Chang, Z. Lv and L. Feng, "Chemistry Triazole derivatives and their anti-tubercular activity," *Eur J Med Chem*, vol. 138, pp. 501–513, 2017. https://doi.org/10.1016/j.ejmech.2017.06.051.

[18] P. C. Chen, V. Patil, W. Guerrant, P. Green, A. K. Oyelere, Synthesis and structure-activity relationship of histone deacetylase (HDAC) inhibitors with triazole-linked cap group," vol. 16, pp. 4839–4853, 2008. https://doi.org/10.1016/j.bmc.2008.03.050.

[19] V. Patil, W. Guerrant, P. C. Chen, B. Gryder, D. B. Benicewicz, S. I. Khan, B. L. Tekwani, and A. K. Oyelere, "Antimalarial and antileishmanial activities of histone deacetylase inhibitors with triazole-linked cap group," *Bioorg Med Chem*, vol. 18, pp. 415–425, 2010.

https://doi.org/10.1016/j.bmc.2009.10.042.

[20] N. Boechat, M. de L. G. Ferreira, L. C. S. Pinheiro, A. M. L. Jesus, M. M .M. Leite, C. C. S. Júnior, A. C. C. Aguiar, I. M. de Andrade and A.U. Krettli, "New compounds hybrids 1 h -1,2,3-triazole-quinoline against plasmodium falciparum," *Chem Biol Drug Des*, vol. 84, pp. 325–332, 2014. https://doi.org/https://doi.org/10.1111/cbdd.12321.

[21] S. Pandey, P. Agarwal, K. Srivastava, S. Rajakumar, S. K. Puri, P. Verma, J. K. Saxena, A. Sharma, J. Lal and P. M. S. Chauhan, "Synthesis and bioevaluation of novel 4-aminoquinoline-tetrazole derivatives as potent antimalarial agents," *Eur J Med Chem*, vol. 66, pp. 69–81, 2013. https://doi.org/10.1016/j.ejmech.2013.05.023.

[22] G. Roman, R. Mona, D. Vukomanovic, Z. Jia, K. Nakatsu, W. Szarek, Heme Oxygenase Inhibition by 2-Oxy-substituted 1-Azolyl-4-phenylbutanes : Effect of variation of the azole moiety. X-ray crystal structure of human heme oxygenase-1 in complex with *Chem. Biol. Drug Des*, vol. 75, pp. 68–90, 2010. https://doi.org/10.1111/j.1747-0285.2009.00909.x.

[23] J. Morgan and P.A. Keller, "Antimalarial activity of 2,4-diaminopyrimidines," vol. 5, pp. 277–280, 2008. https://ro.uow.edu.au/scipapers/152

[24] A. Agarwal, K. Srivastava, S. K. Puri and P. M. S. Chauhan, "Syntheses of 2,4,6-trisubstituted triazines as antimalarial agents," *Bioorg Med Chem Lett*, vol. 15, pp. 531–533, 2005) https://doi.org/10.1016/j.bmcl.2004.11.052.

[25] J. A. Badejo, O. O. Abiodun, O. Akinola, C. T. Happi, A. Sowunmi and G. O. Gbotosho, "Interaction between rifampicin, amodiaquine and artemether in mice infected with chloroquine-resistant Plasmodium berghei," *Malar J*, vol. 13, pp. 1–6, 2014. https://doi.org/10.1186/1475-2875-13-299

[26] M. Strath, T. Scott-Finnigan, M. Gardner, D. Williamson and I. Wilson, "Antimalarial activity of rifampicin in vitro and in rodent models," *Trans R Soc Trop Med Hyg*, vol. 87 pp. 211–216, 1993. https://doi.org/10.1016/0035-9203(93)90497-E.

[27] B. Pradines, C. Rogier, T. Fusai, J. Mosnier, W. Daries, E. Barret and D. Parzy, "*In vitro* activities of antibiotics against Plasmodium falciparum are inhibited by iron," *Antimicrob.*

Agents Chemother. vol. 45, pp 1746–1750, 2001. https://doi.org/10.1128/AAC.45.6.1746-1750.2001.

[28] A. Agarwal, K. Srivastava, S. K. Puri and P. M. S. Chauhan, Antimalarial activity of 2,4,6-trisubstituted pyrimidines, *Bioorg Med Chem Lett*, vol. 15, pp. 1881–1883, 2005. https://doi.org/10.1016/j.bmcl.2005.02.015.

[29] E. Bilsland, L. Van Vliet, K. Williams, J. Feltham, M. P. Carrasco, W. L. Fotoran, E. F.G. Cubillos, G. Wunderlich, M. Grøtli, V. Jackson, R. D. King and S. G. Oliver, "Plasmodium dihydrofolate reductase is a second enzyme target for the antimalarial action of triclosan," *Sci Rep*, vol. 8, pp. 1038, 2018. https://doi.org/10.1038/s41598-018-19549-x.

[30] S. Manohar, U. C. Rajesh, S. I. Khan, B. L. Tekwani and D. S. Rawat, " Novel 4-Aminoquinoline-pyrimidine based hybrids with improved *in vitro* and *in vivo* antimalarial Activity," *ACS Med Chem Lett*, no.3 vol 7, pp. 555–559, 2012. doi: 10.1021/ml3000808.

[31] F. Kayamba, C. Dunnill, D. J. Hamnett, A. Rodríguez, N. T. Georgopoulos and W. J. Moran, "Piperolein B, isopiperolein B and piperamide C9:1(8E): Total synthesis and cytotoxicities," *RSC Adv*, vol. 3, pp. 16681–16685, 2013. https://doi.org/10.1039/c3ra42060d.

[32] S. Manohar, M. Tripathi and D. Rawat, 4-Aminoquinoline based molecular hybrids as antimalarials: An Overview," *Curr Top Med Chem*, no. 14, vol. 14, pp. 1706-1733, 2014. https://doi.org/10.2174/1568026614666140808125728.

[33] D. Giles, K. Roopa, F. R. Sheeba, P. M. Gurubasavarajaswamy, G. Divakar, T. Vidhya, "Synthesis pharmacological evaluation and docking studies of pyrimidine derivatives," *Eur J Med Chem*, vol. 58, pp. 478–484, 2012. https://doi.org/10.1016/j.ejmech.2012.09.050.

[34] J. Dickson, L. Flores, M. Stewart, R. Leblanc, H. N. Pati and M. Lee, "Synthesis and cytotoxic properties of chalcones : an interactive and investigative undergraduate laboratory project at the interface of chemistry and biology," *J Chem Educ*, no. 6, vol. 83, pp. 934–936, 2006. https://doi.org/10.1021/ed083p934.

[35] B. Blake, "An Aldol Condensation to synthesize Chalcones," pp. 3–8.

http://sites.psu.edu/sandboxblakeb5606/wp-content/uploads/sites/25494/2015/04/An-Aldol-Condensation-to-synthesize-Chalcones.pdf

[36] P. S. Gribanov, M. A. Topchiy, Y. D. Golenko, Y. I. Lichtenstein, A. V. Eshtukov, V. E. Terekhov, A. F. Asachenko and M. S. Nechaev, "An unprecedentedly simple method of synthesis of aryl azides and 3-hydroxytriazenes," pp. 5984–5988, 2016. https://doi.org/10.1039/c6gc02379g.

[37] A. Trager and J. Jensen, "Human malaria parasites in continuous culture," *J Natl Med Assoc*, vol. 68, pp. 530–533, 1976. doi. 10.1126/science.781840.

[38] C. Lambros and J. P. Vanderberg, "Synchronization of plasmodium falciparum erythrocytic stages in culture," *J Parasitol*, pp. 418–42065, 1979. https://pubmed.ncbi.nlm.nih.gov/383936/.

[39] M. T. Makler, J. M. Ries, J. A. Williams, J. E. Bancroft, R. C. Piper, B. L. Gibbins, D. J. Hinrichs, "Parasite lactate dehydrogenase as an assay for Plasmodium falciparum drug sensitivity," *Am J Trop Med Hyg*, vol. 48, pp. 739–741, 1993. https://doi.org/10.4269/ajtmh.1993.48.739.

[40] A. D. Forkuo, C. Ansah, K. B. Mensah, K. Annan, B. Gyan, A. Theron, D. Mancama, C. W. Wright, In vitro anti-malarial interaction and gametocytocidal activity of cryptolepine, *Malar J*, vol.16, pp. 1–9, 2017. https://doi.org/10.1186/s12936-017-2142-z.

[41] J. Reader, M. Botha, A. Theron, S. B. Lauterbach, C. Rossouw, D. Engelbrecht, M. Wepener, A. Smit, D. Leroy, D. Mancama, T. L. Coetzera and L. M. Birkholtz, "Nowhere to hide: Interrogating different metabolic parameters of Plasmodium falciparum gametocytes in a transmission blocking drug discovery pipeline towards malaria elimination," *Malar J*, vol. 14, pp. 1–17, 2015. https://doi.org/10.1186/s12936-015-0718-z.

[42] T. Mosmann, Rapid colourimetric assay for cellular growth and survival: Application to proliferation and cytotoxicity assays, *J Immunol Methods*, vol 65, pp 55–63, 1983. https://doi.org/10.1016/0022-1759(83)90303-4.

[43] J. C. Domingue, M. Ao, J. Sarathy, A. George, W. A. Alrefai, D. J. Nelson and M. C. Rao,

"HEK-293 cells expressing the cystic fibrosis transmembrane conductance regulator (CFTR): A model for studying the regulation of Cl-transport," *Physiol Rep*, vol 2, pp 1–16, 2014. https://doi.org/10.14814/phy2.12158.

[44] K. M. Krawczyk, D. Matak, L. Szymanski, C. Szczylik, C. Porta and A. M. Czarnecka, "Culture in embryonic kidney serum and xeno-free media as renal cell carcinoma and renal cell carcinoma cancer stem cells research model," *Cytotechnology*, vol 70, pp 761–782, 2018. https://doi.org/10.1007/s10616-017-0181-5.

[45] T. Zininga, O. J. Pooe, P. B. Makhado, L. Ramatsui, "Polymyxin B inhibits the chaperone activity of Plasmodium falciparum Hsp70," *Cell Stress Chaperones*, vol. 22. pp. 707–715 2017. https://doi.org/10.1007/s12192-017-0797-6.

[46] O. J. Pooe, G. Köllisch, H. Heine and A. Shonhai, "Plasmodium falciparum Heat Shock Protein 70 Lacks Immune Modulatory Activity," *Protein Pept Lett*, vol. 24, pp 503–510, 2017. https://doi.org/10.2174/0929866524666170214141909.

[47] T. Zininga, I. Achilonu, H. Hoppe, E. Prinsloo, H. W. Dirr, A. Shonhai, Plasmodium falciparum Hsp70-z, an Hsp110 homologue, exhibits independent chaperone activity and interacts with Hsp70-1 in a nucleotide-dependent fashion, *Cell Stress Chaperones*, vol. 21, pp. 499–513, 2016. https://doi.org/10.1007/s12192-016-0678-4.

[48] T. Zininga, L. Ramatsui, P. B. Makhado, S. Makumire, I. Achilinou, H. Hoppe, H. Dirr and A. Shonhai, "(−)-Epigallocatechin-3-gallate inhibits the chaperone activity of Plasmodium falciparum Hsp70 chaperones and abrogates their association with functional partners," *Molecules*, vol. 22, pp.1–15, 2017. https://doi.org/10.3390/molecules22122139.

CHAPTER 6

6.1 Summary and conclusion

Malaria remains one of the world's leading causes of death and morbidity. *P. falciparum* and *P. vivax* are the deadliest and most widespread malarial parasites, which cause the development of severe malaria, thus attributing to the highest mortality rate worldwide. The spine for the treatment of severe malaria is the immediate commencement of antimalarial treatment. But after a few doses of the treatment, the emergence of resistance in patients becomes imminent. To avoid the limitations, there is a need to focus on adherence to drug prescription, prompt and proper use of medicines, fast-tracked drug discovery and development program, and to identify active molecules that would be useful lead compounds.

This research work aimed to identify novel and potent antimalarial candidates motivated by significant antimalarial compounds such as pyrimethamine and chalcones. Structure modification of pyrimethamine and chalcones gave rise to 4,6-diphenylpyrimidine as a core motif. It was amalgamated with other assorted antimalarial scaffolds, namely quinoline, cinnamoyl, and 1,2,3-triazole, to afford a library of 53 novel hybrids analogue through molecular hybridization strategy. These compounds were characterized using thin-layer chromatography (TLC) and structure elucidation by Fourier-transform infrared spectroscopy (FT-IR), nuclear magnetic resonance spectroscopy (^{1}H, ^{13}C, and 2D NMR) and high-resonance mass spectroscopy (HRMS). The biological evaluation revealed that the synthesized compounds were active with encouraging antimalarial activity, suggesting lead candidates, which would be a standpoint in drug discovery.

Chapter 2 deals with a literature review on lactate dehydrogenase (LDH) and Malate dehydrogenase (MDH) as possible antiparasitic drug discovery targets. LDH is an oxidoreductase enzyme found in a mitochondrion that facilitates the conversion of pyruvate to lactate, simultaneous utilizing NADH as a cofactor. LDH is crucial for the energy generation of the parasite, as it relies on this pathway for energy in the erythrocytes stage of the life cycle, and impeding its activity leads to the death of the parasite. The therapeutic consequences of malate hydrogenase (MDH), an analogue of LDH as potential parasitic targets, is also highlighted. Therefore, LDH and MDH are validated as novel parasitic targets. The review explored the physiological functions, and drug accessibility of LDH and MDH in Plasmodium, Trichomonas, Toxoplasma Gondii, Schistosoma and *Cryptosporidium parvum* and the substantial outcome of

this chapter has emerged as a mini-review manuscript under review in ***Bioorganic and medicinal chemistry letter***.

In chapter 3, following a literature audit, a modified 4,6-diphenylpyrimidine core inspired by pyrimethamine and chalcone was fused with a quinoline scaffold through alkane diamine linker by molecular hybridization approach. The analogues were synthesized in good yield (61-85 percent) following a simple and more versatile synthetic path. The synthesis of the final compounds *N*-(7-chloroquine in-4-yl)-*N*'-(4,6-diphenylpyrimidin-2-yl)methanediamine (**6a-k** and **7a-c**) by amidification reaction of assorted 2-chloro-4,6-diphenylpyrimidine **4** (**a-e**) and *N*-(7-chloro-4a,8a-dihydroquinolin-4-yl) alkane diamine **5**(**a-b**) using K_2CO_3 in DMF as illustrated in **Scheme 2** of the third chapter. The final compounds were structurally elucidated by IR, ^{1}H and ^{13}C NMR and HRMS. These compounds were screened preliminarily for antimalarial against NF54 CQ-susceptible strain performed by the Pharmacology Division, Department of Pharmacy and Pharmacology, Faculty of Health Sciences, University of Witwatersrand, Johannesburg, South Africa. Compound **7c** showed most activity with IC_{50} = 0.33 ± 0.06 µM, with a favourable safety profile of 9.79 to human kidney epithelial (HEK293) cells. The six compounds (**6d**, **6e**, **6f**, **6i**, **7b** and **7c**) displayed decent activity with IC_{50} ranging from 0.50 to 4.30 µM, whereas the remaining compounds (**6a**, **6b**, **6c**, **6h**, **6j** and **6k**) were considered to be inactive with IC_{50} > 5 µM. Also, compound **7a** exhibited the highest binding affinity with K_D in a lower nanomolar range (4.4-11.4 nM) and the highest and lowest binding scores of -9.8 kcal/mol for both PfHsp70s, thus speculated that PfHsp70-1 is one of the targets of these inhibitors. This work was published in the journal ***European Journal of Medicinal*** **Chemistry, volume 217, page 113330** in **2021** (https://www.sciencedirect.com/science/article/abs/pii/S0223523421001793)

In chapter 4, on continuation with the effort to develop new antimalarial candidates. A 4,6-diphenylpyrimidine motif was fused to cinnamoyl scaffold by a piperazine linker through various 4,6-diphenyl-2-(piperazine-1-yl)pyrimidine **5**(**a-e**) intermediates to afford a library of final compounds (*E*)-1-(4-(4,6-diphenylpyrimidin-2-yl)piperazine-1-yl)-3-phenylprop-2-en-1-one hybrid analogues **8**(**a-t**) in excellent yield of 70-90%. The synthesis was achieved through efficient and adaptable synthetic pathways, as described in **Scheme 1** and **2** in the fourth chapter. Structure elucidation of these compounds was performed using IR, ^{1}H and ^{13}C NMR, 2D NMR, and HRMS. *In vitro* antimalarial was performed using NF45 CQ-susceptible strain at Pharmacology Division,

Department of Pharmacy and Pharmacology, Faculty of Health Sciences, University of Witwatersrand, Johannesburg, South Africa. Of the active compounds, two had IC_{50} values of 0.18 ± 0.02 µM and 0.21 ± 0.001 µM with an associated good safety index of 18.59 and 16.75 to human kidney epithelial (HEK293) cells corresponding to **8o** and **8l** respectively. Compounds **8o** and **8l** exhibited an excellent binding affinity for both PfHsp70s with K_D in a lower nanomolar range (1.57 -15.7 nM and 9.69-10.8 nM). Also, this class of hybrids envisioned PfHsp 70-1 as one of their targets. Nine compounds in this family demonstrated decent activity with IC_{50} ranging from 0.5 to 5µM, and the remaining compounds were inactive with IC_{50} > 5 µM. This work has been written in manuscript format, and it is ready for communication.

Lastly, chapter 5 as per a continuation of the ongoing research, 4,6-diphenyl-2-(4-(prop-2-yn-1-yl)piperazine-1-yl)pyrimidine **6**(**a-e**) motif were further hybridized with 1,2,3-triazole scaffold to afford a library of 2-(4-((1H-1,2,3-triazole-4-yl)methyl)piperazine-1-yl)-4,6-diphenylpyrimidine **8(a-t)** analogues which were also characterized as aforementioned in chapter 3 and 4. *In vitro* antimalarial screening against NF54 CQ susceptible were performed by Pharmacology Division, Department of Pharmacy and Pharmacology, Faculty of Health Sciences, University of Witwatersrand, Johannesburg, South Africa. Of the evaluated compounds, seven were active (IC_{50} value < 0.5 µM) with **8p** having IC_{50} values as low as 0.04 ± 2.23 µM specifically **8c, 8e** and **8t** also presenting prominent activity with IC_{50} of 0.18 ± 0.03 µM, 0.22 ± 0.02 µM and 0.29 ± 0.01 µM had a safety profile of 13.40, 9.11 and 61.15 respectively to human kidney epithelial (HEK293) cells. The remaining thirteen compounds displayed moderate activity with IC_{50} values ranging from 0.59 to 2.41 µM. The molecular binding affinities of two vital cytosolic *P. falciparum* heat shock protein 70 homologues, PfHsp70-1 and PfHsp70-z studies, indicated compound **8e** to have the highest binding affinity for both PfHsp70s with K_D in a lower nanomolar range (10-11.3 nM). The finding of this research work shows the significance of molecular hybridization of 4,6-diphenypyrimdine-1,2,3-triazole as a starting point for further lead optimization of antimalarial candidates.

Three new libraries of pyrimidine hybrids amalgamated with quinoline, 1,2,3-triazole and cinnamoyl, were presented, of which the 1,2,3-triazole based hybrids were the most potent. The pyrimidine-1,2,3-triazole family was the more promising with nearly all compounds showed activity with IC_{50} values less than 5 µM and the active one as low as 0.18 µM. The Hsp70 (Hsp70-

z and Hsp70-1) enzyme activity is also good, with activity as low as 11.3 nM. The cinnamoyl series followed the 1,2,3-triazole series, showing promising activity with eight compounds that had moderate activity. Three hybrids were more potent with IC_{50} less than 0.5 µM and Hsp70 activity of 6.99 to 10 nM. Lastly, the quinoline had the least active library with only five compounds with moderate activity and only one more potent; however, it had the highest activity against the Hsp70 as low as 4.4 nM. Pyrimidine-1,2, 3 -triazole emerged as the most potent and promising library of all. All the hybrids showed excellent activity, particularly those of pyrimidine-1,2,3-triazole, which emerged the most potent, suggesting that the pyrimidine and 1,2,3-triazole would serve as the most potent scaffold in the future formulation of new antimalarial compounds. Compound with pyrimidine- quinoline will be a superb lead in targeting the activity Hsp70-z and Hsp70-1.

This work has been written in manuscript format, and it is ready for communication.

6.2 Future work

Following the potential antimalarial activities demonstrated by the pyrimidine-based analogues, computer stimulations, namely 3D QSAR (three-dimensional quantitative structure-activity relationship) and 3D QSPR (three dimensional quantitively structure properties relationship) can be employed for *in silico* optimization of the lead compounds to attain drug-like compounds with improved activity, bioavailability and efficacy profiles.

Aligned to those described above, a promising antimalarial pharmacophore can be produced from the available database of biologically active molecules using 3D QSAR. Further, virtual screening of the database such as ZINC, Mobridge, Cambridge and NCL could be done to identify drug-like ligands with more potent antimalarial properties that can be considered a new set of hit molecules for chemical synthesis.

Also, together with the bioassay of Hsp70, the enzyme activity of the active compounds can be performed Lactate dehydrogenase and malate dehydrogenase, which forms another class of promising antimalarial targets in a quest to establish a mode of action of the compounds.

In addition, a comparative solution to identify and optimize antimalarial lead can also be achieved through molecular docking studies (structure-based drug design) of the second (chapter 4) and third (chapter) series. These will permit a comprehensive exploration into the interaction of drug-

protein targets available in protein data bank (PDB). Nonetheless, the pyrimidine pharmacophore has shown important biological properties, including antimalarial properties, which could further be explored for prospective biological activity with the view to offering an antimalarial lead.

The current work will be significant in advancing, exploring, and developing a new class of pyrimidine-based compounds as potential antimalarial candidates.

APPENDIX - I

SUPPLEMENTARY INFORMATION

CHAPTER 3

Design and synthesis of quinoline-pyrimidine inspired hybrids as potential plasmodial inhibitors

Representative NMR Spectrum for chalcone derivatives

(E)-1-(4-chlorophenyl)-3-(p-tolyl)prop-2-en-1-one **(1b)**

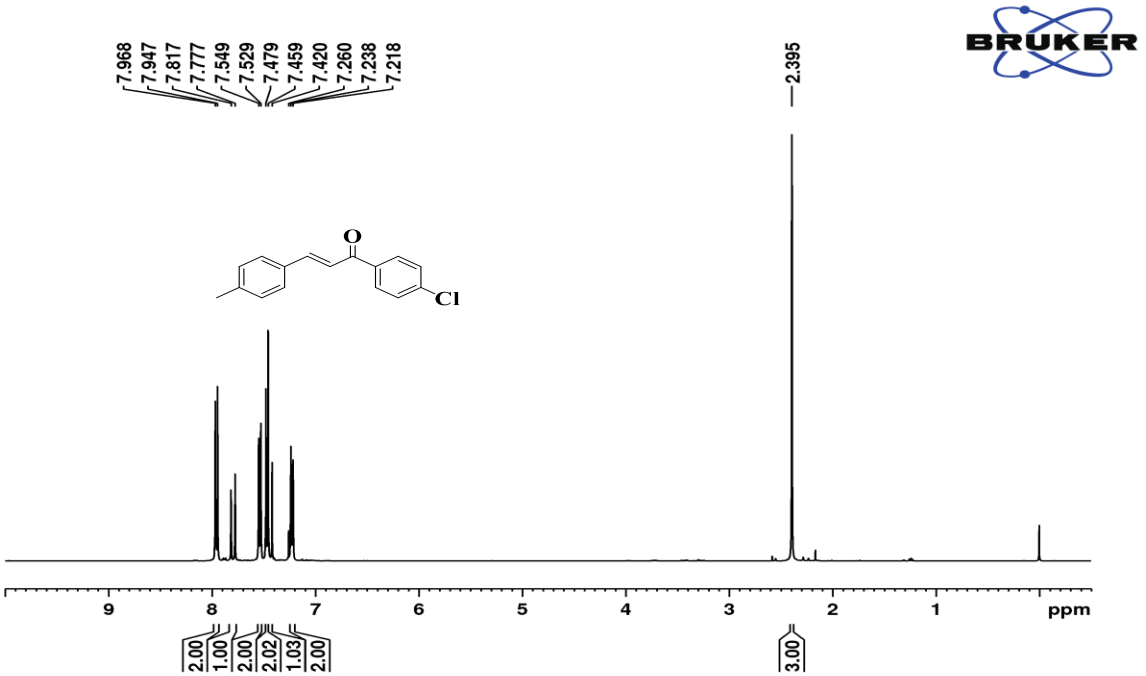

^{1}H NMR (400 MHz, $CDCl_3$)

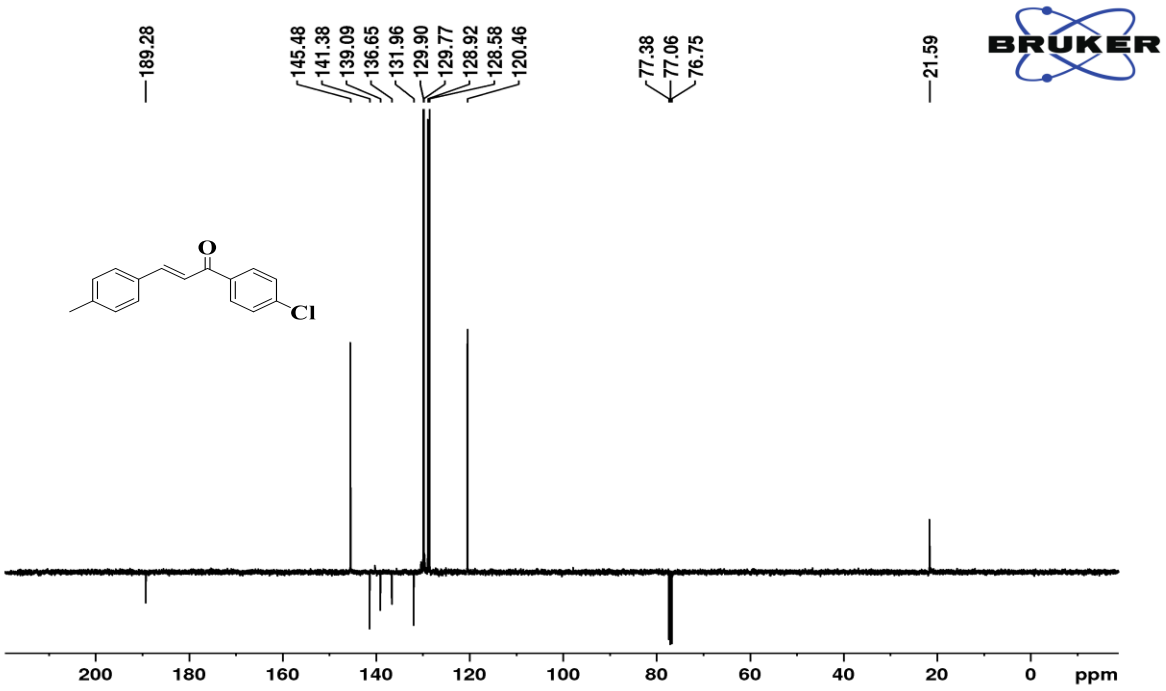

^{13}C NMR (100 MHz, $CDCl_3$)

E)-3-(3,4-dimethoxyphenyl)-1-(4-methoxyphenyl)prop-2-en-1-one (**1e**):

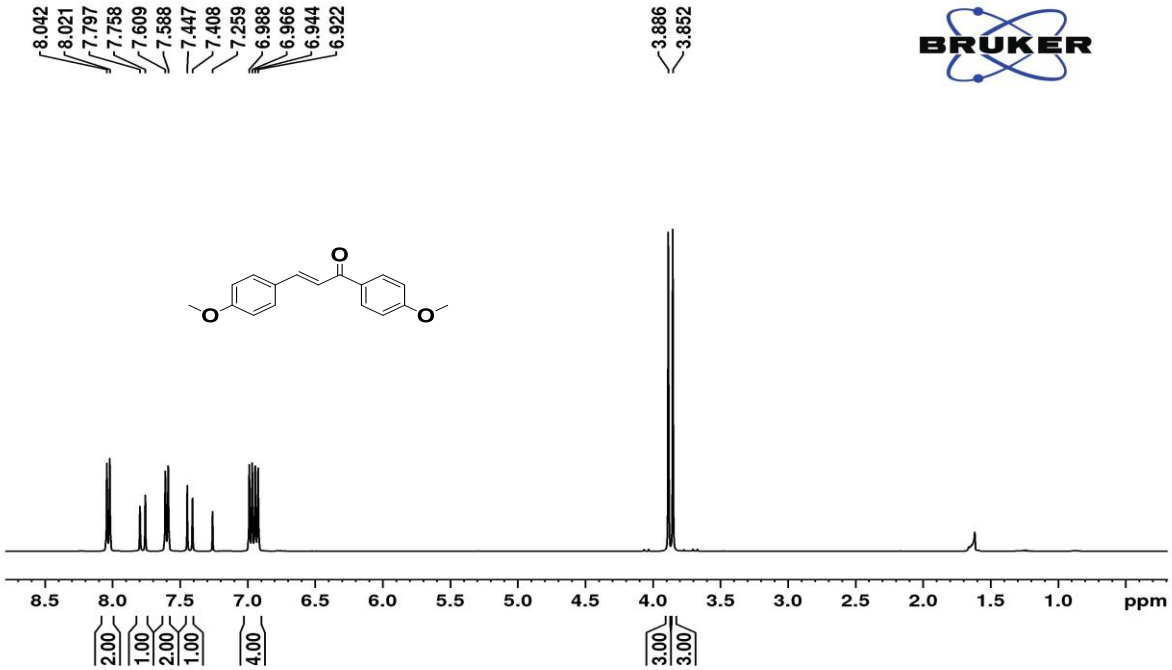

^{1}H NMR (400 MHz, $CDCl_3$, δ, ppm):

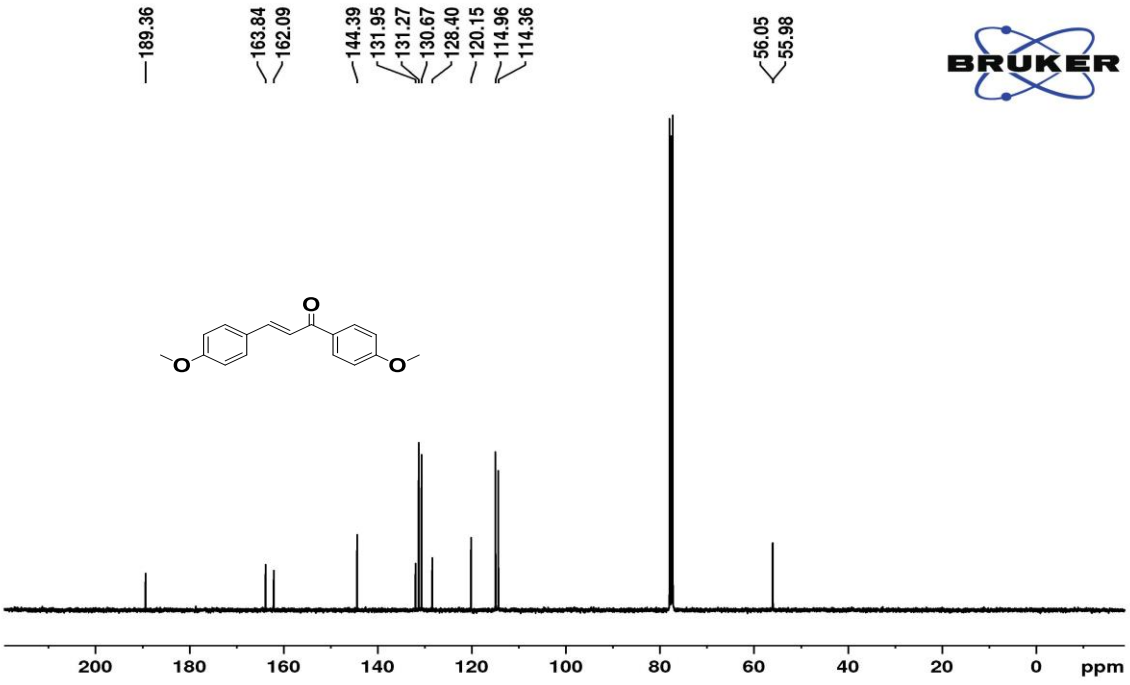

^{13}C NMR (100 MHz, $CDCl_3$)

Representative NMR Spectrums for 2 amino pyrimidine Derivatives

4-(4-methoxyphenyl)-6-(p-tolyl)pyrimidin-2-amine (**2c**):

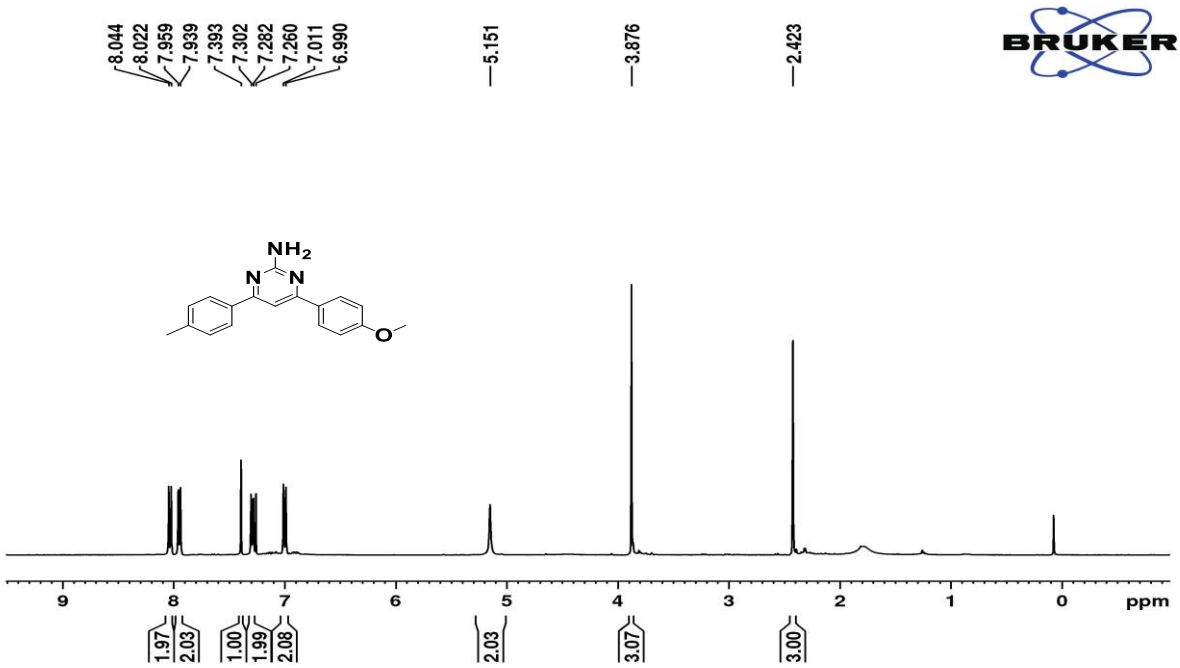

^{1}H NMR (400 MHz, $CDCl_3$)

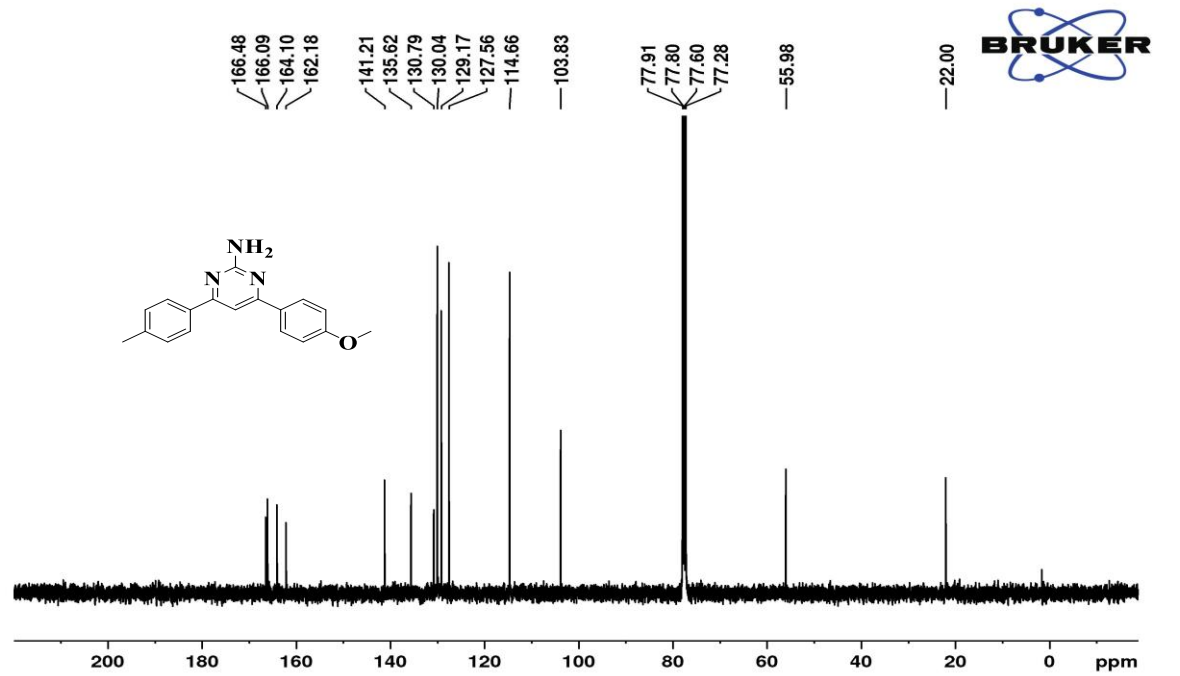

^{13}C NMR (100 MHz, $CDCl_3$)

4-(3,4-dimethoxyphenyl)-6-(4-methoxyphenyl) pyrimidin-2-amine (**2e**)

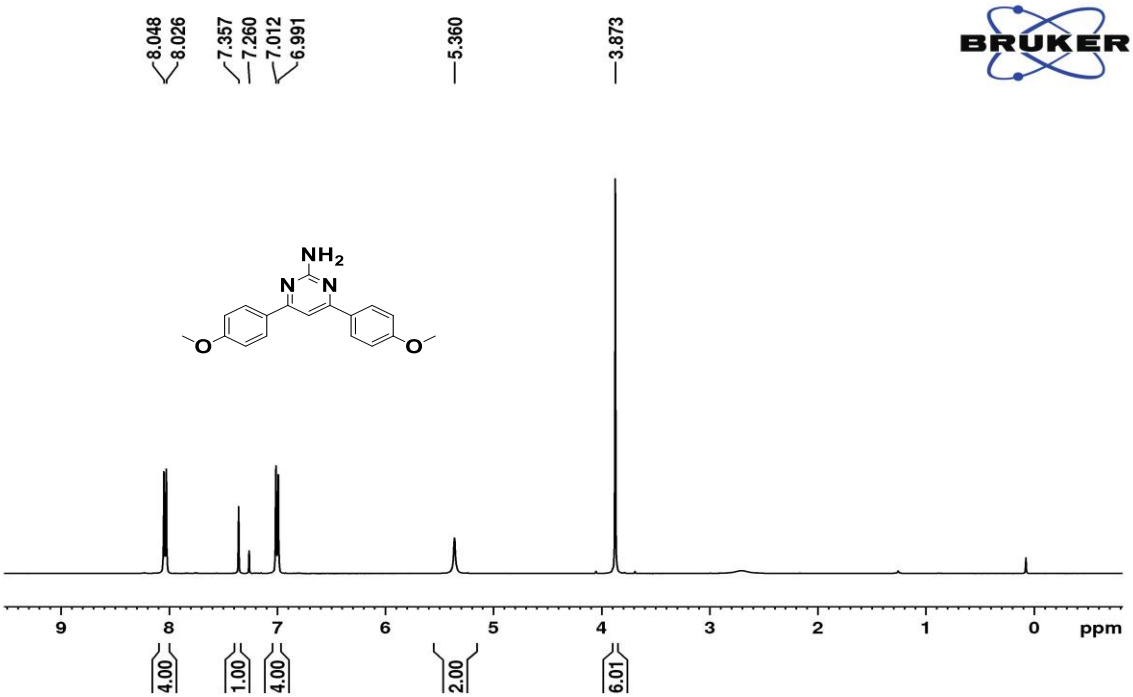

^{1}H NMR (400 MHz, $CDCl_3$)

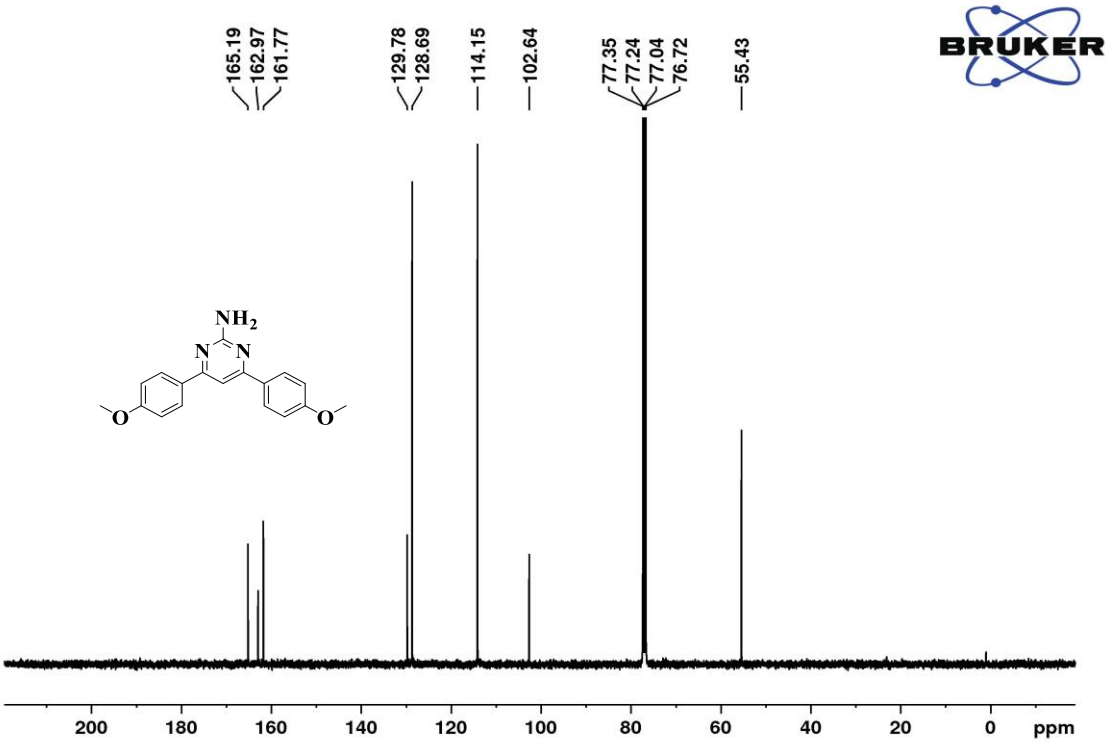

^{13}C NMR (100 MHz, $CDCl_3$)

Representative NMR spectrum for 2-chloro-4, 6-pyrimidine derivatives

2-chloro-4,6-bis(4-methoxyphenyl)pyrimidine (**4d**):

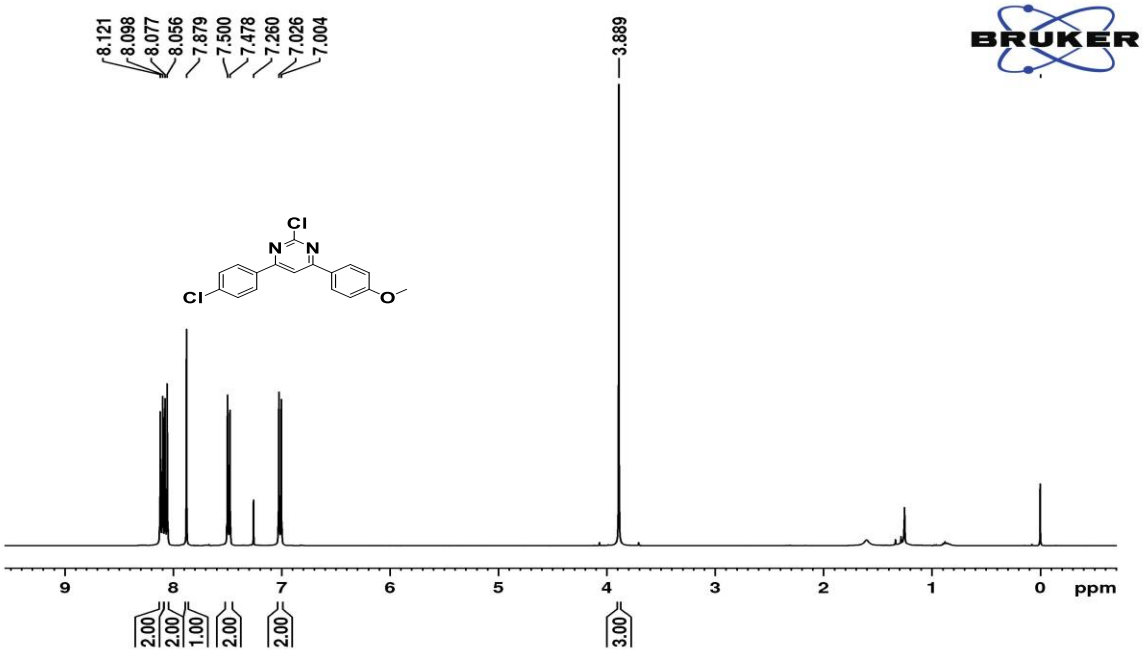

^{1}H NMR (400 MHz, $CDCl_3$)

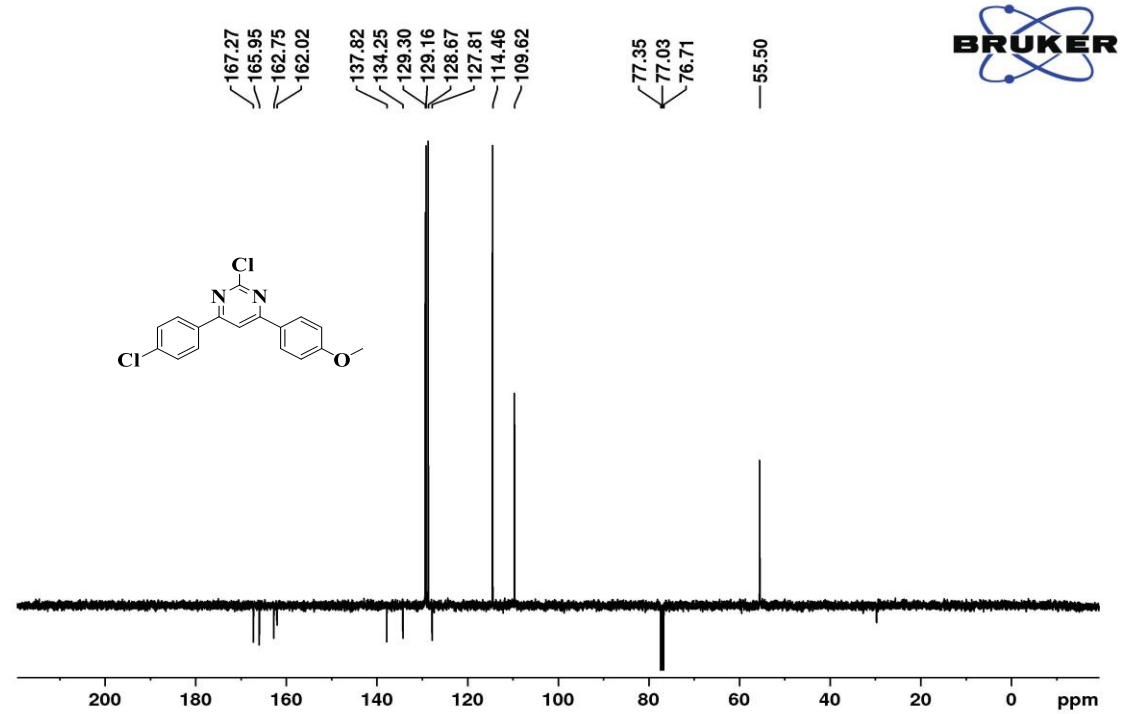

^{13}C NMR (100 MHz, $CDCl_3$)

2-chloro-4-(3,4-dimethoxyphenyl)-6-(4-methoxyphenyl)pyrimidine (**4f**):

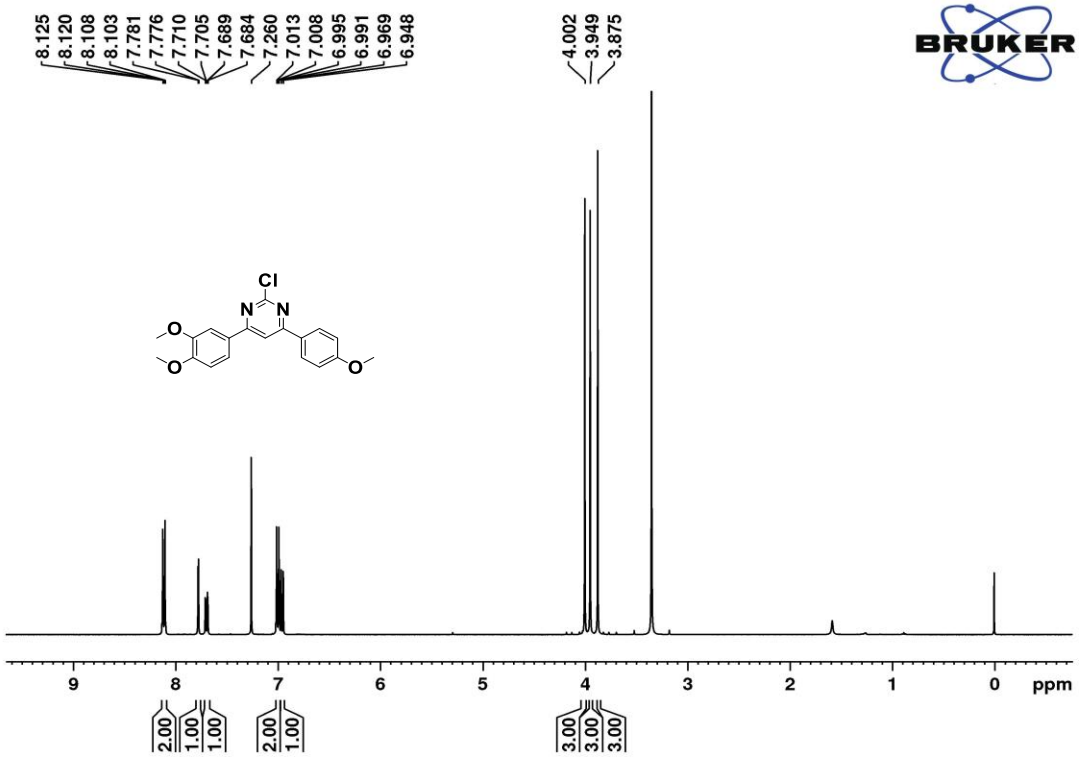

^{1}H NMR (400 MHz, $CDCl_3$)

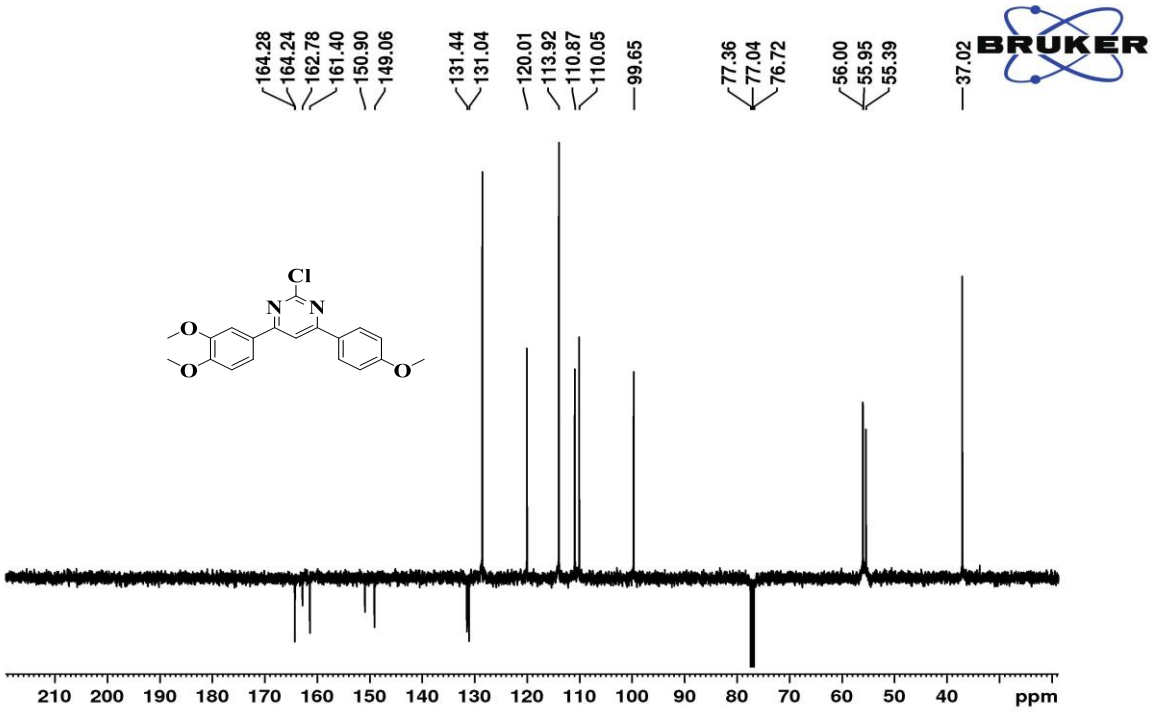

^{13}C NMR (100 MHz, $CDCl_3$)

Representative NMR spectrum for Quinoline diamine derivatives

N^1-(7-chloroquinolin-4-yl)propane-1,3-diamine (**5b**):

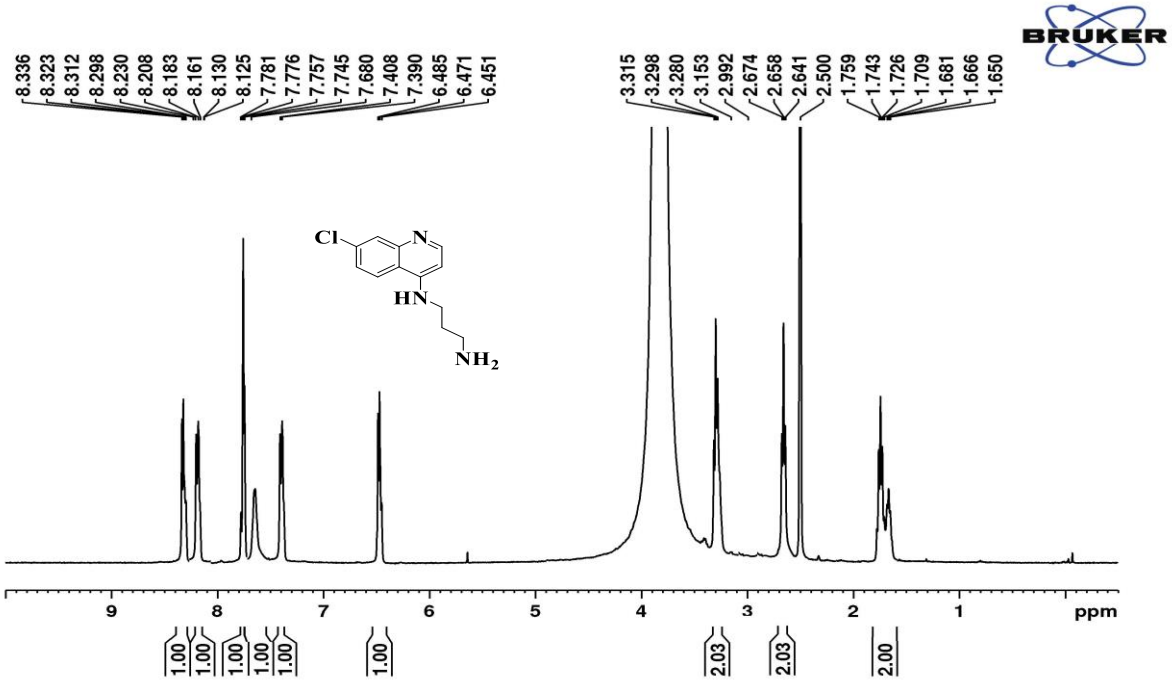

^{1}H NMR (400 MHz, DMSO-d_6)

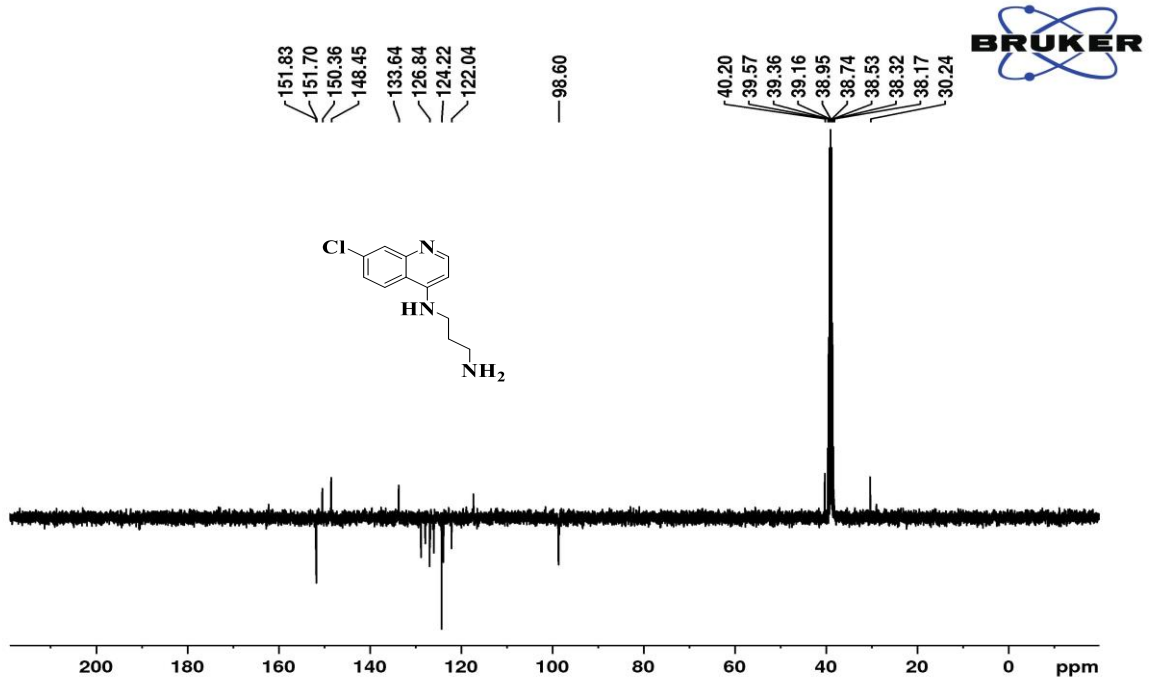

^{13}C NMR (100 MHz, DMSO-d_6)

7-chloro-4-(piperazin-1-yl)quinoline (**5d**):

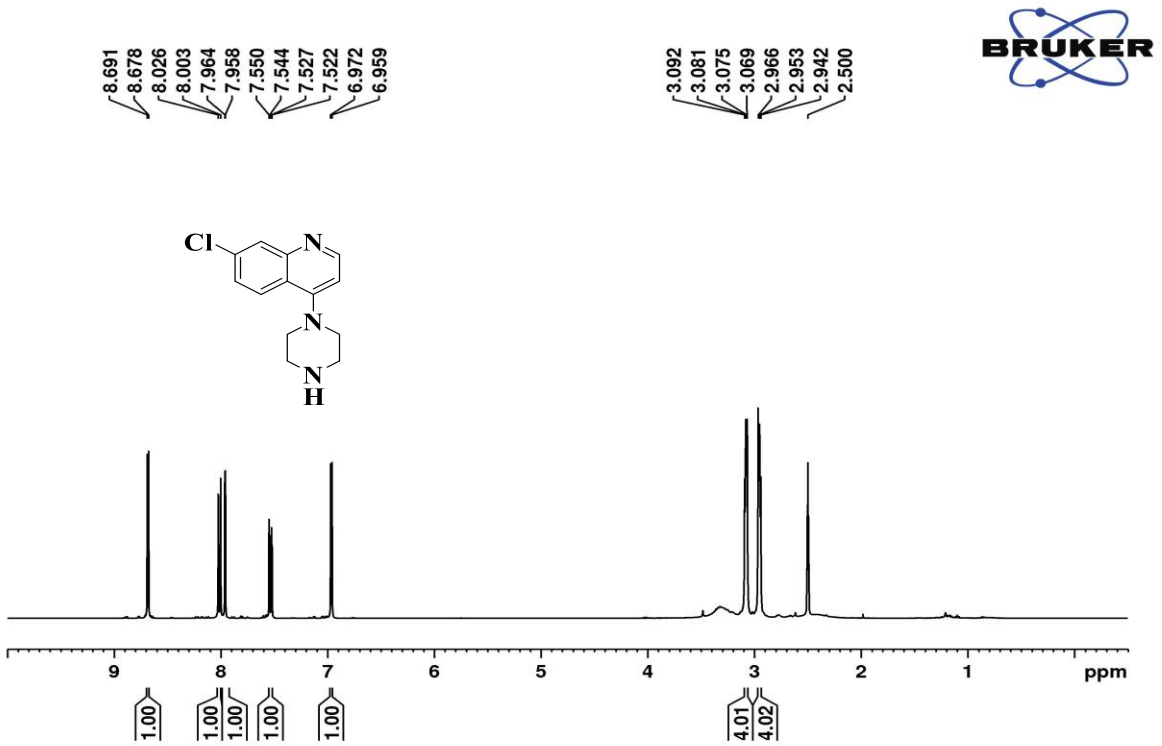

^{1}H NMR (400 MHz, DMSO-d_6)

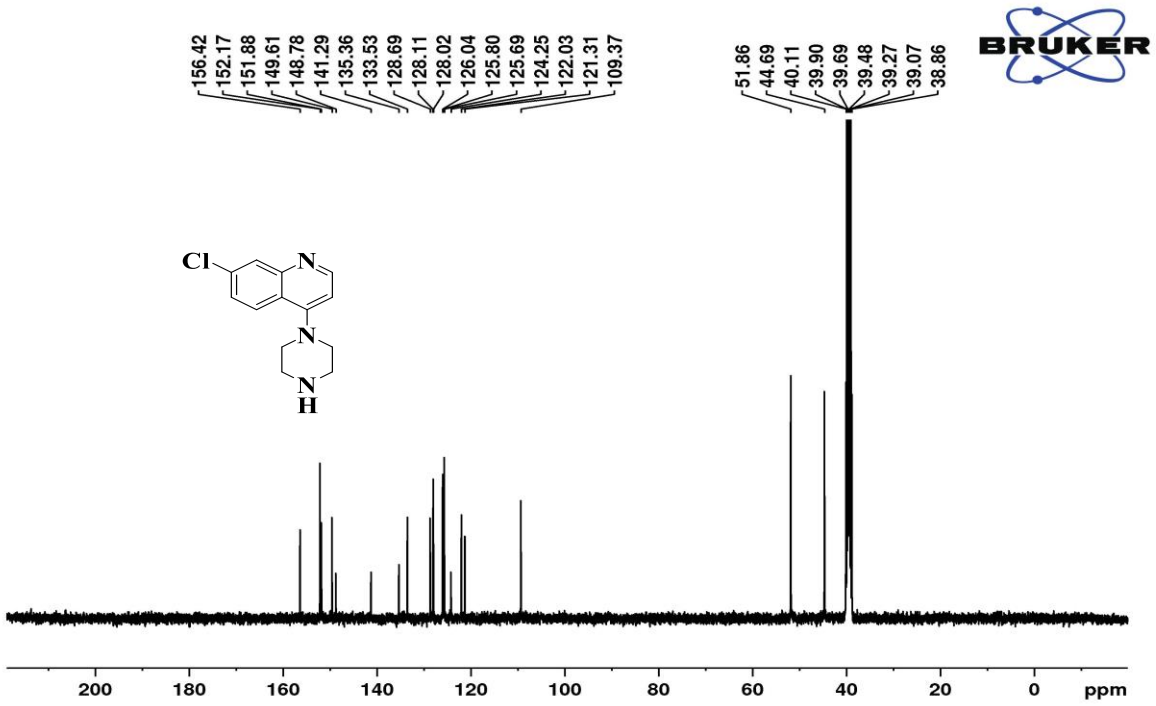

^{13}C NMR (100 MHz, DMSO-d_6)

Spectrums for final compounds (6(a-k) and 7(a-b))

7-chloro-4-(4-(4,6-diphenylpyrimidin-2-yl)piperazin-1-yl)quinoline (**6a**):

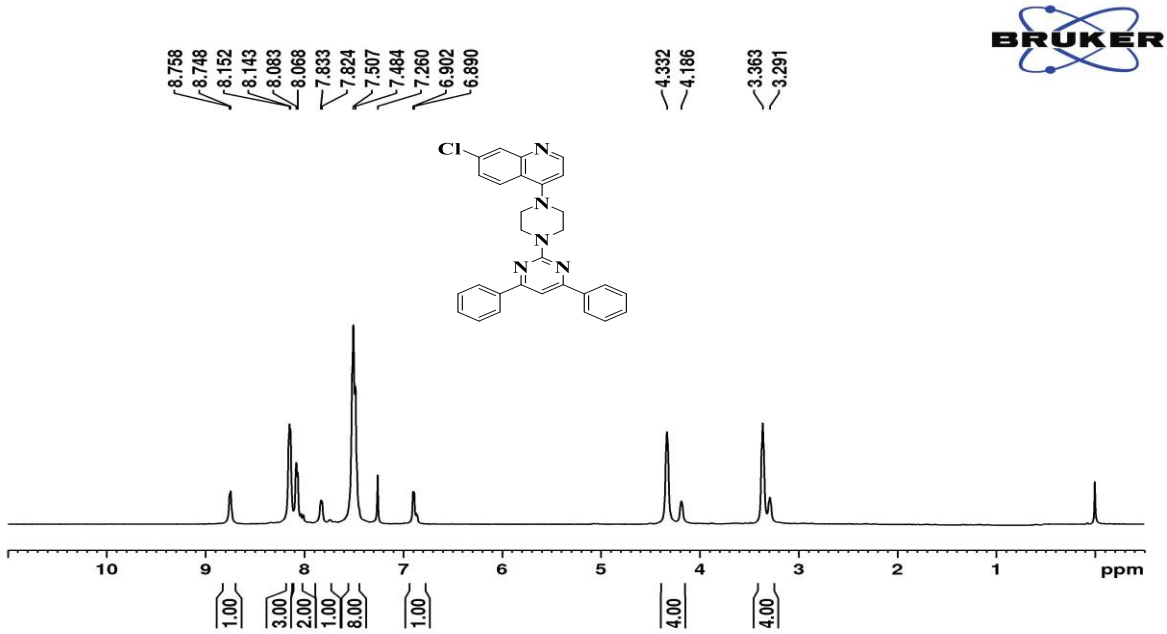

^{1}H NMR (400 MHz, $CDCl_3$)

N^1-(4-(4-chlorophenyl)-6-(p-tolyl)pyrimidin-2-yl)-N^4-(7-chloroquinolin-4-yl)butane-1,4-diamine (**6b**):

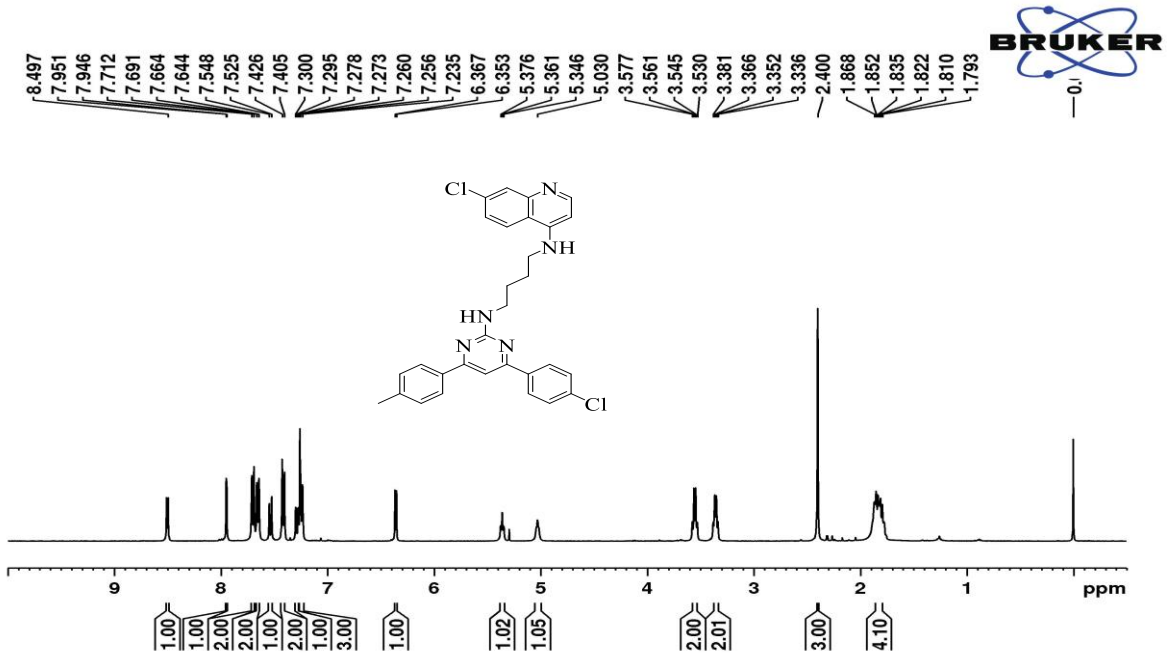

^{1}H NMR (400 MHz, $CDCl_3$)

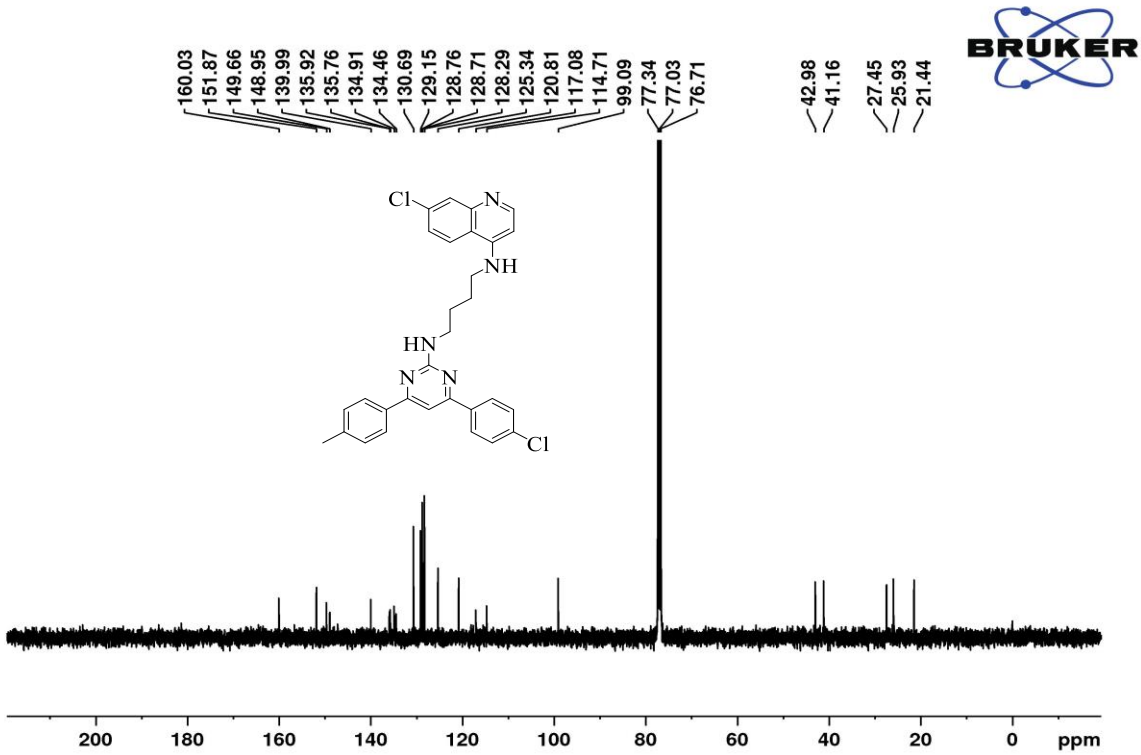

^{13}C NMR (100 MHz, $CDCl_3$)

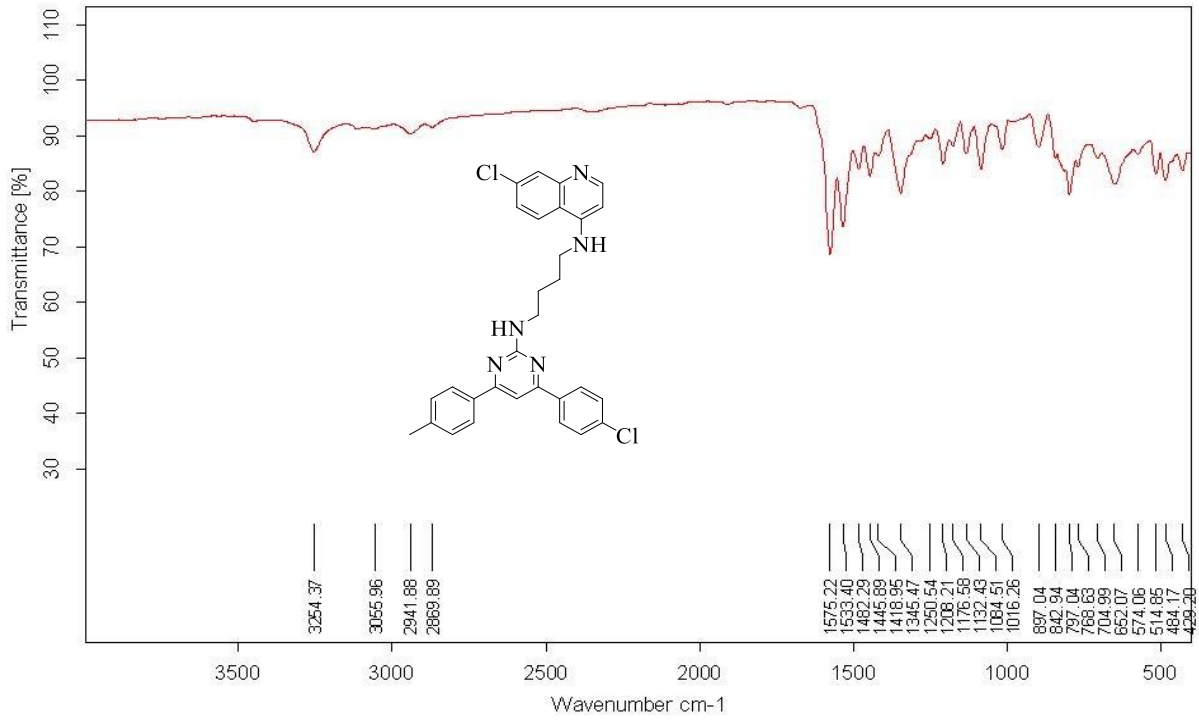

IR spectra

7-chloro-4-(4-(4-(4-chlorophenyl)-6-(p-tolyl)pyrimidin-2-yl)piperazin-1-yl)quinoline (**6c**)*:*

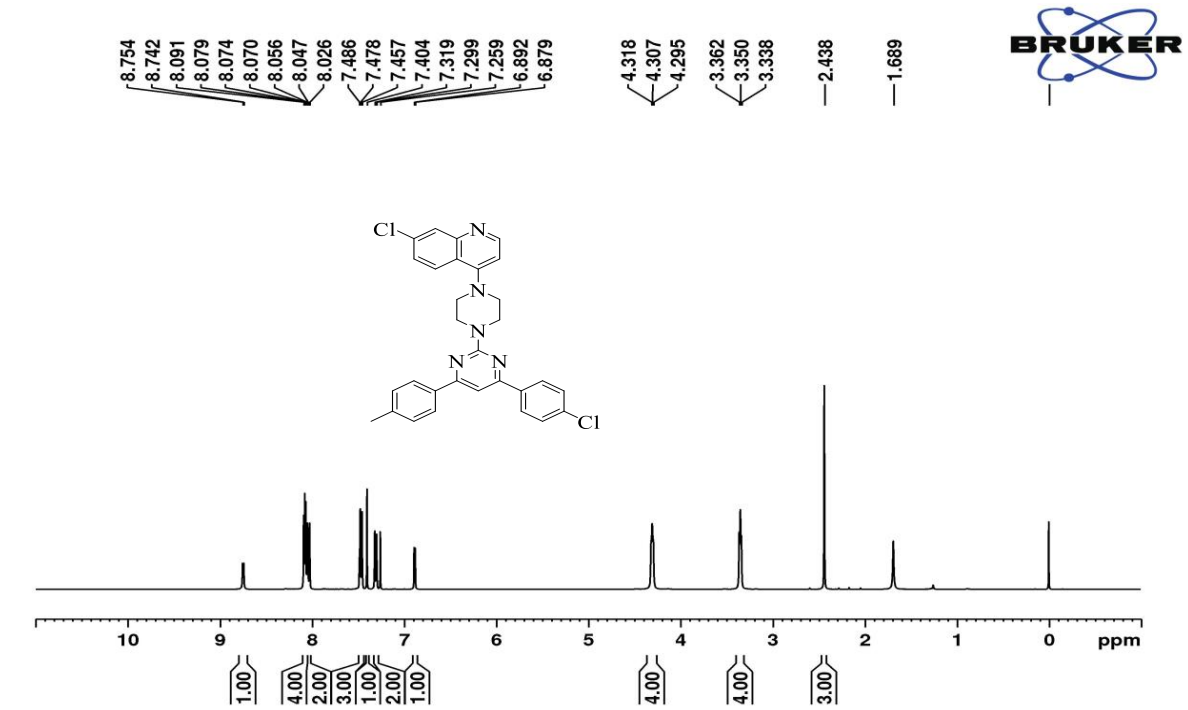

^{1}H NMR (400 MHz, $CDCl_3$)

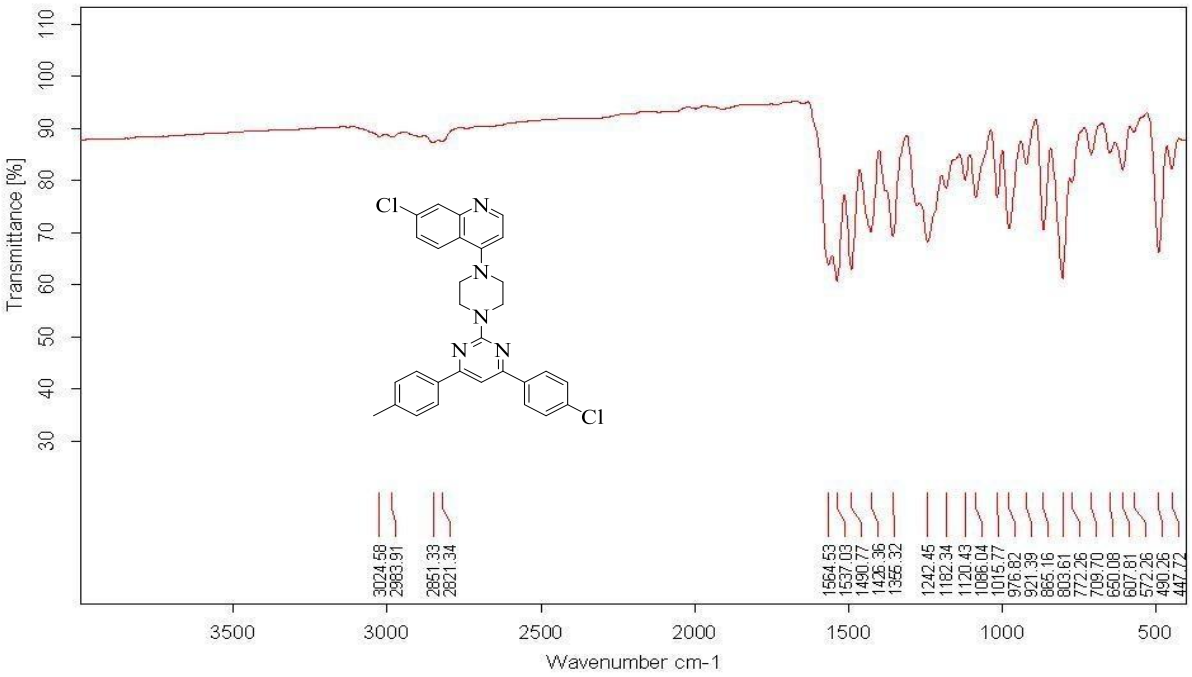

IR spectra

N^1-(7-chloroquinolin-4-yl)-N^2-(4-(4-methoxyphenyl)-6-(p-tolyl)pyrimidin-2-yl)ethane-1,2-diamine **(6d)**:

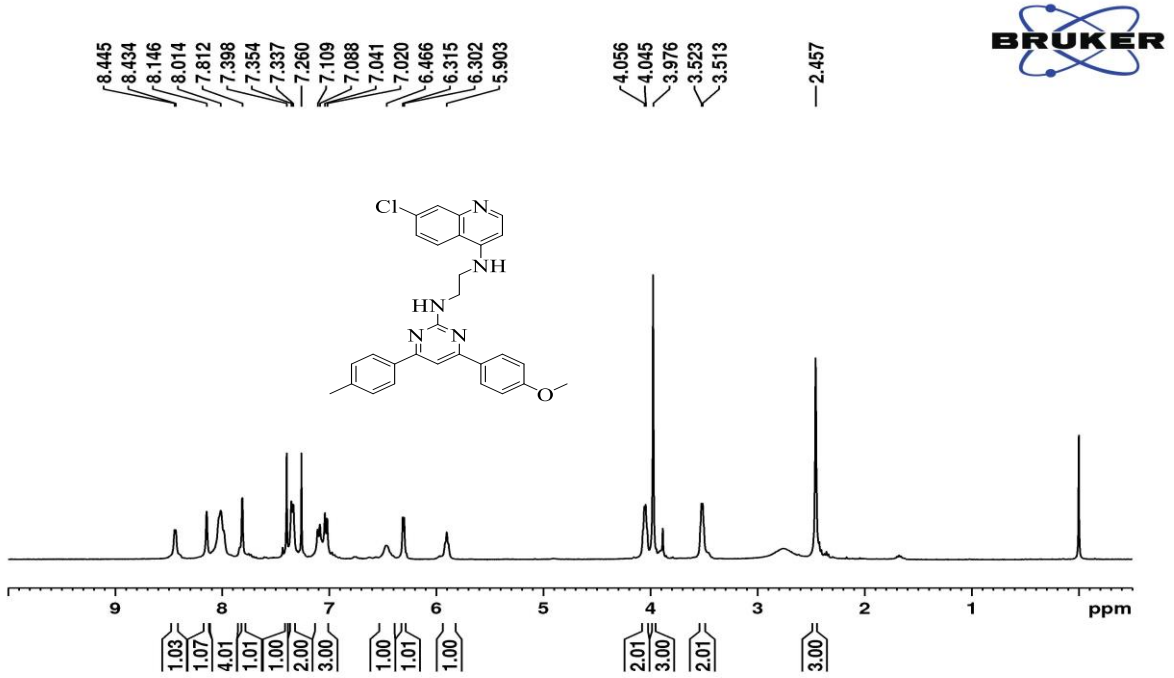

^{1}H NMR (400 MHz, $CDCl_3$)

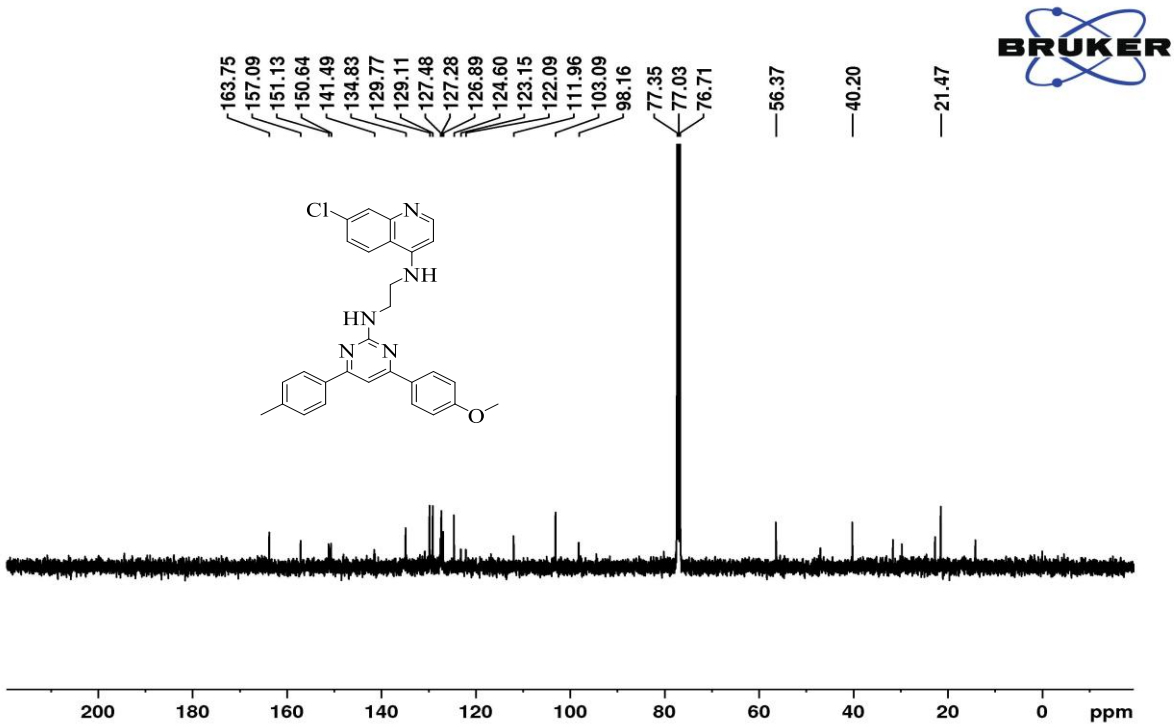

^{13}C NMR (100 MHz, $CDCl_3$)

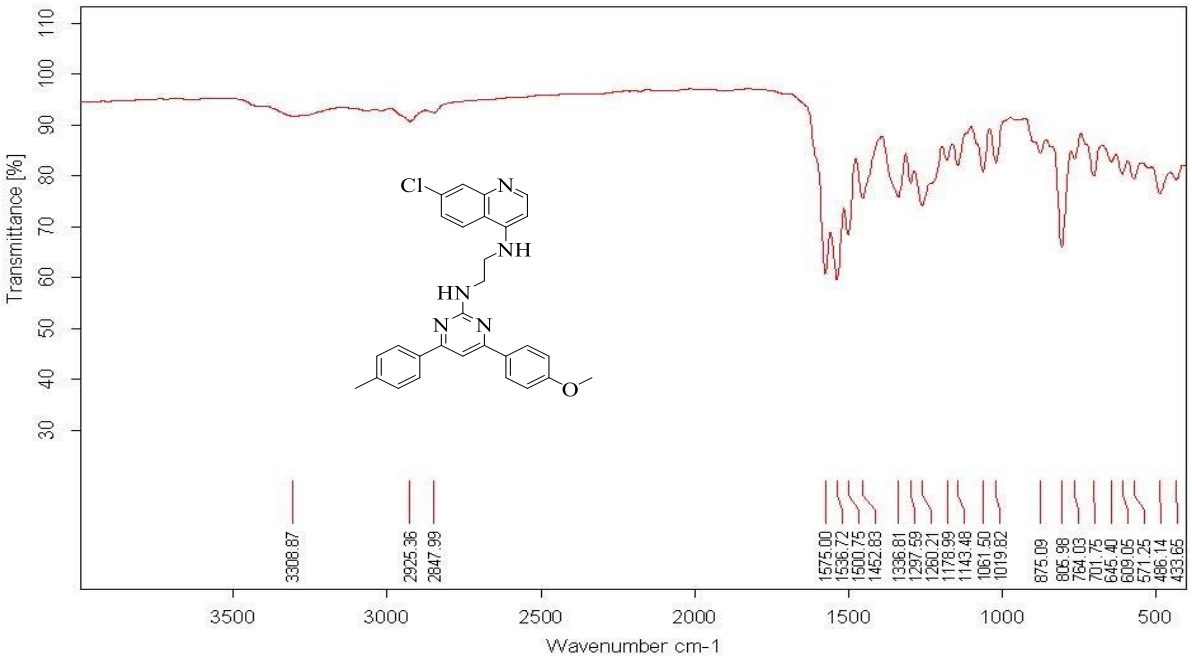

IR spectra

N[1]*-(7-chloroquinolin-4-yl)-N*[3]*-(4-(4-methoxyphenyl)-6-(p-tolyl)pyrimidin-2-yl)propane-1,3-diamine* (**6e**)

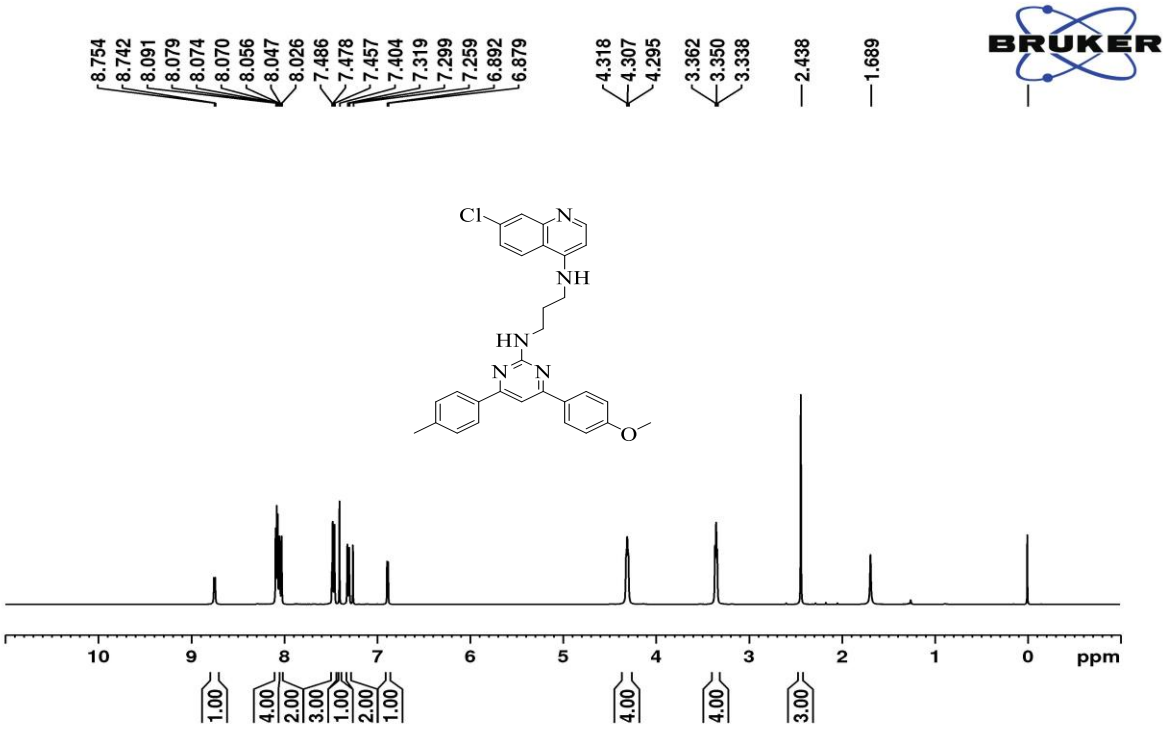

^{1}H NMR (400 MHz, $CDCl_3$)

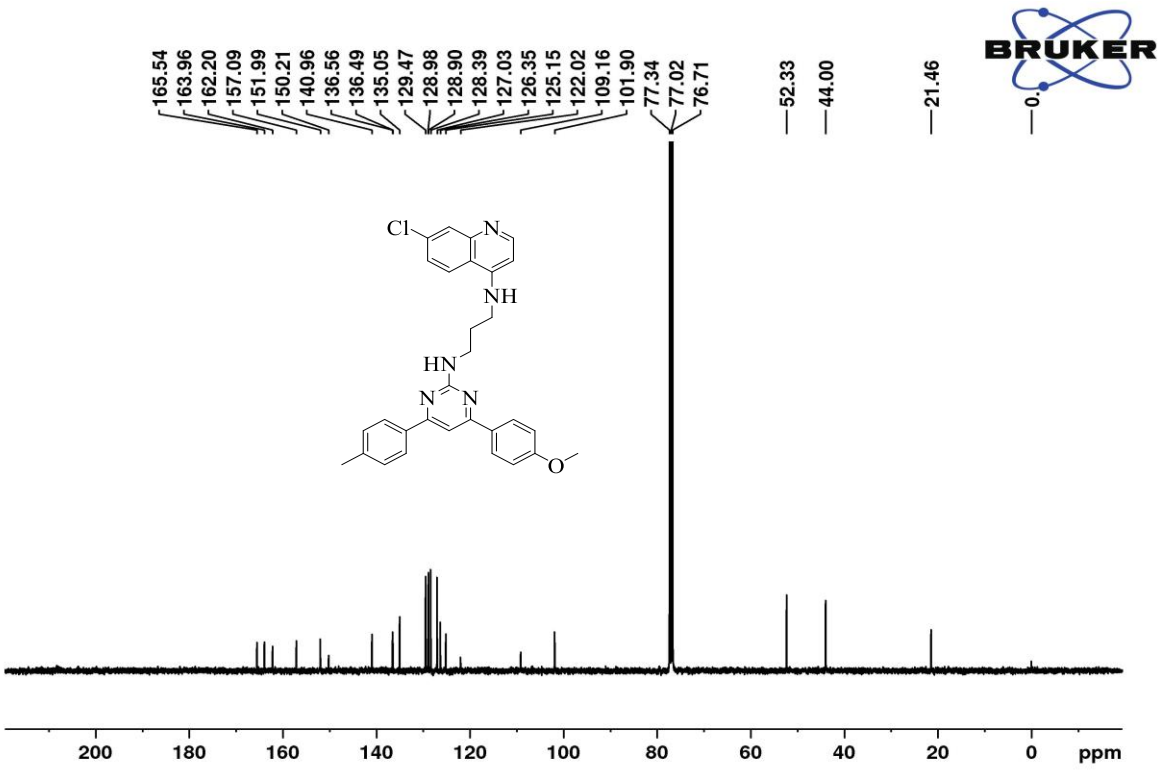

^{13}C NMR (100 MHz, $CDCl_3$)

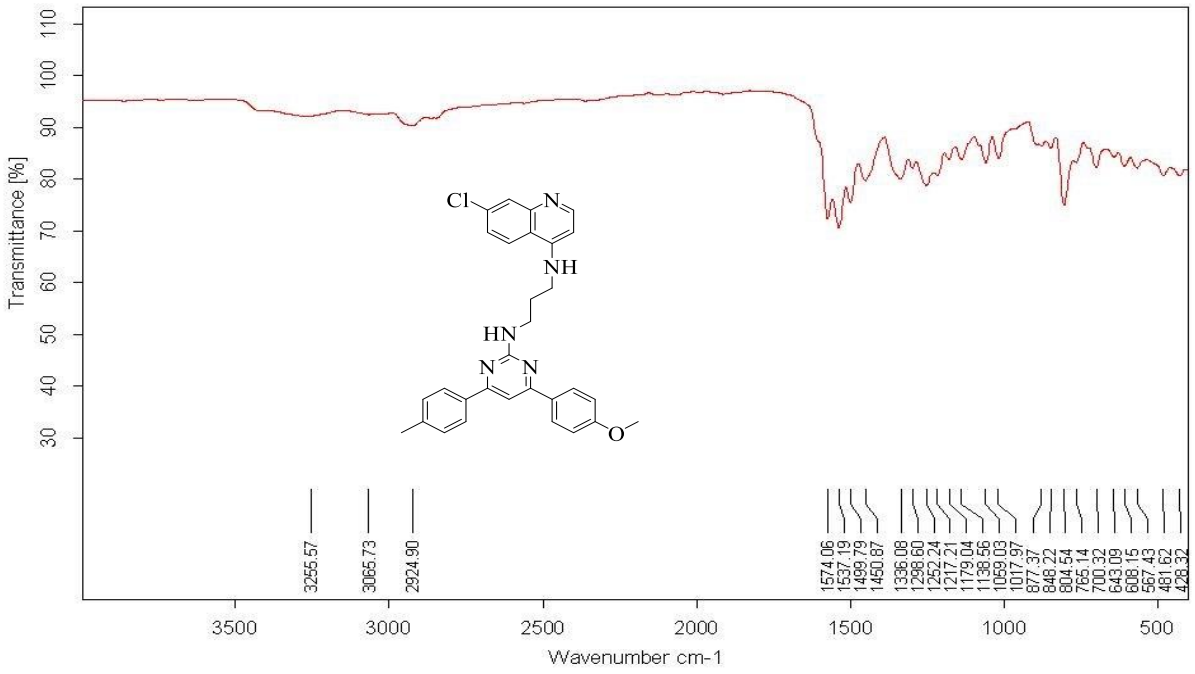

IR spectra

N^1-(4,6-bis(4-methoxyphenyl)pyrimidin-2-yl)-N^4-(7-chloroquinolin-4-yl)butane-1,4-diamine (**6g**)

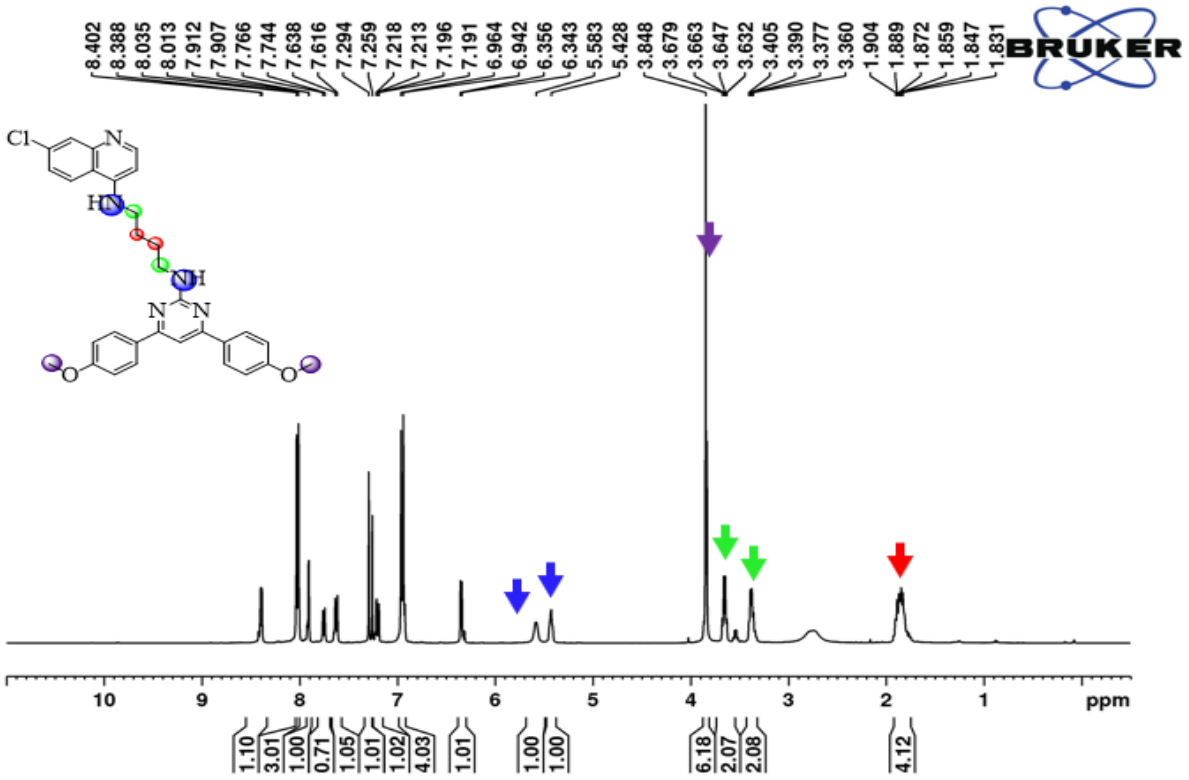

^{1}H NMR (400 MHz, $CDCl_3$)

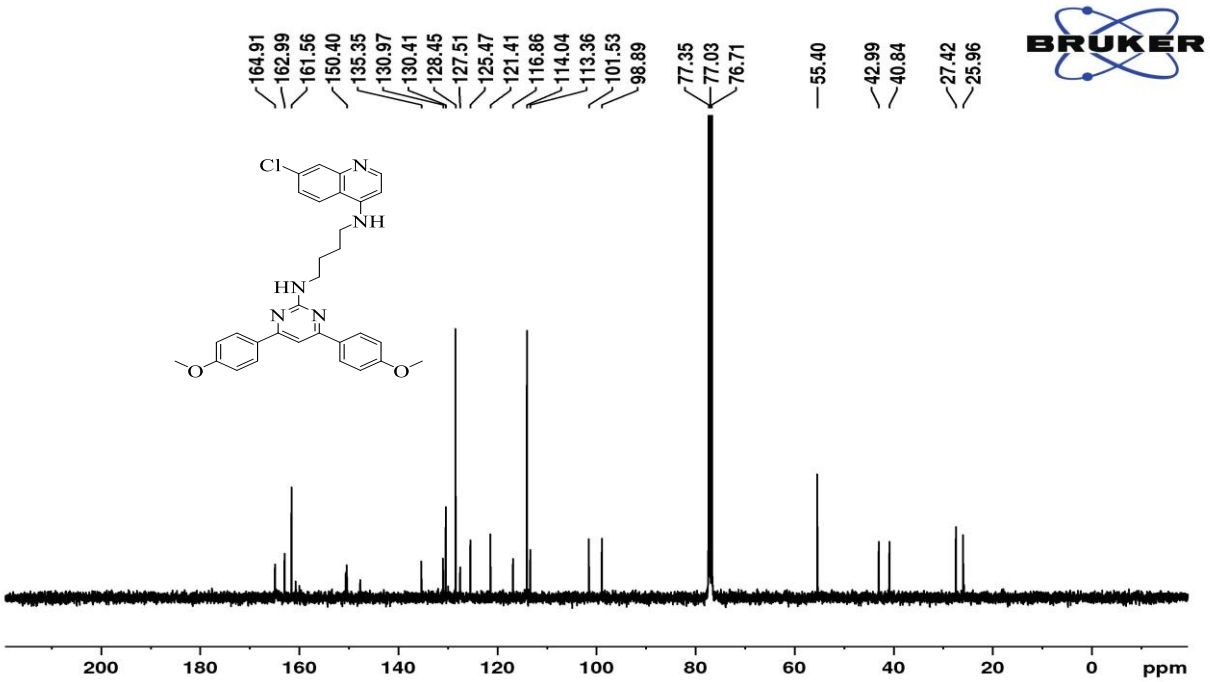

^{13}C NMR (400 MHz, $CDCl_3$)

Elemental Composition Report **Page 1**

Single Mass Analysis
Tolerance = 5.0 PPM / DBE: min = -1.5, max = 50.0
Element prediction: Off
Number of isotope peaks used for i-FIT = 3

Monoisotopic Mass, Even Electron Ions
17 formula(e) evaluated with 1 results within limits (all results (up to 1000) for each mass)
Elements Used:
C: 30-35 H: 30-35 N: 0-5 O: 0-5 Na: 1-1 Cl: 0-1

FK-1 5 (0.135) Cm (1:61)
TOF MS ES+

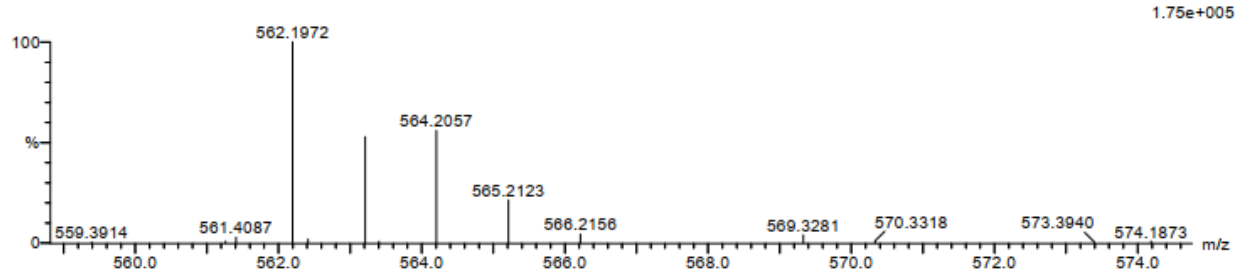

Minimum:				-1.5						
Maximum:		5.0	5.0	50.0						
Mass	Calc. Mass	mDa	PPM	DBE	i-FIT	i-FIT (Norm)	Formula			
562.1972	562.1986	-1.4	-2.5	18.5	66.6	0.0	C31	H30	N5	O2	Na	Cl

HRMS spectra

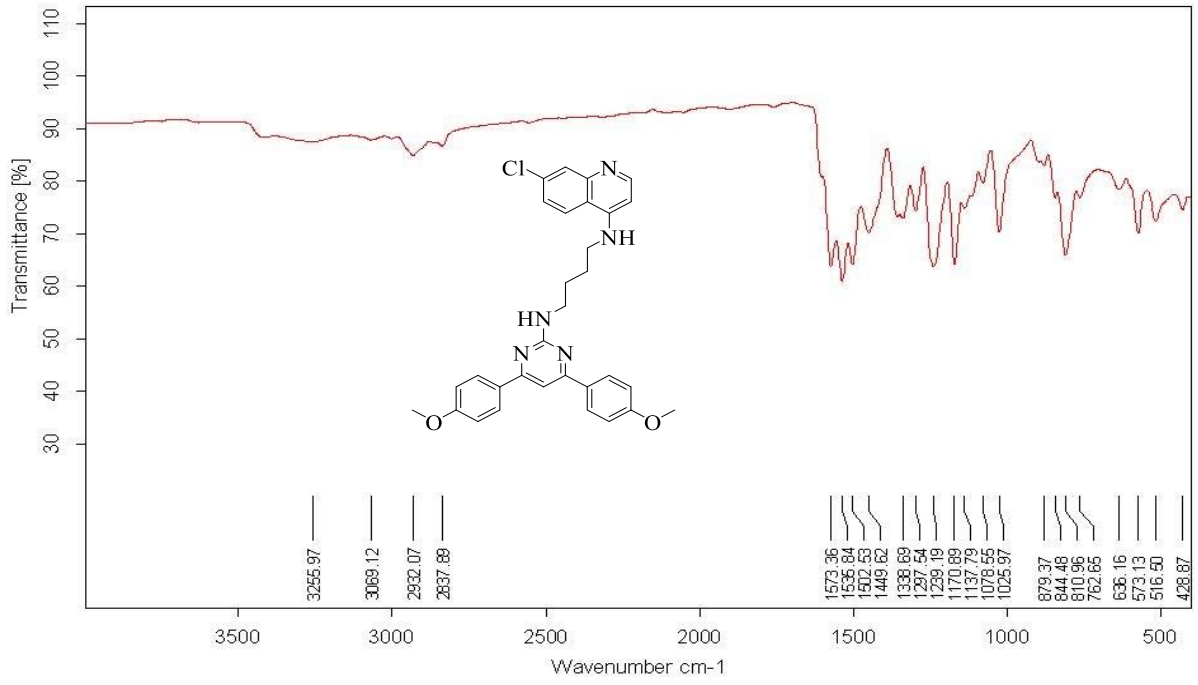

IR spectra

7-chloro-4-(4-(4-(4-methoxyphenyl)-6-(p-tolyl)pyrimidin-2-yl)piperazin-1-yl)quinoline **(6f)**:

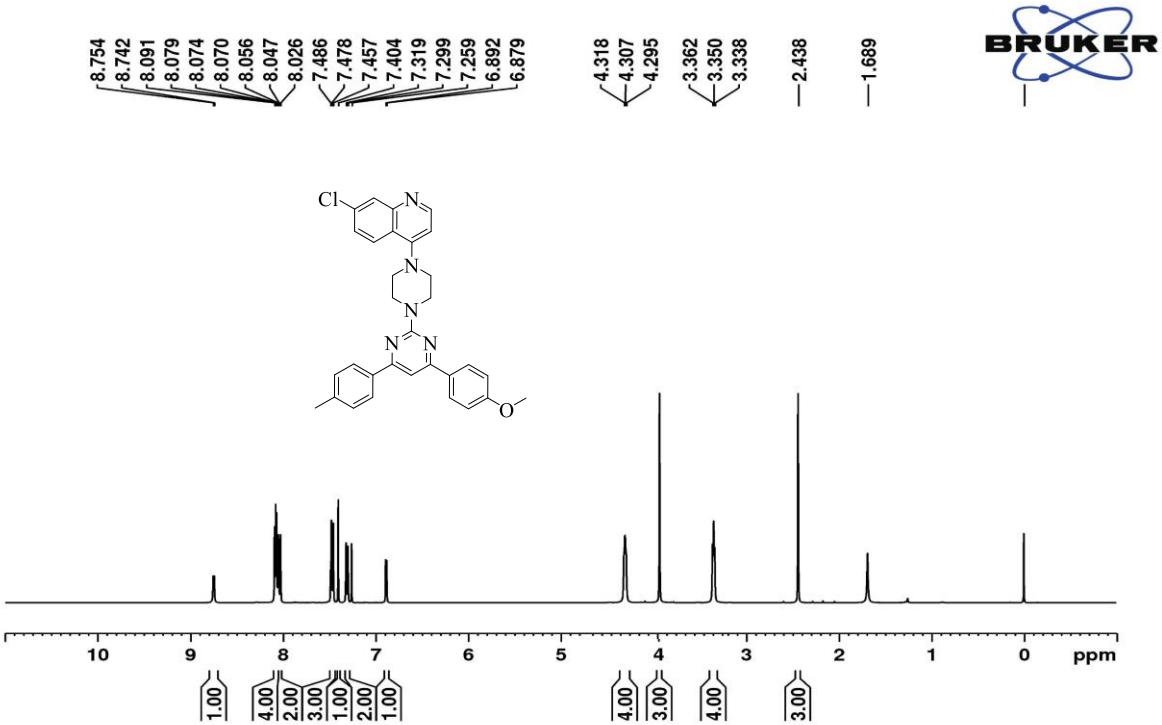

^{1}H NMR (400 MHz, $CDCl_3$)

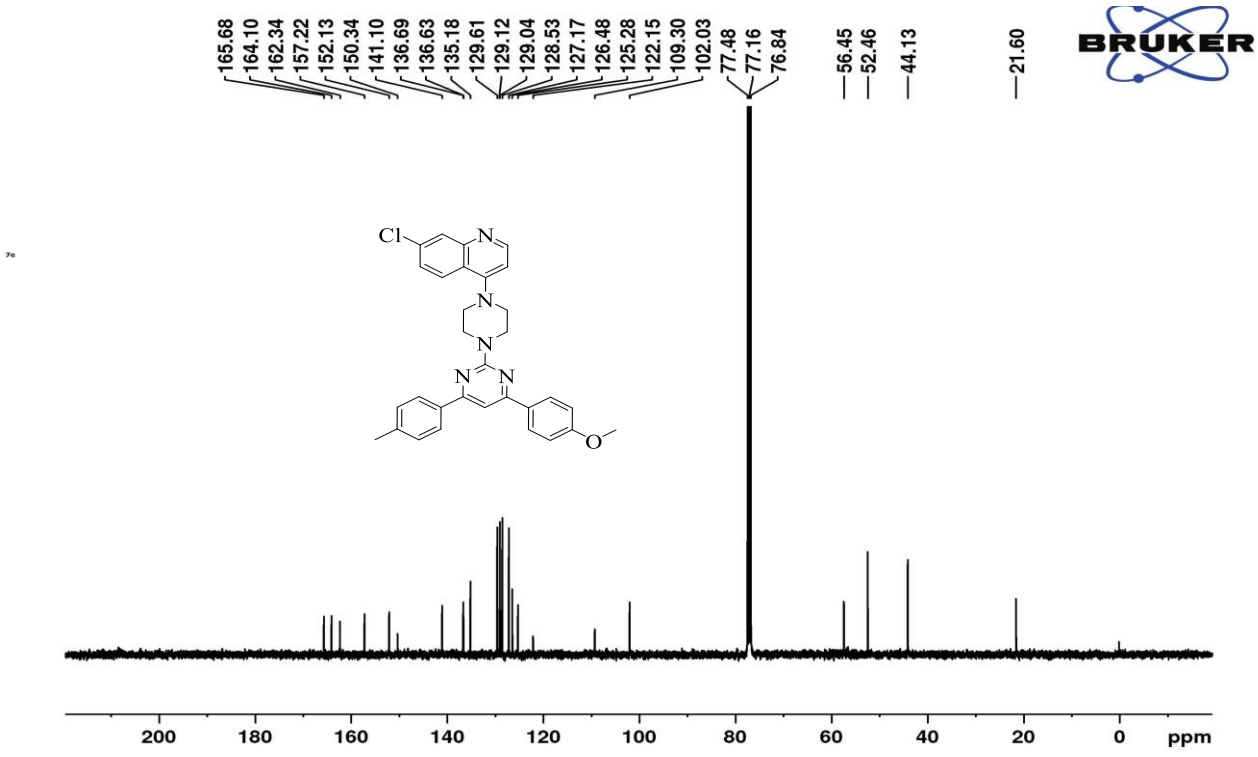

^{13}C NMR (100 MHz, $CDCl_3$)

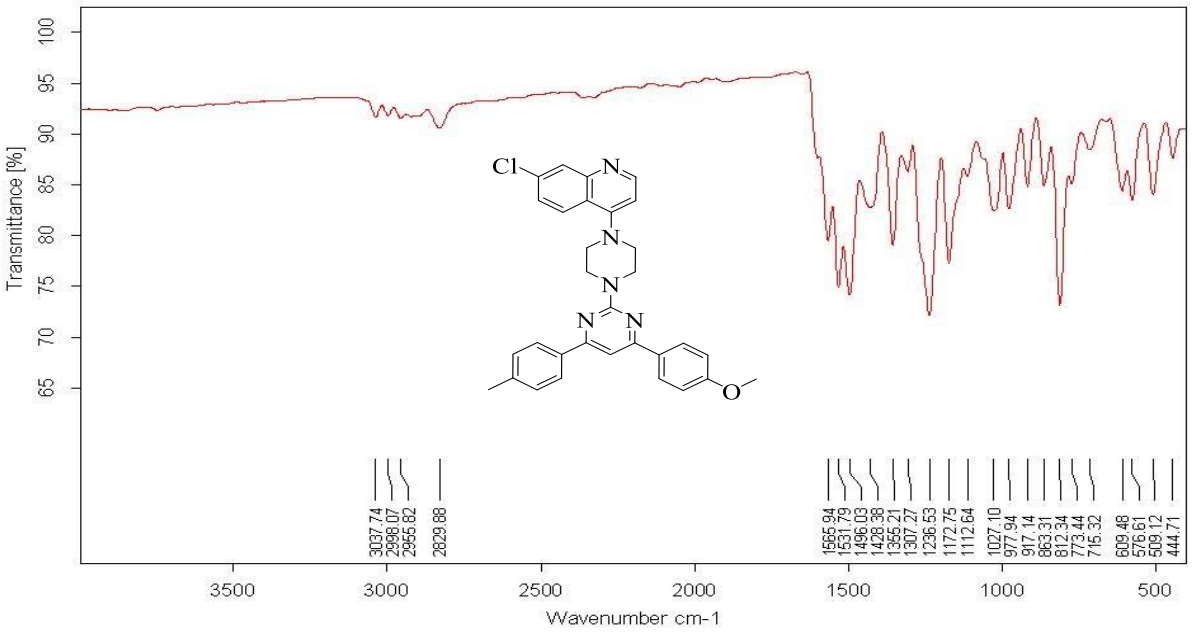

IR spectra

7-chloro-4-(4-(4-(3,4-dimethoxyphenyl)-6-(4-methoxyphenyl)pyrimidin-2-yl)piperazin-1-yl)quinoline (**6j**):

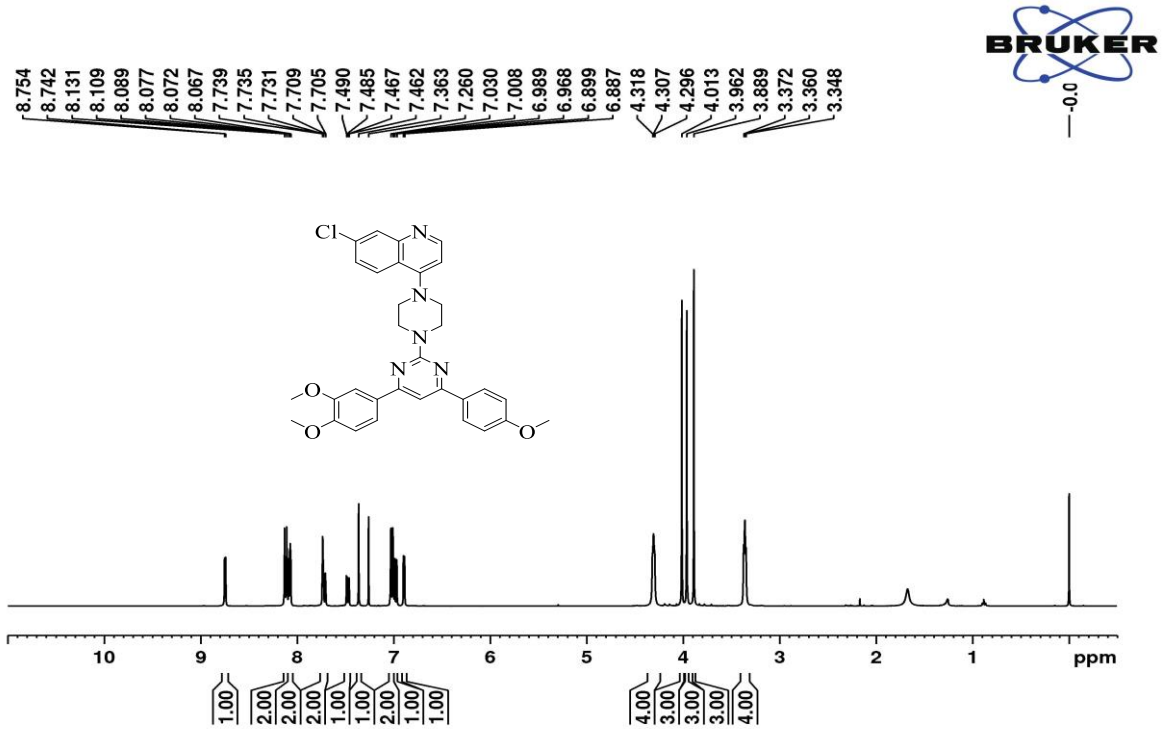

^{1}H NMR (400 MHz, $CDCl_3$)

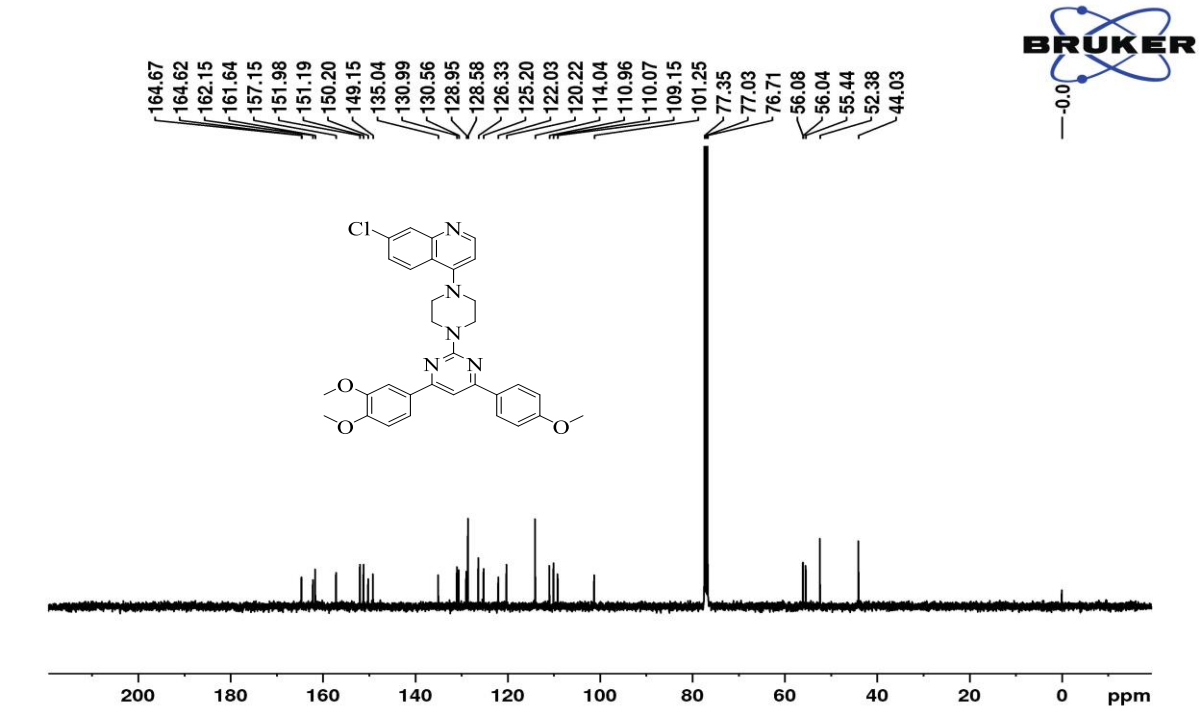

^{13}C NMR (100 MHz, $CDCl_3$)

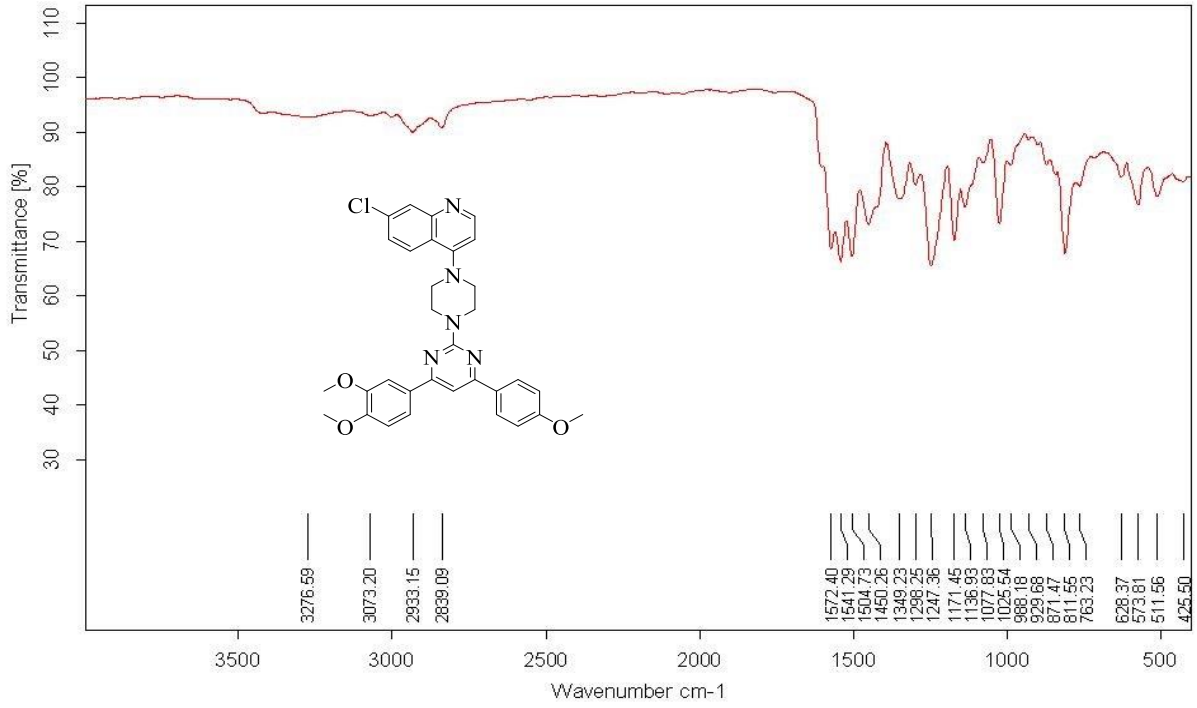

IR spectra

4-(4-(4,6-bis(3,4-dimethoxyphenyl)pyrimidin-2-yl)piperazin-1-yl)-7-chloroquinoline (**6k**):

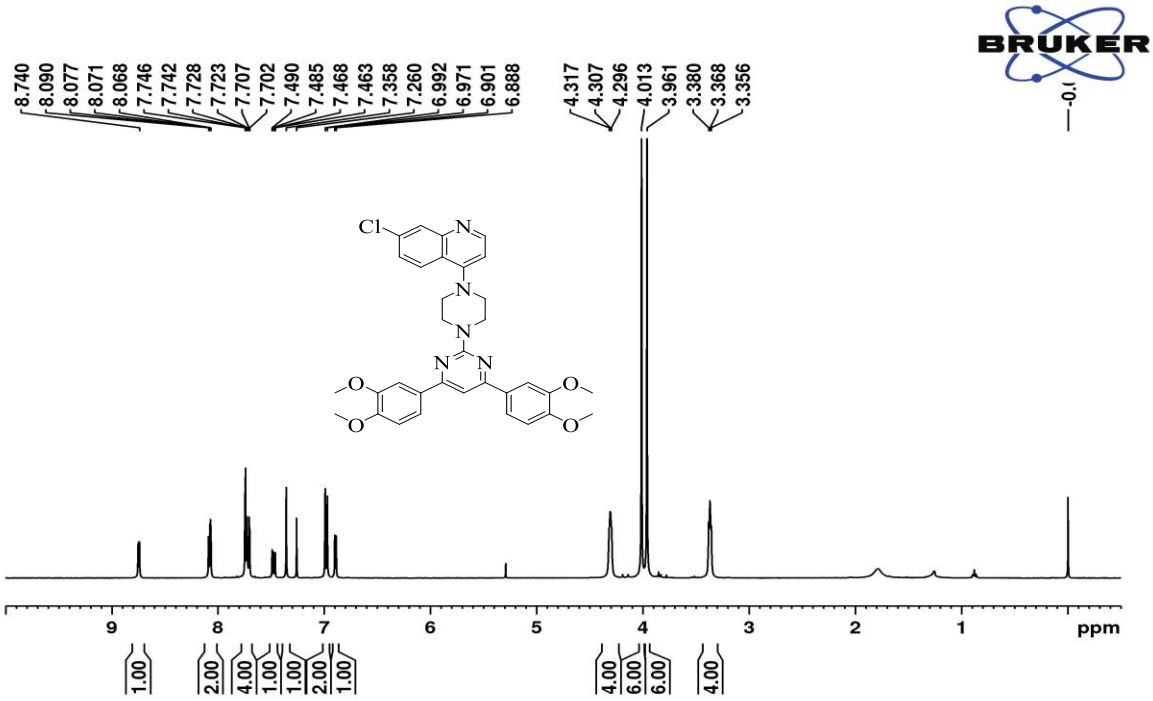

^{1}H NMR NMR (400 MHz, $CDCl_3$)

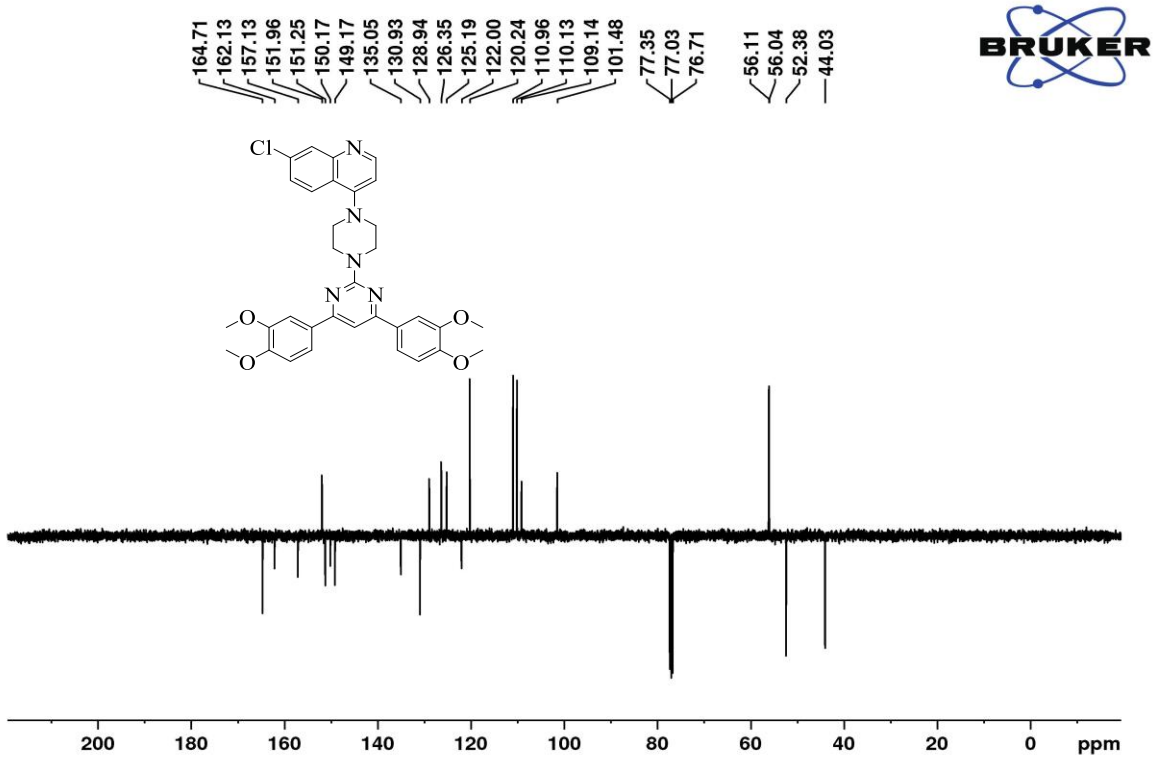

^{13}C NMR (100 MHz, $CDCl_3$)

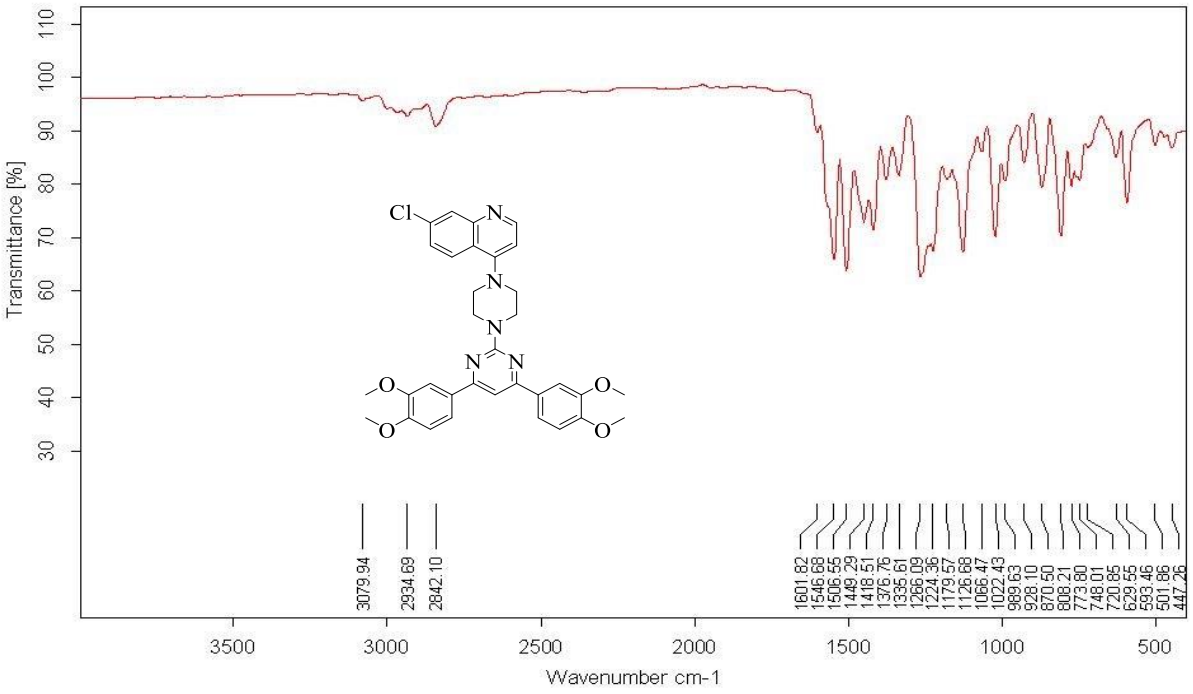

IR spectrum

4,4'-(2-((4-((7-chloroquinolin-4-yl)amino)butyl)amino)pyrimidine-4,6-diyl)diphenol **(7a)**

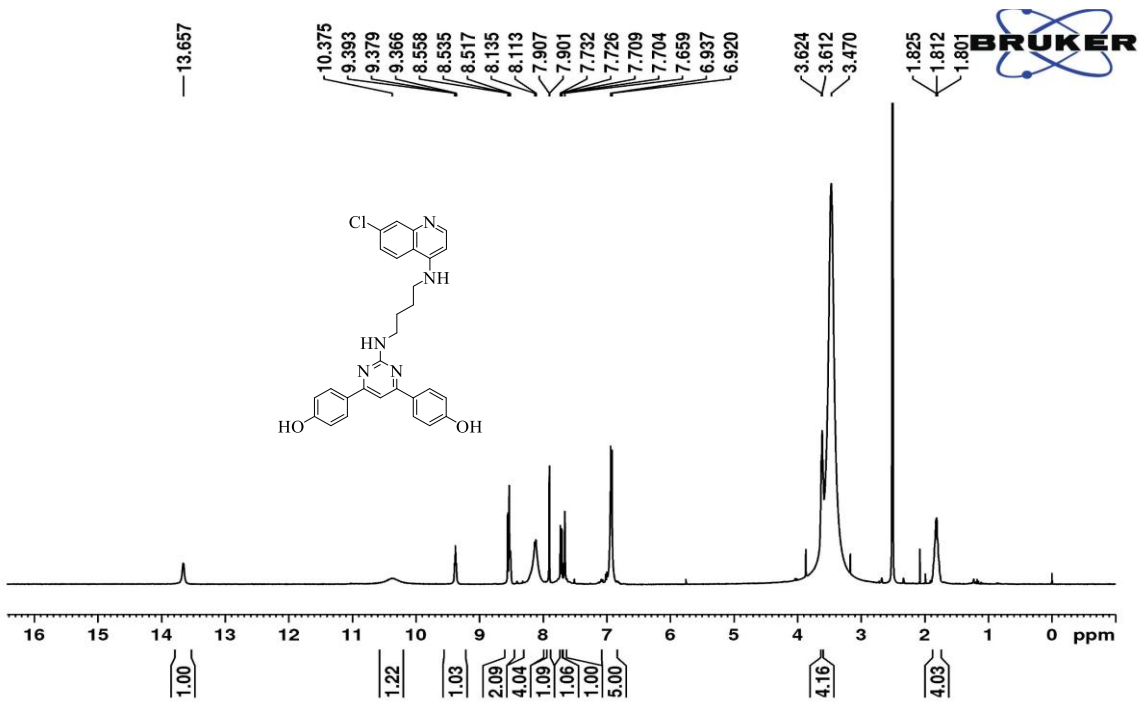

^{1}H NMR (400 MHz, DMSO-*d6*)

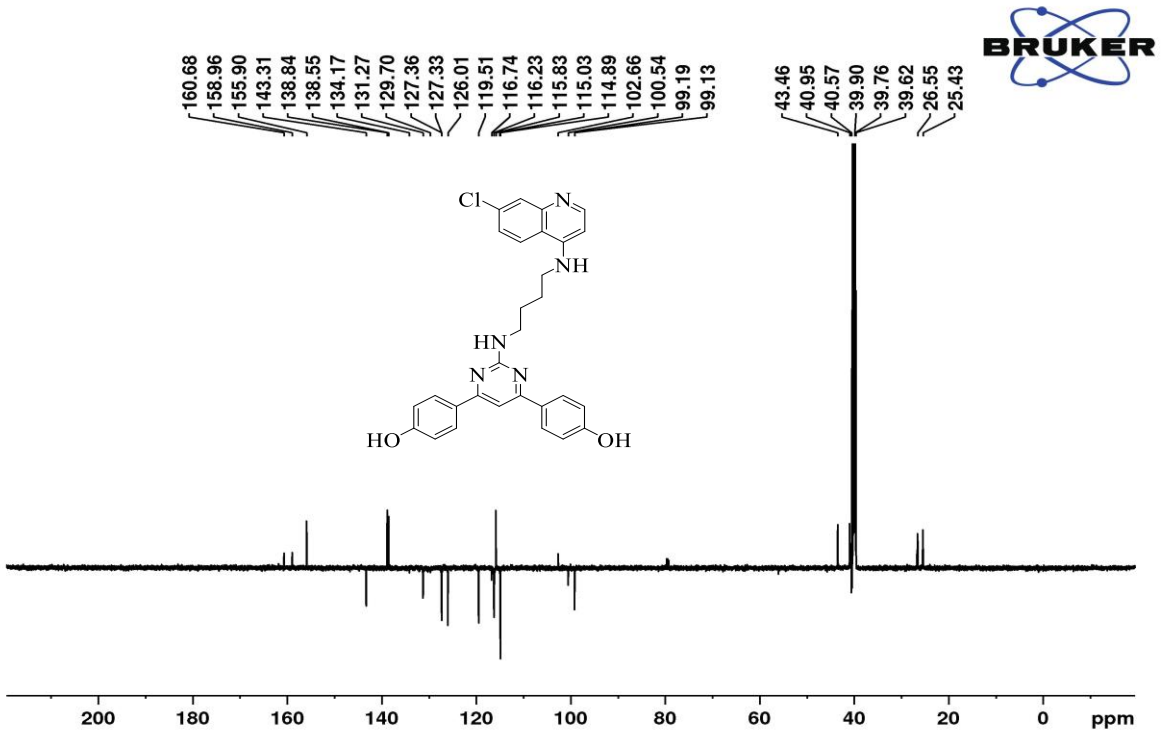

^{13}C NMR (100 MHz, DMSO-*d6*)

Elemental Composition Report **Page 1**

Single Mass Analysis
Tolerance = 5.0 PPM / DBE: min = -1.5, max = 50.0
Element prediction: Off
Number of isotope peaks used for i-FIT = 3

Monoisotopic Mass, Even Electron Ions
26 formula(e) evaluated with 1 results within limits (all results (up to 1000) for each mass)
Elements Used:
C: 25-30 H: 25-30 N: 0-5 O: 0-5 Cl: 0-1
FK3 5 (0.135) Cm (1:61)
TOF MS ES+

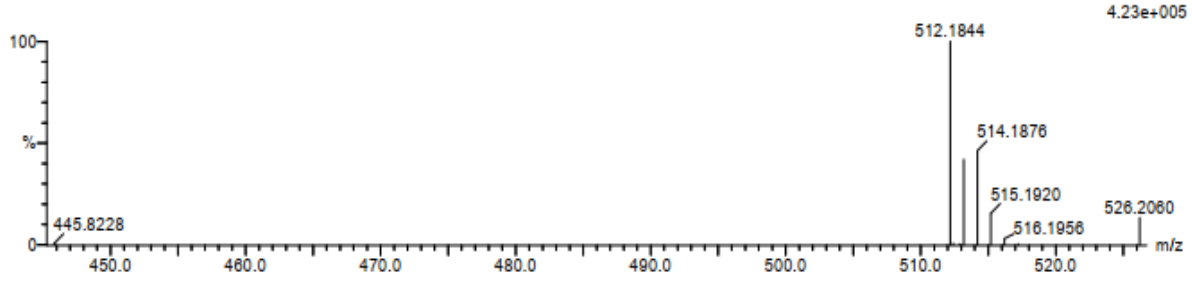

Minimum:				-1.5			
Maximum:		5.0	5.0	50.0			
Mass	Calc. Mass	mDa	PPM	DBE	i-FIT	i-FIT (Norm)	Formula
512.1844	512.1853	-0.9	-1.8	18.5	63.9	0.0	C29 H27 N5 O2 Cl

HRMS spectra

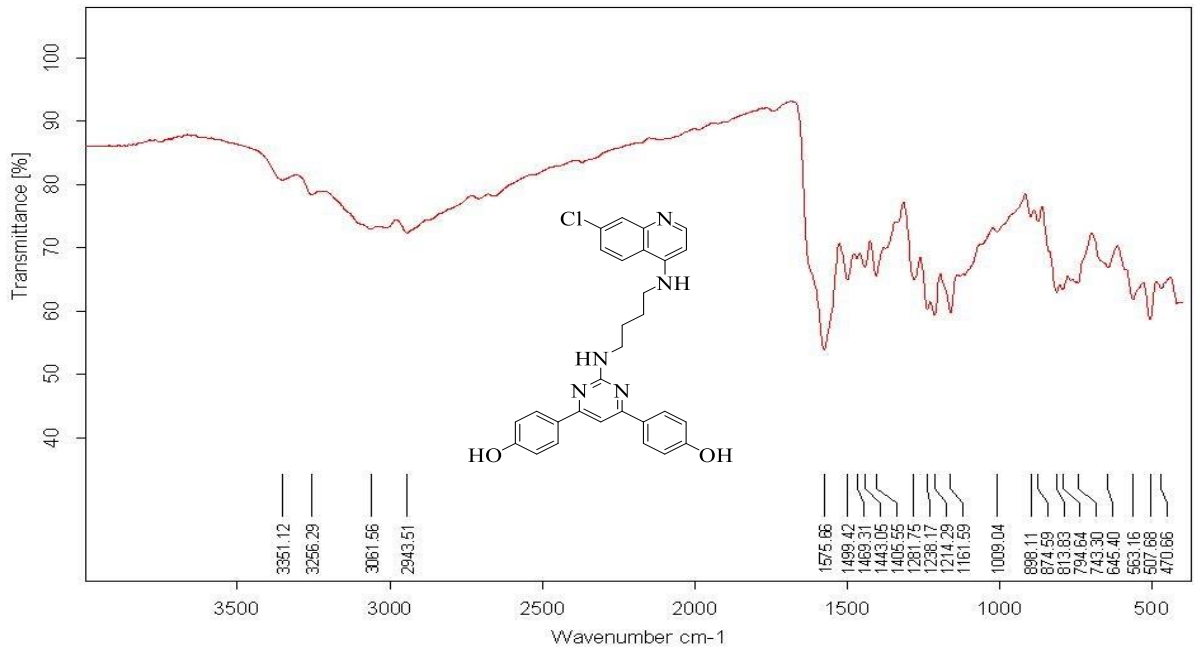

IR Spectra

4-(2-((4-((7-chloroquinolin-4-yl)amino)butyl)amino)-6-(4-hydroxyphenyl)pyrimidin-4-yl)benzene-1,2-diol (**7b**):

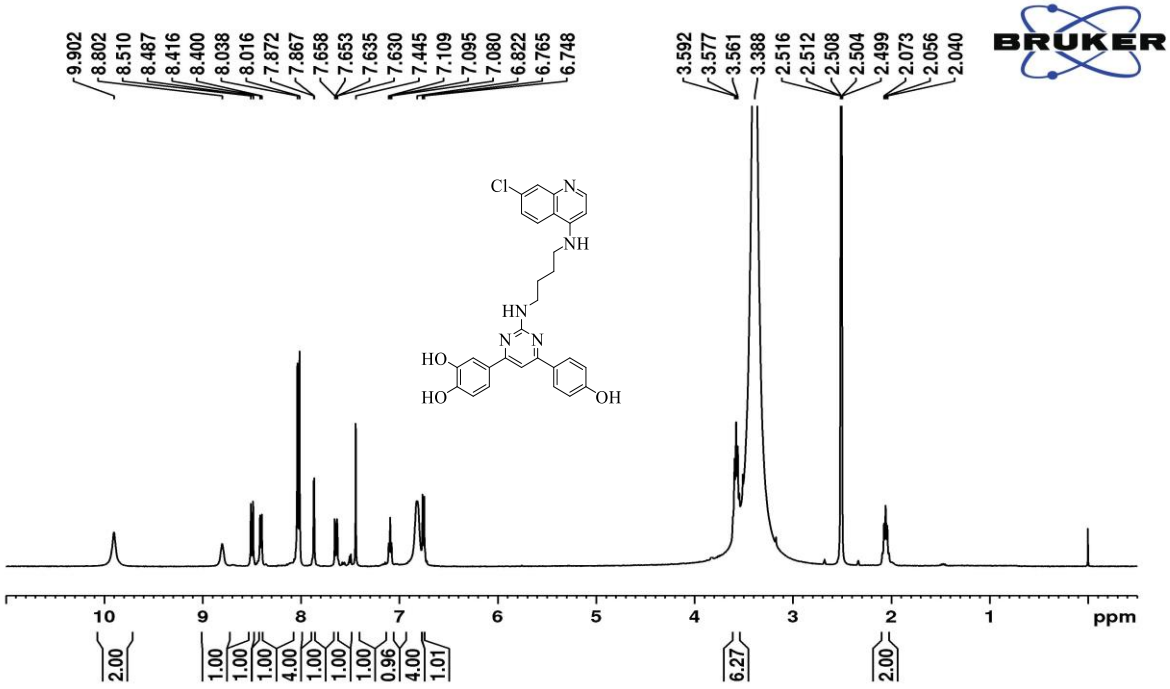

^{1}H NMR (400 MHz, DMSO-*d6*)

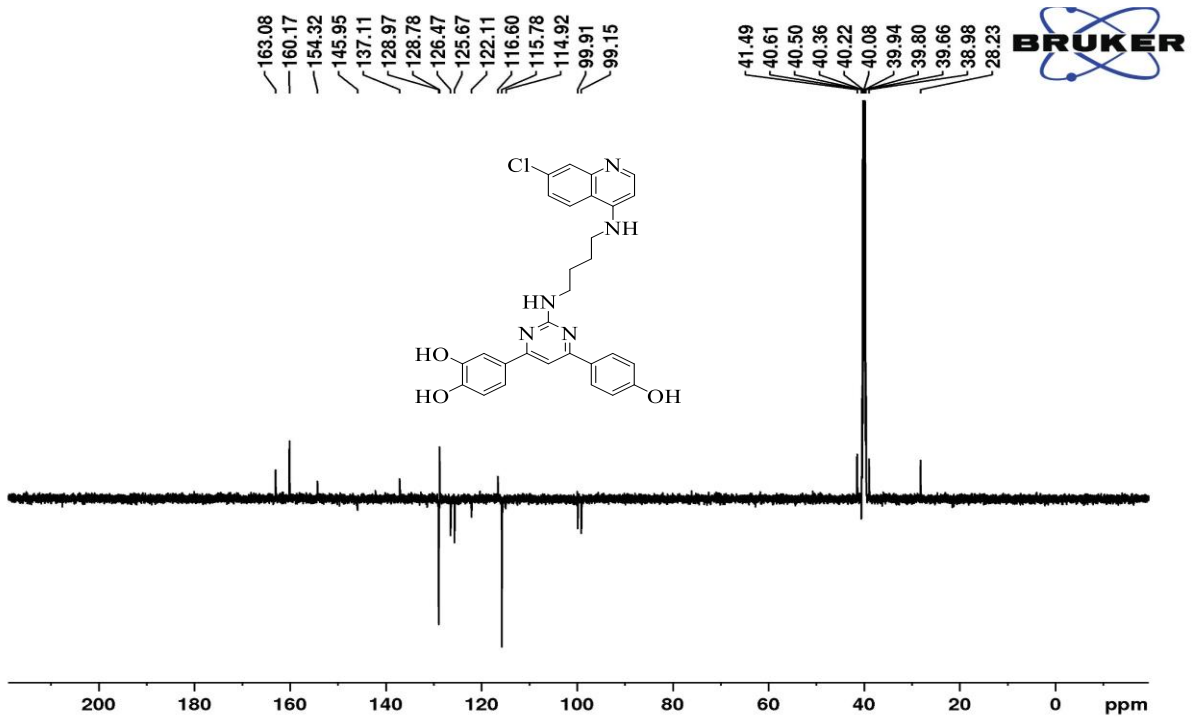

^{13}C NMR (400 MHz, DMSO-*d6*)

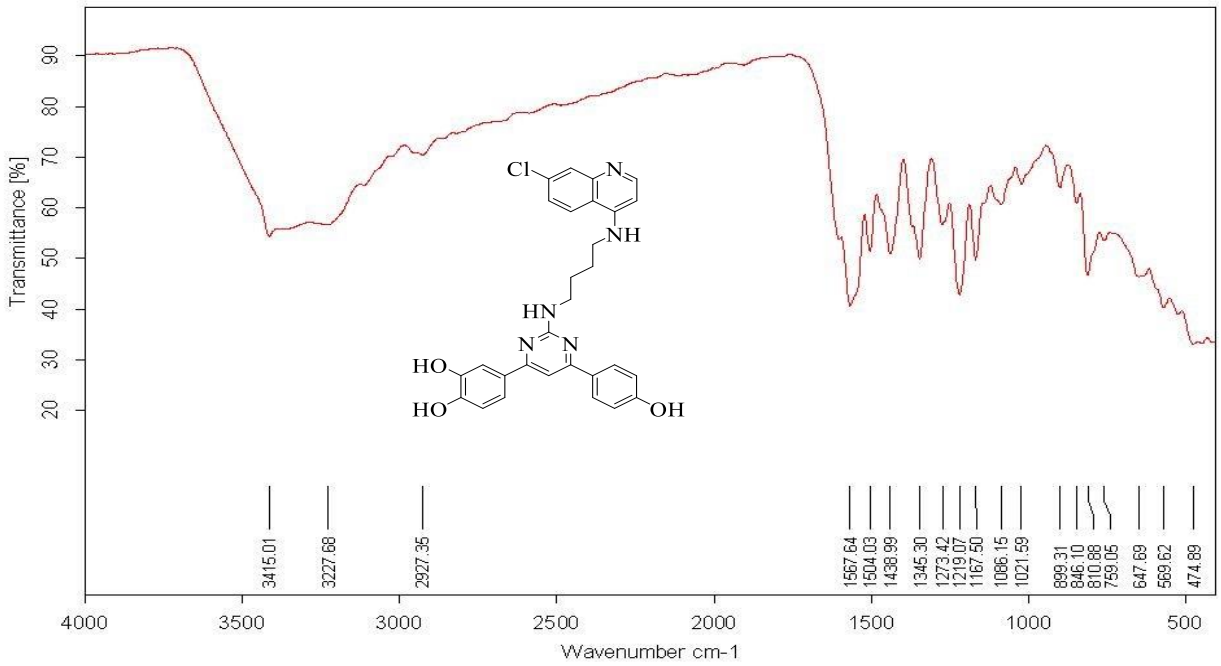

IR spectra

4-(2-(4-(7-chloroquinolin-4-yl)piperazin-1-yl)-6-(4-hydroxyphenyl)pyrimidin-4-yl)benzene-1,2-diol (**7c**):

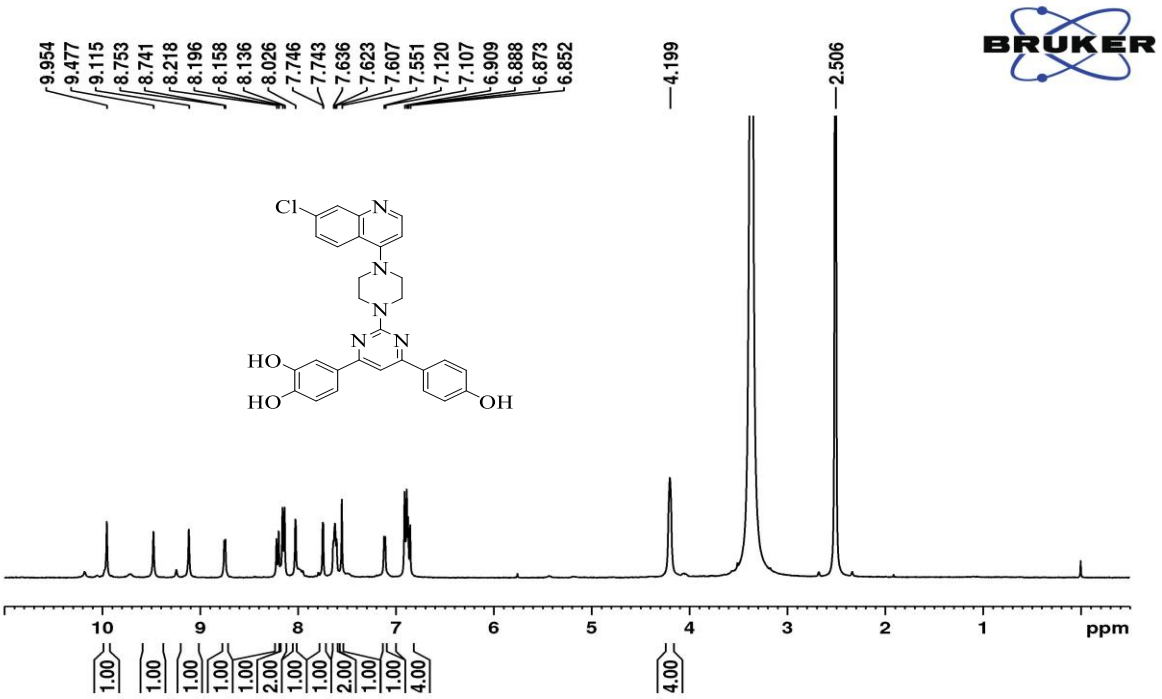

^{1}H NMR (400 MHz, DMSO-*d6*)

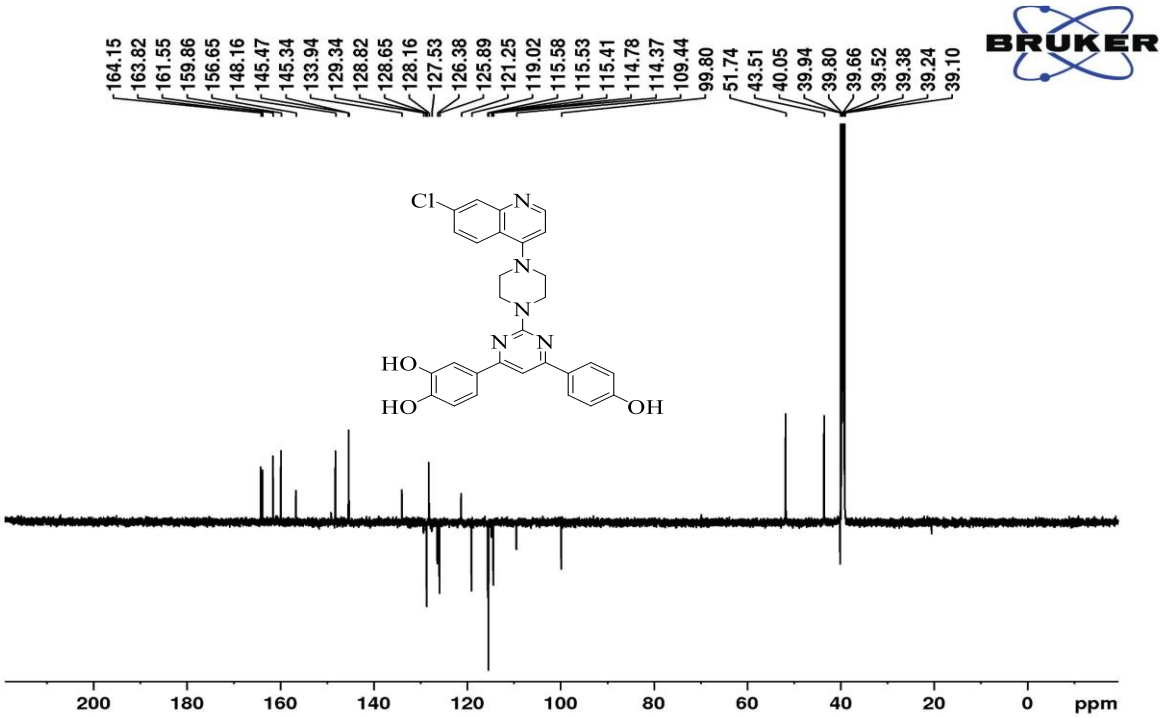

^{13}C NMR (100 MHz, DMSO-d_6)

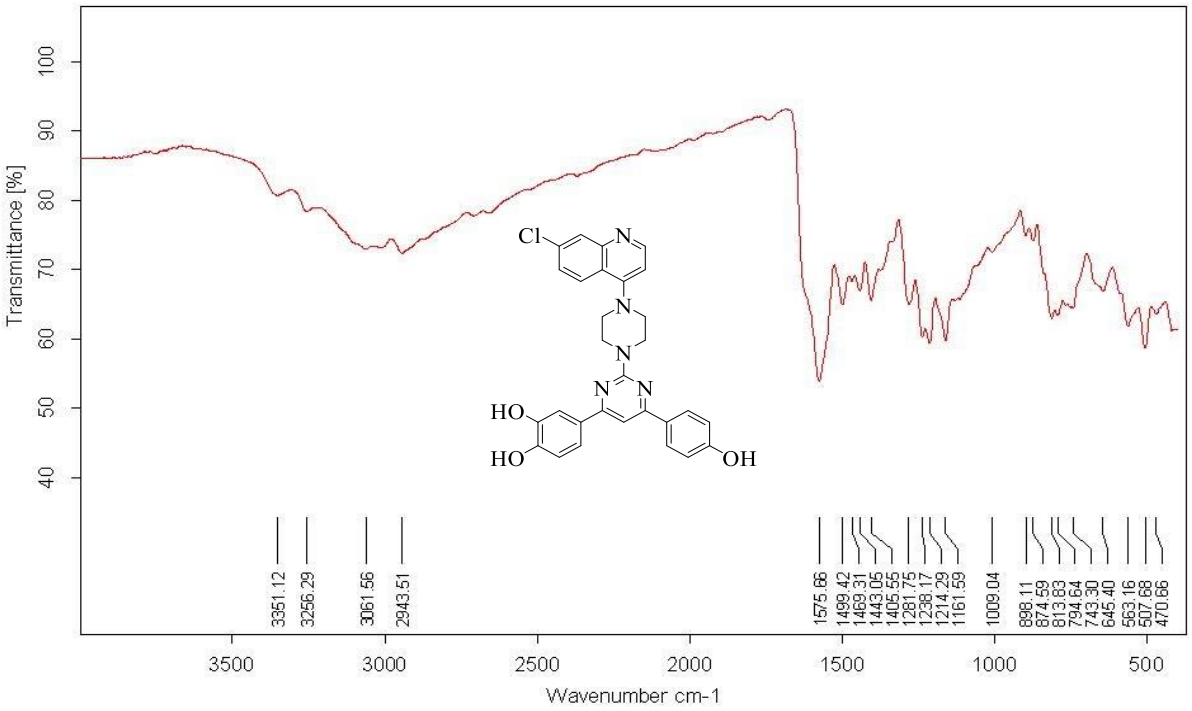
Transmittance [%]
100
90
80
70
60
50
40
3500
3000
2500
2000
1500
1000
500
Wavenumber cm-1
3351.12
3256.29
3061.56
2943.51
1575.66
1499.42
1469.31
1443.05
1405.55
1281.75
1238.17
1214.29
1161.59
1009.04
898.11
874.59
813.83
794.64
743.30
645.40
563.16
507.68
470.66
Cl
N
N
N
N
N
HO
HO
OH

IR spectrum

APPENDIX–II

SUPPLEMENTARY INFORMATION

CHAPTER 4

Promising class of antiprotozoal agents; **Design and synthesis of novel pyrimidine–cinnamyl hybrids**

Representative spectra 4,6-diphenyl-2-(piperazin-1-yl)pyrimidine derivative

4,6-bis(4-methoxyphenyl)-2-(piperazin-1-yl)pyrimidine **(c)**

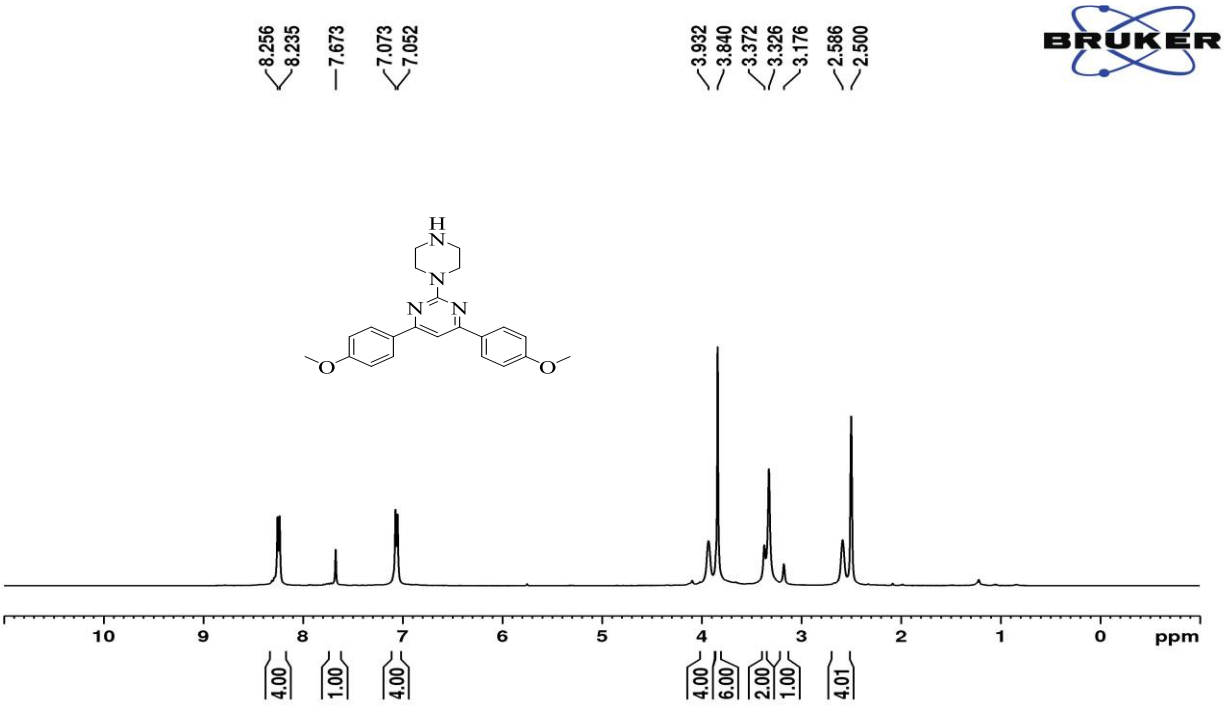

^{1}H NMR (400 MHz, DMSO-d_6)

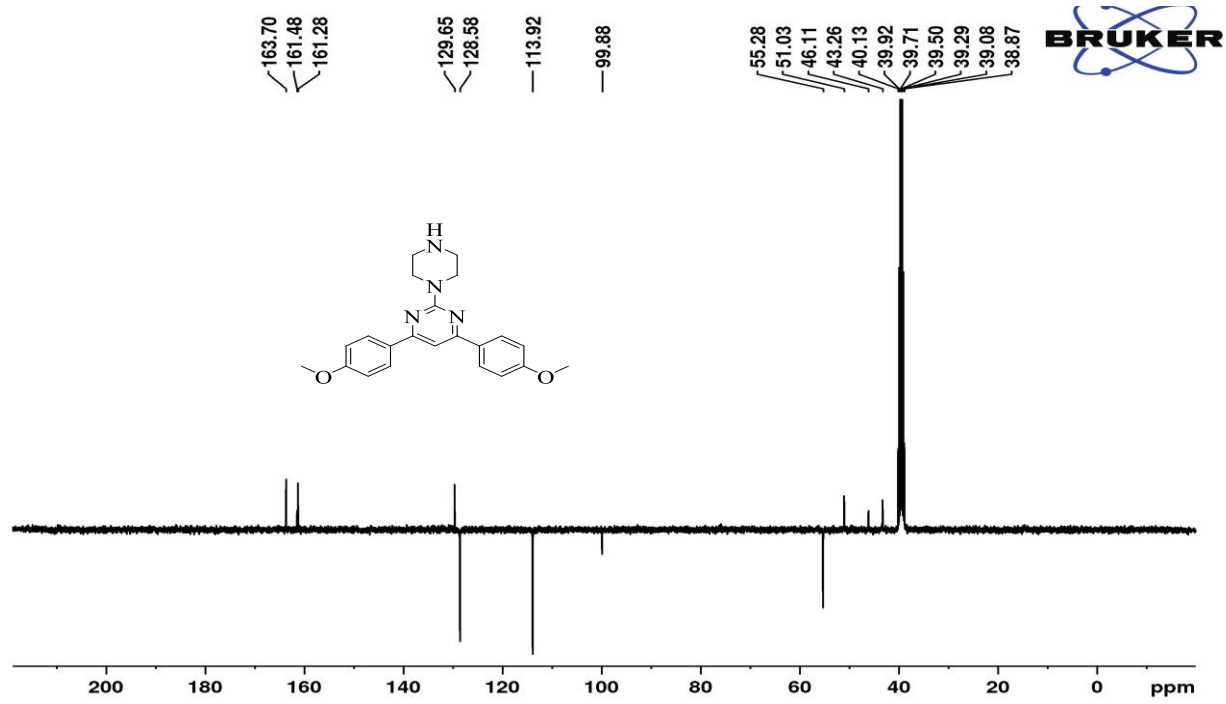

^{13}C NMR (100 MHz, DMSO-d_6)

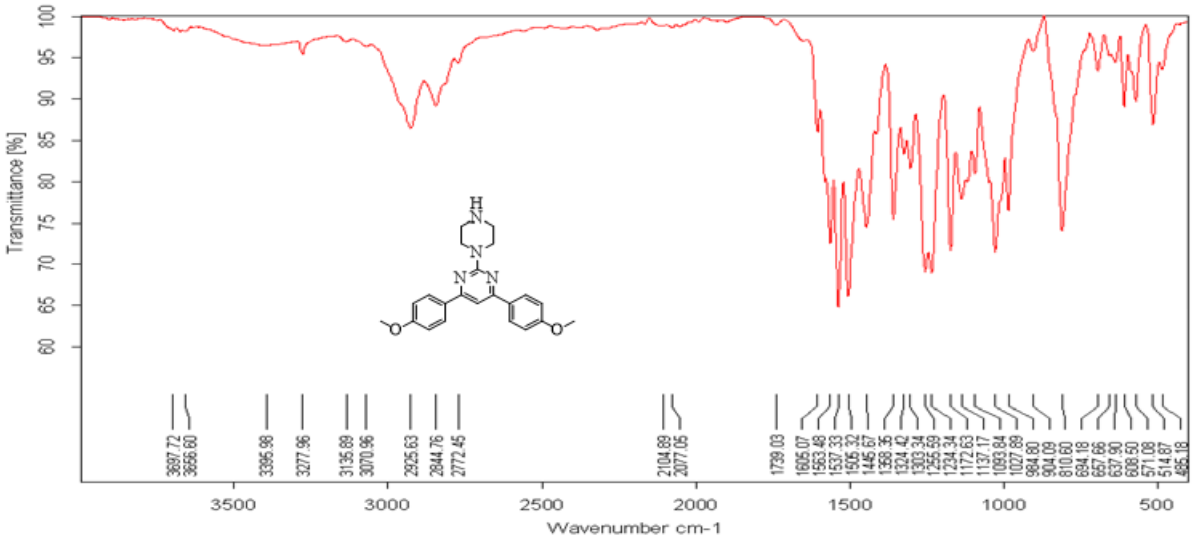

IR spectra

Spectra of the final compounds(8a-8t)

(E)-1-(4-(4-(4-chlorophenyl)-6-(4-methoxyphenyl)pyrimidin-2-yl)piperazin-1-yl)-3-phenylprop-2-en-1-one (**8a**):

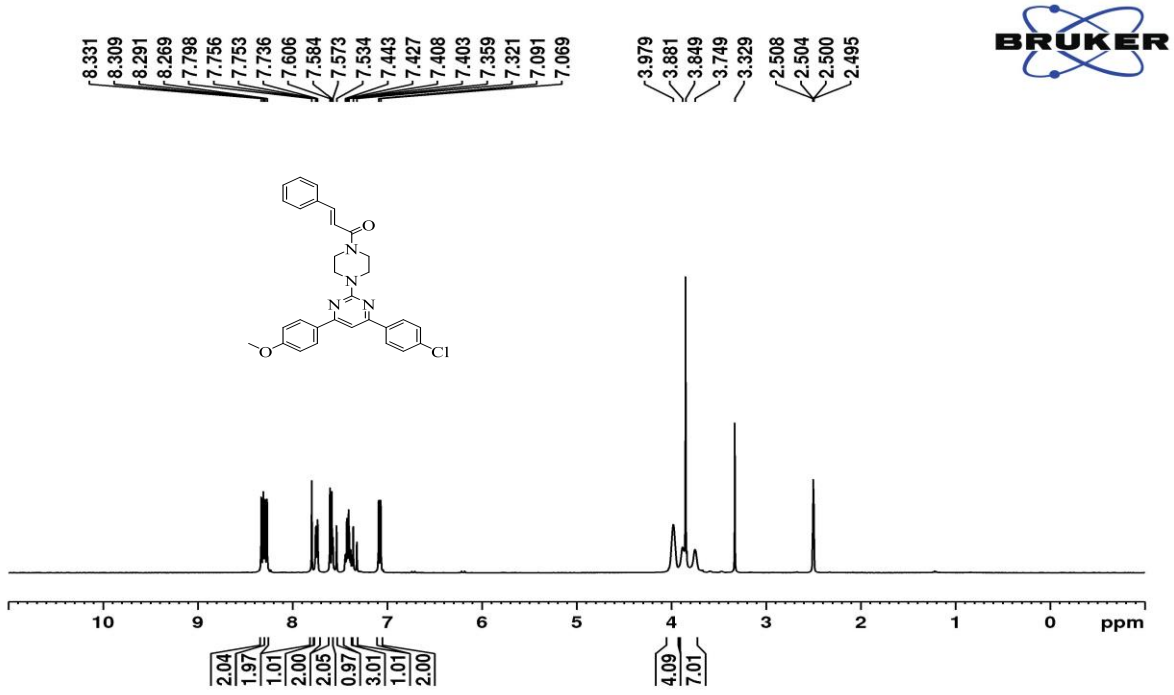

^{1}H NMR (400 MHz, $CDCl_3$)

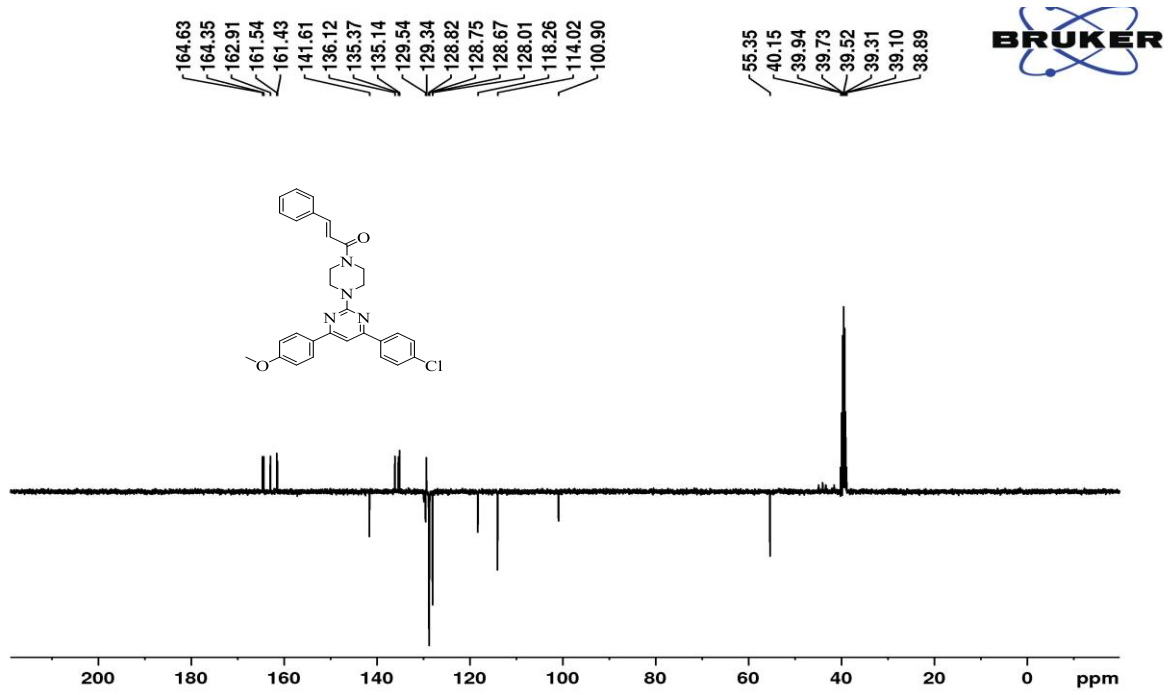

^{13}C NMR (100 MHz, DMSO-d_6)

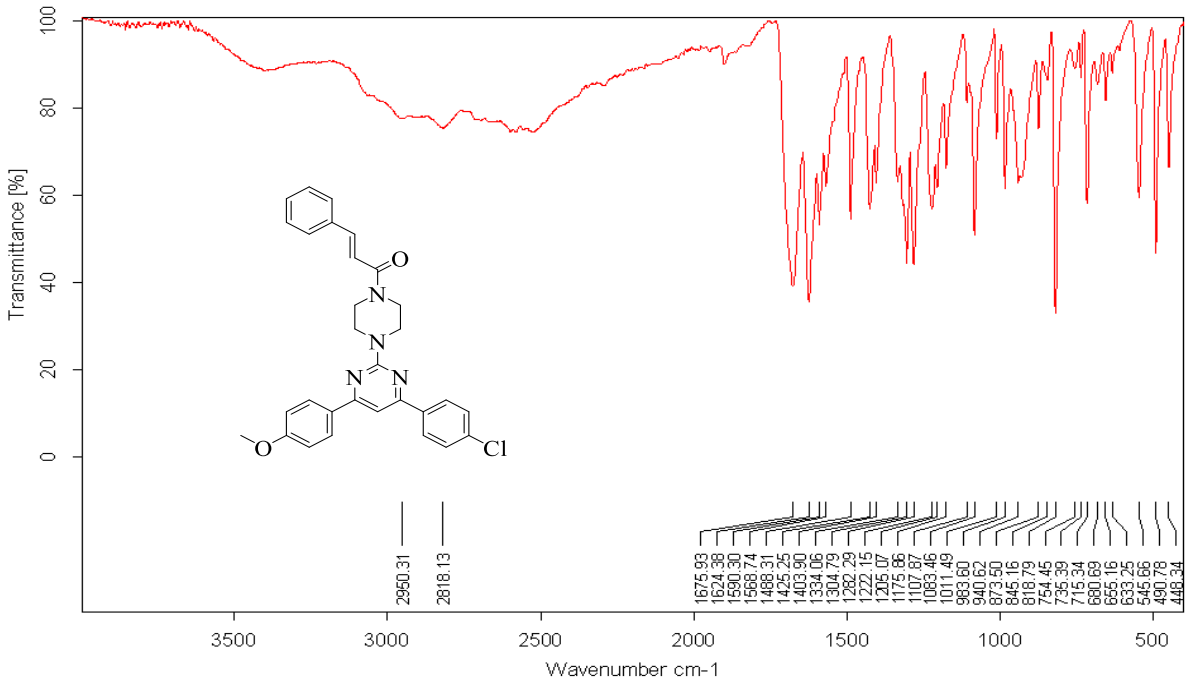

IR spectra

(E)-1-(4-(4-(4-chlorophenyl)-6-(4-methoxyphenyl)pyrimidin-2-yl)piperazin-1-yl)-3-(p-tolyl)prop-2-en-1-one (**8b**):

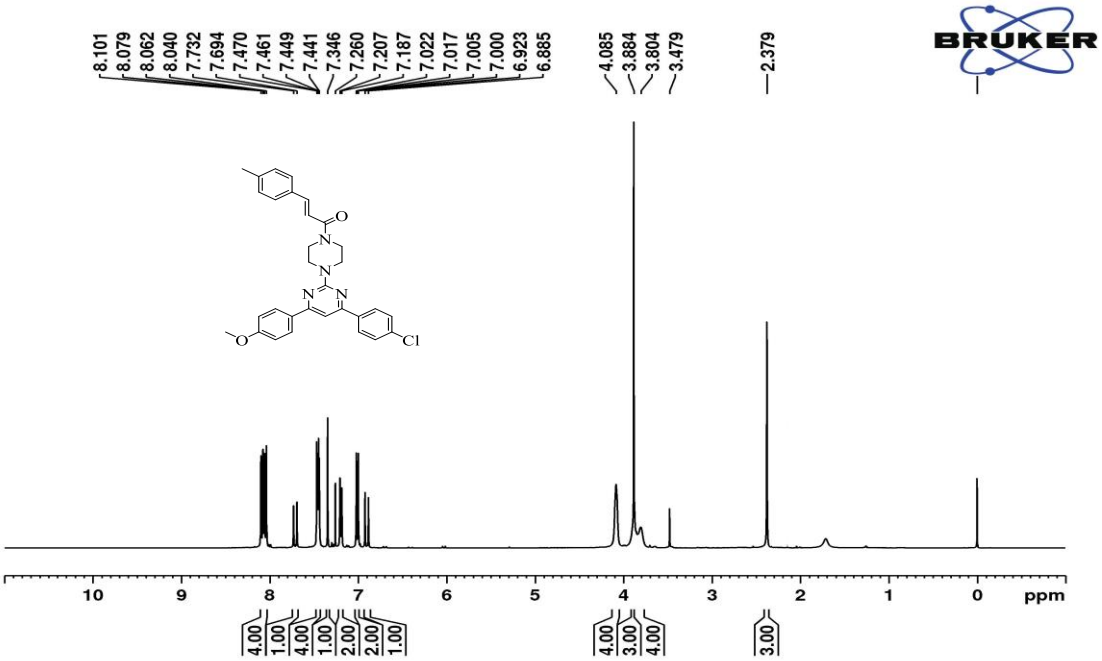

^{1}H NMR (400 MHz, $CDCl_3$)

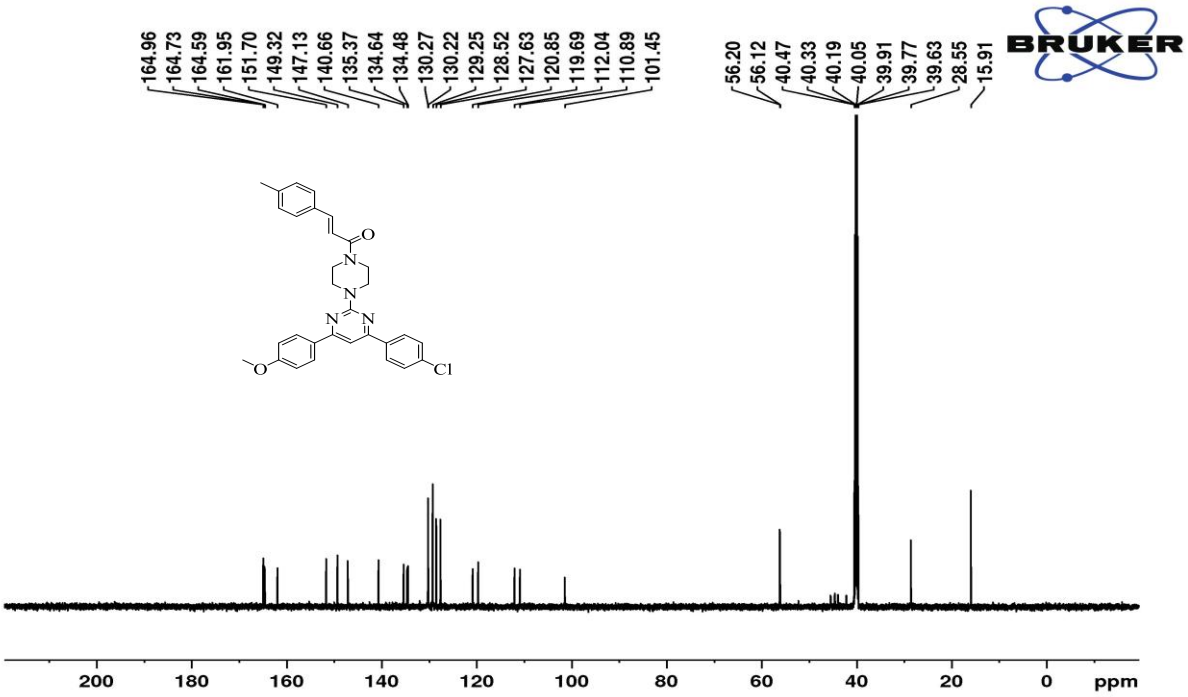

^{13}C NMR (100 MHz, $CDCl_3$)

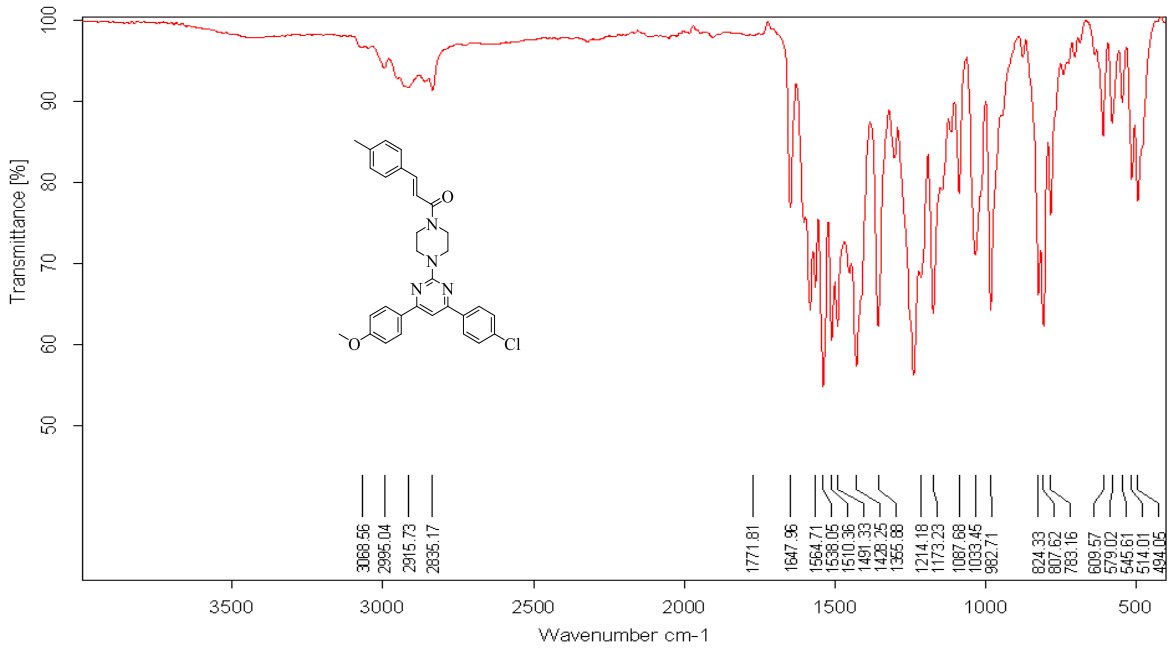

IR spectra

(E)-1-(4-(4-(4-methoxyphenyl)-6-(p-tolyl)pyrimidin-2-yl)piperazin-1-yl)-3-phenylprop-2-en-1-one (**8c**):

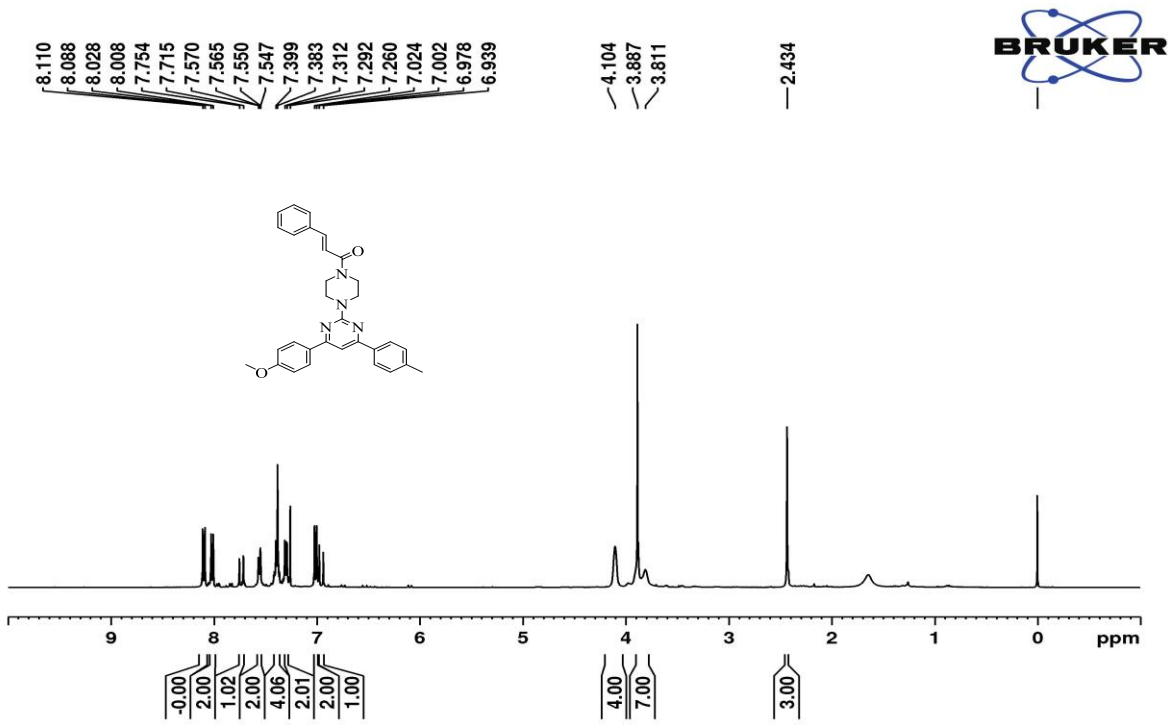

^{1}H NMR (400 MHz, $CDCl_3$)

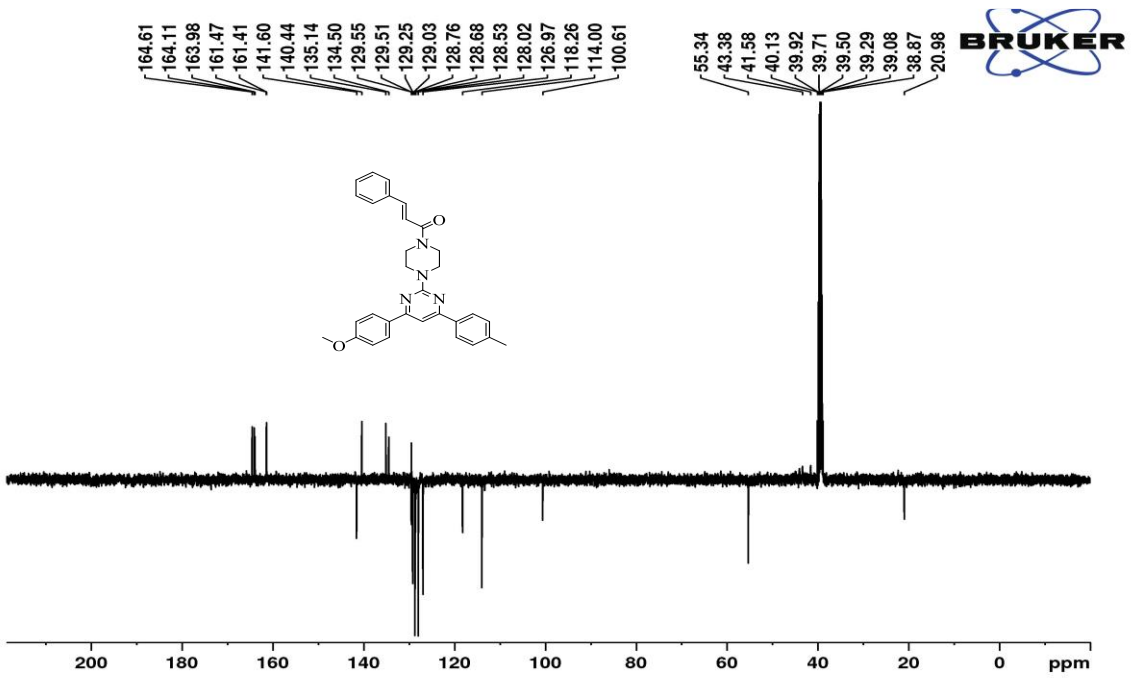

^{13}C NMR (100 MHz, $CDCl_3$)

Elemental Composition Report **Page 1**

Single Mass Analysis
Tolerance = 5.0 PPM / DBE: min = -1.5, max = 50.0
Element prediction: Off
Number of isotope peaks used for i-FIT = 3

Monoisotopic Mass, Even Electron Ions
13 formula(e) evaluated with 1 results within limits (all results (up to 1000) for each mass)
Elements Used:
C: 30-35 H: 25-30 N: 0-5 O: 0-5 Na: 1-1
FK4 9 (0.270) Cm (1:61)
TOF MS ES+

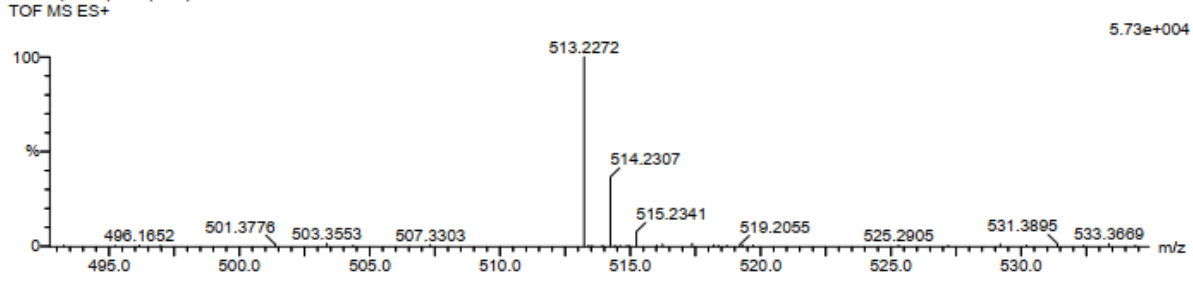

Minimum:				-1.5			
Maximum:		5.0	5.0	50.0			
Mass	Calc. Mass	mDa	PPM	DBE	i-FIT	i-FIT (Norm)	Formula
513.2272	513.2266	0.6	1.2	18.5	86.1	0.0	C31 H30 N4 O2 Na

HRMS spectra

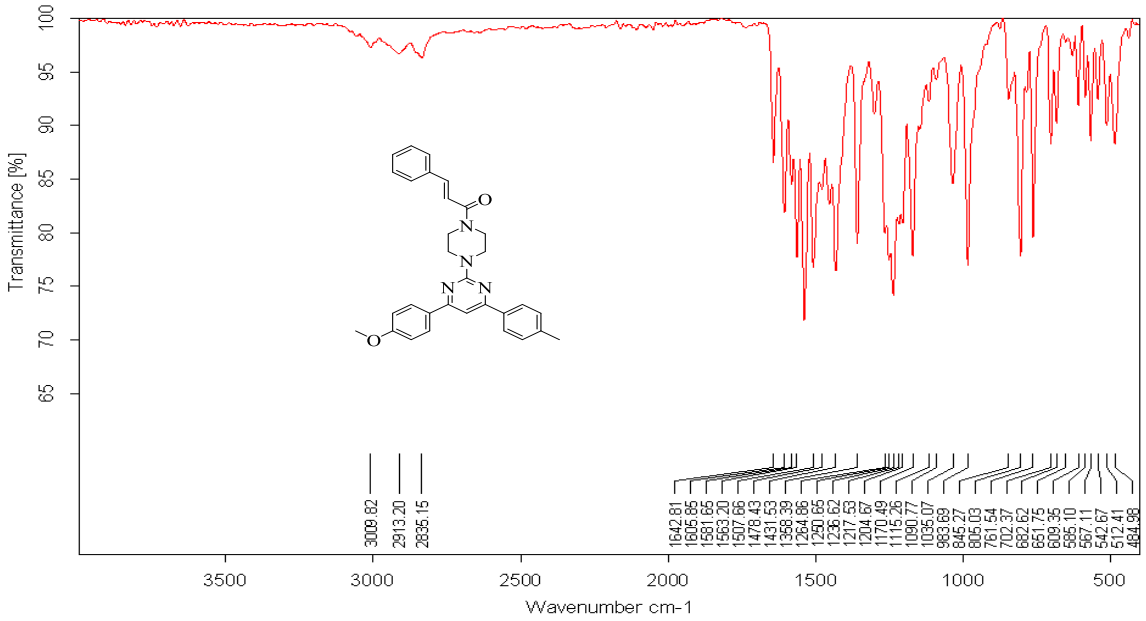

IR spectra

(E)-3-(4-chlorophenyl)-1-(4-(4-(4-methoxyphenyl)-6-(p-tolyl)pyrimidin-2-yl)piperazin-1-yl)prop-2-en-1-one (**8d**):

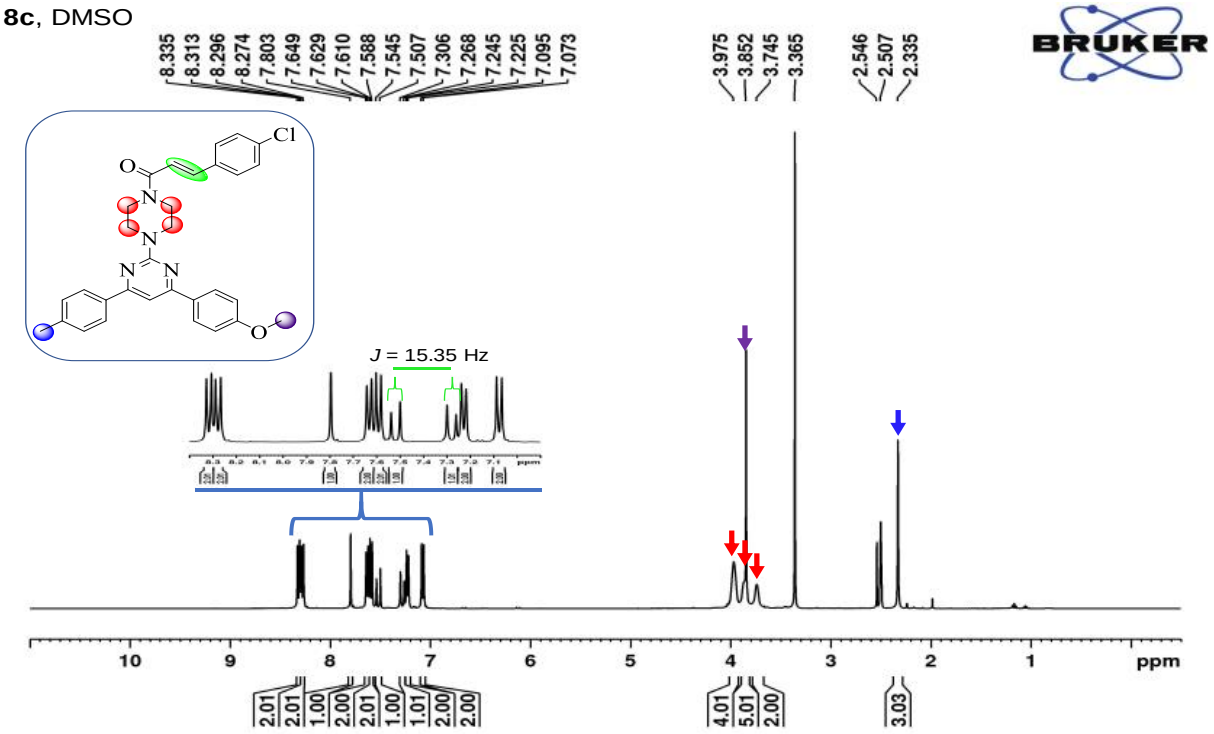

^{1}HNMR (400 MHz, $CDCl_3$)

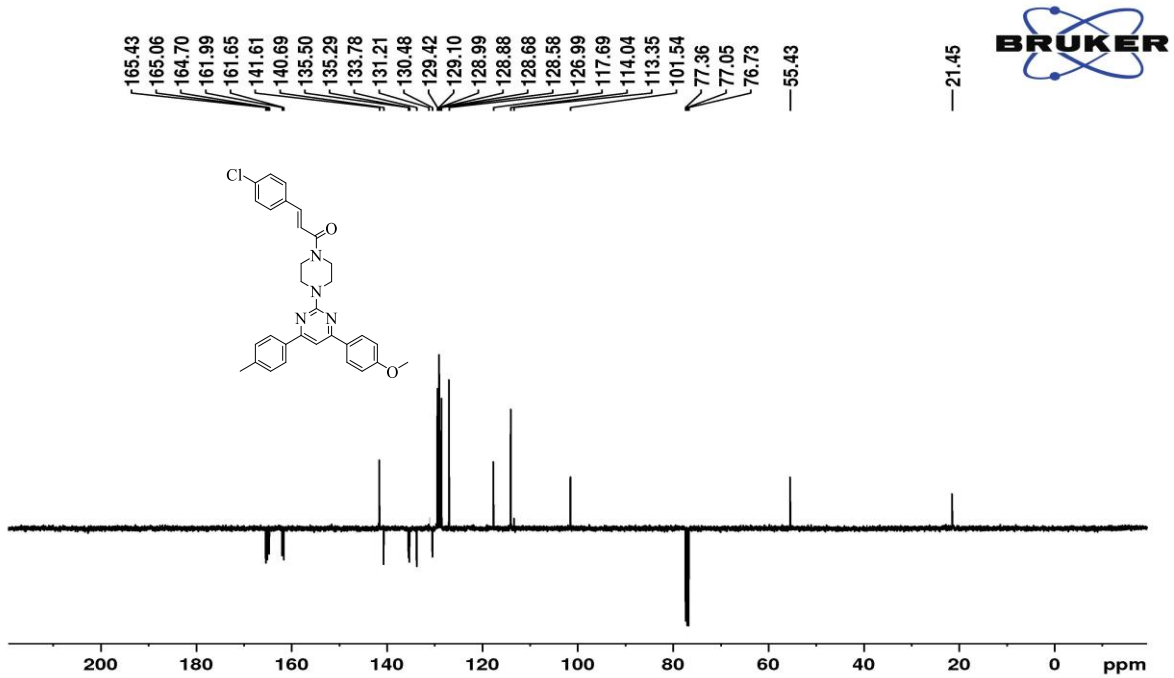

^{13}C NMR (100 MHz, $CDCl_3$)

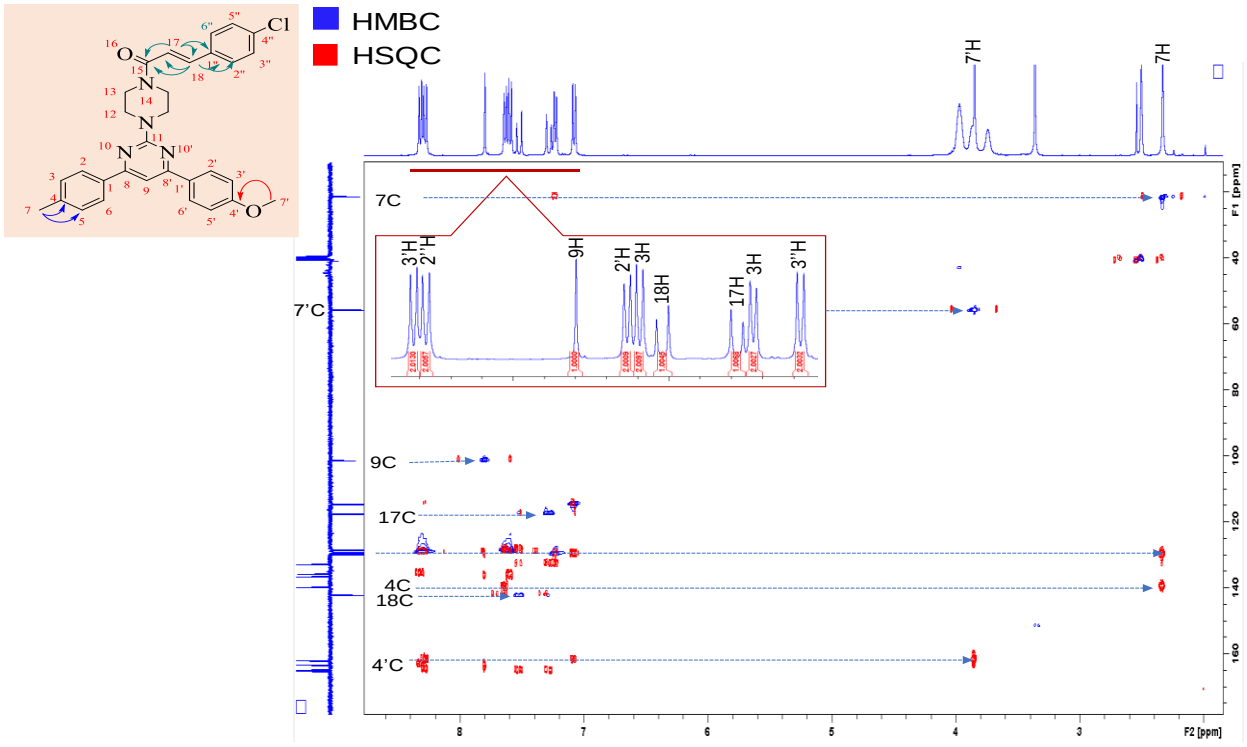

HMBC and HSQC spectra

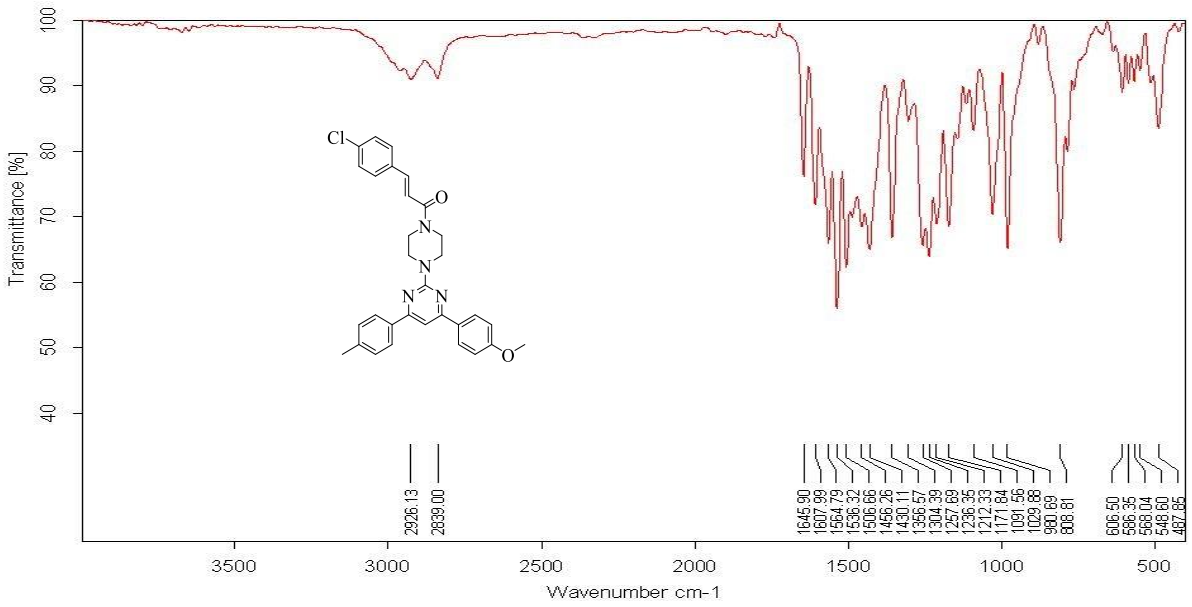

IR spectra

(E)-3-(3,4-dimethoxyphenyl)-1-(4-(4-(4-methoxyphenyl)-6-(p-tolyl)pyrimidin-2-yl)piperazin-1-yl)prop-2-en-1-one (**8e**):

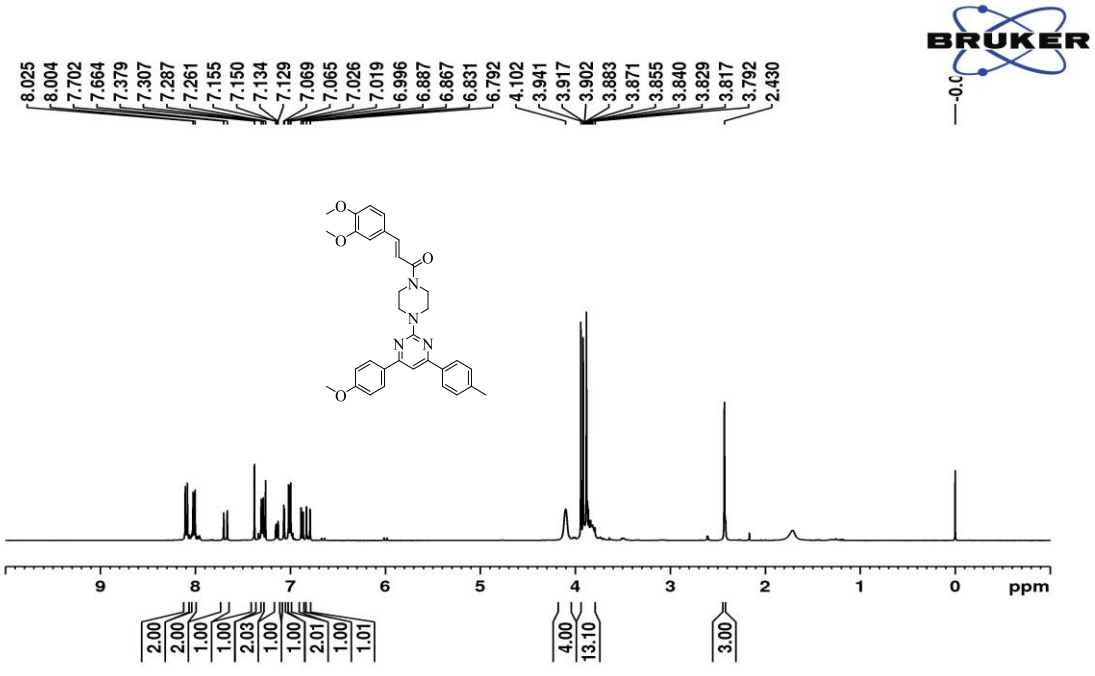

^{1}HNMR (400 MHz, $CDCl_3$)

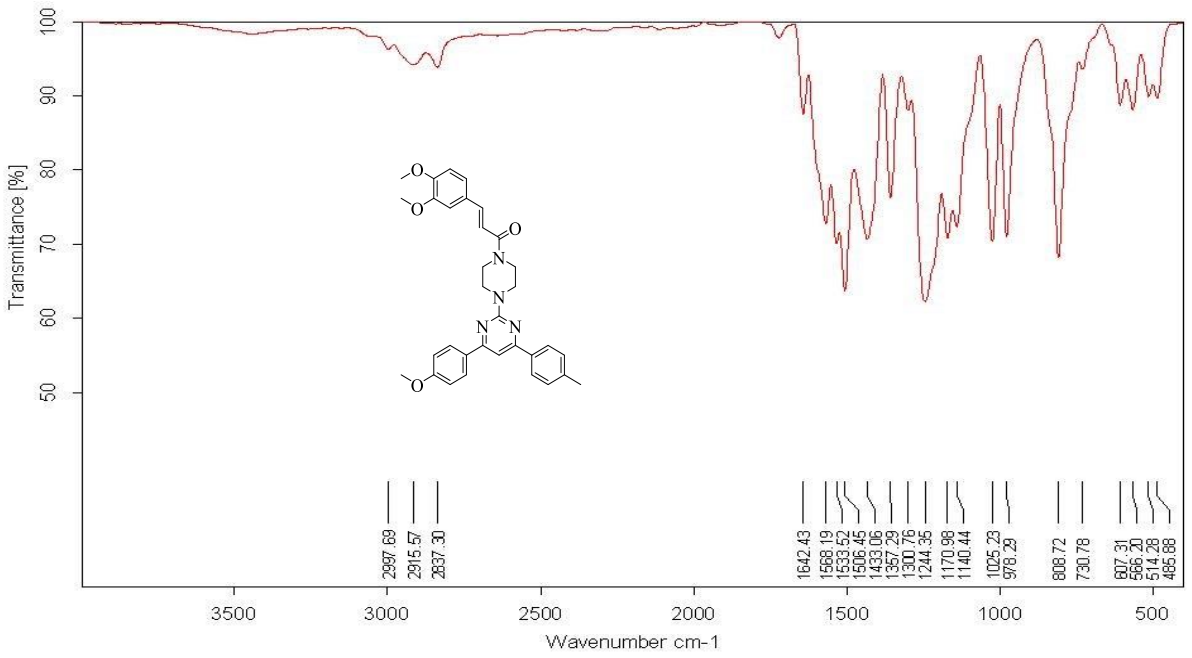

IR NMR spectra

(E)-1-(4-(4,6-bis(4-methoxyphenyl)pyrimidin-2-yl)piperazin-1-yl)-3-phenylprop-2-en-1-one (**8f**):

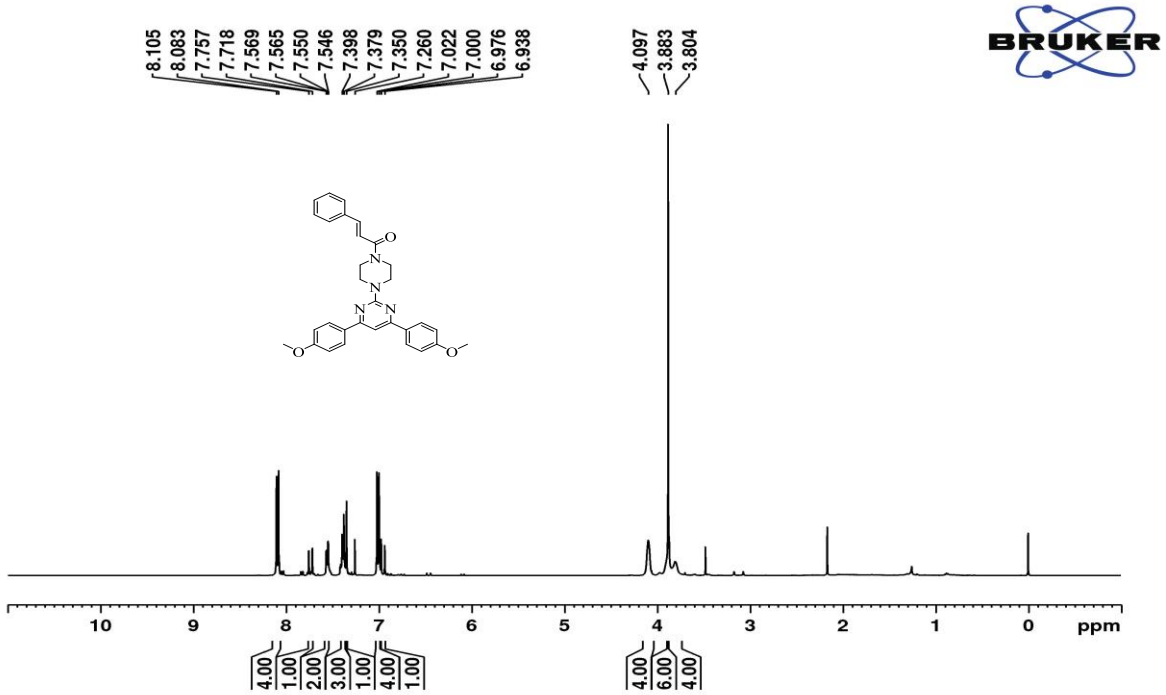

^{1}HNMR (400 MHz, $CDCl_3$)

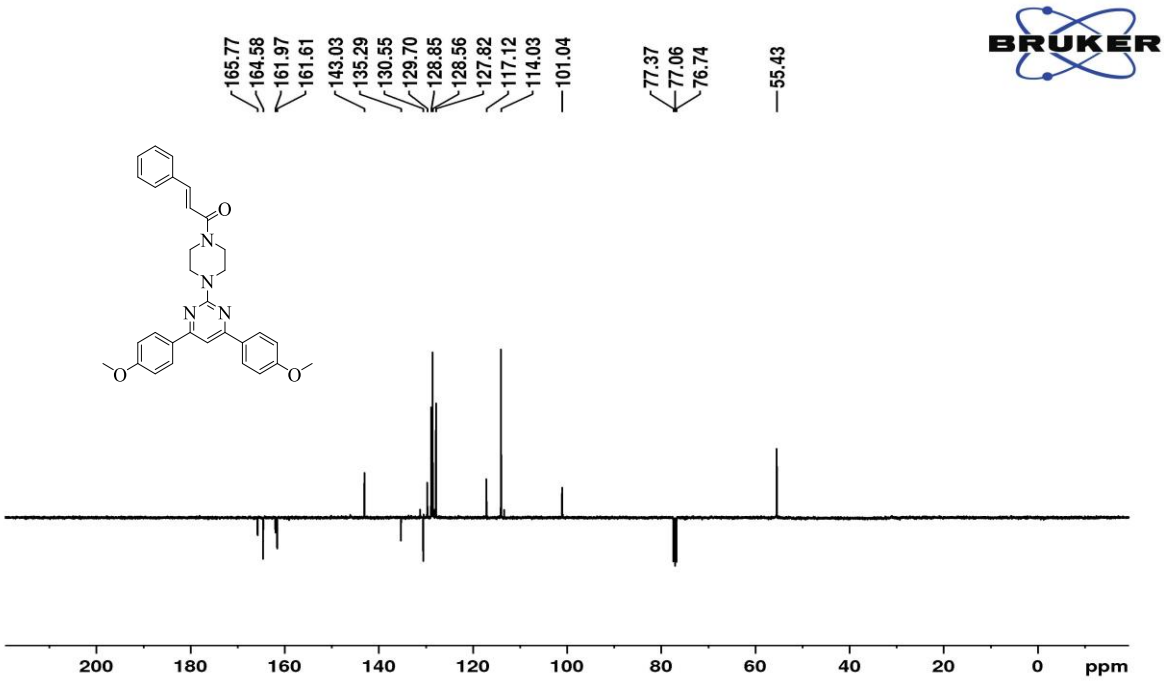

^{13}C NMR (100 MHz, $CDCl_3$)

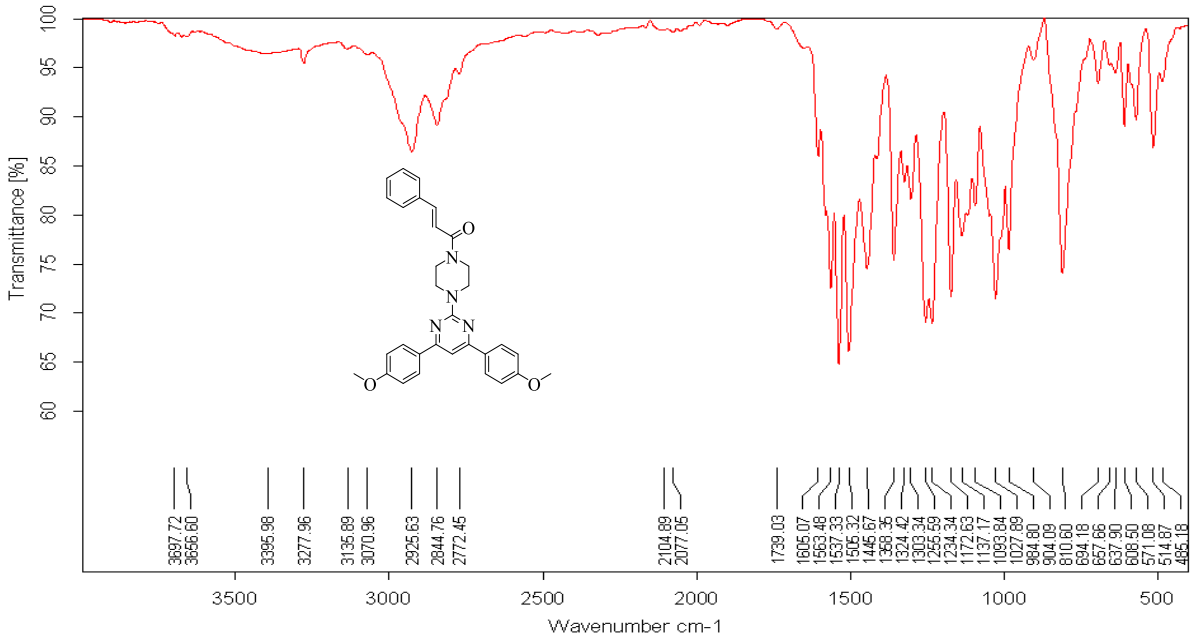

IR spectra

(E)-1-(4-(4,6-bis(4-methoxyphenyl)pyrimidin-2-yl)piperazin-1-yl)-3-(4-chlorophenyl)prop-2-en-1-one (**8g**):

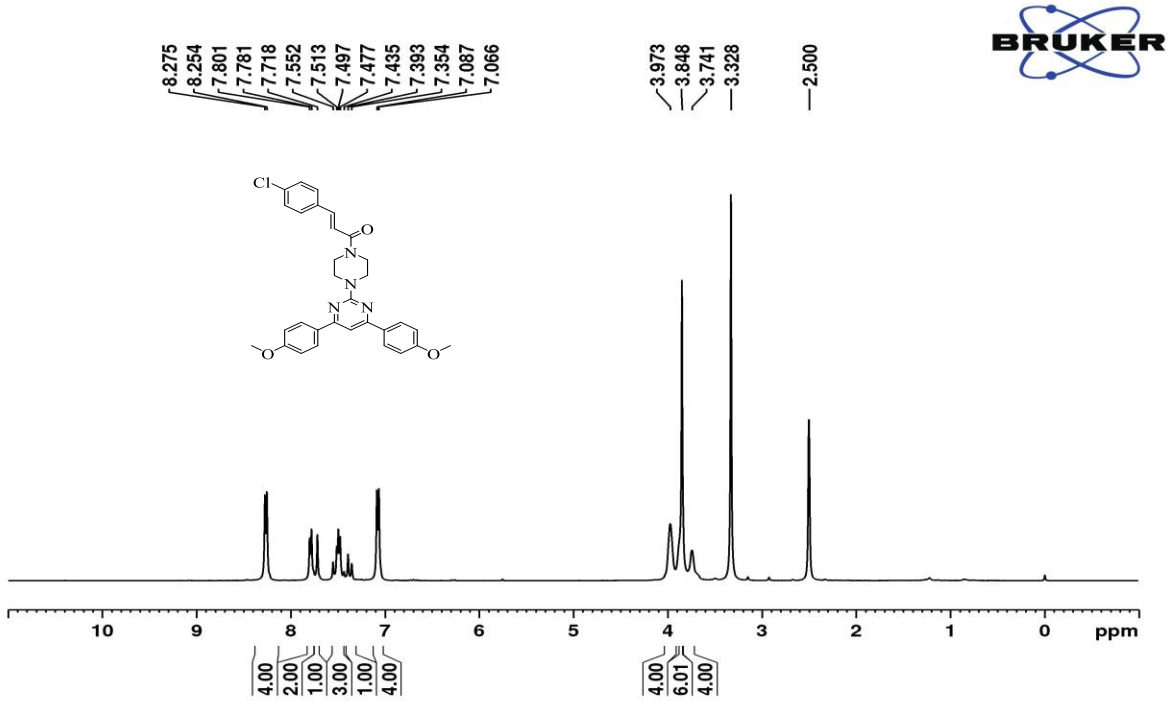

^{1}H NMR (400 MHz, DMSO-d$_6$)

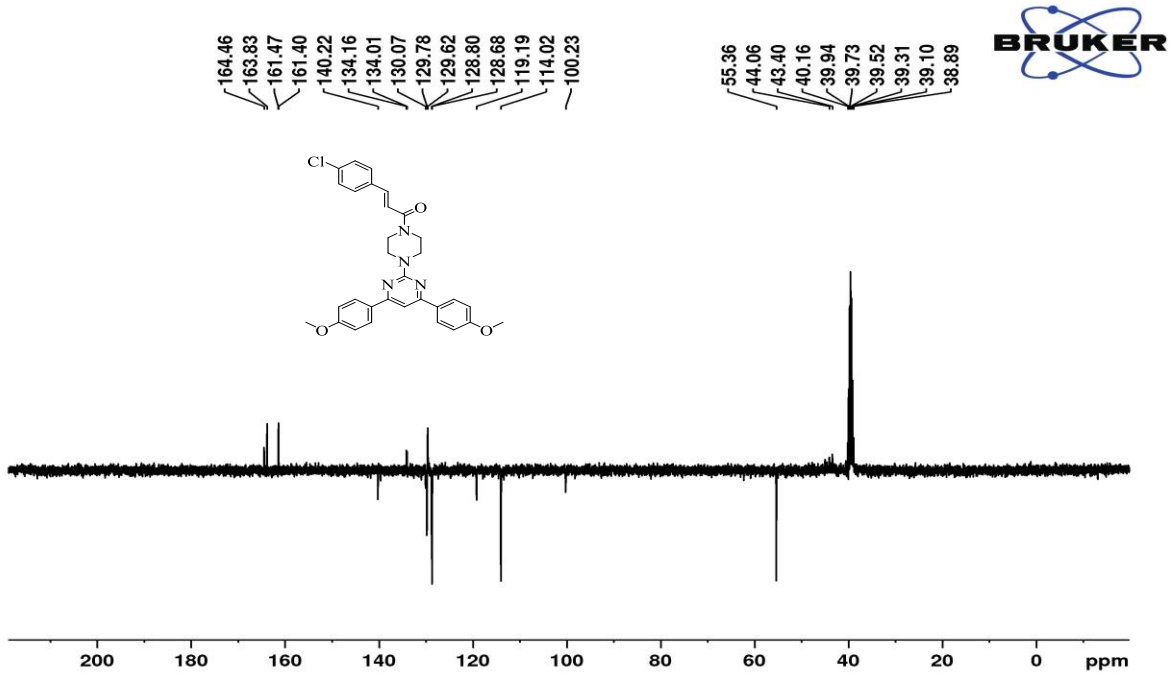

^{13}C NMR (100 MHz, DMSO-d$_6$)

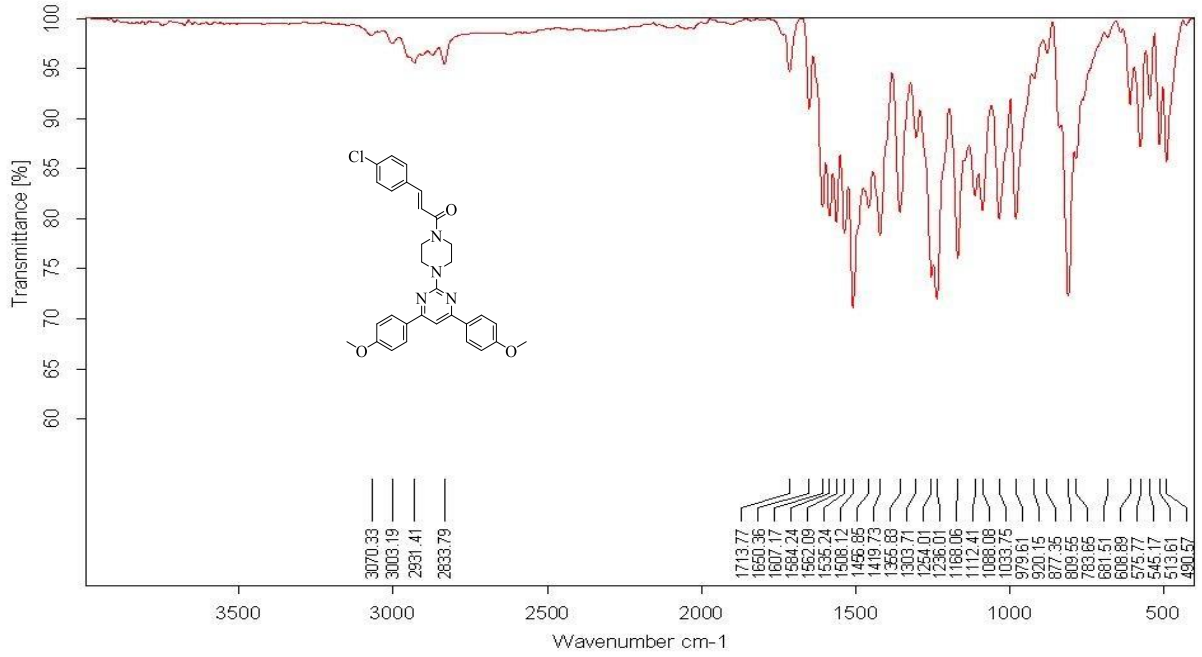

IR spectra

(E)-1-(4-(4,6-bis(4-methoxyphenyl)pyrimidin-2-yl)piperazin-1-yl)-3-(p-tolyl)prop-2-en-1-one (**8h**):

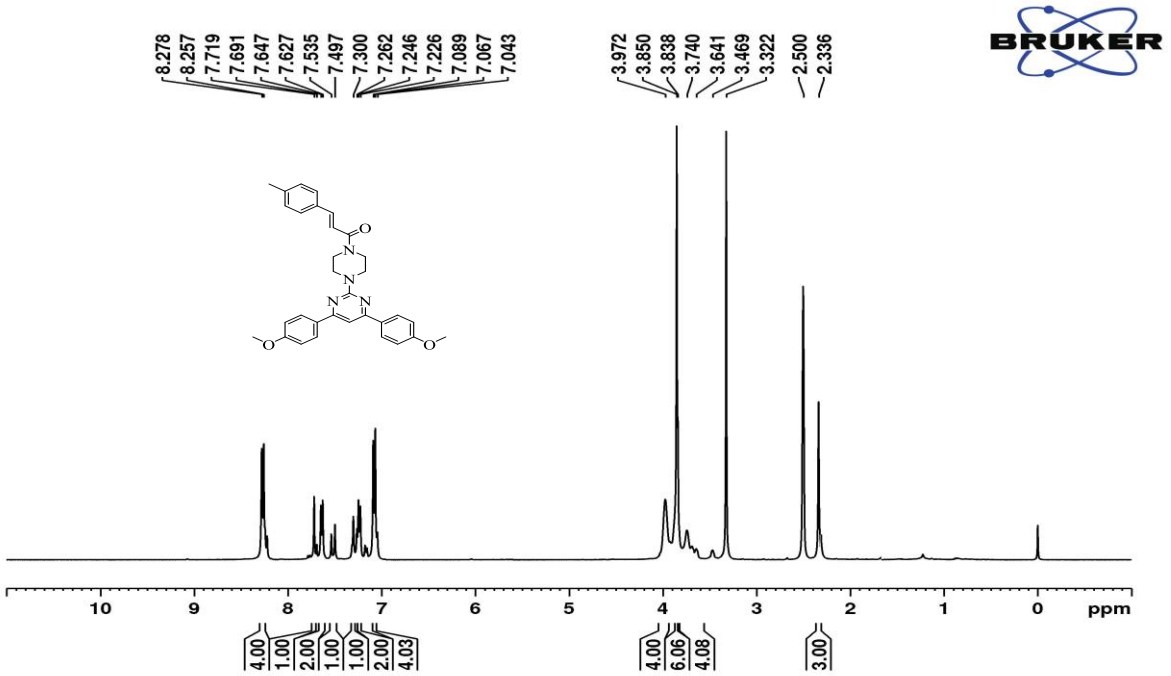

^{1}H NMR (400 MHz, DMSO-d_6)

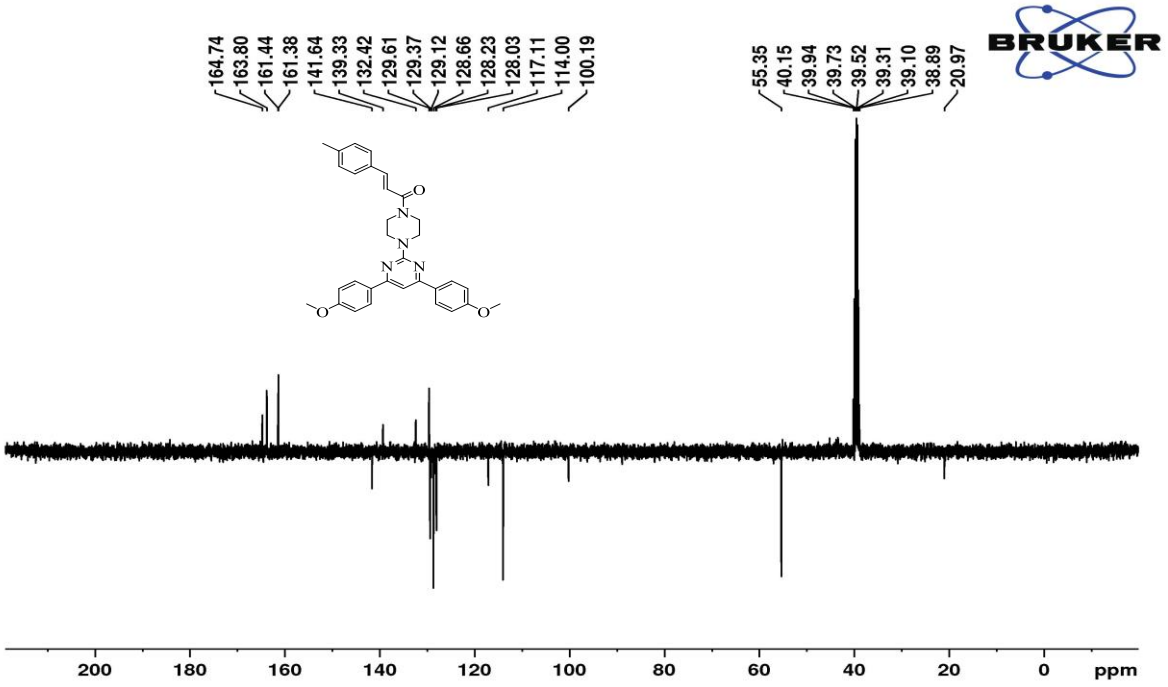

^{13}C NMR (100 MHz, DMSO-d$_6$)

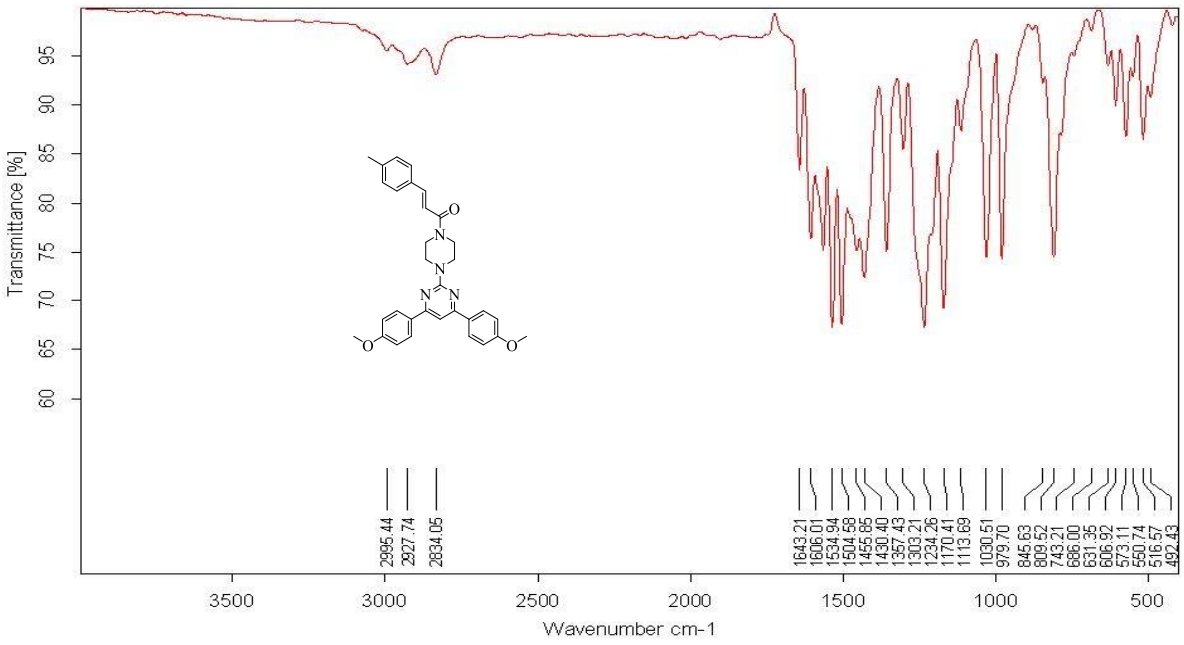

IR spectra

(E)-1-(4-(4,6-bis(4-methoxyphenyl)pyrimidin-2-yl)piperazin-1-yl)-3-(4-methoxyphenyl)prop-2-en-1-one (**8i**):

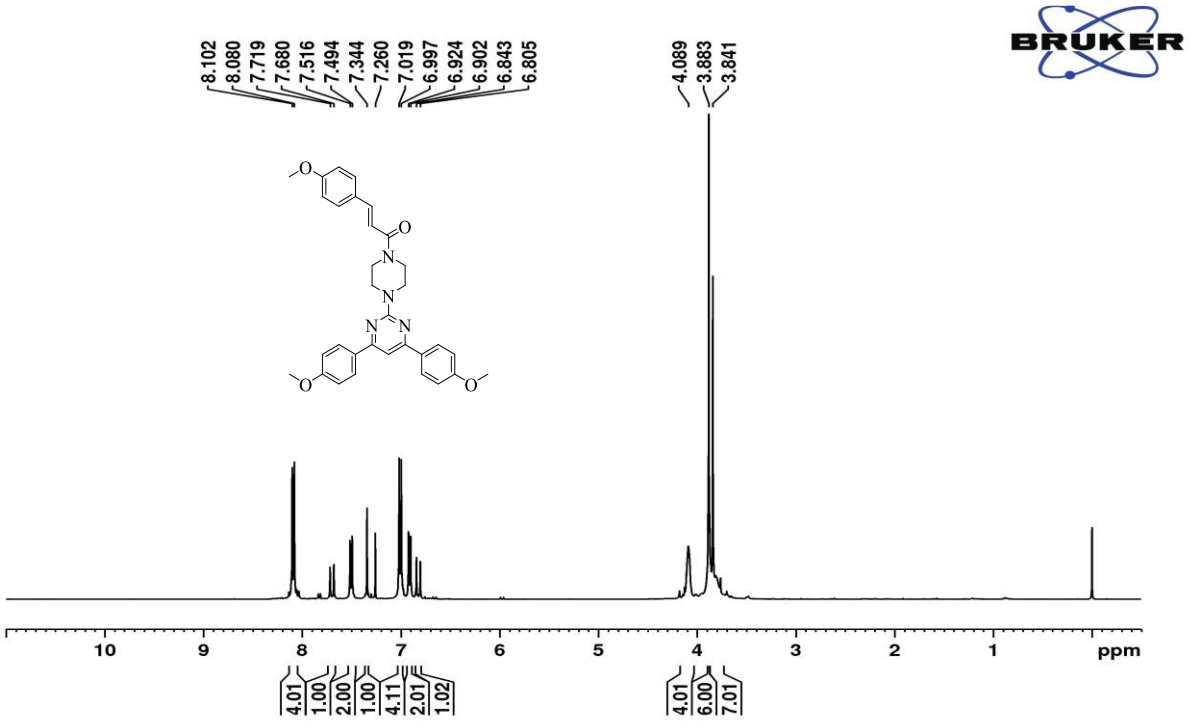

^{1}H NMR (400 MHz, $CDCl_3$)

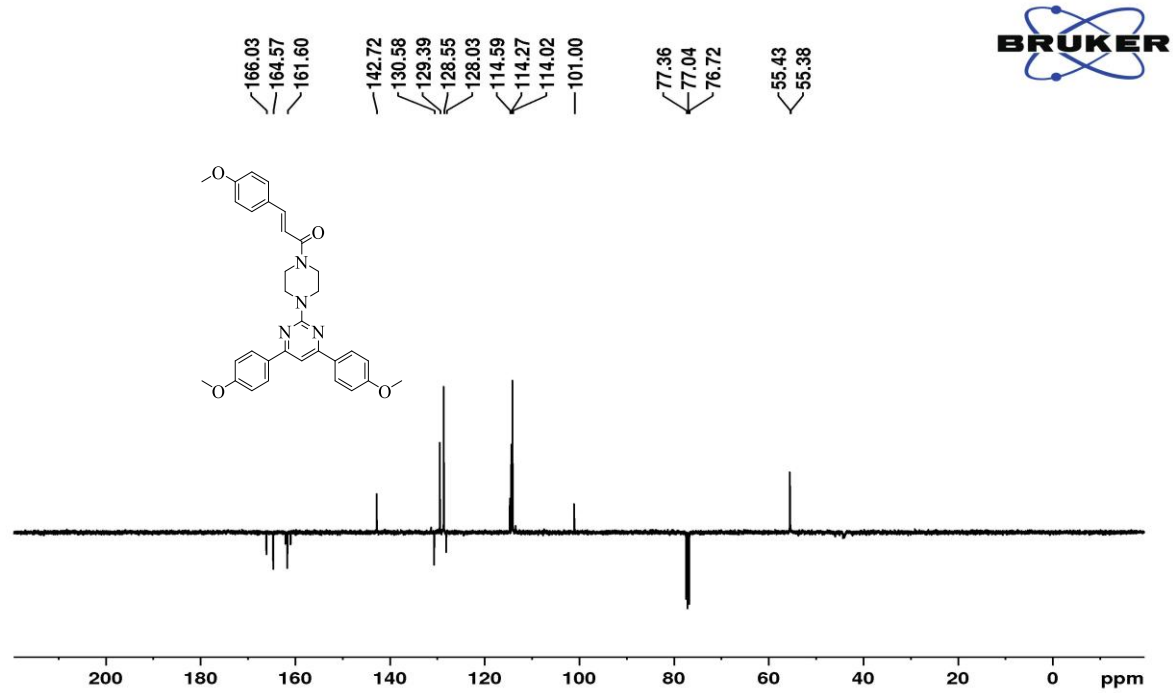

^{13}C NMR (100 MHz, $CDCl_3$)

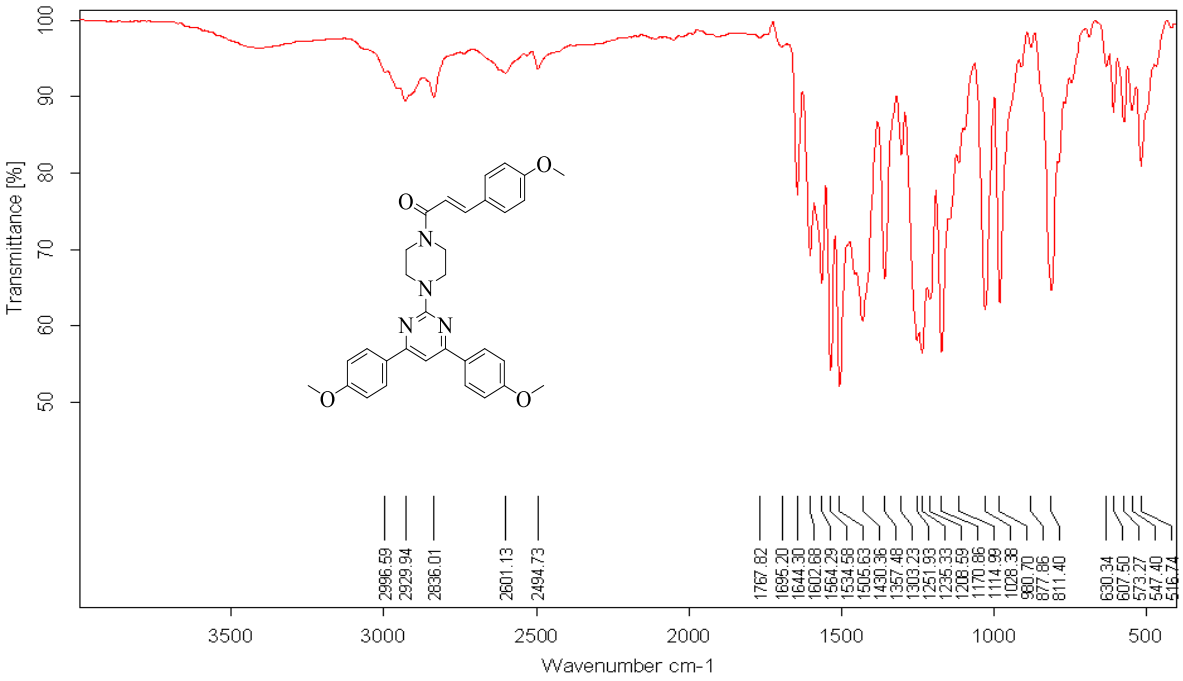

IR spectra

(E)-1-(4-(4,6-bis(4-methoxyphenyl)pyrimidin-2-yl)piperazin-1-yl)-3-(3,4-dimethoxyphenyl)prop-2-en-1-one (**8j**):

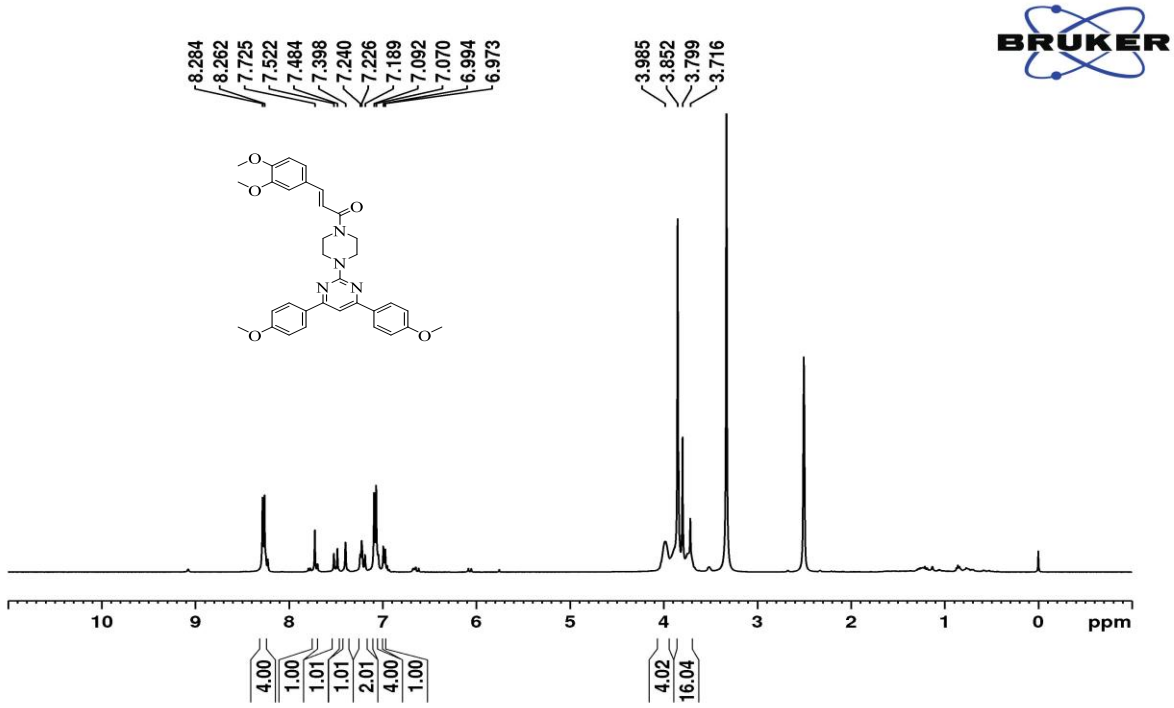

^{1}H NMR **(**400 MHz, DMSO-d$_6$)

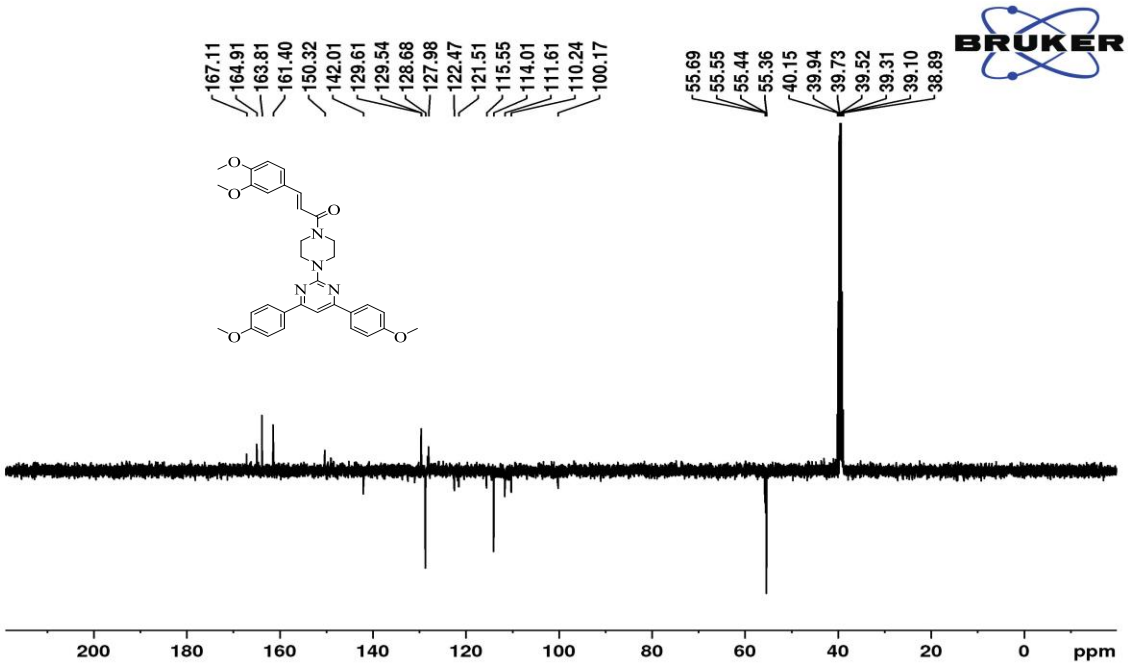

^{13}CNMR (100 MHz, DMSO-d_6)

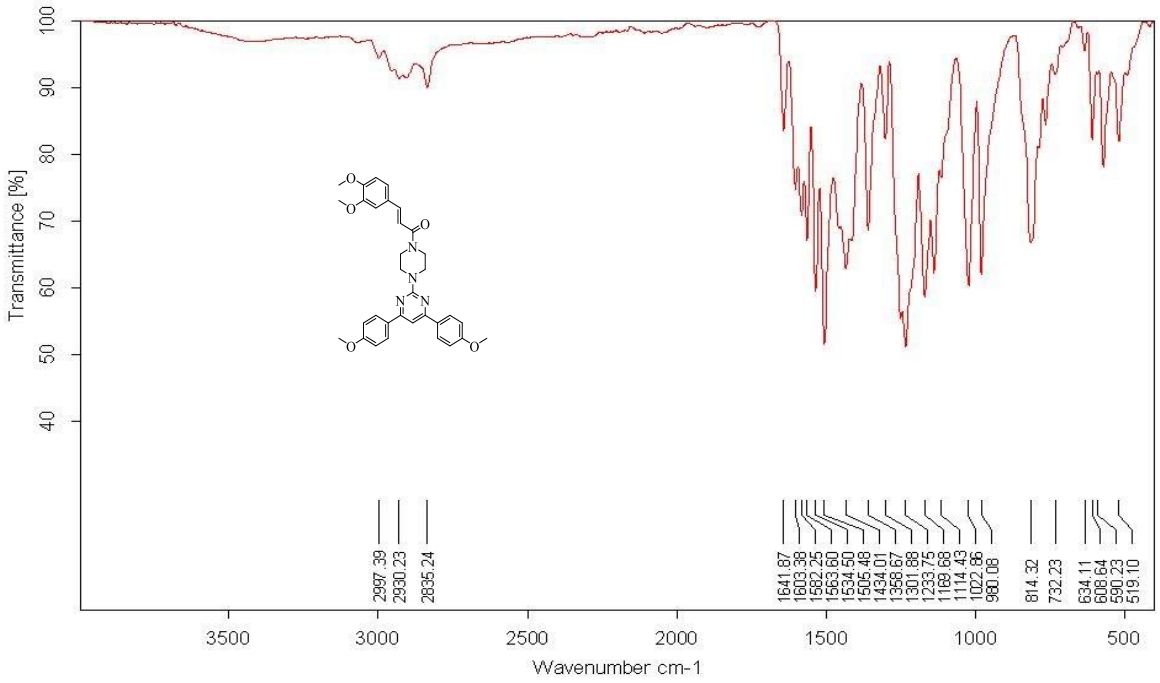

IR spectra

(E)-1-(4-(4,6-bis(4-methoxyphenyl)pyrimidin-2-yl)piperazin-1-yl)-3-(furan-2-yl)prop-2-en-1-one (**8k**):

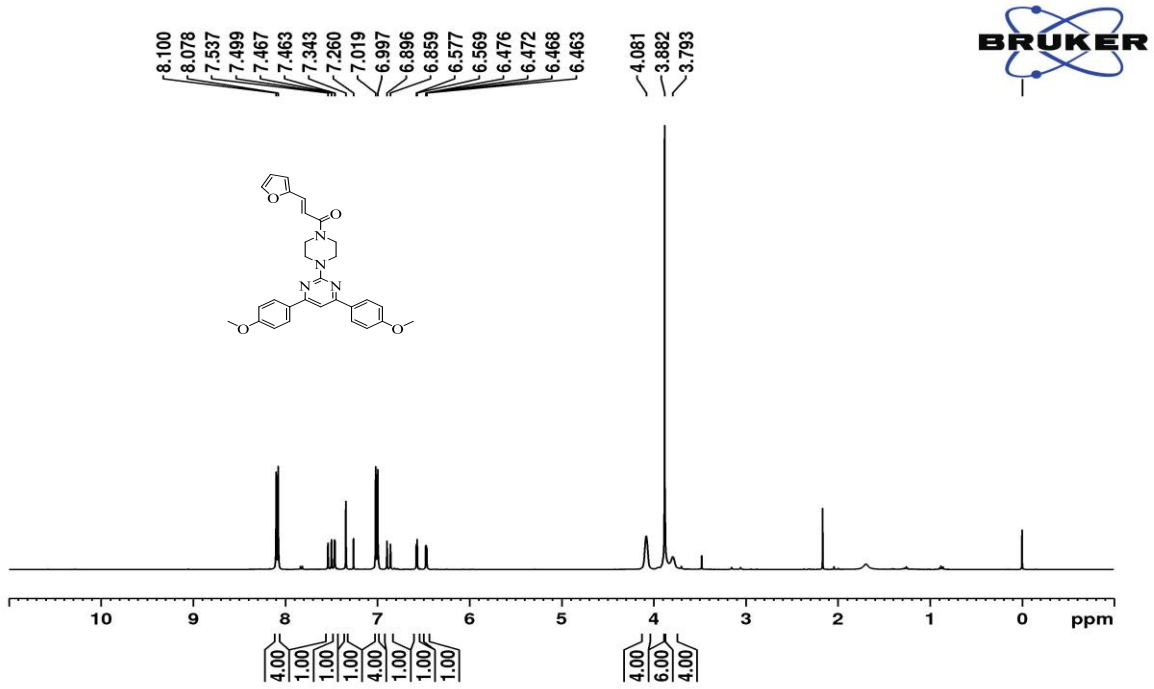

^{1}H NMR (100 MHz, $CDCl_3$)

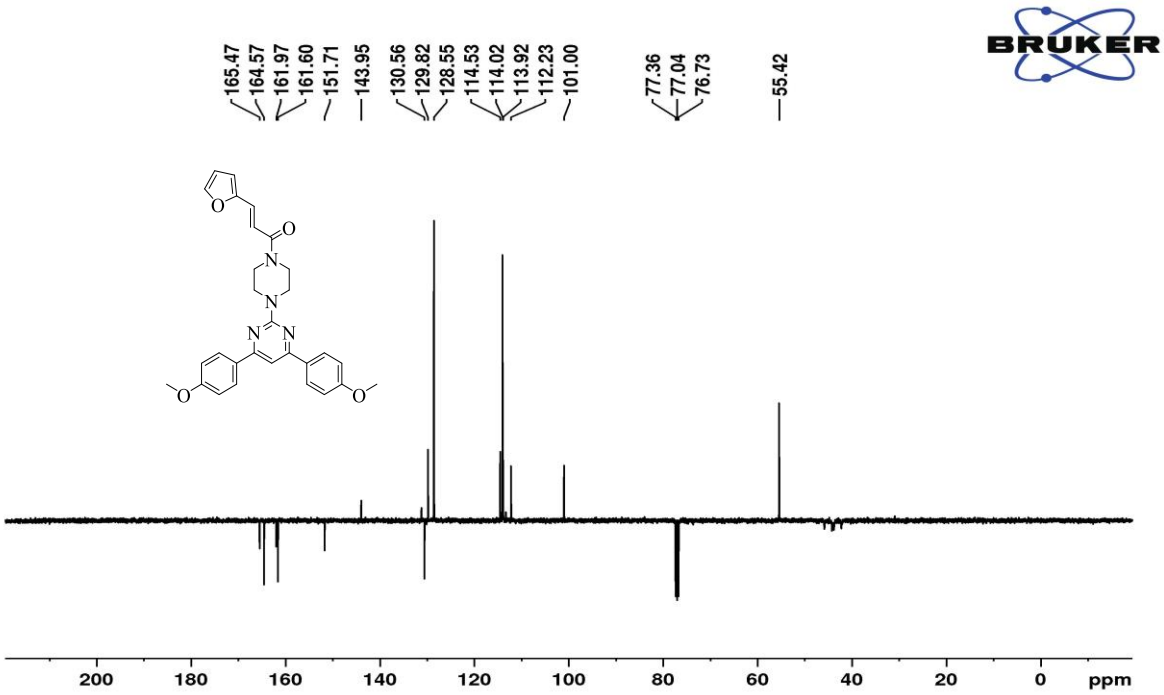

^{13}C NMR (100 MHz, $CDCl_3$)

Elemental Composition Report **Page 1**

Single Mass Analysis
Tolerance = 5.0 PPM / DBE: min = -1.5, max = 50.0
Element prediction: Off
Number of isotope peaks used for i-FIT = 3

Monoisotopic Mass, Even Electron Ions
13 formula(e) evaluated with 1 results within limits (all results (up to 1000) for each mass)
Elements Used:
C: 25-30 H: 25-30 N: 0-5 O: 0-5 Na: 1-1
FK6 4 (0.102) Cm (1:61)
TOF MS ES+

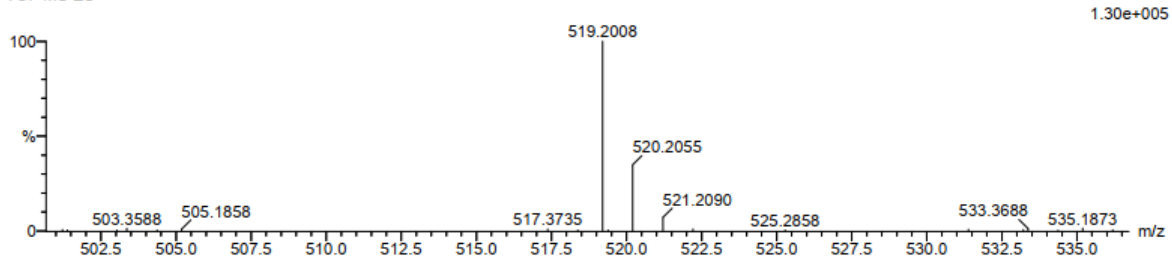

Minimum:				-1.5			
Maximum:		5.0	5.0	50.0			
Mass	Calc. Mass	mDa	PPM	DBE	i-FIT	i-FIT (Norm)	Formula
519.2008	519.2008	0.0	0.0	17.5	29.1	0.0	C29 H28 N4 O4 Na

HRMS spectra

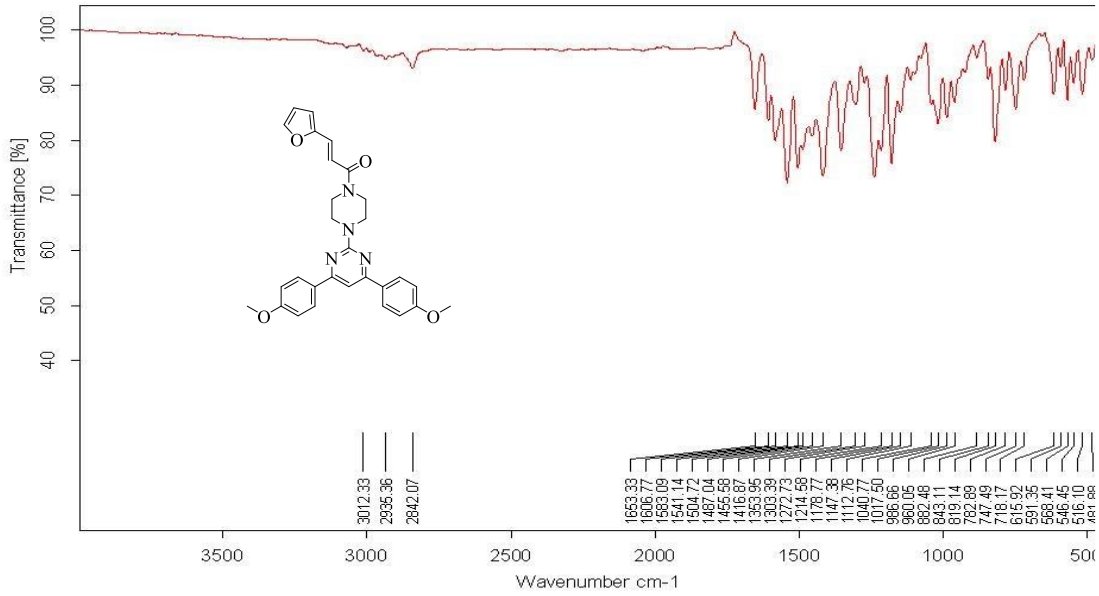

IR spectra

(E)-1-(4-(4-(3,4-dimethoxyphenyl)-6-(4-ethylphenyl)pyrimidin-2-yl)piperazin-1-yl)-3-phenylprop-2-en-1-one (**8l**):

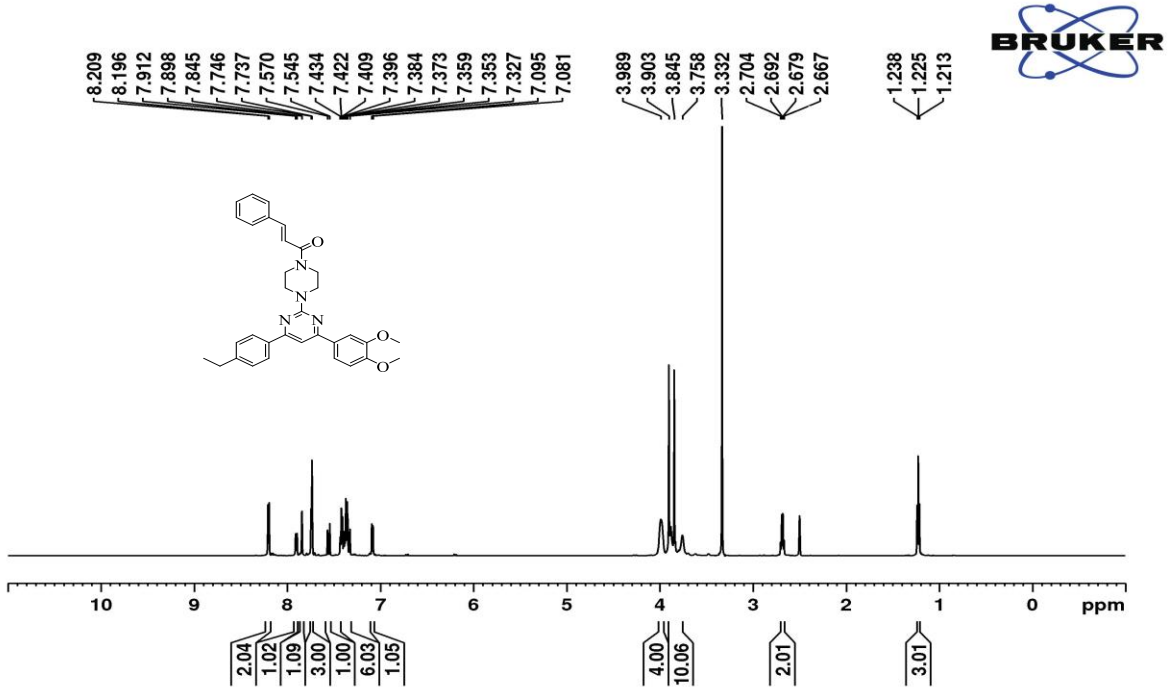

^{1}H NMR (400 MHz, DMSO-d$_6$)

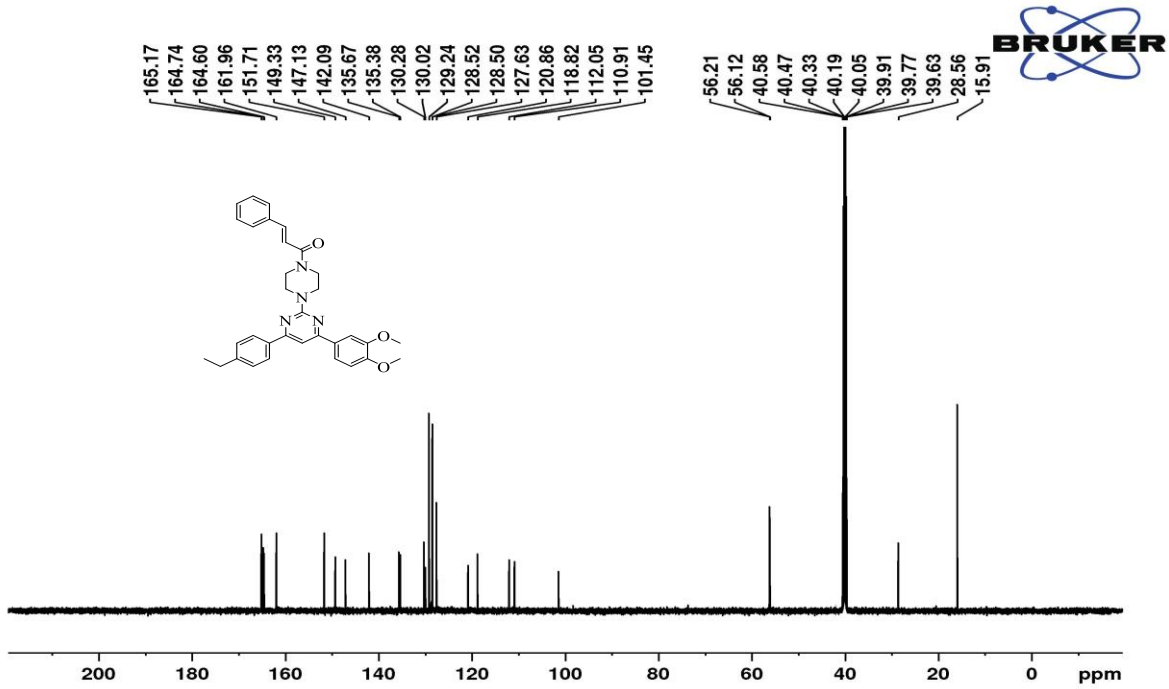

^{13}C NMR (100 MHz, DMSO-d$_6$)

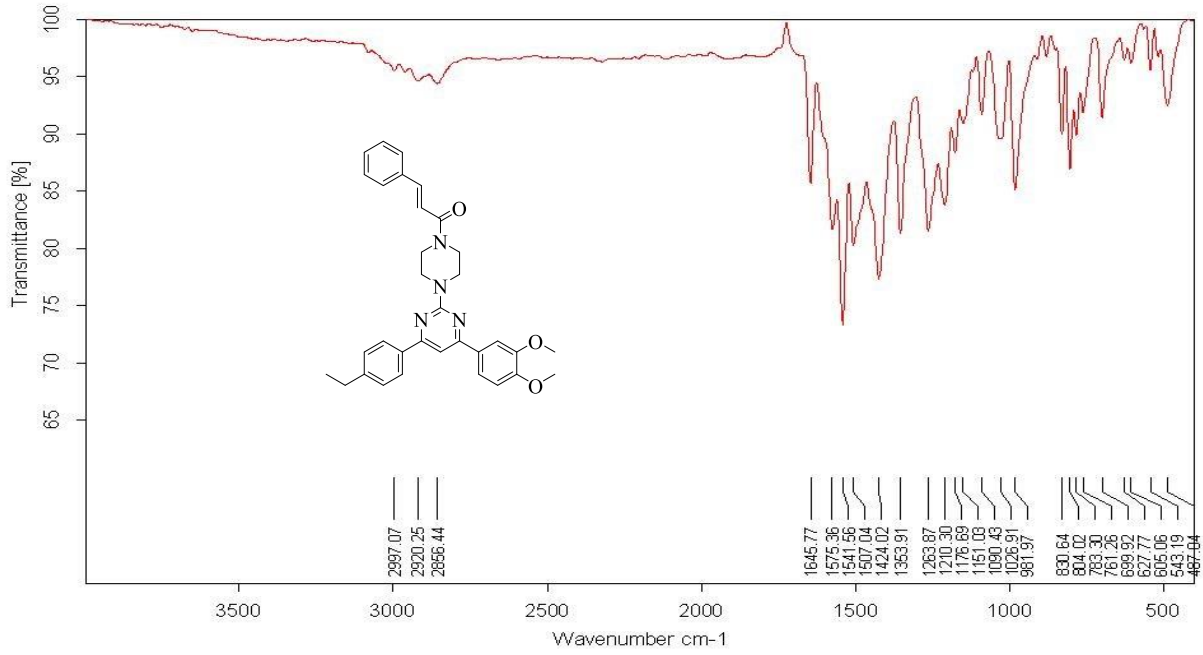

IR spectra

(E)-3-(4-chlorophenyl)-1-(4-(4-(3,4-dimethoxyphenyl)-6-(4-ethylphenyl)pyrimidin-2-yl)piperazin-1-yl)prop-2-en-1-one (**8m**):

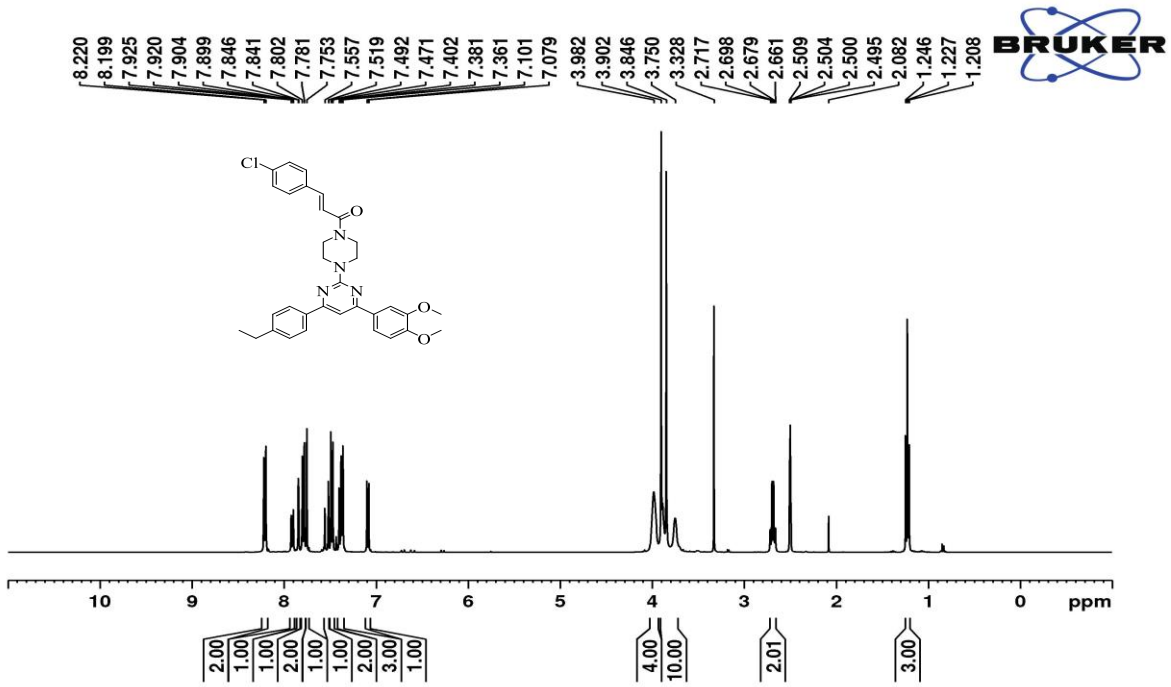

^{1}H NMR (400 MHz, DMSO-d_6)

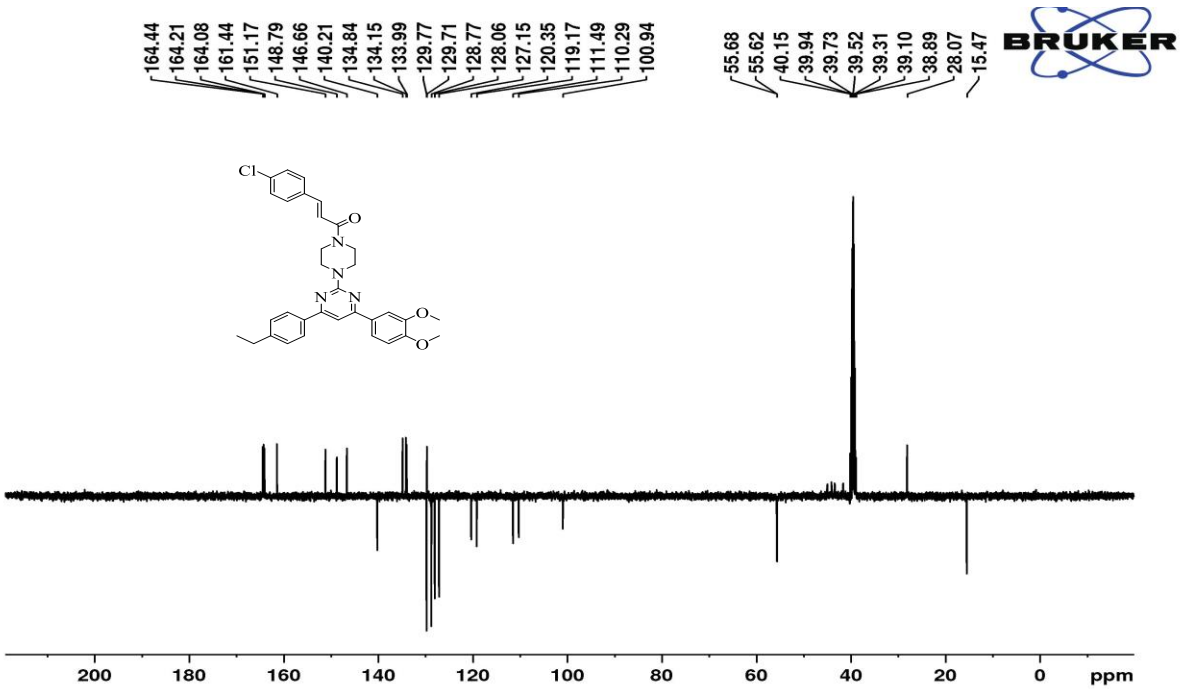

^{13}C NMR (100 MHz, DMSO-d$_6$)

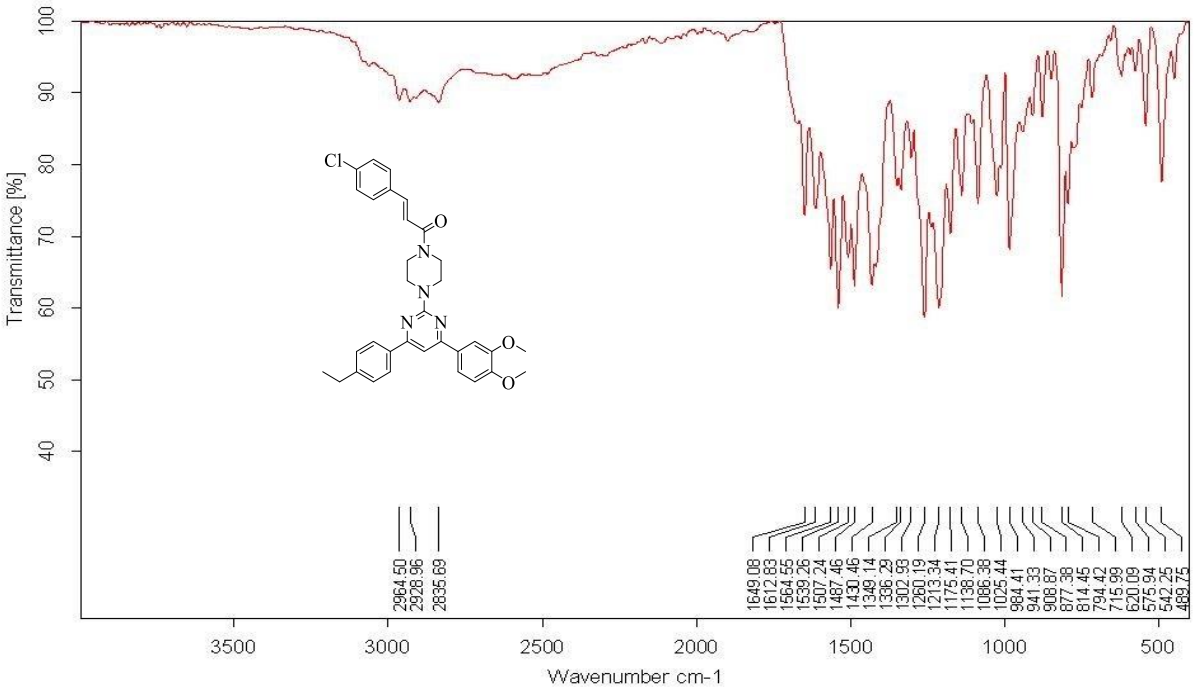

IR spectra

(E)-1-(4-(4-(3,4-dimethoxyphenyl)-6-(4-ethylphenyl)pyrimidin-2-yl)piperazin-1-yl)-3-(p-tolyl)prop-2-en-1-one (**8n**):

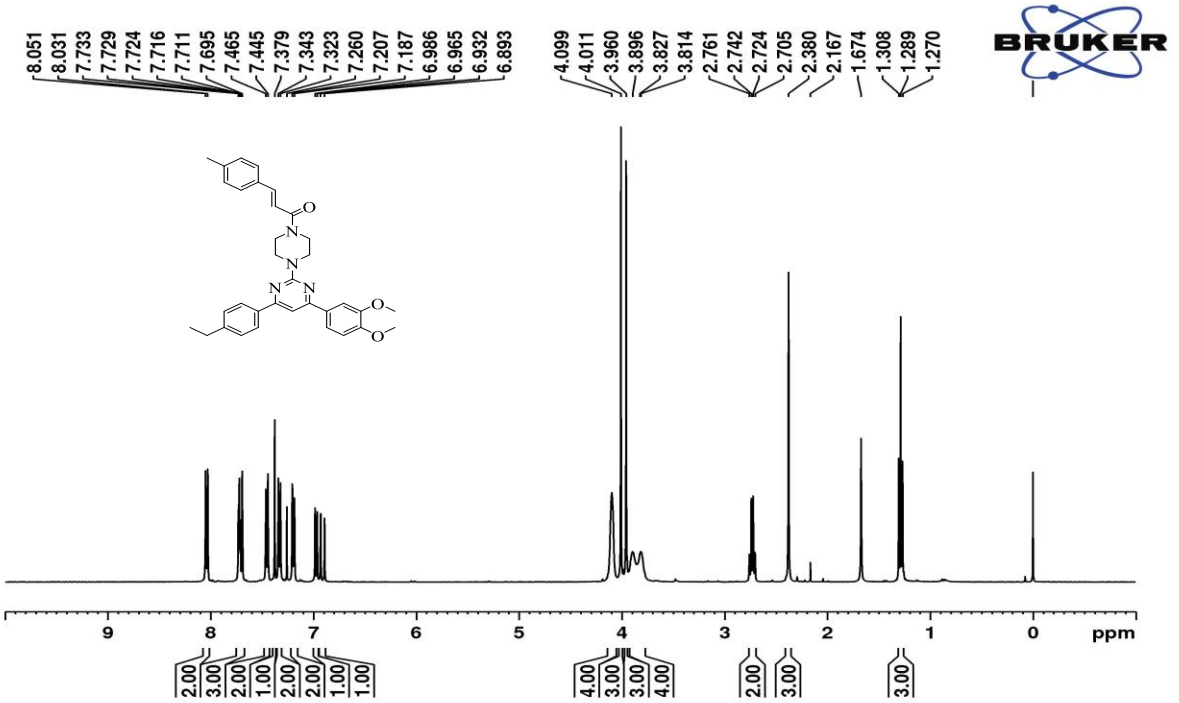

^{1}H NMR (400 MHz, $CDCl_3$)

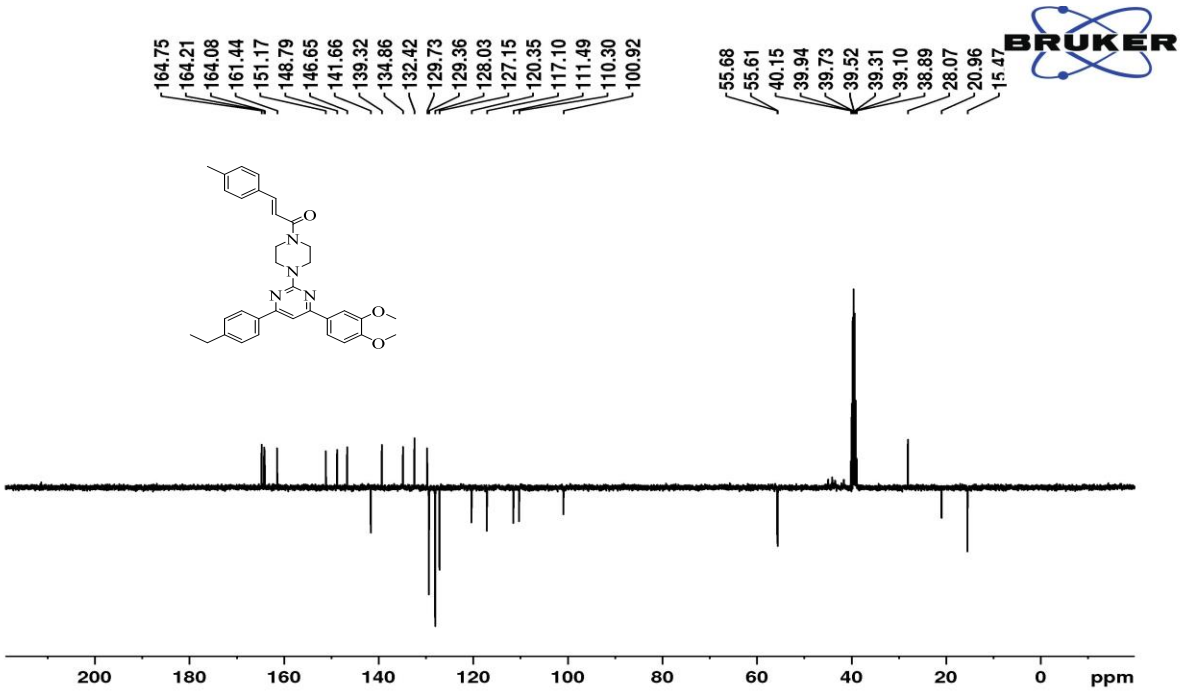

^{13}C NMR (100 MHz, $CDCl_3$)

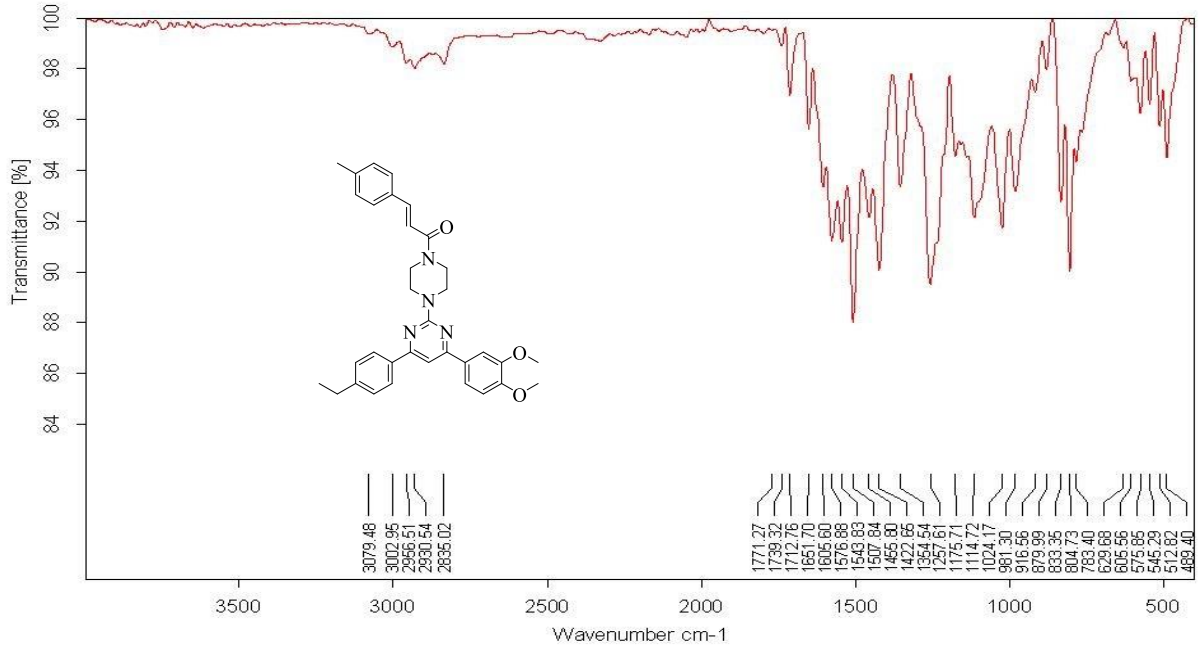

IR spectra

(E)-1-(4-(4-(3,4-dimethoxyphenyl)-6-(4-ethylphenyl)pyrimidin-2-yl)piperazin-1-yl)-3-(4-methoxyphenyl)prop-2-en-1-one (**8o)**:

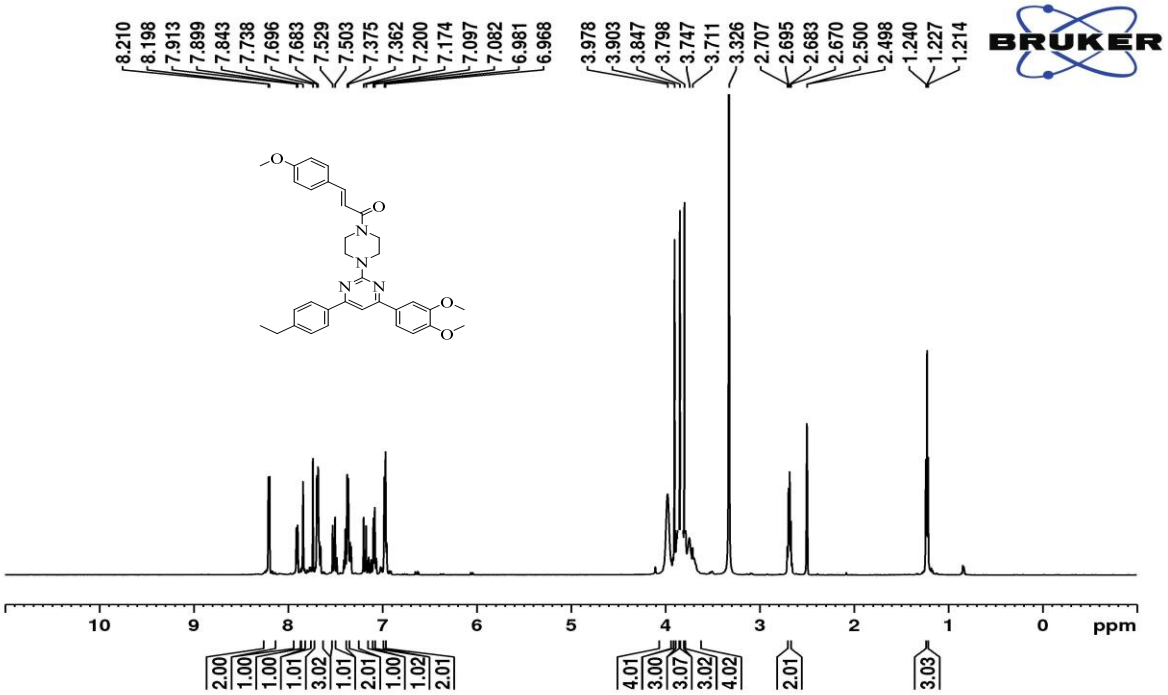

^{1}H NMR (400 MHz, $CDCl_3$)

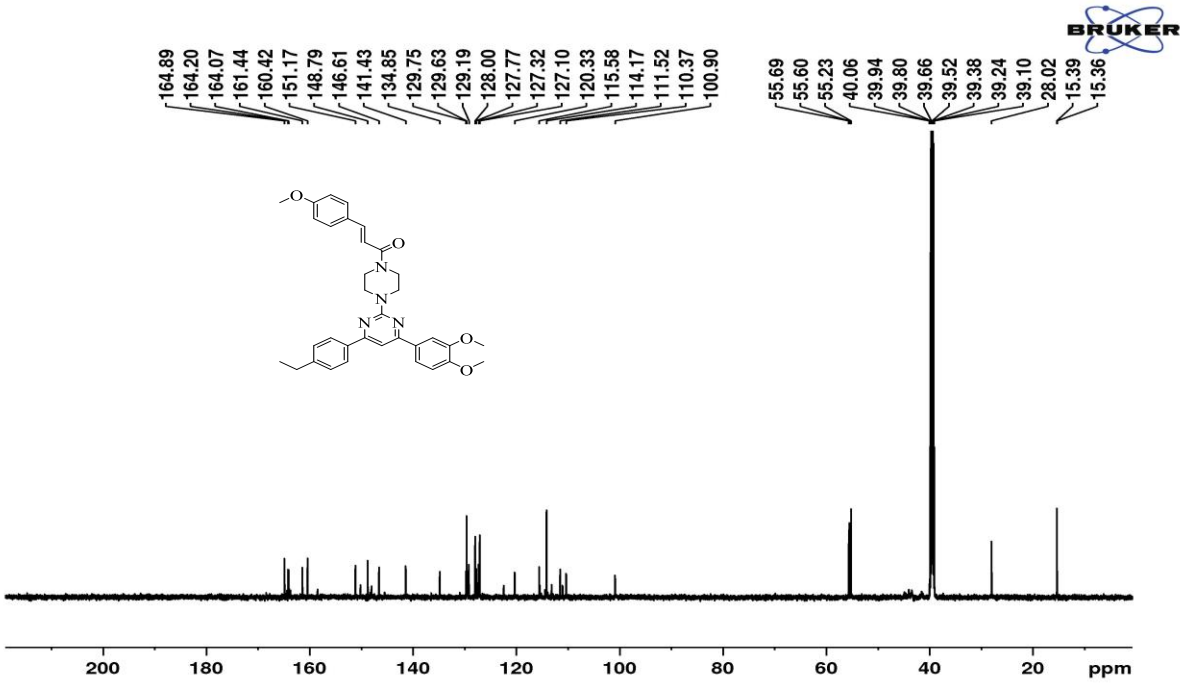

^{13}C NMR (100 MHz, $CDCl_3$)

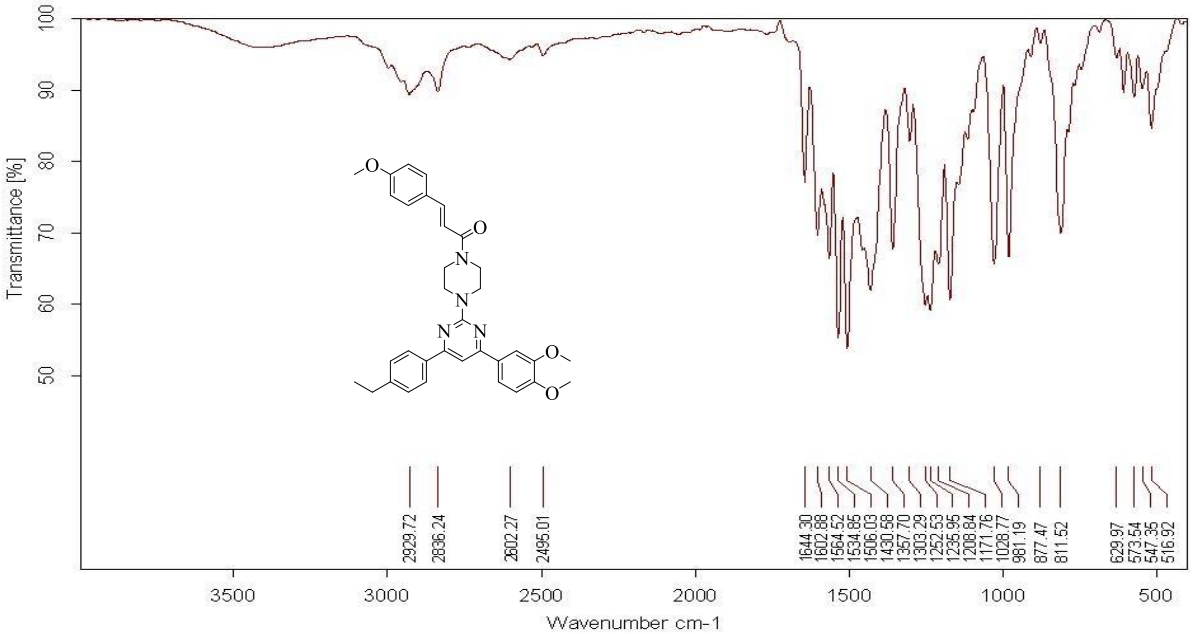

IR spectra

(E)-1-(4-(4-(3,4-dimethoxyphenyl)-6-(4-ethylphenyl)pyrimidin-2-yl)piperazin-1-yl)-3-(furan-2-yl)prop-2-en-1-one (**8p**):

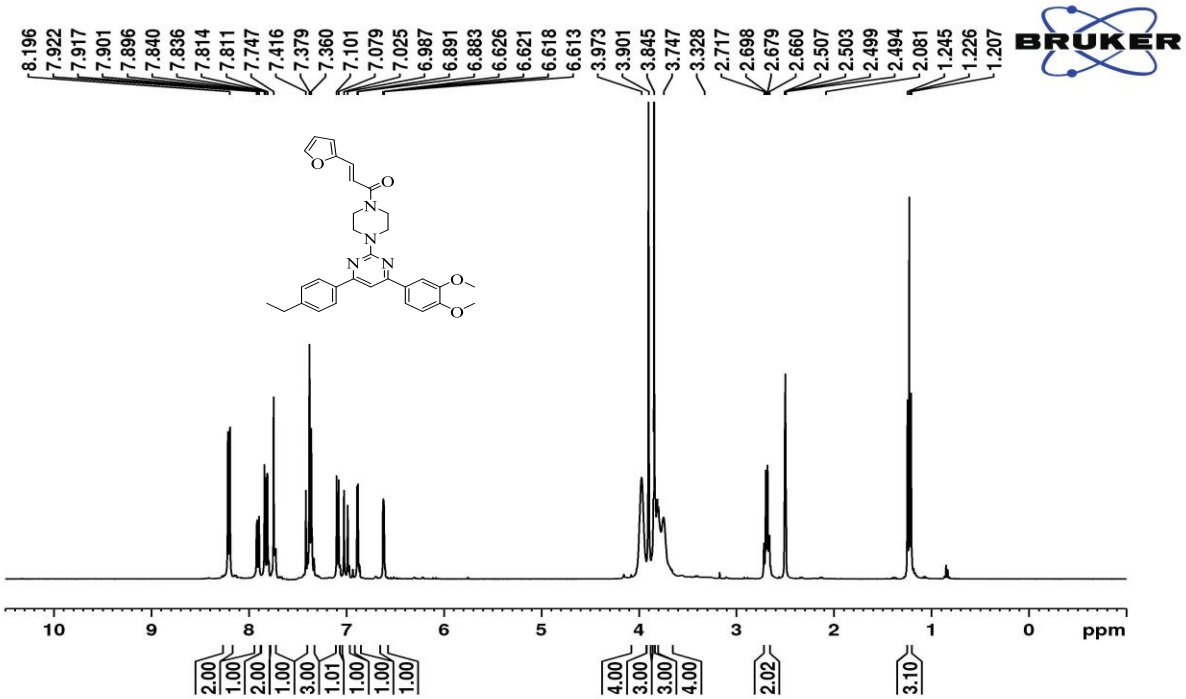

^{1}H NMR **(**400 MHz, DMSO-d$_6$**)**

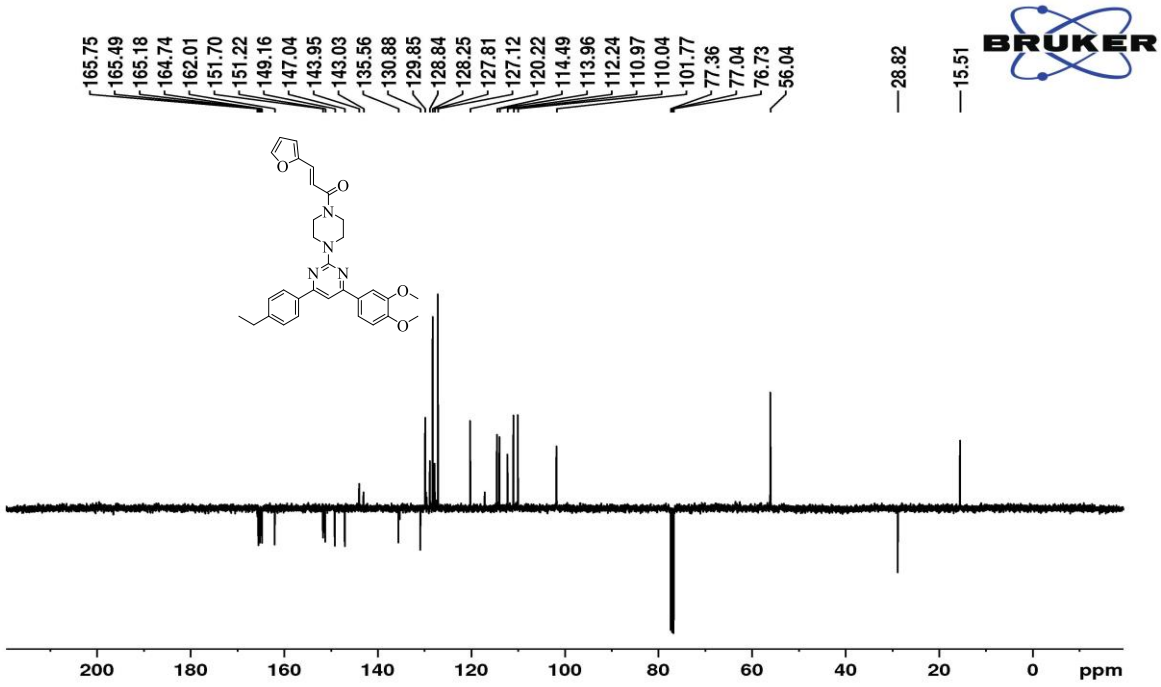

^{13}C NMR (100 MHz, DMSO-d$_6$**)**

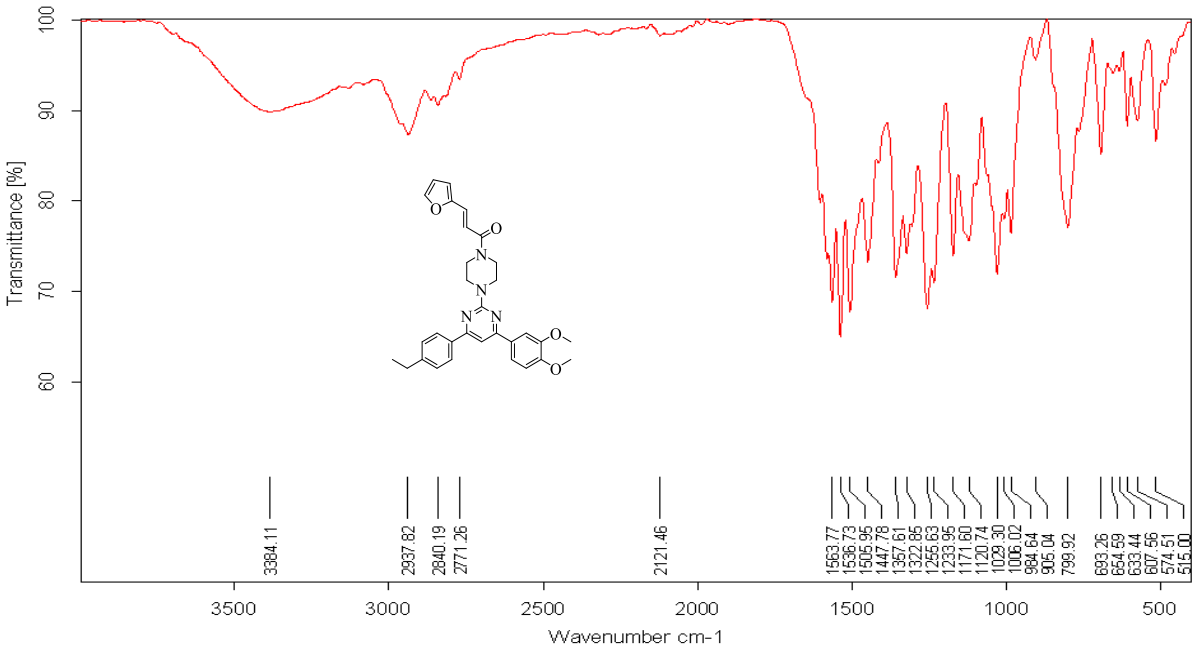

IR spectra

(E)-1-(4-(4-(4-chlorophenyl)-6-(pyridin-3-yl)pyrimidin-2-yl)piperazin-1-yl)-3-(p-tolyl)prop-2-en-1-one (**8q**):

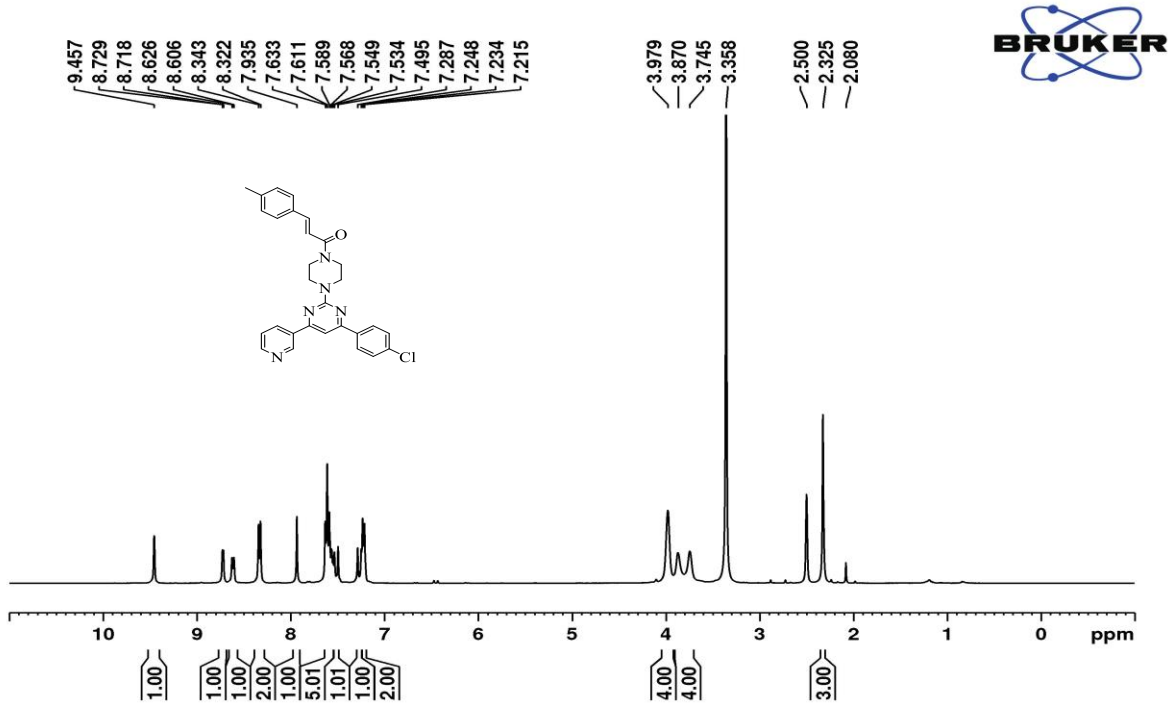

^{1}H NMR (400 MHz, DMSO-d$_6$)

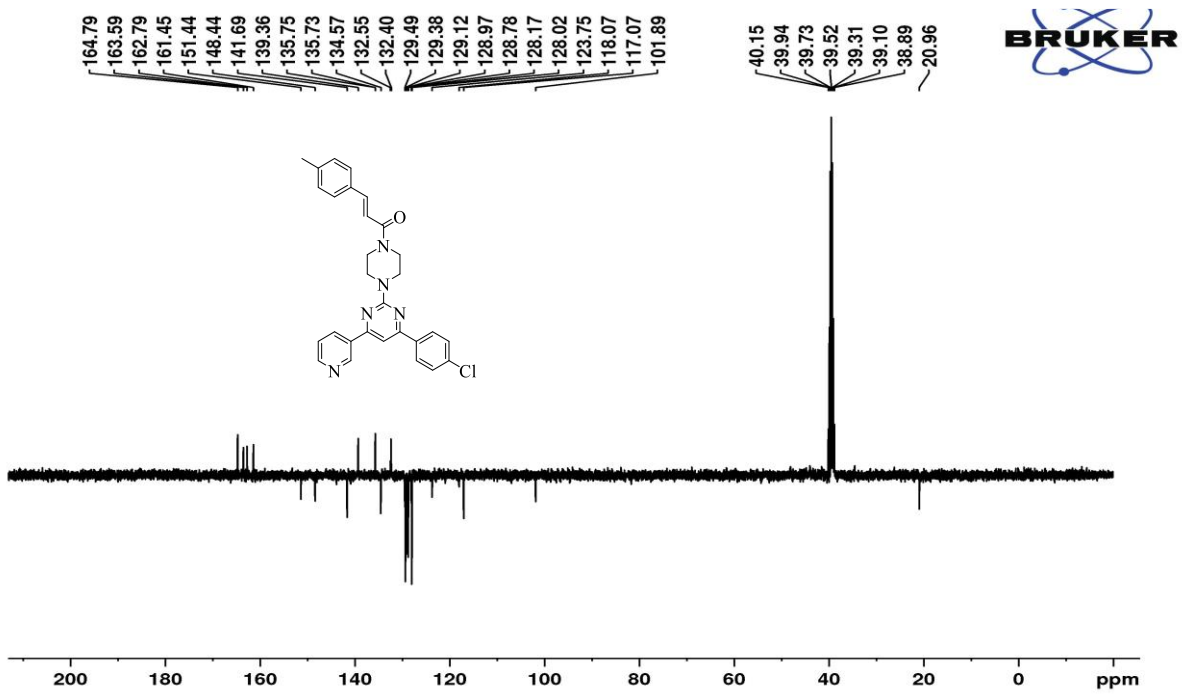

^{13}C NMR (100 MHz, DMSO-d$_6$)

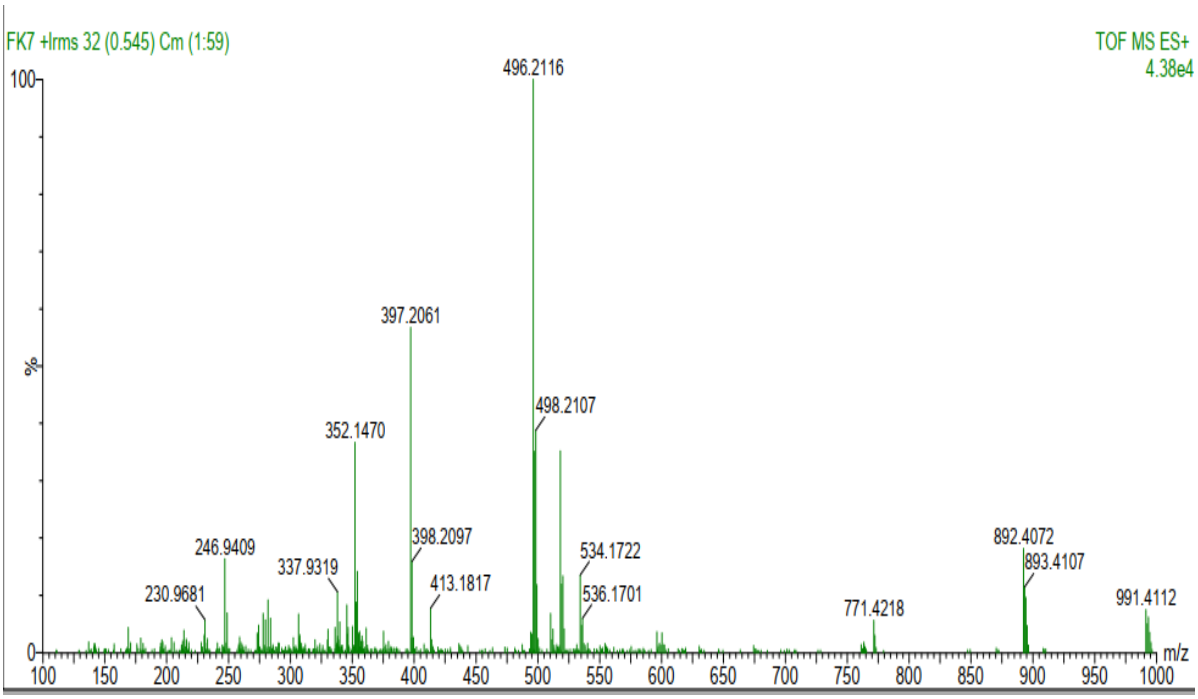

HRMS spectra

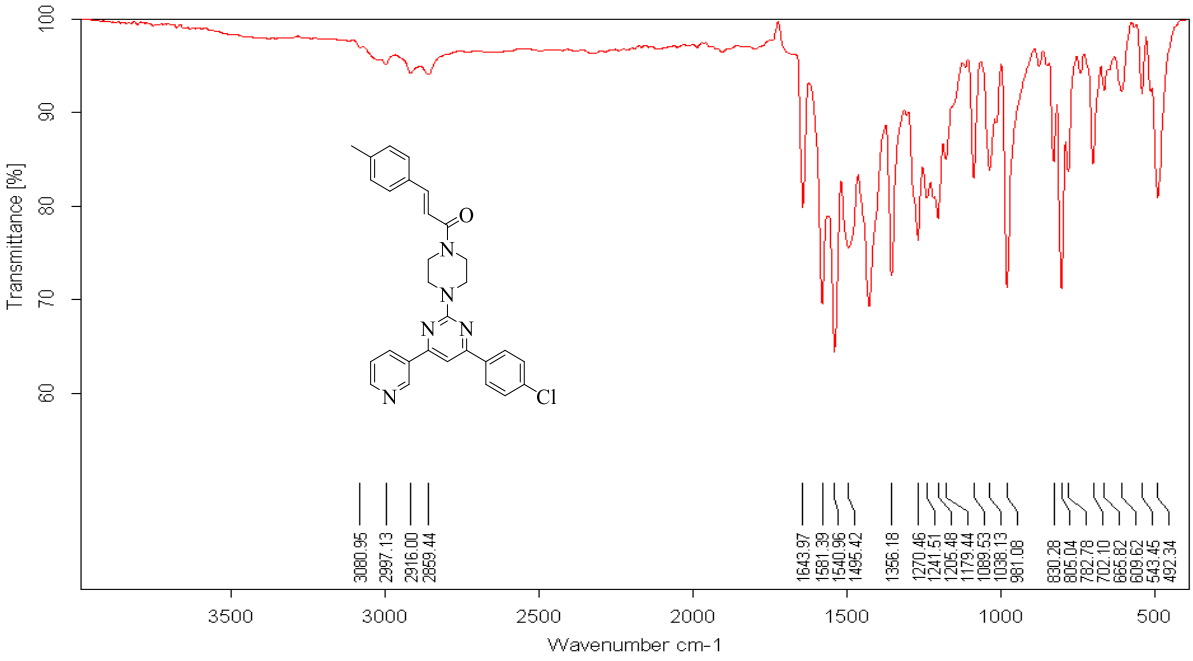

IR spectra

(E)-1-(4-(4-(furan-3-yl)-6-(pyridin-3-yl)pyrimidin-2-yl)piperazin-1-yl)-3-phenylprop-2-en-1-one (**8r**):

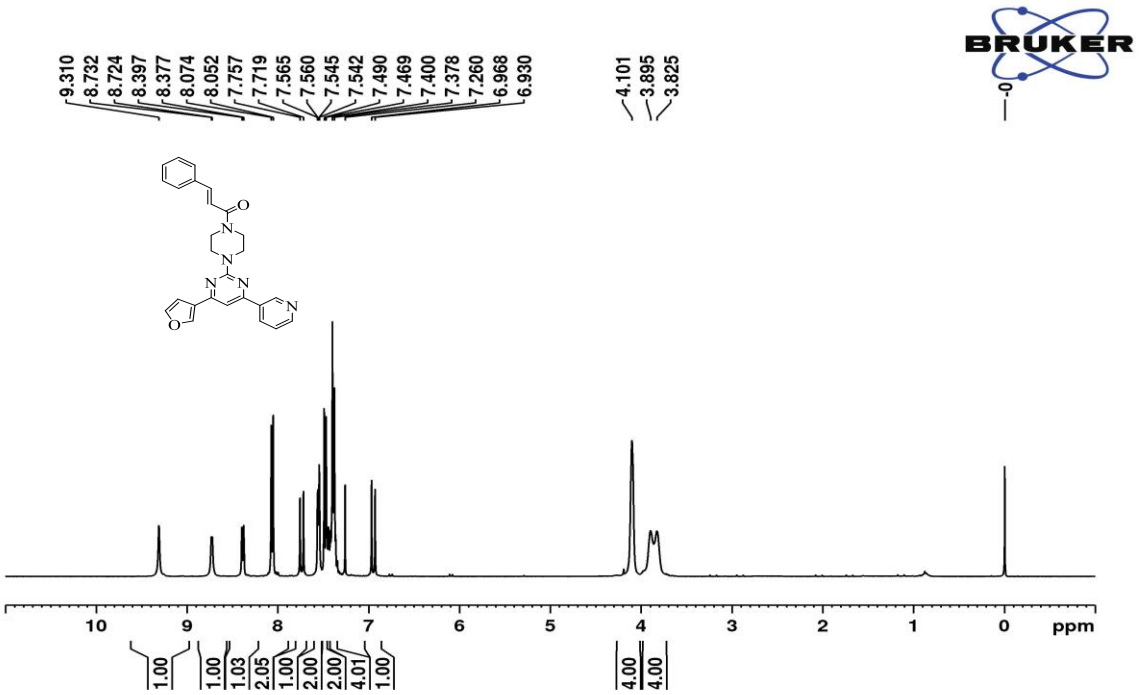

^{1}H NMR (400 MHz, $CDCl_3$)

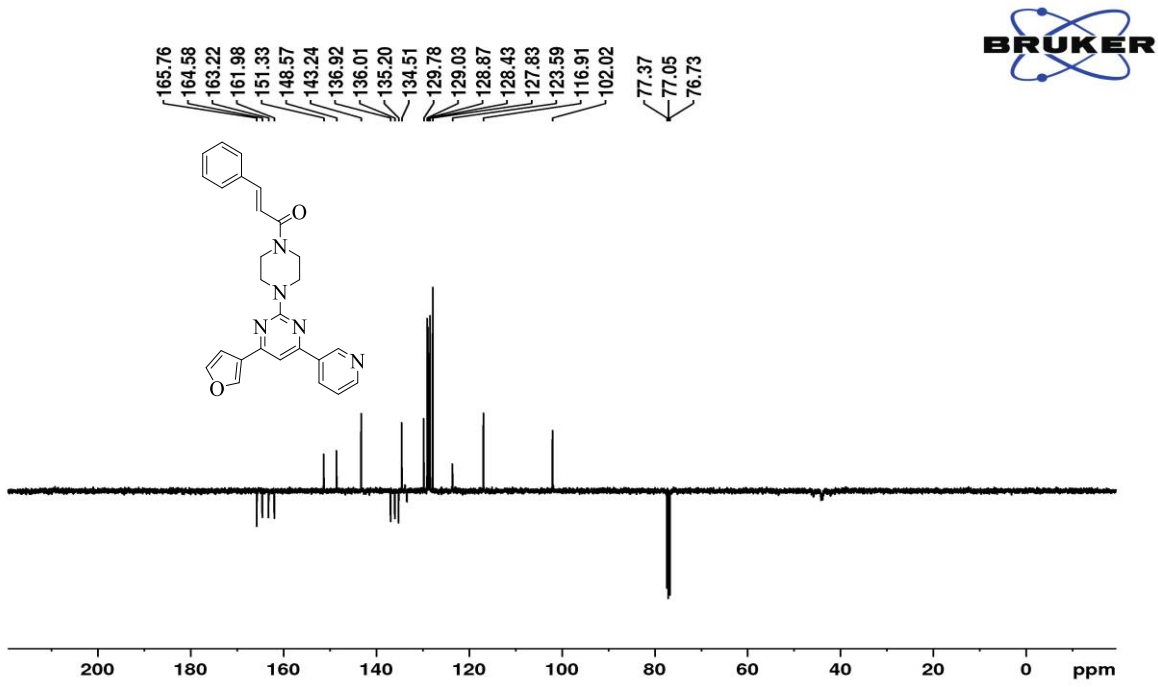

^{13}C NMR (100 MHz, DMSO-d$_6$)

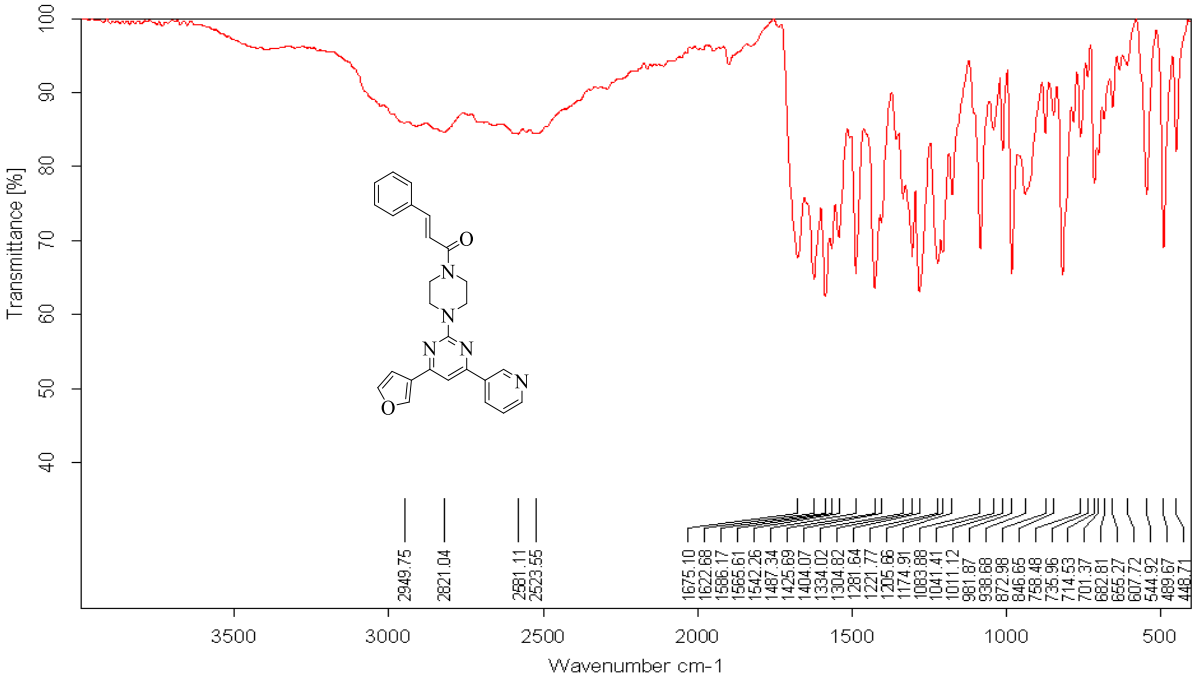

IR spectra

APPENDIX – III

SUPPLEMENTARY INFORMATION

CHAPTER 5

Synthesis and antimalarial activity of novel 1,2,3-triazole-pyrimidine hybrids

4-(4-methoxyphenyl)-2-(4-(prop-2-yn-1-yl)piperazin-1-yl)-6-(p-tolyl)pyrimidine (6b)

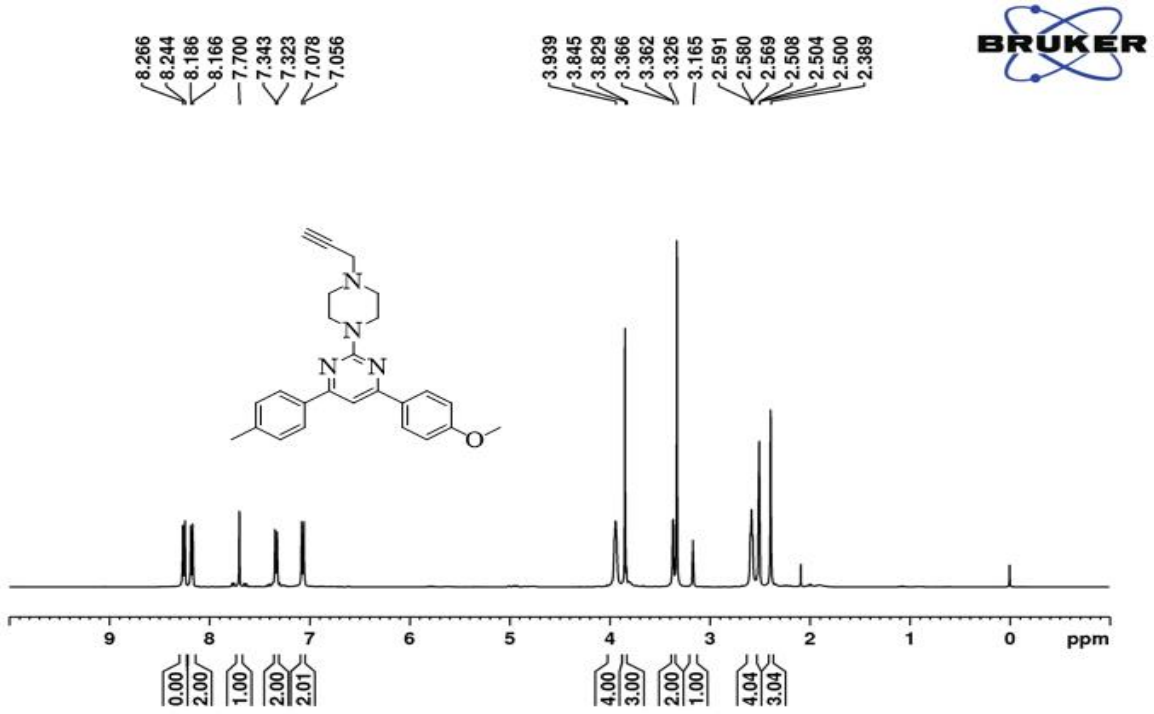

^{1}H NMR (400 MHz, DMSO-d_6)

4,6-bis(4-methoxyphenyl)-2-(4-(prop-2-yn-1-yl)piperazin-1-yl)pyrimidine (**6c**)

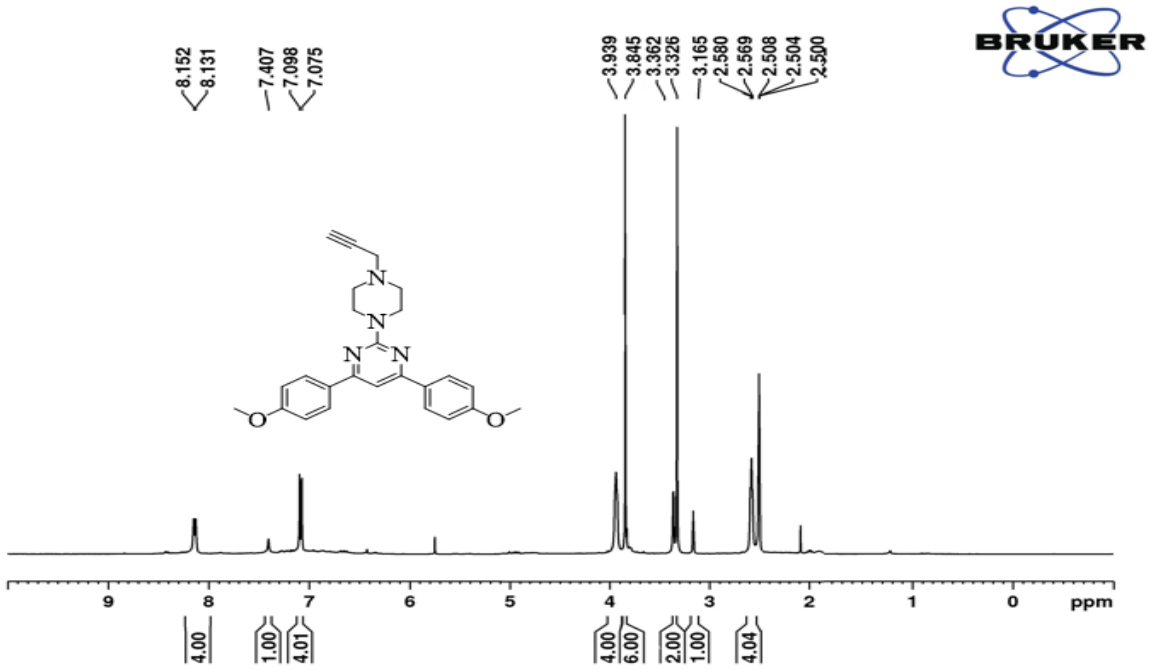

^{1}H NMR (400 MHz, DMSO-d_6)

4-(3,4-dimethoxyphenyl)-6-(4-ethylphenyl)-2-(4-(prop-2-yn-1-yl)piperazin-1-yl)pyrimidine(**6d**)

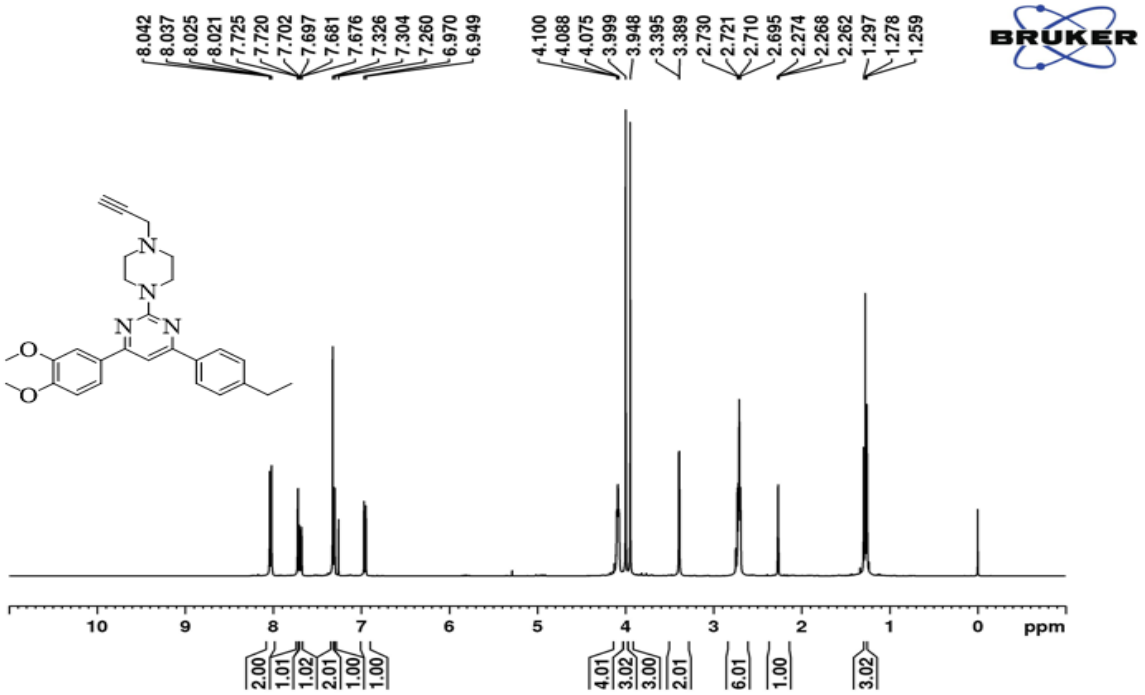

^{1}H NMR (100 MHz, DMSO-d_6)

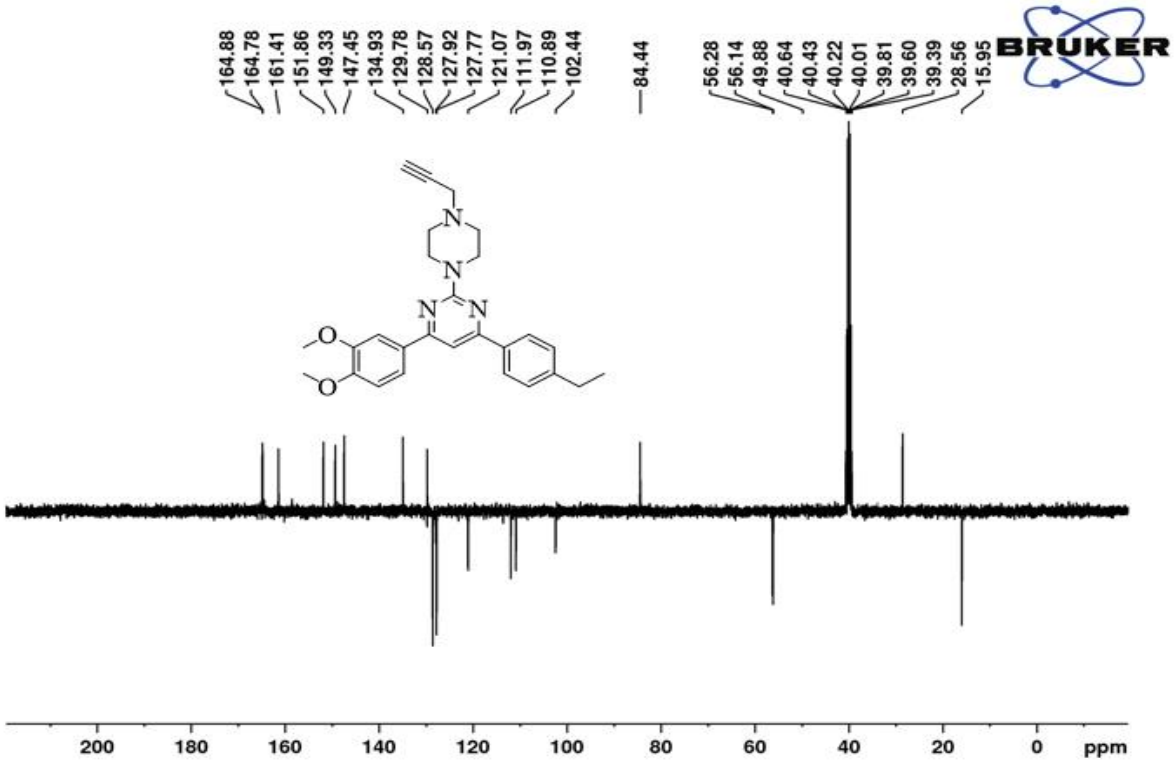

^{1}H NMR (400 MHz, CDCl3)

Spectrums for final compounds 8(a-t)

4-(4-chlorophenyl)-2-(4-((1-(4-fluorophenyl)-1H-1,2,3-triazol-4-yl)methyl)piperazin-1-yl)-6-(4-methoxyphenyl)pyrimidine **(8b)**:

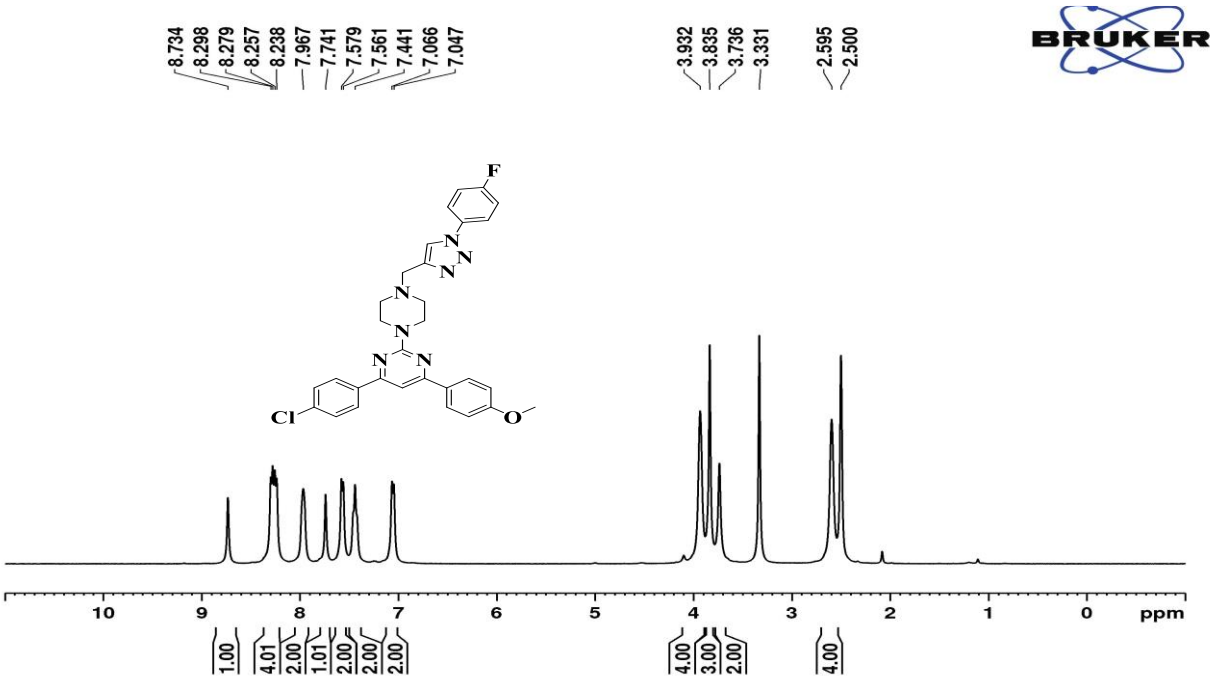

^{1}H NMR (400 MHz, CDCl3)

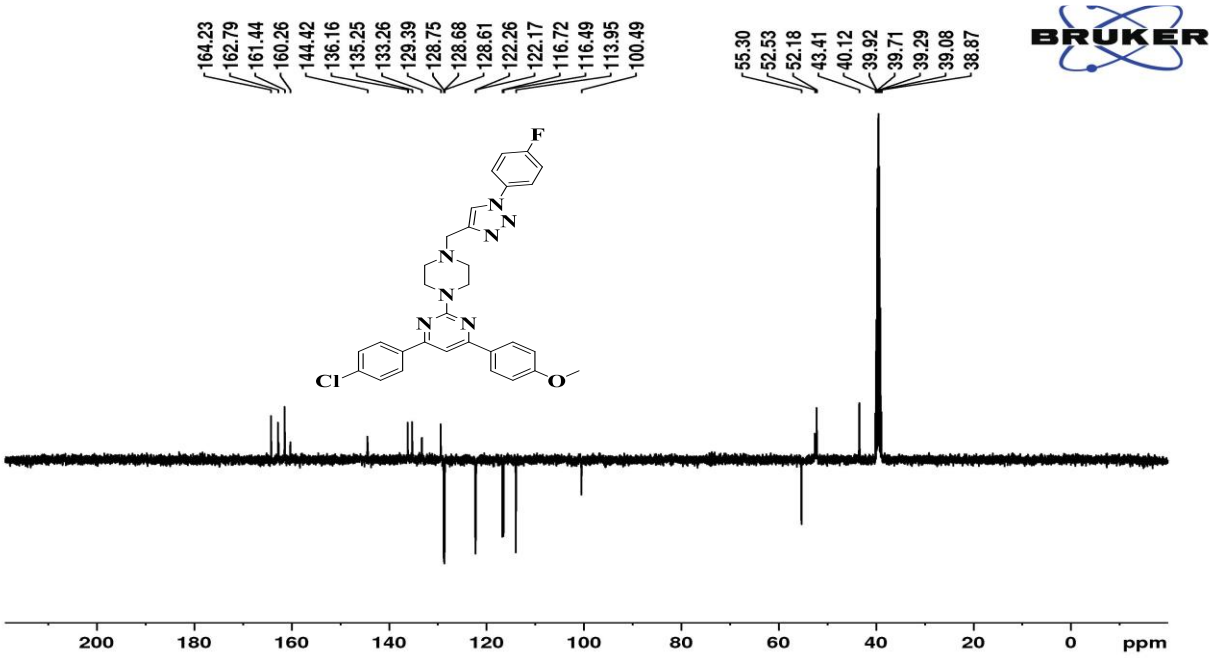

^{13}C NMR (100 MHz, CDCl3)

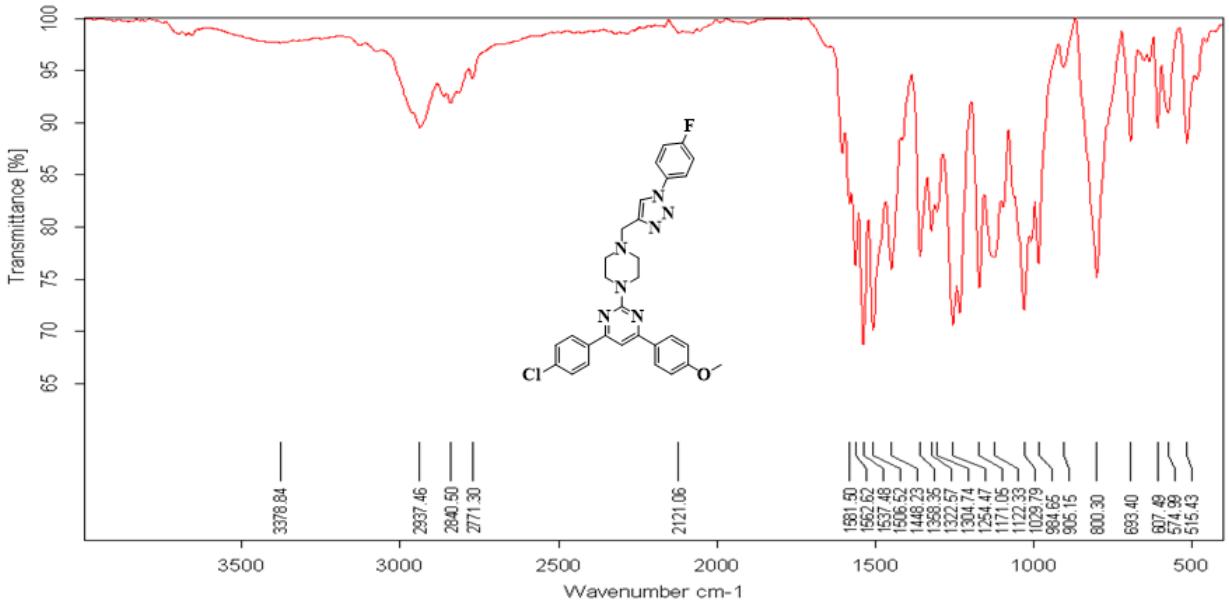

IR spectra

4-(4-chlorophenyl)-2-(4-((1-(4-chlorophenyl)-1H-1,2,3-triazol-4-yl)methyl)piperazin-1-yl)-6-(4-methoxyphenyl)pyrimidine (**8c**):

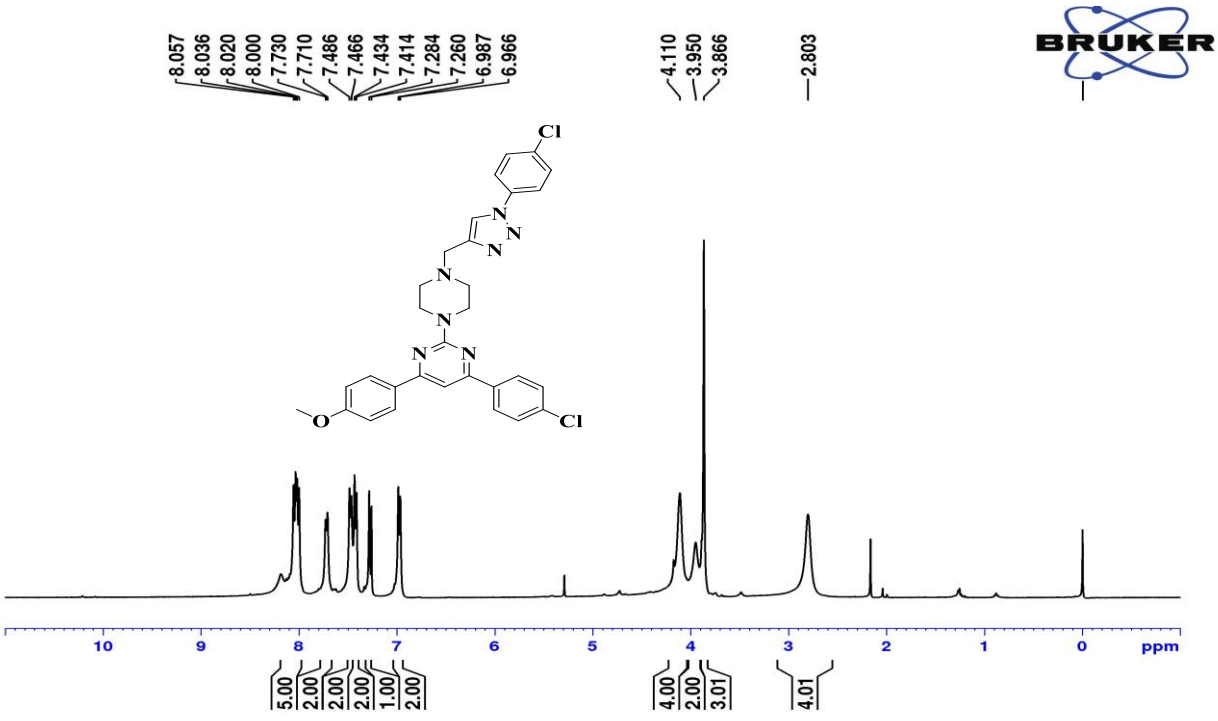

^{1}H NMR (400 MHz, CDCl3)

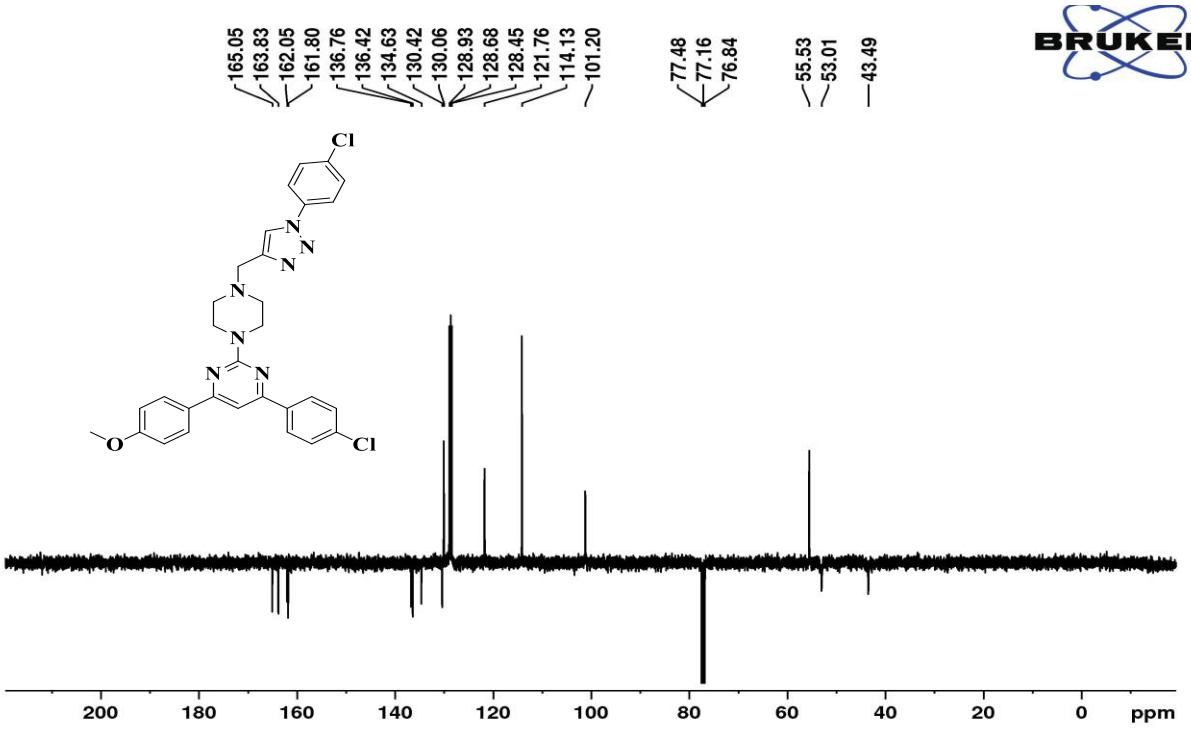

^{13}C NMR (100 MHz, CDCl3)

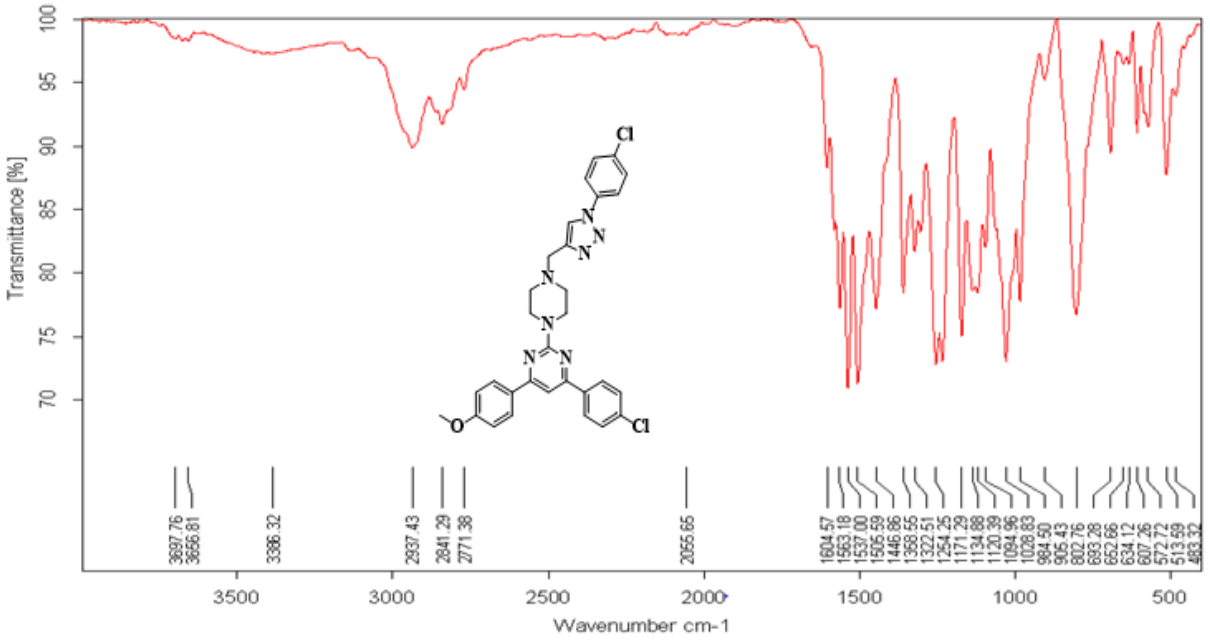

IR spectra

4-(4-chlorophenyl)-6-(4-methoxyphenyl)-2-(4-((1-(4-nitrophenyl)-1H-1,2,3-triazol-4-yl)methyl)piperazin-1-yl)pyrimidine (**8e**)

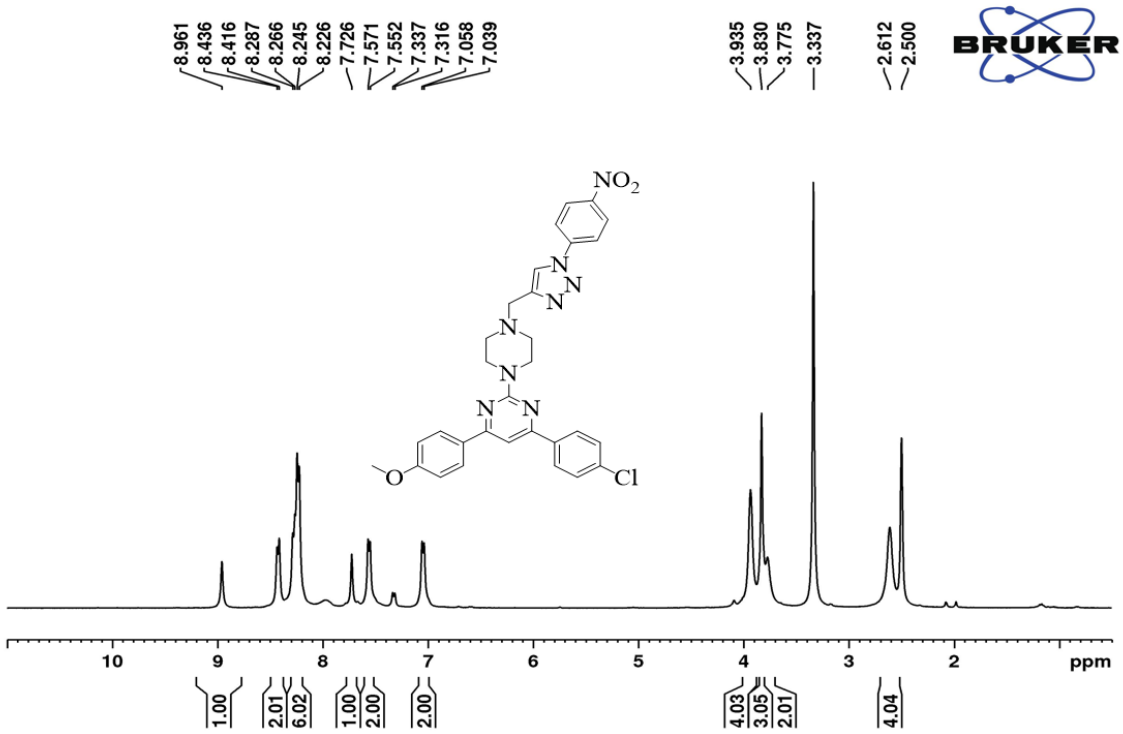

^{1}H NMR (400 MHz, CDCl3)

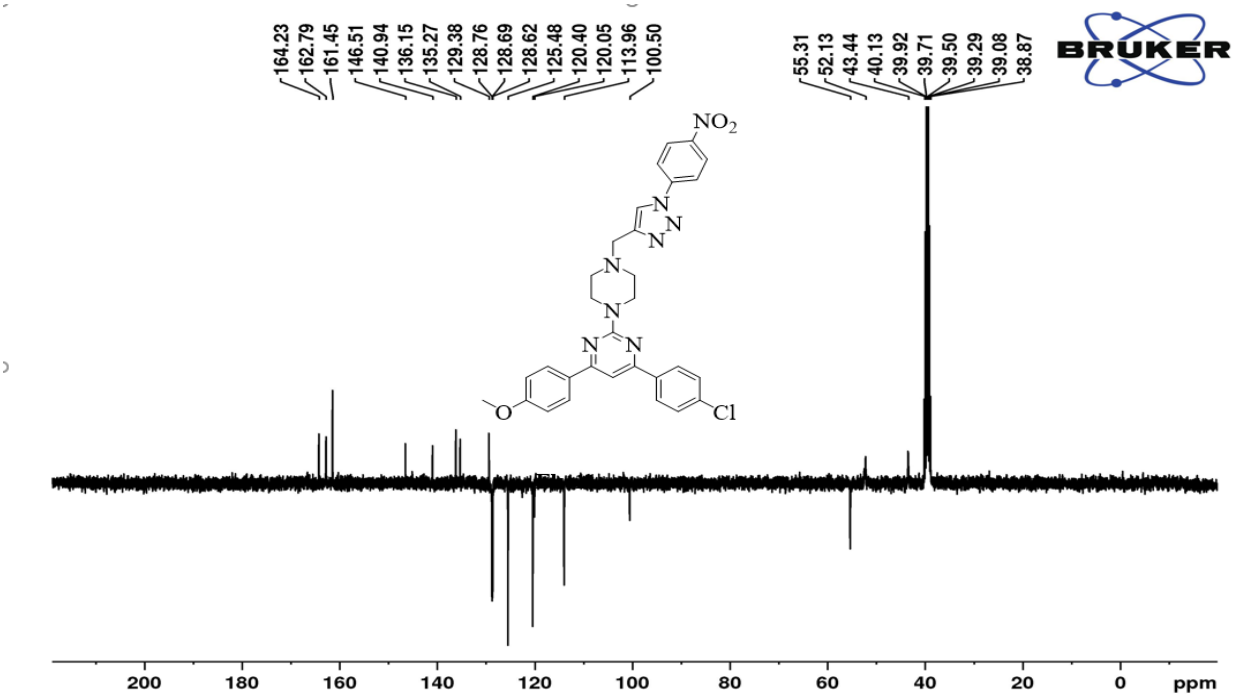

^{13}C NMR (100 MHz, CDCl3)

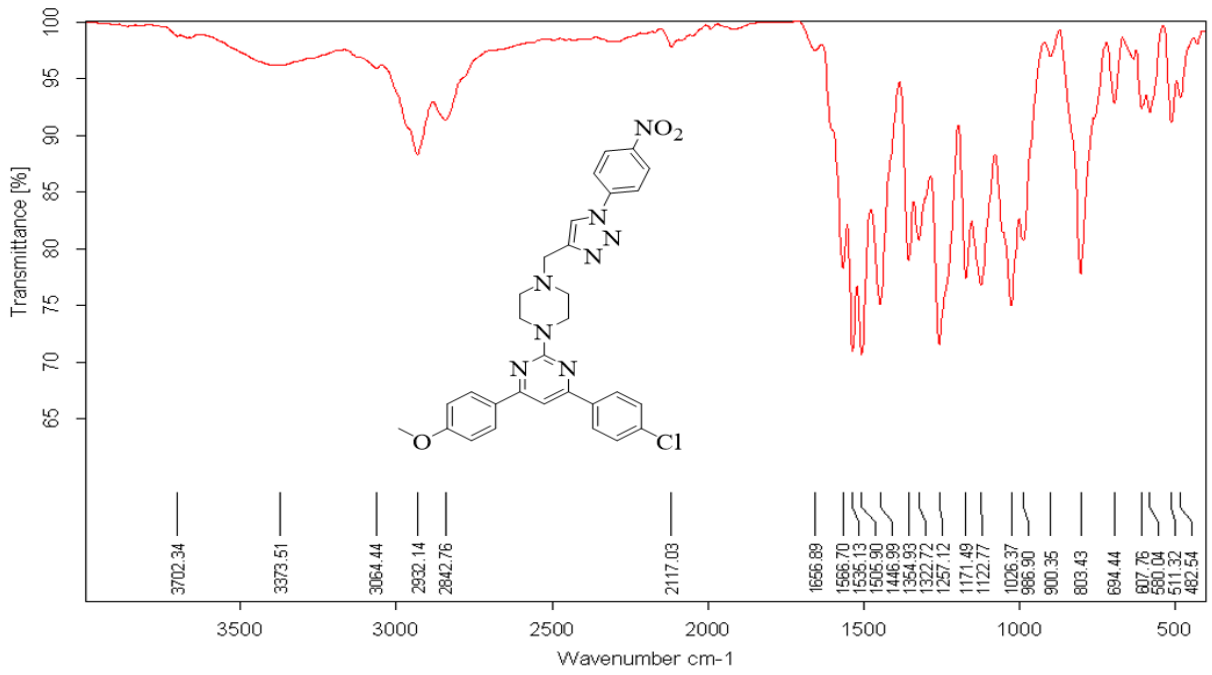

IR spectra

4-(4-chlorophenyl)-6-(4-methoxyphenyl)-2-(4-((1-(3-(trifluoromethyl)phenyl)-1H-1,2,3-triazol-4-yl)methyl)piperazin-1-yl)pyrimidine (**8e**)

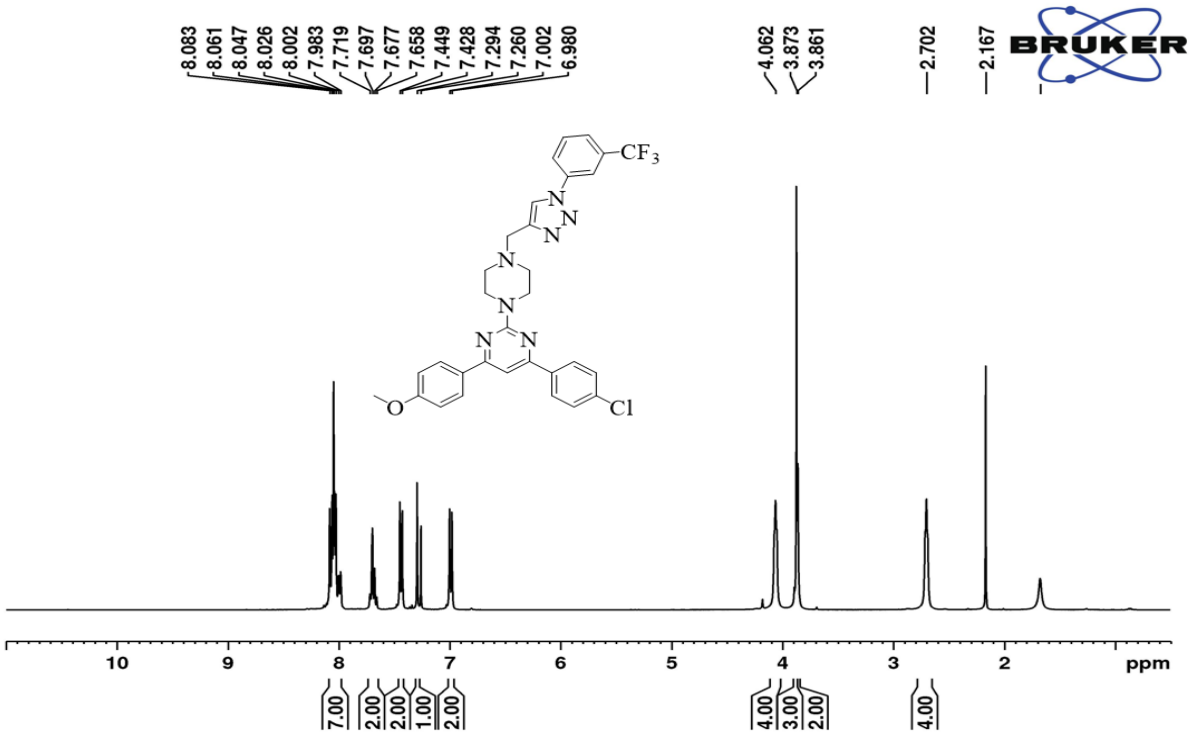

^{1}H NMR (400 MHz, CDCl3)

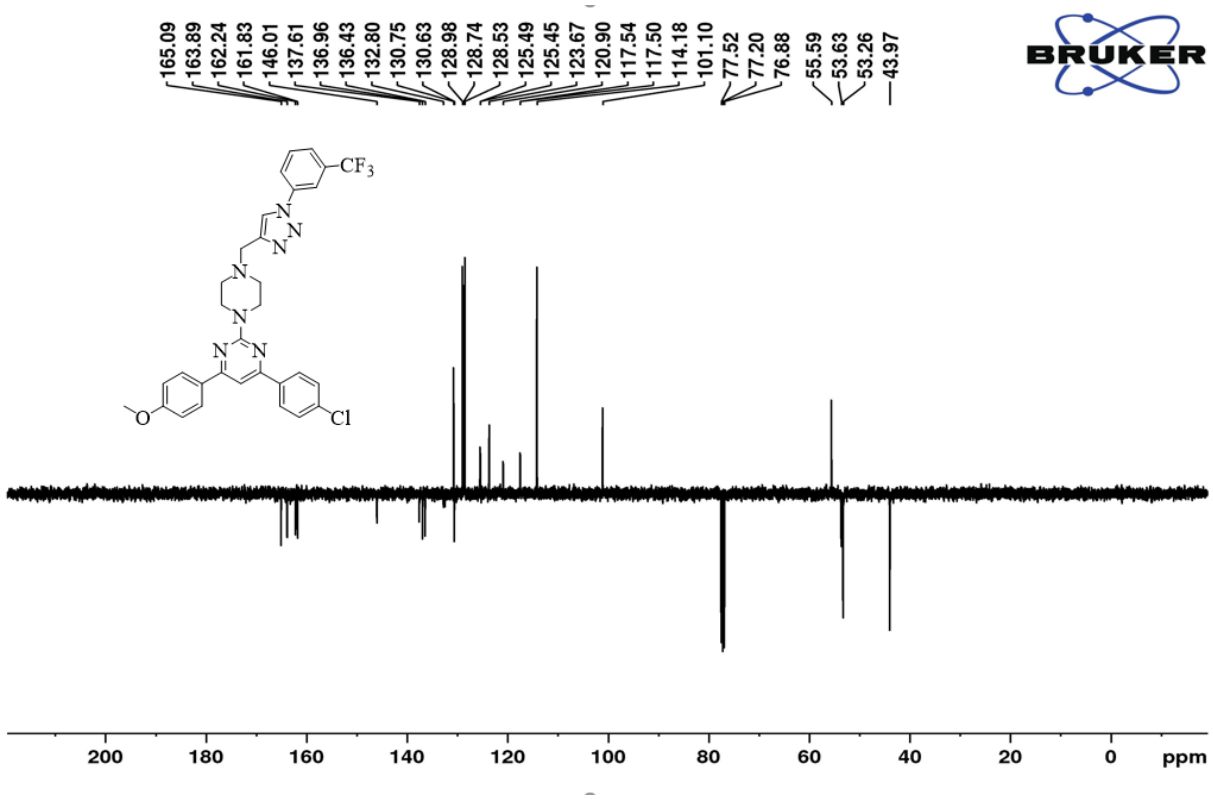

^{13}C NMR (100 MHz, CDCl3)

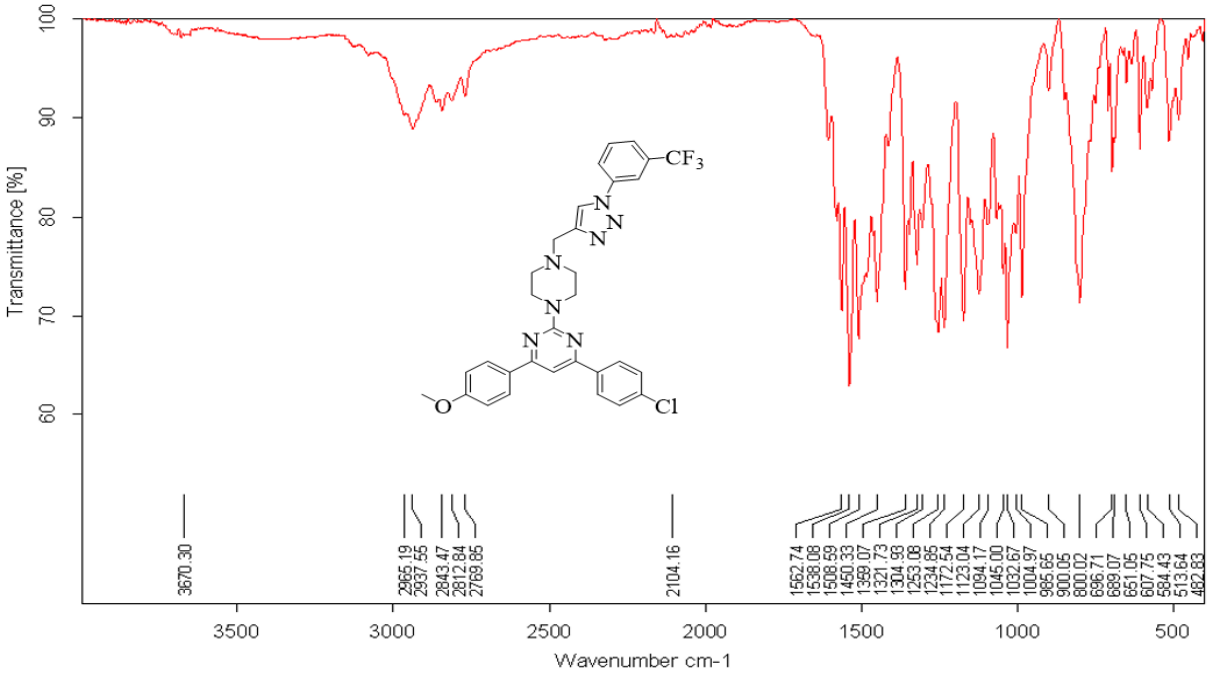

IR spectra

4-(4-chlorophenyl)-2-(4-((1-cyclohexyl-1H-1,2,3-triazol-4-yl)methyl)piperazin-1-yl)-6-(4-methoxyphenyl)pyrimidine (**8f**)

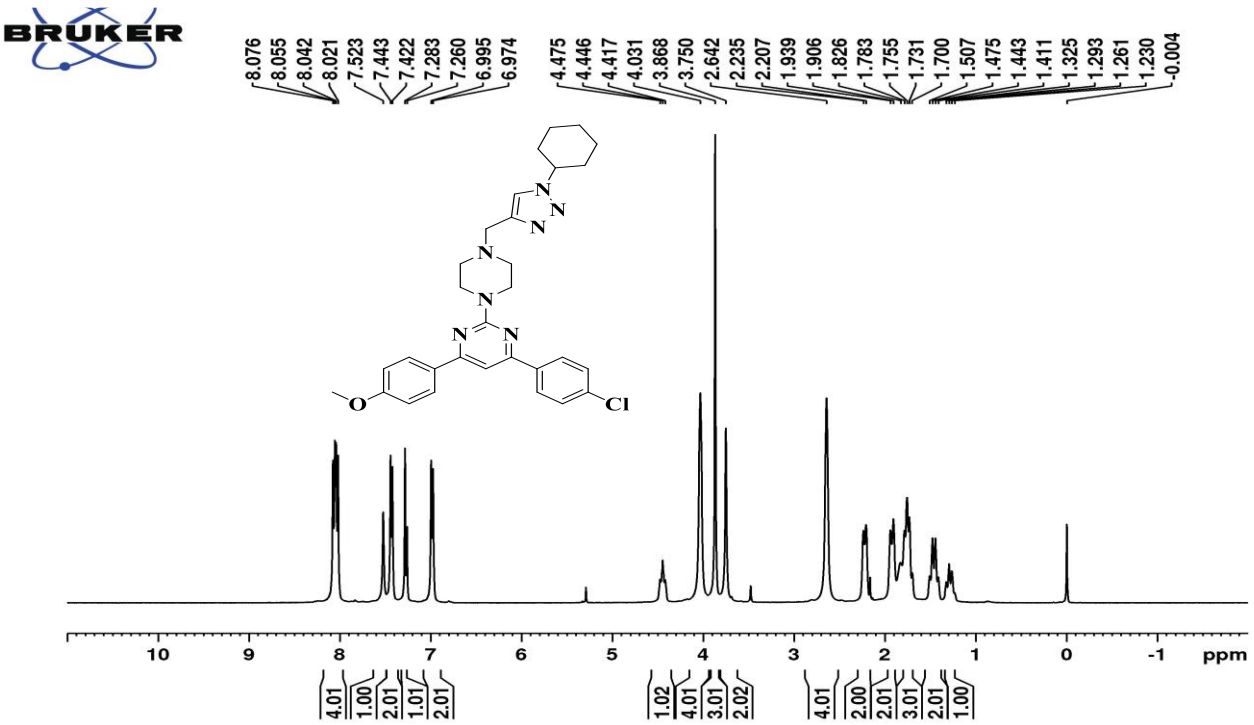

^{1}H NMR (400 MHz, CDCl3)

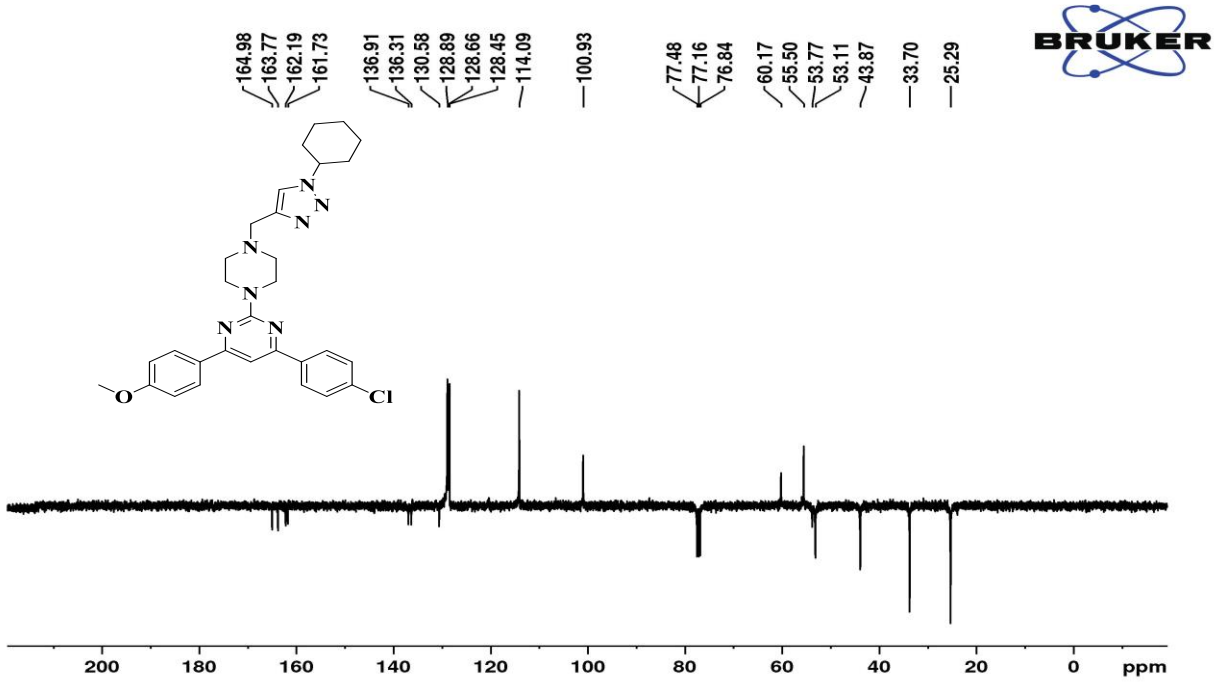

^{13}C NMR (100 MHz, CDCl3

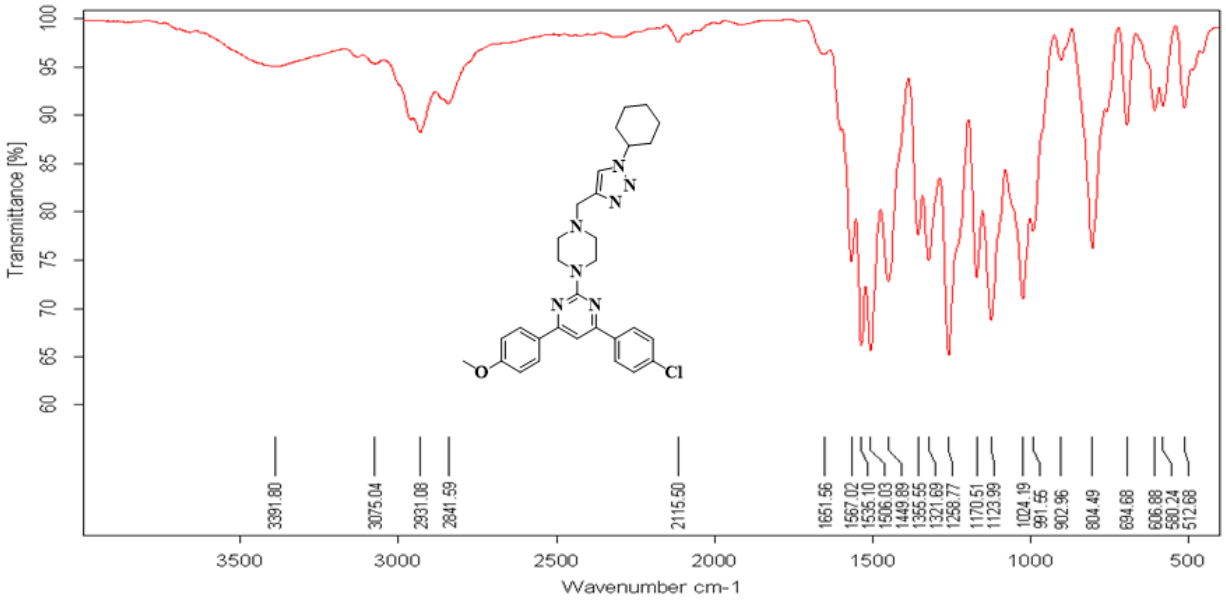

IR spectra

4-(4-methoxyphenyl)-2-(4-((1-phenyl-1H-1,2,3-triazol-4-yl)methyl)piperazin-1-yl)-6-(p-tolyl)pyrimidine **(8g)**

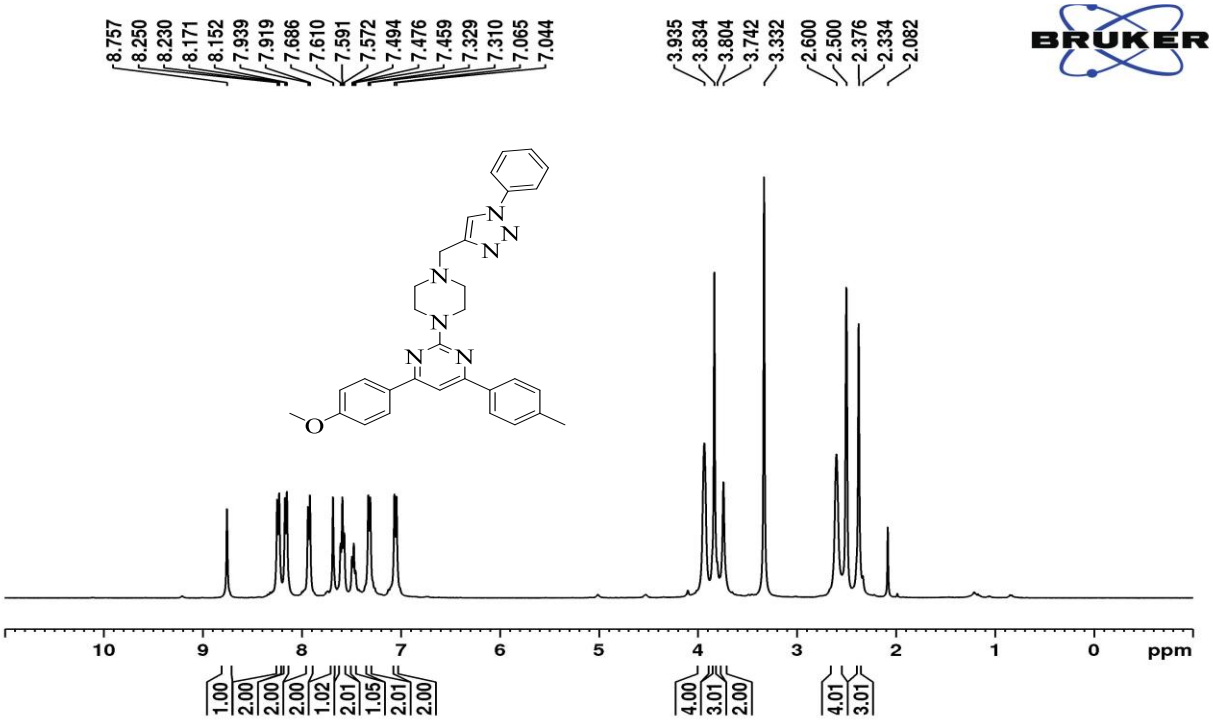

^{1}H NMR (400 MHz, CDCl3)

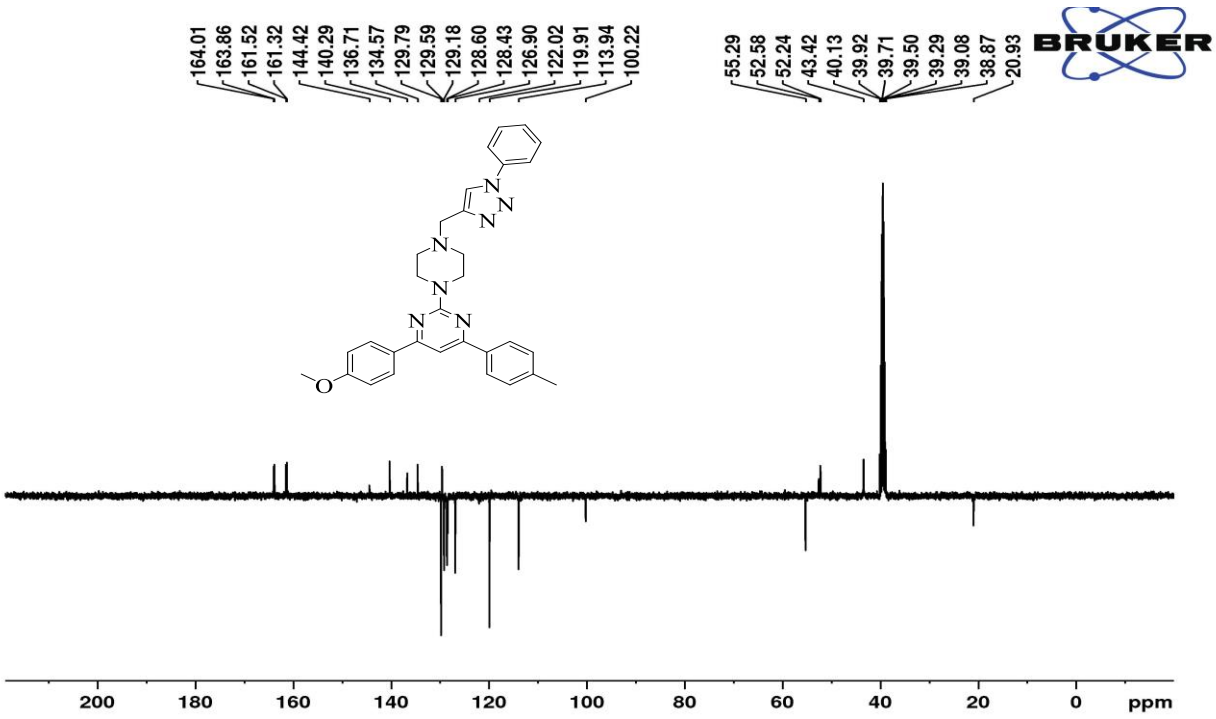

^{13}C NMR (100 MHz, CDCl3)

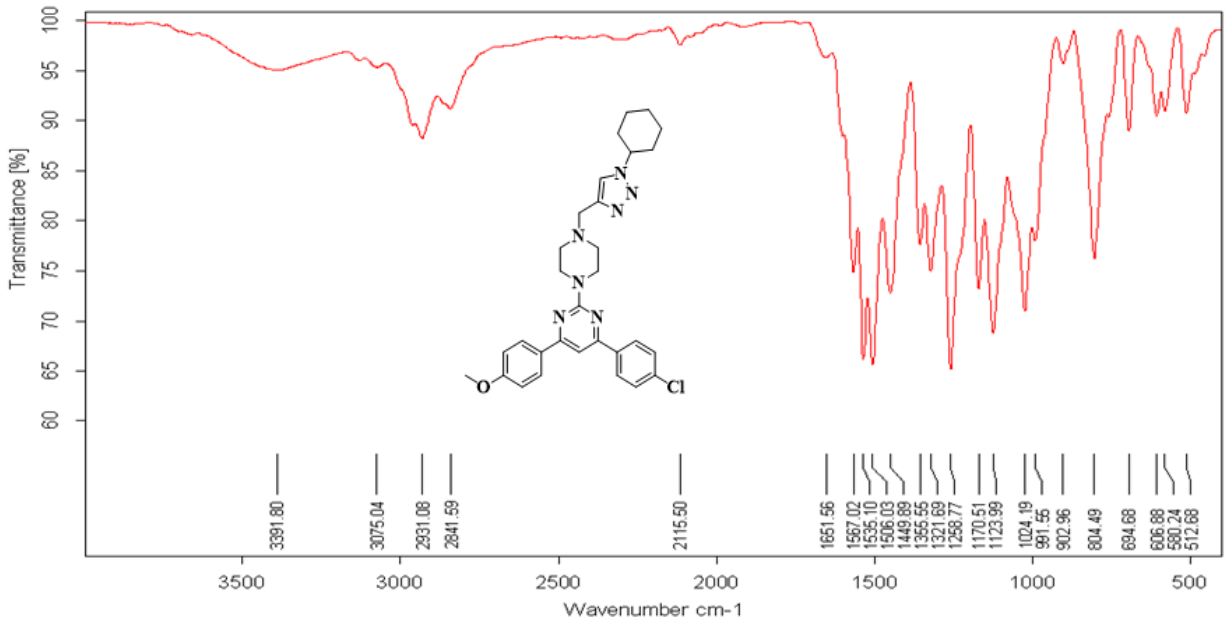

IR spectra*2-(4-((1-(4-fluorophenyl)-1H-1,2,3-triazol-4-yl)methyl)piperazin-1-yl)-4-(4-*

methoxyphenyl)-6-(p-tolyl)pyrimidine (**8h**)

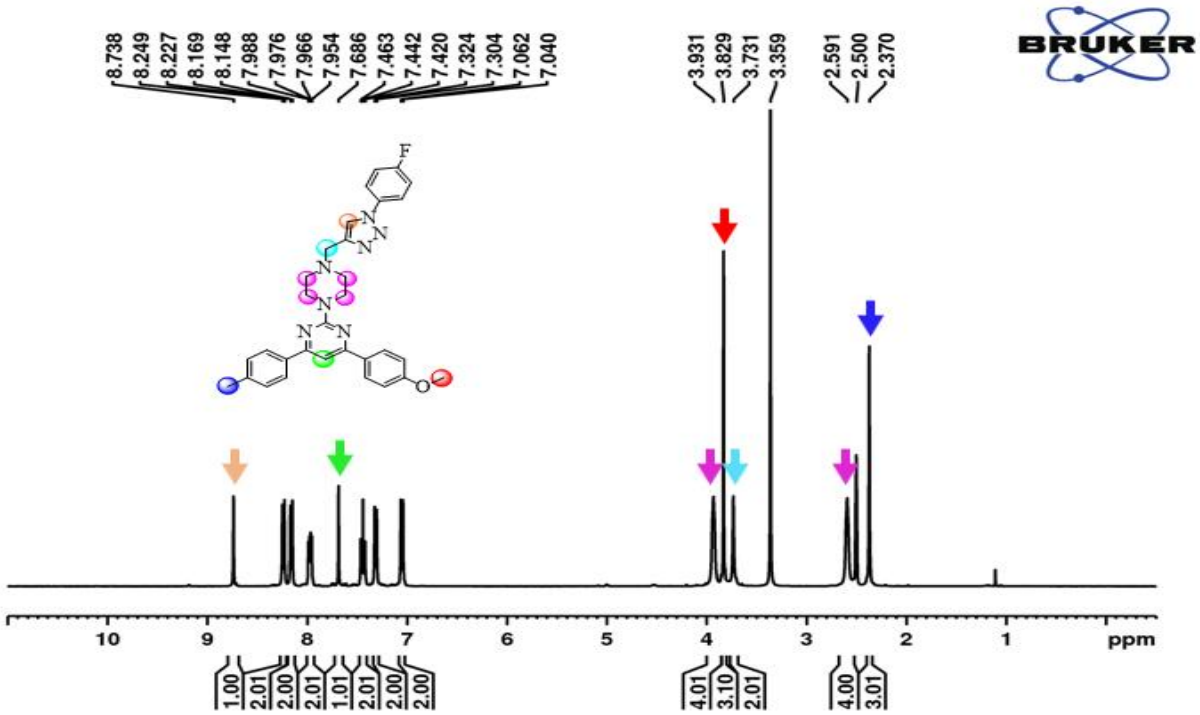

^{1}H NMR (400 MHz, DMSO-d_6)

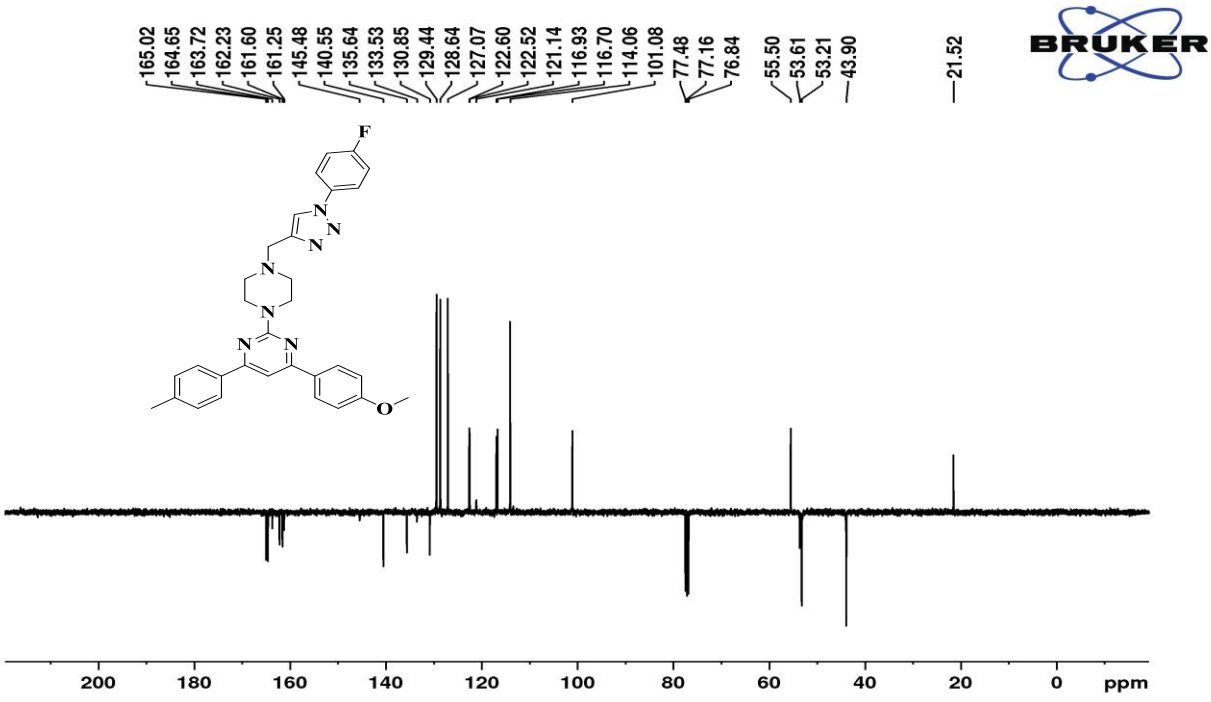

^{13}C NMR (100 MHz, CDCl3)

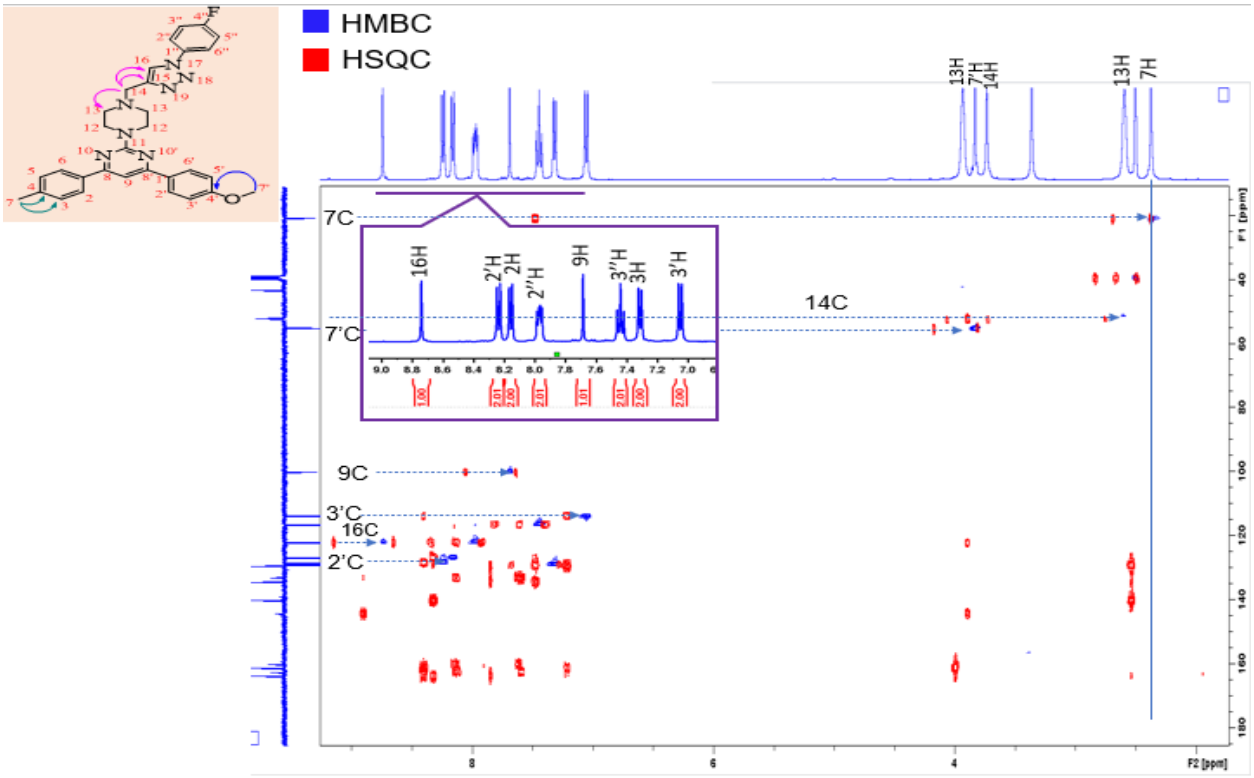

HMBC/ HSQC Spectra

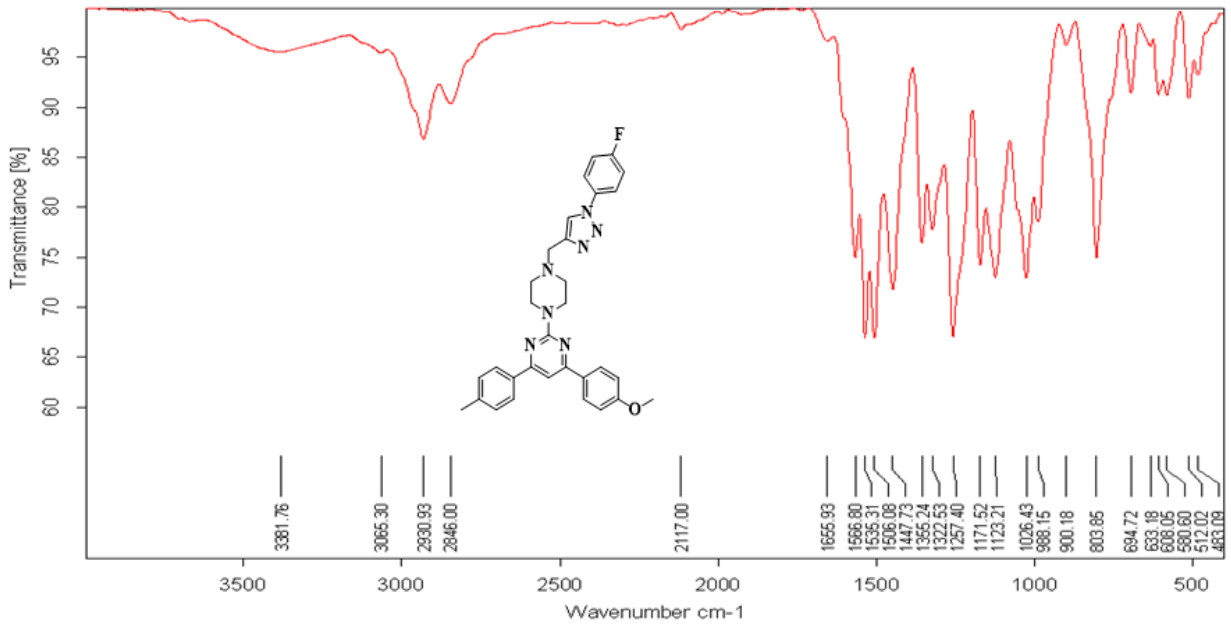

IR spectra

2-(4-((1-(4-chlorophenyl)-1H-1,2,3-triazol-4-yl)methyl)piperazin-1-yl)-4-(4-methoxyphenyl)-6-(p-tolyl)pyrimidine **(8i)**

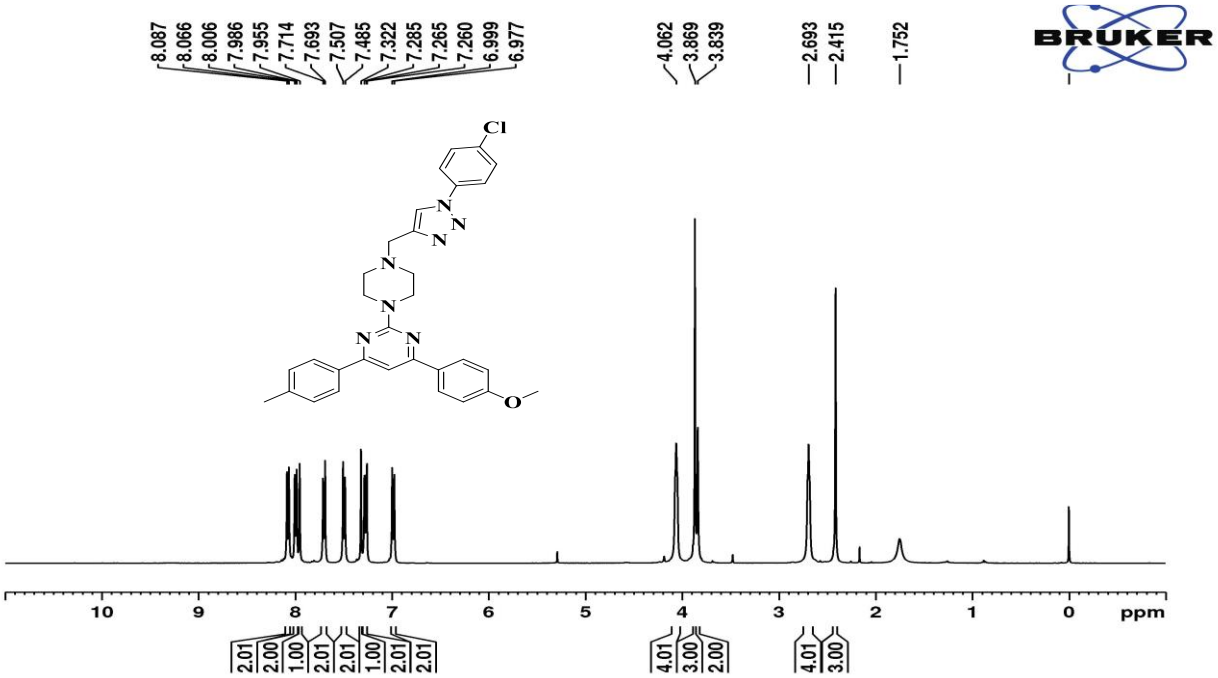

^{1}H NMR (400 MHz, DMSO-d_6)

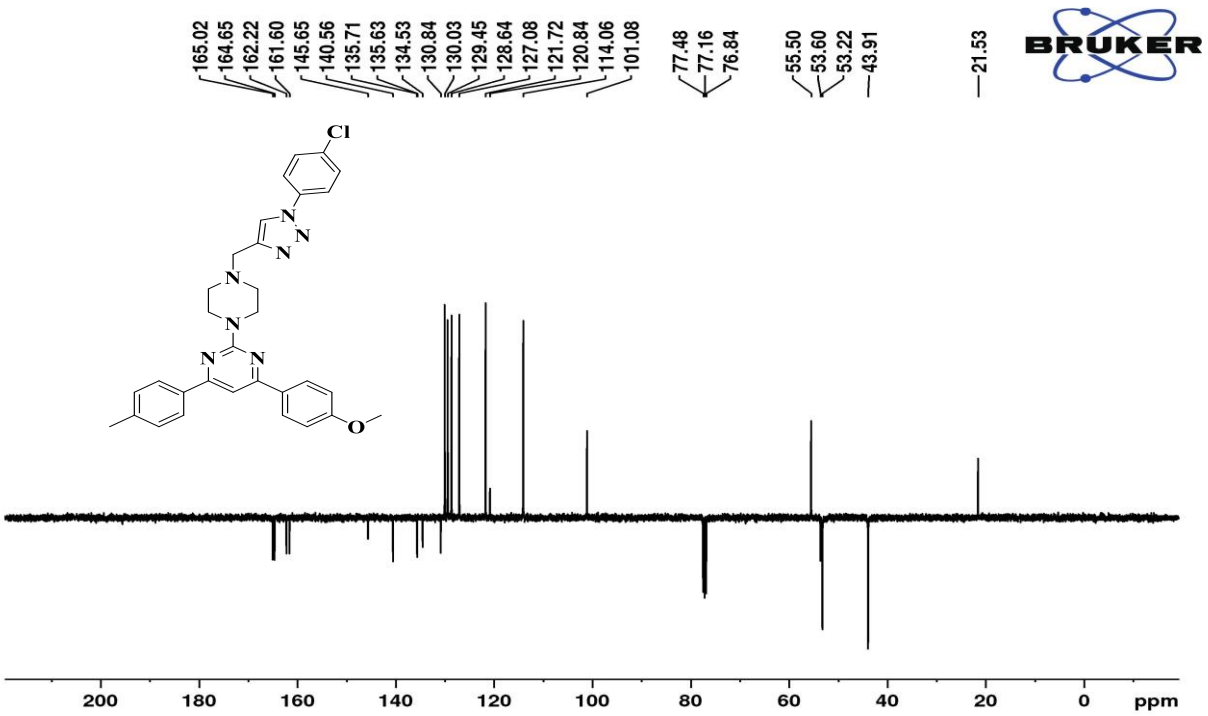

^{13}C NMR (100 MHz, DMSO-d_6)

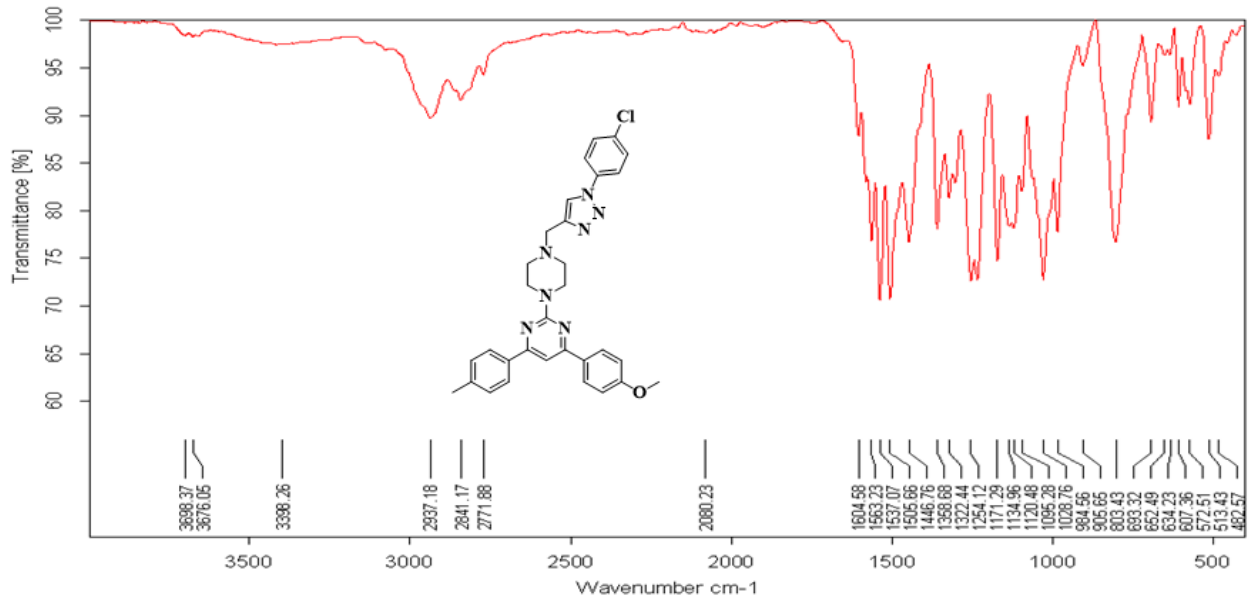

IR spectra

4-(4-methoxyphenyl)-2-(4-((1-(4-nitrophenyl)-1H-1,2,3-triazol-4-yl)methyl)piperazin-1-yl)-6-(p-tolyl)pyrimidine **(8j)**

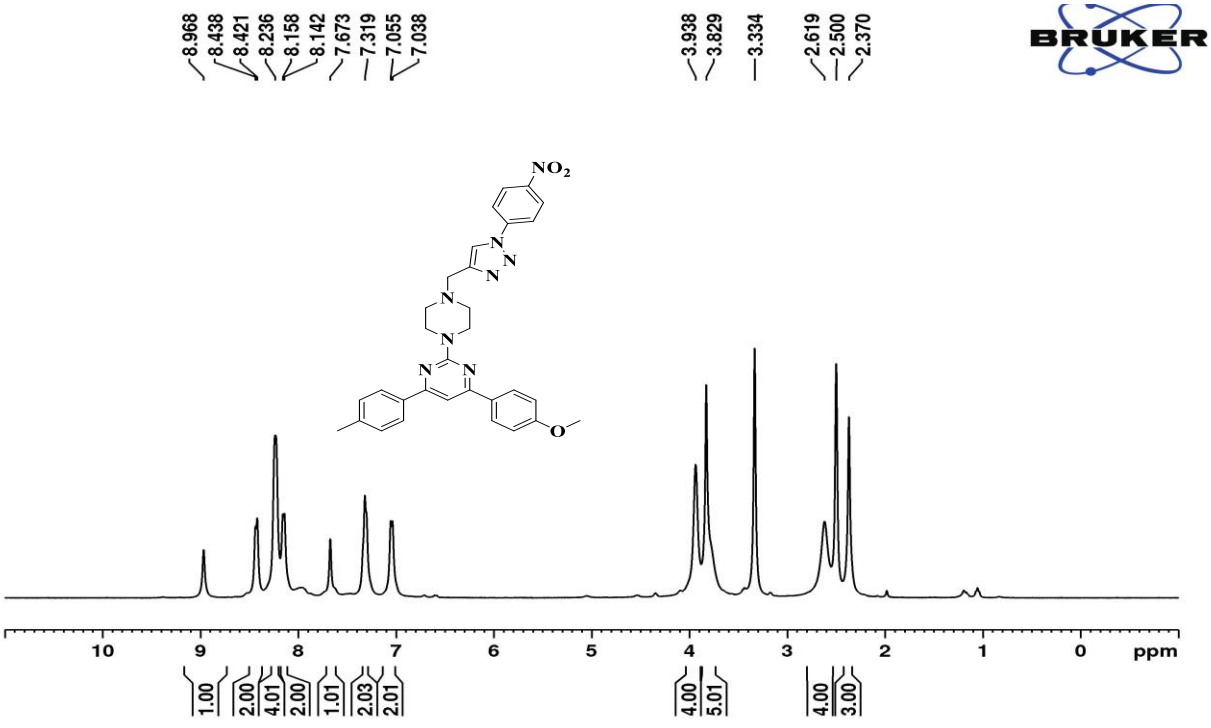

^{1}H NMR (400 MHz, DMSO-d_6)

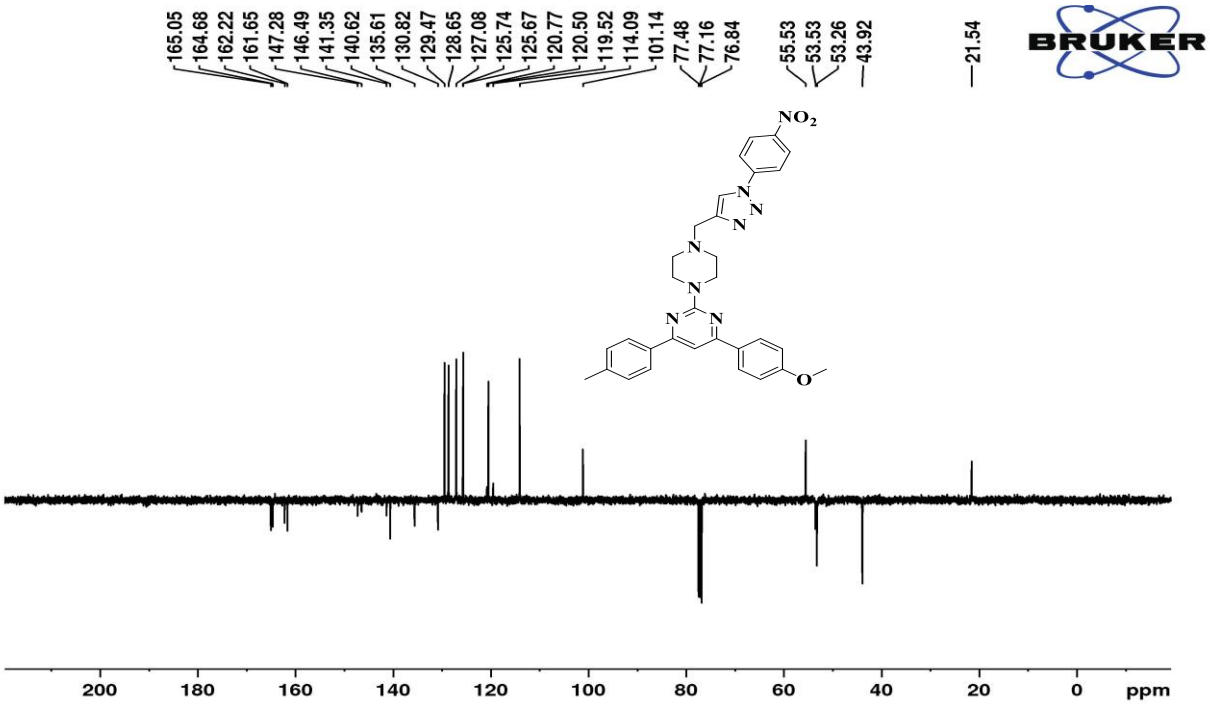

^{13}C NMR (100 MHz, DMSO-d_6)

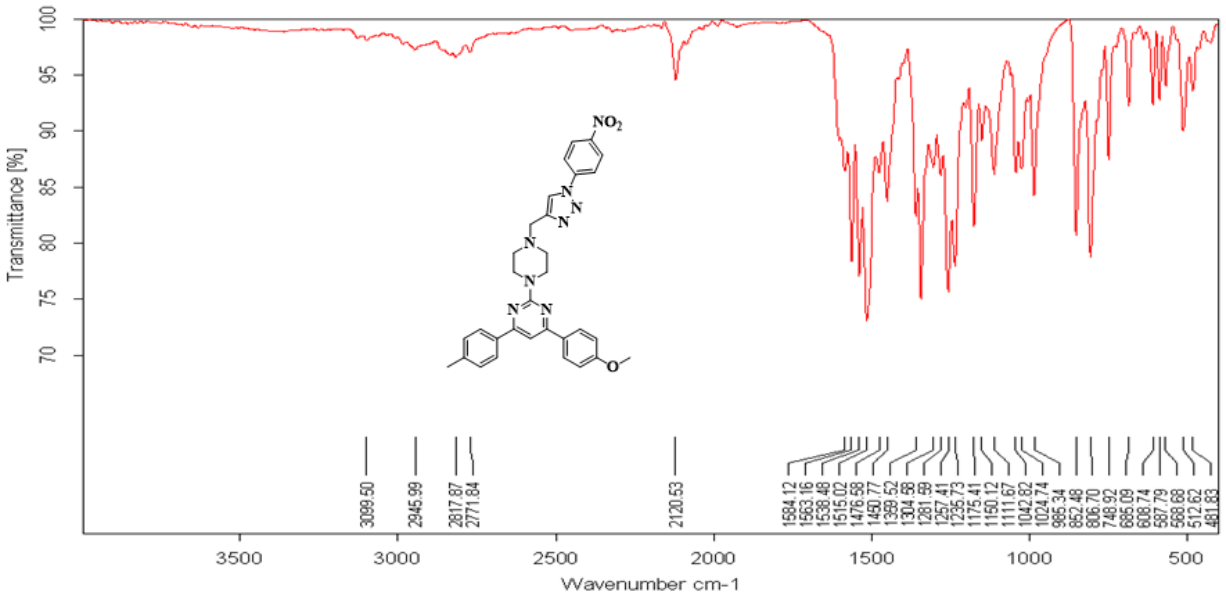

IR spectra

4-(4-methoxyphenyl)-6-(p-tolyl)-2-(4-((1-(3-(trifluoromethyl)phenyl)-1H-1,2,3-triazol-4-yl)methyl)piperazin-1-yl)pyrimidine (**8k**)

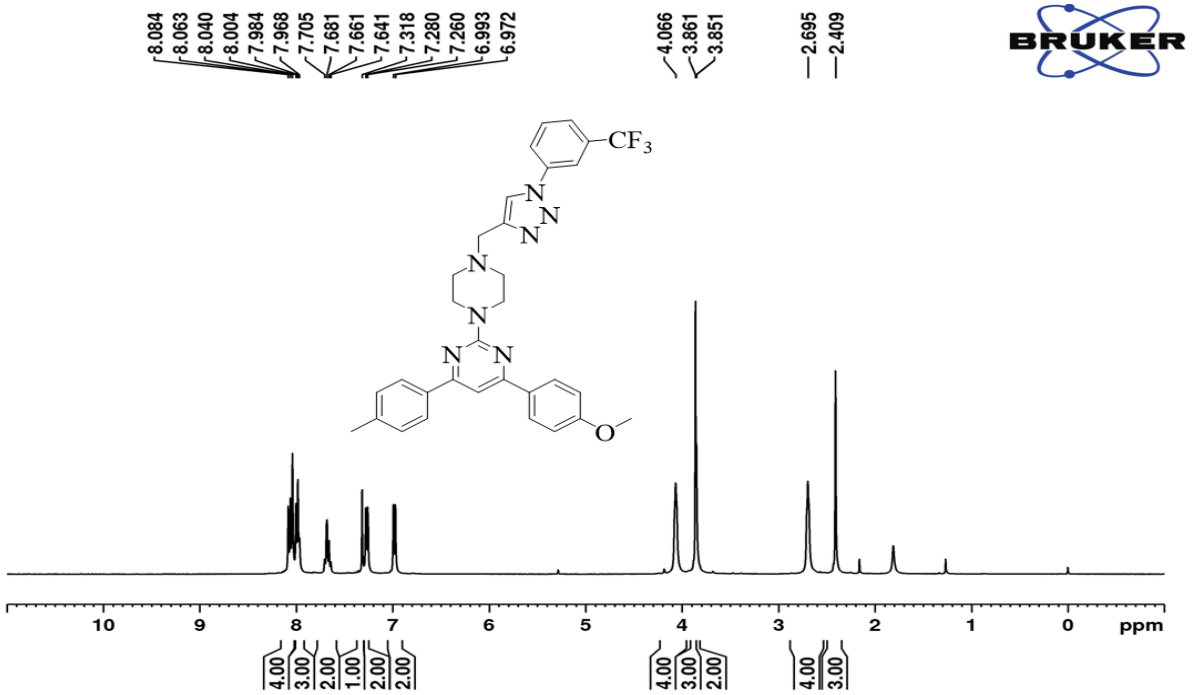

^{1}H NMR (400 MHz, $CDCl_3$)

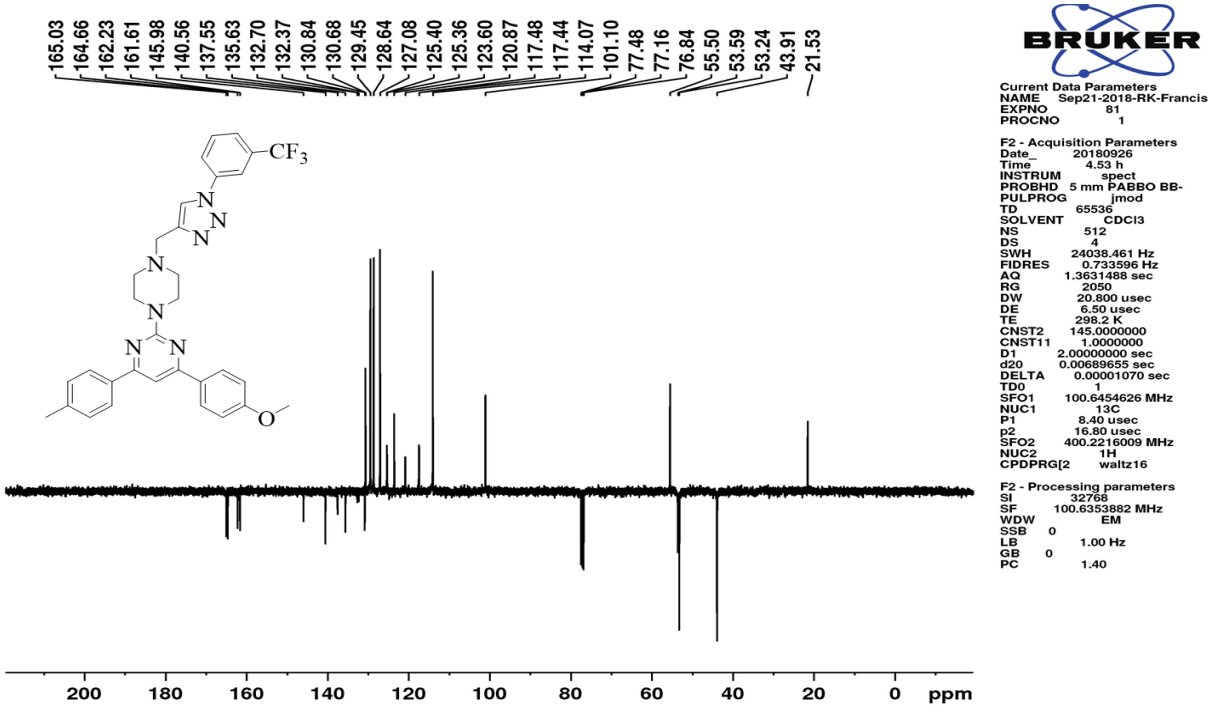

^{13}C NMR (100 MHz, $CDCl_3$)

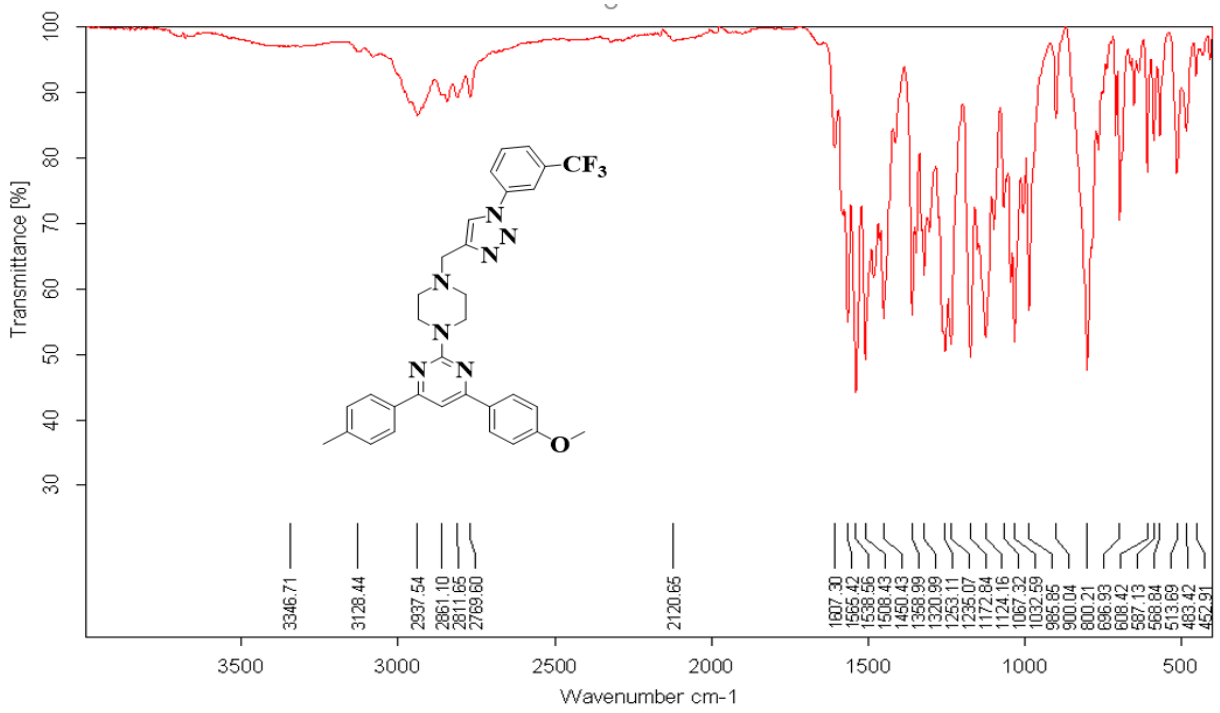

IR spectra

2-(4-((1-cyclohexyl-1H-1,2,3-triazol-4-yl)methyl)piperazin-1-yl)-4-(4-methoxyphenyl)-6-(p-tolyl)pyrimidine **(8l)**

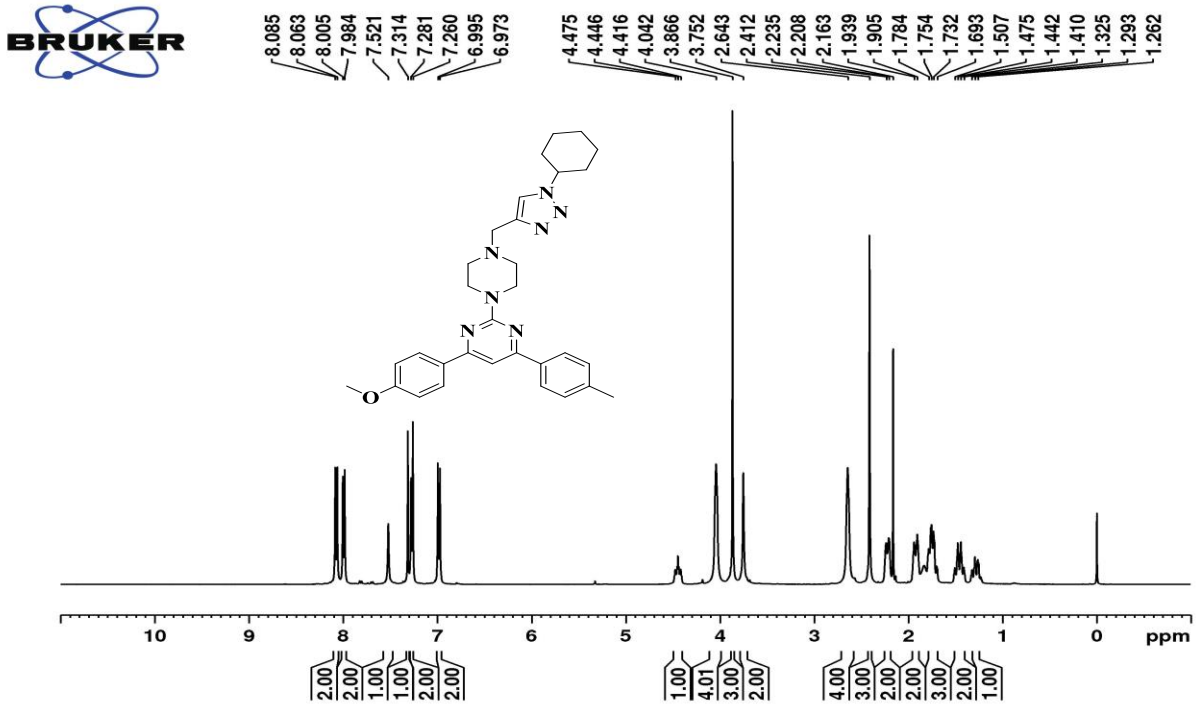

^{1}H NMR (400 MHz, $CDCl_3$)

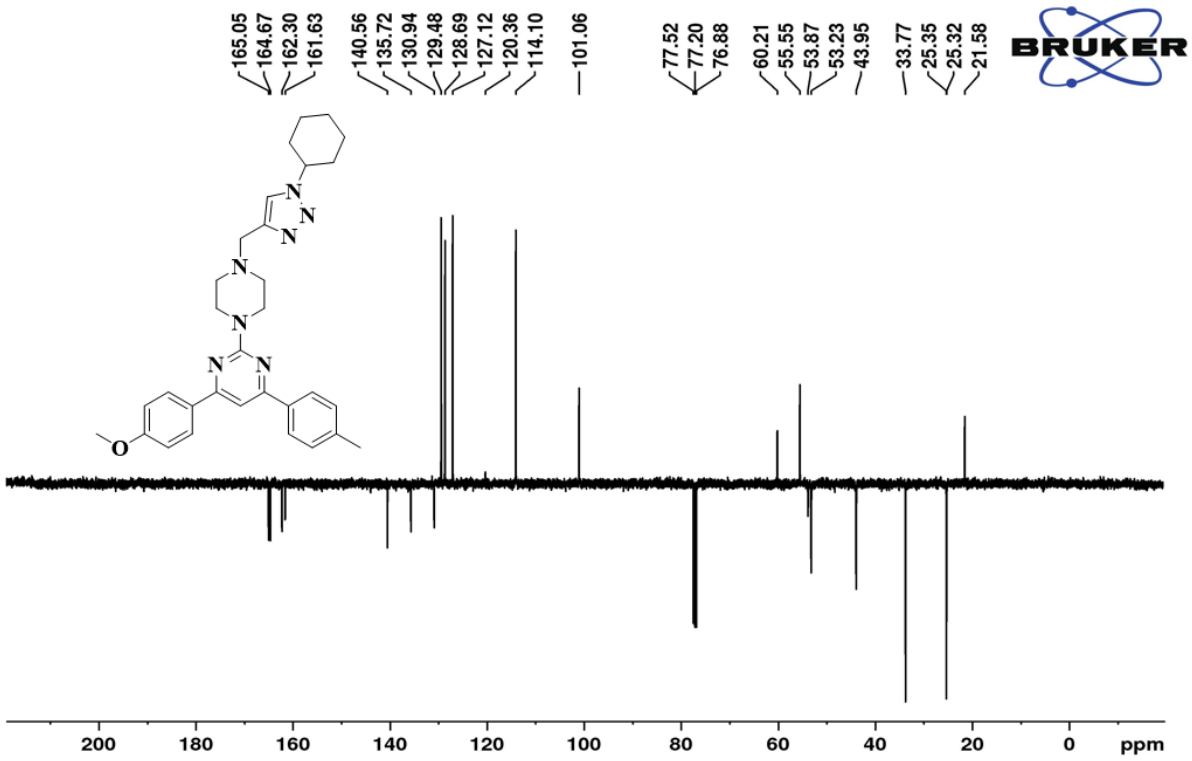

^{13}C NMR (100 MHz, $CDCl_3$)

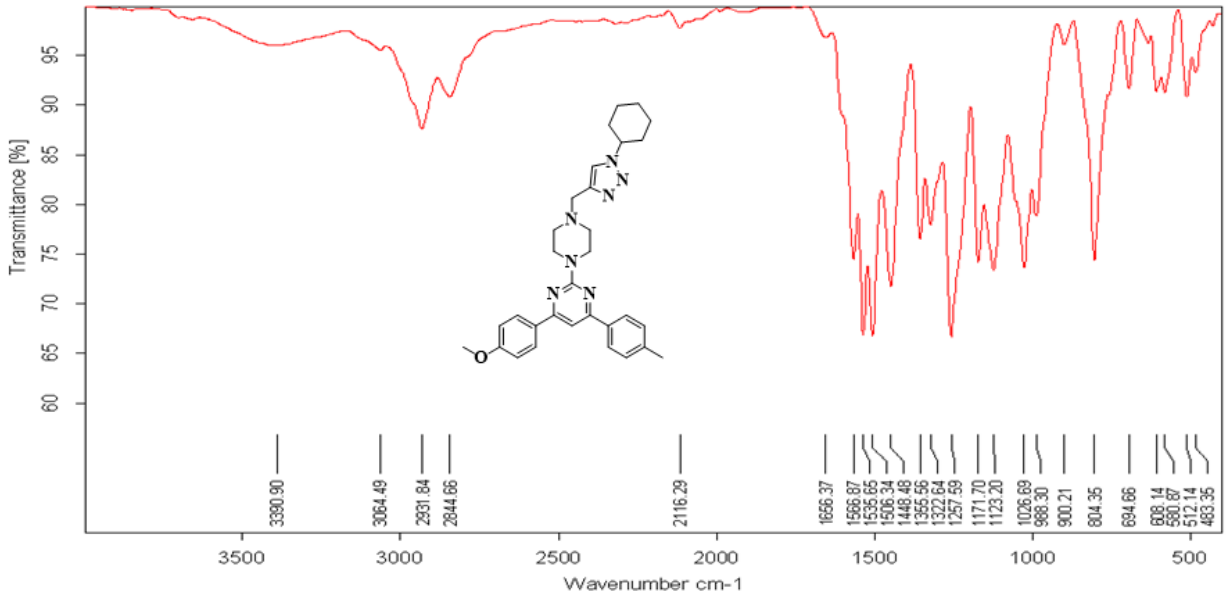

IR spectra

4,6-bis(4-methoxyphenyl)-2-(4-((1-phenyl-1H-1,2,3-triazol-4-yl)methyl)piperazin-1-yl)pyrimidine **(8m)**

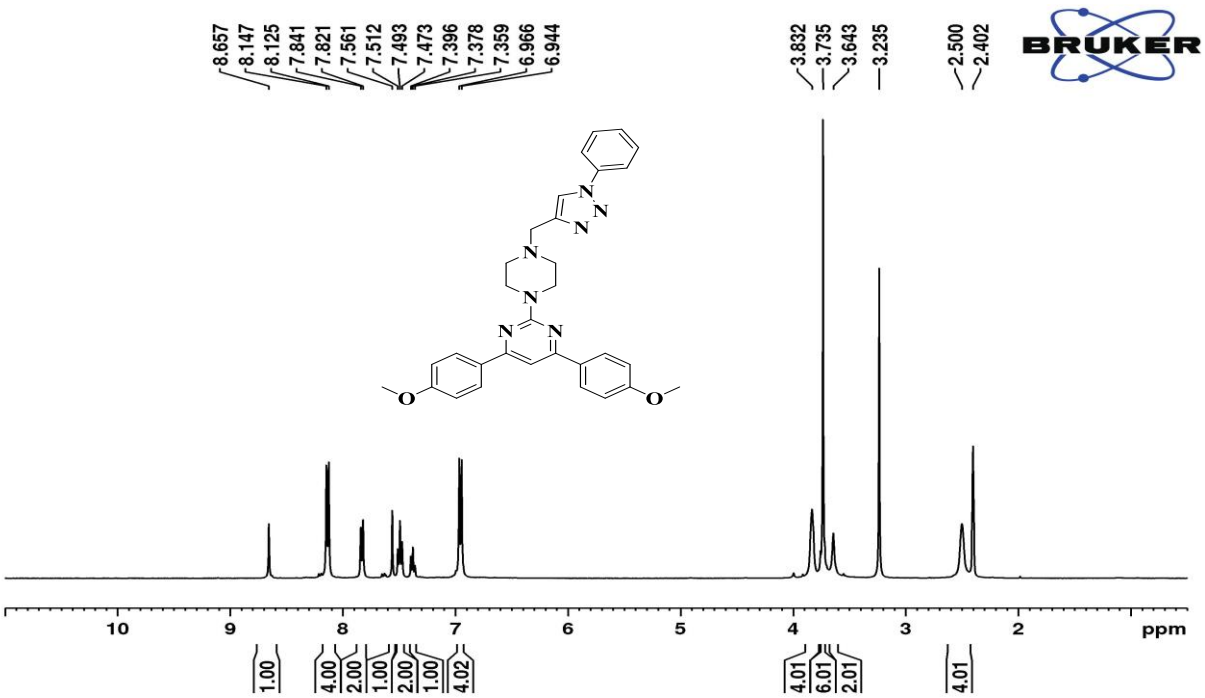

^{1}H NMR (100 MHz, DMSO-d_6)

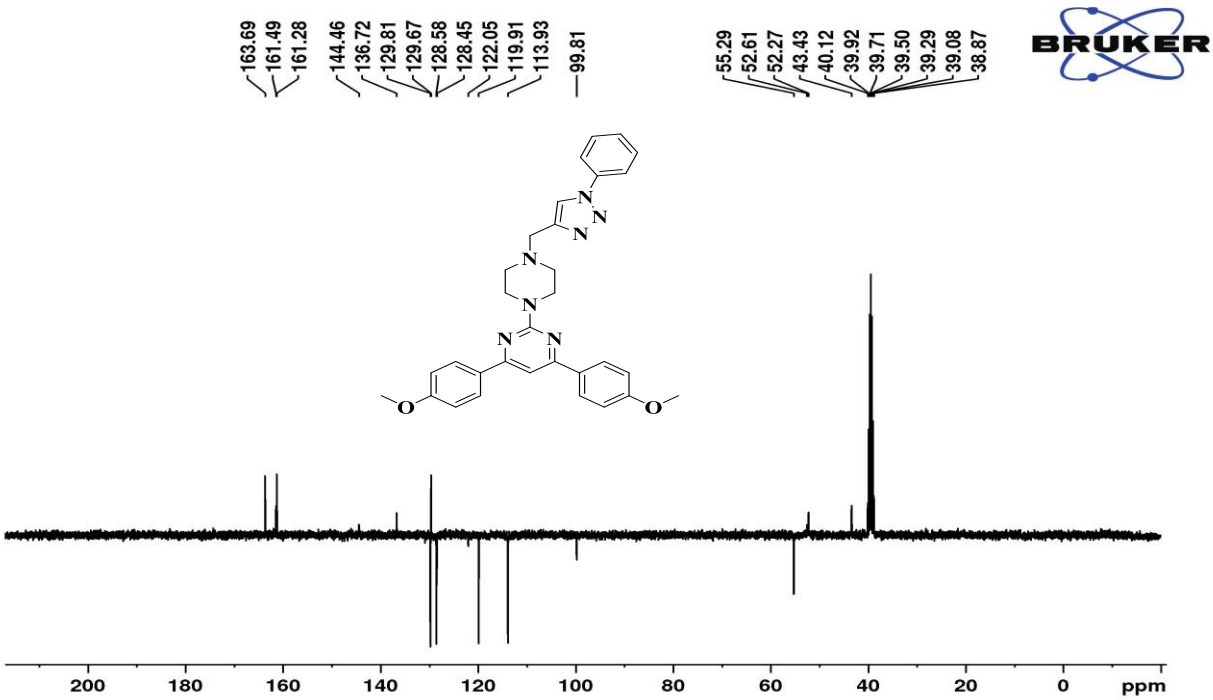

^{13}C NMR (100 MHz, DMSO-d_6)

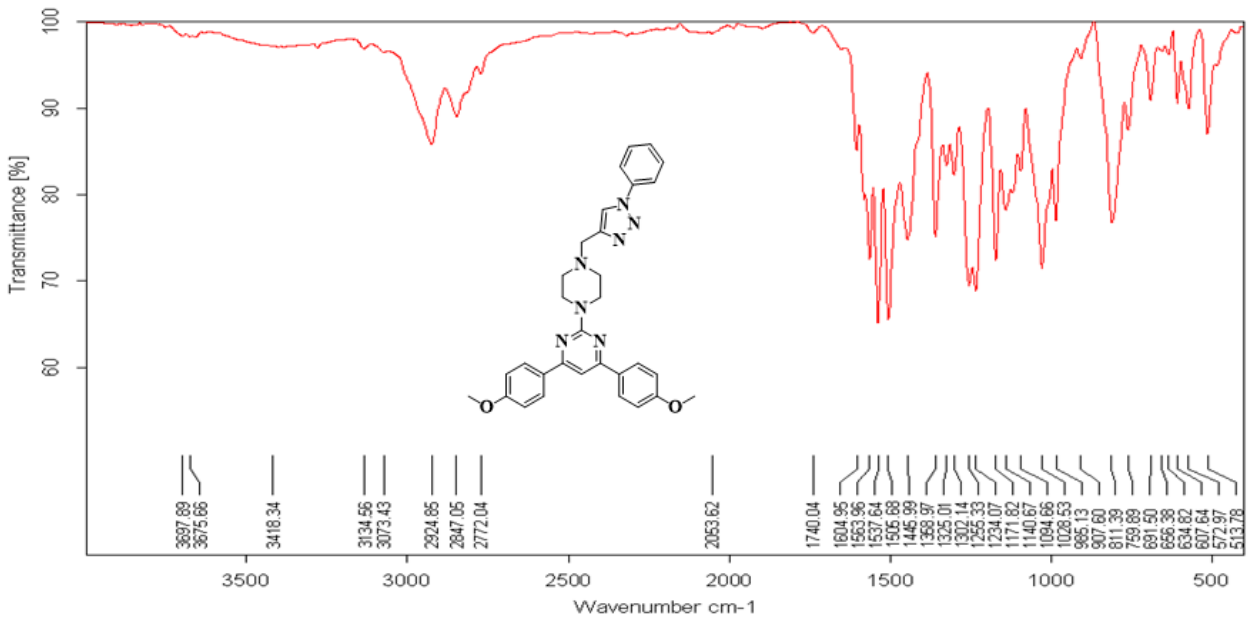

IR spectra

2-(4-((1-(4-fluorophenyl)-1H-1,2,3-triazol-4-yl)methyl)piperazin-1-yl)-4,6-bis(4-methoxyphenyl)pyrimidine **(8n)**

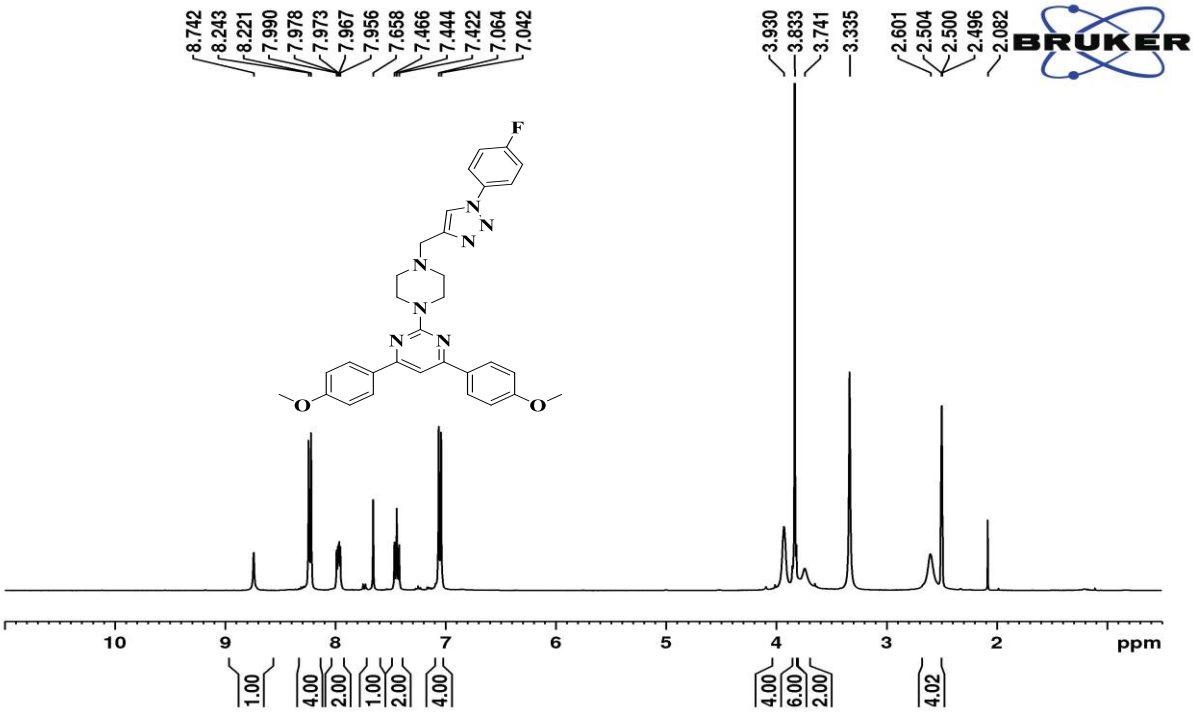

^{1}H NMR (400 MHz, DMSO-d_6)

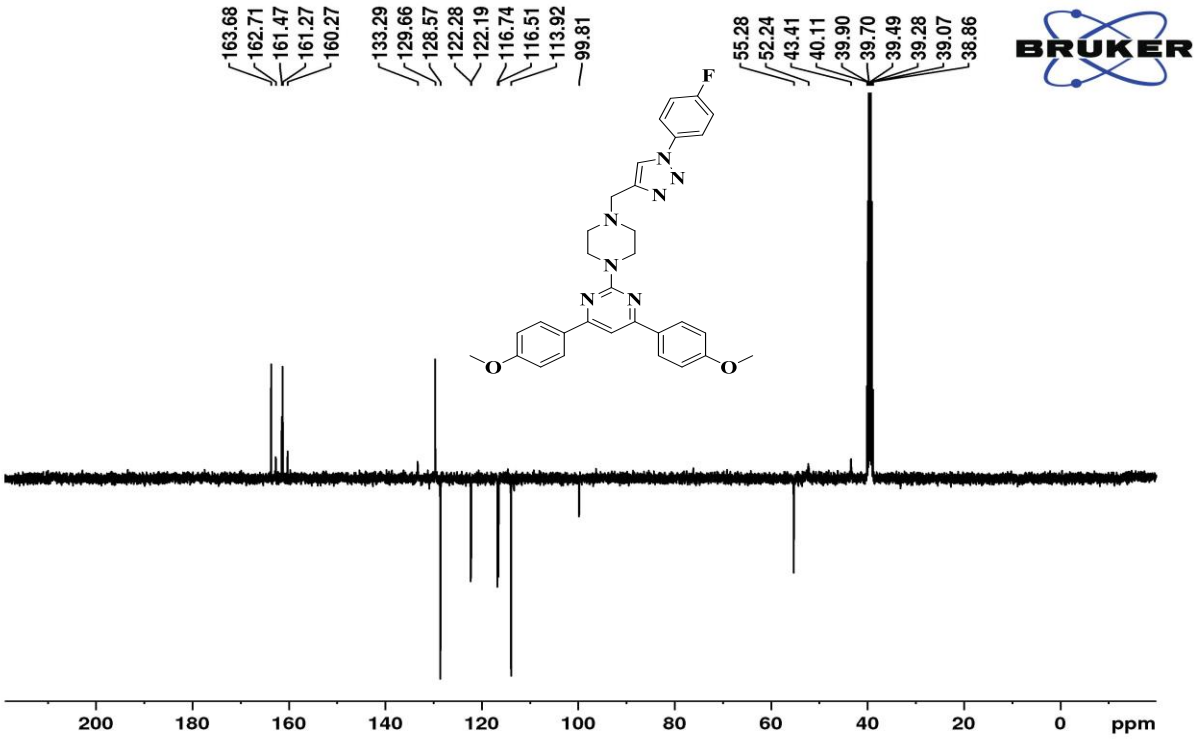

^{13}C NMR (100 MHz, DMSO-d_6)

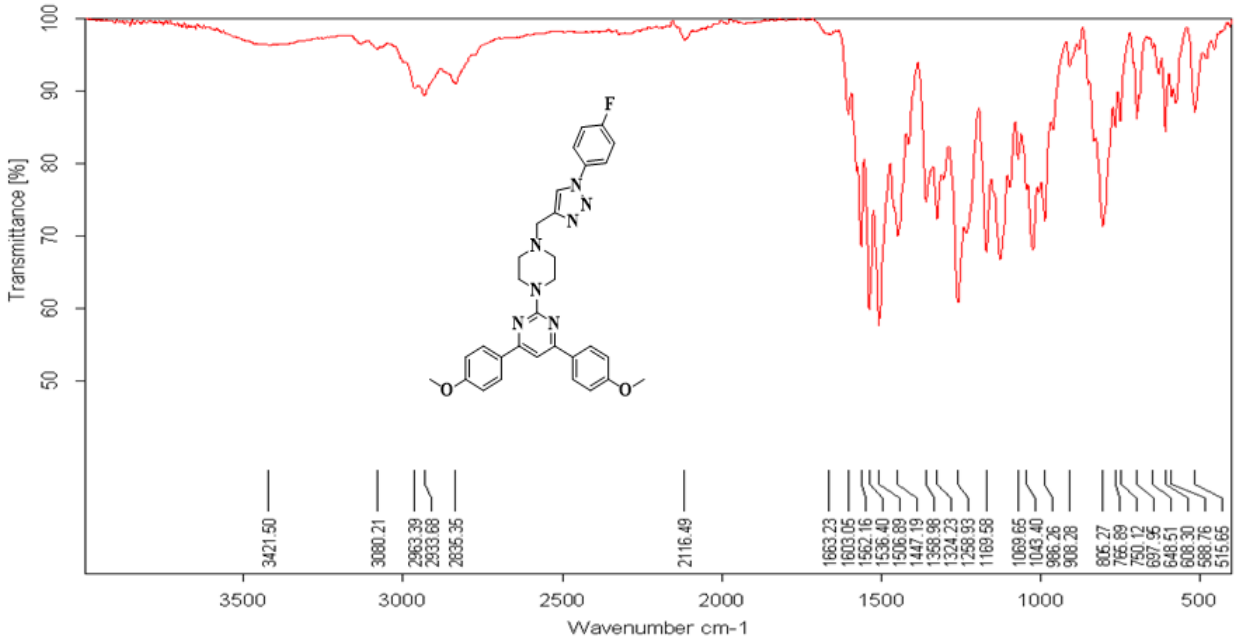

IR spectra

4,6-bis(4-methoxyphenyl)-2-(4-((1-(4-nitrophenyl)-1H-1,2,3-triazol-4-yl)methyl)piperazin-1-yl)pyrimidine (**8o**)

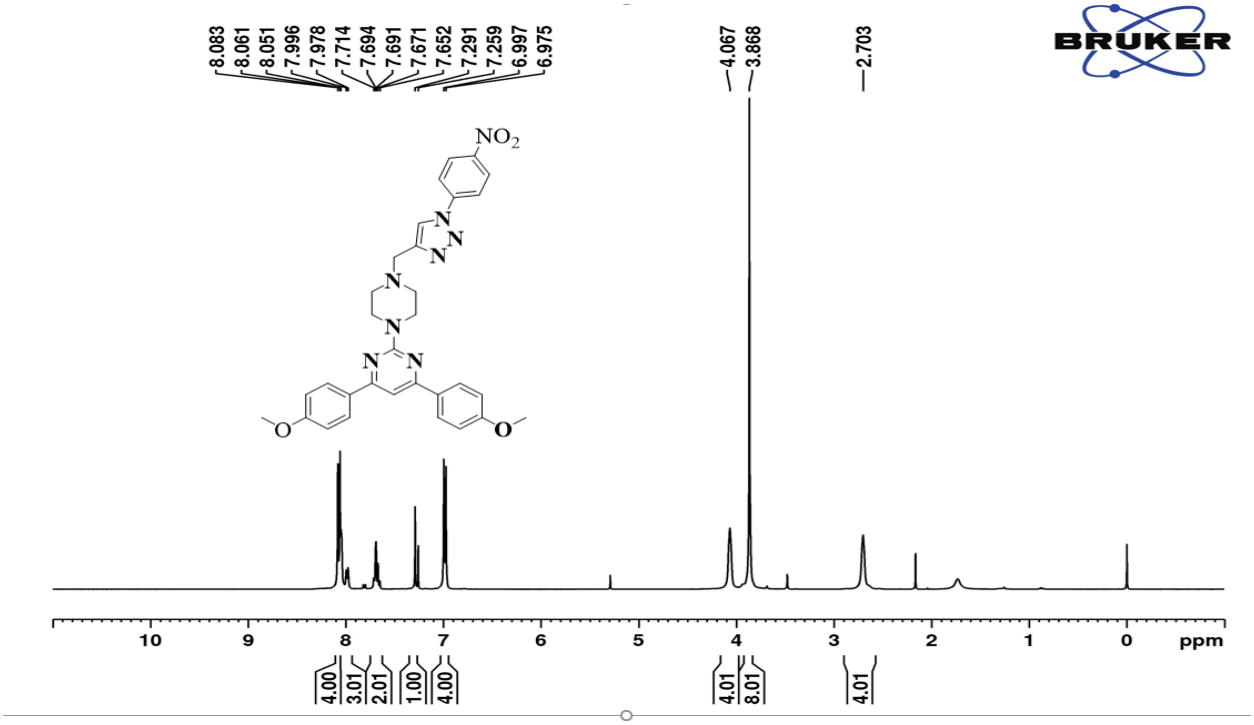

^{1}H NMR (400 MHz, $CDCl_3$)

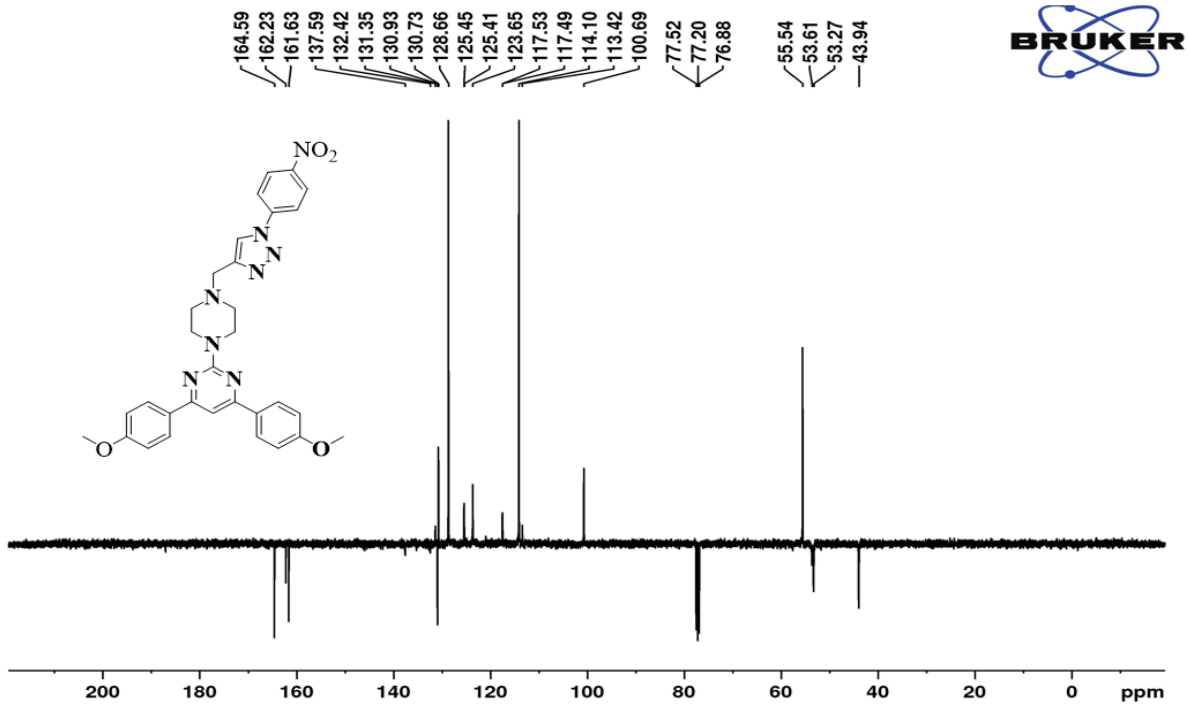

^{13}C NMR (400 MHz, $CDCl_3$)

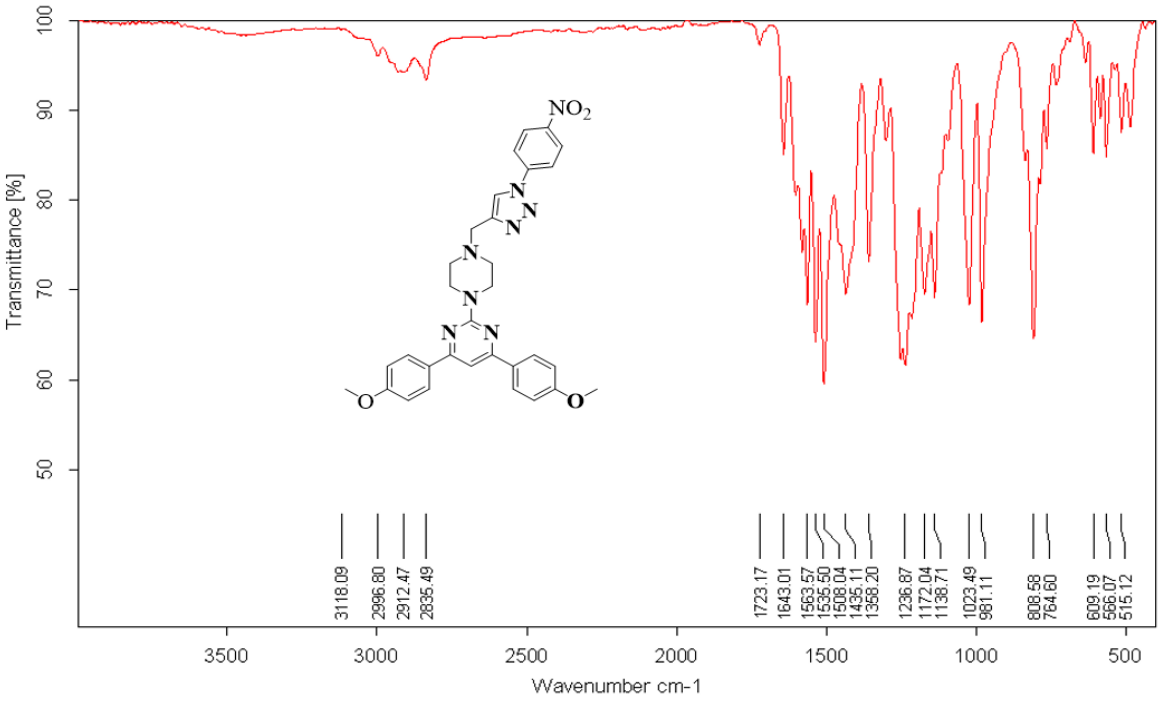

IR spectra

4,6-bis(4-methoxyphenyl)-2-(4-((1-(3-(trifluoromethyl)phenyl)-1H-1,2,3-triazol-4-yl)methyl)piperazin-1-yl)pyrimidine (**8p**)

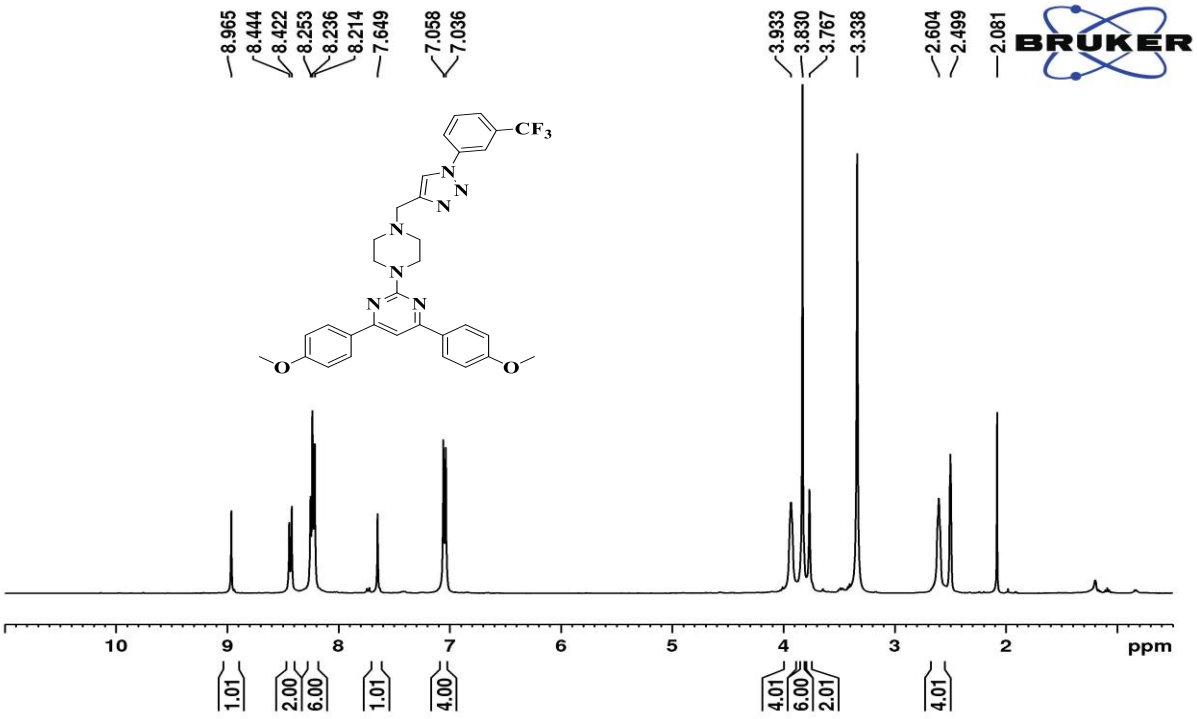

^{1}H NMR (400 MHz, DSMO-d_6)

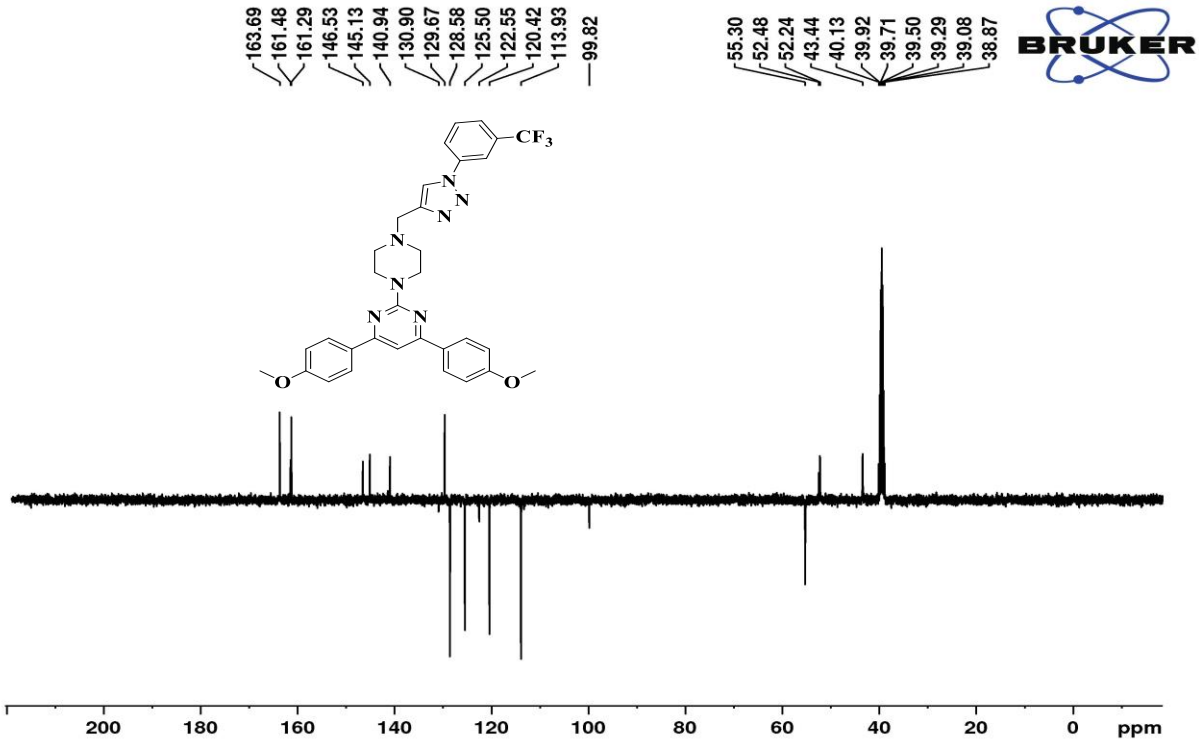

^{13}C NMR (100 MHz, DSMO-*d*$_6$)

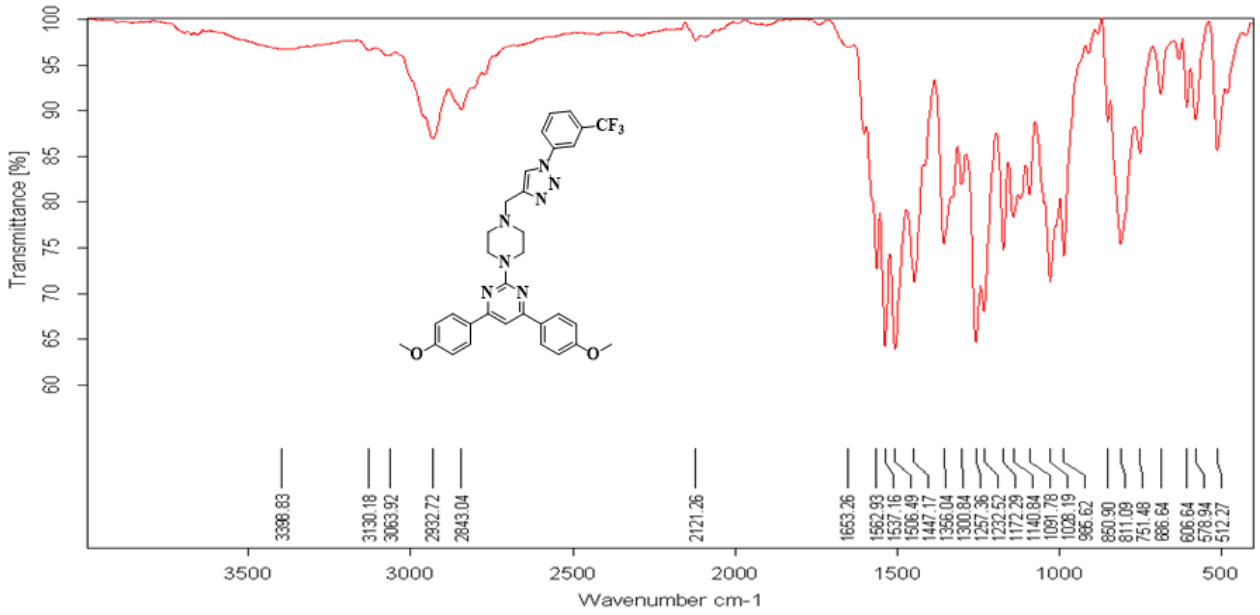

IR spectra

4-(3,4-dimethoxyphenyl)-6-(4-ethylphenyl)-2-(4-((1-phenyl-1H-1,2,3-triazol-4-yl)methyl)piperazin-1-yl)pyrimidin **(8q)**

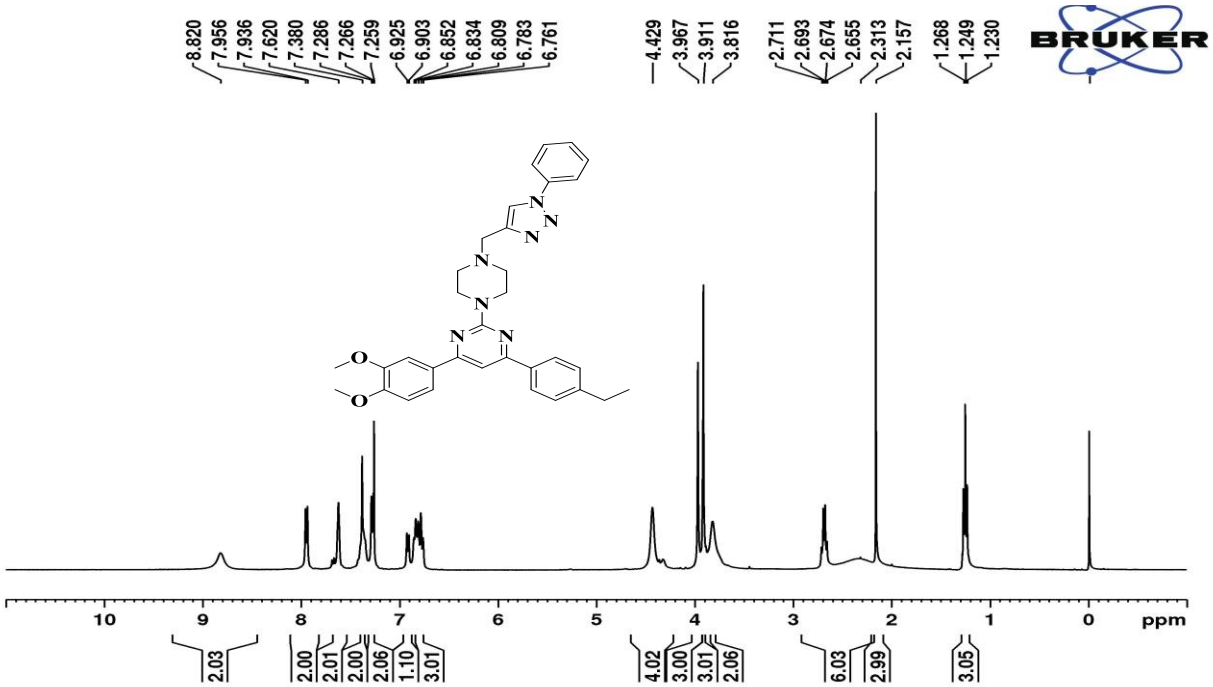

^{1}H NMR (400 MHz, DSMO-d_6)

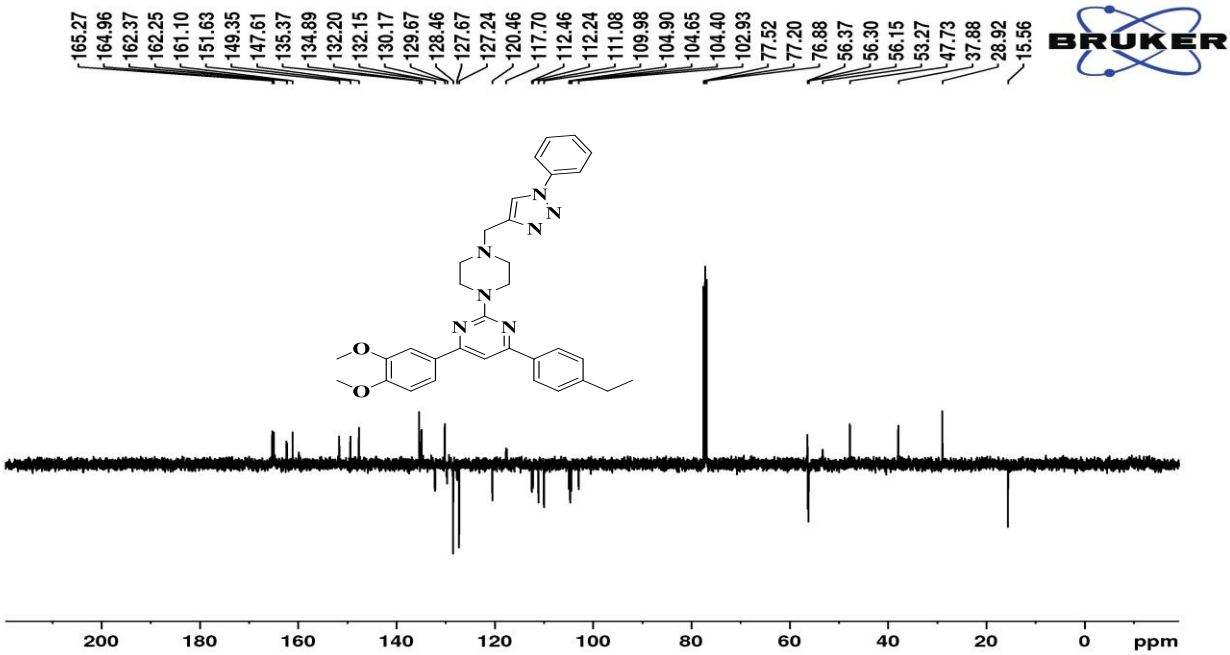

^{13}C NMR (100 MHz, DSMO-d_6)

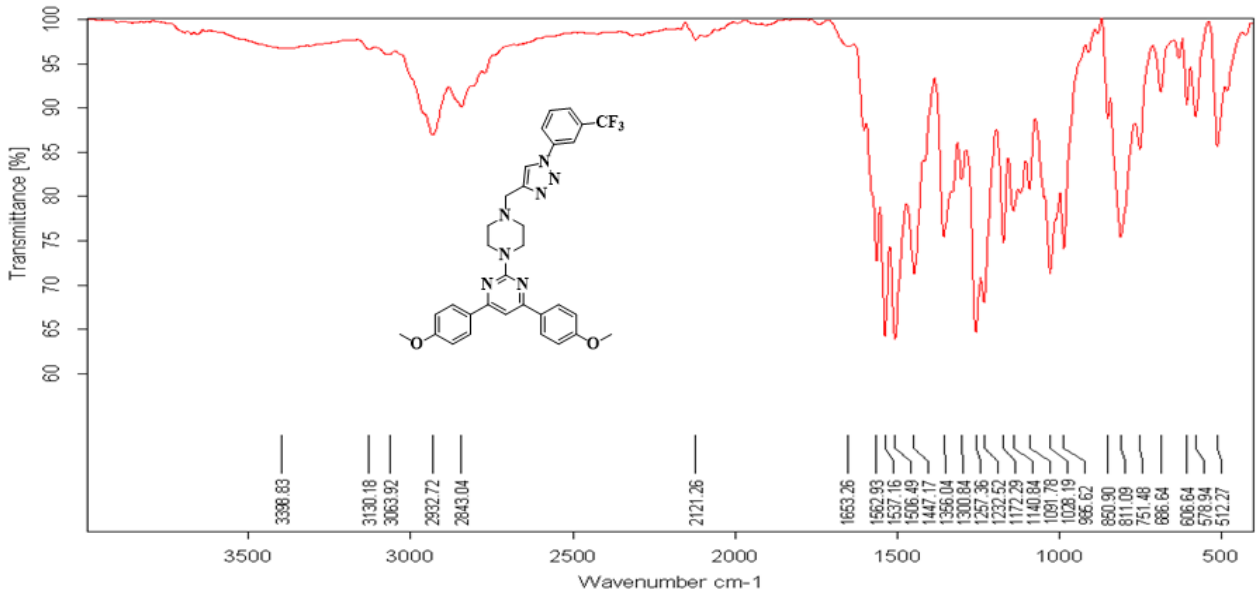

IR spectra

2-(4-((1-(4-chlorophenyl)-1H-1,2,3-triazol-4-yl)methyl)piperazin-1-yl)-4-(3,4-dimethoxyphenyl)-6-(4-ethylphenyl)pyrimidine (**8r**)

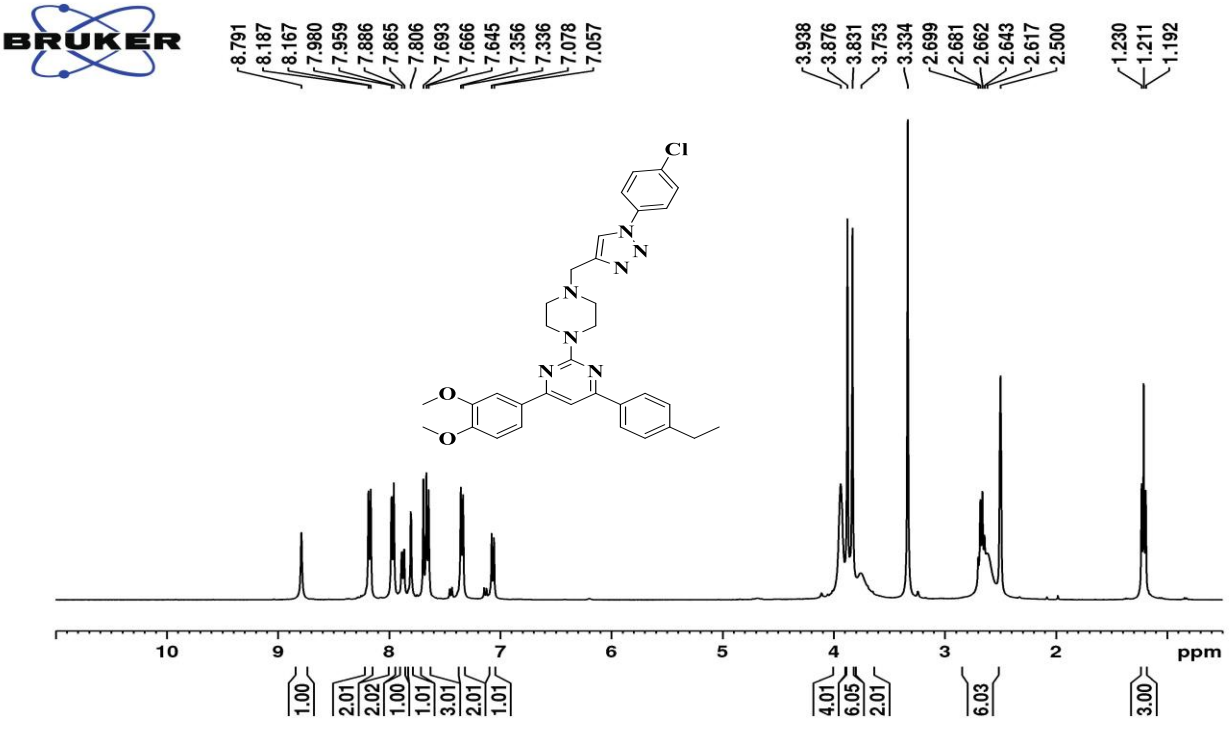

^{1}H NMR (400 MHz, DSMO-d_6)

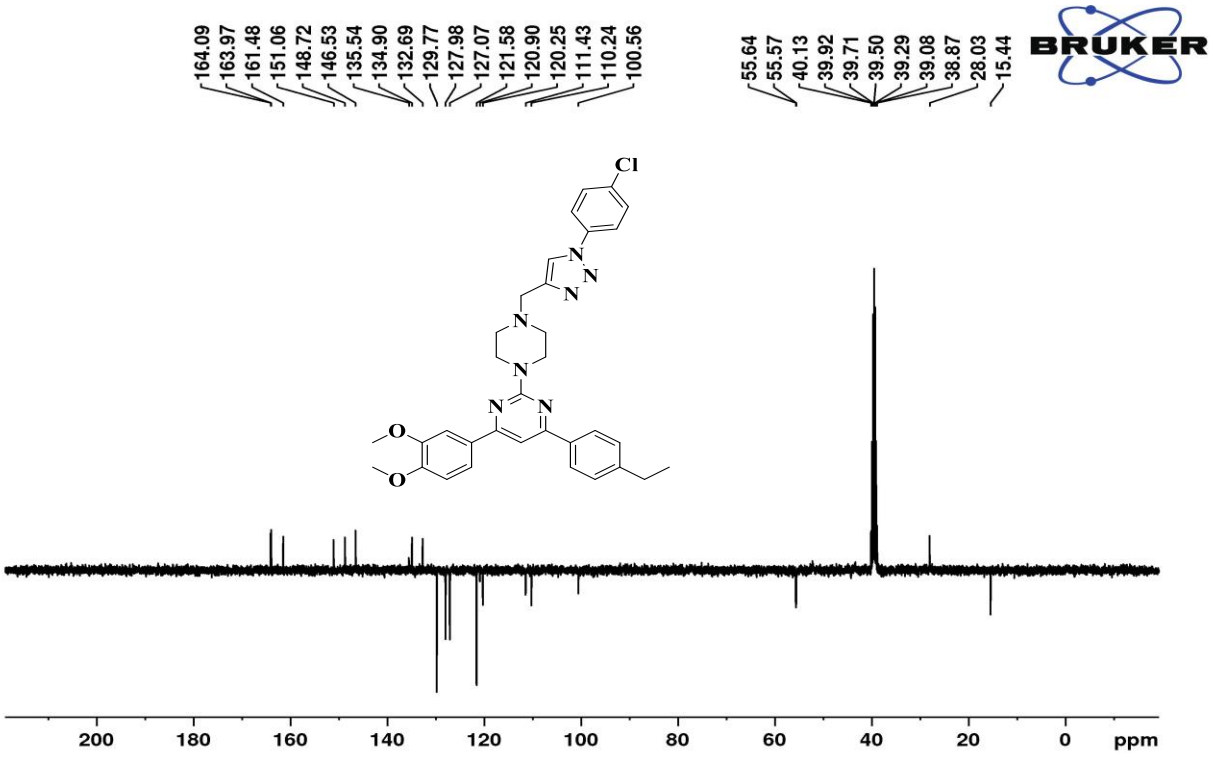

^{13}C NMR (100 MHz, DSMO-d_6)

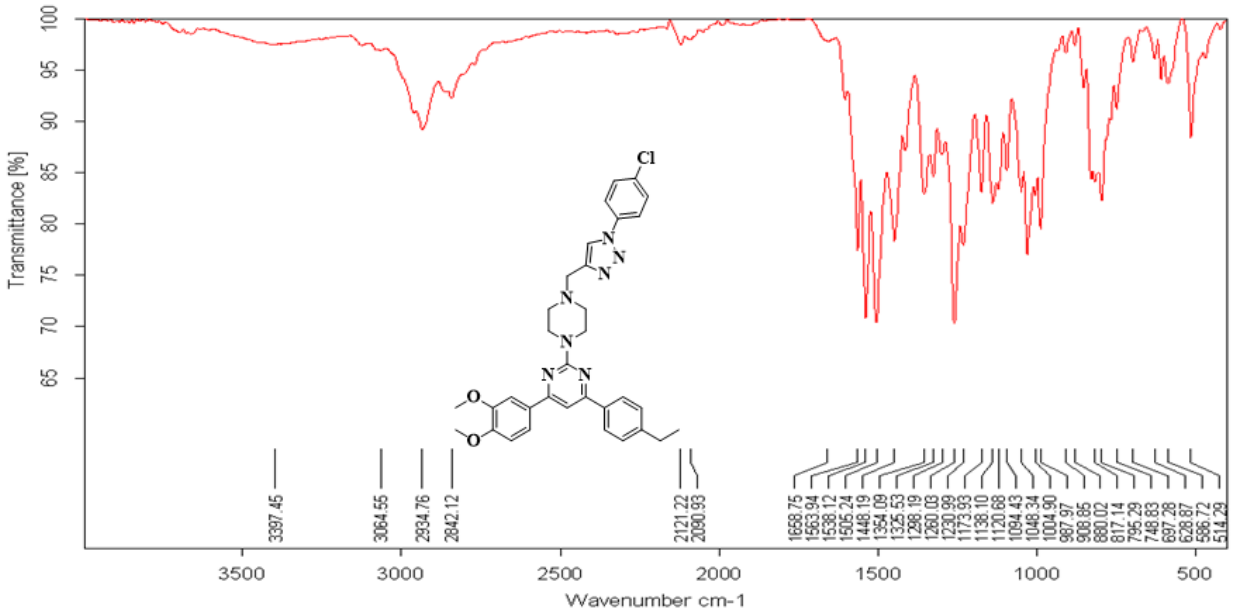

IR spectra

4-(3,4-dimethoxyphenyl)-6-(4-ethylphenyl)-2-(4-((1-(4-(trifluoromethyl)phenyl)-1H-1,2,3-triazol-4-yl)methyl)piperazin-1-yl)pyrimidine **(8s)**

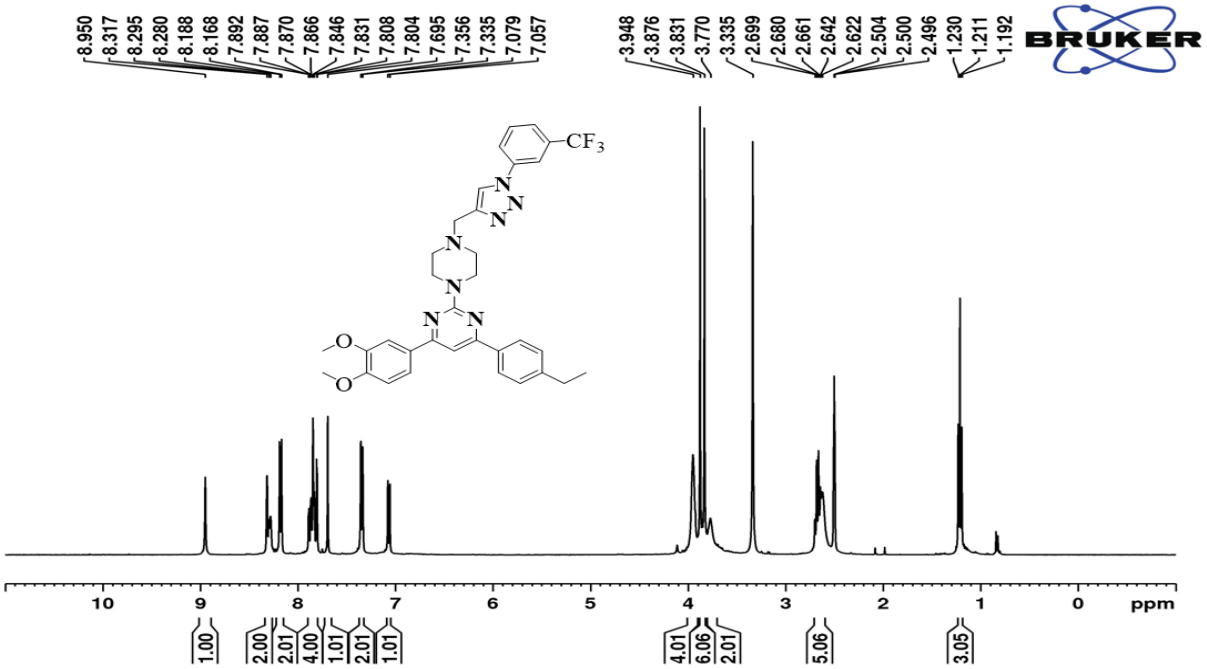

^{1}H NMR (400 MHz, $CDCl_3$)

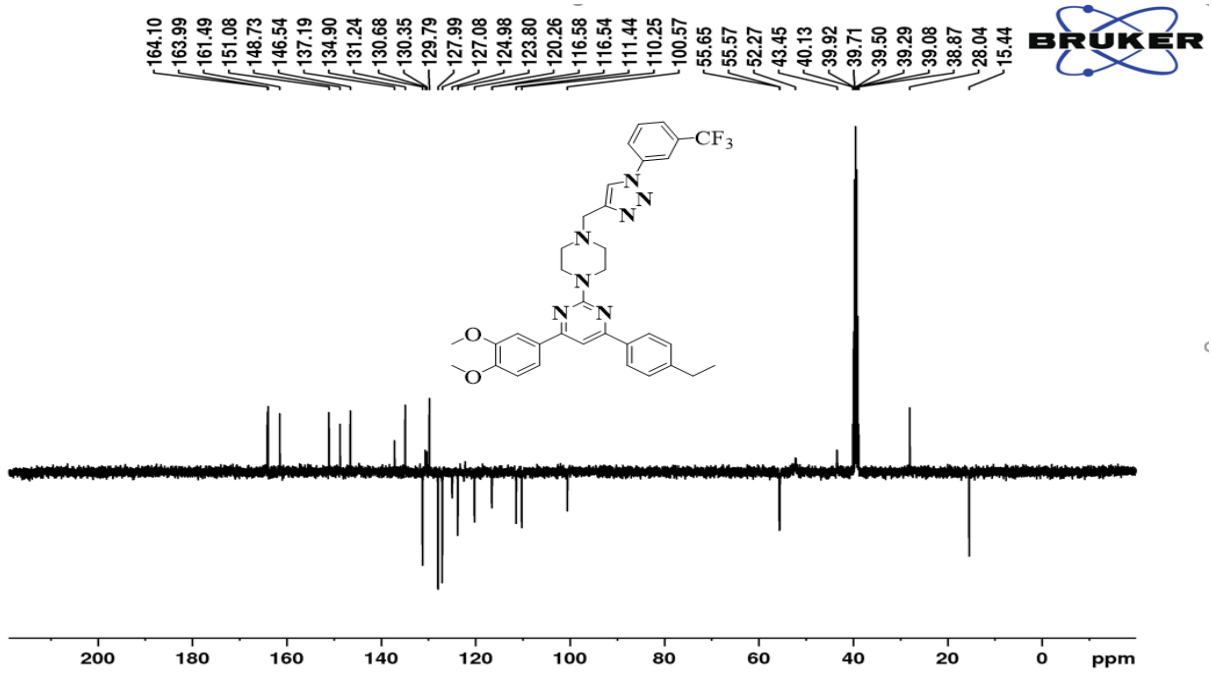

^{13}C NMR (400 MHz, $CDCl_3$)

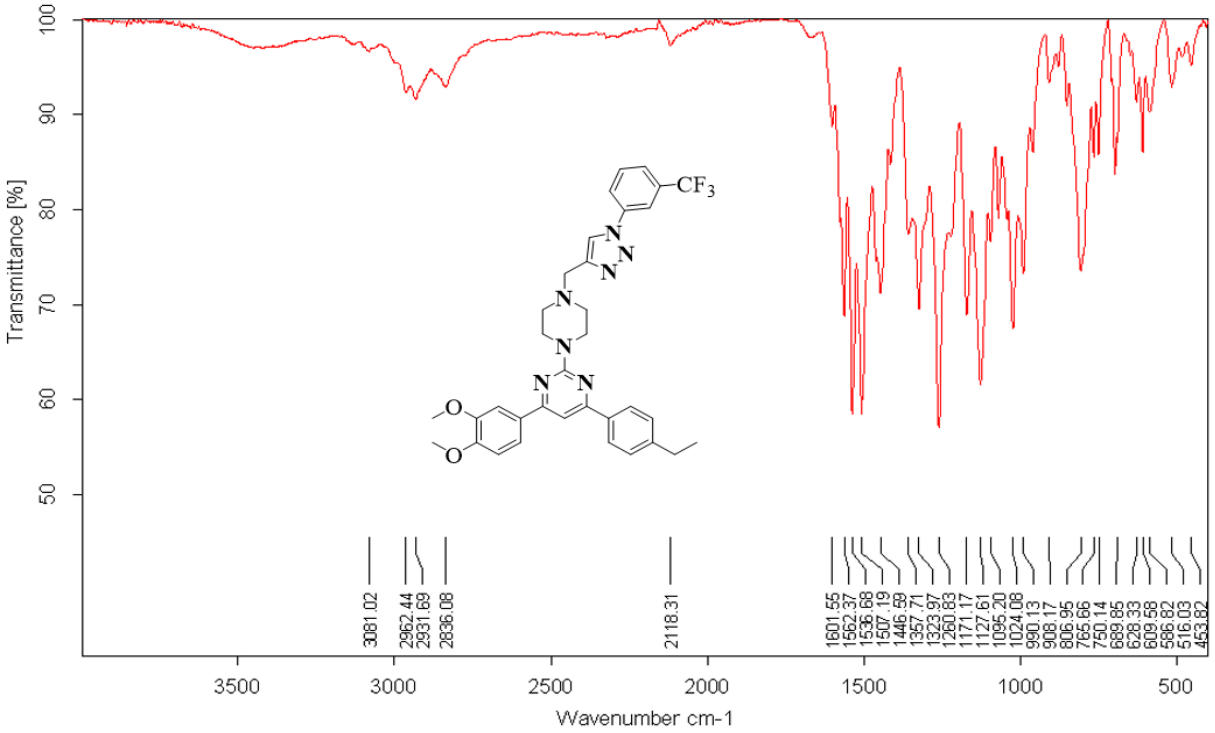

IR spectra

2-(4-((1-(3,5-difluorophenyl)-1H-1,2,3-triazol-4-yl)methyl)piperazin-1-yl)-4-(3,4-dimethoxyphenyl)-6-(4-ethylphenyl)pyrimidine **(8t)**

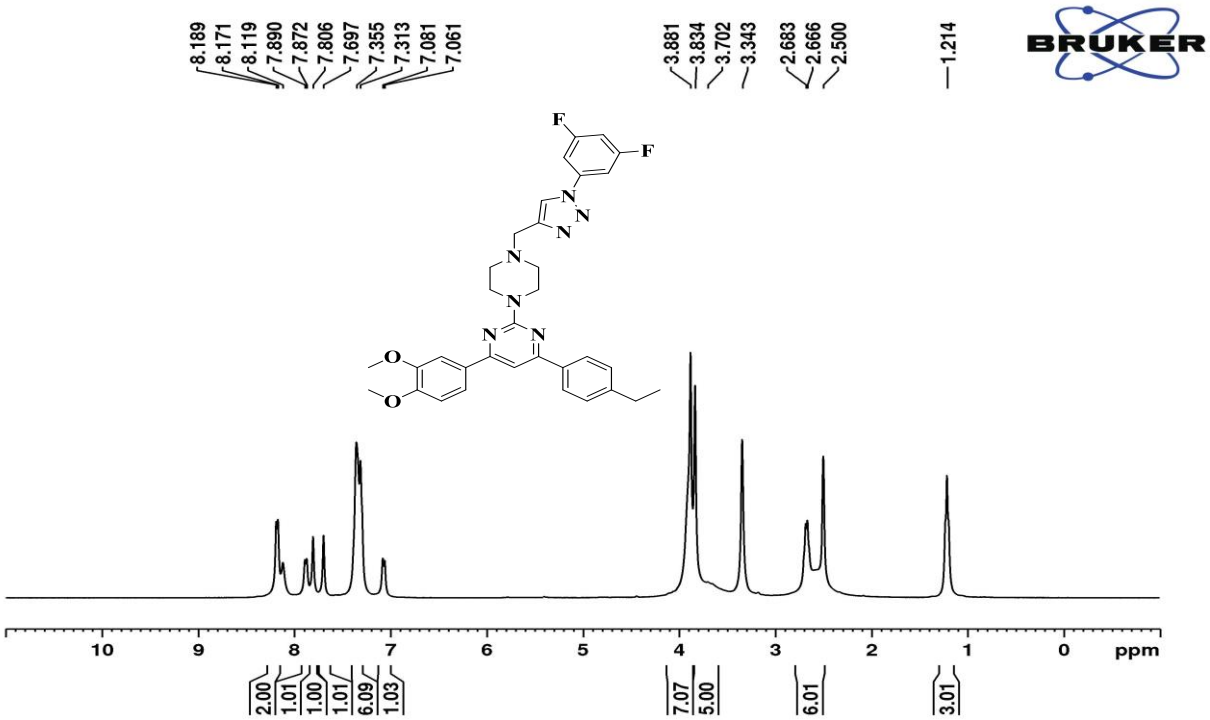

^{1}H NMR (400 MHz, $CDCl_3$)

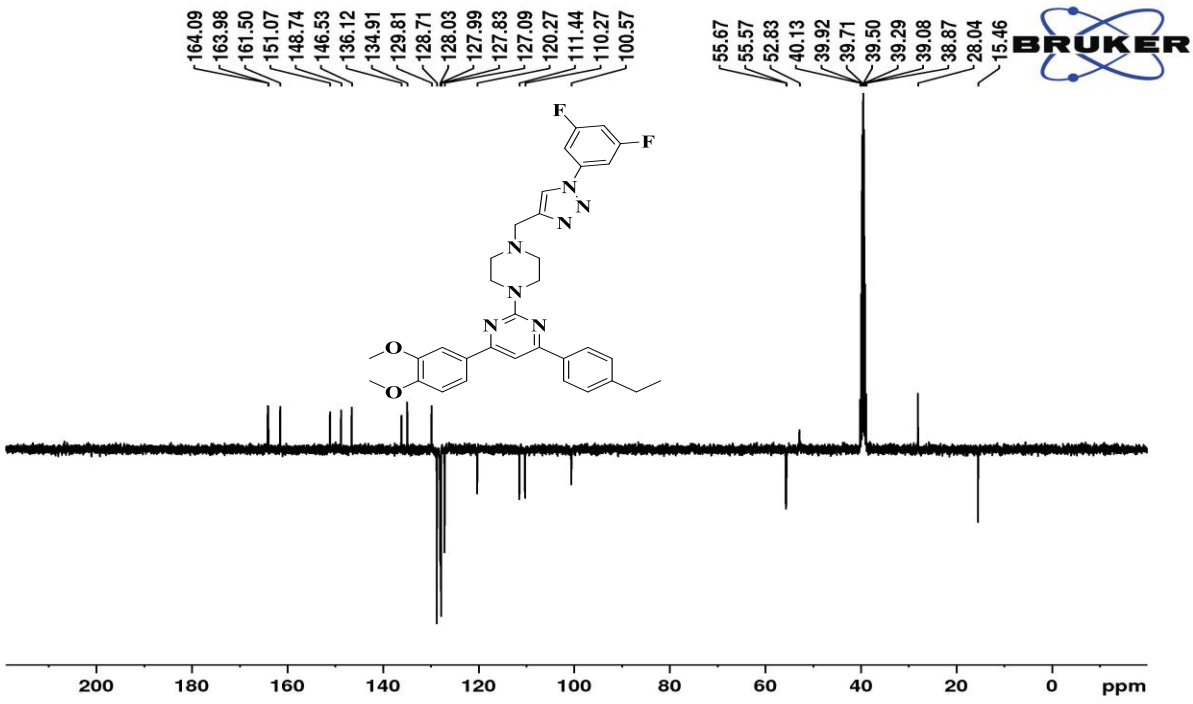

^{13}C NMR (100 MHz, $CDCl_3$)

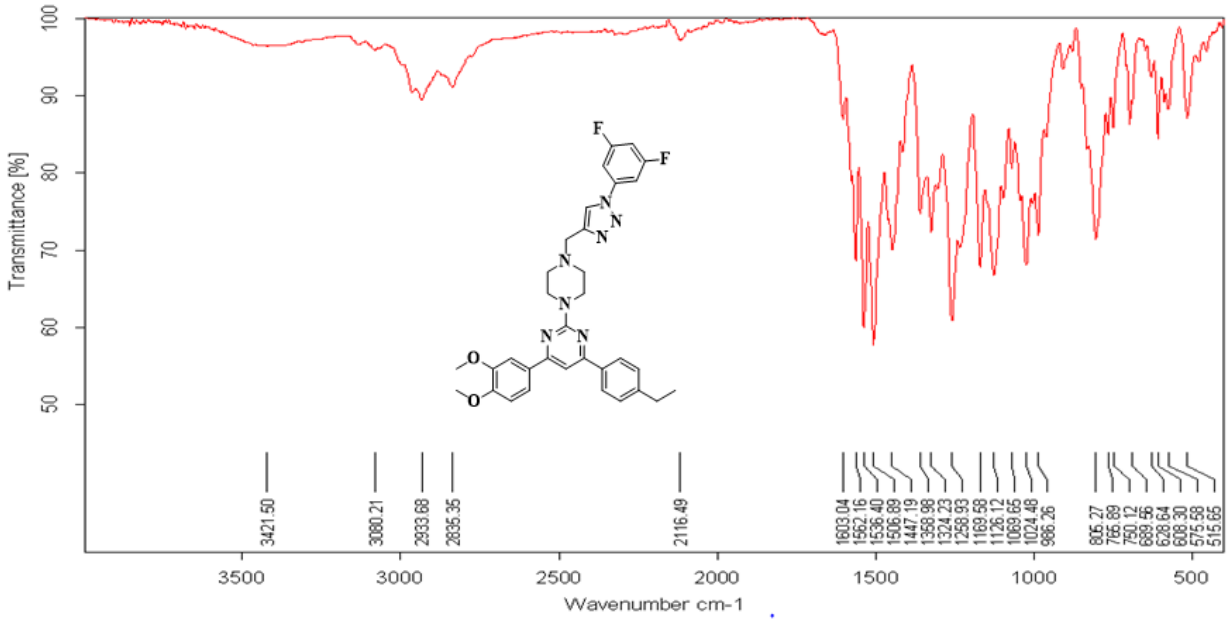

IR spectra

APPENDIX – IV

PUBLISHED PAPERS

APPENDIX-IV

European Journal of Medicinal Chemistry 217 (2021) 113330

Contents lists available at ScienceDirect

European Journal of Medicinal Chemistry

journal homepage: http://www.elsevier.com/locate/ejmech

Design and synthesis of quinoline-pyrimidine inspired hybrids as potential plasmodial inhibitors

Francis Kayamba [a], Teboho Malimabe [b, c], Idowu Kehinde Ademola [d], Ofentse Jacob Pooe [e], Narva Deshwar Kushwaha [a], Mavela Mahlalela [a], Robyn L. van Zyl [b, c], Michelle Gordon [d], Pertunia T. Mudau [f], Tawanda Zininga [f, g], Addmore Shonhai [g], Vincent O. Nyamori [h], Rajshekhar Karpoormath [a, *]

[a] Department of Pharmaceutical Chemistry, College of Health Sciences, University of KwaZulu-Natal, Durban, 4000, South Africa
[b] Pharmacology Division, Department of Pharmacy and Pharmacology, Faculty of Health Sciences, University of Witwatersrand, Johannesburg, 2193, South Africa
[c] WITS Research Institute for Malaria (WRIM), Faculty of Health Sciences, University of Witwatersrand, Johannesburg, 2193, South Africa
[d] School of Laboratory Medicine and Medical Sciences, College of Health Science, University of KwaZulu-Natal, Durban, 4000, South Africa
[e] Discipline of Biochemistry, School of Life Sciences, University of KwaZulu-Natal, Durban, 4000, South Africa
[f] Department of Biochemistry University of Venda, School of Mathematical and Natural Sciences, Thohoyandou, 0950, South Africa
[g] Department of Biochemistry, Stellenbosch University, Stellenbosch, 7600, South Africa
[h] School of Chemistry and Physics, University of KwaZulu-Natal, Westville Campus, Durban, 4000, South Africa

ARTICLE INFO

Article history:
Received 29 October 2020
Received in revised form
18 February 2021
Accepted 24 February 2021
Available online 3 March 2021

Keywords:
Molecular hybrids
Quinoline
Pyrimidine
Antimalarial agents
Malaria
Antiprotozoal
Piperazine
PfHsp70

ABSTRACT

Presently, artemisinin-based combination therapy (ACT) is the first-line therapy of *Plasmodium falciparum* malaria. With the emergence of malaria parasites that are resistant to ACT, alternative antimalarial therapies are urgently needed. In line with this, we designed and synthesised a series of novel *N*-(7-chloroquinolin-4-yl)-*N'*-(4,6-diphenylpyrimidin-2-yl)alkanediamine hybrids (**6a-7c**) and evaluated their inhibitory activity against the NF54 chloroquine-susceptible strain as a promising class of antimalarial compounds. The antiplasmodial screening revealed that seven analogues showed promising to good activity with half-maximal inhibitory concentration (IC_{50}) = 0.32 μM–4.30 μM. Compound **7a** with 1,4-diamine butyl linker and 4-hydroxyl phenyl on fourth and sixth position of pyrimidine core showed the most prominent activity with an IC_{50} value of 0.32 ± 0.06 μM, with a favourable safety profile of 9.79 to human kidney epithelial (HEK293) cells. The remaining six analogues showed moderate activity with IC_{50} values ranging from 7.50 μM to 83.01 μM. We further investigated the binding affinities of the molecules to two essential cytosolic *P. falciparum* heat shock protein 70 homologues; PfHsp70-1 and PfHsp70-z. Compound **7a** exhibited the highest binding affinity for both PfHsp70s with K_D in a lower nanomolar range (4.4–11.4 nM). Furthermore, molecular docking revealed that compounds **6**, **6k**, **7b** and **7a** exhibited better fitness in PfHsp70-1 with compound **7a** showing the highest and lowest binding scores of −9.8 kcal/mol. Therefore, we speculate that PfHsp70-1 is one of the targets of these inhibitors. The bioisoteric replacement of the groups at phenyl ring at the fourth and sixth position of the pyrimidine core had a constructive association with antiplasmodial activity. The promising antiplasmodial activity of the synthesised analogues illustrates how crucial molecular hybridisation is as a strategy in the development of quinoline-pyrimidine hybrids as prospective antiprotozoal agents.

1. Introduction

The evolution of *Plasmodium* strains has caused uncertainty in the treatment of malaria, and thousands of people are still dying as a result of the advent of resistance on current treatment such as artemisinin combination therapies (ACTs) and chloroquine (CQ) [1]. Malaria is predominately spread by *P. falciparum* which is more prevalent in Africa. An estimate of 228 million people were infected with malaria in 2018, killing approximately 405 000 people, of which over 90% were in Sub-Saharan Africa. Children under the age

* Corresponding author.
E-mail address: karpoormath@ukzn.ac.za (R. Karpoormath).

https://doi.org/10.1016/j.ejmech.2021.113330
0223-5234/

of five and pregnant women are the major victims of the scourge, especially those in poor tropical regions. About 3.2 billion people remain at risk of the epidemic [2,3]. Thus, necessitating the need for alternative therapy in the absence of an efficient antimalarial vaccine [4].

An audit of antimalarial pharmacophores revealed that, in addition to other vast medicinal properties, the pyrimidine moiety displayed admirable antimalarial properties. It has proven to be key in some drugs and lead antimalarial candidates at an advanced stage of clinical trials. Amongst the leading antimalarial pharmacophores are proguanil, pyrimethamine, P218 and WR9920. Most antimalarial pyrimidine-based drugs hold prospects as prophylactic agents. These compounds target *P. falciparum* dihydrofolate reductase, which is implicated in the folic acid pathway that is essential for DNA biosynthesis [5]. Chalcones are another class of analogues well-known for excellent antimalarial therapy; where for example, licochalcone, a natural flavonoid product was active against CQ-susceptible (3D7) and CQ-resistance (Dd2) strains [6,7]. The phenyl groups of chalcone were important for antiplasmodial activity as indicated by SAR studies, and as such, we tried to integrate these pharmacophores into the modified potent molecule [8]. Given this context, we expected that a promising antiplasmodial agent would be the combination of active pharmacophores inspired by pyrimethamine and chalcone to produce a 4,6-diphenylpyrimidine. Fig. 1 shows CQ and other potential antimalarial compounds that were crucial in designing this novel series.

While antimalarial drugs, such as piperaquine and CQ, based on a quinoline backbone are inexpensive with a robust therapeutic index, they have lost efficacy as stand-alone drugs due to the emergence of resistance [9,10] mediated by a mutated form of the *Plasmodium falciparum* chloroquine resistance "transporter" [11,12]. Although prospects for CQ reapplication as an antimalarial remain [13], it is its roles as an agent against avian influenza H5N1 and ZIKV viral infections that is gaining more attention [14–16]. SAR studies of CQ revealed that the basic chain is crucial for antimalarial activity by improving the drug's lipophilic, which allows easy passage through the malarial plasma membrane [2]. In light of this, the incorporation of various linkers such as piperazine and different alkyl diamine holds promise towards making effective antimalarial agents. In view of the aforementioned, we synthesised a hybrid molecule, as illustrated in Fig. 2, by a molecular hybridisation approach using two robust moieties viz pyrimidine and quinoline, with the aim of presenting a safer and alternative therapy for malaria. We anticipated presenting an antimalarial candidate effective against both the liver and blood-stages of *Plasmodium*; for potential use for both treatment and prophylaxis.

2. Chemistry

The novel library of quinoline-pyrimidine hybrids **6(a-t**) was synthesised using a versatile synthetic pathway. The intermediate *(E)*-chalcones **1(a–e)** were prepared by aldol condensation reaction as previously reported, using assorted commercially available benzaldehydes and acetophenones using sodium hydroxide basic condition in a good yield of 95% [17]. The cyclisation of chalcone using guanidine hydrochloride and sodium hydroxide base afforded numerous 4,6-diphenylpyrimidin-2-amine **2(a–e)** analogues. Known **Sandmeyer reaction** applies to the substitution of an aromatic amine of compound **2** to hydroxyl (4,6-diphenylpyrimidin-2-ol **3(a–e)** via diazonium salt intermediate formation. Sodium nitrate in acetic acid initiates the diazonium salt formation and then substitution of diazo salt with water. 2-Chloro-4,6-diphenylpyrimidine analogues **4(a–e)** were synthesised from assorted **3** analogues using $POCl_3$ with catalytic DMF as illustrated in Scheme 1.

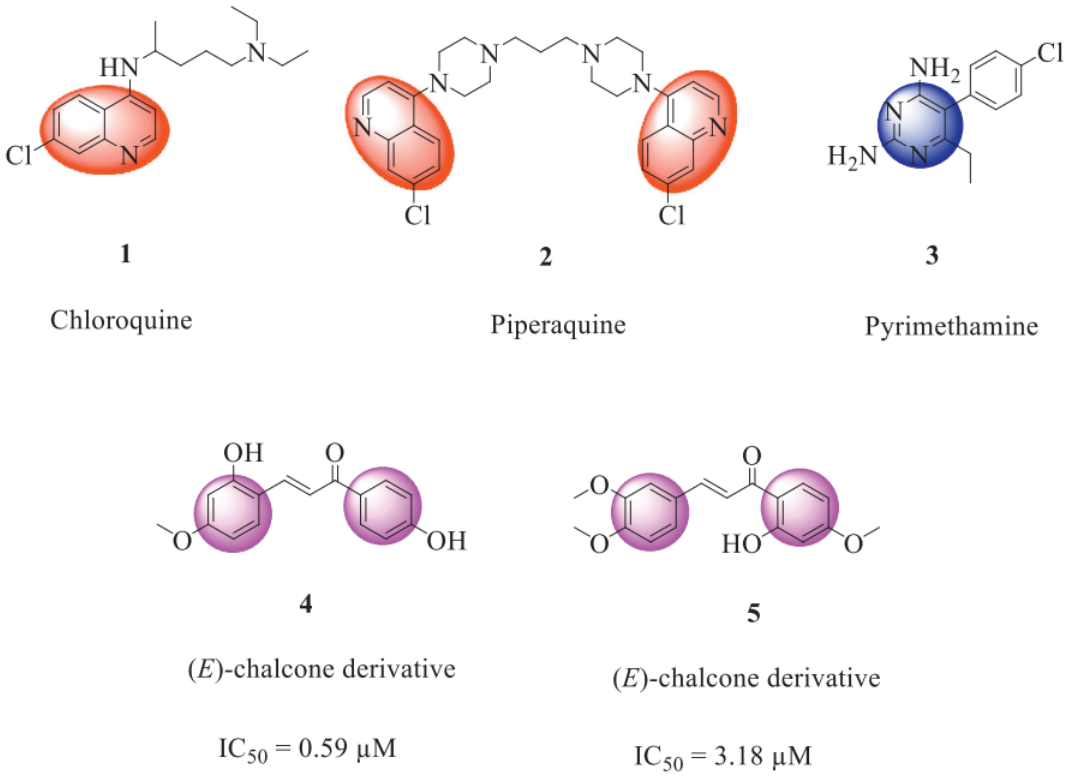

Fig. 1. Marketed drugs and chalcone based potential antimalarial compounds.

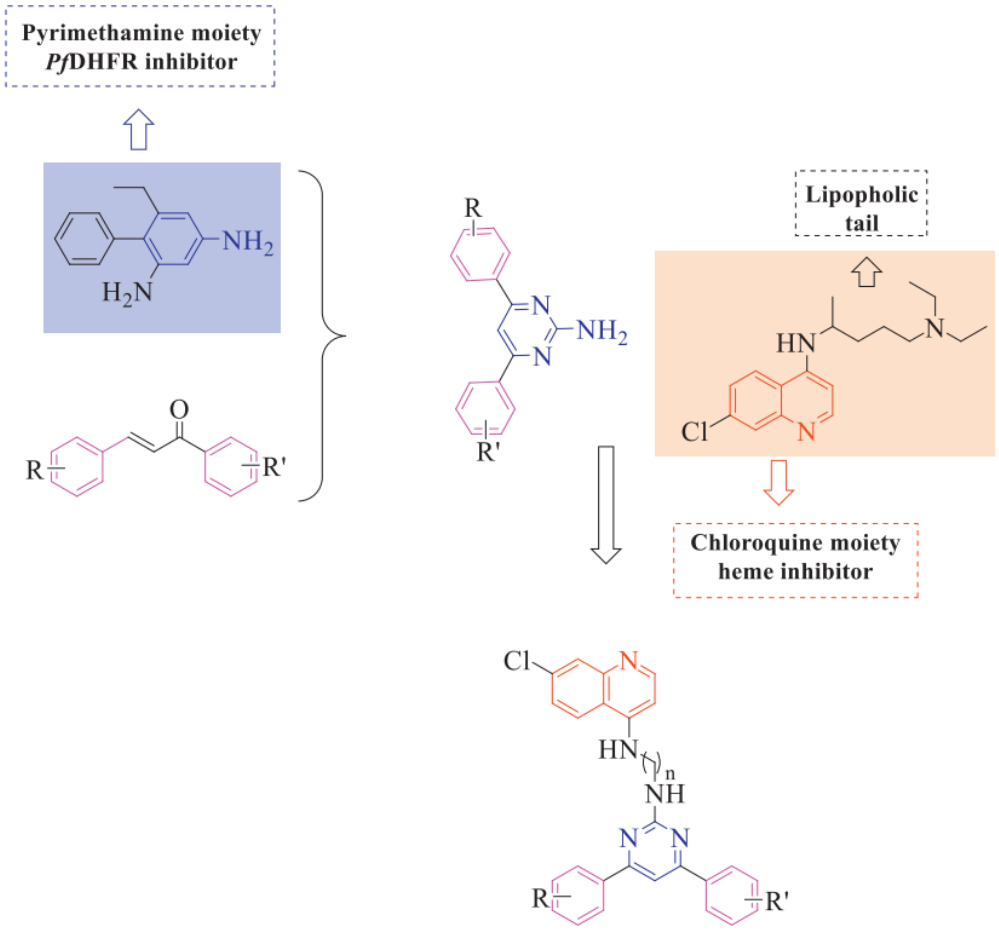

Fig. 2. Rational design of pyrimidine-quinoline hybrid molecules.

The synthesis and characterisation of a series of quinoline-diamine compounds **5(a–d)** were as per reported methods [1]. Various **5(a–d)** compounds were further coupled with various **4(a–e)** compounds using K_2CO_3 to afford a library of the targeted pyrimidine-quinoline hybrids analogues (**6a-7c**). The methoxy substituents on the phenyl group of final compounds **6g**, **6i** and **6j** were further demethylated using HBr acid in a microwave to afford compounds **7a, 7b and 7c,** respectively, in good yield as depicted in Scheme 2.

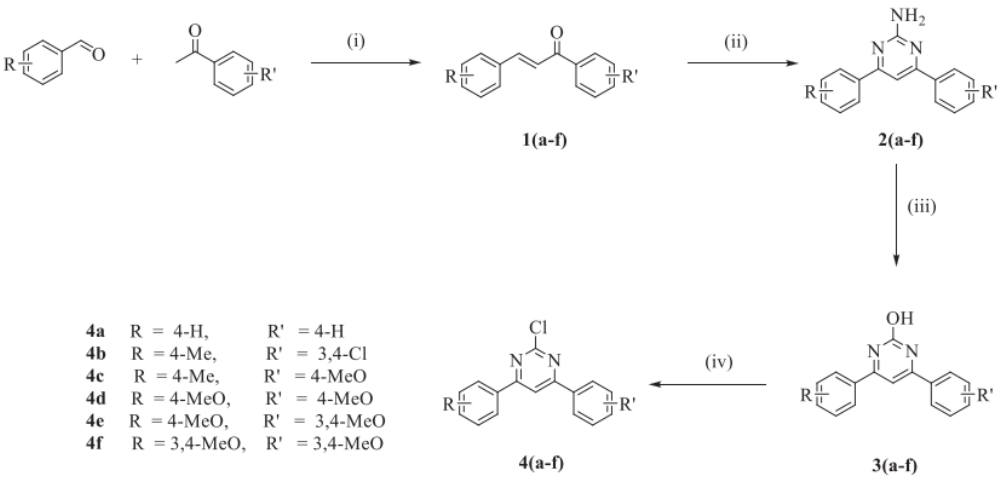

Scheme 1. Reaction conditions: (i) EtOH, NaOH, sonicate, 35 °C, 1 h; (ii) Guandine hydrochloride, NaOH, EtOH, reflux, 24 h; (iii) Acetic acid, $NaNO_2$, H_2O, rt, 3 h; (iv) $POCl_3$, DMF, 100 °C, reflux, 6 h.

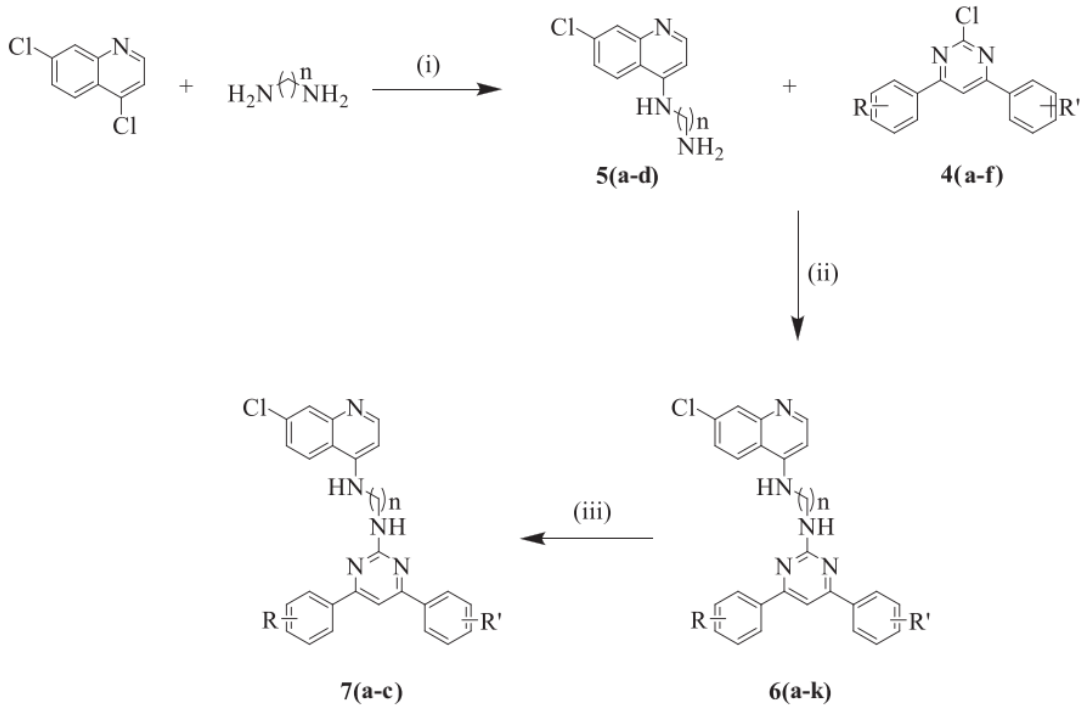

Scheme 2. Reaction conditions: (i) Isopropanol (IPA), reflux, 100 °C, 16 h; (ii) K_2CO_3, Dimethylformamide (DMF), Microwave (MW), 120 °C, 40 min; (iii) HBr, MW, 100 °C, 20 min.

3. Results and discussion

3.1. Synthesis and spectral studies

Structural analysis based on proton nuclear magnetic resource (^{1}H NMR) spectrum of compound **1b** revealed two characteristic doublets resonating at chemical shifts (δ) 7.80–7.77 ppm (Ph-CH=CH) and 7.52–7.49 ppm (Ph-CH=CH) with J = 15.62 Hz and 15.61 Hz, respectively, signifying the formation of a *trans*-olefinic conformation. Other resonating signals were observed on the spectrum at δ 3.89 and 2.39 ppm representing methoxy and methyl substituents on the phenyl groups of the (*E*)-chalcone. The two doublet signals of the olefin disappear on the ^{1}H NMR spectrum of compound **2b**, and two distinctive singlets at signal δ 7.35 ppm (pyr-H) in the aromatic region and the amino signal at δ 5.22 ppm (pyr-NH_2) appeared indicating the formation of a pyrimidine core. The structure of 2-hydroxyl pyrimidine analogue is signified by the vanishing of the amino signal and presence of hydroxyl (OH) signal downfield at δ 11.89 ppm on the H^1 NMR spectrum of compound **3**. The spectrum of the chlorinated compound **4** is characterised by the disappearance of OH signal and minor shifts on pyr-H δ from 7.35 ppm to 7.60 ppm. The ^{1}H NMR spectrum (400 and 600 MHz, DMSO-d_6) of the targeted compound(s), as presented by compound **7d,** is characterised by the presence of two individual peaks; broad singlet resonating at δ 5.04 ppm (-NH) and triplet at 5.55 ppm (-NH) of an aliphatic alkane diamine linker signified coupling of quinoline and pyrimidine motifs. Other distinctive peaks, as aforementioned, included δ 2.46 ppm, 3.52 ppm, 4.06 ppm and 4.07 ppm representing a methyl, methylene, methoxy and methylene, respectively. The outstanding signals from 6.47 to 8.44 ppm represent the aromatic protons for phenyl and piperazine moieties. The spectral properties of the final compound **7g** were confirmed by 2D NMR and further supported by their respective ^{13}C NMR. The most noticeable peak for ^{13}C NMR of the final compound for pyr-H (C9) and methylene for diamine butane line resonate at signal δ ranging from 100.53 to 99.89 pm and 27.42–42.99 ppm, respectively. The methoxy (MeO) peak signal resonates at 55.40 ppm, and the remaining carbon signals correspond to the aromatic carbon. Fig. 3 represents the structures of the final compounds annotated as compound 6 (a-k) and 7 (a-c).

3.2. Antiplasmodial activity

The synthesised novel analogues of (**6a-k** and **7a-c**) were assessed for potency against the NF54 CQ-susceptible strain of *P. falciparum* maintained *in vitro* at the blood stage. Table 1 presents the antiplasmodial activity of the hybrid analogues (**6a-k** and **7a-c**), and standard reference drugs (CQ and quinine). Compound **7a** showed promising activity with IC_{50} values less than 0.5 μM, while the remaining analogues displayed moderate activity in micromolar levels against this CQ-susceptible strain (NF54). The IC_{50} values of the compounds were determined from log sigmoid dose-response curves using GraphPad Prism® 5.0.0 (GraphPad Software, Inc San Diego, CA). Given the antiplasmodial activity, we assessed a reasonable number of analogues to establish a brief structure-activity relationship (SAR) towards identifying the groups accounting for the activity. The bioisosteric replacement on the phenyl rings on the fourth and sixth position of pyrimidine core, and linker coupling the pyrimidine and quinoline positively correlated with the antiprotozoal activity as shown in Table 1.

From the screened compounds, only compounds **7a** showed substantial plasmodial inhibitory activity with $IC_{50} = 0.32 \pm 0.06$ μM, while the other six promising hybrids namely compounds 6**d**, **6e**, **6f**, **6i**, **7b** and **7c** portrayed moderate activity with IC_{50} ranging from 0.50 to 4.30 μM (Table 1). The remaining compounds (**6a**, **6b**, **6c**, **6g**, **6h**, **6j** and **6k**) displaying IC_{50} values < 5 μM were considered inactive. Compound **6i** had a moderate activity with IC_{50} value of 2.61 ± 1.00 μM, and compounds **6g** and **6j** appraised inactive with IC_{50} values of 83.01 ± 1.46 μM and 17.81 ± 1.18 μM, respectively. However, demethylation of the methoxy groups from these compounds resulted into improved aqua solubility that consequently increased the antiplasmodial activity of **7a**, **7b** and **7c** with IC_{50}

APPENDIX-IV

Diamino alkane linker based derivatives

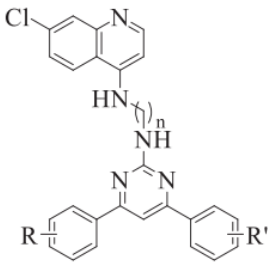

6b n = 4, R = 4-Me, R' = 4-Cl
6d n = 2, R = 4-Me, R' = 4-MeO
6e n = 3, R = 4-Me, R' = 4-MeO
6g n = 4, R = 4-MeO, R' = 4-MeO
6i n = 4, R = 4-MeO, R' = 3,4-MeO
7a n = 4, R = 4-OH, R' = 4-OH
7b n = 4, R = 4-OH, R' = 3,4-OH

Piperazine linker based derivatives

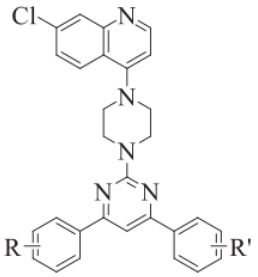

6a R = 4-H, R' = 4-H
6c R = 4-Me, R' = 4-Cl
6f R = 4-Me, R' = 4-MeO
6h R = 4-MeO, R' = 4-MeO
6j R = 4-MeO, R' = 3,4-MeO
6k R = 3,4-MeO, R' = 3,4-MeO
7c R = 4-OH, R' = 3,4-OH

Fig. 3. Structures of the final compounds **6 (a–k)** and **7 (a–c)**.

Table 1
In vitro antiplasmodial activity of compounds (**6a-6k**) and (**7a-7c**).

Compound No	n	R	R′	Antimalarial		Cytotoxicity		Selective Index
				IC_{50} (μM)	SD	IC_{50} (μM)	SD	
6a	p	4-H	4-H	7.50	1.49	nd	nd	Nd
6b	4	4-Me	4-Cl	9.49	1.12	nd	nd	Nd
6c	p	4-Me	4-Cl	13.12	1.28	nd	nd	Nd
6d	2	4-Me	4-MeO	4.30	1.01	nd	nd	Nd
6e	3	4-Me	4-MeO	2.71	1.22	nd	nd	Nd
6f	p	4-Me	4-MeO	2.63	1.28	nd	nd	Nd
6g	4	4-MeO	4-MeO	83.01	1.46	nd	nd	Nd
6h	p	4-MeO	4-MeO	7.69	1.42	nd	nd	Nd
6i	4	3,4-MeO	4-MeO	2.61	1.00	nd	nd	Nd
6j	p	3,4-MeO	4-MeO	17.81	1.18	nd	nd	Nd
6k	p	3,4-MeO	3,4-MeO	6.17	1.22	nd	nd	Nd
7a	4	4-OH	4-OH	0.32	0.06	3.16	0.75	9.79
7b	4	3,4-OH	4-OH	1.62	1.14	nd	nd	Nd
7c	p	3,4-OH	4-OH	2.66	1.04	nd	nd	Nd
Quinine				0.108	0.003	134.35	1.45	1243.98
Chloroquine				0.012	0.002	101.19	25.72	8432.50
Camptothecin				nd	nd	nd	0.20	0.01

IC_{50}: Concentration at 50% inhibition of the parasite's growth.
Selective Index: IC_{50} values of cytotoxic activity/IC_{50} values of antimalarial activity.
nd: not determined.
p: Piperazine.

values of 0.32 ± 0.06 μM, 1.62 ± 1.14 μM and 2.66 ± 1.04 μM, respectively of which compound **7a** had the most prominent activity.

As observed, compound **6a, 6c**, **6h** and **6k** owning a piperazine linker were considered inactive with IC_{50} values < 5 μM. However, compounds **6g** and **7c** with piperazine linker revealed moderate activity with IC_{50} values of 2.63 ± 1.28 μM and 2.66 ± 1.04 μM, respectively. It can be suggested that the piperazine linker could have been significant and the difference in activity could allude to bioisosteric replacements at phenyl groups of the 4,6-diphenylpyrimidine core. Of the piperazine linker-based compounds, **6j** had the least activity with an IC_{50} value of 17.81 ± 1.18 μM, but its demethylation boosted the activity by almost seven-fold as illustrated by compound **7c** with IC_{50} of 2.66 ± 1.04 μM. In addition, substituting chloro with a methoxy group of the 4-(4-chlorophenyl)-6-(p-tolyl)pyrimidine core of compound **6c** yielded improved activity four-fold as illustrated by compound **6f**. Insignificant variation in activity is observed as more methoxy groups are added as shown by compound **6h** and **6k** with IC_{50} values of 7.69 ± 1.42 μM and 6.17 ± 1.22 μM individually. Compounds **6d** and **6e** respectively bearing 1,3-diamino propane and 1,2-diamino ethane, and both containing a 4-(4-methoxyphenyl)-6-(p-tolyl)pyrimidine motif only displayed moderate activity with IC_{50} values of 4.30 ± 1.01 μM and 2.71 ± 1.22 μM. Compounds **6b**, **6g**, **6i**, **7a** and **7b** having a 1,4-diamino butane linker presented a broader variation in the activity. Note that compound **6g** bearing two methoxy substituents on fourth positions of the phenyl groups of the 4,6-diphenylpyrimidine core had the least activity (Table 1). Adding an extra methoxy group on the third position increased the activity by nine-fold as defined by compound **6i** (IC_{50} = 2.61 ± 1.00 μM). Compound **6b** housing a

methyl and chloro substituents on 4-(4-chlorophenyl)-6-(p-tolyl) pyrimidine core was nine times more active than compound **6g**, though four times less active than **6i** despite both having methoxy substituents on the 4,6-diphenypyrimindine nucleus. The demethylation of methoxy groups of 4,6-bis(4-methoxyphenyl)pyrimidine of compound **6g** core heightened the activity by over two hundred-fold as demonstrated by **7a,** the most active compound. Although compound **6i** showed moderate activity, demethylation of the methoxy groups of the 4-(3,4-dimethoxyphenyl)-6-(4-methoxyphenyl)pyrimidine core compounds only mildly improved the activity of compound **7b** (2.61 vs 1.62 μM).

It should be noted that, in contrast to other substituents such as methyl, chlorine and methoxy, the hydroxyl significantly influenced the antiplasmodial activity as defined in the activity of compounds **6b**, **6g**, **6i**, **7a** and **7b** analogues with the same 1,4-diamino butane linker (Fig. 4). Given the above, it can be concluded that diamino alkane linkers, particularly 1,4-diamino butane and piperazine were crucial for the activity. Also, substitution on the phenyl groups of 4, 6-diphenylprimidine core with electron-donating groups, particularly hydroxyl groups, positively correlated with antiplasmodial activity.

Pyrimidinones have previously been shown to possess the antiplasmodial activity and target the essential parasite protein folding pathway of *P. falciparum* Hsp70 [18]. As such, we investigated the binding affinities of these compounds against the recombinant forms of two essential cytosolic *P. falciparum* Hsp70s; PfHsp70-1 and PfHsp70-z [17]. To determine binding kinetics, we employed surface plasmon resonance (SPR) analysis, as previously conducted [19,20]. The SPR sensorgrams generated (Fig. 5), were fitted to a simple 1:1 Langmuir kinetic binding model (Table 2). Generally, both parasite Hsp70s interacted with the four molecules in a concentration-dependent manner (Fig. 5). The rates of dissociation were comparable for all the molecules. Estimated K_D values were within the lower micromolar to the upper nanomolar range, suggesting a fairly high affinity of the compounds for the two essential cytosol localized *P. falciparum* Hsp70s (Table 2). Interestingly, PfHsp70-1 exhibited higher binding affinity (K_D values within lower nanomolar range) for compounds **6h** and **6k** compared to PfHsp70-z, which exhibited a four and two orders of magnitude reduction in affinity for the same compounds, respectively (Table 2). Compound **7a** exhibited higher binding affinity for PfHsp70-z with one order of magnitude difference in comparison to its affinity for PfHsp70-1 (Table 2). On the other hand, compound **7b** had a lower affinity (K_D = 0.281 μM) for PfHsp70-1; and higher affinity (K_D = 4.75 μM) for PfHsp70-z, respectively. Altogether, this suggests that compound **7a** showed the highest propensity to recognize both proteins. Notably, the observed varied preference of some of the compounds for the two PfHsp70 proteins highlights that despite their apparent sequence conservation, PfHsp70s possess unique motifs for selective targeting.

Shown in Fig. 5 are the representative SPR sensorgrams representing direct protein-compound interaction. The sensorgrams were analysed to generate the kinetics in Table 2. Binding affinity was evaluated as follows: (A) PfHsp70-1-**6h** (K_D = 2.19 nM) and PfHsp70-z-**6h** (K_D = 0.137 μM); (B) PfHsp70-1-**6k** (K_D = 0.261 nM) and PfHsp70-z-**6k** (K_D = 2.05 μM); (C) PfHsp70-1-**7a** (K_D = 0.114 nM) and PfHsp70-z-**7a** (K_D = 4.43 nM); (D) PfHsp70-1-**7b** (K_D = 0.281 μM) and PfHsp70-z-**7b** (K_D = 4.75 μM); , respectively.

SPR based kinetics for the direct interaction of PfHsp70-1 and Hsp70-z with the various compounds are represented by the rate of association (*Ka*), rate of dissociation (Kd) and the steady-state affinity (K_D), respectively. The ligand represents the respective immobilised protein on the CMD 3D 500L chip surface to which the analyte was injected at a flow rate of 50 μl/min in triplicate. Data was analysed after double referencing (refractive index changes on-chip surface without protein immobilised and for buffer injected without analyte) as a baseline. Data are represented as mean ± standard error of measurement. Chi-square (χ^2) values show the 1:1 Langmuir curve fitting residuals.

Furthermore, the cytotoxicity screening of the most potent molecule, **7a**, against human embryonic kidney epithelial (HEK-293) cells was studied (Table 1). The selective index (SI) of 9.79 was calculated for the most potent compound by dividing the IC_{50} value of the cytotoxic activity divided by the IC_{50} value of the antimalarial activity. The observed activity suggests that while selectively killing

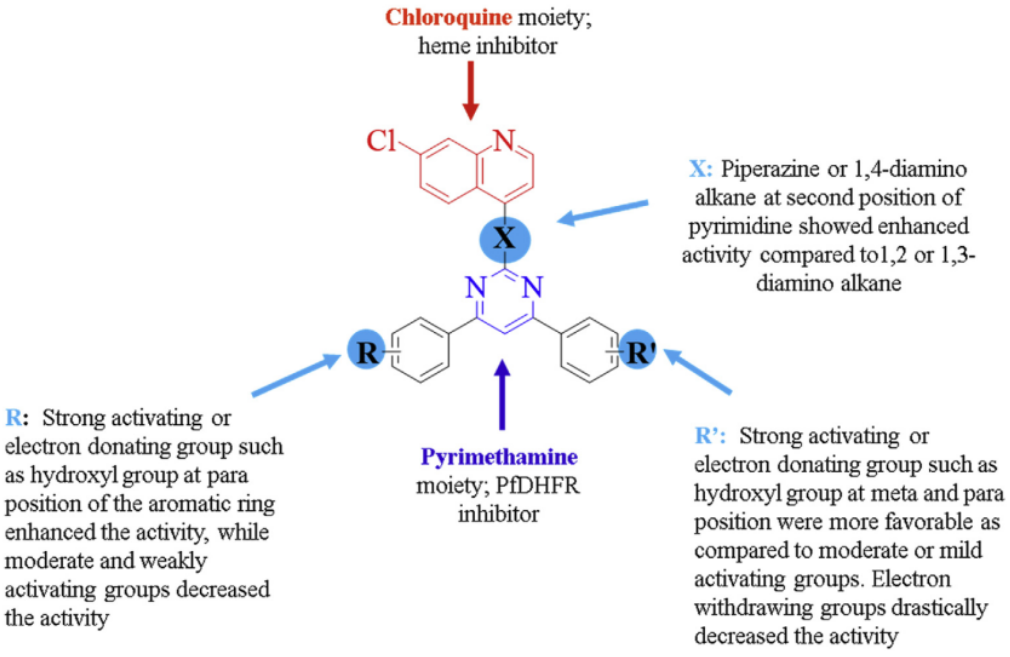

Fig. 4. Structure Activity Relationship (SAR) for quinioline-pyrimidine derivatives.

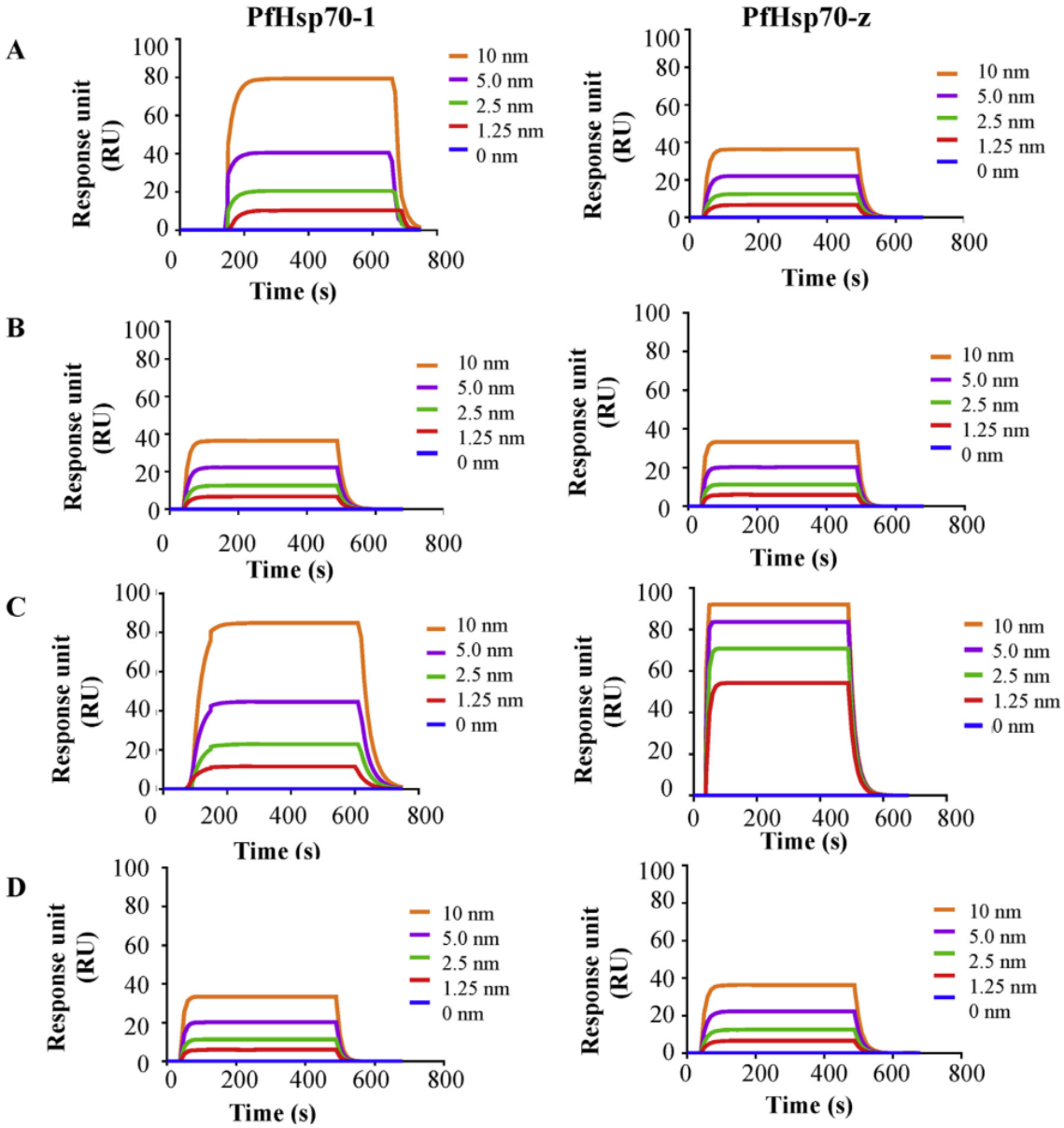

Fig. 5. Selected synthetic compounds bind *P. falciparum* Hsp70s directly. Plots represent interaction of PfHsp70-1 or PfHsp70-z) as investigated against varying levels of the selected compounds (**6h, 6k, 7a or 7b**).

the parasite, compound **7a** has a limited cytotoxic effect against mammalian cells at therapeutic dosages; where a safety index of 10 is regarded as safe.

4. Molecular docking scores

To measure the compounds' fitness at the active catalytic sites of the two enzymes, molecular docking analysis was performed. The four compounds were docked into the ATPase active sites of the

Table 2
Kinetics data for the interaction of molecules with P. falciparum recombinant Hsp70 proteins.

Analyte	Ligand	K_a (1/(M*s)) ± est. error	K_d (1/s) ± est. error	K_D (M) ± est. error	X^2
6h	PfHsp70-1	3.30 (±0.67) e^{+06}	1.32 (±0.12) e^{-02}	2.19 (±0.70) e^{-09}	1.1
	PfHsp70-z	5.99 (±0.90) e^{+03}	8.24 (±0.76) e^{-02}	1.37 (±0.89) e^{-05}	7.1
6k	PfHsp70-1	2.68 (±0.68) e^{+06}	7.00 (±0.11) e^{-02}	2.61 (±0.57) e^{-08}	2.4
	PfHsp70-z	1.34 (±0.99) e^{+04}	7.48 (±0.60) e^{-02}	2.05 (±0.59) e^{-06}	6.9
7a	PfHsp70-1	7.73 (±0.54) e^{+06}	8.81 (±0.24) e^{-02}	1.14 (±0.44) e^{-08}	4.7
	PfHsp70-z	2.70 (±0.53) e^{+07}	1.20 (±0.44) e^{-01}	4.43 (±0.92) e^{-09}	3.2
7b	PfHsp70-1	2.79 (±0.67) e^{+05}	7.84 (±0.92)e^{-02}	2.81 (±0.35) e^{-07}	8.8
	PfHsp70-z	1.91 (±0.77) e^{+04}	9.06 (±0.83)e^{-02}	4.75 (±0.55) e^{-06}	7.9

APPENDIX-IV

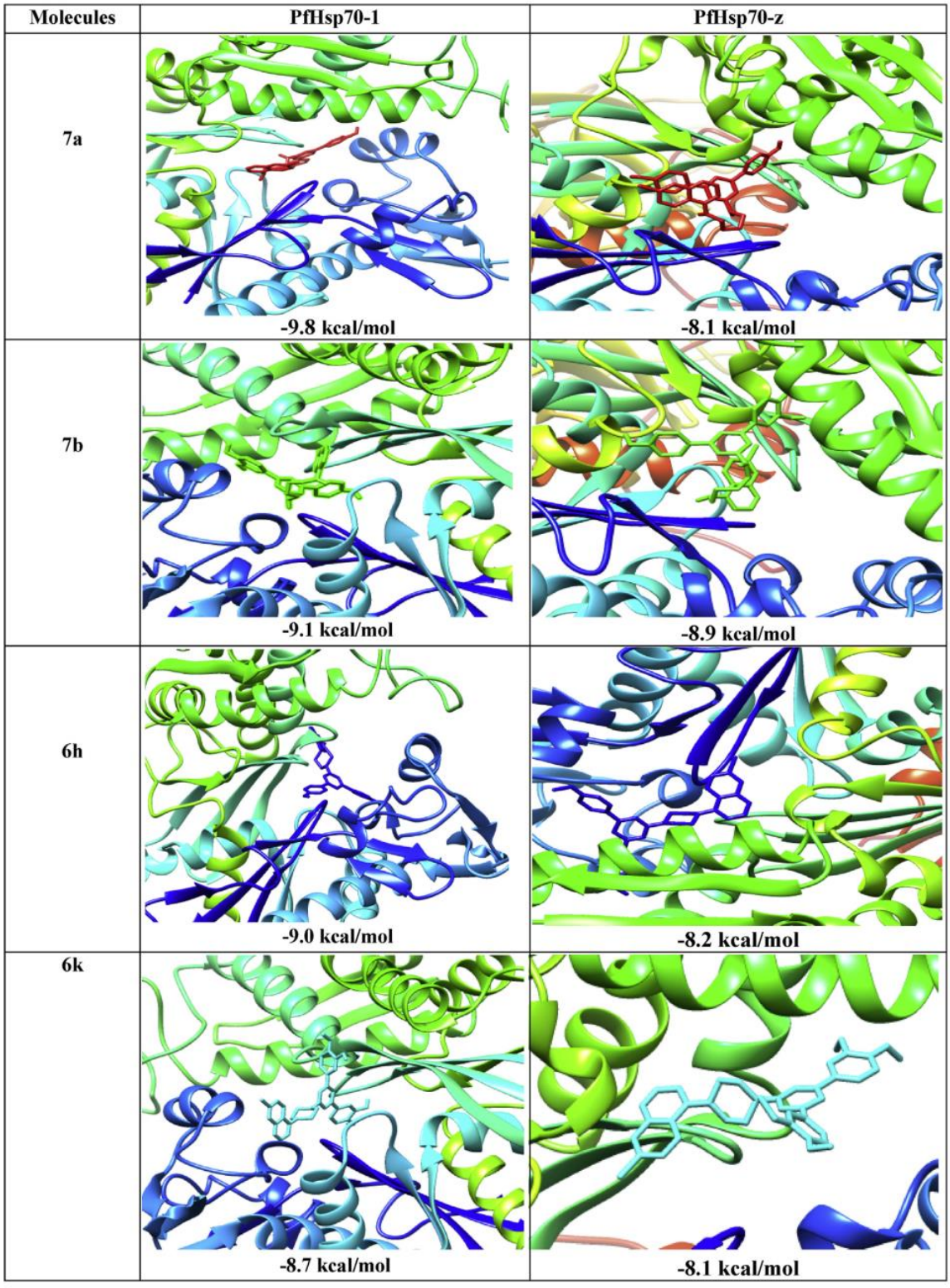

Fig. 6. Binding modes and docking scores of the molecules to PfHsp70-1 and PfHsp70-z.

enzymes (PfHsp70-1 and PfHsp70-z) to calculate and examine the fitness/affinity of the compounds. Based on the computational data, it is likely that the compounds bind to the ATPase domain for both proteins in a similar fashion to ATP binding. Suggesting that they could be competitive inhibitors to ATP binding for PfHsp70-1 and PfHsp70-z. Fig. 6 represents the binding modes and docking results of the compounds for each enzyme. Notably, the four compounds showed relatively good binding scores for PfHsp70-1. Compounds **7a** and **6k** showed the highest and lowest binding scores of −9.8 kcal/mol and −8.7 kcal/mol, respectively. The docking result for PfHsp70-z revealed that compound **7b** exhibited the highest docking score of −8.9 kcal/mol; while, compounds **7a** and **6k** showed the lowest values of −8.1 kcal/mol. The results suggest that the four compounds exhibited better fitness in PfHsp70-1 than PfHsp70-z. To better understand the binding affinity and structural mechanisms of inhibition of the four compounds against the two enzymes, molecular dynamics study on the compounds' best binding modes to the enzymes were investigated since molecular docking scores might give a false positive results.

4.1. Binding energies/affinities of the molecules to PfHsp70-1 and PfHsp70-z

To calculate the binding free energies of all the finals compounds to the enzymes, Molecular Mechanics/Generalized Born Surface Area (MMGBSA) computational technique was employed. Table 3 shows the results of the thermodynamic binding free energy profiles for the compounds to the two enzymes. All the compounds showed high binding energies/affinity for PfHsp70-1, ranging from −46.752 to −56.270 kcal/mol, with compounds **7a** and **7b** having the highest free energies of −56.270 kcal/mol and −53.968 kcal/mol, respectively. Compound **6k** exhibited higher binding energy (−49.182 kcal/mol) than **6h** (−46.752 kcal/mol). This result is in consistent with the docking results indicating that compounds **7a** and **7b** had the highest docking score for PfHsp70-1. In the PfHsp70-z systems, compounds **7b** and **6k** showed the highest binding affinities of −52.097 kcal/mol and −49.122 kcal/mol. This is also in consistent with the docking result that showed compound **7b** to have the highest docking score.

Furthermore, as shown in Table 3, compounds **6k** and **7b** showed no difference in their binding affinities for the two enzymes. Generally PfHsp70-1 showed strong binding energies for compounds, **6h**, **6k**, **7a** and **7b**, than PfHsp70-z. The high binding affinities recorded suggest possible inhibitory activities of compounds (**6h**, **6k**, **7a** and **7b**) against the protein folding role of PfHsp70-1.

4.2. Ligand-receptor interaction profiles of the molecules

The receptor-ligand interaction plots examined the molecular interactions between the bound compounds and the amino acid residues at the active sites of an enzyme [21]. To examine the mechanistic inhibitory characteristics of the four compounds, the interaction between the compounds and the active site amino residues of the enzymes were assessed. Fig. 7 and Fig. 8 shows the 2D representation of the interactions plots between the compounds and the different amino acid residues of PfHsp70-1 and PfHsp70-z, respectively. Van der Waals, H-bond, pi-anion and pi-akyl are the interactions observed in the PfHsp70-1 complexes. Structurally related compounds **6k** and **6h** showed pi-anion interactions with cysteine residues, Cys206 and Cys77, respectively (Fig. 7).

While compound **7a** had pi-anion interaction with Asp5, however, compound **6h** showed no pi-anion interaction, but had a pi-

Table 3
Thermodynamic binding free energy profiles for the compounds.

Energy Components (kcal/mol)					
Complex	Δ E_{vdW}	ΔE_{elec}	ΔG_{gas}	ΔG_{solv}	ΔG_{bind}
PfHsp70−1					
6a	−48.805 ± 4.167	−10.005 ± 3.324	−46.179 ± 8.117	20.574 ± 1.104	−41.485 ± 7.544
6b	−33.255 ± 4.705	−8.775 ± 2.751	−39.685 ± 2.216	15.111 ± 2.212	−37.323 ± 4.245
6c	−37.742 ± 4.235	−9.155 ± 1.545	−41.331 ± 4.114	17.008 ± 2.101	−40.137 ± 3.038
6d	−38.188 ± 7.884	−9.288 ± 6.002	−42.078 ± 4.555	21.000 ± 2.414	−36.685 ± 5.422
6e	−42.131 ± 7.134	−38.322 ± 10.231	64.111 ± 9.313	40.120 ± 4.223	−47.363 ± 4.205
6f	−35.777 ± 6.155	−19.578 ± 3.688	−58.124 ± 4.574	25.435 ± 2.585	−34.898 ± 5.985
6g	−37.903 ± 3.241	−21.588 ± 2.411	−60.004 ± 2.660	27.747 ± 2.575	−35.999 ± 4.257
6h	−58.681 ± 4.387	−8.298 ± 6.244	−66.978 ± 7.441	20.226 ± 4.431	−46.752 ± 5.806
6i	−35.113 ± 4.585	−22.200 ± 3.471	−51.745 ± 3.747	24.155 ± 3.886	−33.219 ± 3.888
6j	−35.989 ± 5.100	−24.681 ± 3.812	−57.818 ± 5.558	24.988 ± 4.515	−34.910 ± 4.378
6k	−59.352 ± 5.864	−21.389 ± 6.159	−80.741 ± 7.015	31.559 ± 5.613	−49.182 ± 6.582
7a	−65.317 ± 4.753	−36.744 ± 10.146	−102.061 ± 12.488	45.791 ± 5.010	−56.270 ± 9.413
7b	−58.507 ± 4.406	−42.327 ± 13.445	100.834 ± 12.429	46.867 ± 6.614	−53.968 ± 7.005
7c	−60.688 ± 3.181	−31.581 ± 8.435	−87.481 ± 7.700	39.928 ± 6.781	−42.823 ± 7.880
PfHsp70-z					
6a	−40.243 ± 2.723	−23.212 ± 3.104	−72.126 ± 4.332	31.432 ± 3.424	−32.073 ± 3.023
6b	−34.123 ± 4.111	−14.423 ± 3.933	−44.133 ± 2.811	21.331 ± 5.121	−30.332 ± 1.932
6c	−41.272 ± 3.928	−23.092 ± 7.834	−73.023 ± 4.933	34.422 ± 5.474	−41.324 ± 3.339
6d	−37.223 ± 3.983	−21.223 ± 7.215	−51.443 ± 4.113	30.551 ± 5.441	−37.525 ± 5.251
6e	−35.245 ± 4.145	−23.254 ± 5.444	−47.982 ± 2.254	32.268 ± 4.141	−33.125 ± 3.331
6f	−21.113 ± 3.112	−17.723 ± 2.863	−32.141 ± 4.223	19.321 ± 2.113	−29.222 ± 3.432
6g	−22.343 ± 4.422	−19.424 ± 2.128	−28.321 ± 3.252	20.441 ± 3.938	−26.234 ± 2.224
6h	−47.397 ± 3.501	−16.487 ± 5.949	−63.884 ± 7.430	28.353 ± 5.285	−35.531 ± 4.910
6i	−23.111 ± 2.165	−22.214 ± 3.819	−19.231 ± 4.122	17.654 ± 4.525	−24.212 ± 2.333
6j	−42.785 ± 3.423	−18.447 ± 4.551	−55.957 ± 5.541	25.415 ± 5.998	−31.258 ± 4.233
6k	−61.985 ± 4.948	−23.126 ± 9.433	−85.111 ± 11.737	35.990 ± 8.178	−49.122 ± 6.131
7a	−48.129 ± 4.947	−28.574 ± 12.986	−76.703 ± 14.429	41.877 ± 7.891	−34.826 ± 9.645
7b	−60.543 ± 3.675	−33.094 ± 9.310	−93.636 ± 8.713	41.539 ± 5.474	−52.097 ± 5.016
7c	−29.105 ± 5.500	−20.117 ± 2.234	−45.777 ± 424	23.425 ± 4.646	−30.411 ± 4.008

ΔEele electrostatic energy, ΔEvdW van der Waals energy, ΔGbind total binding free energy, ΔGsol solvation free energy, ΔEgas gas-phase free energy.

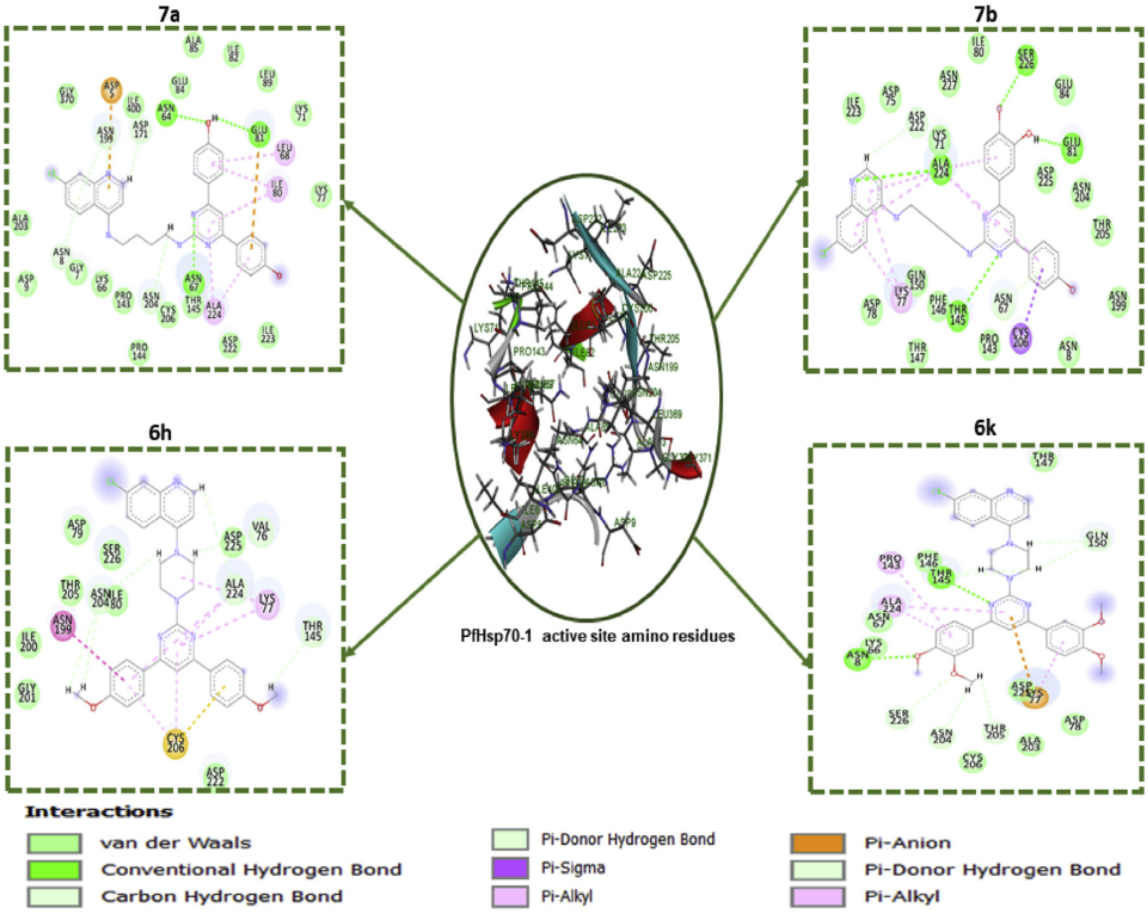

Fig. 7. A depiction of protein-ligand interactions plots with different amino acid residues.

sigma interaction with Cys206. These data revealed that binding energies are proportional to the number of H-bond and the total number of interactions observed in the four compounds, where compounds **7a**, **7b**, **6k** and **6h** have total interaction numbers of 29, 23, 17 and 15, respectively. A slightly different interaction was observed in PfHsp70-z complexes. Unlike the pi-anion interaction observed in PfHsp70-1, a pi-cation interaction was observed in PfHsp70-z. Furthermore, pi-pi stacked and donor-donor interactions were also observed. All the compounds showed a significant number of H-bond interactions required for stability. A donor-donor interaction was only observed in compound **7b**. The difference in the number and type of interactions observed for the two proteins (PfHsp70-1 and PfHsp70-z) could explain the higher binding energies observed in the PfHsp70-1 complexes.

4.3. Stability and flexibility of the enzymes bound complexes

To examine the stability and dynamics of enzymes-ligand complexes, 100 ns molecular dynamic (MD) simulations were performed. Root means square deviation (RMSD), radius of gyration (RoG), root means square fluctuation (RMSF) and solvent accessible surface area (SASA) of alpha carbon (Cα) atoms were monitored and analysed along with the entire duration of 100 ns of the MD simulation for the unbound and bound enzyme systems. For PfHsp70-1, the RoG plots revealed the binding of the four compounds lowers the mean RoG values of the four compounds (**7a**; 35.243 Å, **7b**; 34.553 Å, **6h**; 34.183 Å, **6k**; 31.432 Å) when compared to the unbound PfHsp70-1 systems; 35.973 Å (Fig. 9–1a). A similar reduction in average RoG values after the binding of the Brath goo compounds (**7a**; 28.272 Å, **7b**; 28.231 Å, **6h**; 28.354 Å, **6k**; 27.642 Å) was also observed in PfHsp70-z complexes when compared with the average value of the unbound PfHsp70-z system, 28.321 Å (Fig. 9–1). This finding suggests the binding of the compounds stabilizes the enzymes.

Fig. 9–2 shows the plot of the RMSD values, which is a measurement of the enzyme complexes' convergence and stability [22]. The plot shows that all the four compounds and the unbound systems reach convergence after about 8 ns. The RMSD plots for the complexes revealed that the four complexes are more stable (lower RMSD values) than the unbound systems of PfHsp70-1 and PfHsp70-z. This also suggests that the alpha carbon fluctuation of the compounds converged well during MD simulation. Likewise, the RMSF of the complexes were studied to examine the flexibility and stability of individual amino residues of the proteins. RMSF monitors the behaviour of the active residues of a protein. Higher and lower fluctuation values indicated more and less flexible movements, respectively. As shown in Fig. 9–2. c, residues 200–300, 305–345 and 5525 - 600 fluctuate more in all the four compounds and the unbound PfHsp70-1 systems. While most of the residues (150–250) involved in ligand binding fluctuate less. The plot further revealed that the average RMSF values of the compounds (**7b** (3.743 Å), **7a** (3.771 Å), **6h** (3.989 Å) and **6k** (4.023 Å)) were lower (less fluctuation) than the unbound system with average RMSF value of 4.212 Å. For the PfHsp70-z systems, more flexibility was observed at residues 230–260, 375–400 and 450–475. Unlike the PfHsp70-1 system, compounds **7a** and **7b**

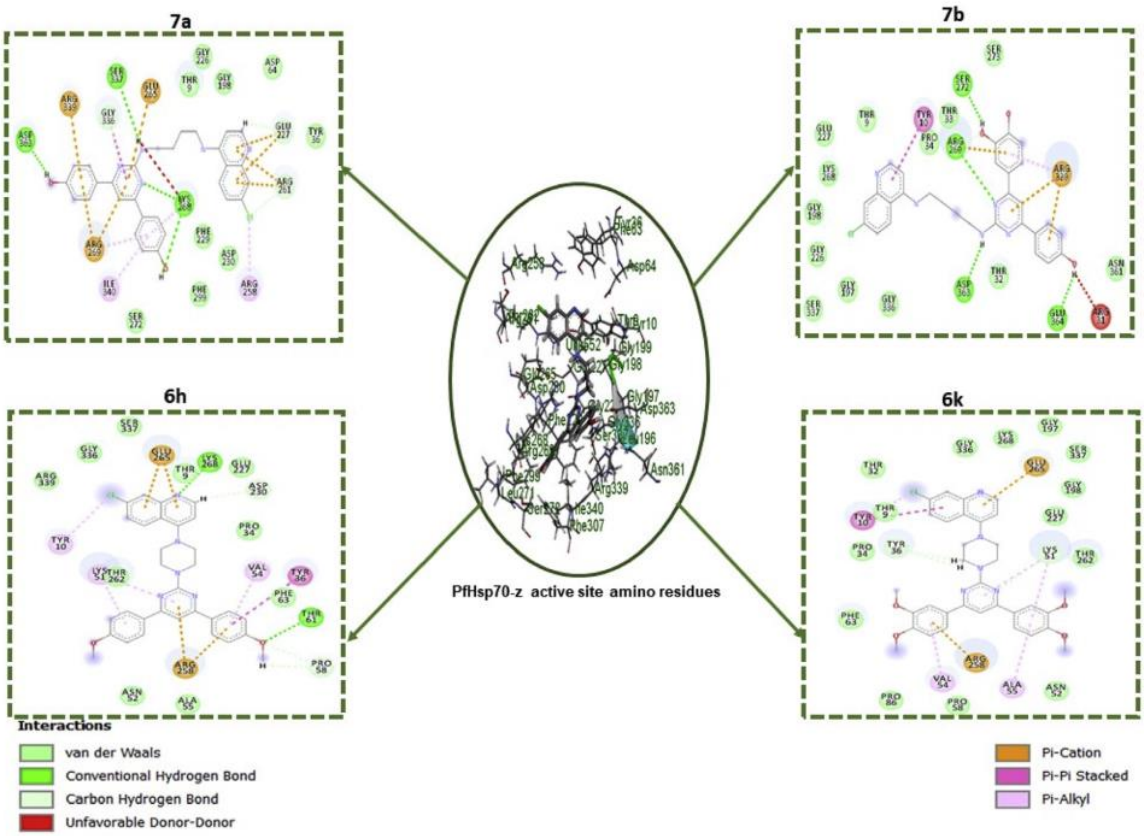

Fig. 8. A depiction of protein-ligand interactions plots with different amino acid residues.

exhibited higher average RMSF values (2.942 Å and 2.729 Å, respectively) than registered by unbound PfHsp70-1 (2.547 Å). Compounds **6h** and **6k** exhibited less fluctuation than the unbound enzyme with average values of 2.4675 Å and 2.501 Å, respectively.

SASA is another parameter to quantify the enzymes' exposure to the solvent environment [23]. The four compounds exhibited an increase in the exposure of the enzyme to solvent molecules, as their respective bindings raised the average SASA values when compared to the unbound PfHsp70-1 (Fig. 9–2d). SASA mean values of 35100 $Å^2$, 34200 $Å^2$, 34550 $Å^2$, 33800 $Å^2$ and 33700 $Å^2$ were recorded for compounds **7a**, **7b**, **6h**, **6k** and unbound PfHsp70-1. The average SASA values for compounds **7a**, **7b**, **6h**, **6k** and the unbound PfHsp70-z systems are 25900 $Å^2$, 25100 $Å^2$, 25600 $Å^2$, 24700 $Å^2$ and 24800 $Å^2$ (Fig. 9–2d). The increased SASA values reported for the compounds showed the binding of the compounds further exposed the enzyme to a solvent molecule. This suggests that the structural integrity of the enzyme was not distorted after 100 ns.

4.4. Assessing the drug-likeness of the compounds

Pharmacokinetic properties of the compounds were predicted using the SwissADME serve [24]. The Lipinski's rule of five is a set of rules that assess both the physical and chemical properties of potential drugs to ascertain its safety as an orally active drug [25]. As shown in Table 4, the four compounds (**6h**, **6k**, **7a** and **7b**) had no more than 5 hydrogen bond donors, no more than 10 hydrogen bond acceptors, thus passed the drug-likeness test and are poorly soluble in water. The result showed that the four compounds' partition coefficients (logP) are around 5. Greater logP usually indicates the probability of a drug to permeate the lipid membrane is low [26]. Compounds **7a** and **7b** were predicted to be lowly absorbed in the gastrointestinal tract (GIT), while compounds **6h** and **6k** were predicted to be highly absorbed. This suggests that the highly absorbed compounds would attain optimal concentrations in the systemic circulation than the lowly absorbed compounds. The blood-brain barrier (BBB) is a protective gate that prevents the passage of toxic compounds into the brain or the central nervous system [24]. For the four test compounds (6h, 6j, 7a and 7b) the number of hydrogen donors ranged between 0 and 5 while hydrogen acceptors 5 to 7. Thus, indicating that all the test compounds could be considered orally active. None of the four compounds were predicted to permeate the BBB. Bioavailability score is a measurement of the rate of absorption and quantity of a given amount of unchanged drug that goes to the systemic circulation [27]. The four compounds showed a relatively high score of 0.55, which suggests they all might reach their sites of active with higher concentrations required for therapeutic effect.

5. Conclusion

In summary, pyrimidine-quinoline analogy inspired chloroquine and pyrimethamine antimalarial drugs were designed, synthesised by molecular hybridisation approach and screened for their antiplasmodial activity. The facile preparation with excellent yields of these compounds makes synthetic pathway attractive and versatile. Among the tested compounds, only compound **7a** displayed the best antiplasmodial activity (IC_{50} = 0.32 ± 0.06 μM), with a selectivity index of 9.79, which is considered safe. Interestingly, compound **7a** bound to both parasite Hsp70 chaperones with significant affinity, suggesting that one possible mechanism of action of this compound could be to abrogate the protein folding

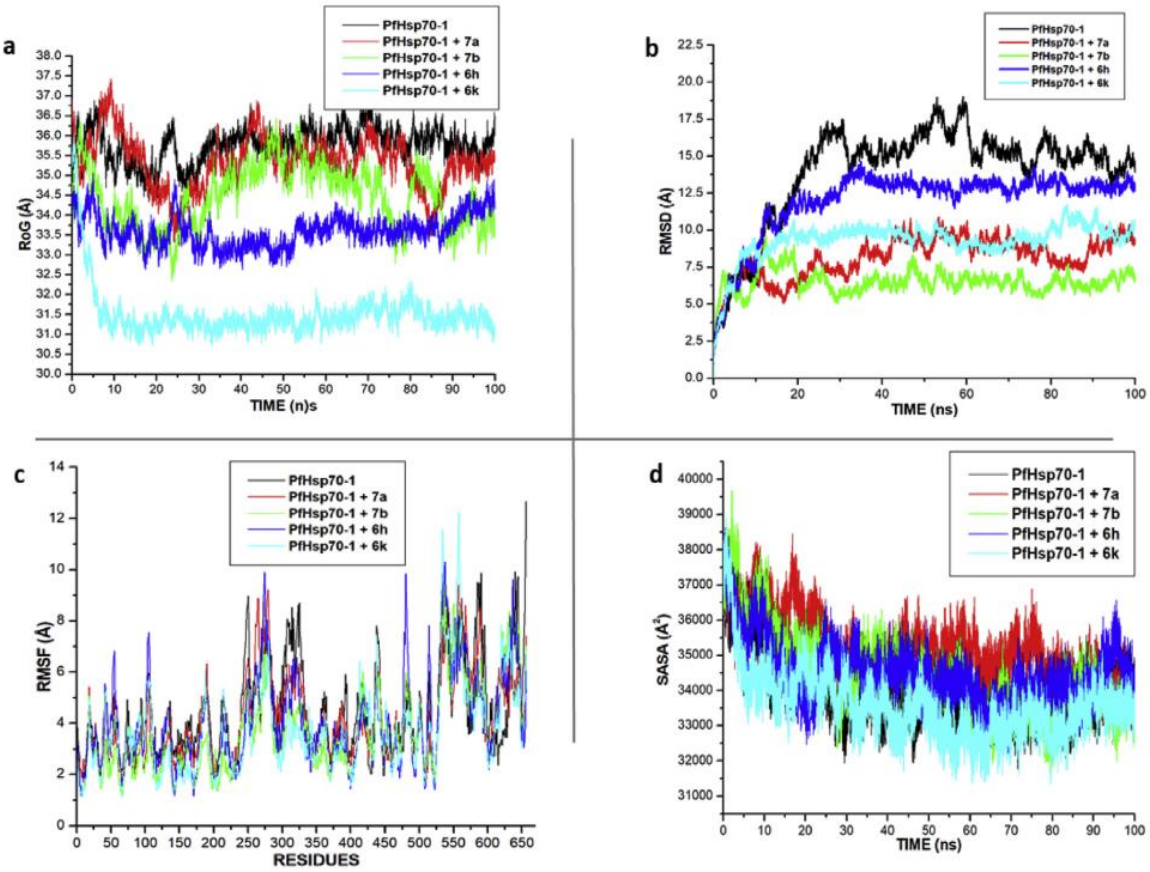

Fig. 9-1. Plots of alpha C atoms of the PfHsp70-1, 7**a**, 7**b**, **6h** and **6k**, a) RoG plots b) RMSD, c) RMSF and d) SASA plots systems calculated throughout 100 ns MD simulations.

pathway of the parasite. This hypothesis was further supported by the observed molecular docking scores. Brief SAR studies revealed that strong activating or electron-donating groups on the meta and para position of the aromatic group enhanced the activity. Similarly piperazine or 1,4-diamino butane linkers were essential for the activity. The authors believe that the outcome or observation of this research work would assist in the researchers in designing potent antimalarial agents.

6. Experimental

All the chemicals used in this research work were purchased from Sigma-Aldrich and Merck Millipore, South Africa. The commercially available chemicals benzaldehyde and acetophenone were purchased from Sigma-Aldrich (South Africa). All the solvents, except those of laboratory-reagent grade, were dried and purified when necessary according to previously published methods. The progress of the reactions and the purity of the compounds were monitored by thin-layer chromatography (TLC) on pre-coated silica gel plates procured from E. Merck and Co. (Darmstadt, Germany) using 36% ethyl acetate in n-hexane as the mobile phase and iodine vapour as the visualising agent.

The melting points of the synthesised compounds were determined using a Thermo Fisher Scientific (IA9000, UK) digital melting point apparatus and are uncorrected. The IR spectra were recorded on a Bruker Alpha FT-IR spectrometer (Billerica, MA, USA) using the ATR technique. The ^{1}H NMR and ^{13}C NMR spectra were recorded on a Bruker AVANCE 400 and 600 MHz (Bruker, Rheinstetten/Karlsruhe, Germany) spectrometers using $CDCl_3$ and DMSO-d_6. The chemical shifts are reported in units with respect to TMS as an internal standard. HRMS spectra were recorded on an Autospec mass spectrometer with electron impact at 70 eV.

6.1. A typical procedure for the synthesis of (E) chalcone (1b-1f)

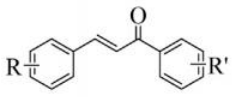

1b	R = 4-Me,	R' = 4-Cl
1c	R = 4- Me,	R' = 4-MeO
1d	R = 4-MeO,	R' = 4-MeO
1e	R = 3,4-MeO,	R' = 4-MeO
1f	R = 3,4-MeO,	R' =3,4-MeO,

To a stirring solution of acetophenone (5 g, 32.34 mmol) in EtOH (30 ml), a 60% NaOH solution (12 g $NaOH/H_2O$ (20 mL)) was added. The reaction was stirred at room temperature for 30 min. Benzaldehyde (4.7 g, 38.81 mmol) was then added and the reaction sonicated for 1 h at 35 °C. The progression of the reaction was monitored by TLC. Excess ethanol was removed under vacuum, and the reaction mixture was added into 100 g of ice and stirred. The precipitates formed were filtered, washed with excess water and dried under vacuum. The crude product was purified by recrystallized in EtOH to obtain the following pure compounds in good yield.

(E)-1-(4-chlorophenyl)-3-(p-tolyl)prop-2-en-1-one **(1b)**: Yellow solid, yield: 90%, mp = 162–164 °C; ^{1}H NMR (400 MHz, $CDCl_3$, δ, ppm): 7.96 (d, J = 8.57 Hz, 2H, ArH), 7.78 (d, J = 15.65 Hz, 1H, ph,-CH=C**H**), 7.54 (d, J = 8.08 Hz, 2H, ArH), 7.47 (d, J = 8.36 Hz, 2H, ArH), 7.46-7.42 (d, J = 15.65 Hz, 1H, ph,-C**H**=CH), 7.23 (d,

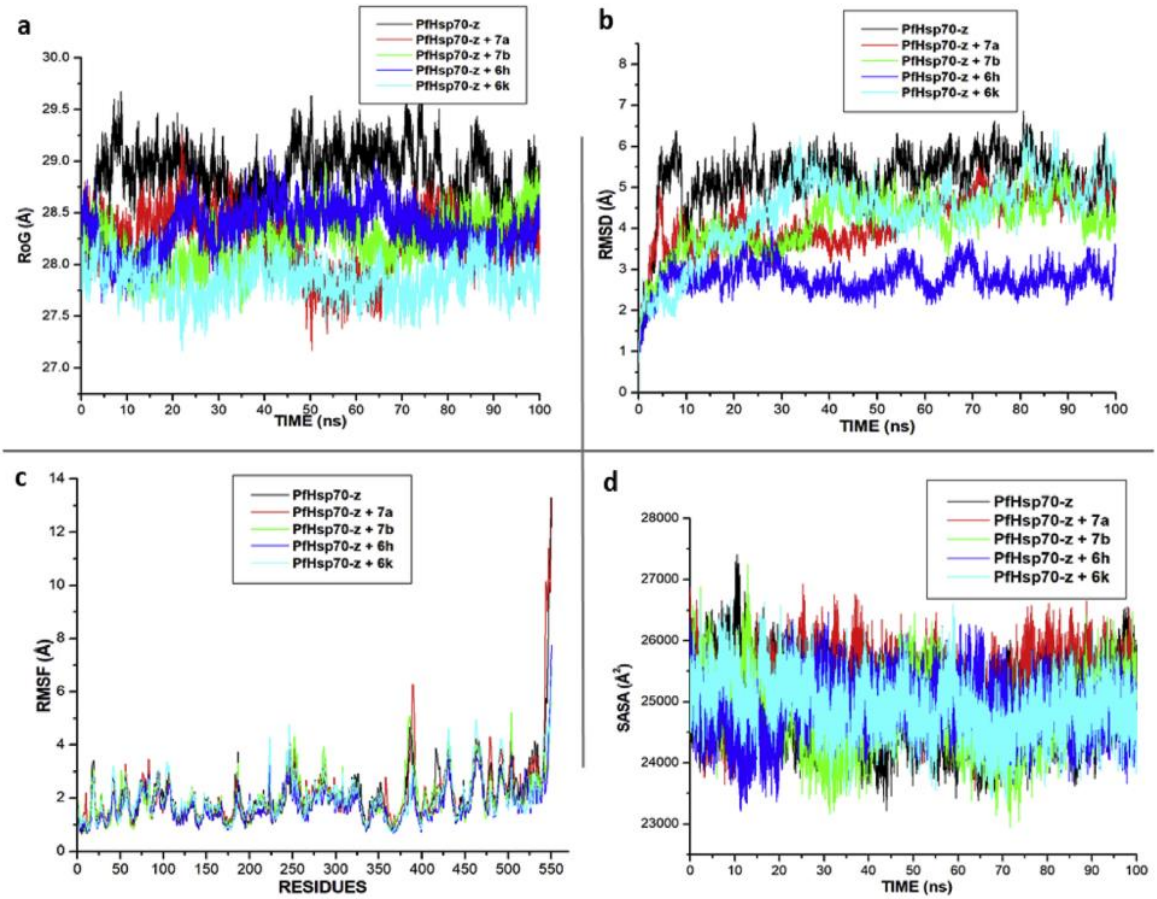

Fig. 9-2. Plots of alpha C atoms of the PfHsp70-z, **7a**, **7b**, **6h** and **6k,** a) RoG plots b) RMSD, c) RMSF and d) SASA plots systems calculated throughout 100 ns MD simulations.

Table 4
Pharmacokinetic and physicochemical properties of the molecules.

Comp	M. Formula	M. Weight (g/mol)	H-bond donar	H-bond acceptor	*Lipophilicity (iLOGP*	Water Solubility	GIT Absorption	BBB Permeability	Bioavailability Score	*Drug likeness (Lipinski)*
7a	$C_{29}H_{26}ClN_5O_2$	512.00	4	5	5.03	Poor	Low	No	0.55	Yes
7b	$C_{29}H_{26}ClN_5O_3$	528.00	5	6	4.69	Poor	Low	No	0.55	Yes
6h	$C_{31}H_{28}ClN_5O_2$	538.04	0	5	5.20	Poor	High	No	0.55	Yes
6k	$C_{33}H_{32}ClN_5O_4$	598.09	0	7	5.16	Poor	High	No	0.55	Yes

J = 7.96 Hz, 2H ArH), 2.40 (s, 3H, CH_3); ^{13}C NMR (400 MHz, $CDCl_3$, δ, ppm): 189.28, 145.48, 141.38, 139.09, 136.09, 136.65, 131.96, 129.90, 129.77, 128.92, 128.58, 120.46, 21.59 (CH_3).

(E)-1-(4-methoxyphenyl)-3-(p-tolyl)prop-2-en-1-one (**1c**): Yellow solid, yield: 96.3%, mp = 125–128 °C; ^{1}H NMR (400 MHz, $CDCl_3$, δ, ppm): 8.04 (d, J = 8.76 Hz, 2H, ArH), 7.89 (d, J = 15.60 Hz, 1H, ph-C**H**=CH), 7.54 (d, J = 7.95 Hz, 2H, ArH), 7.51 (d, J = 15.63 Hz, 1H, ph-CH=C**H**), 7.22 (d, J = 7.97, Hz, 2H ArH), 6.98 (d, J = 8.77 Hz, 2H, ArH), 3.88 (s,3H, CH_3), 2.39 (s, 3H,CH_3); ^{13}C NMR (400 MHz, $CDCl_3$, δ, ppm): 189.43, 163.92, 144.64, 141.40, 132.92, 131.81, 131.34, 130.24, 128.96, 121.46, 114.39, 56.06(OCH_3), 22.09 (CH_3).

(E)-1,3-bis(4-methoxyphenyl)prop-2-en-1-one (**1d**): yellow solid, yield: 85.7%, mp = 102–104 °C; ^{1}H NMR (400 MHz, $CDCl_3$, δ, ppm): 8.03 (d, J = 8.75 Hz, 2H, ArH), 7.78 (d, J = 15.58 Hz, 1H, ph-C**H**=CH), 7.60 (d, J = 8.66 Hz, 2H, ArH), 7.43 (d, J = 15.58 Hz, 1H, ph-CH=C**H**), 6.96 (dd, J = 17.58, 8.72 Hz, 4H, ArH), 3.89 (s,3H, OCH_3), 3.85 (s, 3H, OCH_3); ^{13}C NMR (400 MHz, $CDCl_3$, δ, ppm): 189.39, 163.84, 162.09, 162.09, 144.39, 131.95, 131.28, 130.67, 128.40, 120.15, 114.96, 114.36, 56.05 (OCH_3), 55.98 (OCH_3).

(E)-3-(3,4-dimethoxyphenyl)-1-(4-methoxyphenyl)prop-2-en-1-one (**1e**): Yellow solid, yield: 80.6%, mp = 92–94 °C; ^{1}H NMR (400 MHz, $CDCl_3$, δ, ppm): 8.03 (d, J = 8.81 Hz, 2H, ArH), 7.75 (d, J = 15.56 Hz, 1H, ph,-CH=C**H**), 7.40 (d, J = 15.56 Hz, 1H, ph-C**H**=CH), 7.23 (dd, J = 8.31, 1.64 Hz, 1H, ArH), 7.16 (s, 1H, ArH,), 6.98 (d, J = 8.81 Hz, 1H, ArH), 6.89 (d, J = 8.27 Hz, 1H, ArH), 3.94 (s, 3H, OCH_3), 3.92 (s, 3H, OCH_3), 3.88 (s, 3H, OCH_3); ^{13}C NMR (400 MHz, $CDCl_3$, δ, ppm): 189.37, 163.86, 151.83, 149.80, 144.71, 131.89, 131.29, 128.65, 123.53, 120.42, 114.36, 111.70, 110.68, 56.56 (OCH_3), 56.54 (OCH_3), 56.05 (OCH_3).

(E)-1,3-bis(3,4-dimethoxyphenyl)prop-2-en-1-one (**1f**): Yellow solid, yield: 99%, mp = 109–111 °C; ^{1}H NMR (400 MHz, $CDCl_3$, δ, ppm): 7.76 (d, J = 15.54 Hz, 1H, ph,-CH=C**H**), 7.69 (d, J = 8.36 Hz, 1H, ArH), 7.62 (s, 1H, ArH) 7.41 (d, J = 15.54 Hz, 1H, ph-C**H**=CH), 7.24 (d, J = 8.44 Hz, 1H, ArH), 7.16 (s, 1H, ArH), 6.92 (dd, J = 11.73, 8.31 Hz, 2H, ArH), 3.89–3.95 (m, 9H, CH_3), 3.92 (s, 3H, CH_3); ^{13}C NMR (400 MHz, $CDCl_3$, δ, ppm): 189.26, 153.70, 151.86, 149.81, 144.73, 132.13, 128.64, 123.46, 123.43, 120.25, 111.72, 111.43, 110.81, 110.50, 56.65 (2OCH_3), 56.57 (2OCH_3).

APPENDIX-IV

6.2. A typical procedure for the synthesis of 4,6-diphenylpyrimidin-2-amine(2a-2f)

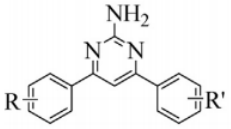

2a	R = 4-H,	R' = 4-H
2b	R = 4-Me,	R' = 4-Cl
2c	R = 4- Me,	R' = 4-MeO
2d	R = 4-MeO,	R' = 4-MeO
2e	R = 3,4-MeO,	R' = 4-MeO
2f	R = 3,4-MeO,	R' =3,4-MeO,

The reaction mixture of (*E*)-chalcone (**1**) (8 g, 31.16 mmol), guanidine hydrochloride (4.8 g, 49. 86 mmol) and 60% NaOH (12 g $NaOH/H_2O$ (20 mL)) in EtOH (30 mL) was refluxed for 24 h. The progression of the reaction was monitored using TLC. Excess ethanol was removed under vacuum using rotavapor, and the reaction mixture was then added in 100 g ice water. The precipitate formed was filtered, washed with excess water and dried. The crude compound was purified by column chromatography using EtOAc/hexane (1:4) eluent to obtain the following pure compounds.

4,6-diphenylpyrimidin-2-amine **(2a)**: Yellow solid, yield: 65%, mp = 136–138 °C; ^{1}H NMR (400 MHz, $CDCl_3$, *δ*, ppm): 8.07-8.05 (m, 4H, ArH), 7.51-7.49 (m, 6H, ArH), 7.46 (s, 1H, ArH), 5.35 (s, 2H, NH_2).

4-(4-chlorophenyl)-6-(p-tolyl)pyrimidin-2-amine (**2b**): Yellow solid, yield: 62%, mp = 162–165 °C; ^{1}H NMR (400 MHz, $CDCl_3$, *δ*, ppm): 8.00 (d, *J* = 8.36 Hz, 2H, ArH), 7.95 (d, *J* = 7.96 Hz, 2H, ArH), 7.46 (d, *J* = 8.36 Hz, 2H, ArH), 7.369 (s, 1H, ArH), 7.30 (d, *J* = 7.380 Hz, 2H, ArH), 5.31 (s, 2H, NH_2), 2.43 (s, 3H, CH_3); ^{13}C NMR (400 MHz, $CDCl_3$, *δ*, ppm): 166.40, 164.76, 163.63, 140.93, 136.52, 136.25, 134.74, 129.53, 128.95, 128.42, 127.04, 103.64, 21.44 (CH_3).

4-(4-methoxyphenyl)-6-(p-tolyl)pyrimidin-2-amine (**2c**): Yellow solid, yield: 58%, mp = 127–129 °C; 8.03 (d, *J* = 8.64 Hz, 2H, ArH), 8.00 (d, *J* = 8.36 Hz, 2h, ArH), 7.46 (d, *J* = 8.36 Hz, 2H, ArH), 7.37 (s, 1H, Pyr-H), 7.00 (d, *J* = 8.56 Hz, 2H, ArH) 5.20 (s, 2H, NH_2), 3.88 (s, 3H, CH_3); ^{13}C NMR (400 MHz, $CDCl_3$, *δ*, ppm): 165.88, 164.64, 163.55, 161.76, 136.47, 136.47, 129.91, 128.96, 128.64, 128.40, 114.14, 103.18, 55.43 (OCH_3).

4,6-bis(4-methoxyphenyl) pyrimidin-2-amine (**2d**); Yellow solid, yield: 65%, mp = 171–173 °C; ^{1}H NMR (400 MHz, $CDCl_3$, *δ*, ppm): 8.04 (d, *J* = 8.66 Hz, 4H, ArH), 7.36 (s, 1H, Pyr-H) 7.00 (d, *J* = 8.69 Hz,4H, ArH), 5.36 (s, 2H, NH_2), 3.87 (s, 6H, $2CH_3$); ^{13}C NMR (400 MHz, $CDCl_3$, *δ*, ppm): 165.19, 162.97, 161.77, 129.78, 128.69, 114.15, 102.64, 55.43 (OCH_3).

4-(3,4-dimethoxyphenyl)-6-(4-methoxyphenyl) pyrimidin-2-amine (**2e**): Yellow solid, yield: 61%, mp = 157–159 °C; ^{1}H NMR (400 MHz, $CDCl_3$, *δ*, ppm): 8.04 (d, *J* = 8.86 Hz, 2H, ArH), 7.71 (d, *J* = 1.92 Hz, 1H, ArH), 7.63 (dd, *J* = 8.55, 2.0 Hz,1H, ArH), 7.36 (s, 1H, Pyr-H), 7.00 (d, *J* = 8.84 Hz, 1H, ArH), 6.96 (d, *J* = 8.45 Hz, 1H, ArH), 5.35 (s, 2H, NH_2), 4.00 (s, 3H, CH_3), 3.95 (s, 3H, CH_3), 3.87 (s, 3H, CH_3).

4,6-bis(3,4-dimethoxyphenyl)pyrimidin-2-amine (**2f**): Yellow solid, yield: 67%, ^{1}H NMR (400 MHz, $CDCl_3$, *δ*, ppm): 7.71 (s, 2H, ArH), 7.62 (dd, *J* = 8.45, 1.69 Hz, 2H, ArH), 7.37 (s, 1H, Pyr-H), 6.96 (d, *J* = 8.40 Hz, 1H, ArH), 5.25 (s, 2H, NH_2), 4.00 (s, 6H, $2CH_3$), 3.95 (s, 6H, $2CH_3$).

6.3. A typical procedure for the synthesis of 4,6-diphenylpyrimidin-2-ol (3a-3f)

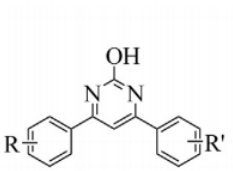

3a	R = 4-H,	R' = 4-H
3b	R = 4-Me,	R' = 4-Cl
3c	R = 4- Me,	R' = 4-MeO
3d	R = 4-MeO,	R' = 4-MeO
3e	R = 3,4-MeO,	R' = 4-MeO
3f	R = 3,4-MeO,	R' =3,4-MeO,

4,6-Diphenylpyrimidin-2-amine (**2**) (4 g, 12.76 mmol) was dissolved in acetic acid (100 mL), and whilst stirring a solution of 10 eq $NaNO_2$ dissolved in H_2O (50 ml) was slowly added at room temperature. The reaction mixture was further stirred for 3 h. The progression of the reaction was monitored using TLC. The precipitate formed was filtered and washed with excess water and dried under vacuum. The crude product was recrystallized in EtOH to obtain the following pure compounds in good yield.

4,6-diphenylpyrimidin-2-ol (**3a**): Yellow solid, yield: 85%, mp = 231–234 °C; , ^{1}H NMR (400 MHz, DMSO-d_6, *δ*, ppm): 11.96 (s, 1H, Pyr-O**H**), 8.17 (d, *J* = 6.56 Hz, 4H, ArH), 7.57-7.55 (m, 7H, ArH); ^{13}C NMR (400 MHz, DMSO-d_6, *δ*, ppm): 134.78, 131.42, 128.79, 127.54, 100.40.

4-(4-chlorophenyl)-6-(p-tolyl)pyrimidin-2-ol (**3b**): Yellow solid, yield: 89%, mp = <300 °C; ^{1}H NMR (400 MHz, DMSO-d_6, *δ*, ppm): 11.83 (s, 1H, Pyr-O**H**), 8.14 (d, *J* = 8.56 Hz, 1H, ArH), 8.13 (d, *J* = 8.76 Hz, 2H, ArH), 7.79-7.77 (m, 1H, ArH), 7.69 (d, *J* = 1.56 Hz, 2H, ArH), 7.08 (d, *J* = 8.84 Hz, 2H, ArH), 3.88 (s, 3H, OCH_3), 3.85 (s, 6H, $2OCH_3$).

4-(4-methoxyphenyl)-6-(p-tolyl)pyrimidin-2-ol (**3d**): Yellow solid, yield: 91%, mp = 235–237 °C; , ^{1}H NMR (400 MHz, DMSO-d_6, *δ*, ppm): 11.85 (s, 1H, Pyr-O**H**), 8.16 (d, *J* = 8.74 Hz, 2H, ArH), 8.04 (d, *J* = 7.97 Hz, 2H, ArH), 7.44 (s, 1H, pyr-H), 7.35 (d, *J* = 7.98 Hz, 2H, ArH), 7.09 (d, *J* = 8.97 Hz, 2H, ArH), 3.85 (s, 3H, OCH_3), 2.39 (s, 3H, CH_3); ^{13}C NMR (400 MHz, DMSO-d_6, *δ*, ppm): 162.05, 141.51, 129.39, 129.35, 127.46, 114.18, 55.46 (OCH_3), 55.99 (CH_3).

4,6-bis(4-methoxyphenyl)pyrimidin-2-ol (**3d**): Yellow solid, yield: 90%, mp = <300 °C; ^{1}H NMR (400 MHz, DMSO-d_6, *δ*, ppm): 11.82 (s, 1H, Pyr-O**H**), 8.14 (d, *J* = 8.53 Hz, 2H, ArH), 7.41 (s, 1H, pyr-H), 7.09 (d, *J* = 8.91 Hz, 2H, ArH), 3.85 (s, 6H, $2OCH_3$), ^{13}C NMR (400 MHz, DMSO-d_6, *δ*, ppm): 162.00, 129.32, 114.18, 55.46 ($2OCH_3$).

4-(3,4-dimethoxyphenyl)-6-(4-methoxyphenyl)pyrimidin-2-ol **(3e)**: Yellow solid, yield: 89%, mp = 235–237 °C; ^{1}H NMR (400 MHz, DMSO-d_6, *δ*, ppm): 11.83 (s, 1H, Pyr-O**H**), 7.79 (d, *J* = 7.29 Hz, 2H, ArH), 7.70 (d, *J* = 7.71 Hz, 2H, ArH), 7.41 (s, 1H, ArH), 7.10 (d, *J* = 8.2 Hz, 2H, ArH), 3.88 (s, 3H, OCH_3), 3.85 (s, 3H, OCH_3); ^{13}C NMR (400 MHz, DMSO-d_6, *δ*, ppm): 162.00, 151.74, 148.77, 129.37, 129.31, 121.10, 114.7, 111.47, 110.43, 97.91, 55.71 (OCH_3), 55.45 ($2OCH_3$).

4,6-bis(3,4-dimethoxyphenyl)pyrimidin-2-ol **(3f)**: Yellow solid, yield: 93%, mp = <300 °C; ^{1}H NMR (400 MHz, DMSO-d_6, *δ*, ppm): 11.83 (s, 1H, Pyr-O**H**), 7.79 (d, *J* = 7.29 Hz, 2H, ArH), 7.70 (d, *J* = 7.71 Hz, 2H, ArH), 7.41 (s, 1H, ArH), 7.10 (d, *J* = 8.2 Hz, 2H, ArH), 3.88 (s, 6H, $2OCH_3$), 3.85 (s, 6H, $2OCH_3$); ^{13}C NMR (400 MHz, DMSO-d_6, *δ*, ppm): 151.73, 148.72, 121.18, 111.42, 110.43, 55.66 ($4OCH_3$); HRMS (ESI, *m/z*) [M+Na] calculated for $C_{20}H_{20}N_2O_5$, 391.1270; found 391.1279.

6.4. A typical procedure for the synthesis of 2-chloro-4,6-diphenylpyrimidine

APPENDIX-IV

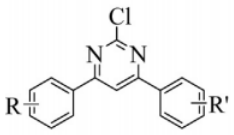

4a	R = 4-H,	R' = 4-H
4b	R = 4-Me,	R' = 4-Cl
4c	R = 4- Me,	R' = 4-MeO
4d	R = 4-MeO,	R' = 4-MeO
4e	R = 3,4-MeO,	R' = 4-MeO
4f	R = 3,4-MeO,	R' =3,4-MeO

A solution of 4,6-diphenylpyrimidin-2-ol (4g, 16.11 mmol) and 0.4 mL DMF in $POCl_3$ (20 mL) was refluxed for 6 h. The reaction completion was monitored by TLC. The reaction was added into ice water, and the precipitate formed was filtered, washed with water and dried under vacuum. The crude compound was purified by column chromatography using EtOAc/hexane (1:9) eluent to obtain pure compounds.

2-chloro-4,6-diphenylpyrimidine (**4a**): yellow solid, yield: 93%, mp = 115–116 °C; ^{1}H NMR (400 MHz, $CDCl_3$, δ, ppm): 8.07-8.05 (m, 4H, ArH), 7.51-7.49 (m, 6H, ArH), 7.46 (s, 1H, ArH), 5.35 (s, 2H, NH_2).

2-chloro-4-(4-chlorophenyl)-6-(p-tolyl)pyrimidine (**4b**): Yellow solid, yield: 89%, ^{1}H NMR (400 MHz, $CDCl_3$, δ, ppm): 8.09 (d, J = 8.52 Hz, 2H, ArH), 8.04 (d, J = 8.16 Hz, 2H, ArH), 7.94 (s, 1H, Pyr-H), 7.50 (d, J = 8.52 Hz, 2H, ArH), 7.33 (d, J = 8.00 Hz, 2H, ArH), 2.44 (s, 3H, CH_3); ^{13}C NMR (400 MHz, $CDCl_3$, δ, ppm): 166.77, 165.13, 161.05, 141.46, 136.88, 133.16, 131.65, 128.83, 128.30, 127.68, 126.37, 109.20, 20.51(CH_3).

2-chloro-4-(4-chlorophenyl)-6-(4-methoxyphenyl)pyrimidine (**4c**): Yellow solid, yield: 95%, ^{1}H NMR (400 MHz, $CDCl_3$, δ, ppm): 8.11 (d, J = 8.84 Hz, 2H, ArH), 8.07 (d, J = 8.56 Hz, 2H, ArH), 7.88 (s, 1H, Pyr-H), 7.49 (d, J = 8.68 Hz, 2H, ArH), 7.02 (d, J = 8.92 Hz, 2H, ArH), 3.89 (s, 3H, OCH_3); ^{13}C NMR (400 MHz, $CDCl_3$, δ, ppm): 167.27, 165.95, 162.75, 162.02, 137.82, 134.25, 129.30, 129.16, 128.67, 127.81, 114.46, 109.62, 55.50 (OCH_3).

2-chloro-4,6-bis(4-methoxyphenyl)pyrimidine (**4d**): Yellow solid, yield: 93%, mp = 187–190 °C; ^{1}H NMR (400 MHz, $CDCl_3$, δ, ppm): 8.10 (d, J = 8.48 Hz, 3H, ArH), 7.87 (d, J = 8.84 Hz, 1H, ArH), 7.85 (s, 1H, Pyr-H), 7.01 (dd, J = 8.50 Hz, 1.74 Hz, 4H, ArH), 3.88 (s, 6H, 2OCH_3); ^{13}C NMR (400 MHz, $CDCl_3$, δ, ppm): 166.74, 166.52, 162.51, 161.84, 161.58, 131.61, 129.10, 128.19, 127.90, 114.39,113.67, 109.01, 55.49(OCH_3), 55.44 (OCH_3).

2-chloro-4,6-bis(4-methoxyphenyl)pyrimidine (**4e**): Yellow solid, yield: 93%, mp = 187–190 °C; ^{1}H NMR (400 MHz, $CDCl_3$, δ, ppm): 8.10 (d, J = 8.48 Hz, 3H, ArH), 7.87 (d, J = 8.84 Hz, 1H, ArH), 7.85 (s, 1H, Pyr-H), 7.01 (dd, J = 8.50 Hz, 1.74 Hz, 4H, ArH), 3.88 (s, 6H, 2OCH_3); ^{13}C NMR (400 MHz, $CDCl_3$, δ, ppm): 166.74, 166.52, 162.51, 161.84, 161.58, 131.61, 129.10, 128.19, 127.90, 114.39, 113.67, 109.01, 55.49(OCH_3), 55.44 (OCH_3).

2-chloro-4-(3,4-dimethoxyphenyl)-6-(4-methoxyphenyl)pyrimidine (**4f**): Yellow solid, yield: 89%, mp = 138–141 °C; ^{1}H NMR (400 MHz, $CDCl_3$, δ, ppm): 8.12 (d, J = 8.88 Hz, 2H, ArH), 7.87 (d, J = 8.84 Hz, 1H, ArH), 7.85 (s, 1H, Pyr-H), 7.01 (d, J = 8.88, 2H, ArH), 6.96 (d, J = 8.36, 1H, ArH), 4.00 (s, 3H, OCH_3), 3.95 (s, 3H, OCH_3), 3.88 (s, 3H, OCH_3); ^{13}C NMR (400 MHz, $CDCl_3$, δ, ppm): 164.28, 164.24, 162.78, 161.40, 150.90, 149.06, 131.44, 131.04, 120.01, 113.92, 110.87, 110.05, 99.65, 56.00 (OCH_3), 55.95 (OCH_3), 55.39 (OCH_3).

2-chloro-4,6-bis(3,4-dimethoxyphenyl)pyrimidine (**4g**): Yellow solid, yield: 78%, mp = 180–183 °C; ^{1}H NMR (400 MHz, $CDCl_3$, δ, ppm): 7.86 (s, 1H, ArH), 7.74 (s, 2H, ArH), 7.69 (d, J = 7.12 Hz, 2H, ArH), 6.97 (d, J = 7.76 Hz, 2H, ArH), 4.00 (s, 6H, 2OCH_3), 3.96 (s, 6H, 2OCH_3).

6.5. A typical procedure for the synthesis of 4,6-diphenyl-2-(piperazin-1-yl)pyrimidine

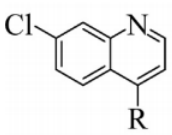

5a	R = ethane-1,2-diamine
5d	R = propane-1,3-diamine
5c	R = butane-1,4-diamine
5d	R = piperazin-1-yl

A reaction mixture of 2-chloro-4,6-diphenylpyrimidine (4.0 g, 15 mmol) and piperazine (13.92 g, 150 mmol) in isopropanol (20 mL) was refluxed for 20 h. The progression of the reaction was monitored by TLC. The reaction mixture was added to 2 M NaOH (100 ml) solution, and the precipitate formed was filtered, washed with water and diethyl ether, and dried under vacuum. The crude product was purified by recrystallized in EtOAc to obtain the following pure compounds.

N^1-(7-chloroquinolin-4-yl*)ethane-1,2-diamine* (**5a**): Yellow solid, yield: 97%, mp = 137–139 °C; ^{1}H NMR (400 MHz, DMSO-d_6, δ, ppm): 8.33 (d, J = 5.48 Hz, 1H, ArH), 8.20 (d, J = 9.01 Hz, 1H, ArH), 7.76 (d, J = 1.84 Hz, 1H, ArH), 7.40 (dd, J = , 9.00 Hz, 1.85 Hz, 1H, ArH), 7.26 (s, 1H, -NH), 6.50 (d, J = 5.56 Hz, 1H, ArH), 3.27 (br.s, 2H, CH_2), 2.79 (t, J = 6.38 Hz, 2H, CH_2); ^{13}C NMR (400 MHz, DMSO-d_6, δ, ppm): 152.35, 152.27, 150.06, 149.02, 134.24, 127.41, 124.78, 117.80, 99.25, 45.58.

N^1-(7-chloroquinolin-4-yl*)propane-1,3-diamine* (**5b**): Yellow solid, yield: 98%, mp = 88–90 °C; ^{1}H NMR (400 MHz, DMSO-d_6, δ, ppm): 8.32 (d, J = 5.06 Hz, 1H, ArH), 8.17 (d, J = 8.92 Hz, 1H, ArH), 7.75 (d, J = 4.92Hz, 1H, ArH), 7.68 (br.s, 1H, -NH), 7.40 (d, J = 7.20 Hz, 1H, ArH), 6.48 (d, J = 5.54 Hz, 1H, ArH), 3.30 (t, J = 6.90Hz, 2H, ArH), 2.66 (t, J = 6.60 Hz, 2H, CH_2), 1.74 (q, J = 6.75 Hz, 2H, CH_2), ^{13}C NMR (400 MHz, DMSO-d_6, δ, ppm): 151.83, 151.70, 150.36,148.45, 133.64, 126.84, 126.84, 124.22, 123.89, 122.04, 98.61, 40.20.

N^1-(7-chloroquinolin-4-yl*)butane-1,4-diamine* (**5c**): White solid, yield: 99%, mp = 121–124 °C; ^{1}H NMR (400 MHz, DMSO-d_6, δ, ppm): 8.32 (d, J = 5.48 Hz, 1H, ArH), 8.19 (d, J = 9.01 Hz, 1H, ArH), 7.76 (d, J = 1.64 Hz, 1H, ArH), 7.39 (dd, J = 8.94, 1.64, Hz, 1H, ArH), 7.36 (br.s, 1H, -NH), 6.44 (d, J = 5.56 Hz, 1H, ArH), 3.23 (t, J = 6.90 Hz, 2H, CH_2), 2.54 (t, J = 6.98 Hz, 2H, CH_2), 1.62 (q, J = 6.98 Hz, 2H, CH_2), 1.44 (p, J = 7.35 Hz, 2H, CH_2); ^{13}C NMR (400 MHz, DMSO-d_6, δ, ppm): 151.25, 149.91, 148.02, 133.19, 126.38, 123.72, 123.43, 116.77, 98.13, 41.79(CH_2), 40.88 (CH_2), 29.49 (CH_2), 24.67 (CH_2).

7-chloro-4-(piperazin-1-yl*)quinoline* (**5d**): Yellow solid, yield: 100%, mp = 113–115 °C;^{1}H NMR (400 MHz, DMSO-d_6, δ, ppm): 8.68 (d, J = 5.00 Hz, 1H, ArH), 8.01 (d, J = 9.00 Hz, 1H, ArH), 7.96 (d, J = 2.16 Hz, 1H, ArH), 7.53 (dd. J = 8.98 Hz, 2.26 Hz, 1H, ArH), 3.09-3.07 (m, 4H, 2CH_2), 2.97-2.94 (m, 4H, 2CH_2); ^{13}C NMR (400 MHz, DMSO-d_6, δ, ppm): 156.42, 151.17, 151.88, 149.61, 148.78, 141.29, 135.36, 133.53, 128.69, 128.11, 128.02, 126.04, 125.80, 125.69, 124.25, 122.03, 121.31, 109.37, 109.37, 51.86, 44.69.

6.6. A typical procedure for the synthesis of N^1-(7-chloroquinolin-4-yl)-N2-(4,6-diphenylpyrimidin-2-yl) ethane-1,2-diamine

APPENDIX-IV

A solution of 2-chloro-4,6-diphenylpyrimidine **(6)** (120.65 mg, 0.45 mmol), **N^1-(7-**chloroquinolin-4-yl) ethane-1,2-diamine **(5)** (100 mg, 0.45 mmol) and K_2CO_3 (125.03 mg, 0.91 mmol) in DMF (2 mL) was discharged to a microwave at temperature 120 °C, pressure 150 Psi and power 150 Watts for 40 min. The progression of the reaction was monitored using TLC. The reaction mixture was added to ice water. The precipitate formed was filtered, washed with water and dried under vacuum. The compound was purified using silica gel in a chromatographic column with eluent 1% MeOH in DCM to afford the following pure compounds.

*7-chloro-4-(4-(4,6-diphenylpyrimidin-2-*yl*)piperazin-1-*yl*)quinoline* (**6a**): Yellow solid, yield: 65%, mp = 169–172 °C; ^{1}H NMR (400 MHz, $CDCl_3$, *δ*, ppm): 8.76 (d, *J* = 4.35 Hz, 1H, ArH), 8.14 (d, *J* = 3.63 Hz, 3H, ArH), 8.08-8.07 (m, 2H, ArH), 7.82 (d, *J* = 3.44 Hz, 1H, ArH), 7.51-7.48 (m, 8H, ArH), 6.89 (d, *J* = 8.45 Hz, 1H, ArH), 4.33-4.19 (m, 4H, $2CH_2$), 3.36-3.29 (m, 4H, $2CH_2$); ^{13}C NMR (400 MHz, $CDCl_3$, *δ*, ppm): 163.76, 157.09, 151.13, 150.64, 414.49, 134.83, 129.77, 129.11, 127.48, 127.28, 126.89, 124.60, 123.09, 122.09, 111.96, 103.09, 98.16, 56.37, 40.20, 21.47.

*N^1-(4-(4-chlorophenyl)-6-(p-tolyl)pyrimidin-2-*yl*)-N^4-(7-chloroquinolin-4-*yl*)butane-1,4-diamine* (**6b**): Yellow solid, yield: 84%, mp = 192–194 °C; ^{1}H NMR (400 MHz, $CDCl_3$, *δ*, ppm): 8.50 (d, *J* = 5.32 Hz, 1H, ArH), 7.94 (d, *J* = 1.99 Hz, 1H, ArH), 7.70 (d, *J* = 8.43 Hz, 2H, ArH), 7.65 (d, *J* = 7.97 Hz, 2H, ArH), 7.54 (d, *J* = 8.96 Hz, 1H, ArH), 7.41 (d, *J* = 8.44 Hz, 2H, ArH), 7.29 (dd, *J* = 8.92, 2.07 Hz, 1H, ArH), 7.24 (d, *J* = 8.24 Hz, 3H, ArH), 6.36 (d, *J* = 5.34 Hz, 1H, ArH), 5.36 (t, *J* = 5.95 Hz, 1H, NH), 5.03 (br.s, 1H, NH), 3.55 (q, *J* = 3.55 Hz, 2H, CH_2), 3.55 (q, *J* = 5.55 Hz, 2H, CH_2), 2.40 (s, 3H, CH_3), 1.85-1.79 (m, 4H, $2CH_2$) ^{13}C NMR (400 MHz, $CDCl_3$, *δ*, ppm): 160.03, 151.87, 149.66, 148.95, 139.99, 135.92, 135.76, 134.91, 134.46, 130.69, 129.15, 128.76, 128.29, 125.81, 117.08, 114.71, 99.03, 42.98(CH_2), 41.16(CH_2), 27.45(CH_2), 25.93 (CH_2), 21.44. (CH_3).

*7-chloro-4-(4-(4-(4-chlorophenyl)-6-(p-tolyl)pyrimidin-2-*yl*) piperazin-1-*yl*)quinoline* (**6c**): Yellow solid, yield: 82%, mp = 215–217 °C; ^{1}H NMR (400 MHz, $CDCl_3$, *δ*, ppm): 8.74 (d, *J* = 4.90 Hz, 1H, ArH), 8.07 (m, 4H, ArH), 8.04 (d, *J* = 8.16 Hz, 2H, ArH), 7.47 (d, *J* = 8.49 Hz, 3H, ArH), 7.40 (s, 1H, ArH), 7.31 (d, *J* = 8.04 Hz, 2H, ArH), 6.88 (d, *J* = 5.00 Hz, 1H, ArH), 4.31 (t, *J* = 4.58 Hz, 4H, $2CH_2$), 3.35 (t, *J* = 4.86 Hz, 4H, $2CH_2$), 2.44 (s, 3H, CH_3); ^{13}C NMR (400 MHz, $CDCl_3$, *δ*, ppm): 163.96, 162.21, 157.09, 151.99, 150.21, 140.96, 136.56, 136.49, 135.05, 129.47, 128.98, 128.39, 127.03, 126.35, 125.15, 122.02, 1032.16, 101.90, 52.33, 44.00, 21.46.

*N^1-(7-chloroquinolin-4-*yl*)-N^2-(4-(4-methoxyphenyl)-6-(p-tolyl) pyrimidin-2-*yl*)ethane-1,2-diamine* (**6d**): Yellow solid, yield: 88%, mp = 154–157 °C; ^{1}H NMR (400 MHz, $CDCl_3$, *δ*, ppm): 8.43 (d, *J* = 3.67 Hz, 1H, ArH), 8.15 (s, 1H, ArH), 8.01 (br, s, 4H, ArH), 7.81 (s, 1H, ArH), 7.40 (s, 1H, ArH), 7.34 (d, *J* = 7.09 Hz, 3H, ArH), 7.11-7.02 (m, 3H, ArH), 6.46 (br, s, 1H, NH), 6.30 (d. *J* = 5.28 Hz, 1H, ArH), 5.90 (s.br, 1H, NH), 4.05-4.04 (m, 2H, CH_2), 3.97 (s, 3H, CH_3), 3.51-3.50 (m, 2H, CH_2), 2.46 (s, 3H, CH_3); ^{13}C NMR (400 MHz, $CDCl_3$, *δ*, ppm): 163.89, 157.23, 151.26, 150.77, 134.97, 129.90, 129.24, 127.62, 127.42, 127.02, 124.74, 112.10, 103.23, 98.29, 56.50, 40.33, 21.60, 14.25.

*N^1-(7-chloroquinolin-4-*yl*)-N^3-(4-(4-methoxyphenyl)-6-(p-tolyl) pyrimidin-2-*yl*)propane-1,3-diamine* (**6e**): Yellow solid, yield: 76%, mp = 97–99 °C; ^{1}H NMR (400 MHz, $CDCl_3$, *δ*, ppm): 8.42 (s, 1H, ArH), 8.09 (d, *J* = 1.99 Hz, 1H, ArH), 7.91 (t, *J* = 16.44 Hz, 5H, ArH), 7.42 (d, *J* = 8.73 Hz, 1H, ArH), 7.28 (s, 2H, ArH), 7.00-6.94 (m, 2H, ArH), 6.37 (d, *J* = 4.89 Hz, 1H, ArH), 5.69 (br.s, 1H, -NH), 5.48 (t, *J* = 4.89 Hz, 1H, -NH), 3.96 (s, 3H, OCH_3), 3.81 (q, *J* = 6.16 Hz, 2H, CH_2), 3.52-3.48 (m, 2H, ArH), 2.44 (s, 3H, CH_3), 2.10 (q, *J* = 6.09 Hz, 2H, CH_2); ^{13}C NMR (400 MHz, $CDCl_3$, *δ*, ppm): 166.06, 164.01, 163.17, 156.82, 140.94, 135.07, 129.58, 128.99, 127.06, 126.68, 125.26, 122.97, 121.37, 111.83, 102.59, 56.32 (OCH_3), 40.59 (C–NH_2), 38.75(C–NH_2), 28.89(CH_2), 21.44 (CH_3).

7-chloro-4-(4-(4-(4-methoxyphenyl)-6-(p-tolyl)pyrimidin-2-yl)piperazin-1-yl)quinoline (**6f**): Yellow solid, yield: 83%, mp = 191–193 °C; FTIR (ATR, *νmax*, cm-1): 3038 (C–H), 2998 (C–H of CH_3), 2956 (C–H of CH_3), 1438–1565 (C=C of Ar), 1237 (C–O), 773 (C–Cl), ^{1}H NMR (400 MHz, $CDCl_3$, *δ*, ppm): 8.74 (d, *J* = 4.96 Hz, 1H, ArH),), 8.12 (d, *J* = 8.80 Hz, 2H, ArH), 8.08 (s, 1H, ArH), 8.06 (d, *J* = 5.69 Hz, 1H, ArH), 8.04 (d, *J* = 8.09 Hz, 3H, ArH) 7.47 (dd, *J* = 8.99, 1.99 Hz, 1H, ArH), 7.40 (s, 2H, CH_2), 7.30 (d, *J* = 8.04 Hz, 2H, ArH), 7.01 (d, *J* = 8.79 Hz, 2H, ArH), 6.88 (d, *J* = 5.02 Hz, 1H, ArH), 4.31-4.29 (m, 4H, $2CH_2$), 3.89 (s, 3H, OCH_3), 3.35 (t, q = 4.83 Hz,4H, $2CH_2$) 2.43 (s, 3H, CH_3); ^{13}C NMR (400 MHz, $CDCl_3$, *δ*, ppm): 164.71, 162.12, 157.13, 151.96, 151.25, 150.17, 149.17, 135.06, 130.93, 128.94, 126.35, 125.19, 122.00, 120.24, 110.96, 110.13, 109.14, 101.48, 56.11(2OMe), 56.04 (2OMe), 52.38 ($2CH_2$), 44.03 ($2CH_2$), 21.44 (CH_3).

*N^1-(4,6-bis(4-methoxyphenyl)pyrimidin-2-*yl*)-N^4-(7-chloroquinolin-4-*yl*)butane-1,4-diamine* (**6g**): Yellow solid, yield: 83%, mp = 144–145 °C; FTIR (ATR, *νmax*, cm-1): 3256 (N–H), 3069, 2932 (C–H, CH_3), 1573-1450 (C=C, Ar) 1239 (C–O), 763 (C–Cl); ^{1}H NMR (400 MHz, $CDCl_3$, *δ*, ppm): 8.38 (d, *J* = 5.57 Hz, 1H, ArH),), 8.03 (d, *J* = 8.81 Hz, 3H, ArH), 7.91 (d, *J* = 2.10 Hz, 1H, ArH), 7.76 (d, *J* = 8.69 Hz, 1H, ArH), 7.62 (d, *J* = 8.97 Hz, 1H, ArH), 7.30 (s, 1H, ArH), 7.21 (dd, *J* = 7.20, 2.04 Hz, 1H, ArH) 6.96 (d, *J* = 8.72 Hz, 5H, ArH), 6.35 (d, *J* = 5.61 Hz, 1H, ArH), 5.55 (br.s, 1H, NH), 5.40 (t, *J* = 6.01Hz, 1H, NH), 3.85 (s, 6H, $2OCH_2$), 3.66 (m, 1H, NH),), 5.56- 5.48 (m, 1H, NH), 3.19 (s, 6H, $2CH_3$), 3.81-3.60 (m, 2H, CH_2), 3.51 (q, *J* = 6.27 Hz, 2H, CH_2), 3.51 (q, *J* = 6.10 Hz, 2H, CH_2), 1.91-1.82 (m, 4H, $2CH_2$); ^{13}C NMR (400 MHz, $CDCl_3$, *δ*, ppm): 164.91, 162.99, 161.58, 150.40, 135.35, 130.97, 130.41, 128.45, 127.51, 125.47, 212.41, 116.86, 114.03, 113.37, 101.53, 99.89, 55.40 2(OCH_3), 42.99 (C–NH), 40.84 (C–NH), 27.42 (CH_2), 25.96 (CH_2); HRMS (ESI, *m/z*) $[M+Na]^+$; calculated for $C_{31}H_{30}ClN_5O_2$, 562.1972, found 562.1986.

*4-(4-(4,6-bis(4-methoxyphenyl)pyrimidin-2-*yl*)piperazin-1-*yl*)-7-chloroquinoline* (**6h**): Yellow solid, yield: 87%, mp = 191–195 °C; FTIR (ATR, *νmax*, cm-1): 3037, 2996 (C–H, CH_3), 1604-1419 (C=C, Ar) 1242 (C–O), 812. (C–Cl); ^{1}H NMR (400 MHz, $CDCl_3$, *δ*, ppm): 8.74 (d, *J* = 4.98 Hz, 1H, ArH), 8.11 (d, *J* = 8.85 Hz, 3H, ArH), 8.13-8.01 (m, 2H, ArH), 7.86 (d, *J* = 8.84 Hz, 1H, ArH) 7.47 (dd, *J* = 9.05, 2.01 Hz, 1H, ArH), 7.37 (s, 1H, ArH), 7.01 (d, *J* = 8.81 Hz, 4H, ArH), 6.88 (d, *J* = 5.03 Hz, 1H, ArH), 4.31-4.29 (m, 4H, $2CH_2$), 3.88 (s, 6H, $2CH_3$), 3.35 (t, *J* = 4.88 Hz, 4H, $2CH_3$), 1.29 (s, 3H, CH_3); ^{13}C NMR (400 MHz, $CDCl_3$, *δ*, ppm): 164.71, 162.12, 157.13, 151.96, 151.25, 150.17, 149.17, 135.06, 130.93, 128.94, 126.35, 125.19, 122.00, 120.24, 110.96, 110.13, 109.14, 101.48, 56.11(2OMe), 56.04 (2OMe),52.38 ($2CH_2$), 44.03 ($2CH_2$); HRMS (ESI, *m/z*) $[M+H]^+$; calculated for $C_{31}H_{28}ClN_5O_2$, 538.2010, found 538.2030.

*N1-(7-chloroquinolin-4-*yl*)-N4-(4-(3,4-dimethoxyphenyl)-6-(4-methoxyphenyl)pyrimidin-2-*yl*)butane-1,4-diamine* (**6i**); Yellow solid, yield: 93% mp = 130–132 °C; FTIR (ATR, *νmax*, cm^{-1}): 3080 (C–H), 2935 (C–H of CH_3), 2956 (C–H of CH_3), 1438–1601 (C=C of Ar), 1179, 1260 (C–O), 773 (C–Cl), ^{1}H NMR (400 MHz, $CDCl_3$, *δ*, ppm): 8.39 (d, *J* = 5.52 Hz, 1H, ArH), 7.99 (d, *J* = 8.77 Hz, 3H, ArH), 7.89 (brs.1H, ArH), 7.73 (d, *J* = 8.72 Hz, 1H, ArH), 7.46-7.42 (m, 1H, ArH), 7.28 (s, 1H, ArH) 6.96 (d, *J* = 8.80 Hz, 1H, ArH), 6.35 (t, *J* = 4.47 Hz, 1H, ARH), 5.83-5.76 (m, 1H, NH), 5.56-5.49 (m, 1H, NH), 3.87 (s, 6H, $2OCH_3$), 3.85 (s, 3H, OCH_3), 3.78 (t, *J* = 5.76 Hz, 2H, $2CH_2$), 3.48 (t, *J* = 5.81 Hz, 2H, CH_2), 2.07 (q, *J* = 5.81 Hz, 2H, CH_2);

^{13}C NMR (400 MHz, $CDCl_3$, δ, ppm): 164.71, 162.13, 157.13, 151.96, 151.25, 150.17, 149.17, 135.06, 130.93, 128.94, 126.35, 125.19, 122.00, 120.24, 110.96, 110.13, 109.14, 101.48, 56.11 (2OMe), 56.04 (OMe), 52.38 ($2CH_2$), 44.03 ($2CH_2$).

7-chloro-4-(4-(4-(3,4-dimethoxyphenyl)-6-(4-methoxyphenyl) pyrimidin-2-yl)piperazin-1-yl)quinoline (**6j**): Yellow solid, yield: 79% mp = 201–204 °C; FTIR (ATR, *νmax*, cm-1): 3276 (C–N), 3073, 2839 (C–H of CH_3), 1572-1430 (C=C Ar) 1298 (C–O), 763 (C–Cl), ^{1}H NMR (400 MHz, $CDCl_3$, δ, ppm): 8.74 (d, J = 4.97 Hz, 1H, ArH), 8.12 (d, J = 8.81 Hz, 2H, ArH), 8.08 (m, 2H, ArH), 7.74-7.70. (m, 2H, ArH), 7.47 (dd. J = 9.01, 1.99 Hz, 1H, ArH), 7.36 (s, 1H, ArH), 7.02 (d, J = 8.77 Hz, 2H, ArH), 6.98 (d, J = 8.27 Hz, 1H, ArH), 6.89 (d, J = 5.02 Hz, 1H, ArH), 4.31 (t, J = 4.40 Hz, 4H, $2CH_2$), 4.01 (s, 3H, CH_3), 3.96 (s, 3H, CH_3), 3.89 (s, 3H, CH_3), 3.36 (t, J = 4.40 Hz, 4H, $2CH_2$); ^{13}C NMR (400 MHz, $CDCl_3$, δ, ppm): 161.64, 157.15, 151.98, 151.19, 150.20, 149.15, 135.04, 130.99, 130.56, 128.95, 128.58, 126.33, 125.20, 122.03, 120.22, 114.04, 110.96, 110.07, 109.15, 101.25, 56.08, 56.04, 52.38, 44.03.

4-(4-(4,6-bis(3,4-dimethoxyphenyl)pyrimidin-2-yl)piperazin-1-yl)-7-chloroquinoline (**6k**): Yellow solid, yield: 88%, mp = 249–251 °C; FTIR (ATR, *νmax*, cm-1): 3080 (C–H), 2935 (C–H of CH_3), 2956 (C–H of CH_3), 1438–1601 (C=C of Ar), 1179, 1260 (C–O), 773 (C–Cl), ^{1}H NMR (400 MHz, $CDCl_3$, δ, ppm): 8.74 (d, J = 4.96 Hz, 1H, ArH), 8.08 (m, 2H, ArH), 7.75-7.70 (m, 4H, ArH) 7.47 (dd, J = 9.01, 1.99 Hz, 1H, ArH), 7.36 (s, 1H, ArH), 6.98 (d, J = 8.40 Hz, 2H, ArH), 6.89 (d, J = 5.01 Hz, 1H, ArH), 4.30 (t, J = 4.10Hz, 4H, $2CH_2$), 4.01 (s, 6H, $2OCH_3$), 3.96 (s, 6H, $2OCH_3$), 3.36 (t, J = 4.73 Hz, 4H, $2CH_2$); ^{13}C NMR (400 MHz, $CDCl_3$, δ, ppm): 164.71, 162.13, 157.13, 151.96, 151.25, 150.17, 149.17, 135.06, 130.93, 128.94, 126.35, 125.19, 122.00, 120.24, 110.96, 110.13, 109.14, 101.48, 56.11(2OMe), 56.04 (2OMe), 52.38 ($2CH_2$), 44.03 ($2CH_2$).

6.7. A typical procedure for the synthesis of 4-(2-(4-(7-chloroquinolin-4-yl)piperazin-1-yl)-6-(4-hydroxyphenyl) pyrimidin-4-yl)benzene-1,2-diol

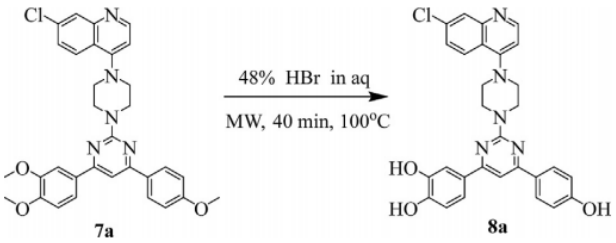

7a (50 mg, 0.10 mmol) in 48% aqueous HBr (2 mL) was discharged into a microwave and radiated at temperature 100 °C, pressure 300 PSI and power 300 W for 40 min. Using TLC, the development of the product was monitored. The precipitate formed was filtered and washed with water and diethyl ether. The crude product was recrystallized in ethanol to afford the following pure compounds in good yield.

4,4'-(2-((4-((7-chloroquinolin-4-yl)amino)butyl)amino)pyrimidine-4,6-diyl)diphenol (**7a**); Yellow solid, yield: 93%, mp = 214–216 °C; FTIR (ATR, ν_{max}, cm^{-1}): 3351 (O–H), 3256 (N–H), 3061, 2944 (C–H, CH_3), 1443–1576 (C=C, Ar), 1281 (C–O), 791 (C–Cl);^{1}H NMR (400 MHz, $CDCl_3$, δ, ppm): 13.06 (s, 1H, ph-OH), 10.37 (br, s, 1H, ph-OH), 9.39-9.37 (m, 1H, NH), 8.55 (d, J = 9.21 Hz, ArH), 8.52 (br, s, 1H, NH), 8.24-8.05 (m, 4H, ArH), 7.90 (d, J = 2.05 Hz, 1H, ArH) 7.71 (dd, J = 9.08, 2.07 Hz, 1H, ArH), 7.66 (s, 1H, ArH), 7.30-7.23 (m, 4H, ArH), 6.36 (d, J = 5.32 Hz, 1H, ArH), 5.36 (t, J = 5.94 Hz, 1H, ArH), 6.93 (d, J = 7.16Hz, 5H, ArH), 5.62-2.61 (m, 4H, $2CH_2$), 1.83 -1.80 (m, 4H, $2CH_2$); ^{13}C NMR (400 MHz, $CDCl_3$, δ, ppm): 160.68, 158.96, 155.90, 143.31, 138.84, 138.55, 134.17, 131.27, 129.70, 127.36, 127.33, 126.01, 119.51, 116.74, 115.83, 115.03, 114.89, 102.66, 100.54, 99.19, 99.13, 43.45, 40.95, 26.55, 25.43; HRMS (ESI, *m/z*) $[M+H]^+$; calculated for $C_{29}H_{26}ClN_5O_2$, 512.1853; found 512.1844.

4-(2-((4-((7-chloroquinolin-4-yl)amino)butyl)amino)-6-(4-hydroxyphenyl)pyrimidin-4-yl)benzene-1,2-diol (**7b**): Yellow solid, yield: 89%, mp = 221–223 °C; FTIR (ATR, *νmax*, cm^{-1}): 3418 (O–H), 3228 (N–H), 2927 (C–H of CH_3), 1439–1568 (C=C of Ar), 1273 (C–O), 759 (C–Cl); ^{1}H NMR (400 MHz, $CDCl_3$, δ, ppm): 9.90 (br.s, 2H, 2ph-OH), 8.80 (br, s, 1H, ph-OH) 8.50 (d, J = 9.13 Hz, 1H, ArH), 8.41 (d, J = 6.64 Hz, 1H, ArH), 8.03 (d, J = 8.66 Hz, 4H, ArH), 8.24-8.05 (m, 4H, ArH), 7.87 (d, J = 1.96 Hz, 1H, ArH), 7.64 (dd, J = 9.12, 2.12 Hz, 1H, ArH), 7.44 (s, 1H, ArH), 7.09 (t, J = 5.87 Hz, 1H, NH), 6.82 (br, s, 4H, (1NH, 3ArH)), 6.76 (d, J = 6.66 Hz, 1H, ArH), 3.59-3.194 (m, 6H, $2CH_2$), 2.06 (t, J = 6.60 Hz, 2H, ArH); ^{13}C NMR (400 MHz, $CDCl_3$, δ, ppm): 163.08, 160.17, 154.32, 145.95, 137.11, 128.97, 128.78, 126.47, 125.67, 122.67, 116.60, 115.78, 114.92, 99.91, 99.15, 41.49, 40.61, 38.98, 28.23.

4-(2-(4-(7-chloroquinolin-4-yl)piperazin-1-yl)-6-(4-hydroxyphenyl)pyrimidin-4-yl)benzene-1,2-diol (**7c**): Yellow solid, yield: 94%, mp = < 300 °C; FTIR (ATR, *νmax*, cm^{-1}): 3418 (O–H), 3228 (N–H), 2927 (C–H of CH_3), 1439–1568 (C=C of Ar), 1273 (C–O), 759 (C–Cl); ^{1}H NMR (400 MHz, $CDCl_3$, δ, ppm): 9.93 (s, H, ph-OH), 9.43 (br, s, 1H, ph-OH),), 9.08 (s, H, 2ph-OH), 8.73 (d, J = 4.96 Hz, 1H, ArH), 8.20 (d, J = 9.00 Hz, 1H, ArH), 8.13 (d, J = 8.55 Hz, 2H, ArH), 8.01 (d, J = 1.97 Hz, 1H, ArH), 7.73 (d, J = 2.04 Hz, 1H, ArH), 7.62-7.56 (m, 2H, ArH), 7.53 (s, 1H, ArH), 7.10 (d, J = 5.12 Hz, 1H, ArH), 6.90 (d, J = 8.56 Hz, 2H, ArH), 6.87 (d, J = 8.28 Hz, 1H, ArH), 4.19 (br.s, 4H, $2CH_2$); ^{13}C NMR (400 MHz, $CDCl_3$, δ, ppm): 164.63, 164.30, 162.03, 160.36, 157.13, 148.64, 145.95, 134.42, 129.81, 129.30, 129.13, 128.01, 126.86, 128.01, 126.86, 126.37, 121.73, 119.50, 116.06, 116.00, 115.89, 115.24, 114.85, 109.92, 100.28, 52.22, 43.99, 40.53.

7. Pharmacological evaluation

7.1. Antiplasmodial activity

The chloroquine-sensitive strain of *P. falciparum* (NF54) was maintained continuously *in vitro* in supplemented RPMI-1640 culture media at 37 °C and gassed with a mixture of 5% CO_2, 3% O_2 and 92% N_2 [28]. 5% D-sorbitol was used to synchronise the culture in the ring stage [29]. To determine the antimalarial activity of the compounds, the synchronised ring-stage parasites were adjusted to a final parasitaemia of 2% and 2% haematocrit, to which serial dilutions of the compounds and positive control, quinine were added after a 24 h incubation. Negative controls included uninfected erythrocytes and drug-free parasitised erythrocytes. Following a further 48 h incubation period, the plates were frozen at −70 °C for 1 h and thawed for 1 h. Lysate (25 μl) were transferred to a second plate, to which 100 μl Malstat™ and 20 μl nitroblue tetrazolium-phenazine ethosulphate (1:1) mixture was added to each well and incubated for 40 min at 37 °C to quantify the parasite lactate dehydrogenase (pLDH) activity [30]. Thereafter, 5% acetic acid was added to each well, and the absorbance of the formazan products read at 620 nm, as an indicator of parasite viability. The percentage parasite growth, taking the appropriate controls into account, were calculated and used to determine the concentration required to inhibit parasite growth by 50% (IC_{50} value) from log sigmoid dose-response curves using the GraphPad Prism® 5.0.0 software. Each experiment was repeated in triplicate [31,32].

8. Toxicity assays

8.1. Cell viability assay

Human embryonic kidney epithelial (HEK-293) cells were maintained at 37 °C in a humidified environment with a 5% CO_2 as a monolayer in Dulbecco's modified Eagle's medium (DMEM) supplemented with 10% fetal bovine serum, 100 IU/ml penicillin and 100 μg/ml streptomycin. A cell suspension (10 000 cells/well) was incubated at 37 °C for 48 h with serial dilutions of compounds/positive control. A final concentration of less than 1% DMSO had no effect on the viability of the cells. Thereafter, 40 μl of (3-(4, 5-dimethylthiazolyl-2)-2, 5-diphenyltetrazolium bromide (MTT; 5 mg/ml in phosphate buffer saline (pH 7.3)) was added to each well and incubated for a further 2 h. DMSO was used to dissolve the formazan crystals and then quantified spectrophotometrically at an absorbance of 540 nm with a reference wavelength of 690 nm (Labsystems Multiskan RC) [33]. Percent cellular viability was determined using the appropriate controls and used to calculate the IC_{50} values which were compared to the positive control, camptothecin. The experiment was repeated in triplicate [34,35].

8.2. Determination of binding affinity of select synthetic compounds to P. falciparum Hsp70

Recombinant forms of two essential cytosol localized *P. falciparum* Hsp70s; PfHsp70-1 and PfHsp70-z were expressed in *E. coli* and purified using nickel affinity chromatography following a previously described approach [20]. The binding affinities of the proteins for four selected compounds were determined by SPR analysis using the BioNavis™ 420A ILVES MP-SPR (BioNavis, Tampere, Finland) at 25 °C as previously described [20]. A running buffer, degassed PBS Tween 20 (4.3 mM Na_2HPO_4, 1.4 mM KH_2PO_4, 137 mM NaCl, 3 mM KCl, 0.005% (v/v) Tween 20, and 20 mM EDTA; pH 7.4) was used. The recombinant proteins were immobilised as ligands at 0.5 μg/ml onto functionalized 3D carboxymethyl dextran sensors (CMD 3D 500L; BioNavis, Tampere, Finland). Immobilization of ligands was achieved through amine coupling after 1-ethyl-3-(3-dimethylaminopropyl) carbodiimide (EDC) [Sigma Aldrich, Germany] and N-hydroxy-succinimide (NHS) [Sigma Aldrich, Germany] activation following a protocol provided by the manufacturer (BioNavis, Tampere, Finland) to achieve <200 RUs. A reference channel without immobilised protein served as a control for non-specific binding and changes in refractive index. As analyte, compounds (**6h**, **6k**, **7a**, and **7b**) were prepared into aliquots of 0, 1.25, 2.5, 5 and 10 nM injected three times at a flow rate of 50 μl/min into each flow cell. Injections with buffer only were used as controls. Association between ligand and analyte was allowed for 3 min, and dissociation was monitored for a total of 10 min. Kinetics steady-state equilibrium constant data was processed after double referencing of the sensorgrams and concatenating the responses of all five analyte concentrations by global fitting using TraceDrawer software version 1.8 (Ridgeview Instruments, Sweden).

8.3. Molecular docking

The molecular docking software utilized in this study was the Autodock Vina Plugin available on Chimera [36], with default docking parameters. Homology model of PfHsp70-1 (PlasmoDB accession number: PF3D7_0818900) and PfHsp70-z (PlasmoDB accession number: PF3D7_0708800.1) were also built using chimera software [37]. Gasteiger charges were added to the compounds, and the non-polar hydrogen atoms were merged to carbon atoms. The PCs were then docked into the active site pocket of PfHsp70-1 and PfHsp70-z (by defining the grid box with a spacing of 1 Å and size of 35 × 43 × 45 and 43 x 40 x 32 pointing in x, y and z directions respectively). The four compounds' systems were then subjected to molecular dynamics simulations.

8.4. Molecular dynamic (MD) simulations

The MD simulation was performed as described by Idowu et al. (2019) with little modification. The simulations were performed using the GPU version provided with the AMBER package (AMBER 18), in which the FF18SB variant of the AMBER force field [38] was used to describe the systems.

ANTECHAMBER was used to generate atomic partial charges for the compounds by utilizing the Restrained Electrostatic Potential (RESP) and the General Amber Force Field (GAFF) procedures. The Leap module of AMBER 18 allowed for the addition of hydrogen atoms, as well as Na^+ counter ions for neutralization all (both PfHsp70-1 and PfHsp70-z) systems. The amino acids were numbered, numbering residues 1–658 for PfHsp70-1 and 1–567 for PfHsp70-z. The systems were then suspended implicitly within an orthorhombic box of TIP3P water molecules such that all atoms were within 8 Å of any box edge [39].

An initial minimization of 2000 steps were carried out with an applied restraint potential of 500 kcal/mol for both solutes, were performed for 1000 steps using the steepest descent method followed by 1000 steps of conjugate gradients. An additional full minimization of 1000 steps were further carried out using the conjugate gradient algorithm without restraint. A gradual heating MD simulation from 0 K to 300 K was executed for 50 ps, such that the systems maintained a fixed number of atoms and fixed volume. The solutes within the systems were imposed with a potential harmonic restraint of 10 kcal/mol and collision frequency of 1.0 ps. Following heating, an equilibration estimating 500 ps of each system was conducted; the operating temperature was kept constant at 300 K. Additional features such as several atoms and pressure were also kept constant mimicking an isobaric-isothermal ensemble. The system's pressure was maintained at 1 bar using the Berendsen barostat [40,41].

The total time for the MD simulations conducted were 100 ns. In each simulation, the SHAKE algorithm was employed to constrict the bonds of hydrogen atoms [42]. The step size of each simulation was 2 fs, and an SPFP precision model was used. The simulations coincided with the isobaric-isothermal ensemble (NPT), with randomized seeding, the constant pressure of 1 bar maintained by the Berendsen barostat [40], a pressure-coupling constant of 2 ps, a temperature of 300 K and Langevin thermostat [43] with a collision frequency of 1.0 ps.

8.5. Post-dynamic analysis

Analysis of Root Mean Square Deviation (RMSD), Root Means Square Fluctuation (RMSF), Solvent accessible surface area (SASA) and Radius of Gyration (RoG) was done using the CPPTRAJ module employed in the AMBER 18 suit. All raw data plots were generated using the Origin data analysis software [44].

8.6. Binding free energy calculations

To estimate and compare the binding affinity of the systems, the free binding energy was calculated using the Molecular Mechanics/GB Surface Area method (MM/GBSA) (Ylilauri, M., Pentikäinen, 2013). Binding free energy was averaged over 100000 snapshots extracted from the 100 ns trajectory. The free binding energy (ΔG) computed by this method for each molecular species (complex, ligand, and receptor) can be represented as:

APPENDIX-IV

$$\Delta G_{bind} = G_{complex} - G_{receptor} - G_{ligand} \quad (1)$$

$$\Delta G_{bind} = E_{gas} + G_{sol} - TS \quad (2)$$

$$E_{gas} = E_{int} + E_{vdw} + E_{ele} \quad (3)$$

$$G_{sol} = G_{GB} + G_{SA} \quad (4)$$

$$G_{SA} = \gamma SASA \quad (5)$$

The term E_{gas} denotes the gas-phase energy, which consists of the internal energy E_{int}; Coulomb energy E_{ele} and the van der Waals energies E_{vdw}. The E_{gas} was directly estimated from the FF14SB force field terms. Solvation free energy, G_{sol}, was estimated from the energy contribution from the polar states, GGB, and non-polar states, G. The non-polar solvation energy, SA. GSA, was determined from the solvent-accessible surface area (SASA), using a water probe radius of 1.4 Å. In contrast, the polar solvation, GGB, the contribution was estimated by solving the GB equation. S and T denote the total entropy of the solute and temperature, respectively.

Declaration of competing interest

The authors declare that they have no known conflicting financial or personal interests that could have appeared to influence the work reported in this paper.

Acknowledgment

The authors would like to express the heartflet gratitude to the Discipline of Pharmaceutical Sciences, College of Health Sciences, University of KwaZulu-Natal (UKZN), Durban, South Africa, for providing all the necessary facilities. R.K. gratefully acknowledges National Research Foundation-South Africa (NRF-SA) for funding this project (grant nos. 103728, 112079 and 129247). The authors would also like to acknowledge Dr. Vuyisa Mzozoyana (UKZN) for NMR spectroscopic experimental data.

Appendix A. Supplementary data

Supplementary data to this article can be found online at https://doi.org/10.1016/j.ejmech.2021.113330.

References

[1] Lancet, Accelerated evolution and spread of multidrug-resistant Plasmodium falciparum takes down the latest first-line antimalarial drug in southeast Asia, Lancet Comment 3099 (2019) 916–917, https://doi.org/10.1016/S1473-3099(19)30394-9.
[2] E.G. Tse, M. Korsik, M.H. Todd, The past, present and future of antimalarial medicines, Malar. J. 18 (2019) 1–21, https://doi.org/10.1186/s12936-019-2724-z.
[3] Global Malaria Programme: WHO Global, World Malaria Report 2019, 2019. https://www.who.int/news-room/fact-sheets/detail/malaria.
[4] P. Adepoju, RTS, S malaria vaccine could provide major public health benefits, Lancet 394 (2019) 735–736, https://doi.org/10.1016/S0140-6736(19)31567-3.
[5] M.V. Raimondi, O. Randazzo, M. La Franca, G. Barone, E. Vignoni, D. Rossi, S. Collina, DHFR Inhibitors : reading the past for discovering novel anticancer agents, Molecules 24 (2019) 1–19, https://doi.org/10.3390/molecules24061140.
[6] L.C. Mishra, A. Bhattacharya, V.K. Bhasin, Phytochemical licochalcone A enhances antimalarial activity of artemisinin in vitro, Acta Trop. 109 (2009) 194–198, https://doi.org/10.1016/j.actatropica.2008.11.006.
[7] M. Chen, T.G. Theander, S.B. Christensen, L. Hviid, L.I.N. Zhai, A. Kharazmil, Licochalcone A, a New Antimalarial Agent, Inhibits in vitro growth of the human malaria parasite plasmodium falciparum and protects mice from P. yoelii Infection, Antimicrob. Agents Chemother. 38 (1994) 1470–1475.
[8] K. Devi, V. Rajendran, Ayushee, T.M. Rangarajan, R.P. Singh, P.C. Ghosh, M. Singh, Synthesis and evaluation of antiplasmodial activity of 2,2,2-trifluoroethoxychalcones and 2-fluoroethoxy chalcones against plasmodium falciparum in culture, Molecules 23 (2018) 1–28, https://doi.org/10.3390/molecules23051174.
[9] L. Sitali, M.C. Mwenda, J.M. Miller, D.J. Bridges, M.B. Hawela, E. Chizema-Kawesha, J. Chipeta, B. Lindtjørn, En-route to the "elimination" of genotypic chloroquine resistance in Western and Southern Zambia, 14 years after chloroquine withdrawal, Malar. J. 18 (2019) 1–8, https://doi.org/10.1186/s12936-019-3031-4.
[10] N.C. Phong, M. Chavchich, H.H. Quang, N.N. San, G.W. Birrell, I. Chuang, N.J. Martin, N.D. Manh, M.D. Edstein, Susceptibility of plasmodium falciparum to artemisinins and plasmodium vivax to chloroquine in Phuoc Chien Commune, Ninh Thuan Province, south-central Vietnam 11 medical and health Sciences 1108 medical Microbiology 11 medical and health Sciences 1103 Cli, Malar. J. 18 (2019) 1–11, https://doi.org/10.1186/s12936-019-2640-2.
[11] M. Mishra, V. Singh, S. Singh, Structural insights into key plasmodium proteases as therapeutic drug targets, Front. Microbiol. 10 (2019) 1–13, https://doi.org/10.3389/fmicb.2019.00394.
[12] S. Pulcini, H.M. Staines, A.H. Lee, S.H. Shafik, G. Bouyer, C.M. Moore, D.A. Daley, M.J. Hoke, L.M. Altenhofen, H.J. Painter, J. Mu, D.J.P. Ferguson, M. Llinás, R.E. Martin, D.A. Fidock, R.A. Cooper, S. Krishna, Mutations in the plasmodium falciparum chloroquine resistance transporter, PfCRT, enlarge the parasite's food vacuole and alter drug sensitivities, Sci. Rep. 5 (2015) 1–16, https://doi.org/10.1038/srep14552.
[13] Z.O. Ibraheem, R.A. Majid, H.M. Sidek, S.M. Noor, M.F. Yam, M.F. Abd Rachman Isnadi, R. Basir, In vitro antiplasmodium and chloroquine resistance reversal effects of andrographolide, evidence-based complement, Alternative Med. (2019) 1–16, https://doi.org/10.1155/2019/7967980.
[14] S. Zhang, C. Yi, C. Li, F. Zhang, J. Peng, Q. Wang, X. Liu, X. Ye, P. Li, M. Wu, Q. Yan, W. Guo, X. Niu, L. Feng, W. Pan, L. Chen, L. Qu, Chloroquine inhibits endosomal viral RNA release and autophagy-dependent viral replication and effectively prevents maternal to fetal transmission of Zika virus, Antivir. Res. 169 (2019) 1–8, https://doi.org/10.1016/j.antiviral.2019.104547.
[15] R. Delvecchio, L.M. Higa, P. Pezzuto, A.L. Valadão, P.P. Garcez, F.L. Monteiro, E.C. Loiola, A.A. Dias, F.J.M. Silva, M.T. Aliota, E.A. Caine, J.E. Osorio, M. Bellio, D.H. O'Connor, S. Rehen, R.S. De Aguiar, A. Savarino, L. Campanati, A. Tanuri, Chloroquine, an endocytosis blocking agent, inhibits zika virus infection in different cell models, Viruses 8 (2016) 1–15, https://doi.org/10.3390/v8120322.
[16] S. Oha, J.H. Shina, E.J. Janga, H.Y. Wona, H.K. Kima, M.-G. Jeonga, K.S. Kimb, E.S. Hwanga, Anti-inflammatory activity of chloroquine and amodiaquine through p21-mediated suppression of T cell proliferation and Th1 cell differentiation, Biochem. Biophys. Res. Commun. 474 (2017) 345–350, https://doi.org/10.1016/j.physbeh.2017.03.040.
[17] C.L. Perrin, K. Chang, The complete mechanism of an aldol condensation the complete mechanism of an Aldol condensation, J. Org. Chem. 81 (2016) 1–16, https://doi.org/10.1021/acs.joc.6b00959.
[18] A.N. Chiang, J.C. Valderramos, R. Balachandran, R.J. Chovatiya, B.P. Mead, C. Schneider, S.L. Bell, M.G. Klein, D.M. Huryn, X.S. Chen, B.W. Day, D.A. Fidock, P. Wipf, J.L. Brodsky, Select pyrimidinones inhibit the propagation of the malarial parasite, Plasmodium falciparum, Bioorg. Med. Chem. 17 (2009) 1527–1533, https://doi.org/10.1016/j.bmc.2009.01.024.
[19] I. Achilinou, H. Hoppe, H. Dirr, A. Shonhai, Chaperone activity of Plasmodium falciparum Hsp70 functional partners, Molecules 22 (2017) 1–15, https://doi.org/10.3390/molecules22122139.
[20] T. Zininga, O.J. Pooe, P.B. Makhado, L. Ramatsui, Polymyxin B inhibits the chaperone activity of Plasmodium falciparum Hsp70, Cell Stress Chaperones 22 (2017) 707–715, https://doi.org/10.1007/s12192-017-0797-6.
[21] M. Idowu, K. Ramharack, P. Nlooto, M. Gordon, Molecular dynamic mechanism(s) of inhibition of bioactive antiviral phytochemical compounds targeting cytochrome P450 3A4 and P-gly coprotein, Biomol. Struct. Dyn. (2020) 1221–1233.
[22] B. Hess, Convergence of sampling in protein simulations, Phys. Rev. E. 65 (2002) 1–10, https://doi.org/10.1103/PhysRevE.65.031910.
[23] S.E. Boyce, N. Tirunagari, A. Niedziela-Majka, J. Perry, M. Wong, E. Kan, L. Lagpacan, O. Barauskas, M. Hung, M. Fenaux, T. Appleby, W.J. Watkins, U. Schmitz, R. Sakowicz, Structural and regulatory elements of HCV NS5B polymerase - β-loop and C-terminal tail - are required for activity of allosteric thumb site II inhibitors, PLoS One 9 (2014), https://doi.org/10.1371/journal.pone.0084808.
[24] D.J. Begley, M.W. Brightman, Structural and functional aspects of the blood-brain barrier, Prog. Drug Res. 61 (2003) 39–78, https://doi.org/10.1007/978-3-0348-8049-7_2.
[25] C.A. Lipinski, F. Lombardo, B.W. Dominy, P.J. Feeney, Experimental and computational approaches to estimate solubility and permeability in drug discovery and development settings, Adv. Drug Deliv. Rev. 64 (2012) 4–17, https://doi.org/10.1016/j.addr.2012.09.019.
[26] M. Remko, A. Boháč, L. Kováčiková, Molecular structure, pKa, lipophilicity, solubility, absorption, polar surface area, and blood-brain barrier penetration of some antiangiogenic agents, Struct. Chem. 22 (2011) 635–648, https://doi.org/10.1007/s11224-011-9741-z.
[27] R.P. Heaney, Bioavailability of nutrients and other bioactive components from dietary supplements factors influencing the measurement of bioavailability, taking calcium as a model 1, J. Nutr. 131 (2001) 1344–1348. https://academic.

APPENDIX-IV

oup.com/jn/article-abstract/131/4/1344S/4686862.
[28] A. Trager, J. Jensen, Human malaria parasites in continuous culture, J. Natl. Med. Assoc. 68 (1976) 530–533.
[29] C. Lambros, J.P. Vanderberg, Synchronization of plasmodium falciparum erythrocytic stages in culture, J. Parasitol. 65 (1979) 418–420.
[30] M.T. Makler, J.M. Ries, J.A. Williams, J.E. Bancroft, R.C. Piper, B.L. Gibbins, D.J. Hinrichs, Parasite lactate dehydrogenase as an assay for Plasmodium falciparum drug sensitivity, Am. J. Trop. Med. Hyg. 48 (1993) 739–741, https://doi.org/10.4269/ajtmh.1993.48.739.
[31] A.D. Forkuo, C. Ansah, K.B. Mensah, K. Annan, B. Gyan, A. Theron, D. Mancama, C.W. Wright, In vitro antimalarial interaction and gametocytocidal activity of cryptolepine, Malar. J. 16 (2017) 1–9, https://doi.org/10.1186/s12936-017-2142-z.
[32] J. Reader, M. Botha, A. Theron, S.B. Lauterbach, C. Rossouw, D. Engelbrecht, M. Wepener, A. Smit, D. Leroy, D. Mancama, T.L. Coetzer, L.M. Birkholtz, Nowhere to hide: interrogating different metabolic parameters of Plasmodium falciparum gametocytes in a transmission blocking drug discovery pipeline towards malaria elimination, Malar. J. 14 (2015) 1–17, https://doi.org/10.1186/s12936-015-0718-z.
[33] T. Mosmann, Rapid colorimetric assay for cellular growth and survival: application to proliferation and cytotoxicity assays, J. Immunol. Methods 65 (1983) 55–63, https://doi.org/10.1016/0022-1759(83)90303-4.
[34] J.C. Domingue, M. Ao, J. Sarathy, A. George, W.A. Alrefai, D.J. Nelson, M.C. Rao, HEK-293 cells expressing the cystic fibrosis transmembrane conductance regulator (CFTR): a model for studying regulation of Cl- transport, Phys. Rep. 2 (2014) 1–16, https://doi.org/10.14814/phy2.12158.
[35] K.M. Krawczyk, D. Matak, L. Szymanski, C. Szczylik, C. Porta, A.M. Czarnecka, Culture in embryonic kidney serum and xeno-free media as renal cell carcinoma and renal cell carcinoma cancer stem cells research model, Cytotechnology 70 (2018) 761–782, https://doi.org/10.1007/s10616-017-0181-5.
[36] Z. Yang, K. Lasker, D. Schneidman-Duhovny, B. Webb, C.C. Huang, E.F. Pettersen, T.D. Goddard, E.C. Meng, A. Sali, T.E. Ferrin, UCSF Chimera, MODELLER, and IMP: an integrated modelling system, J. Struct. Biol. 179 (2012) 269–278, https://doi.org/10.1016/j.jsb.2011.09.006.
[37] A. Sali, T. Blundell, A. Sali, T.L. Blundell, Comparative modelling by satisfaction of spatial restraints, J. Mol. Biol. 234 (1994) 779–815, https://doi.org/10.1006/jmbi.1993.1626. J. Mol. Biol. 234, 779-815.
[38] P.C. Nair, J.O. Miners, Molecular dynamics simulations: from structure function relationships to drug discovery, Silico Pharmacol. 2 (2014) 1–4, https://doi.org/10.1186/s40203-014-0004-8.
[39] W.L. Jorgensen, J. Chandrasekhar, J.D. Madura, R.W. Impey, M.L. Klein, Comparison of simple potential functions for simulating liquid water, J. Chem. Phys. 79 (1983) 926–935, https://doi.org/10.1063/1.445869.
[40] J.E. Basconi, M.R. Shirts, Effects of temperature control algorithms on transport properties and kinetics in molecular dynamics simulations, J. Chem. Theor. Comput. 9 (2013) 2887–2899, https://doi.org/10.1021/ct400109a.
[41] P. Gonnet, P-SHAKE: a quadratically convergent SHAKE in O (n2), J. Comput. Phys. 220 (2007) 740–750, https://doi.org/10.1016/j.jcp.2006.05.032.
[42] J.P. Ryckaert, G. Ciccotti, H.J.C. Berendsen, Numerical integration of the cartesian equations of motion of a system with constraints: molecular dynamics of n-alkanes, J. Comput. Phys. 23 (1977) 327–341, https://doi.org/10.1016/0021-9991(77)90098-5.
[43] J.A. Izaguirre, D.P. Catarello, J.M. Wozniak, R.D. Skeel, Langevin stabilization of molecular dynamics, J. Chem. Phys. 114 (2001) 2090–2098, https://doi.org/10.1063/1.1332996.
[44] E. Seifert, OriginPro 9.1: Scientific data analysis and graphing software - software review, J. Chem. Inf. Model. 54 (2014) 1552, https://doi.org/10.1021/ci500161d.